

Multi-Purpose Detector

Solenoidal Magnet

Technical Design Report

August 2019

CONTENTS

| | | |
|-----------|---|----|
| 1 | INTRODUCTION | 4 |
| 2. | MPD MAGNET | 5 |
| 2.1 | Purpose | 5 |
| 2.2 | Technical Characteristics | 5 |
| 2.3 | Components | 8 |
| 2.4 | Design and Operation | 9 |
| 2.4.1 | Structural arrangement | 9 |
| 2.4.2 | Superconducting coil | 13 |
| 2.4.2.1 | Superconducting cable | 13 |
| 2.4.2.2 | Turn-to-turn and ground wall insulation | 16 |
| 2.4.2.3 | Conductor Joints | 16 |
| 2.4.2.4 | Support cylinder | 16 |
| 2.4.2.5 | SC Coil | 17 |
| 2.4.2.5.1 | Coil manufacturing | 17 |
| 2.4.2.5.2 | Static structural strength of the SC coil | 20 |
| 2.4.2.6 | Coil cooling | 22 |
| 2.4.3 | Cryostat of the Solenoid | 24 |
| 2.4.3.1 | Vacuum vessel of the Cryostat | 25 |
| 2.4.3.2 | Cold mass | 27 |
| 2.4.3.3 | Thermal insulation of the cryostat cold mass | 27 |
| 2.4.3.4 | Cold mass suspension | 29 |
| 2.4.3.5 | Thermal shield | 33 |
| 2.4.3.6 | Control Dewar | 34 |
| 2.4.3.7 | Chimney | 37 |
| 2.4.3.8 | Vapor cooled current leads | 39 |
| 2.4.3.9 | Connecting bus lines and feedthrough insulators | 39 |
| 2.4.3.10 | Assembling the cryostat | 40 |
| 2.4.3.11 | Fixating the cryostat to the yoke | 41 |
| 2.4.3.12 | Busbar on the cryostat outer surface to compensate the stray field of the reverse coil current lead | 43 |
| 2.4.4 | Vacuum system | 45 |
| 2.4.5 | Cryogenic safety system for the vacuum vessel | 48 |
| 2.4.6 | Cryostatting system for the superconducting coil | 48 |
| 2.4.7 | Superconducting coil protection system | 51 |
| 2.4.7.1 | Emergency de-energizing of the superconducting coil | 53 |
| 2.4.7.2 | Accelerated de-energizing of the superconducting coil | 55 |
| 2.4.8 | Yoke | 55 |
| 2.4.8.1 | Yoke barrel | 60 |
| 2.4.8.2 | Magnet poles | 63 |
| 2.4.8.3 | Positioning of the MPD magnet for assembly and operation | 68 |
| 2.4.8.4 | Magnet and pole supports | 75 |
| 2.4.8.5 | Yoke and pole transport systems | 78 |
| 2.4.8.6 | Roller skates for moving the magnet and the poles | 80 |
| 2.4.8.7 | Rail tracks for moving the magnet and the poles | 82 |
| 2.4.9 | Adjusting the spatial position of the magnet | 84 |
| 2.4.10 | Fixing poles into borings of the yoke support rings | 85 |
| 2.4.11 | Hydraulic systems of the MPD magnet | 86 |
| 2.4.11.1 | Hydraulic jacks of the magnet | 87 |

| | | |
|----------|--|-----|
| 2.4.11.2 | Yoke movement hydraulic system | 87 |
| 2.4.11.3 | Pole movement hydraulic system | 90 |
| 2.4.12 | Pole trim coils | 92 |
| 2.4.13 | Power supply of the magnet coils | 97 |
| 2.4.13.1 | Power supply system of the magnet coils | 97 |
| 2.4.13.2 | Superconducting coil power supply | 99 |
| 2.4.13.3 | Power supplies of the pole trim coils | 100 |
| 2.4.14 | Seismic safety of the magnet | 101 |
| 2.4.15 | Passages for running cabling and tubing out of the magnet aperture | 101 |
| 2.4.16 | The upper platform for the equipment of the magnet | 105 |
| 2.5 | Assembling the magnet | 105 |
| 2.5.1 | Test assembly of the yoke at the manufacturer's | 105 |
| 2.5.1.1 | Assembling the poles | 105 |
| 2.5.1.2 | Assembling the yoke barrel in the vertical position | 105 |
| 2.5.1.3 | Acceptance tests of the yoke in the horizontal position | 109 |
| 2.5.2 | Disassembly and transportation of the yoke | 109 |
| 2.5.3 | Final assembly of the magnet in Dubna | 109 |
| 2.5.3.1 | Assembling the magnet with the cryostat | 109 |
| 2.5.3.2 | Acceptance tests of the assembled magnet | 113 |
| 3 | Cryogenic system of the MPD magnet | 114 |
| 3.1 | Components of the cryogenic system | 114 |
| 3.2 | Coil cryostatting equipment | 114 |
| 3.2.1 | Helium SATELLITE refrigerator | 114 |
| 3.2.2 | Nitrogen re-condenser for cooling (heating) and cryostatting the thermal screens | 115 |
| 3.2.3 | Transfer lines | 115 |
| 3.3 | Operating regimes | 116 |
| 3.3.1 | Cooling from 300 to 4.5 K | 116 |
| 3.3.2 | Steady-state regime | 118 |
| 3.3.3 | Warming-up regime | 119 |
| 3.3.4 | Emergency regime I (sc coil quenching) | 120 |
| 3.3.5 | Cooling of the coil after quenching | 121 |
| 3.3.6 | Emergency regime II (staelite refrigerator failure) | 121 |
| 3.3.7 | Emergency regime III (on site power failure) | 122 |
| 3.3.8 | Emergency regime IV (current lead voltage rise above allowable level) | 122 |
| 3.3.9 | Emergency regime V (loss of vacuum) | 123 |
| 3.3.10 | Emergency regime VI (nitrogen re-condenser failure) | 123 |
| 3.4 | Controlled parameters and control actions | 124 |
| 4 | control system of the Magnet | 129 |
| 4.1 | Purpose | 129 |
| 4.2 | General structure | 129 |
| 4.3 | Lower level structure (transducers and actuators) | 131 |
| 4.4 | Middle level structure (master controllers) | 131 |
| 4.5 | Upper level structure (servers) | 131 |
| 5 | Transportation of the magnet | 132 |
| | References | 133 |
| | Appendix 1. Superbolts | 135 |
| | appendix 2. Roller skates | 137 |
| | appendix 3. Instrumentation system hardware | 140 |
| | appendix 4. Reconfigurable instrumentation system software | 143 |
| | appendix 5. ASSEMBLY DRAWINGS OF THE SOLENOID | 145 |
| | appendix 6. ASSEMBLY DRAWINGS OF THE YOKE | 151 |

| | |
|---|-----|
| appendix 7. THERMAL CALCULATION | 156 |
| appendix 8. Magnetic verification | 182 |
| appendix 9. Magnet Power Supply System | 204 |
| appendix 10. Power supplies general specifications and performances | 220 |
| appendix 11. Quench Calculation | 232 |
| appendix 12. HELIUM REFRIGERATOR DESCRIPTION | 257 |

1 INTRODUCTION

The multipurpose detector (MPD) is a 4π spectrometer to be used for studying charged hadrons, electrons, and photons generated in heavy ion collisions at energies provided by the NICA collider of the Joint Institute for Nuclear Research (Dubna). Figure 1.1 shows the general 3D view of the MPD with the inner detectors.

A constituent part of the MPD is a superconducting solenoid magnet with a superconducting NbTi coil and a steel flux return yoke. All magnet interfaces, including those for inner detectors, are described in [1].

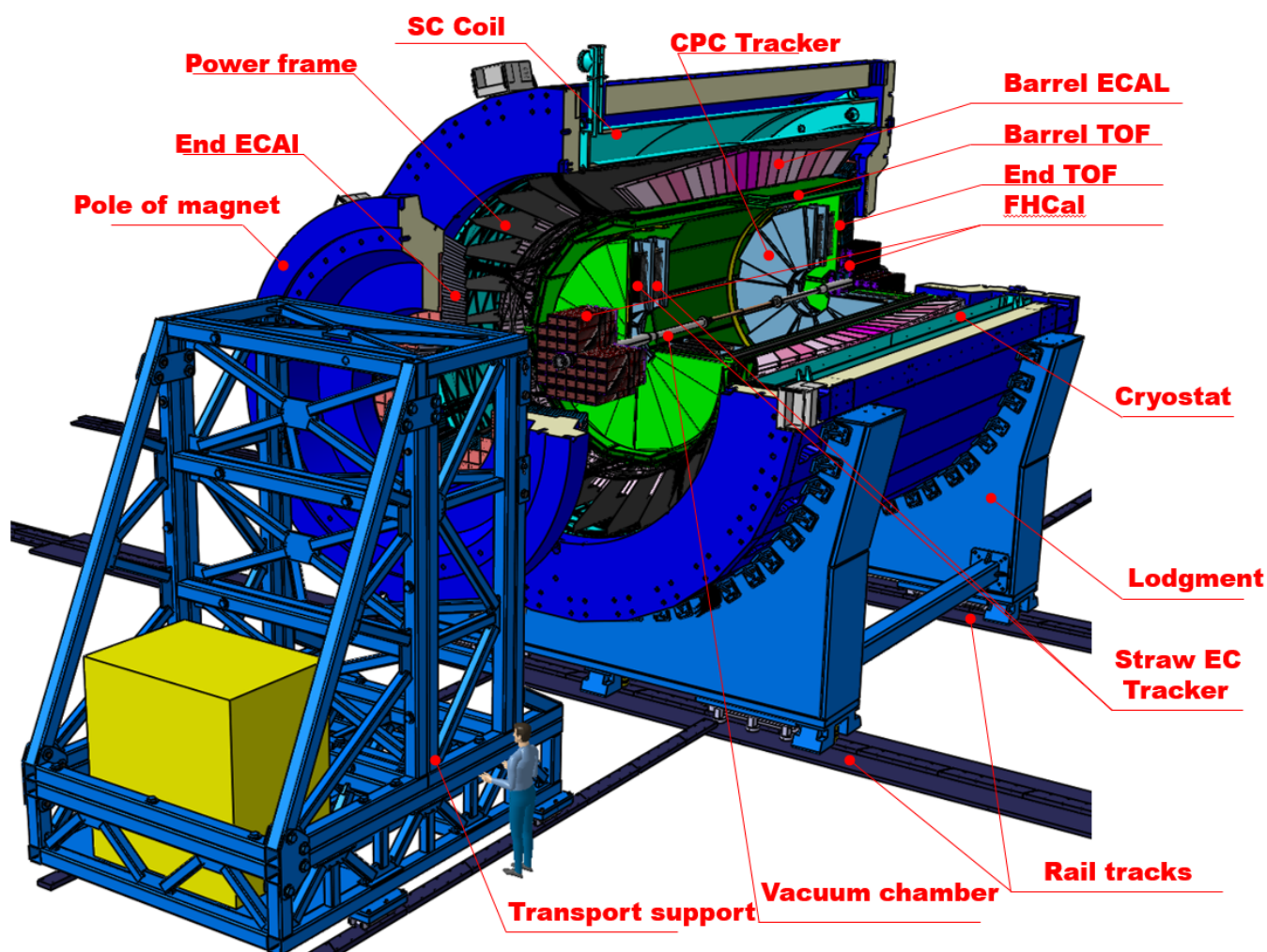


Fig. 1.1. 3D view of the MPD

2. MPD MAGNET

2.1 PURPOSE

The superconducting magnet of MPD is intended for providing a highly homogeneous magnetic field of 0.57 T in an aperture 4596 mm in diameter to ensure the transverse momentum resolution within the range of 0.1–3 GeV/c at NICA.

2.2 TECHNICAL CHARACTERISTICS

The main parameters of the MPD magnet are listed in Table 2.2.1. General view drawing 3HM1002.00.000BO of the solenoid is given in [2]. Requirements to the radial magnetic field component of the MPD solenoid in the cylindrical volume of the Charged Particle Tracker (TPC) are listed in Table 2.2.2. The field inhomogeneity in the TPC region must be less than 10^{-3} .

According to the calculations, the integral of the radial component of the magnetic induction in the TPC region for the nominal dimensions of the magnet system is

$$Int = \int_z^{z_{max}} \frac{B_r}{B_z} dz \leq 0.08 \text{ mm}$$

and the inhomogeneity of the magnetic field is

$$\delta = \frac{|B|_{\max} - |B|_{\min}}{2B_0} = 3 \cdot 10^{-4}$$

However, the real inhomogeneity and the integral of the radial component appear to be greater due to the technological deviations in dimensions that arise during the manufacture and assembly of the magnet. Nevertheless, the calculations show that even with the deviations, the homogeneity remains better than 10^{-3} and the integral of the radial component is $Int \leq 1.5$ mm. The influence of possible deviations from the nominal geometrical dimensions due to technological manufacture and mounting inaccuracy on the integral of the radial magnetic induction component is illustrated in Table 2.2.3.

The main dimensions of the cryostat and the magnet yoke are listed in Table 2.2.4.

Rated current of the magnet is 1790 A (it corresponds to a field in the aperture of 0.5 T). The maximum magnet field at which the specified value of the integral of the radial component of the induction in the area of TPC $Int \leq 1.5$ mm is maintained, and which can be achieved with a maximum level of technological deviations from the optimized geometry of the magnetic system, is 0.57 T. Maximum level of deviation is accepted as the simultaneous shift of SC coil in the axial direction by 20mm, the symmetrical increase of the interpole distance of $2 \times 5 = 10$ mm, the linear change of the current density along the SC coil by 2%, SC coil radial offset by 20 mm, and the radial offset of one of the poles 1 mm. These values were obtained by expert judgment based on analysis of current manufacturing technologies of the detector magnets. Restriction on the field adjustment at the maximum level of the technology deviations for the induction above 0.57 T is imposed by allowable value of the trim coil currents - 151 kA-turns. The maximum field which can be achieved without any technological deviations from the optimized geometry is 0.64 T. This means that in the field interval 0.57 - 0.64 T the specified value of the integral of the radial component of induction can be achieved by reducing to zero the level of technological deviations. The maximum design current of the magnet is 2388 A, which corresponds to a field 0.66 T. Assuming that the maximum test current is equal to the

maximum design current and shall be 5% above the maximum operating current, we find that the maximum operating field of the magnet is 0.629 T. However, it is unlikely that the actual level of technological deviations would provide this field while maintaining a given value of the radial component of induction. The practical value of the maximum operating field will be clarified after the magnet test and measuring of the magnetic field distribution in the tracker area.

The design life of the MPD magnet is 15 years.

Table 2.2.1. Main characteristics of the MPD magnet

| | |
|---|------------|
| Rated current, kA | 1.79 |
| Rated induction, T | 0.5 |
| Maximum design current, kA | 2.4 |
| Maximum flux density in the coil at maximum design current, T | 1.2 |
| Total current (ampere-turns) at the rated induction, MA | 3.0 |
| Stored energy at the rated induction, MJ | 14.6 |
| Stored energy at the maximum design current, MJ | 25.4 |
| Bare SC cable cross section, mm ² | 4.1 x 20 |
| Insulated SC cable cross section, mm ² | 4.5 x 20.4 |
| Number of turns in the SC coil | 1674 |
| Inductivity of the SC coil, H | 8.7 |
| Inductivity of the trim coil, H | 0.007 |
| Mutual inductivity of the SC coil and each of the trim coils, H | 0.05 |
| Decentering axial force density dF_z/dz , kN/cm | 61 |
| Decentering radial force density dF_r/dr , kN/cm | 5.4 |
| Rated current density in the trim coil at the nominal induction $B=0.5$ T, A/mm ² | 1.142 |
| Total current (ampere-turns) in the trim coil at the nominal induction $B=0.5$ T, kA | 104 |
| Maximum current density in the trim coil for compensation of technological deviation in dimensions, A/mm ² | 1.507 |
| Number of turns in each of the trim coils | 34 |
| Hollow aluminum cable cross section in the trim coil, mm ² | 42 x 42 |

Table 2.2.2. Requirements to the MPD magnetic field homogeneity in the TPC volume

| | | |
|--|---|--------------------------|
| Radial magnetic field component $z \geq 0,$ $z_{max} = +1700 \text{ mm}$ $403 \text{ mm} < r < 1203 \text{ mm}$ | $Int = \int_z^{z_{max}} \frac{B_r}{B_z} dz$ | $ Int < 1.5 \text{ mm}$ |
| Radial magnetic field component $z \leq 0,$ $z_{min} = -1700 \text{ mm}$ $403 \text{ mm} < r < 1203 \text{ mm}$ | $Int = \int_z^{z_{min}} \frac{B_r}{B_z} dz$ | $ Int < 1.5 \text{ mm}$ |

Table 2.2.3. Characteristics of the MPD magnet with variation in geometrical dimensions

| Nature of deviation from nominal position | Integral of the radial component B_r/B_z [mm] | Current density in the trim ₁ / trim ₂ coils [A/mm ²] |
|---|---|---|
| None | 0.08 | 1.142/1.142 |
| Complex axial deviation* | 0.41=0.08+0.33 | 0.851/1.507 |
| Radial shift of SC coil by 20 mm | 0.27=0.08+0.19 | 1.142/1.142 |
| Radial shift of a pole by 1 mm | 0.21=0.08+0.13 | 1.142/1.142 |
| Total complex deviation | 0.73=0.08+0.33+0.19+0.13 | 0.851/1.507 |

- * Simultaneous shift of the SC coil in the axial direction by 20 mm, symmetrical increase of the interpole distance by $2 \times 5 = 10$ mm, and linear change in the current density along the SC coil by 2%

Table 2.2.4. Main dimensions of the cryostat and the yoke

| Cryostat | |
|--------------------------------|------|
| Inner diameter (warm hole), mm | 4656 |
| Outer diameter, mm | 5443 |
| Length, mm | 7910 |
| Yoke | |
| Inscribed diameter, mm | 5883 |
| Circumscribed diameter, mm | 6583 |
| Interpole distance, mm | 7390 |
| Length, mm | 8970 |

2.3 COMPONENTS

The MPD magnet consists of (Fig. 2.3.1)

- A cryostat with a superconducting coil and a control Dewar
- A flux return yoke with two support rings, 28 bars, and two poles with trim coils
- Magnet support cradles
- Auxiliary platforms for moving the poles
- Stationary supports
- Hydraulic actuators for displacement of the yoke and poles
- Roller skates for movement of the magnet and its poles.

In addition, there are power supplies for the superconducting coil and for the trim coils in the poles, a SC coil quenching protection system, a cryogenic system with the cryogenic pipeline, a vacuum system, helium refrigerator and a magnet control system.

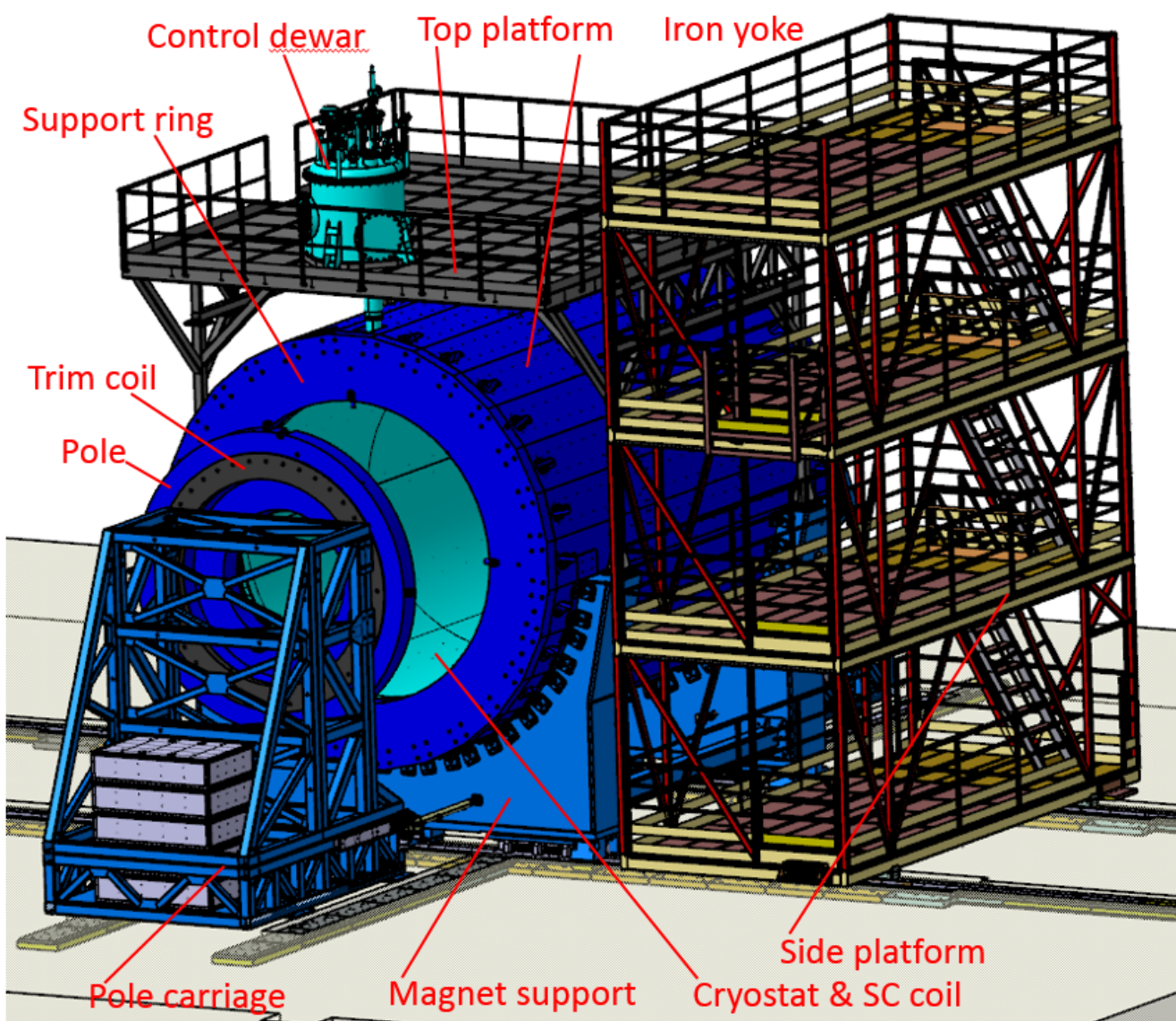


Fig. 2.3.1. MPD magnet

2.4 DESIGN AND OPERATION

2.4.1 STRUCTURAL ARRANGEMENT

The set of drawings of the main MPD magnet assemblies [2] contains assembly drawings of the main units of the magnet yoke and the cryostat with the superconducting coil.

Structurally, the MPD magnet yoke is a cylindrical barrel-like structure, which consists of 28 beams that return the magnetic flux of the coil, two support rings, two poles, and two support cradles that carry the total weight of the detector (Fig. 2.3.1, Fig. 2.4.1.1). The MPD yoke design is similar to that of the STAR magnet [3]. The support rings are made as single forged pieces. In general, the adopted structural arrangement of the yoke guarantees high rigidity of the whole magnet and will ensure the required field homogeneity (integral of the radial magnetic induction component) in the TPC region after subsequent withdrawals of the poles and multiple movements of the magnet to the assembly site for updating or repair.

The cryostat with the superconducting coil is placed inside the flux return yoke (Fig. 2.3.1). After alignment of the coil with the support rings, the cryostat is rigidly fixed inside the yoke barrel.

The weight load of the inner detectors is transferred directly to the support rings and further to the support cradles. The weight of the cryostat, as well as the decentering magnetic forces caused by the coil installation uncertainty, is transferred to the yoke beams and further to the support rings.

When being assembled and when installed in the accelerator, the magnet rests on ten stationary supports. Roller skates and rail tracks are used for moving it with the cryostat and inner detectors from the assembly site to the operating position. Ten hydraulic jacks in the stationary supports allow transferring the magnet from the stationary supports to the roller skates and back again. The yoke and the completely assembled magnet are moved along the rail track using two bidirectional hydraulic cylinders and removable stops.

Two end caps installed within the support rings form a magnet poles. The magnet poles equipped with the trim coils are assembled and mounted on individual platforms with roller skates. Each platform with the magnet poles can be moved on its own rail track in the collider axis direction by two hydraulic cylinders (see section 2.4.8.2). The disc calorimeters (ECal) are fixed on the poles. Their weight loads are transferred to the tips of the poles.

The assembled flux return yoke is moved along the rail track to the intermediate position, where the poles are mounted. In this place the poles are moved up to the yoke and fixed to the support rings by pole stops with M48 bolts (Fig.2.3.1). Relative parallelism of the poles planes, positions of poles axes relative to the central magnet axis, and positions of the poles relative to the magnet center are corrected by inserting spacers between the pole stops and the support rings. The final positions of the poles are fixed by the locking pins.

Any time when the yoke barrel with the internal detectors is moved to the assembly site for repair or maintenance, the poles are pulled out of the magnet and stay on the platforms on their rail tracks.

A control Dewar is installed on the upper beam of the yoke barrel. It is connected to the cryostat by a demountable connecting pipe through the slot in the upper barrel beam. The control Dewar is connected to the forward and backward liquid Helium and Nitrogen pipelines

by bayonet-type joints on its side wall. The top plate of the control Dewar is supplied by the terminals of the gas-cooled current leads to which the SC coil power supply is connected, relief valves, and other valves and electrical connectors of the coil protection and control system. At the outer sides of the magnet poles there are electrical terminals for the power supplies and connecting pipes for the hydraulic cooling system of the trim coils.

On top of the magnet there is a platform to accommodate vacuum pumps, a power supply and protection system of the SC coil (Fig. 2.4.1.2).

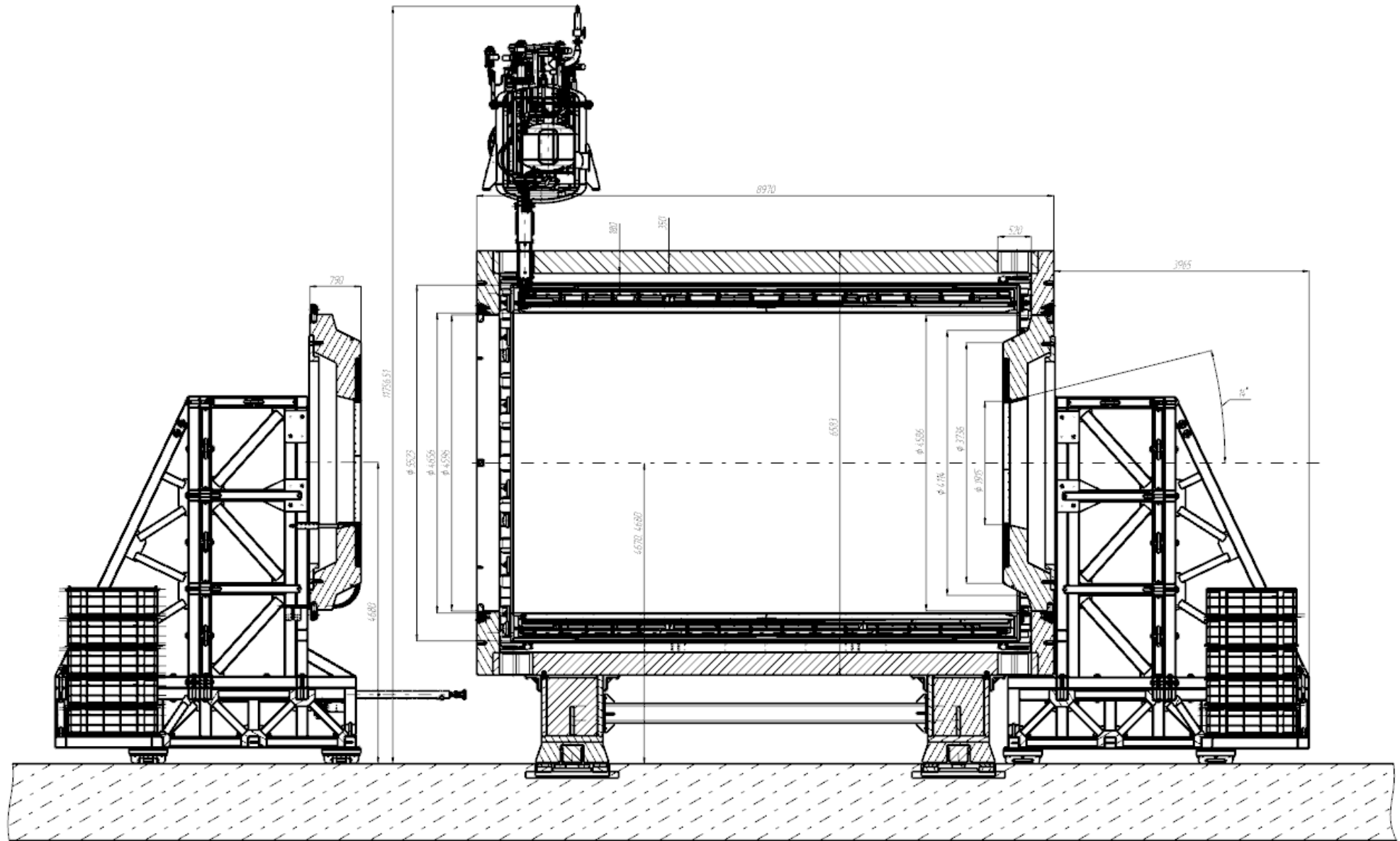


Fig. 2.4.1.1. Longitudinal cross section of the MPD magnet

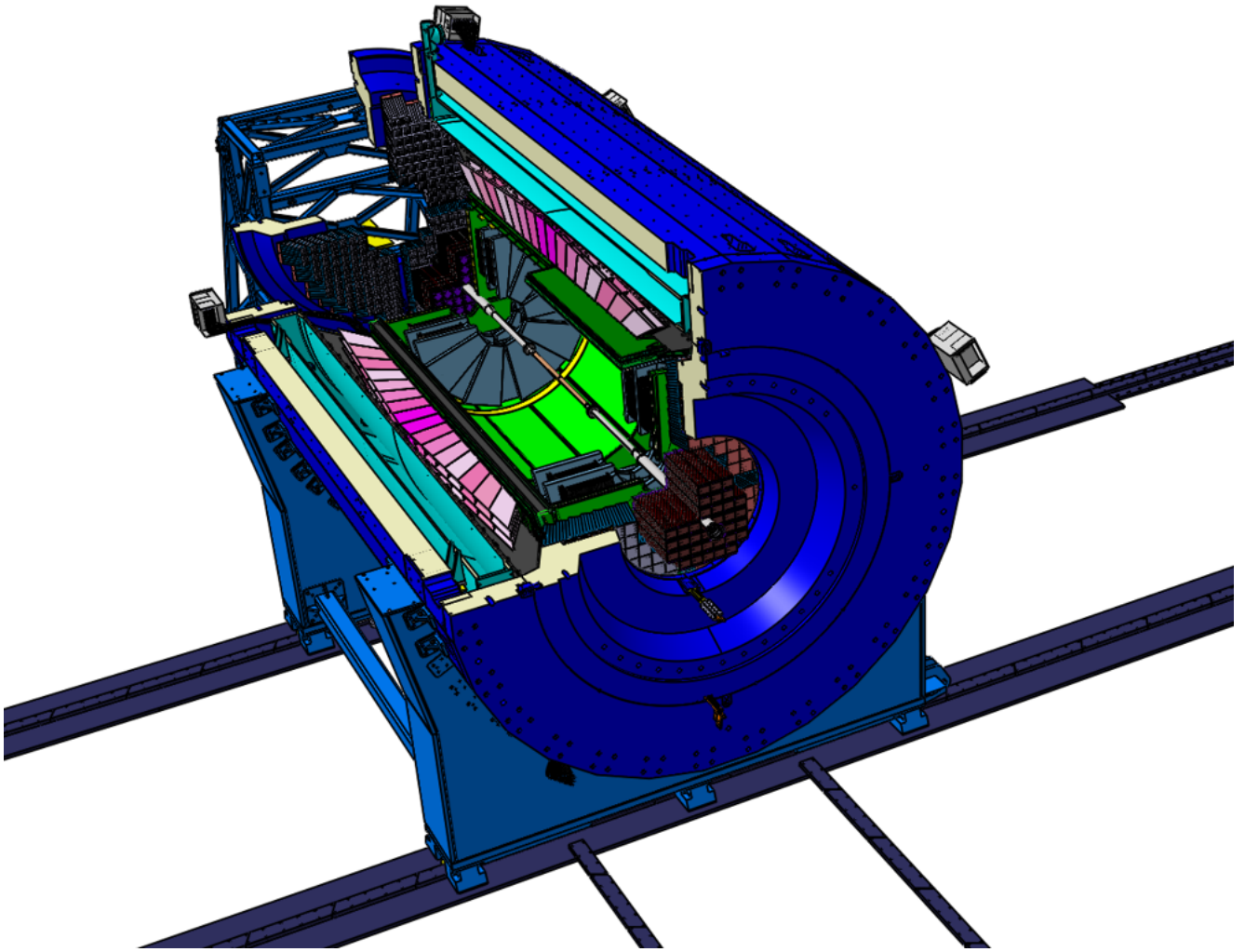


Fig. 2.4.1.2. Assembled magnet on the stationary supports

2.4.2 SUPERCONDUCTING COIL

2.4.2.1 SUPERCONDUCTING CABLE

A conductor with a bare cross section of $4.1 \times 20 \text{ mm}^2$ is used for winding the superconducting coil (the insulated conductor cross section is $4.5 \times 20.4 \text{ mm}^2$). The conductor is manufactured by co-extrusion of stabilizing high-purity aluminum (purity 99.999%, RRR>1000) and a superconducting NbTi wire 1.5 mm in diameter (Cu/SC ratio =0.9/1). Highly pure aluminum ensures high stability of the coil due to the low matrix resistance at the helium temperature, which allows the premature propagation of the normal zone to be avoided when local heat emissions occur in the coil due to mechanical disturbances during the energizing and de-energizing of the magnet. The cross section of the MPD solenoid superconducting coil is shown in Fig. 2.4.2.1.1.

A distinctive feature of this solenoid is that the main superconducting coil has no correcting coils at its ends. This is because maintaining the needed value of the radial component integral would require rigid adherence to the relationship between the numbers of the turns in the main and correcting coils within the given coil dimensions, which is hardly possible in view of the manufacturing tolerances on the conductor cross section.

The choice of the conductor parameters is presented in [4]. The main parameters are listed in Table 2.4.2.1.1.

The radial thickness of the conductor was chosen to be 20 mm for the reason of limiting the maximum temperature rise after all stored magnetic energy is released in the coil at the unprotected quench process.

The maximum design current of 2388 A (Table 2.2.1) at the maximum magnetic induction of 1.2 T in the coil corresponds to the critical conductor temperature of $\sim 6.8 \text{ K}$ and is approximately 2.9 times lower than the critical current in the conductor at a temperature of 4.5 K and the same induction. The safety margin of the maximum current in relation to the critical current according to the critical parameter curve at $T=4.5 \text{ K}$ is ~ 1.9 (Fig.2.4.2.1.2).

The stability level of the chosen conductor corresponds to that of other similar magnetic systems. The minimum energy necessary for the superconducting-normal transition of the coil (Minimum Quench Energy) is $\text{MQE} \approx 3 \text{ J}$. Calculations of the MQE and the length of the minimal propagating zone MPZ using the QUENCH code are given in [5].

Table 2.4.2.1.1. Main parameters of the cable

| | |
|---|------------------|
| Superconductor | NbTi/Cu |
| Stabilizer | Pure Al |
| RRR of stabilizer | >1000 |
| Strand diameter, mm | 1.75 ± 0.005 |
| Filament diameter, μm | ~20 |
| Number of filaments | ~2000 |
| Twist pitch, mm | ~20 |
| RRR of copper matrix | >100 |
| SC/Cu/Al ratio | 1:0.9:100 |
| Outer dimensions of bare conductor, mm^2 | 4.1 x 20 |
| Edge radius, mm | 0.2 |
| Insulated conductor dimensions, mm^2 | 4.5 x 20.4 |
| Current density in aluminum matrix of coil conductor for design current, A/mm^2 | 29.8 |
| Critical current density $J_c(5 \text{ T}, 4.2 \text{ K}), \text{A}/\text{mm}^2$ | 2800 |
| Critical current (1.2 T, 4.5 K), kA | >6.9 |
| Number of turns in winding | 1674 |
| Conductor length, km | ~27 |
| Conductor weight, kg | ~6350 |

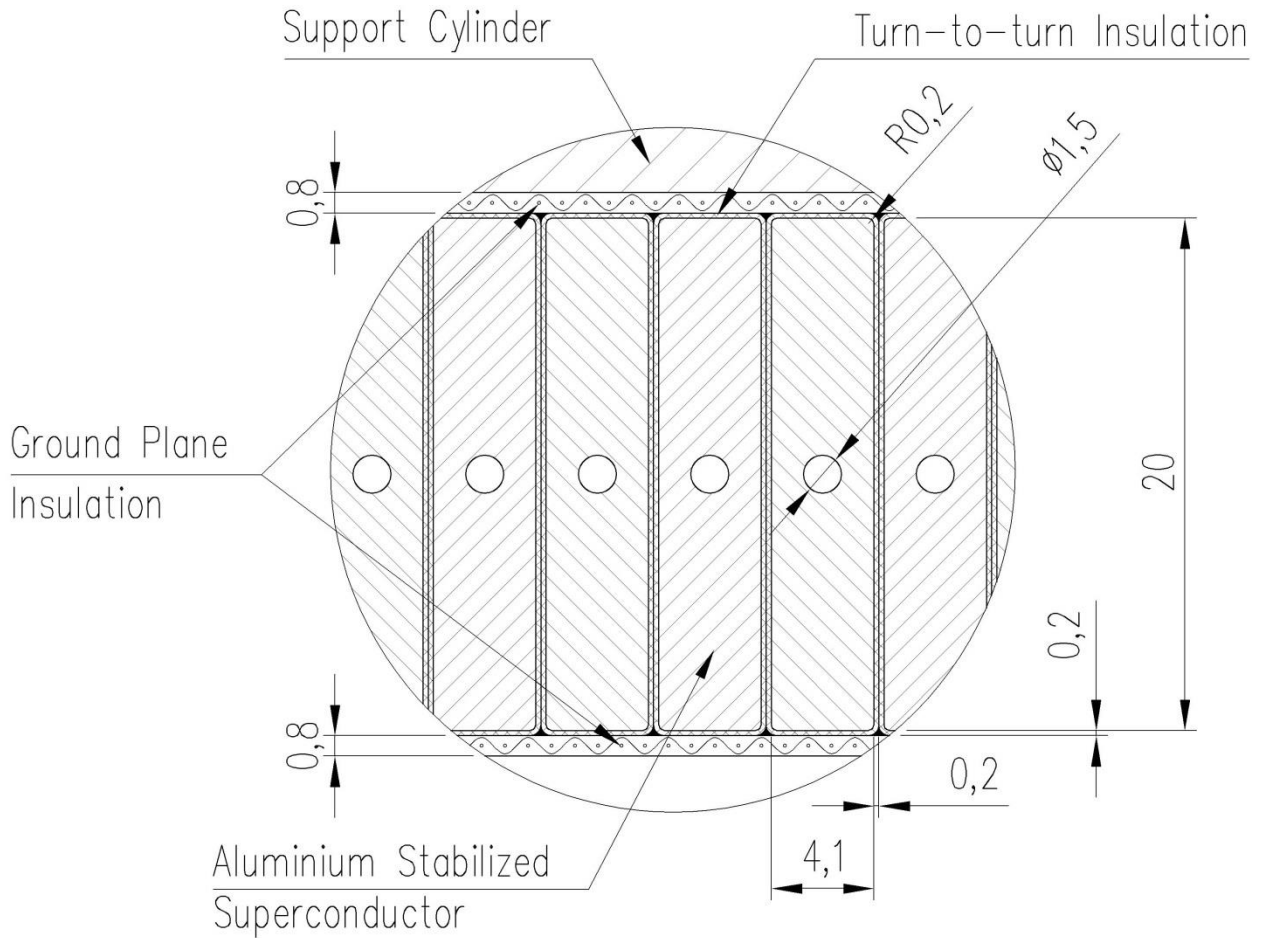


Fig. 2.4.2.1.1. Cross section of the superconducting coil of the MPD solenoid

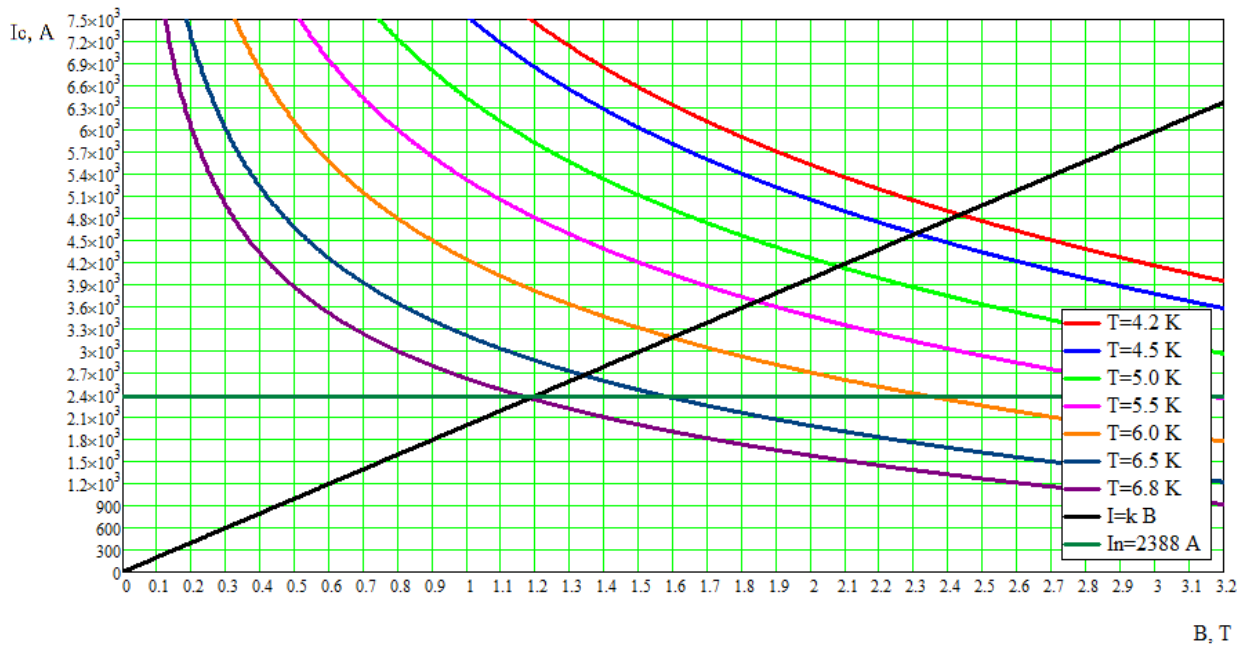


Fig. 2.4.2.1.2. Magnet load line $I(B)$ for the point with the maximum induction in the coil and the critical parameter curves of the conductor with $d=1.5$ mm at a temperature from 4.2 K to 6.8 K for $J_c(4.2$ K, 5 T) $=2800$ A/mm²

2.4.2.2 TURN-TO-TURN AND GROUND WALL INSULATION

The coil insulation consists of the turn-to-turn insulation, which separates coil turns, and the ground wall insulation between the coil and the support cylinder. The insulation is designed for the maximum voltage up to 500 V relative to the support cylinder at the energy release during the quench. The ground wall insulation is made of G10 fiberglass 0.8 mm thick applied to the inner surface of the aluminum support cylinder before the coil winding begins. The turn-to-turn insulation is made by the fiberglass tape wrapping the conductor with half-width overlap before winding the coil. After vacuum impregnation with epoxy compound and thermal treatment, the conductor gets turn insulation with a total thickness of 0.2 mm per side of the conductor (Fig. 2.4.2.1.1).

2.4.2.3 CONDUCTOR JOINTS

There will be several joints of superconductor pieces in the coil. These joints will be made by soft-alloy soldering over the whole turn length. The resistance of each joint must be $< 1e-9$ Ohm @ $B = 1$ T to ensure that losses in a joint no higher than a few mW.

According to calculations, the presence of the joints doesn't virtually effect on the values of the integral of the radial component of induction and the field homogeneity in the TPC area [10].

Thickness of a finished length of the conductor can vary in the range of $1 \div 2\%$ (it is determined by the process of extrusion).

Pieces of the superconducting cable when winding should be placed so that the directions of the turn width variation would interchange along the winding. It is necessary to reduce the influence of the current density variation along the coil on the integral of the radial induction component and on the force acting on the coil.

Two nonsuperconducting joints will be placed on the feedthrough insulators at the entrance of the lead-ins into the He volume of the control Dewar.

2.4.2.4 SUPPORT CYLINDER

The support cylinder serves to limit the azimuthal stresses in the aluminum matrix of the superconducting cable, which result from magnetic pressure, provide indirect cooling of the coil, and fix the coil inside the cryostat against weight load and magnetic decentering forces (Fig. 2.4.2.4.1). The cylinder will be made of the Al 5083 aluminum alloy. The weight of the cylinder is 6950 kg. The cylinder length is 7598 mm; its outer diameter is 5092 mm, the thickness is 18 mm in the central part and 45 mm at the ends, where tie rods are attached for suspending the cylinder on the outer vacuum shell of the cryostat and keeping it stable against the axial shifts.

Fabrication of an aluminum cylinder as large as this with machine treatment of its inner surface for laying the conductor is a difficult task that requires complicated auxiliary equipment. Before the final machine treatment of the inner cylinder surface, a heat exchanger tube is welded to the cylinder outer surface and the axial and radial tie rod fixation units are placed there.

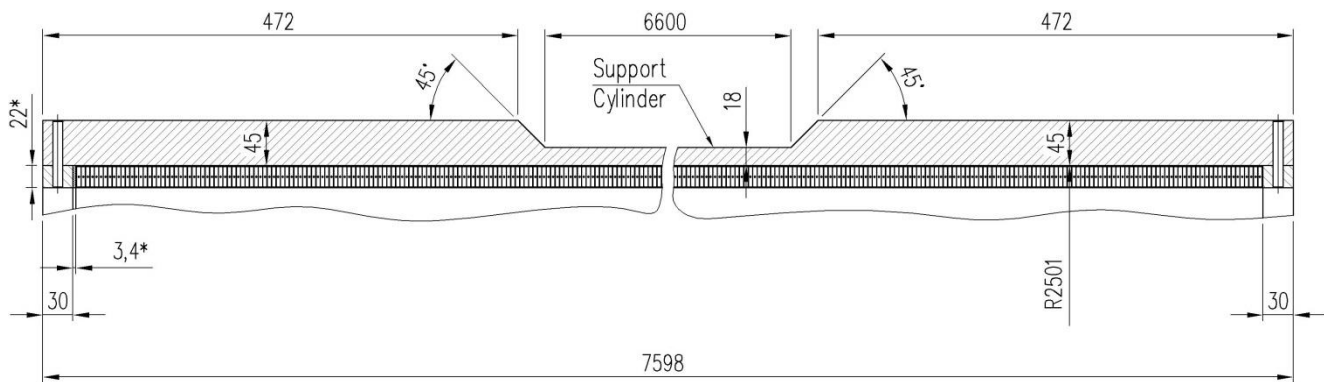


Fig. 2.4.2.4.1. Support cylinder with the superconducting coil (the dimensions are given for the “warm” state)

2.4.2.5 SC COIL

2.4.2.5.1 COIL MANUFACTURING

The coil is a one-layer solenoid made of a superconducting NbTi cable in the aluminum matrix. The conductor preinsulated by dry fiberglass tape is wound onto inside the support cylinder with the larger side of its cross section kept radially directed. Internal winding and indirect conductor cooling simplify the cryostat design and allow the amount of liquid He in the coil to be minimized, thus avoiding the risk of emergency pressure increase in the cryostat.

The ground-wall insulation is made by applying a fiberglass layer a few millimeters thick to the inner surface of the support cylinder. This layer, consisting of several prepreg layers, is compressed for having a high glass filling factor and then polymerized at the prescribed temperature. The inner surface of the insulation is machined to the final ground-wall insulation thickness of about 0.8 mm (Fig. 2.4.2.1.1).

To prevent unexpected quenching due to the local inelastic shifts of the conductor, the coil turns must be monolithically connected to each other and to the ground-wall insulation to avoid separation of the conductor and the insulation and the coil and the support cylinder.

At the several stations that the conductor will pass before being wound inside the cylinder, degreasing and sandblasting will be performed and the turn insulation (dry fiberglass tape) will be applied. The final station will be the caterpillar-type tensioner, which will help wind the conductor with slight compression (about few MPa) applied along the conductor axis. During the winding process, permanent axial compression will be applied to the coil with the aid of roller holders to ensure uniform winding density.

After the winding process is accomplished, a pressure of 10 MPa is applied to the coil in the axial direction using the aluminum end rings. Then a fiberglass ground plane insulation layer is applied to the inner surface of the coil and radially pressurized. Then vacuum compounding of the coil by epoxy resin with its high-temperature polymerization at a constant pressure is carried out.

Since it is a single-layer winding, its lead-out cable must come to the beginning of the winding to pass through the vacuum chimney to the cooled current leads in the control Dewar. This cable is directed strictly along the solenoid axis and is attached to the inner surface of the aluminum cylinder close to the cooling tube.

The inner diameter of the finished coil is 4958 mm and its length is 7534.6 mm (Fig. 2.4.2.5.1).

In the cooling-down mode and at the quenching the maximum allowed temperature gradient in the coil must be no higher than 20–30 K to avoid considerable thermomechanical stresses.

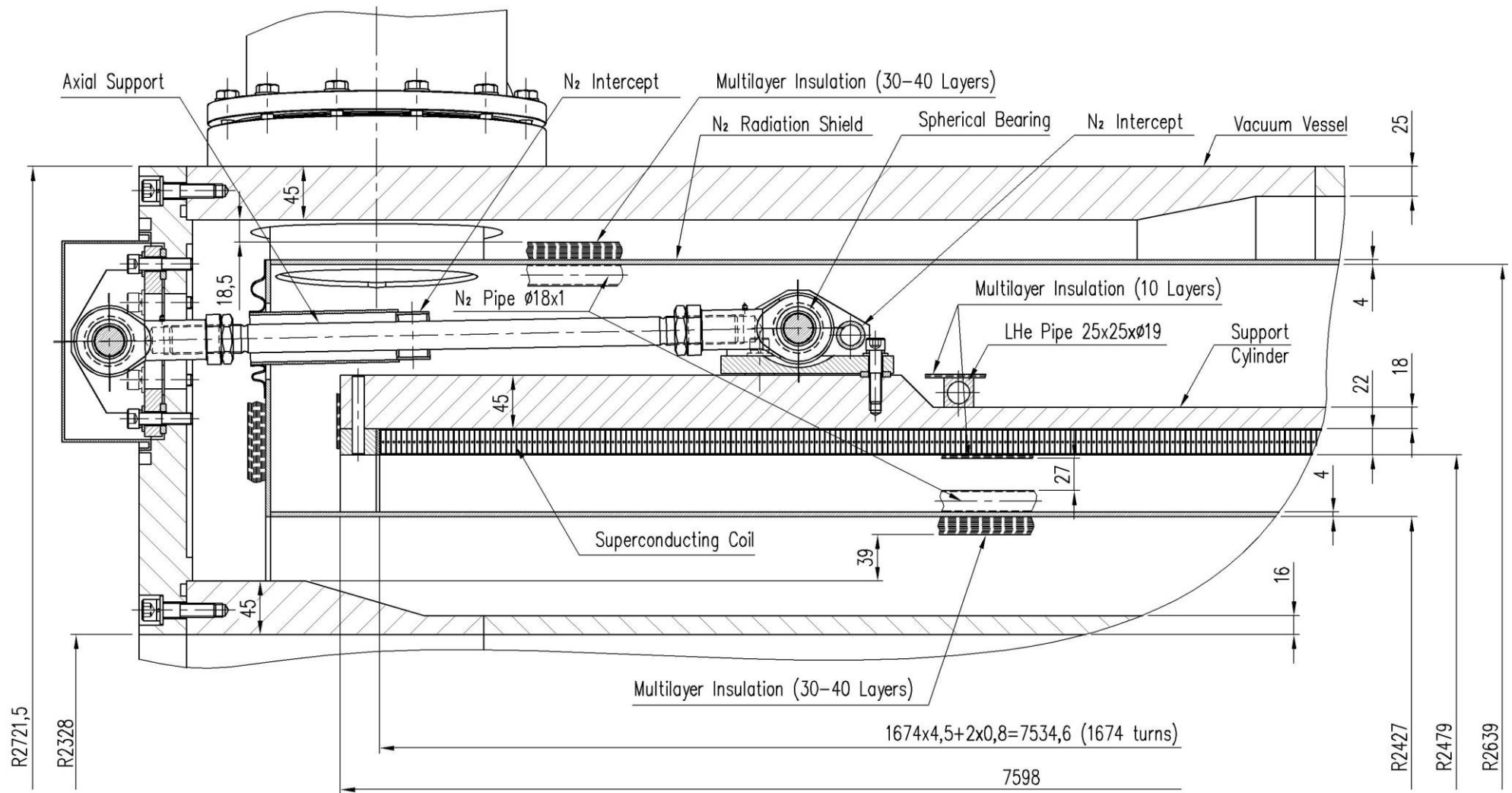


Fig. 2.4.2.5.1. Superconducting coil within the cryostat (the dimensions are given for the “warm” state)

2.4.2.5.2 STATIC STRUCTURAL STRENGTH OF THE SC COIL

The superconducting coil is a rather stressed component of the magnet. Its cooling is accompanied by appreciable thermal stresses arising from the difference of the thermal expansion coefficients of its constituent materials. The operating magnet produces a radial magnetic pressure of 0.1–0.175 MPa on the inner surface of the support cylinder. The axial magnetic force compressing the coil is as high as ≈ 688 kN at the central cross section of the coil. The axial forces acting on the coil are partially transmitted to the support cylinder through the ground-wall insulation.

The results of the SC coil stress-strain computation with allowance for the influence of the axial after-winding compression, cooling-down to the helium temperature, and action of the magnetic forces after the energizing are presented in [6]. The inelastic deformation of the aluminum matrix of the conductor is also taken into account.

The radius of the cooled coil decreases by 9.9–10.4 mm (the larger deformation corresponds to the end of the support cylinder). The magnetic pressure increases the coil radius by no more than 0.4 mm; the axial shortening of the coil after the cooling is 33.3 mm. In addition, magnetic forces make the coil ~ 0.5 mm shorter.

According to the computations, the maximum overall equivalent stresses in the support cylinder arise in its central part. The thickness-averaged equivalent stresses (von Mises) in the cylinder and the pressing rings after the cooling are 8.3 MPa, and those due to the joint influence of the temperature deformations and the magnetic force are 18.9 MPa, which is less than the allowable stress for Al5083 $[\sigma_m] = 92$ MPa. The maximum equivalent stresses that locally arise in areas of contact between the pressing rings and the coil turns in the cylinder and in the pressing rings do not exceed 117 MPa in all operation modes, which is less than the allowable value $[\sigma_{eq}] = 120$ MPa.

The temperature field gives rise to maximum equivalent stresses, which are 183 MPa $< [\sigma]$, in the superconducting NbTi cable at the coil ends. The cable is compressed due to the difference of the thermal expansion coefficients of the cable material and aluminum. At the center of the coil these stresses come to a lower value of 173 MPa (the cross section of the support cylinder is smaller in this region).

In the conductor matrix the maximum elasto-plastic equivalent stresses in a small region around the superconducting cable in the end turns of the coil are as high as 21 MPa, and at the center of the coil these stresses have a lower value of 19.7 MPa.

The average equivalent stresses in the conductor matrix at the coil center are ~ 4.3 MPa after cooling and increase to 14.6 MPa when the maximum design current is applied. At the coil ends these stresses do not exceed ~ 11.2 MPa in both cases.

The maximum tensile detaching stresses in the insulation do not exceed the adopted allowable value $[\sigma_{otp}] = 6.6$ MPa over the entire coil structure, except for the local areas of contact between the last coil turns and the pressing rings. For example, in the connection region of the pressing ring insulation and the cylindrical surface insulation the maximum detaching stress is

higher than the ultimate strength of the insulation. However, the region where this value is exceeded is smaller than 0.9 mm. The insulation can split in this region. In the rest of the contact zone between the pressing ring insulation and the turn-to-turn insulation the detaching stresses are below the allowable limit. In addition, stresses in this part of the coil exceed the allowable value in the ground-wall insulation on the surface of the support cylinder. The maximum stresses in this area are 8.7 MPa, but this area is smaller than 1.1 mm.

The preliminary compression of the coil in the axial direction by a pressure of 10 MPa reduces the average tensile stresses in the turn-to-turn insulation. At the center of the coil the average/maximum tensile stresses decrease from 7.7/9.5 MPa to -0.7/0.7 MPa. At the coil end, near the pressing ring, they decrease from 6.7/9.8 MPa to 2.3/4.3 MPa. The influence of the magnetic forces on the axial stresses in the turn-to-turn insulation at the coil end is insignificant while at the coil center it is higher: the average compressive stresses increase from -0.7 MPa to -1.6 MPa.

The shear stresses in the insulation do not exceed the allowable value $[\tau] = 7$ MPa in practically the whole coil structure, except for the local regions around the end turn contact with the pressing ring, as in the case of detaching stresses. The shear stresses exceed their ultimate strength in the contact area (~ 2.3 mm) of the ground wall insulation on the pressing ring with the ground wall insulation on the support cylinder. In all other local areas with heightened shear stresses in the insulation they do not exceed the shear strength, and the average shear stresses are below the allowable value.

Thermal cycling affects the level of stresses in the coil. Most dependent on the number of thermal cycles are radial stresses in the end turns of the coil. After the 8th thermal cycle the radial stress at the outer surface of the end turn near the pressing ring increases within the range from 20% (farther from the pressing ring) to 75% (nearer to the compressing ring). However, in the next coil turns this effect is practically negligible.

Therefore, according to the calculations, glue splitting between the ground wall insulation and the support cylinder and between the end turns of the coil and the pressing rings is only possible in local areas about 2 mm large within the contact zone of the pressing ring insulation with the ground wall insulation. Considering that local deformations in this zone are restricted to the areas where stresses do not exceed the allowable values, no significant propagation of this splitting can be expected.

It should be noted that the stresses caused by the magnetic forces are appreciably lower than those arising from the thermal deformations due to the low rated magnetic field.

According to the calculations, the maximum temperature difference in the ground wall insulation during the unprotected quench will not exceed 30 K.

The results of the computations confirm that it is correct to choose the coil design that has already been used in other similar magnets and proved to operate appropriately.

2.4.2.6 COIL COOLING

The cooling method chosen for the MPD magnet is based on the natural convection of liquid helium flow (thermosyphon mode). The coil conductor is cooled indirectly via the thermal contact with the aluminum support cylinder and heat removal through the cylinder to the square aluminum tubes of “rib-cage” type heat exchanger, where vapor-liquid helium mixture circulates. The cross section of a tube is 25x25 mm with a hole of 19 mm. There are 28 parallel branches attached to the external surface of the cylinder by epoxy glue (Fig. 2.4.2.6.1, 2.4.2.6.2).

The volume of liquid helium in the tubes is about 70 L. After a quench the evaporating helium will be expelled from the tube through the relief valves to the gaseous helium collection and storage system.

Heat interceptors are used (strips of pure aluminum RRR 1000) to reduce the maximum temperature rise in the superconducting coil because of heat inflow through the cold mass supports. These interceptors shunt the thermal resistance from the suspension tie foots to the cooling tube).

The maximal temperature rise in the sc coil ~ 4.99 K corresponds to the current ramping. The results of computing the maximal temperature in superconducting coil are presented in [21].

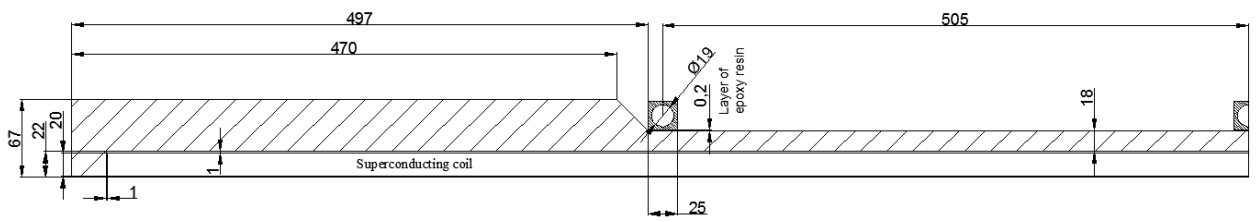


Fig. 2.4.2.6.1. Cooling tube glued to the support cylinder surface

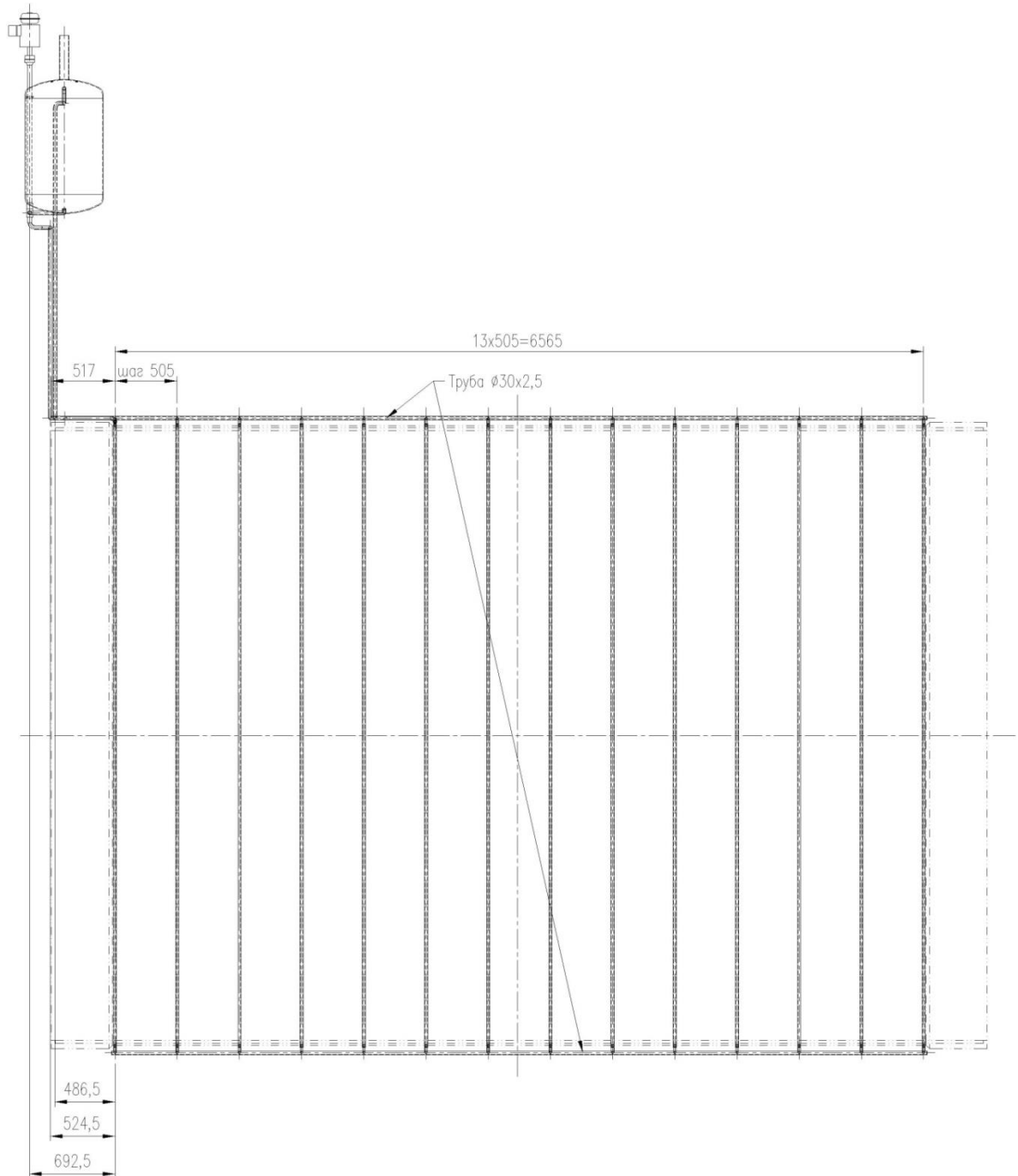


Fig. 2.4.2.6.2. Layout of the tubes of the "rib-cage" type heat exchanger on the support cylinder surface

2.4.3 CRYOSTAT OF THE SOLENOID

Since there are no requirements on radiation transparency, the vacuum vessel of the solenoid cryostat (Fig. 2.4.3.1) can be made of stainless steel. The cryostat should be designed, manufactured, and tested in accordance with the Rostekhnadzor requirements [14, 15].

The cryostat consists of

- A vacuum vessel with a support system for fixating the cryostat to the yoke.
- A cold mass with a system for suspending it inside the vacuum vessel.
- A thermal shield.
- A control Dewar with a system of valves and gas-cooled current leads.
- A connecting tube (chimney).

The computation of stresses which arise in the cryostat shells as the magnet is moved or operates is given in [8].

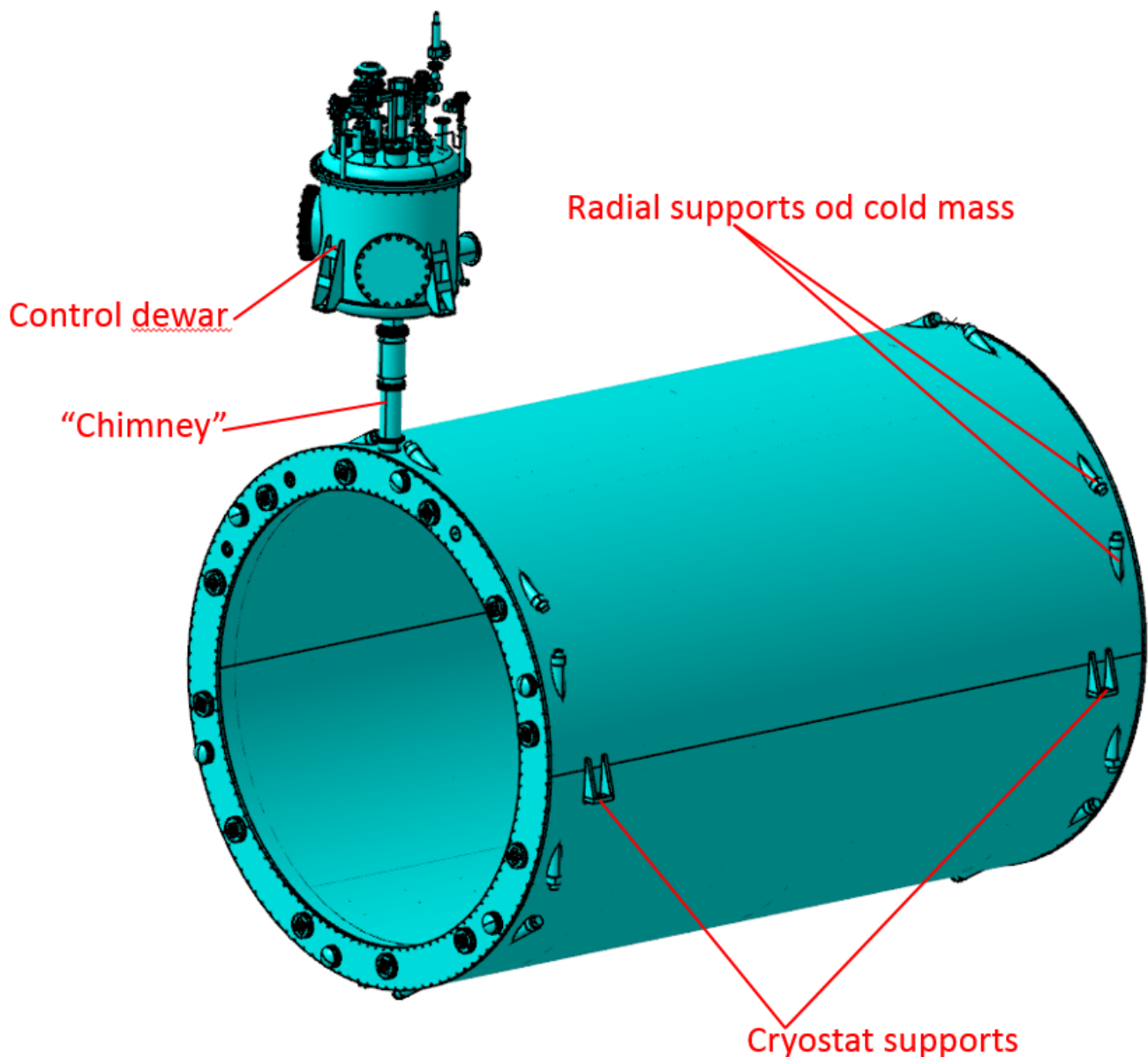


Fig. 2.4.3.1. General view of the cryostat of the solenoid

2.4.3.1 VACUUM VESSEL OF THE CRYOSTAT

The cryostat vacuum vessel (Fig. 2.4.3.1.1) is made of stainless steel. It consists of an inner and an outer shell 16 mm and 25 mm thick respectively. At the ends of the shells there are beads 45 mm thick, to which the cryostat flanges are attached. Two collars of the radial suspension are connected to the outer shell thickenings. Axial tie rods of the coil are fixed at the cryostat flange on the chimney side.

The vacuum vessel is designed

- To withstand the ambient air pressure in accordance with the requirements [16].
- To bear the weight of the cold mass and the thermal shield that is attached to the radial ties during the transportation of the magnet (including load handling), movement together with the magnet from the assembly site to the operating position (and back), and operation of the magnet.
- To withstand the magnet decentering forces when the SC coil deviates from the prescribed position (in the normal and emergency modes of operation).

The weight of the vacuum cryostat vessel is 49.1 t. Under all loads, the change in the outer cryostat dimensions (diametric or axial) must not exceed 2 mm.

Under the normal operation conditions the inner volume of the cryostat is pumped out, which results in membrane compressing stresses at the outer shell due to the external atmospheric pressure. In addition, during the magnet operation an emergency situation of an overpressure up to 0.7 bar in the inner cryostat volume can occur, giving rise to membrane compressing stresses in the inner cryostat shell. The buckling analysis of both cryostat shells in various operation modes of the MPD magnet is given in [8]. Negative tolerances on the shell thickness specified at the computations are -0.8 mm for the inner shell with $t=16$ mm and -1 mm for the outer shell with $t=25$ mm.

The minimum acceptable safety margin in the buckling analysis was taken to be 2.86, identical for the normal operation mode and for the emergency mode. According to the calculations, the shell stability is guaranteed both in the normal operation mode and in the emergency mode. The safety margins for the inner and outer shells in the modes considered were 5.82 and 2.9 respectively.

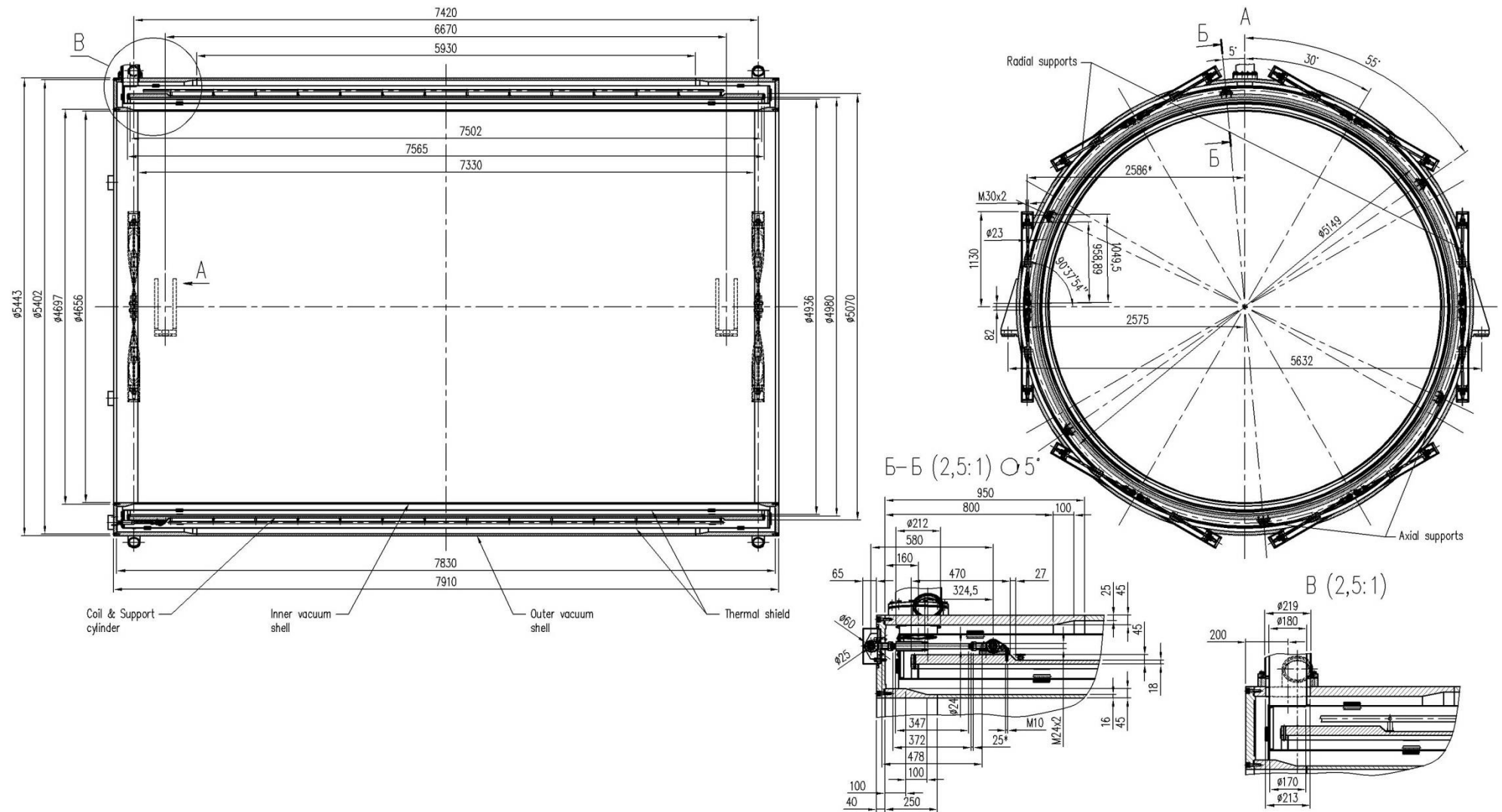


Fig. 2.4.3.1.1. Main dimensions of the cryostat

2.4.3.2 COLD MASS

The cold part of the cryostat includes a superconducting coil with a support cylinder. After winding the coil is impregnated with epoxy compound together with the support cylinder, which makes them into a single solid unit. The cold mass weight is 13.3 t.

When cooled down to the operation temperature, the support cylinder with the coil shrinks radially by 9.9–10.4 mm. The total shortening of the coil is 33.3 mm. The increase in the outer radius of the support cylinder due to magnetic pressure (0.1–0.175 MPa) does not exceed 0.51 mm.

The support cylinder with the coil is installed inside the cryostat and fixed by axial ties so that after cooling it takes a position symmetric about the magnet poles.

The minimum gap between the end of the support cylinder and the thermal shield on the antichimney side for the warm coil and the cold shield is 36 mm (without the thickness of the multilayer shield-vacuum insulation). The minimum radial gap between the support cylinder and the external thermal shield is 11 mm after the cooling of the coil and the shield.

2.4.3.3 THERMAL INSULATION OF THE CRYOSTAT COLD MASS

To ensure thermal stability, the cold mass of the cryostat is effectively insulated between the inner and outer vacuum shells of the cryostat and fixed with radial and axial ties of low heat conductivity.

At the surface of the cold mass the specific heat flow is generated due to radiation. The heat is transmitted to the cold mass due to heat conduction of six axial ties, which carry the axial load, and 12x12 radial ties, which fix the coil in the radial direction. Heat is also transmitted to the cold mass through the current leads cooled by the boiling helium vapor. Heat inflow in the cold mass also arises from heat losses in the superconducting cable junctions, a heat flow along the measurement cables, and heat losses in the aluminum cylinder due to eddy currents during energizing and de-energizing of the magnet.

The coil is indirectly cooled by the two-phase helium flow in the heat exchanger tube fixated on the outer surface of the aluminum support cylinder. Between the inner surface of the vacuum cryostat shell and the cold mass there is a thermal shield, which is cooled by liquid Nitrogen at an the temperature of ~80 K. Approximately 30 layers of superinsulation separate the shield surface from the vacuum shell of the cryostat.

The calculated values of the heat inflow to the cryostat cold mass and to the thermal shields are given in Table 2.4.3.3.1 [21].

Table 2.4.3.3.1. Thermal loads to the cold mass and the thermal shield

| T=4.5 K | | Thermal load, W |
|--|---|------------------|
| <i>Cryostat</i> | | |
| | Radiation ($0.07 \text{ W/m}^2 \times 240 \text{ m}^2$) | 16.8 |
| | Heat inflow to the cold mass supports | 11.2 |
| | Conductor joints and wires | 1 |
| | Eddy current losses in the Al cylinder | 4.2 |
| <i>Cryogenic chimney and Control Dewar</i> | | |
| | LHe vessel, tubing, valves, supports | 3.9 |
| <i>Transfer line</i> | | |
| | | 3.8 |
| | Total (normal/transit regime): | 36.7/40.9 |
| | With safety factor 2 | 73.4/81.8 |
| <i>Current leads</i> | | |
| | without current | 4.2 (6.8 l/h) |
| | with current | 7.0 (11.3 l/h) |
| T=80 K | | |
| <i>Cryostat</i> | | |
| | Radiation ($1.3 \text{ W/m}^2 \times 253 \text{ m}^2$) | 326 |
| | Heat intercepts of the coil supports | 69 |
| | Shield supports | 640 |
| <i>Cryogenic chimney and Control Dewar</i> | | |
| | Thermal screen, valves, supports | 21 |
| | | |
| | Total: | 1056 |
| | With safety factor 2 | 2112 |

2.4.3.4 COLD MASS SUSPENSION

At the maximum design Ampere-turns of the SC coil $I_{SC} = 4$ MA, induction $B_0 = 0.66$ T, and total current in each of the trim coils $I_{TRIM} = 151$ kA, the cold mass of the magnet is affected by the coil dead weight 133 kN and the decentering axial and radial magnetic forces 61 kN/cm and 5.4 kN/cm respectively. At the emergency de-energizing of one of the trim coils, the superconducting coil will be exposed to a force of 243 kN directed toward the other (operating) trim coil. If the superconducting coil is displaced by 20 mm, this force will additionally change by ± 128 kN and the linear change in the current density along the SC coil by 2% changes the force by ± 50 kN. Therefore, at the emergency shutdown of one of the trim coils, the force acting on the superconducting coil can be as high as 420 kN.

But in fact, the maximum force has to be significantly less. According to calculations, even when the field in the center of the magnet is 0.64 T the specified value of the integral of the magnetic field radial component can be achieved only for complete absence of technological deviations from the optimized magnetic system configuration. So, the higher values of the magnetic field, up to the induction in the center of the magnet $B_0 = 0.66$ T, is advisable to attain only by switching off the power supply of the correction coils. Furthermore, the power supply circuit in accordance with Section 2.4.13 will be used in order to reduce the maximum value of the axial force acting on the superconducting coil. Taking into account these restrictions, the maximum axial force applied to the superconducting coil during emergency switching off of one of the power supplies of the trim coils is 143 kN.

To avoid contact between the coil and the cryostat shell and prohibitive turning of the magnet axis relative to the TPC axis, the position of the support cylinder should not change in either the axial or the radial direction under the action of all loads in the operation regimes. According to the calculations [10], in order to guarantee the required value of the integral of the radial induction component in the TPC region, the deviation of the coil axis direction from the TPC axis under the action of magnetic forces should not exceed 0.01° . Under this turning the coil ends would be shifted in the radial direction by ± 0.67 mm, and the maximum integral for the nominal dimensions of the magnet system would become two times greater. At the same time, the turning of the coil axis by an angle of $\sim 0.1^\circ$ with respect to the yoke (it corresponds to the radial shift of the coil ends by ± 6.6 mm) would not lead to a significant increase in the integral of the radial component, provided that the TPC axis rotates with the coil by the same angle.

The cold mass is fixed relative to the outer cryostat shell by 2x12 radial and 6 axial tie rods, which are fixed on the thicker parts of the aluminum support cylinder (Fig. 2.4.3.4.1). So many radial rods are needed because the coil must be rigidly fixed in relation to the outer shell of the vacuum vessel and the cylindrical shape of the coil must be maintained under the action of the radial decentering force.

It is accepted that the maximum axial shift of the coil from its nominal position (symmetric about the yoke) due to technological deviations can be ± 20 mm. Since the axial rods are placed on one side of the coil, they can be either tensioned or compressed, according to the coil shift direction. The maximum magnetic force attracting the coil to the magnet poles at the maximum deviation of the coil will be $P_z = \pm 122$ kN (under the Normal Operation Conditions). Since the

hardest operation mode for the rods is compression, when buckling can appear, the coil should be installed with its center displaced from the magnet center towards the antichimney side to provide strictly tensile loads to the rods. To reduce the influence of the current density variation along the coil on the integral of the radial component, the coil should be wound with superconducting cable pieces placed in such a way that the directions of the cable thickness variation in these pieces alternate.

The following loads to the radial tie rods are possible:

1. Dead weight of the cold mass $G=166.7$ kN
2. Operation loads under the normal operation conditions:
 - weight of the cold mass $G=166.7$ kN,
 - radial magnetic decentering force $P_R=9.2$ kN, which can be directed along the circumference in any direction. The maximum stress arises in the vertical rods when the radial decentering magnetic force is directed downwards and in the inclined rods when the force is directed along the X axis
 - the force caused by thermal stresses during the cooling,
 - external pressure on the cryostat, 0.1 MPa ,
 - tightening force Q_z of the threaded rod-nut connection.
3. Dynamical loads as the cryostat is lifted/lowered ($a_y=1.6$ g, $a_x=0.5$ g), which act together with the tightening force $Q_z=40$ kN of the threaded rod-nut connection.

The maximum tension force in the radial tie rod at the maximum design current of the magnet under normal operation conditions is 198 kN. All tie rods of the cold mass suspension are made of the Inconel 718 alloy. The diameter of plain part of the radial rods is taken to be $d=23$ mm. The diameter of their threaded part corresponds to the M30×2 thread. The radial rods are 860 mm long, and their cold part is 480 mm long. The diameter of the axial rods is taken to be $d=24$ mm, and the diameter of their threaded part corresponds to the M24 thread. The total length of the axial rod is 485 mm, and its cold part is 345 mm long.

According to the calculations [9], the chosen radial and axial tie rods are sufficiently strong: under the normal operation conditions the yield and buckling resistance margins with respect to the maximum acting loads are not less than 2.6.

There is no displacement of the cold mass under the action of the thermal load, because of the symmetrical arrangement of the radial tie rods. The downward cold mass shift in relation to the stationary supports, due to caused by elastic deformations of the rods and the cryostat shells under the effect of the vertical loads (cold mass weight $G=166.7$ kN + decentering radial force $P_R=9.2$ kN) is $f_G = 0.2$ mm. The decentering radial force makes a relatively small contribution (≈ 0.01 mm) to the vertical displacement, as compared to the weight of the cold part. According to the calculations, the irregularity of the load on the axial tie rods practically does not have an impact on the turning of the coil axis with respect to the magnet axis. For example, with two neighboring axial ties missing, the displacement of the coil end is no greater than 0.11 mm, which corresponds to the angle $\Delta\varphi=0.0008^\circ$.

Thus, when the magnet operates, the coil will keep its position unchanged under the action of magnetic decentering forces and will not therefore change its position with respect to the TPC.

The design of the radial suspension units is shown in Fig. 2.4.3.4.2, and the design of the axial suspension is shown in Fig. 2.4.3.4.3. To reduce the heat inflow to the cold mass, the tie rods are equipped by heat flow interceptors at the level of 80 K.

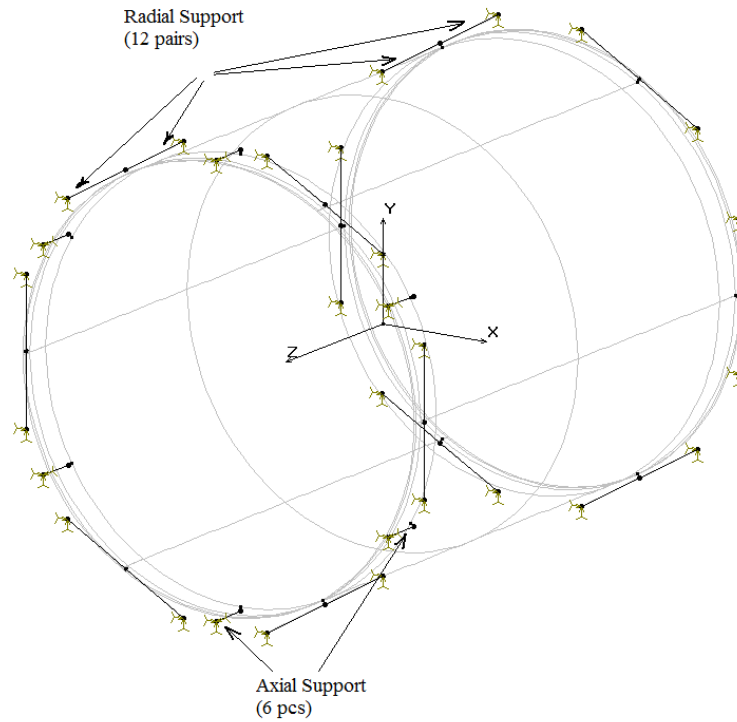


Fig. 2.4.3.4.1. Arrangement of the tie rods of the cold mass suspension system

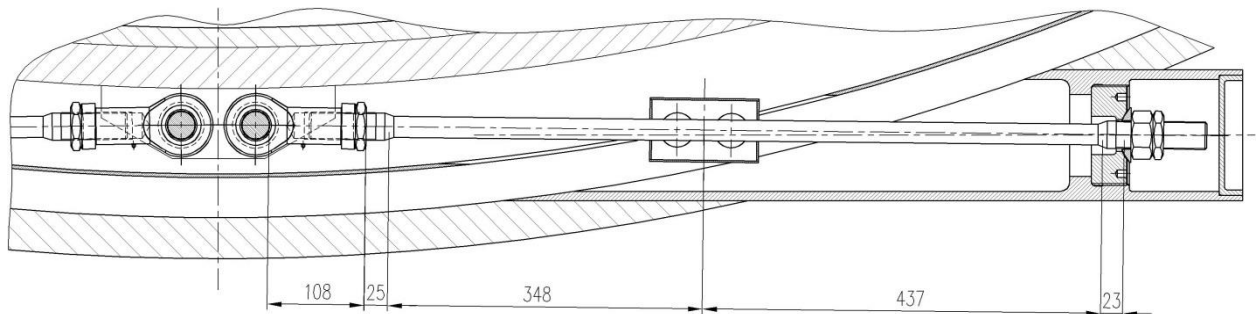


Fig. 2.4.3.4.2. Radial suspension unit of the cryostat cold mass

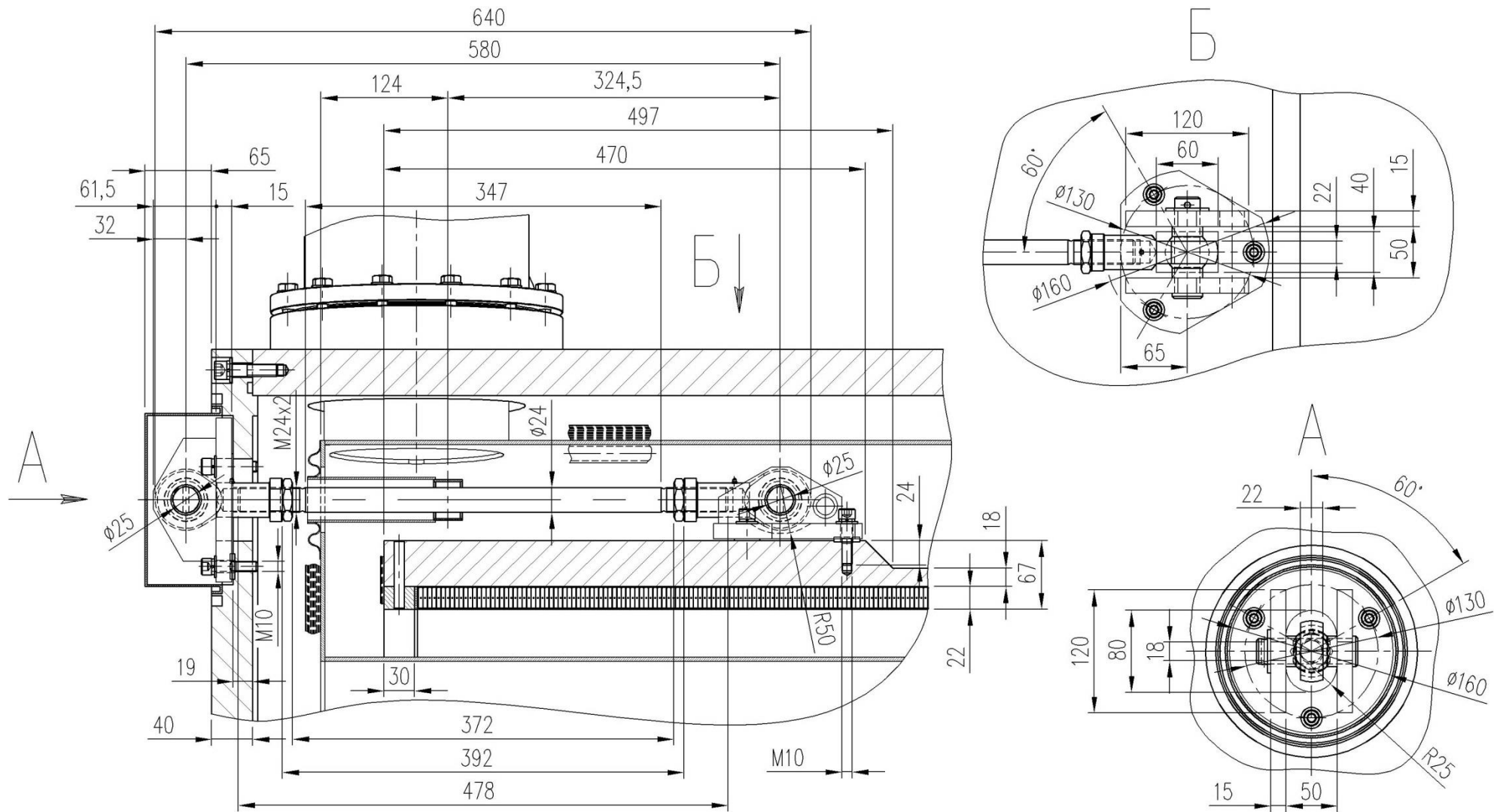


Fig. 2.4.3.4.3. Axial suspension unit of the cryostat cold mass

2.4.3.5 THERMAL SHIELD

The thermal shield cooled by circulated liquid nitrogen consists of an inner and an outer shells connected by two end flanges. It is made of Al 5083 aluminum alloy plates of 3-4 mm in thick (Fig. 2.4.3.5.1). A cooling pipe of Al-1100 is fixed to the shield surfaces facing the superconducting coil. The nitrogen flow (11.5 g/s, 3 bar) comes from the Nitrogen re-condenser at the temperature of 80 K. After passing the shields, the saturated vapor flow returns to the re-condenser.

Nitrogen flow coming from the nitrogen re-condenser is divided into four parallel streams which cool inner and outer thermal screens independently. The end flanges of the shield are cooled by conduction from the heat exchangers of the inner and the outer shields.

To reduce the losses caused by eddy currents at the coil energizing/de-energizing, the shields have longitudinal slits spanned with insulation inserts.

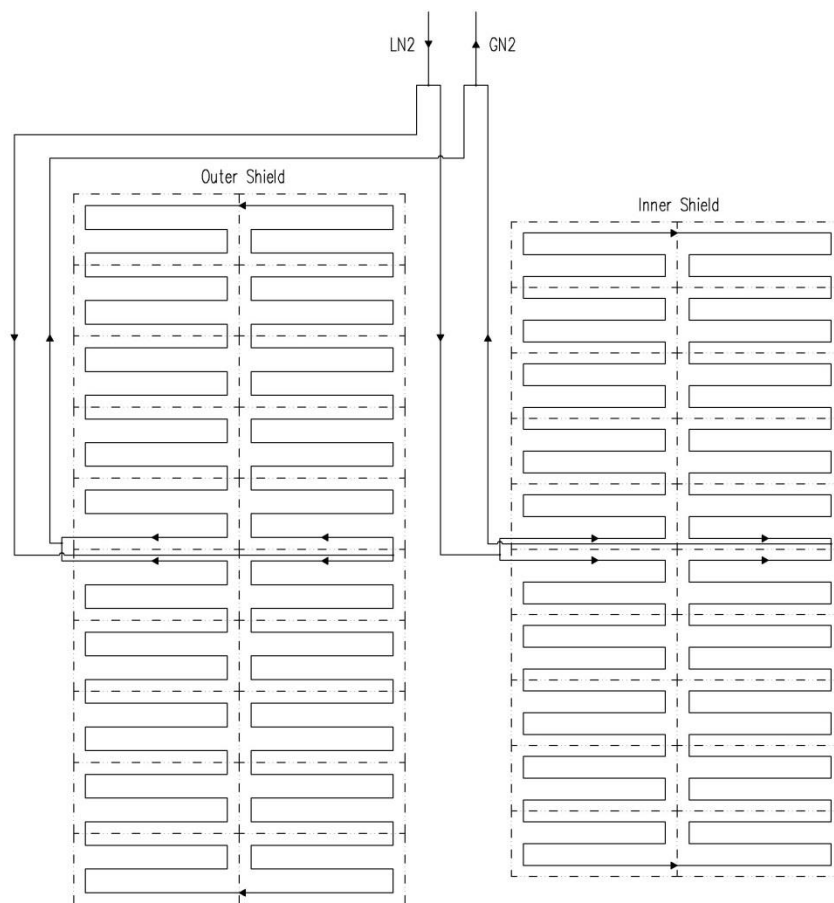


Fig. 2.4.3.5.1. Cooling scheme of the cryostat thermal shields

The shields are fastened to the cryostat body by fiberglass supports of low thermal conductivity. The total number of supports is ~ 1500 . The nitrogen flows are also used for thermal interception on the radial and axial tie rods at a level of 80 K.

To reduce the heat inflow due to radiation, the 30 layers of multilayer insulation are applied to the shield surface facing the cryostat shell.

The weight of the thermal shields is 2 t.

2.4.3.6 CONTROL DEWAR

The control Dewar (fig. 2.4.3.6.1) is a functional unit of the cryogenic system. It is placed between the superconducting coil cryostat and the helium satellite refrigerator. The control Dewar serves to accumulate the liquid helium in the helium bath, maintain the required parameters of the helium and nitrogen flows (flow rate, pressure, temperature), and to provide cooling of the current leads.

The control Dewar is located outside the yoke on its upper barrel beam on the east side of the detector and is connected with the cryostat by the vacuum tube (chimney), which passes through the upper yoke beam (Fig.2.3.1).

The control Dewar of rectangle shape is made of stainless steel. Two large covers on both sides of the control Dewar provide easy access for installation and maintenance of its components. It consists of an outer vacuum housing that encloses a stainless steel vessel for liquid helium. Thermal shield cooled by liquid nitrogen is placed between the outer housing and the helium vessel. Its surfaces facing the cryostat housing are covered by multilayer high-vacuum thermal insulation.

Current leads cooled by vapors of boiling helium, control valves, temperature and pressure sensors are allocated in the vacuum volume of the control Dewar. Safety valves, sensor connectors, bayonet connectors of the transfer lines are placed on the sidewalls and top plate of the control Dewar housing.

The hydraulic volume of the helium vessel is chosen to ensure an essential helium flow for the period needed for safe de-energizing the sc coil if the satellite-refrigerator is stopped. The heat inflows to the helium bath of the control Dewar and to the superconducting coil, including heat losses in current leads, amount to 80 W, which corresponds to the liquid helium flow rate of 130 L/h. Since it takes 60 min for safe de-energizing the coil at the nominal rate, the volume of the helium vessel is chosen to be 300 L with the twofold safety margin.

The flow (4.34 g/s, 1.3 bar, 4.5 K) comes to the helium vessel of the control Dewar from the helium satellite-refrigerator in the steady-state regime.

Electrical heater is located in the helium bath of the control Dewar. It is required to maintain a specified level of the liquid helium bath (maintenance of thermal balance). The heater can also be used for accelerated removal of liquid helium from the bath. Its power is 100W.

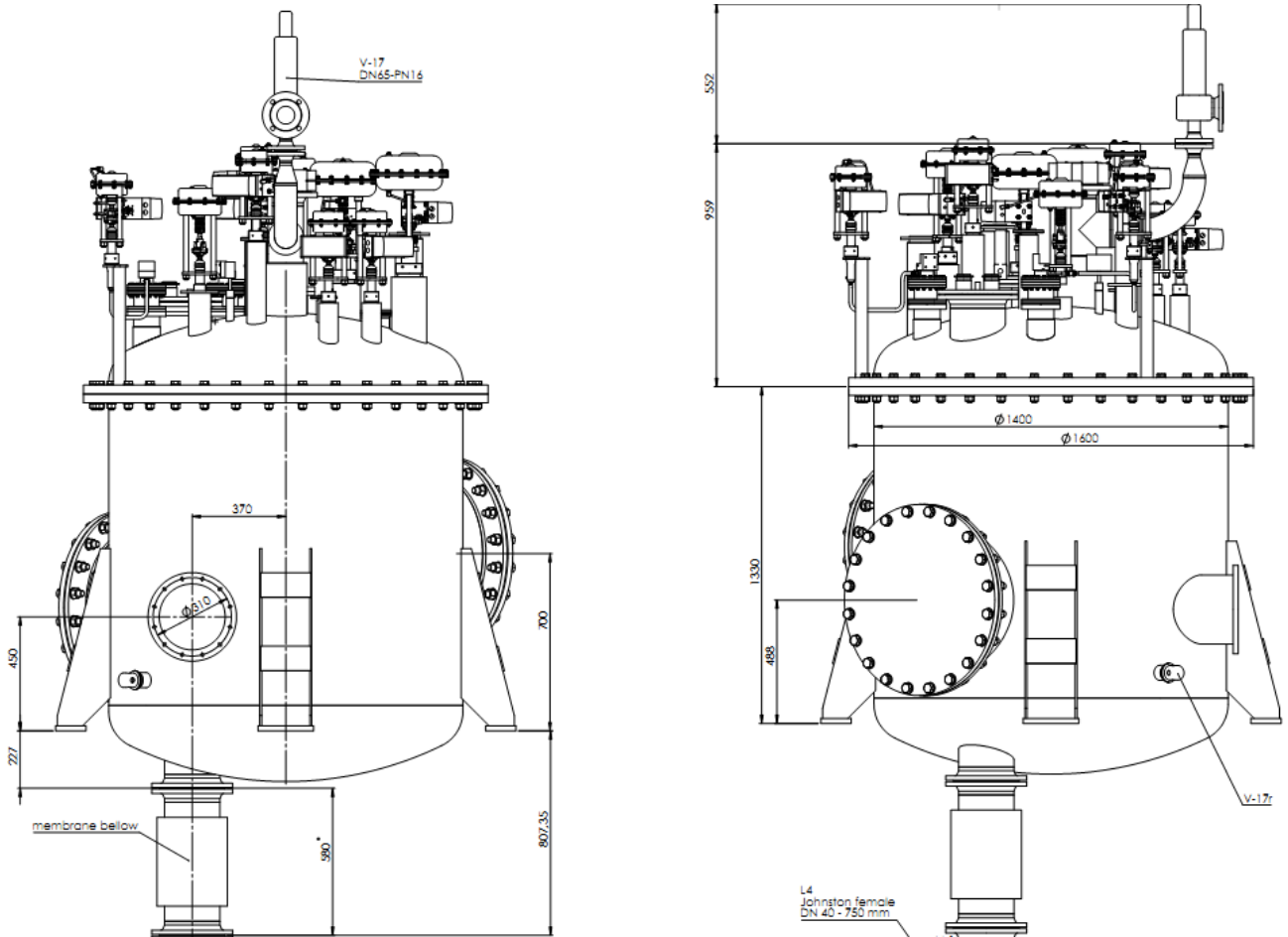


Fig. 2.4.3.6.1. Control Dewar

Figures 2.4.3.6.2 and 2.4.3.6.3 show the schematic pneumohydraulic diagram and the structural layout of the control Dewar.

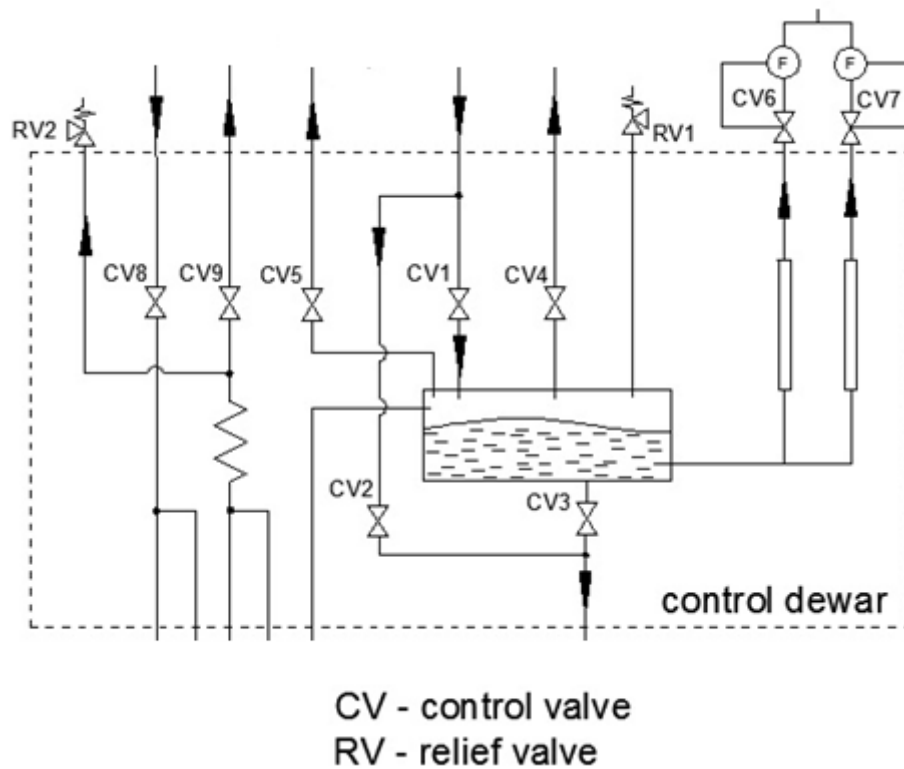


Fig. 2.4.3.6.2. Pneumohydraulic diagram of the control Dewar

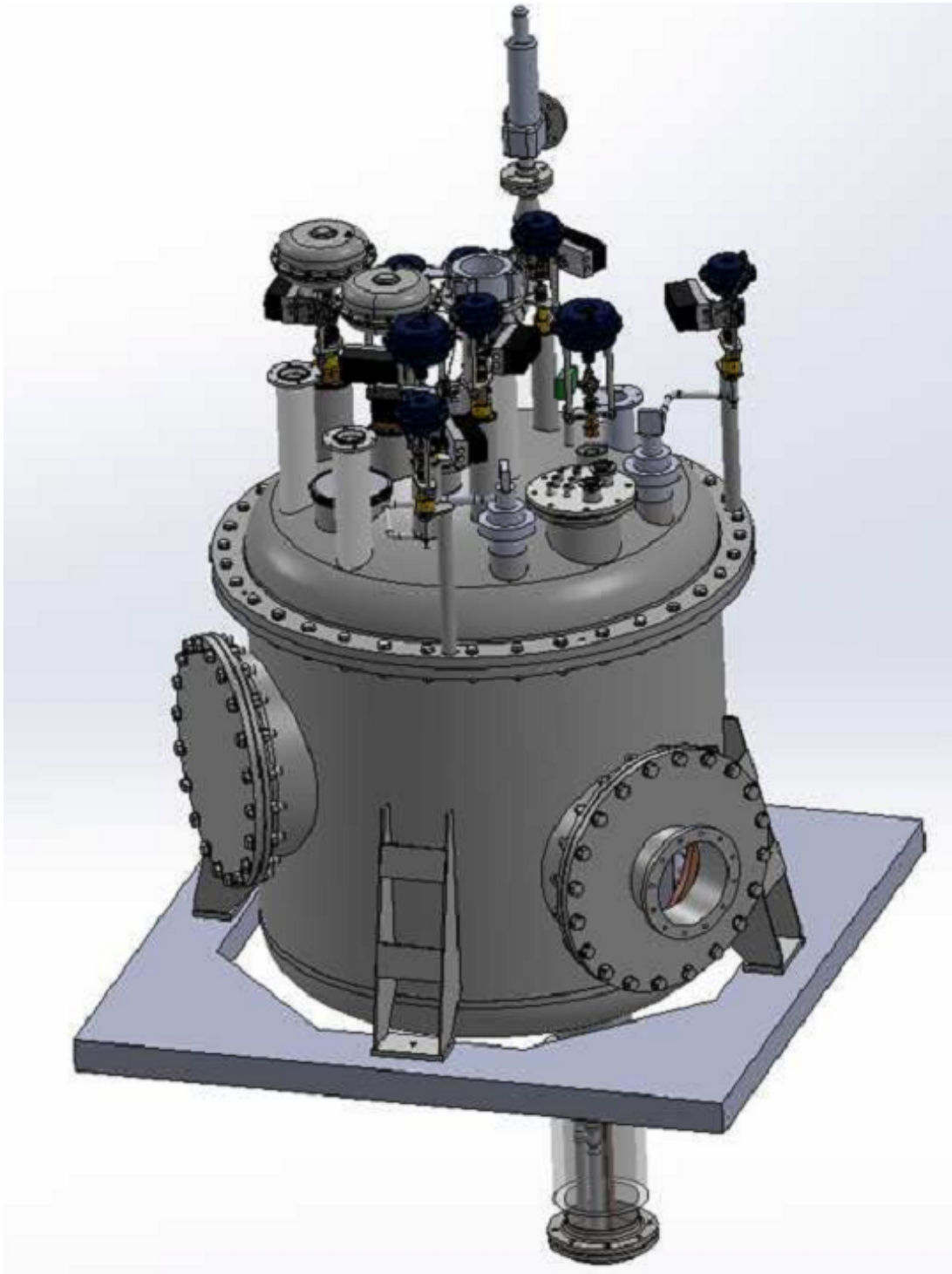


Fig. 2.4.3.6.3. Structural layout of the control Dewar

2.4.3.7 CHIMNEY

The vacuum connecting tube (chimney) connects the vacuum volumes of the cryostat and the control Dewar (Fig. 2.4.3.7.1). Its vacuum jacket of stainless steel encloses superconducting bus bar lines, direct and return helium and nitrogen tubes, measurement cables, and a thermal shield.

Superconducting bus bar lines cooled by a direct liquid helium flow are necessary to connect the superconducting coil lead-outs with the vapor-cooled current leads placed in the control Dewar. The thermal shield of the chimney is cooled by liquid nitrogen, which flows in the tubes welded to its surface and used for liquid nitrogen supply of the thermal shields of the superconducting coil.

The design of the chimney allows detaching the control Dewar from the cryostat for its transportation from the manufacturer to JINR. Besides it has the bellows decoupling at its top which provides the control Dewar montage on the upper platform of the magnet.

Superconducting bus bar lines in the chimney consist of the double superconducting coil cables, which are soldered with each other, insulated with the ground plane insulation, and thermally connected with direct liquid helium flow pipeline. The cross section of the chimney is shown in Fig. 2.4.3.7.2.

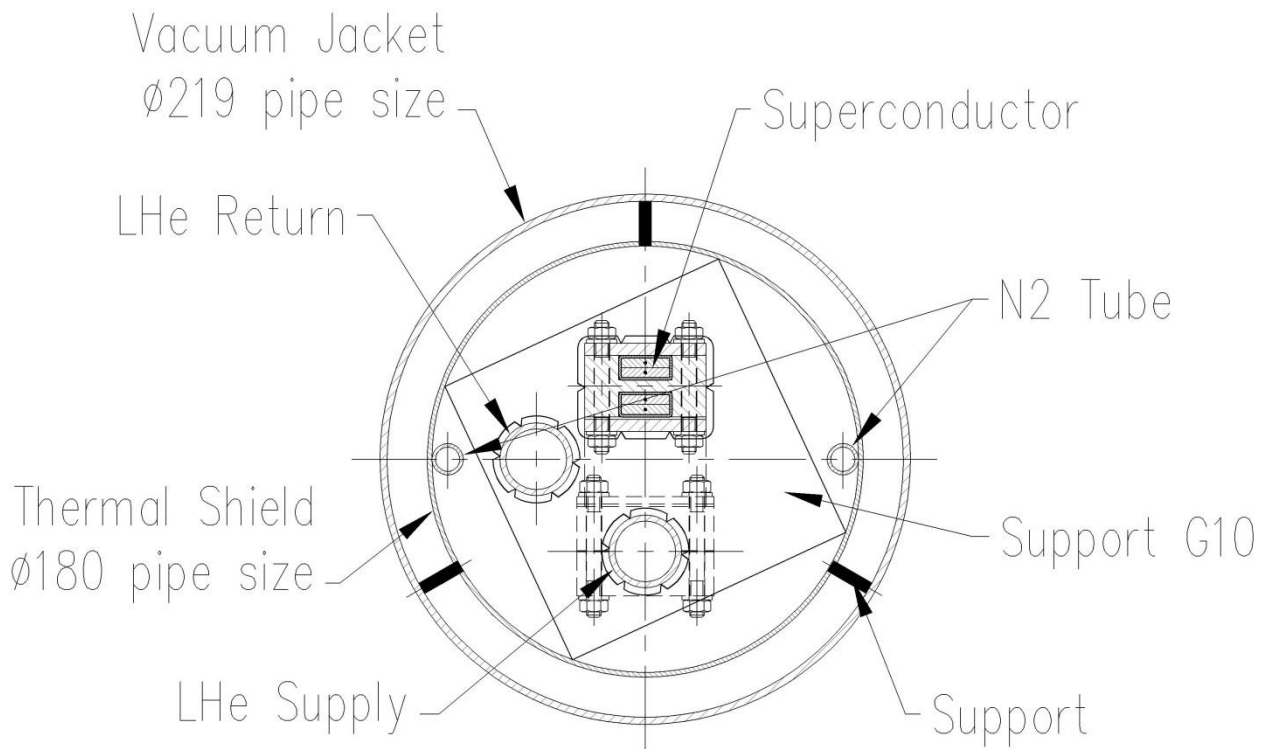


Fig. 2.4.3.7.2. Cross section of the Chimney

2.4.3.8 VAPOR COOLED CURRENT LEADS

A conservative design of the vapor-cooled current leads is used to ensure high reliability of the MPD magnet. The current leads were chosen to provide stably operating of the magnet and to ensure its safe de-energizing in case of cooling stops. They are intended for supplying the maximum design current to the superconducting coil from the temperature level of 300 K to the level of 4.5 K. The nominal current of the superconducting coil is 1790 A and the maximum current is 2388 A. The current leads are mounted at the top plate of the control Dewar housing. The helium flow to cool both current leads is 0.38 g/s at 1792 A and 0.23 g/s at the zero current.

The current leads are of vapor cooled type. They are supplied by helium from the helium vessel through the insulation decoupling. Their “cold” ends are connected with the superconducting bus lines coming from the superconducting coil. The flow of warm helium from the current leads returns to the low pressure line of the satellite refrigerator.

The current lead cooling is monitored by observing the change in the cold gas flow rate through the current leads. The flow rate is measured by flow transducers and controlled by the control valves CV6 and CV7 (Fig. 2.4.3.6.1). On the warm side of the current leads there are terminals for connecting bus lines. They are equipped with heaters to prevent sweating and frosting.

The current leads are insulated from each other, from the control Dewar walls, and from the flange by fiberglass capable of withstanding the output voltage up to 500 V.

2.4.3.9 CONNECTING BUS LINES AND FEEDTHROUGH INSULATORS

To connect the coil lead-outs with the current leads in the control Dewar, the coils lead-outs are reinforced with additional pieces of the superconducting cable soldered to them along the entire length of the bus lines (up to the feedthrough insulators at the helium tight shells of the current leads). The bus lines are insulated by the fiberglass ground-wall insulation. The coil lead-out on the anti-chimney side is mechanically fastened over the entire length of the support cylinder as close as possible to the heat exchanger pipe for indirect cooling of the superconductor. This is also why the bus lines are kept against liquid helium supply tubes in the chimney.

Current leads run into the helium volumes of the current leads through feedthrough insulators rated at 500 V. In the helium volumes the bus lines are soldered and mechanically pressed against the terminations of the gas-cooled current leads.

2.4.3.10 ASSEMBLING THE CRYOSTAT

The cryostat is assembled in the vertical position.

- 2.4.3.10.1. After the cooling pipes are welded to the thermal shields and eddy current insulator inserts are mounted, multilayer vacuum insulation blankets are attached to the shield surfaces facing the vacuum vessel walls. Then the shields are fixed relative to the cryostat vacuum shells with fiberglass supports.
- 2.4.3.10.2 The superconducting coil wound into the support cylinder and impregnated with epoxy compound is installed vertically (lead-outs at the top). Axial suspension tie rods are mounted on the support cylinder.
- 2.4.3.10.3 The outer and inner vacuum shells of the cryostat with the thermal screens fastened to them are fit over the coil from above with the coil end becoming slightly higher than its final position relative to the vacuum shells.
- 2.4.3.10.4 Tie rods of the radial suspension of the cold mass are mounted on the chimney side, and the end thermal shield with multilayer insulation is installed.
- 2.4.3.10.5 The cryogenic pipelines and current buses are passed through the chimney, the cryostat end flange is mounted, and “warm” ends of the axial suspension tie rods are attached to it.
- 2.4.3.10.6 The position of the support cylinder relative to the cryostat shells is measured and the reference marks are made on the outer surface of the cryostat.
- 2.4.3.10.7 The inner and outer shells of the cryostat are lifted to the level of the end flange and fastened with bolts (by welding).
- 2.4.3.10.8 The lower tie rods of the radial suspension and the end thermal shield are mounted (the partially assembled cryostat can be slightly lifted for convenience).
- 2.4.3.10.9 The position of the support cylinder is measured, reference marks are made on the cryostat surface, and the lower flange of the cryostat is mounted.

2.4.3.11 FIXATING THE CRYOSTAT TO THE YOKE

The structural arrangement of the yoke makes it possible to minimize relative displacements of its units as the magnet operates or is moved and thus to fixate rigidly the cryostat to the yoke beams. The cryostat fasteners are four brackets attached to the yoke beams for the cryostat bracket flanges to rest on them (Figs. 2.3.1, 2.4.3.1.1, 2.4.3.11.1). The cryostat is fixed relative to the yoke with four M42 bolts and threaded holes in the 80-mm bracket flanges on the yoke beams. The plane through the surfaces of all support bracket flanges is close to the median plane of the magnet.

The most unfavorable loads in the cryostat fixating bolts occur in an emergency event (the magnet resting on two diagonally located points when running into an obstacle 6 mm high). In this case the maximum stresses are 60 MPa in the shells and flanges and 162 MPa in the supports of the cryostat, which are lower than the allowable value 169 MPa.

The fastening hardware is designed to allow adjustment of the cryostat position in all planes by inserting individually made spacers between the flanges of the brackets on the yoke and the cryostat vacuum shell and securing them in place (Fig. 2.4.3.11.2). The position of the cryostat with respect to the yoke can be varied within ± 20 mm relative to the nominal value along the longitudinal axis of the magnet, ± 10 mm along the transverse axis of the magnet, and from 0 to +20 mm along the vertical axis.

During adjustments the cryostat is supposed to be lifted using a special device (Fig. 2.5.3.1.4).

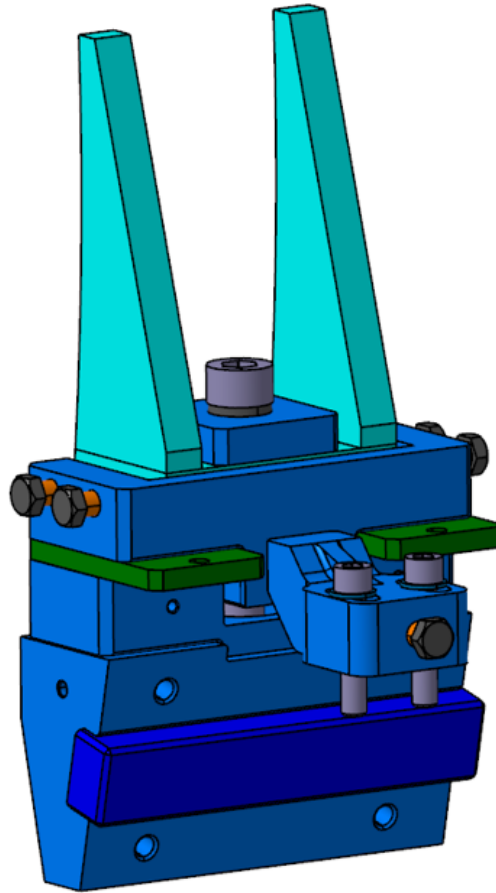


Fig. 2.4.3.11.1. Cryostat-to-yoke fastening unit

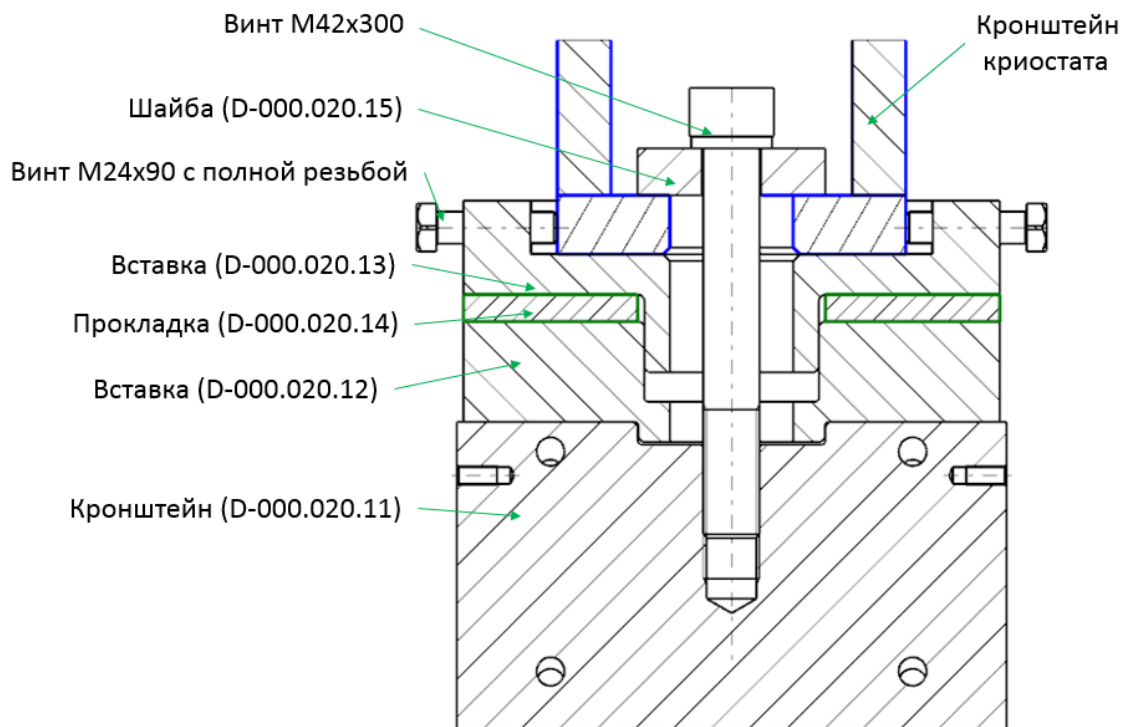


Fig. 2.4.3.11.2. Adjustment of the cryostat position relative to the yoke

2.4.3.12 BUSBAR ON THE CRYOSTAT OUTER SURFACE TO COMPENSATE THE STRAY FIELD OF THE REVERSE COIL CURRENT LEAD

Since the superconducting coil of the MPD magnet is made single layer, the second coil current lead should return to the beginning of the winding to be passed through a vacuum manifold to the vapor cooled current leads located in the control Dewar. This conductor is directed strictly along the solenoid axis and mounted on the outer surface of the aluminum support cylinder in the immediate vicinity of the cooling tube.

In order to compensate the field of this lead an additional conductor with the opposite current direction is used which passes along the outer surface of the cryostat in accordance with Fig. 2.4.3.12.1 [10]. This conductor has also to be strictly directed along the axis of the solenoid, and is attached to the outer vacuum shell of the cryostat. The conductor should be made as a hollow pipe, cooled with demineralized water from the water recycling system. Current carrying capacity of the conductor and its cooling must be considered for the maximal design current of the sc coil 2388 A.

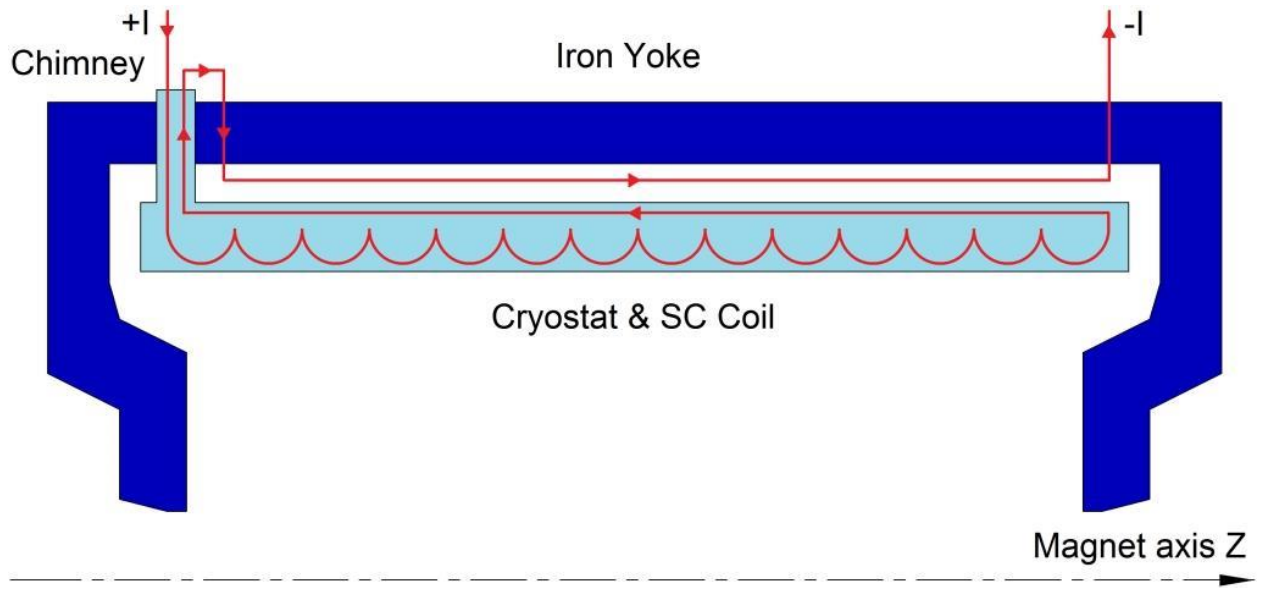


Fig. 2.4.3.12.1. Laying of the compensating conductor

2.4.4 VACUUM SYSTEM

The control Dewar, chimney, and superconducting coil cryostat have a common vacuum volume. The preliminary vacuum pumping is performed by two roughing rotary pumps (main and reserve) and a Roots pump. The high-vacuum pumping will be performed by a turbomolecular pump. The pressure to be obtained by vacuum pumping before cooling is 10^{-5} Torr. Further pumping will be performed in the process of cooling and cryostatting by cryogenic panels mounted on the outer surface of the support cylinder.

On the vacuum casings of the chimney and the control Dewar there are relief valves and a relief diaphragm.

To pump the vacuum volume, a pumping line is connected to the Chimney. Figures 2.4.4.1 show the position of the turbomolecular pump relative to the control Dewar. The forepumps and the Roots pump are placed on the upper platform of the magnet. Two pressure sensors are fitted on the vacuum casings of the chimney and the control Dewar to check the pressure. The block diagram of the vacuum system is shown in Fig. 2.4.4.2.

The main technical and operating characteristics of the vacuum pumps chosen for the preliminary and high-vacuum pumping of the cryostat vacuum volume are presented in Table 2.4.4.1. To pump the vacuum volume, the rate of the turbomolecular pump should be 1000 L/s. The Pfeiffer Vacuum GmbH TPH 1201 pump with a rate of 1200 L/s was chosen. Calculations of the vacuum system parameters and vacuum pump rates for the MPD magnet cryostat are given in [7]. Considering the chosen pumps, the total time for the preliminary and high-vacuum pumping of the superconducting coil cryostat, control Dewar, and chimney vacuum volume is estimated to be about 48 h.

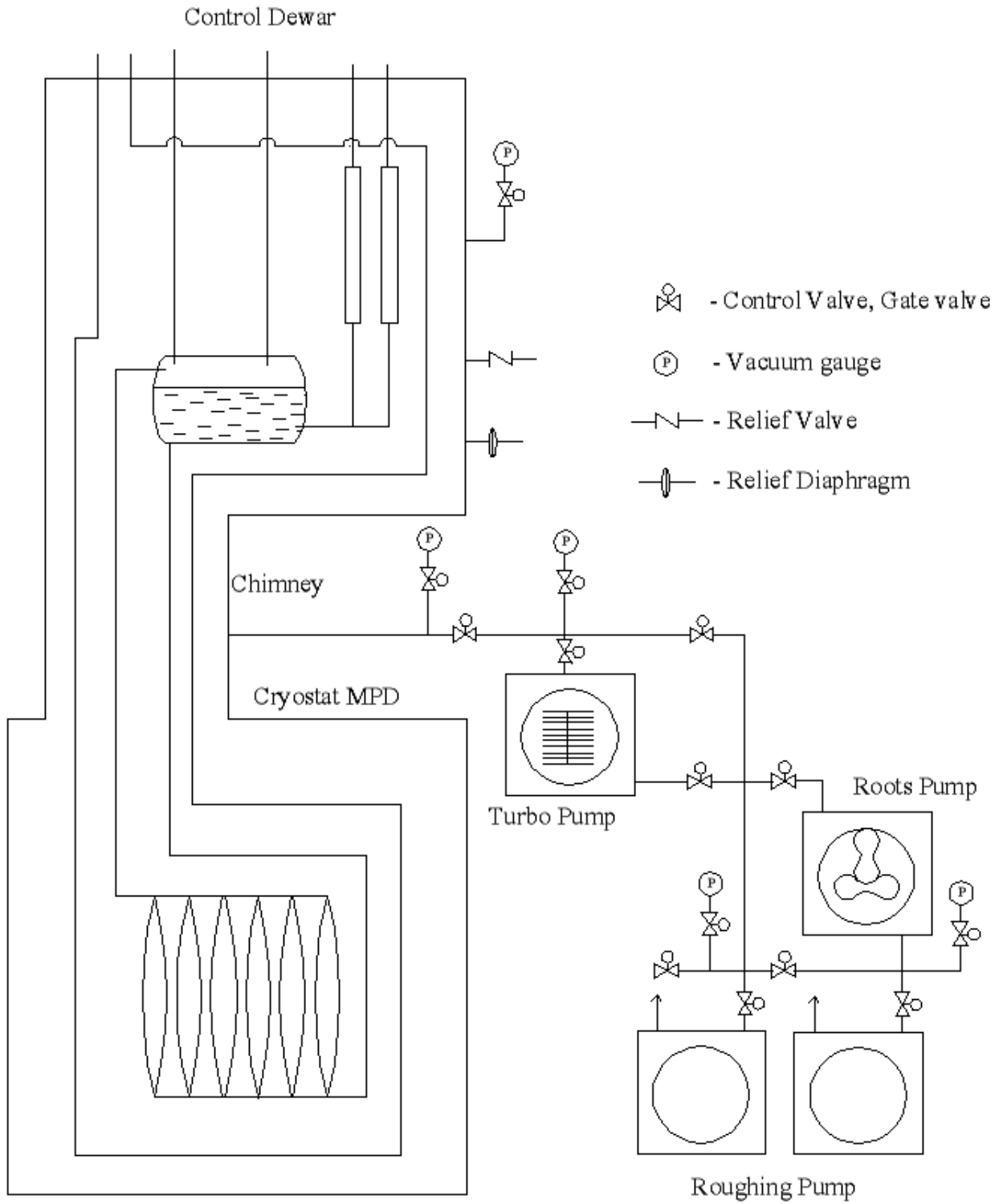


Fig. 2.4.4.2. Block diagram of the MPD solenoid vacuum system

Table 2.4.4.1. Technical and operating characteristics of the vacuum pumps

| Pump | Q-ty | Rate, m ³ /h | Power consumption, kW | Power supply parameters | Mass, kg | Dimensions LxWxH, mm | Cooling parameters |
|------------|------|-------------------------|-----------------------|-----------------------------|----------|----------------------|--|
| DUO 255 | 2 | 255 | 7.5 | 3 phases, 50Hz 220/380 V | 360 | 1360x480x700 | - |
| Okta 250AM | 1 | 250 | 0.75 | 3 phases, 50Hz 220/380 V | 125 | 800x330x280 | - |
| TPH 1201 | 1 | 4320 | 0.9 | 1 phase, 50Hz 220 V | 47 | 300x300x340 | Water, 100L/h, T _{max} =25°C |

2.4.5 CRYOGENIC SAFETY SYSTEM FOR THE VACUUM VESSEL

The cryostat and the control Dewar are designed to comply with the Rostekhnadzor requirements [14, 15, 17]. The most dangerous event in terms of cryostat safety is a cold helium leak in the helium pipelines within the cold volume of the cryostat or control Dewar. The working pressure in the coil cooling circuit is 1.3 bar, and in the cooling circuit of the thermal shield it is 3 bar; i.e., the pressure inside the vacuum volume can increase to higher than the atmospheric pressure, which can result in destruction of the vacuum vessel.

Relief valves are fitted on the vacuum casings of the chimney and control Dewar to protect the cryostat and control Dewar shells. The valves are rated to an internal pressure excess of 0.25 bar. There is also a relief diaphragm on the vacuum casing of the control Dewar, which breaks at a slightly higher pressure excess when the relief valve fails to operate. It is rated to an internal pressure excess of 0.5 bar. The strength of the cryostat vacuum vessel shells was calculated [6] for the emergency pressure excess of 0.7 bar to allow for a possible pressure drop in the chimney.

2.4.6 CRYOSTATING SYSTEM FOR THE SUPERCONDUCTING COIL

Initially the forced two-phase helium circulation using helium refrigerator and control Dewar with a heat-subcooler was selected for cooling the sc coil of MPD magnet [22]. After analyzing the operational characteristics of the regime and in accordance with the recommendations of the independent expertise of the project it was decided to replace the cooling method of the sc coil by natural convection of two-phase helium flow (thermosyphon). As in the previous case the coil is cooled indirectly by removing heat inflows to the liquid helium circulated in the heat exchanger tubes fixed on the outer surface of the coil support cylinder.

Helium cooling capacity at the specified temperature level is provided by a helium satellite refrigerator. Diagram of the cryogenic supply system of the sc coil of the MPD magnet is shown in Fig. 2.4.6.1.

Main components of the cooling system:

1. Cryostat comprising:

- SC coil cooled by indirect heat conduction to liquid helium circulated through heat exchanger tubes fixed on the outer surface of its support cylinder;
- Thermal shield cooled by liquid nitrogen flowing through the tubes fixed on its surface;
- Vacuum casing.

2. Control Dewar, including:

- Vessel with liquid helium;
- Current leads;
- Thermal shield cooled by liquid nitrogen flowing through the tube, fixed on its surface;
- Valve block (valves, sensors);
- Vacuum casing.

3. Vacuum tube (Chimney) connecting the cryostat with sc coil and control Dewar;

4. The helium satellite refrigerator (4.5 K) for cooling (heating) and cryostatting the sc coil;

5. Nitrogen re-condenser for cooling (heating) and cryostatting the thermal screens;

6. Transfer lines between the satellite refrigerator, nitrogen re-condenser and control Dewar.

In the steady state regime liquid helium from the satellite refrigerator enters the helium bath of the control Dewar through the transfer line and the valve CV1 at a pressure of 1.3 bar. From the helium bath liquid Helium through the valve CV3 and supply line enters the lower manifold of the heat exchanger of the rib-cage type on the support cylinder of the sc coil. After passing through the heat exchanger parallel channels vapor-liquid mixture from the upper manifold of the heat exchanger comes into the upper part of the helium vessel of the control Dewar. In the vessel the liquid is separated from the steam and used to cool the current leads and to compensate for heat inflows of the control Dewar helium bath. Backflow in the form of saturated steam at a pressure of 1.25 bar returns through the valve CV4 back to the satellite refrigerator.

Heat influxes to the cold mass due to radiation, through the suspension rods, measuring wiring and due to resistive losses in the joints of the sc cable are taken by the latent heat of vaporization of liquid helium in the tubes of the heat exchanger. The circulation of the helium in the circuit is carried out because of the density difference of the helium flows in the supply and return pipes. Helium gas from the current leads heated up to 300 K is fed into the low pressure line (LP).

Nitrogen re-condenser is used for cooling the thermal screens by flow of liquid nitrogen that enters the control Dewar through the valve CV8. After passing through the thermal shields the

nitrogen vapor-liquid mixture is returned through the valve CV9 to nitrogen re-condenser back, where the vapor phase is condensed and fed for cooling thermal screens (nitrogen closed system).

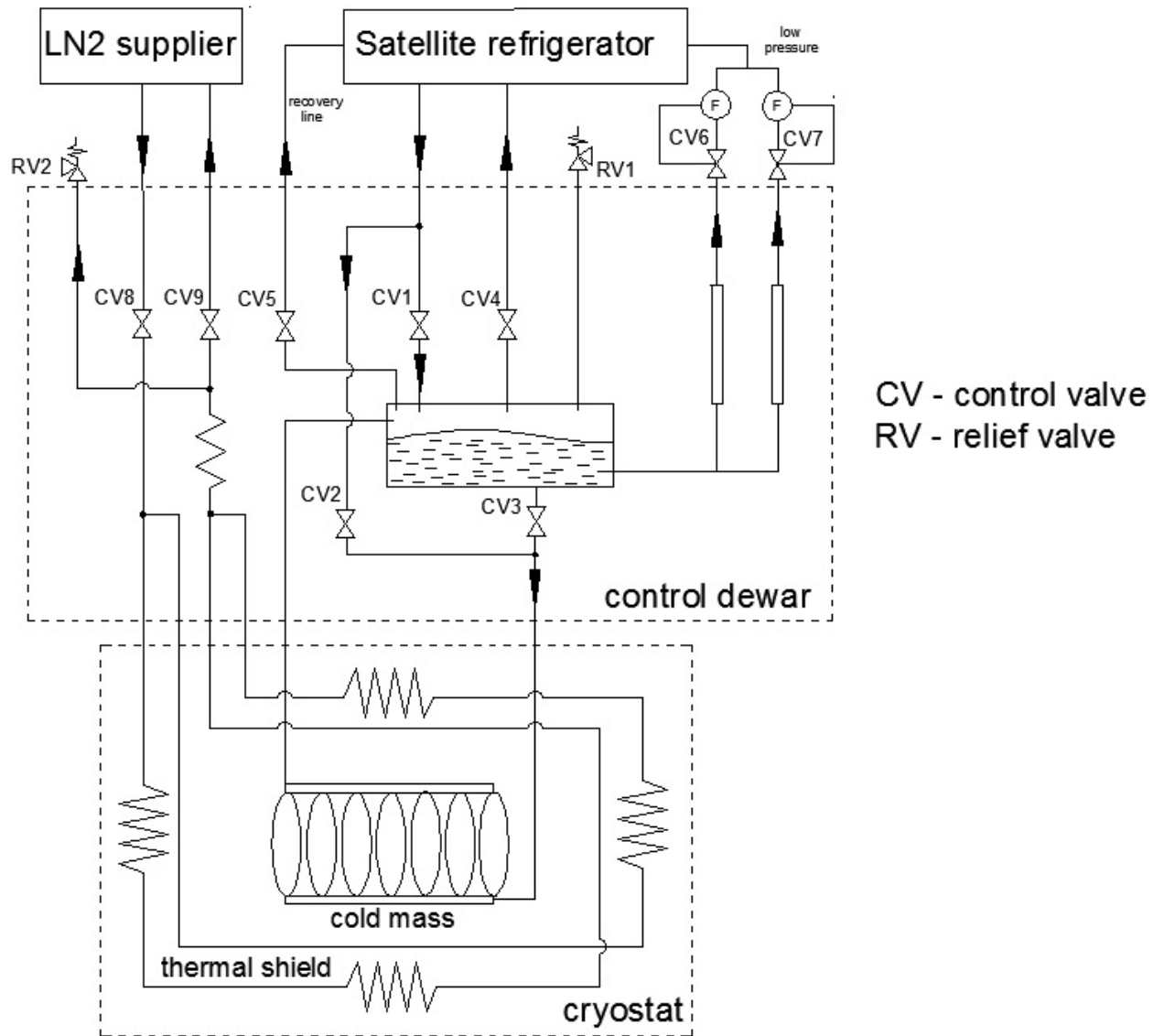


Fig. 2.4.6.1. Cryogenic supply system of the sc coil of the MPD magnet

2.4.7 SUPERCONDUCTING COIL PROTECTION SYSTEM

In superconducting detector magnets the coil and support cylinder thickness should normally be as small as possible to ensure maximum radiation transparency. However, this requirement is in conflict with the necessity to protect the coil after the quench. It is believed that if all the energy stored in the coil is deposited in the cold mass of the cryostat, the cold mass can be kept safe only if the E/M ratio (energy stored in the coil to the conductor and support cylinder mass) is not larger than 6 kJ/kg, which corresponds to the average after-quench temperature of the cold mass ~ 70 K. Since there are no limitations on the coil and cryostat radiation transparency for the MPD detector magnet, the E/M ratio was taken to be appreciably lower, 1.83 kJ/kg, which corresponds to the maximum after-quench average temperature of the cold mass ~ 46 K. A small E/M ratio allows avoiding additional measures for speeding up the propagation of the normal zone over the coil volume, such as gluing strips of pure aluminum to the inner surface of the coil. The maximum temperature rise in the coil remains limited to 108 K.

The protection system of the MPD magnet superconducting coil (Fig. 2.4.7.1) must protect the coil against overheating and decrease the level of mechanical stresses caused by the temperature gradients in the coil during the quench. In addition, the de-energizing system must ensure accelerated de-energizing of the coil without its quench when helium supply stops or power is lost.

After the electronic protection circuit detects quench, switches S_1 and S_2 operate and the superconducting coil with inductance L_s discharges to the series-connected dump resistors R_{d1} and R_{d2} and its energy is partially dissipated in the coil itself and in the aluminum support cylinder (Fig. 2.4.7.1). Doubling of the switches increases the emergency operation reliability of the protection system. The dump resistor $R_{d1} + R_{d2} = 0.104 \Omega$ limits the maximum coil voltage during de-energizing to 250 V.

The switch S_3 allows the discharge resistance to be varied for varying the coil de-energizing rate. When the helium supply stops or a power loss signal comes from the magnet control system, the switches S_1 , S_2 , and S_3 operate and the superconducting coil is rapidly discharged through the dump resistor R_{d1} without quenching.

The discharge resistors R_{d1} and R_{d2} used for energy absorption during the coil discharge are made of stainless steel. The maximum deposited energy is 24.4 MJ in the resistor R_{d1} and ~ 22 MJ in the resistors $R_{d1} + R_{d2}$. The maximum temperature of the resistors during de-energizing will be limited to $\sim 300^\circ\text{C}$. They will be cooled by natural air convection.

The aluminum support cylinder helps decrease the maximum temperature during the coil quench by providing accelerated propagation of the normal zone over the entire coil volume (so-called "quench-back effect"). Accelerated propagation of the normal zone leads to a decrease in the temperature gradients inside the coil and in the voltage drop in the normal zone.

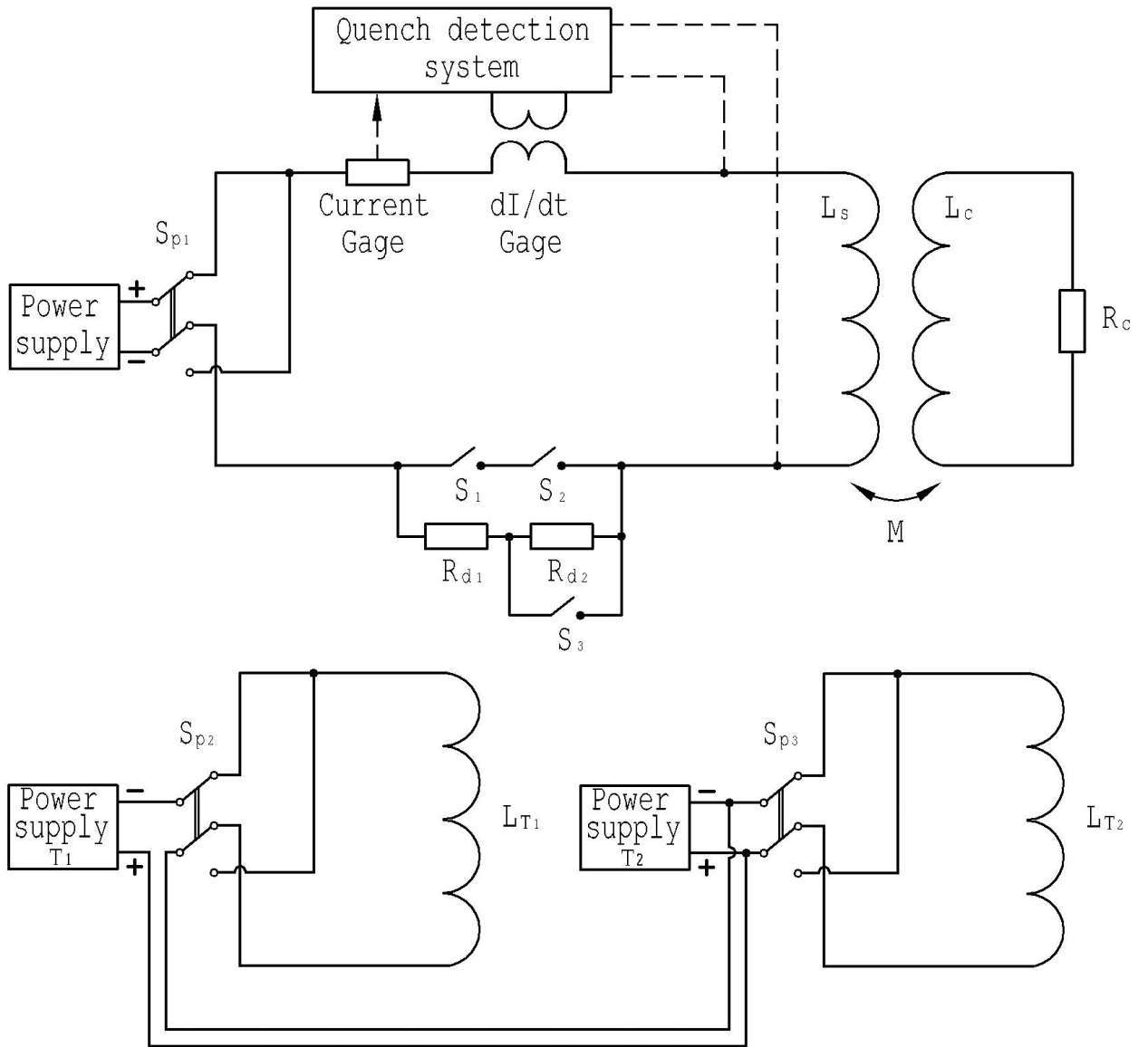


Fig. 2.4.7.1. Superconducting coil protection circuit, MPD magnet power system

2.4.7.1 EMERGENCY DE-ENERGIZING OF THE SUPERCONDUCTING COIL

The operation threshold of the electronic protection circuit will be determined in test low-current energizing of the coil. It is estimated to be 1 V and depend on the noise level in the circuit. Inductance of the MPD superconducting coil with the yoke is 8.7 H, and the stored energy at the maximum current of 2.4 kA is 24.4 MJ.

According to the calculations by the QUENCH code [5], after the protected coil quenching at the maximum current the maximum temperature in the coil is 27 K. The maximum temperature difference in the entire cold mass (winding, insulation, and support cylinder) is in the order of 11 K, which corresponds to a time of ~ 20 s after the beginning of the quenching. If the protection system fails to operate and all the stored energy is deposited in the coil, the maximum temperature of the coil after its quenching will be 108 K when the normal zone originates at the coil edge. The maximum temperature difference in the radial direction across the insulation is ~ 30 K, and the maximum voltage drop in the normal zone is 193 V. When the normal zone originates at the center of the coil, the maximum temperature in the coil will be lower.

Figure 2.4.7.2 shows time variation of the current, voltage drop on the normal zone, and maximum coil temperature during the coil discharge to the protective resistor. Similar plots for the unprotected coil quenching are presented in Fig. 2.4.7.3.

The coil will be energized with the maximum current of 2.4 kA only in the acceptance test of the magnet with the yoke, when failure of the protection system to operate during the coil quenching is hardly possible. If the protection system fails to operate at the rated current of 1.79 kA, the coil temperature will be 74 K.

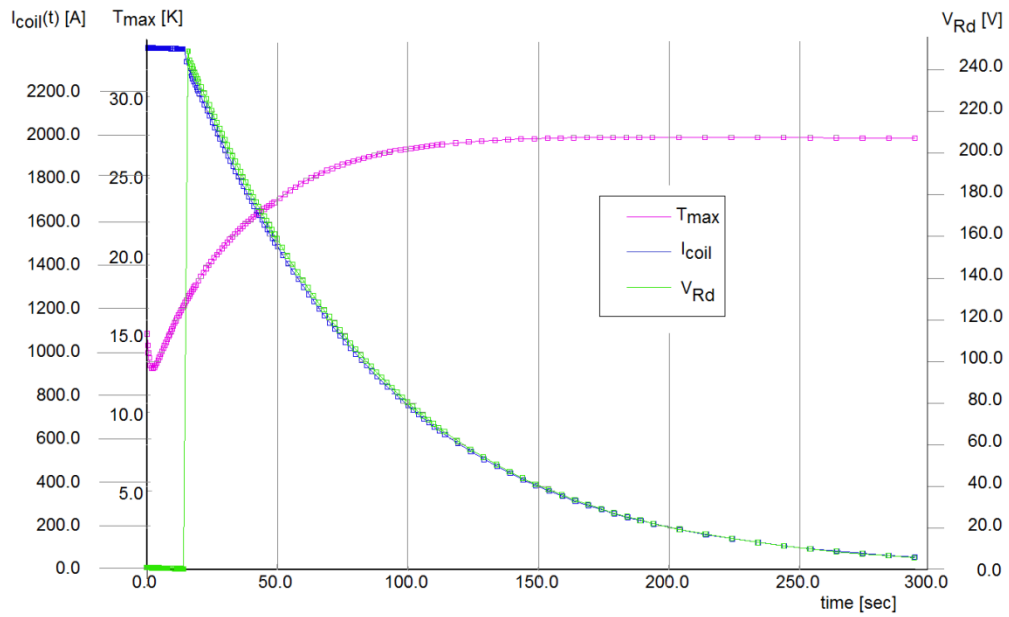


Fig. 2.4.7.2. Maximum coil temperature, coil current, and voltage drop at the current leads when the coil is de-energized through the dump resistor after quenching

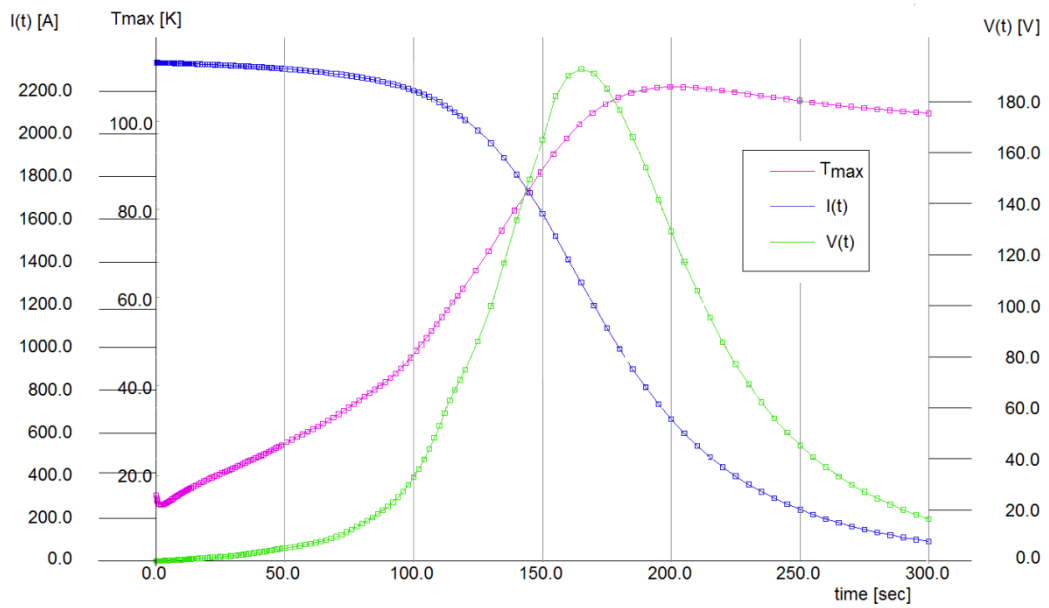


Fig. 2.4.7.3. Maximum temperature, coil current, and voltage drop on the normal zone in the unprotected quench process

2.4.7.2 ACCELERATED DE-ENERGIZING OF THE SUPERCONDUCTING COIL

Accelerated de-energizing is used for rapidly removing energy from the coil without its quenching, e.g., when power is lost to the coil. In this mode de-energizing is not performed using the power supply but rather by discharging to the dump resistor with a resistance lower than in the case of emergency de-energizing.

When the liquid helium circulation in the heat exchanger of the superconducting coil stops and after de-energizing begins, the cold mass of 13 300 kg begins heating due to heat inflows to the coil through the suspension, radiation heat inflows, and eddy current loss in the coil support cylinder. The coil heating time will depend on the cold mass and the vaporization heat and enthalpy of helium that is left in the support cylinder cooling pipe. The cable and support cylinder heat conductance and the liquid helium vaporization heat in the support cylinder cooling pipe should be enough to maintain the winding temperature below the critical value and thus avoid its quenching at the accelerated de-energizing.

According to the calculations, the time for accelerated de-energizing of the coil without its quenching should be limited to 20 min [7], which corresponds to a current decay rate of 2 A/s. A stainless-steel resistor with resistance $R_{d1}=0.0073 \Omega$ will be used for de-energizing. The maximum voltage drop across the resistor during the energy removal will be ~ 18 V, and the maximum power during the energy removal will be about 43 kW.

2.4.8 YOKE

The MPD solenoid yoke (Fig. 2.3.1) is mainly intended for returning the magnetic flux produced by the superconducting solenoid and shielding the environment against the scattered field of the solenoid. In addition, the yoke makes a contribution of about 18% to the total field in the central part of the magnet. The yoke is made of steel similar in composition to steel 10. The chemical composition of steel 10 is presented in Table 2.4.8.1. The main mechanical characteristics of steel 10 are presented in Table 2.4.8.2, and its magnetic characteristics are given in Table 2.4.8.3.

Table 2.4.8.1. Chemical composition of Steel 10

| C | Si | Mn | S | P | Cr | Ni | Cu | N ₂ |
|----------------|---------------|---------------|------|-------|------|------|------|----------------|
| 0.07- 0.014 | 0.17- 0.37 | 0.35- 0.65 | 0.04 | 0.035 | 0.15 | 0.25 | 0.25 | 0.08 |

Table 2.4.8.2. Mechanical properties of Steel 10

| Item | Unit | Value |
|---|-------------------|---------------------|
| Coefficient of thermal expansion at -50-+18°C | Deg ⁻¹ | 13×10 ⁻⁶ |
| Young's module | Gpa | 198 |
| Tensile strength of annealed sample | Mpa | 340 |
| Yield stress of annealed sample | Mpa | 210 |
| Elongation | % | 29 |

Table 2.4.8.3. Magnetic properties of Steel 10

| Induction, T | Magnetizing Field, A/m |
|--------------|------------------------|
| 1.55 | <2179 |
| 2.01 | <23881 |

The yoke comprises two support rings, 24 barrel beams, two poles with trim coils and transportation platforms, and a support structure consisting of two cradles, six stationary supports, and four roller skates (Fig. 2.3.1.). The weights of the main yoke components are presented in Table 2.4.8.4. The total mass of the assembled yoke is 727 t.

The calculation of the magnetic forces applied to the yoke is given in [10]. During the operation at the maximum solenoid current without any technological deviations each yoke beam is pressed against the support rings by an axial magnetic force of 116 kN and radial force of 125 kN. The axial force acting on the pole is $F_z = 2.68$ MN and the corresponding force acting on the pole + support ring is $F_z = 2.79$ MN.

If the SC coil is axially shifted by 20 mm, the axial force acting on the pole from which the coil shifts away is $F_z = 2.61$ MN and the corresponding force acting on the pole + support ring is $F_z = 2.69$ MN. The axial force acting on the pole toward which the coil shifts is $F_z = 2.74$ MN and corresponding force acting on the pole + support ring is $F_z = 2.81$ MN.

Table 2.4.8.4. Weights of the main magnet components

| Item | Dimensions, m | Pcs. | Weight, tons | Sum, tons |
|---|---------------------------------|------|--------------|-----------|
| 1. Iron Yoke Barrel | | | | |
| Support ring | 4.596 I.D., 6.64 O.D., t=0.35 | 2 | 41.8 | 83.6 |
| Barrel beam | 8.47 x 0.866 x 0.35 | 24 | 18.54 | 445 |
| Yoke support | 6.96 x 6.8 x 3.85 | 1 | 92.77 | 92.77 |
| Auxiliary ironware (roller skates, etc) | | | | 9.55 |
| Total (weight of the yoke without poles) | 630.92 | | | |
| 2. Poles | | | | |
| Pole | 1.93 I.D., 4.586 O.D., t=0.79 | 2 | 43.65 | 87.3 |
| Trim coil | 1.93 I.D., 3.592 O.D., t=0.11 | 2 | 2.14 | 4.28 |
| Pole transport platform | 2.54 x 4.03 x 6.433 | 2 | 55 | 110 |
| Auxiliary ironware (roller skates, pole rests, etc) | | | | 6.76 |
| Total (weight of a poles on the transport platforms) | 208.34 | | | |
| Grand Total 1 (weight of the yoke with the poles) | 727.06 | | | |
| 3. Cryostat & sc coil | | | | |
| Vacuum vessel | 4.656 I.D., 5.443 O.D., l=7.945 | 1 | 48.76 | 48.76 |
| Thermal shield | 4.834 I.D., 5.265 O.D., l=7.678 | 1 | 2.68 | 2.68 |
| Coil+Support cylinder | 4.936 I.D., 5.070 O.D., l=7.571 | 1 | 13.9 | 13.9 |
| Control Dewar +chimney | | 1 | | 0.7 |
| Auxiliary ironware (tie rods, rests, etc) | | | | 0.37 |
| Total (cryostat+coil) | 66.41 | | | |
| Grand total 2 (magnet weight) | 793.47 | | | |
| Inner detectors and support cylinder | | | | 166 |
| Magnet top platform with equipment | | | | 20 |
| Grand total 3 (MPD weight) | 979.47≈980 tons | | | |

Static strength calculations for the main yoke components in various modes of MPD magnet operation are given in [8, 20]. The purpose of the calculations was to analyze the strain-stress state of the structural elements of the MPD magnet resulting from weight loads, initial stud/bolt tightening force, and magnetic forces during its movement and under operating conditions. The design load for the MPD magnet moved without poles is the weight load and the initial tightening force applied to the studs of the support ring flange joints. The design load under the operating conditions includes the weight load, the initial tightening force applied to the M48 studs of the support ring flange joints, M48 bolts of pole stops, and M42 fastening bolts of the cryostat, and forces acting on the poles, support rings, and beams due to the magnetic field.

Several possible MPD magnet load regimes during its assembly, movement from the assembly site to the operating position, and operation in the accelerator were considered (see Table 2.4.8.5).

According to the calculations, the maximum bending stress in the yoke beams is 8.7 MPa (regime 5), which is lower than the allowable value 169 MPa. In other structural elements of the magnet (except mounting hardware) the reduced stresses are also below the allowable values. For example, the maximum stresses in the magnet supports are 70 MPa. In the pole rests maximum bending stresses are 22 MPa. In the support rings and magnet poles the total bending stresses are no higher than 17/10 MPa.

During the manufacture of the magnet the end surfaces of the support ring and the beams (especially three lower beams) must be aligned as much as possible for increasing the total rigidity of the magnet structure and thus decreasing the stresses in M48 studs. The tightening force for M48 studs taken to be 296 kN guarantees that the beam will not slip on the support ring surface under the effect of its own weight and magnetic forces. The tightening force for M48 pole stop bolts taken to be 263 kN guarantees that the pole (plus disk calorimeters fixed to the pole tips) will not slip under the effect of its own weight and magnetic forces.

The maximum possible force 270 kN arises in M42 bolts in the case with running into an obstacle 6 mm high. To prevent the contact between the support surface and the cryostat leg from opening, the initial tightening force for M42 bolts was taken to be 290 kN in all calculation cases.

The maximum stresses and strains arise in the structural elements of the magnet during its movement when it comes to rest on two diagonally located support roller skates, e.g., when it runs into an obstacle of 6 mm in high (load case 7 in Table 2.4.8.5). In this case terms of strength are met for all parts of the magnet and correspond to Normal Operating Conditions. The exception is three studs M48 where there is an increased by 11% (σ)_{4w} stress (tensile + bending) with respect to allowable stress. Nevertheless, these increased stresses meet the requirements of the regime of Violation of Normal Operating Conditions. Stresses in these three studs in the subsequent magnet operation in beam position will also exceed by 5.4% stresses corresponded to Normal Operating Conditions, but will meet the requirements of the regime of Violation of Normal Operating Conditions. These circumstance dictates the need for leveling the surface of the rail track with a maximum tolerance of ± 2.25 mm.

Table 2.4.8.5. Calculations of magnet strain-stress state cases

| Case | Description |
|------|--|
| 1. | The yoke without the poles, cryostat, and inner detectors rests on six stationary supports |
| 2. | The yoke without the poles, cryostat, and inner detectors rests on four roller skates |
| 3. | The yoke with the poles, cryostat, and inner detectors rests on six stationary supports |
| 4. | The yoke with the poles, cryostat, and inner detectors rests on four roller skates |
| 5. | The yoke with the poles, cryostat, and inner detectors rests on two diagonally located points (along the other diagonal the contact of the roller skates with the rails is lost) |
| 6. | One of four roller skates carrying the yoke with the poles, cryostat, and inner detectors runs into an obstacle 1 mm high |
| 7. | One of four roller skates carrying the yoke with the poles, cryostat, and inner detectors runs into an obstacle 6 mm high |
| 8. | The yoke with the poles, cryostat, and inner detectors rests on six stationary supports with the maximum decentering magnetic forces (after loading steps 3 and 5) |
| 9. | The yoke with the poles, cryostat, and inner detectors rests on six stationary supports with the maximum decentering magnetic forces (after loading steps 4 and 6) |
| 10. | The yoke with the poles, cryostat, and inner detectors rests on six stationary supports with the maximum decentering magnetic forces (after one loading step) |
| 11. | The yoke with the poles, cryostat, and inner detectors rests on six stationary supports with the maximum decentering magnetic forces (after loading steps 4 and 5) |
| 12. | The yoke with the poles, cryostat, and inner detectors rests on six stationary supports with the maximum decentering magnetic forces (after loading steps 4 and 7) |

2.4.8.1 YOKE BARREL

The barrel of the solenoid yoke (Figs. 2.3.1, 2.4.1.1, 2.4.8.1.1) consists of two end support rings and 24 beams, which are rigidly connected to the rings and make up a cylindrical barrel-like structure, and a support structure. To have the field of the required quality in the TPC region, the relative displacements of the yoke components under loads should be smaller than 1 mm. This is achieved by choosing an appropriate yoke design, precisely fitting the components together, tightly connecting them using studs with supernuts (see Appendix 1) and pin joints of aligned components, and laying a rail track of appropriate quality for moving the magnet (see Section 2.4.8.7).

A support ring (inner diameter 4596 mm, outer diameter 6640 mm, thickness 350 mm, weight 41.8 t) has a 24-face surface at a diameter of 5883 mm for fixing beams (length 8470 mm, thickness 350 mm, trapezoidal section, weight 18.5 t each) in the azimuthal and radial positions. This design involving support rings ensures general stability of the structure and minimum relative displacements of the magnet elements under the effect of weight load and magnetic forces and also during the movement of the assembled magnet, which is necessary for reproduction of highly homogeneous magnetic field in the magnet operation area after each movement.

The weight load of the cryostat with the superconducting coil and the forces produced by the magnetic stress arising from the displacement of the coil axis relative to the yoke axis are transferred to the yoke beams. The weight of the inner detectors is transferred to the yoke support rings.

In the beams there are additional radial slots for bringing cables and pipes of inner detectors out of the magnet aperture (see Section 2.4.15 “Recesses for bringing cables and pipes out of the magnet aperture”).

Each of the yoke beams is rigidly attached by eight M48 studs (four studs on each side) and supernuts (see Appendix 1) to the solid-forged support rings. Supernuts allow avoiding the torque that causes twisting of the stud body as the nut is drawn up. In addition, a small size allows the supernut to be recessed in the support ring body, which decreases the axial dimension of the magnet. The studs are arranged in two radial rows that are 180 mm apart. The studs are spaced at 550 mm in the outer row and at 500 mm in the inner row. The tightening force for each stud is 296 kN.

The yoke barrel rests on two cradles (Fig. 2.4.1.1), each consisting of two vertical steel plates 150 mm thick, which are in contact with the beams at the top and are connected by a horizontal plate 150 mm thick. The cradles are connected to each other by two beams that allow joining them for machining their common plane on the lower horizontal surface to attach four roller skaters for moving the magnet along the rail track and six stationary supports with hydraulic jacks (see Section 2.4.8.4).

Eleven lower beams of the yoke are welded to the support cradles and to each other during the final assembly in Dubna. Thirteen upper beams of the yoke are not connected to each other over their length and have a mounting gap of 2 mm between them.

Terms of strength are met for all elements of the design of the magnet under Normal Operating Conditions after running over an obstacle height of 6 mm. The exception is the M48 studs - their stress for the design group categories of stress $(\sigma)_{4w}$ exceeds the permissible value under Normal Operating Conditions by 5.4% and does not exceed the permissible values for the regime of Violations of Normal Operating Conditions. Terms of strength for these studs under Normal Operating Conditions are to be provided after running over an obstacle of ≤ 4.5 mm in height only.

According to the calculations, the condition of rigidity with respect to mean tangential stresses in the welds connecting the beams is fulfilled in all modes of magnet operation. The maximum mean tangential stress is 33 MPa (in the case of the magnet running into an obstacle 6 mm high as it is moved), which is lower than the allowable stress $[\sigma_{\tau}] = 65$ MPa.

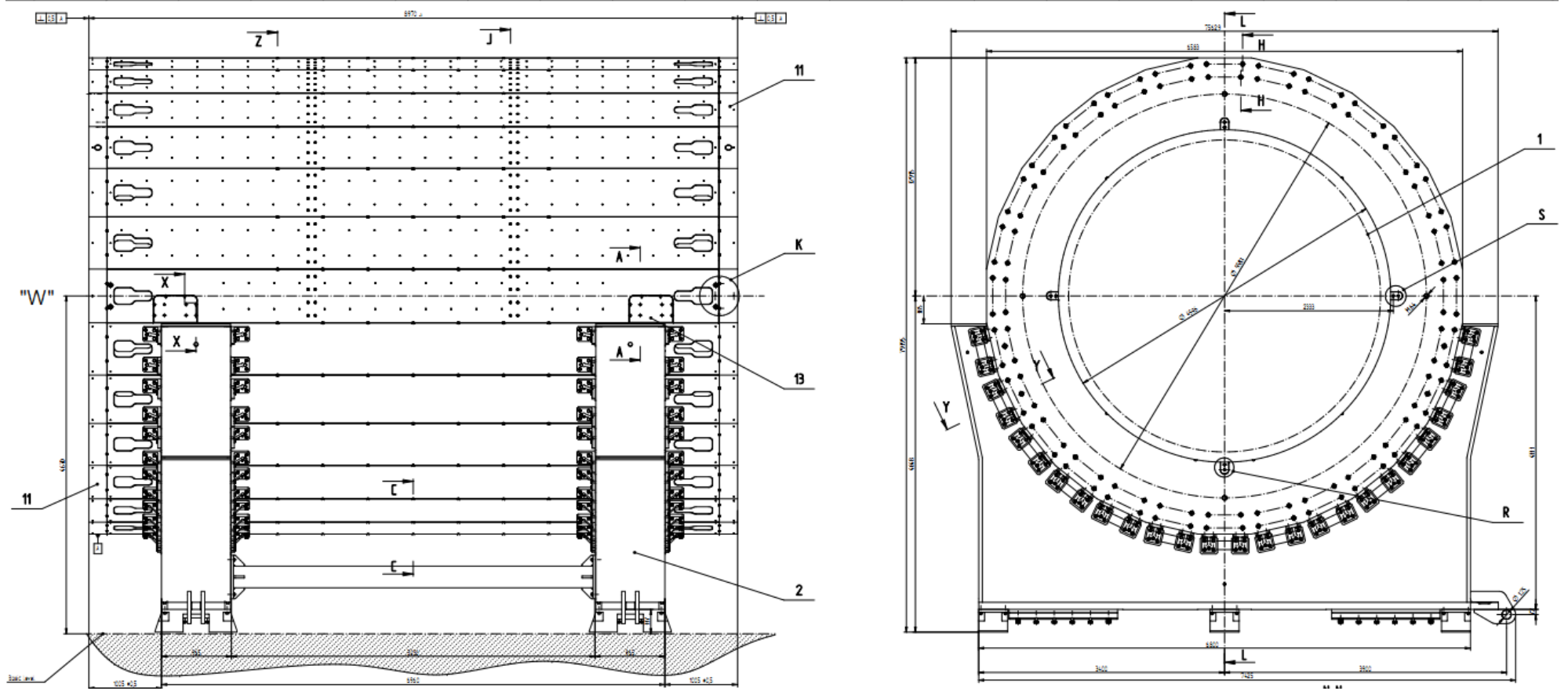


Fig. 2.4.8.1.1. MPD solenoid yoke barrel

2.4.8.2 MAGNET POLES

The poles of the magnet (Figs. 2.3.1, 2.4.8.2.1, 2.4.8.2.2) are made up of two end caps fit into the borings of the support rings. Each pole weighs 43.7 t (without the transport platform and the trim coil). The poles are inserted in the magnet and fixed relative to the yoke support rings by axial stops and radial spacers. The internal recesses of the poles are cone shaped with an angle of 14°.

At the maximum magnet current (with no axial shift of the SC coil) the axial force $F_z = 2.68$ MN acts on the pole. When the SC coil is axially shifted by 20 mm, the axial force acting on the pole from which the coil shifts away is $F_z = 2.61$ MN. The axial force acting on the pole toward which the coil shifts is $F_z = 2.74$ MN.

The disc calorimeters (Ecal) weighing 20 tons each are fixed on the poles. Their weight loads are transferred to the tips of the poles.

When moved on the platform, the pole is fixed in the vertical position using a flange on two vertical knee braces. Flanges allow the planes of the poles and support rings to be aligned as the pole is fitted into the support rings. Relative parallelism of the pole surfaces is obtained using shims between the support ring surfaces and the axial stops.

The pole is fixed relative to the support ring of the magnet barrel using eight stops and 64 bolts M48. The pole and the support ring are precisely aligned using three guide pins 60 mm in diameter with the tapered lead-in parts (Fig. 2.4.8.2.3).

The tightening force for the M48 bolts is taken to be 206 kN, which guarantees that the pole will not slip under the effect of its own weight and magnetic forces. The most unfavorable loads in the bolts occur in an emergency event (the magnet resting on two diagonally located points when transported). In this case the tensile force in a bolt will be 211 kN. The reduced stresses under mechanical exposure determined from the components of the tensile, bending, and torsion stresses in the bolts for the given case are $314 \text{ MPa} < 2.4[\sigma]_w = 1001 \text{ MPa}$.

The friction force between the pole stops and the support ring surfaces is enough to keep the pole immune to the effect of its weight and the magnetic decentering force with a safety factor of 2.2. Nevertheless, wedge-shaped distance pieces are inserted in the gap between the pole and the support ring to fix the pole in the radial direction and keep the gap uniform along the perimeter of the pole (< 0.25 mm). The wedges are exactly positioned using spacers between them and the pole (Fig. 2.4.8.2.3).

According to the calculations, the maximum total bending stresses in the pole stops are 22.3 MPa. The total bending stresses in the magnet poles are no higher than 10.2 MPa.

Roller skates are used to move both the magnet barrel and the poles.

The magnet poles are placed on their own transport platforms that allow them to be moved relative to the yoke along their own rail tracks and stay on the rail tracks when the yoke complete with the poles is moved to the operating position.

To prevent the pole from turning over when moved, there is a counterweight at the opposite end of the platform (the center of gravity of the platform with the pole and the counterweight is 2.92 m high). The pole moves at a speed no higher than 5 mm/s. The mass of the pole with the trim coil, platform, counterweight and disc calorimeter is ~143 t.

The platforms with the poles will be moved using two pairs of hydraulic cylinders. Considering the rolling friction force (the friction factor is taken to be 0.05), the force to move the platform is 50 kN. With a safety margin, the maximum force developed by each cylinder for moving the pole should be about 50 kN. Since the poles are moved on the platforms from the yoke to a minimum distance allowing free movement of the magnet, there is no need for successively transferring stops for pole cylinders from place to place. The maximum distance to which the pole is moved at the full working stroke of the hydraulic cylinder is 1420 mm. It takes about 1 h to move one pole without considering the time for detaching the pole from the barrel.

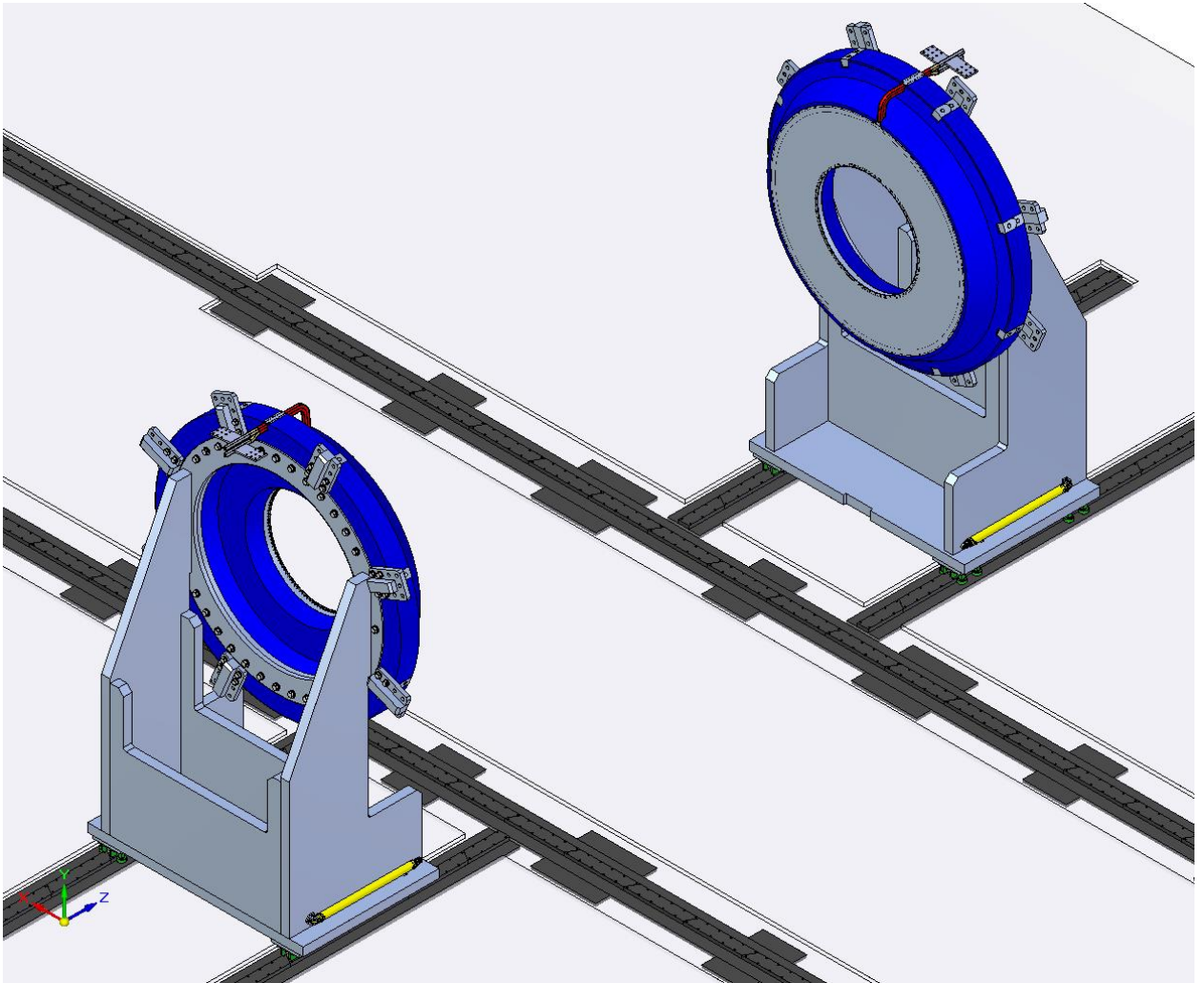


Fig. 2.4.8.2.1. Magnet pole assemblies (hydraulic cylinders for moving the poles are colored yellow)

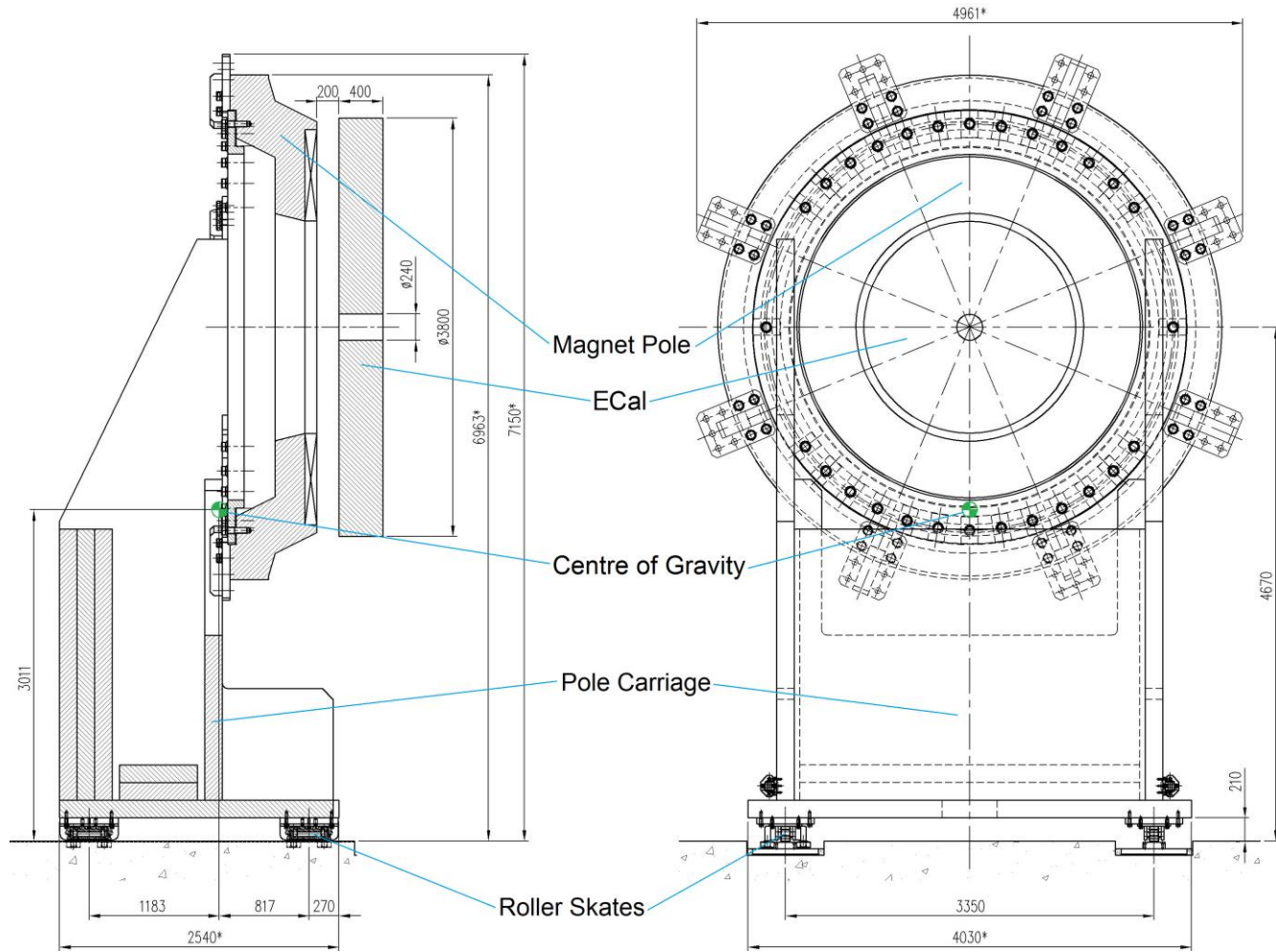


Fig. 2.4.8.2.2. Position of the center of gravity of the pole assembly

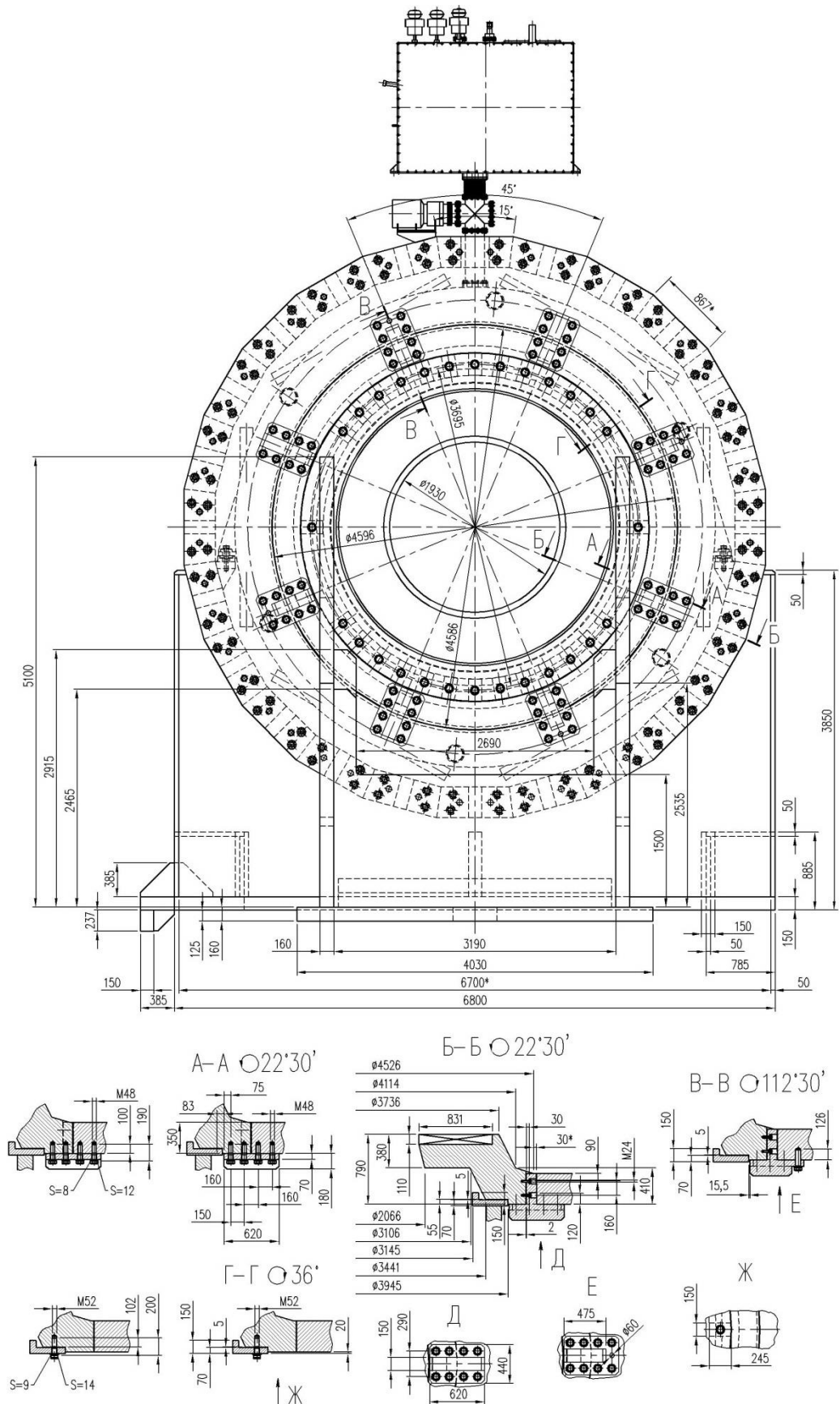


Fig. 2.4.8.2.3. Arrangement of stops and guide elements on the solenoid pole

2.4.8.3 POSITIONING OF THE MPD MAGNET FOR ASSEMBLY AND OPERATION

The magnet yoke barrel with the cryostat and inner detectors is assembled at the assembly site in the experimental building (Fig. 2.4.8.3.1) and then moved to the operating position in the accelerator. In the intermediate position (Fig. 2.4.8.3.2) poles are fixed into the support rings of the yoke. Then the transport platforms are detached from the poles and moved to the parking positions. Figure 2.4.8.3.3 shows the magnet in the operating position

To align the NICA and MPD axes, the floor level in the detector area is lowered to -3.19 m, and the distance from the beam axis to the magnet foundation plane is 4.69 m (Fig. 2.4.8.3.4).

The 3D view of the assembled magnet complete with the inner detectors and an electronics and with top platform for equipment at the assembly site and in the operating position is shown in Figs. 2.4.8.3.5 and 2.4.8.3.6 respectively.

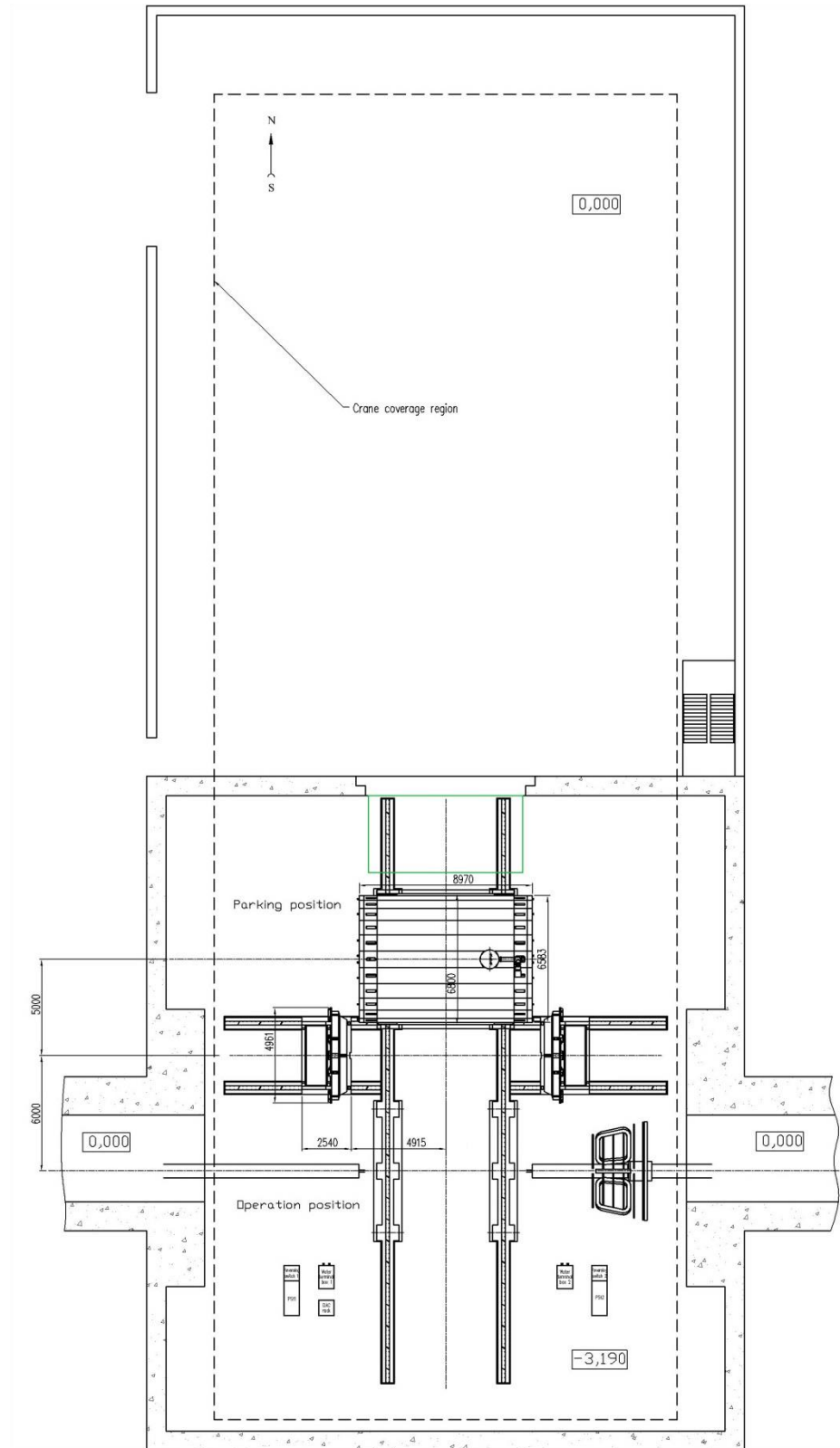


Fig. 2.4.8.3.1. Positioning of the magnet at the assembly site

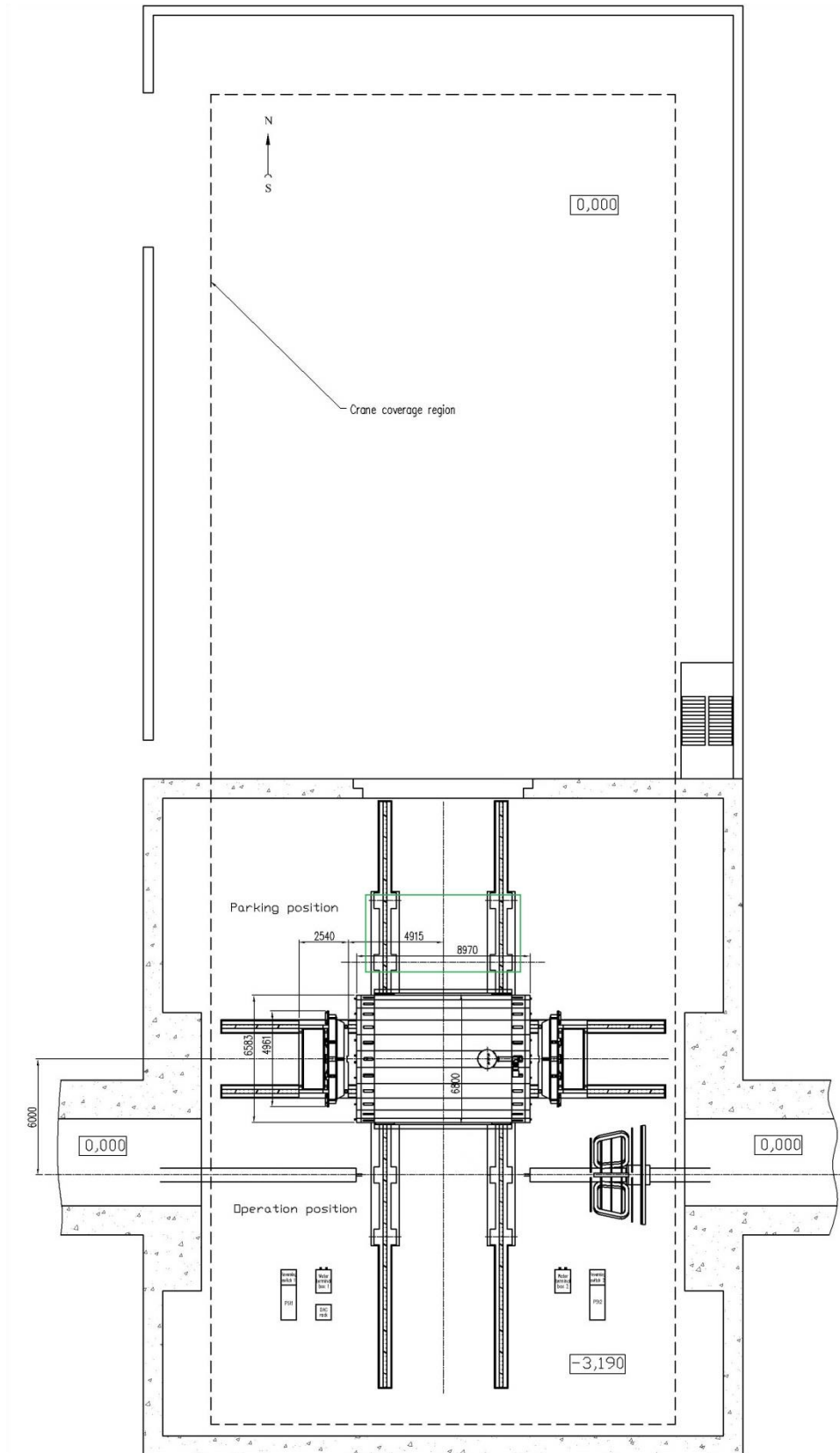


Fig. 2.4.8.3.2. Positioning of the magnet for mounting the poles

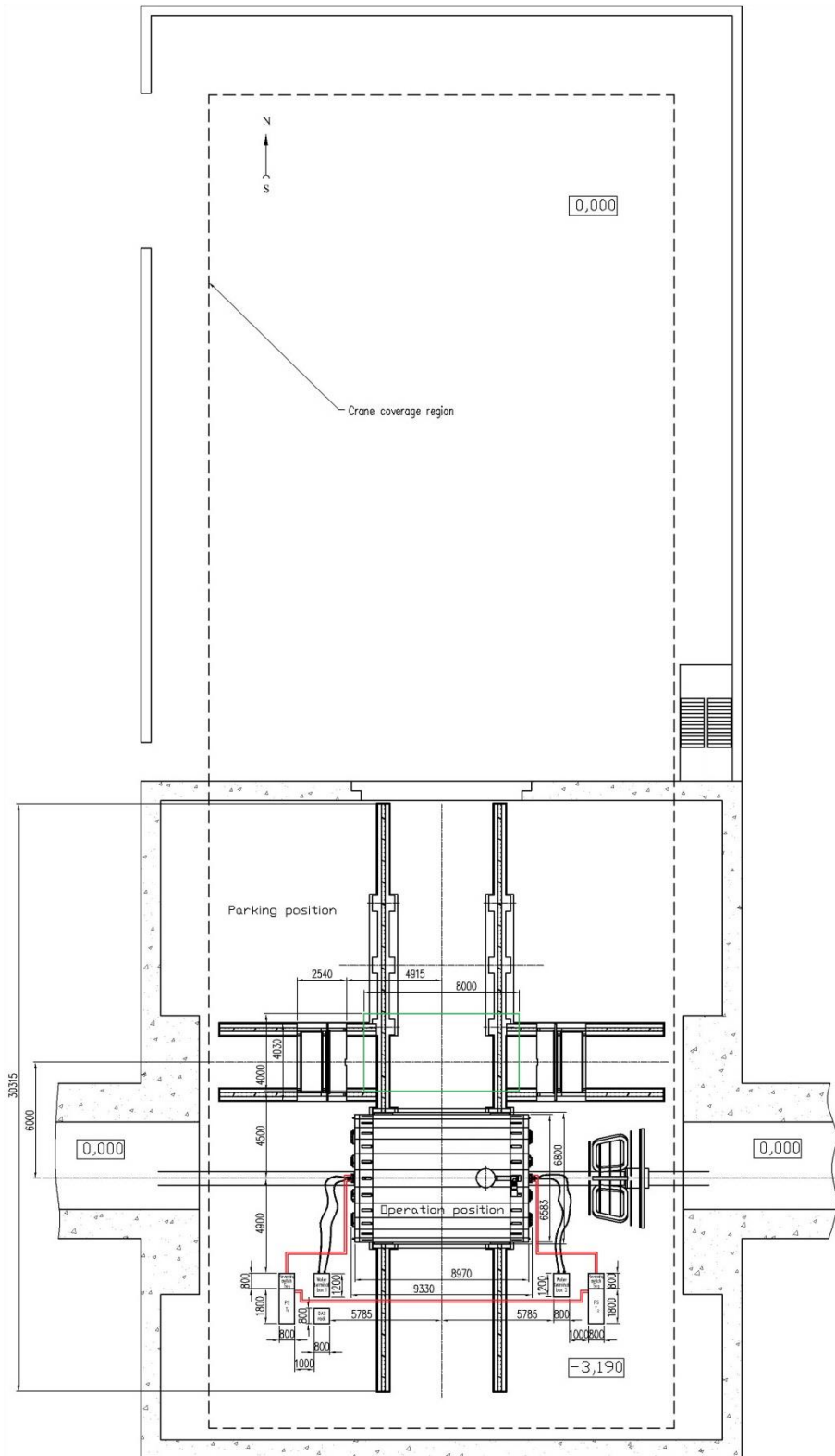


Fig. 2.4.8.3.3. Positioning of the magnet in the accelerator area

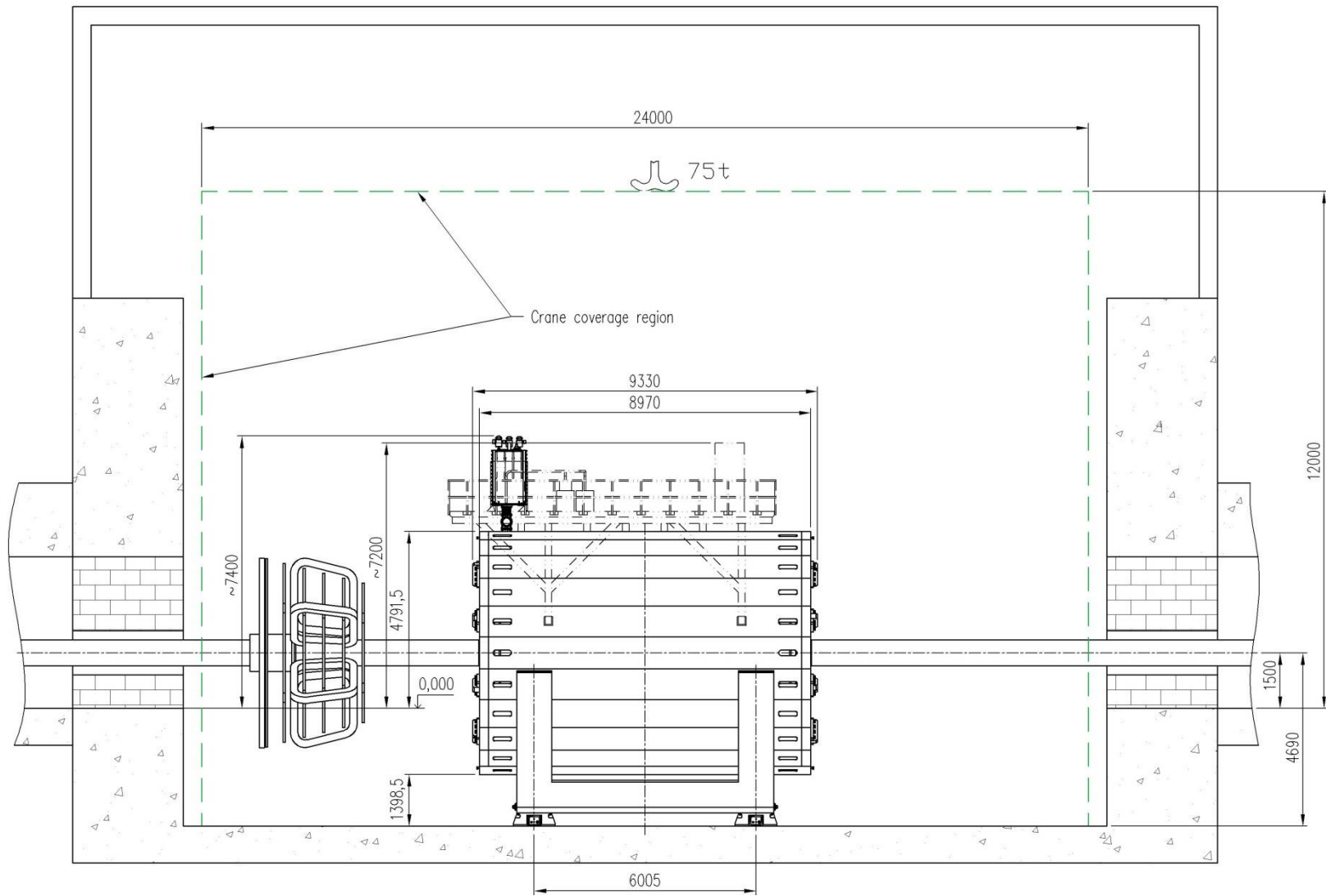


Fig. 2.4.8.3.4. Positioning of the magnet in the accelerator area

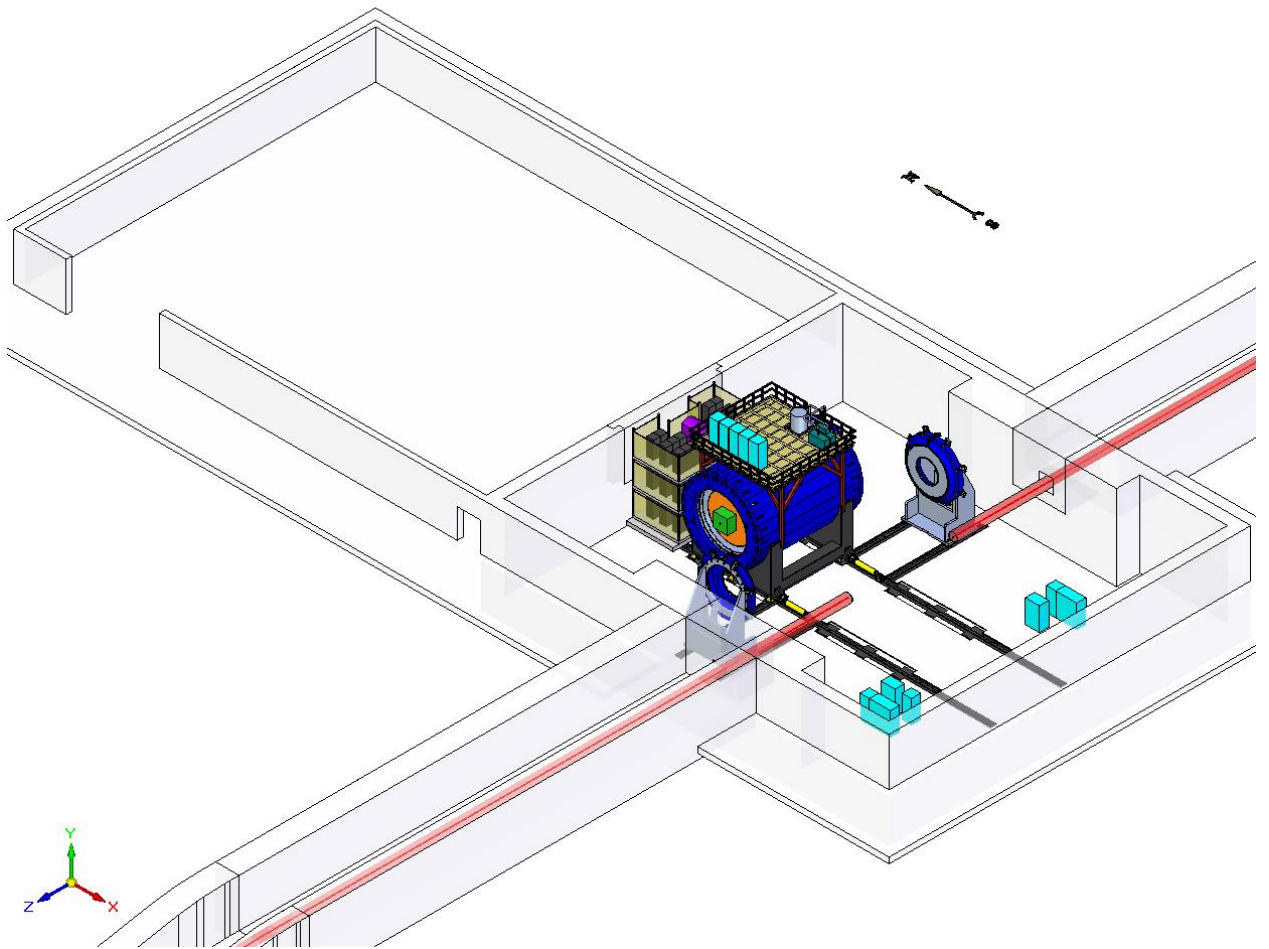


Fig. 2.4.8.3.5. Yoke complete with the cryostat, inner detectors, and platform at the assembly site

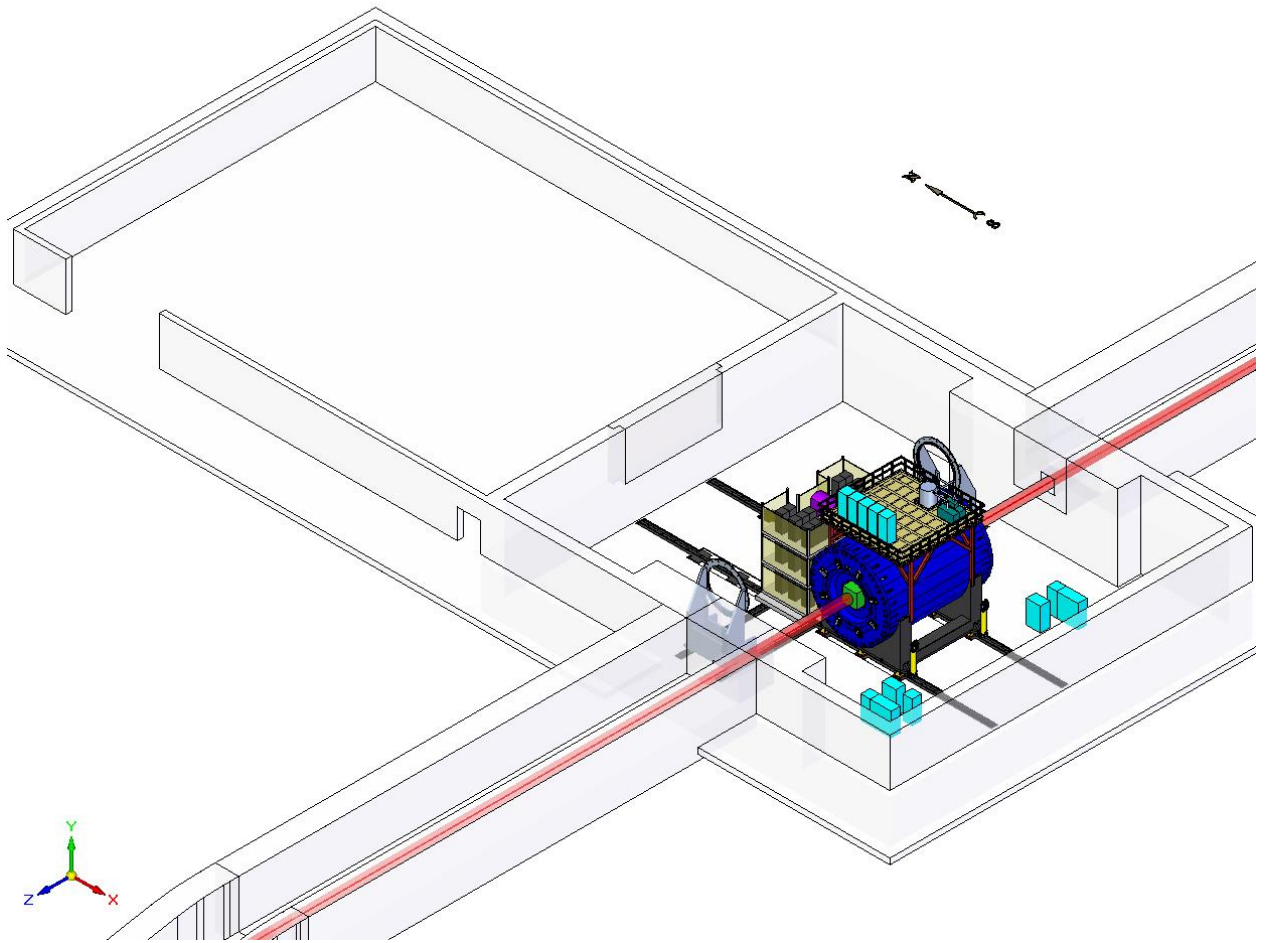


Fig. 2.4.8.3.6. Completely assembled MPD detector in the operating position in the accelerator

2.4.8.4 MAGNET AND POLE SUPPORTS

To transfer the weight load to the foundation, the yoke rests on a support consisting of two cradles joined by box profiles (Fig. 2.3.1). The total mass of the support is ~93 t. Eleven lower beams embraced by the cradles are welded to them and to each other.

At the assembly site the magnet is assembled on six stationary supports (Fig. 2.4.8.4.1.), which are also used later to position it for operation in the accelerator. The magnet is moved on the rail track using four roller skates (Fig. 2.4.8.4.1). The total weight of the yoke complete with the cryostat and inner detectors moved on the rail track is ~870 t (with the upper equipment platform, it amounts to ~890 t). The total weight of the yoke with the cryostat, inner detectors, upper equipment platform, and poles is ~980 t.

The assembled magnet with the detectors is adjusted with respect to the accelerator beam using six hydraulic jacks mounted in the stationary supports (Fig. 2.4.8.4.2) and fixed in position on the stationary supports using shims between them and the foundation baseplate.

The total weight of the pole completed with the trim coil, disc calorimeter (ECal) and the transport platform is ~125 t. The platform is moved on the rail track using four roller skates (see Figs. 2.4.8.2.1 and 2.4.8.2.2).

According to the calculations [18], the foundation plate made from concrete of compressive strength class B25 keeps its strength under the stationary and mobile supports. The allowable load on the stationary support [703 t] is higher than the load under normal operating conditions (250 t) and the emergency load (500 t). The allowable load under the mobile support (roller skate) ~[500 t] is equal to the emergency load on the support (500 t), when the magnet rests on two diagonally located supports.

To keep the bearing load under the jack support at an allowable level of 200 t, a steel distance spacer with a thickness of at least 150 mm, width of 200 mm, and length of 560 mm should be used between the jack rod and the rail plate.

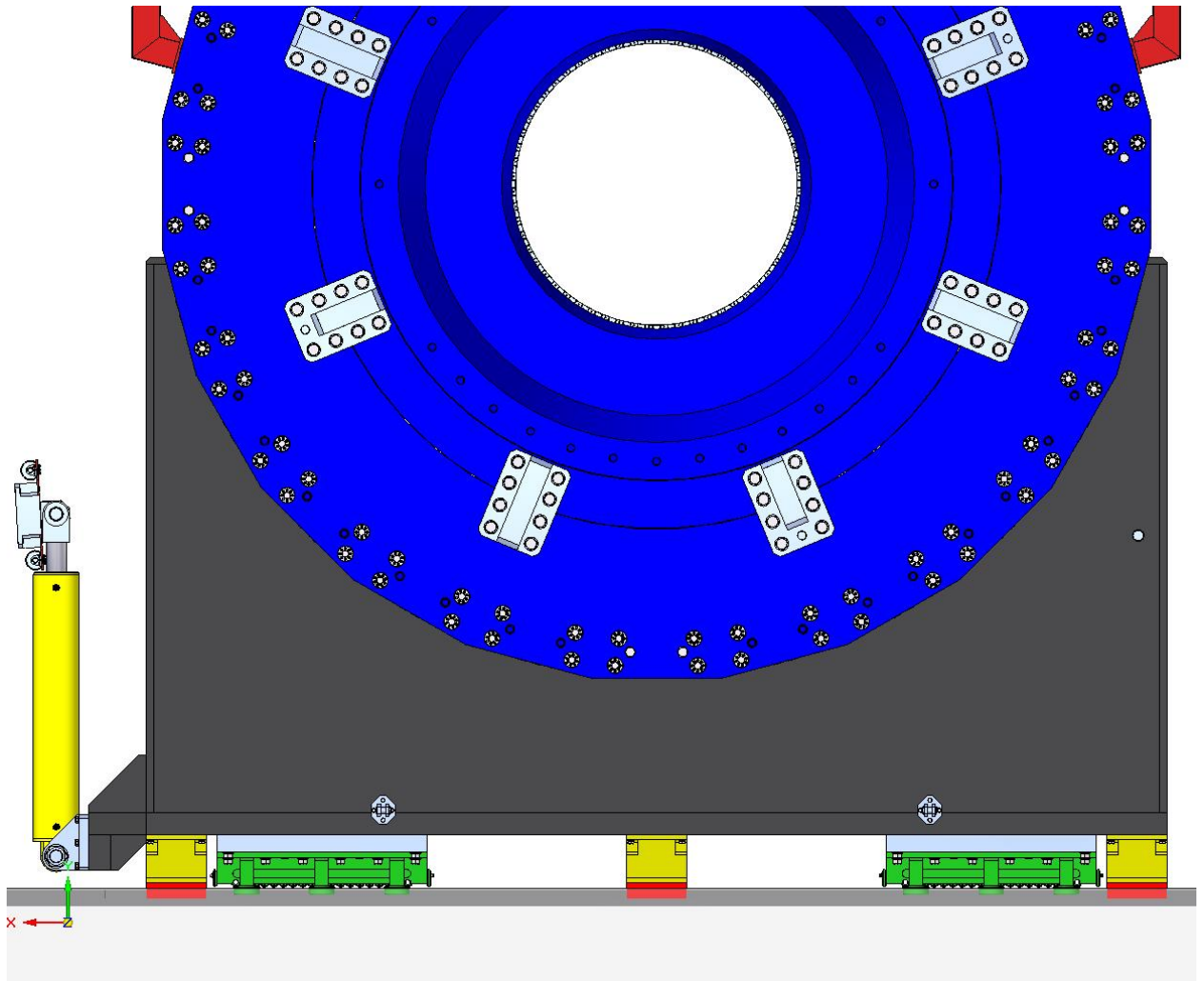


Fig. 2.4.8.4.1. Stationary (yellow) and roller (green) supports of the magnet. Shown in red are the shims under the stationary supports (in the figure the magnet rests on the stationary supports).

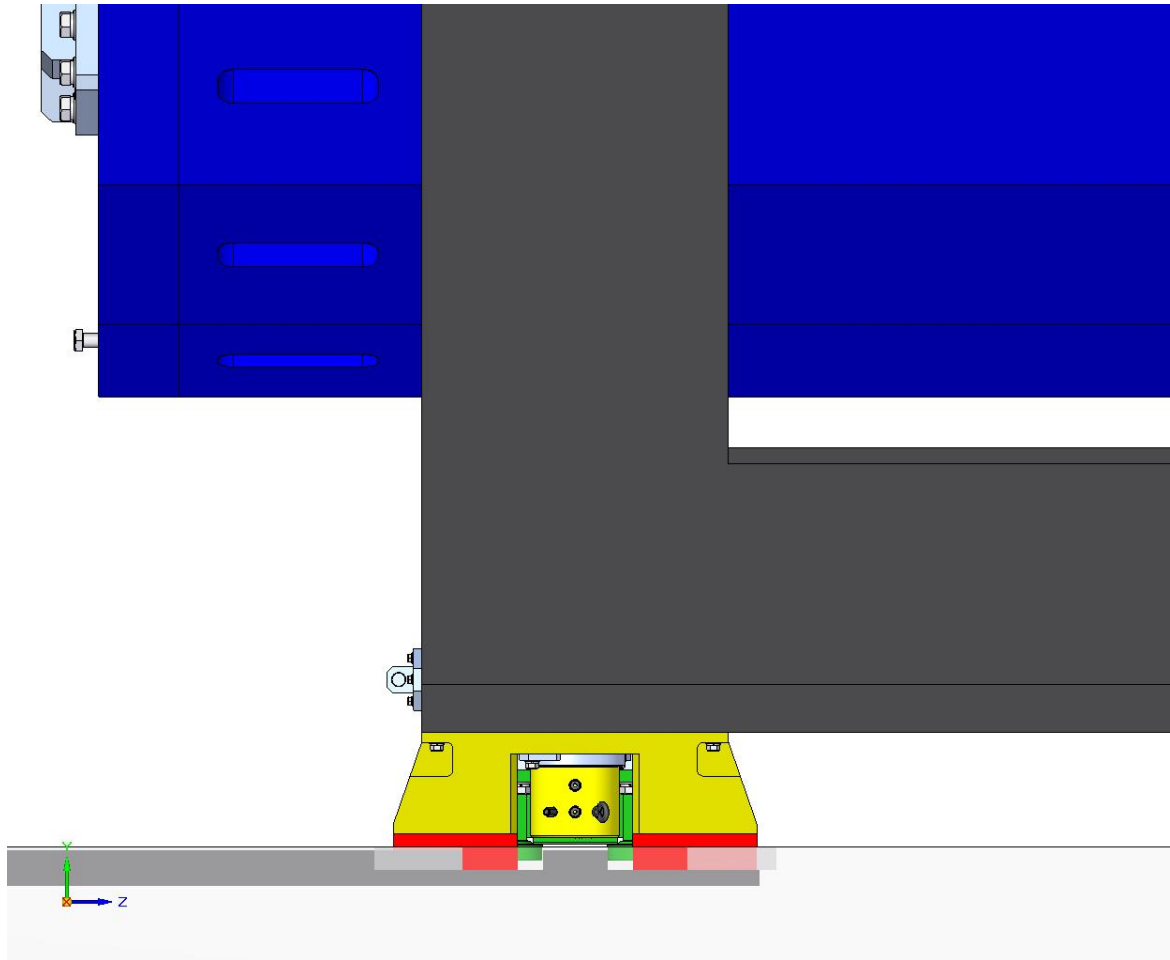


Fig. 2.4.8.4.2. Stationary support of the magnet. At the center of the support there is a hydraulic jack. Shown in red is the shim between the support and the baseplate.

2.4.8.5 YOKE AND POLE TRANSPORT SYSTEMS

The transport system of the assembled magnet with the cryostat and inner detectors is intended for moving it after the assembly or repair at the assembly site to the operating position in the accelerator beam and back for repair or update of the detectors. It is tentatively planned that the magnet complete with the detectors will be moved to the assembly site for repair or adjustment of the detectors and back twice a year for 15 years.

On the way from the assembly site the yoke complete with the cryostat (and the detectors) is stopped at the intermediate site to install the poles that lie on their own individual roller skates moving on their own rail tracks. When the magnet is moved from the operating position to the assembly site, there is also an intermediate stop to remove the poles.

The magnet transport system comprises

- A rail track (two parallel rails attached to the foundation) ~30 m long (Fig. 2.4.8.5.1).
- Four roller skates under two magnet cradles (Fig. 2.4.8.4.1).
- Two hydraulic cylinders to move the magnet (Fig. 2.3.1).

The pole transport system comprises

- Rail tracks for the poles (two pairs of parallel rails attached to the foundation) ~8.1 m long (Fig. 2.4.8.5.1).
- Four roller skates under each pole platform (Fig. 2.4.8.2.2).
- Two pairs of hydraulic cylinders to move the poles (Fig. 2.3.1).

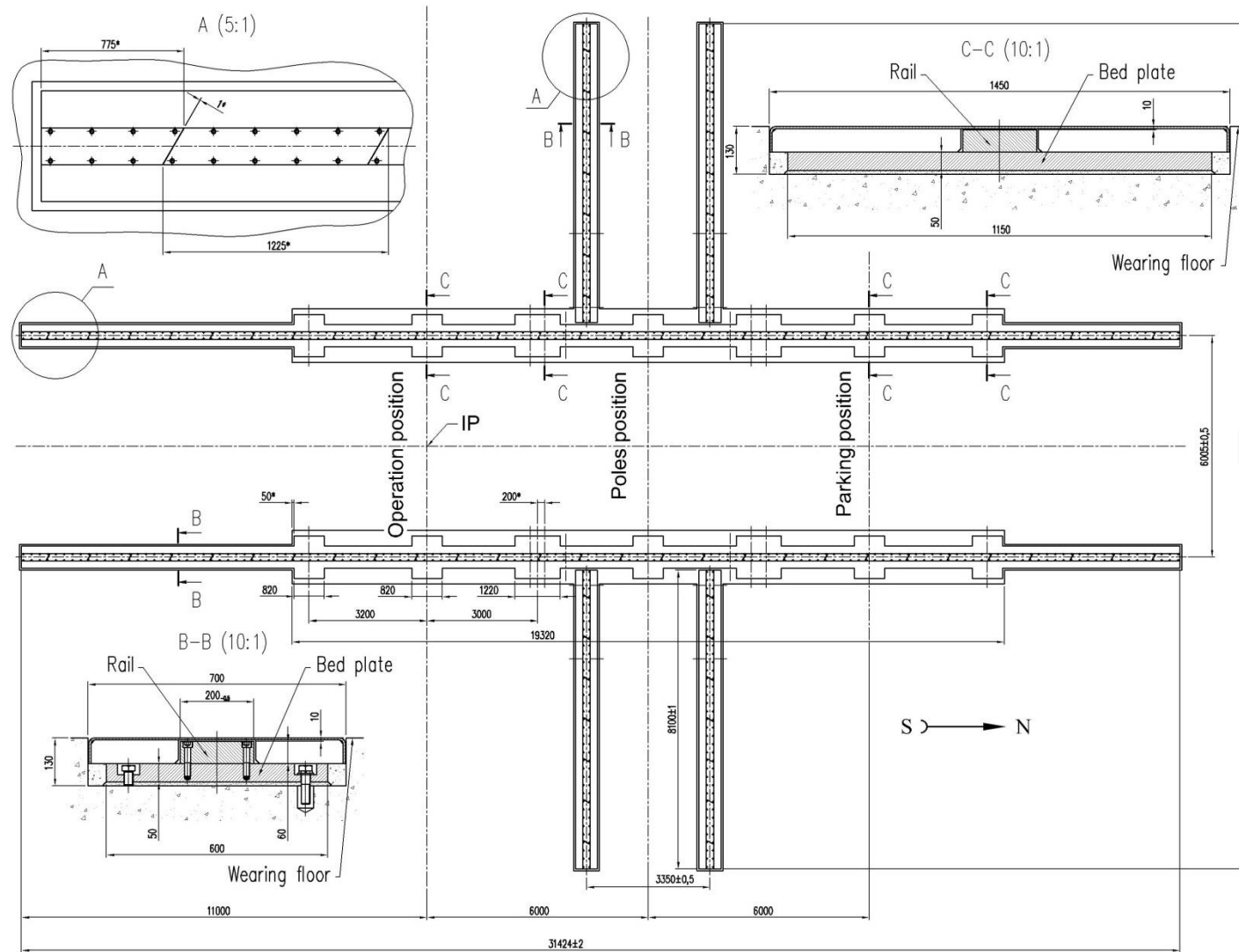


Fig. 2.4.8.5.1. Diagram of the rail track for moving the magnet and the poles

2.4.8.6 ROLLER SKATES FOR MOVING THE MAGNET AND THE POLES

Under each of two yoke cradles there are two roller skates for moving the magnet (Fig. 2.4.8.4.1). Each of the platforms for moving the poles has four roller skates (Figs. 2.4.8.2.1 and 2.4.8.2.2).

Two types of roller skates manufactured by Boerkey (Germany) were chosen as meeting the requirements on the use in the transport systems of the MPD magnet and its poles (see Appendix 2):

- Models Vlv AS-H-50CrV4-FR-K and Vlv AS-H-50CrV4 to carry the 500-t load.
- Models V AS-H-50CrV4-FR-E and V AS-H-50CrV4 to carry the 85-t load.

Both roller skates have guide rollers on one of the two rails and no guide rollers on the other.

The overall dimensions of the roller skates for the magnet and the poles are shown in Figs. 2.4.8.6.1 and 2.4.8.6.2.

Each of the roller skates to be used for moving the magnet is designed for a weight of no smaller than half the weight of the magnet in view of high rigidity of the barrel structure and possible local deviations of the rail surfaces from the common plane. According to the calculations, if one of the magnet supports has a local deviation in height amounting to ~ 5.8 mm, these supports are loaded by a half of the detector weight. This case is treated as a Violation of the Normal Operating Conditions.

The center of gravity of the platform used to move the magnet pole and loaded by pole and disc calorimeter weights is shifted to the pole (see Fig. 2.4.8.2.2). Since the counterweights do not completely compensate the shift of the center of gravity during the motion, the roller skates of the platforms are loaded unevenly (center of gravity position is moved in proportion $\sim 1.137/0.817$, see Fig. 2.4.8.2.2). As a result, the load on a front roller skate can be up to ~ 85 tons.

In the operating position, after alignment with the beam, the magnet is put on the stationary supports, and the roller skates are relieved.

According to the manufacturer's specification, the roller skates allow any cargo to be moved at a speed as high as 10 to 15 m/min, but it is recommended that heavy cargo be moved at a much lower speed to avoid problems arising from the effect of inertia forces on the cargo as the roller skate speeds up or slows down. Considering the experience of moving large detector magnets, the magnet movement speed was chosen to be 2 to 3 mm/s (except for the final step). At the final step it will be decreased to 0.4–0.5 mm/s to allow the detector to be aligned more precisely with to the beam.

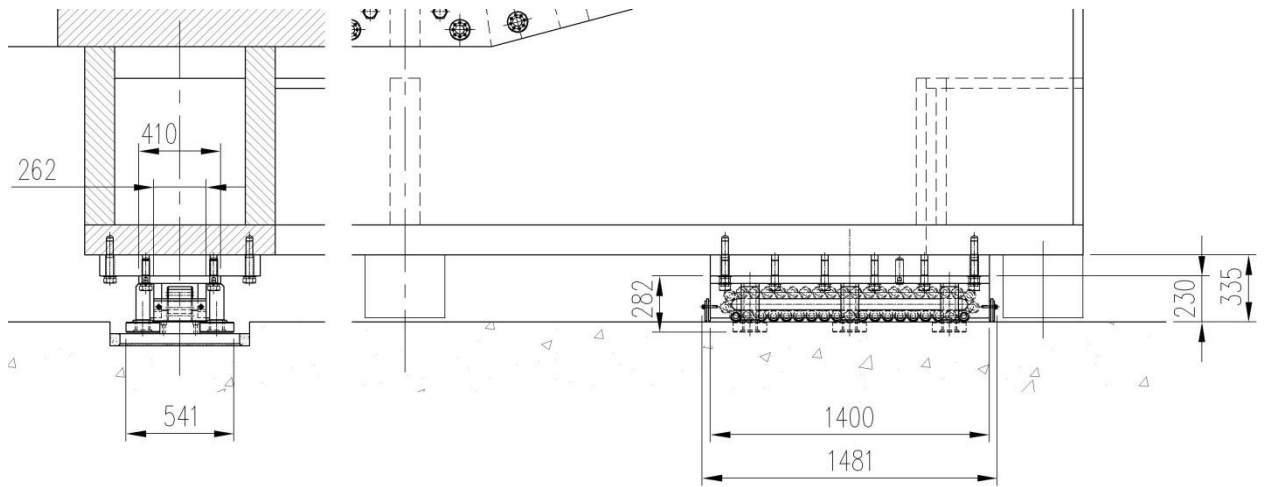


Fig. 2.4.8.6.1. Roller skate to move the magnet

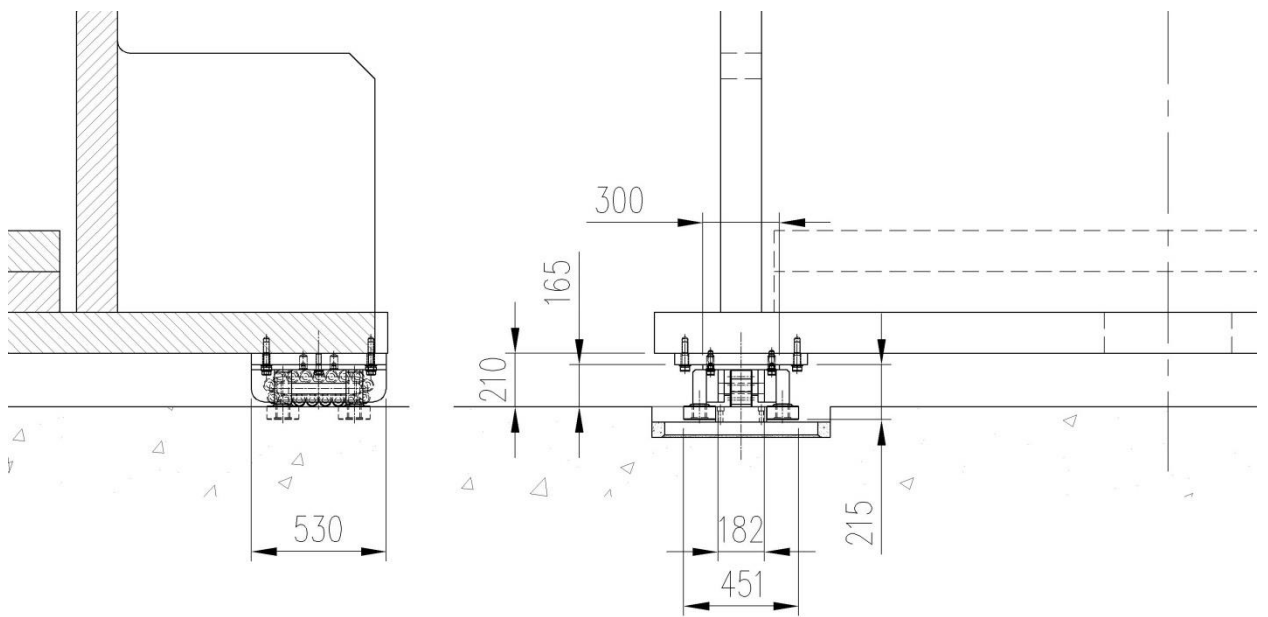


Fig. 2.4.8.6.2. Roller skate to move the pole

2.4.8.7 RAIL TRACKS FOR MOVING THE MAGNET AND THE POLES

The rail tracks for moving the magnet and the poles are shown in Fig. 2.4.8.5.1. In both cases rails of identical dimension will be used. They are laid in the recesses in the foundation. First, a metallic distribution plate (baseplate) is set in the recess and its plane is leveled with the horizon using forcing screws that rest against the recess bottom. Next, the plate is fastened to the foundation by anchor bolts, and the cavities under and around the plate are filled with no-shrink concrete. Then rails made from individual Boerkey segments (Rail Middlepart 1225x200x60) are fastened to the plate surface (Fig. 2.4.8.6.1). The rails are made of high-quality steel C45 (used for skate rollers as well). The rails are thermally treated 3 mm deep. To avoid damage, rails are covered by protective covers for periods between movements of the magnet and the poles.

According to the calculations, when the magnet is set on the stationary supports after one of the roller skates ran into a bump, the load on the supports is different from the load in the case of no bumps on the rails. For example, running into a bump ~ 5.8 mm high leads to an increase in the load on two middle stationary supports by ~ 250 kN and a decrease in the loads on the other supports by ~ 390 kN at maximum because of the mechanical hysteresis effect in the joints of the magnet. This effect has virtually no effect on the geometry of the magnet (with the accuracy of one tenth of a millimeter), that is important to save the mutual position of the magnetic axis of the solenoid and TPC axis after the movement. However, the change in the load in the supports running into a bump can lead to an additional lateral force, which creates an additional burden on the guide rollers of the roller skates. In addition, there is a loading studs M42, connecting barrel beams with end rings by forces close to the maximum allowable values. For this reason, the rail pairs are leveled to a tolerance for horizontal coplanarity not worse than ± 2.5 mm over the entire length of movement (12 m).

As required in Section 2.4.9 “Adjusting the spatial position of the magnet”, the magnetic center of the detector must be positioned in the accelerator beam direction with an accuracy no worse than ± 2.5 mm, which is attained by precisely fixing rails on the foundation and having gaps of ± 0.5 mm between the roller skate guide rollers and rails.

For even loading rollers of roller skates the rail surfaces should be leveled to better than 0.2 mrad in the plane perpendicular to the direction of the rails.

Calculations of the load capacity of the foundation should be performed for the ultimate possible load, when the weight of the magnet in the process of its movement turns out to be distributed between two diagonally located supports (i.e., 490 t on each support). This case is classed as an emergency event and corresponds to having a local rail bump ~ 5.8 mm high.

When the magnet is moved, the rails will not only bear vertical and longitudinal loads but also be affected by a transverse force arising, for example, from the deviation of the roller skate position from the direction of the movement. The calculations yield a rather low value for this force. Given a vertical load of 500 t on the support, the deviation of the roller skate by 1 deg. gives rise to a transverse force of ~ 1 t. However, calculations of the baseplate fasteners for

fixing the rails relative to the foundation should be performed for a local transverse load of ± 45 t, which corresponds to the load-carrying capacity of the roller skate guide rollers for moving the magnet of 500 t. The baseplate fasteners for the pole movement rail track should be calculated for a local transverse load of ± 20 t.

The magnet movement speed was chosen to be 2–3 mm/s. At the final step it will be decreased to 0.4–0.5 mm/s for precise positioning of the detector relative to the beam. Considering the time for transferring stops from place to place, it will take about eight to ten hours to move the magnet from the assembly site to the operating position (or back).

According to the calculations [18], the depth of the groove weld in the rail track base plates will be $t = 22$ mm. To have stability with respect to compression, the length of a free segment between the bolts fastening the support plate to the foundation should not be larger than $L_{\max} = 4.6$ m. The weight load will bend the rail track support plate protruding beyond the skate edge like a beam on an elastic foundation, which is the concrete foundation in this case. According to the calculations, the strength of the solid (seamless) support plate is high enough both under normal operating conditions ($\sigma = 50$ MPa < $[\sigma] = 169$ MPa) and under violated normal operating conditions when the load on the support rises twice as high to 500 t. The weld seam at the junction of the two supporting plates must be carried out with an inclination to the longitudinal axis 30-40°.

The bolts M27 of strength class 10.9 ($\sigma_b \geq 100$ MPa) have to be used for attachment of the hydraulic cylinder stop to the base plate. The distance between the bolts along the rail path must be at least 380 mm. Screwing length in the supporting plate has not to be less than $H = 44$ mm. The diameter of the pins retaining stop of the shift is $d = 45$ mm; depth of entry in the base plate is 20 mm at least. Pin material - steel 45 or 40X with a tensile strength $\sigma_b \geq 600$ MPa.

Anchor bolts securing the base plate should be placed in front of each mounting bolts of the stop. The anchor bolts to attach the base plate to the floor in the area of the stop installation have not to be less than M27 class 10.9. Screwing length in the anchor has not to be less than 45 mm, the tensile strength of the anchor material not less than $\sigma_b = 390$ MPa (design resistance of at least 350 MPa).

2.4.9 ADJUSTING THE SPATIAL POSITION OF THE MAGNET

Apart from specifying the position of the magnet center on the accelerator axis, the spatial position of the magnet is defined by the accuracy of aligning the magnetic axis of the detector and the accelerator axis. According to the tentative estimations of the accelerator designers, the magnet axis should be within a cylinder 5 mm in diameter over the entire length of the TPC region with the center on the accelerator axis.

The position of the center and the magnet axis are adjusted by

- Accurately laying the rail track in the direction of the beam axis (Z axis in Fig. 1.1) within ± 2.5 mm (guaranteed gaps between the guide rollers of the roller skates and the rails ± 0.5 mm, rail making accuracy -0.5 mm).
- Adjusting the height by hydraulic jacks using shims between the stationary supports and the surfaces of the baseplates to compensate for magnet axis deviations in height (Y axis in Fig. 1.1) to within ~ 0.2 mm (after the magnet is set on the stationary supports, the pressure in the hydraulic jacks is relieved) .
- Using hydraulic cylinders intended for moving the magnet to vary the position of the magnet axis in the X direction (see directions of axes in Fig 1.1) to within fractions of a millimeter (oppositely direction action of the cylinders is possible).

Guide locks will be used after each further disassembling for aligning flange joints of the accelerator vacuum pipe in the direction perpendicular to the accelerator axis to within fractions of a millimeter.

When the magnet is transferred from the roller skates to the stationary supports after one of the roller skates ran into a bump, the load on the supports is different from the load in the case of no bumps on the rails due to the mechanical hysteresis effect in the joints of the magnet. According to the calculations, even if one of the roller skates runs into a bump so that contact is lost in two roller skates, the yoke will not suffer any appreciable residual deformation in the process of setting the magnet on the stationary supports. The residual vertical deformation in the region of this roller skate will be no higher than 0.1 mm.

2.4.10 FIXING POLES INTO BORINGS OF THE YOKE SUPPORT RINGS

On the way from the assembly site the yoke complete with the cryostat is stopped at the intermediate site to install the poles that lie on their own individual roller skates moving on their own rail tracks (Fig. 2.4.8.2.1). When the magnet is moved from the operating position to the assembly site, there is also an intermediate stop to remove the poles.

To be fixed into the support ring boring, the pole is moved on its own transport platform to the yoke end by two hydraulic cylinders. When the pole comes close to the yoke end, its axis is aligned with the support ring axis in the horizontal plane by unidirectional or differently directed action of the hydraulic cylinders for movement of the magnet and the poles.

In the vertical longitudinal plane of the magnet the axes of the support ring and the pole are aligned using six hydraulic jacks of the magnet. The height variation range of the jacks allows the magnet tilt angle to be changed within the allowable rod travel range of ± 25 mm ($\pm 14'$) relative to the middle position. A possible azimuthal shift of the pole position relative to the support ring is allowed by separate pressure control in the outermost jacks on the magnet cradle relative to the middle position within the range of $\pm 13'$. The accuracy of vertically adjusting the pole position relative to the support ring by the hydraulic jacks of the magnet is estimated at ± 0.2 mm.

The position of the magnet relative to the pole is fixed and the hydraulic jacks are unloaded using the nuts on the rods of the hydraulic jack cylinders.

After the axes of the pole and the support ring are aligned, the pole is pushed in the support ring using the hydraulic cylinders of the poles. The guide pins on the support ring allow fixing the exact position of the pole relative to the ring. The pole stops are bolted to the support rings by M48 bolts (tightening force 263 MPa). Then spacers are set between the recesses of the pole and the support ring to fix their relative position.

Then the transport platforms are detached from the poles and brought into the parking position using hydraulic cylinders. The magnet is lowered with jacks down onto the roller skates for being moved on the rail track.

The procedure of pulling poles out of the borings of the support rings is similar to the procedure described above. The surface of the support flange on the pole transport platform and the cylindrical support surface on the backside of the pole are aligned using the jacks of the magnet and the hydraulic cylinders for moving the pole and the magnet.

2.4.11 HYDRAULIC SYSTEMS OF THE MPD MAGNET

The hydraulic systems of the MPD magnet are intended for

- Aligning the mounting surfaces of the poles with the borings of the yoke support rings in the vertical and horizontal planes.
- Moving the magnet with the electronics platform attached to it on the rail track from the assembly site to the operating position in the accelerator and back.
- Moving each pole on its transport platform on the rail track from the parking position to the operating position in the yoke and back.
- Aligning the magnet and accelerator axes in the magnet operating position (see 2.4.9).

A hydraulic system of the magnet includes

- Six hydraulic jacks in the stationary supports of the magnet with a load-carrying capacity of 250 t each (Fig. 2.4.8.4.2).
- Two bidirectional cylinders for horizontal movement of the magnet with a maximum force of 35 t (Fig.2.3.1).
- Four bidirectional hydraulic cylinders with a maximum force of 5 t for horizontal movement of the poles (Fig. 2.4.8.2.1).

The hydraulic system of the magnet is driven by an oil station mounted on the magnet support. It also houses commutation elements of the hydraulic system and controllers. Electronically controlled valves are used to perform all commutation. The computer-aided control is exercised over the hydraulic system at all stages with minimum attending personnel.

2.4.11.1 HYDRAULIC JACKS OF THE MAGNET

Six hydraulic jacks of the magnet are mounted in the stationary supports of the magnet upside down (the head of the rod rests against the rail with a spacer between them, see Fig. 2.4.8.4.2). Each jack is designed for a load of 250 t. To lift, an approximately equal pressure corresponding to the total weight of the magnet with the inner detectors (980 t) is set in all supports.

The full piston stroke of a hydraulic jack is 50 mm. With the rod pushed in, the roller skates of the magnet are in contact with the rail. The rod stroke margin is enough to adjust the magnet position within ± 25 mm.

In the operating position the jacks are used to adjust the magnet and accelerator axes in height to within ± 0.2 mm. Each of the cradles is separately adjusted in height, i.e., first one cradle of the magnet is set and then the other. During the adjustment the pressure is simultaneously changed in all three cylinders of each cradle. Metal spacers are used between stationary supports and baseplates to level the position.

2.4.11.2 YOKE MOVEMENT HYDRAULIC SYSTEM

The assembled magnet with the detectors and attached electronics and equipment platform is moved on the rails from the assembly site to the operating position in the accelerator and back using two hydraulic cylinders fixed on the yoke cradles (Figs. 2.4.11.2.1 and 2.4.11.2.2). The full hydraulic cylinder piston stroke is 1500 mm. The magnet is moved on the rails over the total length of 12 m by transferring cylinder stops forward at a step of 1500 mm (Fig. 2.4.13.2.2). The fixing points of the stops are placed on the rail track baseplates a certain distance apart. The stops are transferred to the next position on the foundation together with the hydraulic cylinder rods.

Each of the cylinders develops a pushing/pulling force no less than 35 t. This value has a margin of safety for the total weight of the magnet with the inner detectors and the electronics platform, which is 1000 t, and allows for the manufacturer's recommended roller skate rolling friction factor $k = 0.07$. As the magnet moves, the pressure is checked in each cylinder.

The maximum deviation of the yoke position relative to the rails in the direction parallel to the accelerator beam axis is kept within ± 0.5 mm over the entire way due to guide rollers. The yoke is moved on the rails at a speed of 2–3 mm/s, which decreases to 0.4–0.5 mm/s as the magnet approaches the operating position.

When the magnet arrives at the final position, the cylinder rods are fully pushed in and the cylinders are set in the vertical position lest they hinder magnet operation (Fig. 2.4.8.4.1).

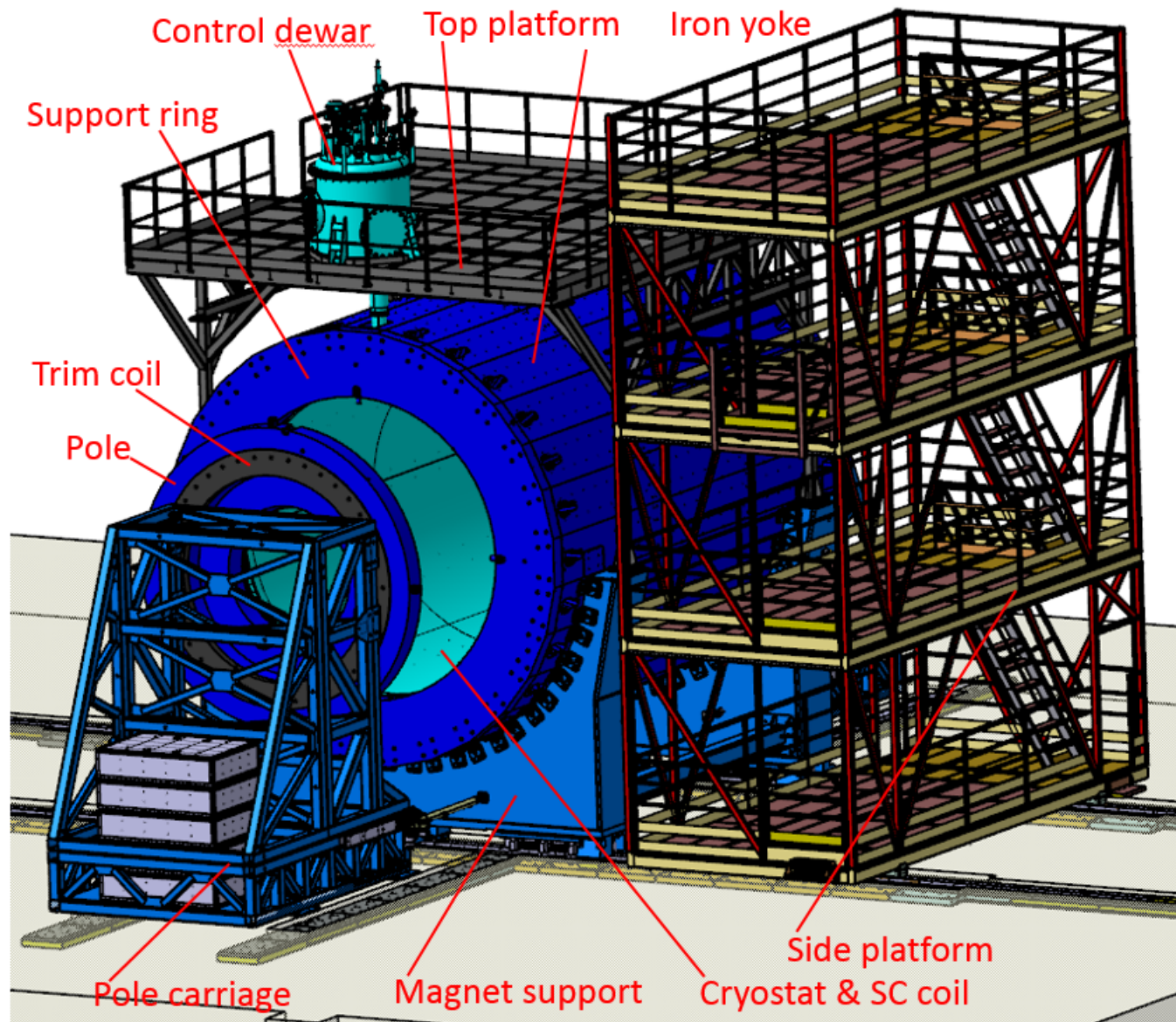


Fig. 2.4.11.3.1. Magnet with the attached platform for electronics and equipment

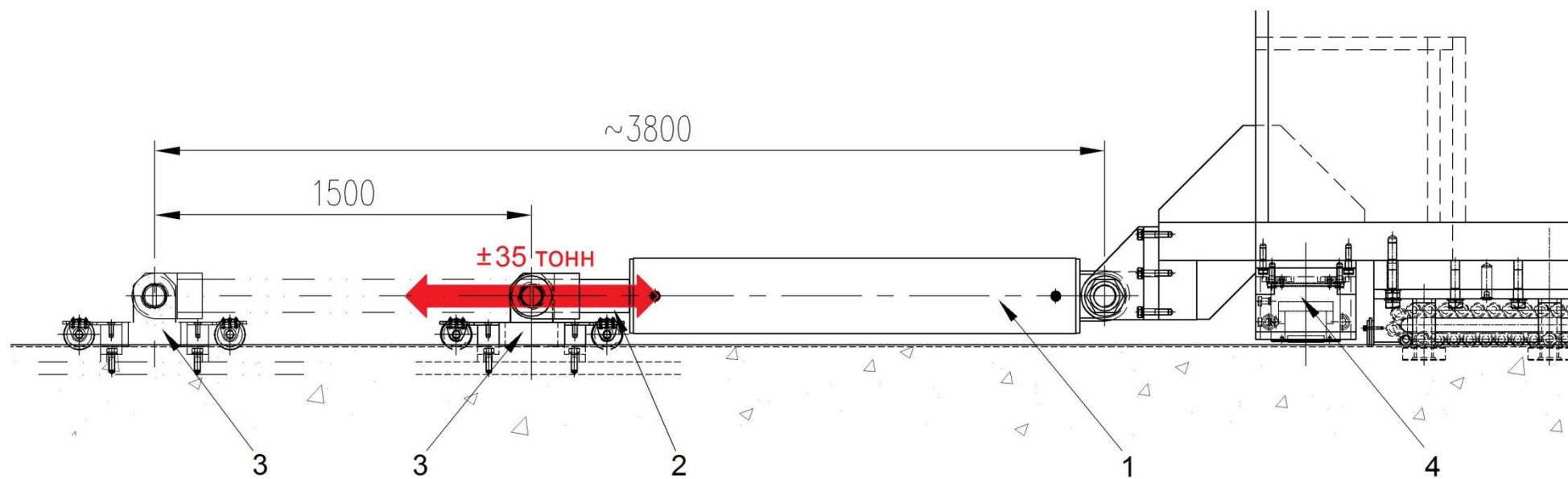


Fig. 2.4.11.3.2. Installation of the hydraulic cylinder for moving the yoke:

(1) magnet drive hydraulic cylinder; (2) hydraulic cylinder rod; (3) hydraulic cylinder rod stop; (4) stationary support of the magnet

2.4.11.3 POLE MOVEMENT HYDRAULIC SYSTEM

Two pairs of hydraulic cylinders fixed on the pole transport platforms are used to move poles on the roller skates on the rail track from the parking to the operating position and back (Fig. 2.4.8.2.1).

Each of the cylinders develops a pushing/pulling force no less than 5 t. The full piston stroke of the hydraulic cylinder is 1545 mm, and the working stroke is 1420 mm (Fig. 2.4.11.4.1). The accuracy of the movement direction is maintained by separately controlling the pressure in each cylinder. The maximum deviation of the pole position relative to the rails in the direction perpendicular to the accelerator beam direction is kept below ± 0.5 mm over the entire way due to the gaps between the guide rollers and rails. The accurate alignment of the pole plane with the support ring plane can be obtained by differently directed action of the horizontal drive cylinders.

The maximum allowable speed of the pole moving on the rails is limited to 2–3 mm/s in view of a danger of its turning-over at a sudden stop. Close to the magnet, the speed is decreased to 0.5 mm/s.

On arrival at the final position, the cylinder rods are detached from the ears on the magnet and fully pushed in lest they hinder magnet operation.

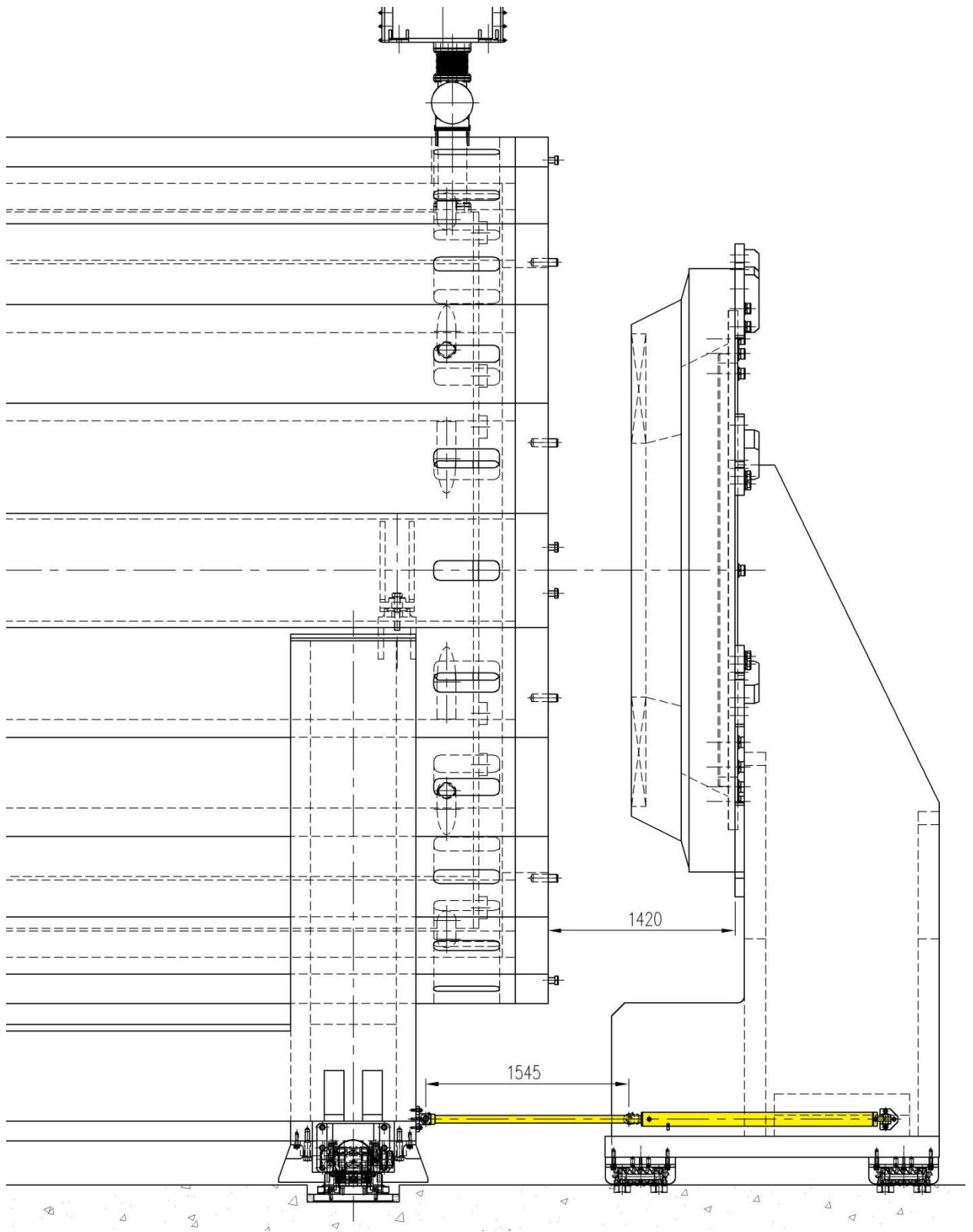


Fig. 2.4.11.4.1. Pole fully pulled out

2.4.12 POLE TRIM COILS

To correct the magnetic field in the TPC region, there are trim coils fixed in the pole recesses (Figs. 2.3.1 and 2.4.12.1). They are wound using a hollow aluminum conductor $42 \times 42 \text{ mm}^2$ in cross section with a hole 27 mm in diameter and an edge round-off radius of 2 mm. The calculations of the trim coil parameters are given in [11]. The trim coils will be cooled by demineralized return water circulating in a closed loop. The maximum possible temperature of the cooling water is taken to be $T = 25 \text{ K}$ at the entrance to the trim coil and $T = 55 \text{ K}$ at the exit (temperature difference $T = 30 \text{ K}$).

The dimensions of the recess in the pole tip for mounting the trim coil are as follows:

| | |
|--------------|-------------------------|
| Inner radius | $R_i = 965 \text{ mm}$ |
| Outer radius | $R_e = 1796 \text{ mm}$ |
| Depth | $Z_s = 110 \text{ mm}$ |

Structurally, the trim coils are two-layer pancakes wound from the center, which are fixed in the circular recess. The trim coils lead-outs are at the outer radius. The turn insulation of glass tape vacuum impregnated with epoxy compound is 1 mm thick on the conductor side. The ground-wall insulation is 5 mm thick. A fiber glass plastic sheet 1.0 mm thick is sandwiched between two pancakes of the coil. The number of turns in the trim coil is 34. The inner diameter of the trim coil is 1.95 m, its outer diameter is 3.466 m, the axial thickness of the coil is 0.099 m, and the weight of a trim coil is 1.12 t.

The calculations of the magnetic forces applied to a trim coil are given in [10]. At the maximum superconducting coil current forces of 6.8 kN act on the trim coils and press them against the poles. When the superconducting coil is shifted by 20 mm, a pole-directed force of 7.9 kN acts on the trim coil in the pole from which the superconducting coil shifts away. In the pole toward which the superconducting coil shifts a pole-directed force of 5.8 kN acts on the trim coil.

When the superconducting coil shifts by 20 mm along the beam axis, each of the poles shifts by 5 mm in the axial direction away from the center of the magnet, and the current density in the superconducting coil linearly varies by 2%, a separating force of $\sim 11 \text{ kN}$ can act on one of the pole trim coils. In an emergency event, when one of the trim coil power supplies is suddenly off, the maximum force acting on the trim coil and tending to separate it from the pole surface can be as high as 14.2 kN.

Calculations of the trim coil fixation in the recess on the pole tip are given in [19]. The trim coils are secured in place by 5-mm-thick caps of stainless steel on the side facing the detectors (Fig. 2.4.12.1). The caps prevent the trim coils from moving under the action of electromagnetic forces directed toward the magnet center.

Between a stainless-steel cap and the trim coil surface there is a rubber gasket 6 mm thick. The trim coil is packed out relative to the recess walls at the outer radius by fiberglass wedges.

The total length of the cable in one trim coil is 294 m. The resistance of each trim coil at 20°C is 0.007299 Ohm and at 40°C - 0.007883 Ω. The total flow rate from the return water system over the two trim coils is 2476 cm³/s at a maximum pressure of 7.7 bar. The diagram of connection of the solenoid pole trim coils to the return water system is shown in Fig. 2.4.12.2. A 3D view of the trim coil lead-outs is given in Fig. 2.4.12.3.

The maximum current density in the trim coil aluminum in the basic mode of operation 3.27 A/mm². The maximum ampere-turns in the each magnet pole trim coil are 151 kA. The overall loss power in both trim coils can be as high as 310 kW with a maximum loss power up to 155 kW in one of the trim coils.

The trim coil inductance is 7×10^{-3} H. Mutual inductance of a trim coil and the superconducting coil is 0.05 H, and the mutual inductance of two trim coils is 7×10^{-9} H. When there are no technological deviations to be compensated by the trim coils, the rated current of the trim coils is 3059 A. The maximum trim coil current that can be set when it is necessary to compensate for a technological deviation is 4441 A at a trim coil voltage drop of 35 V.

The trim coils are connected to the return water supply system by flexible pipes and to the power supply system by aluminum buses to be disconnected during movement.

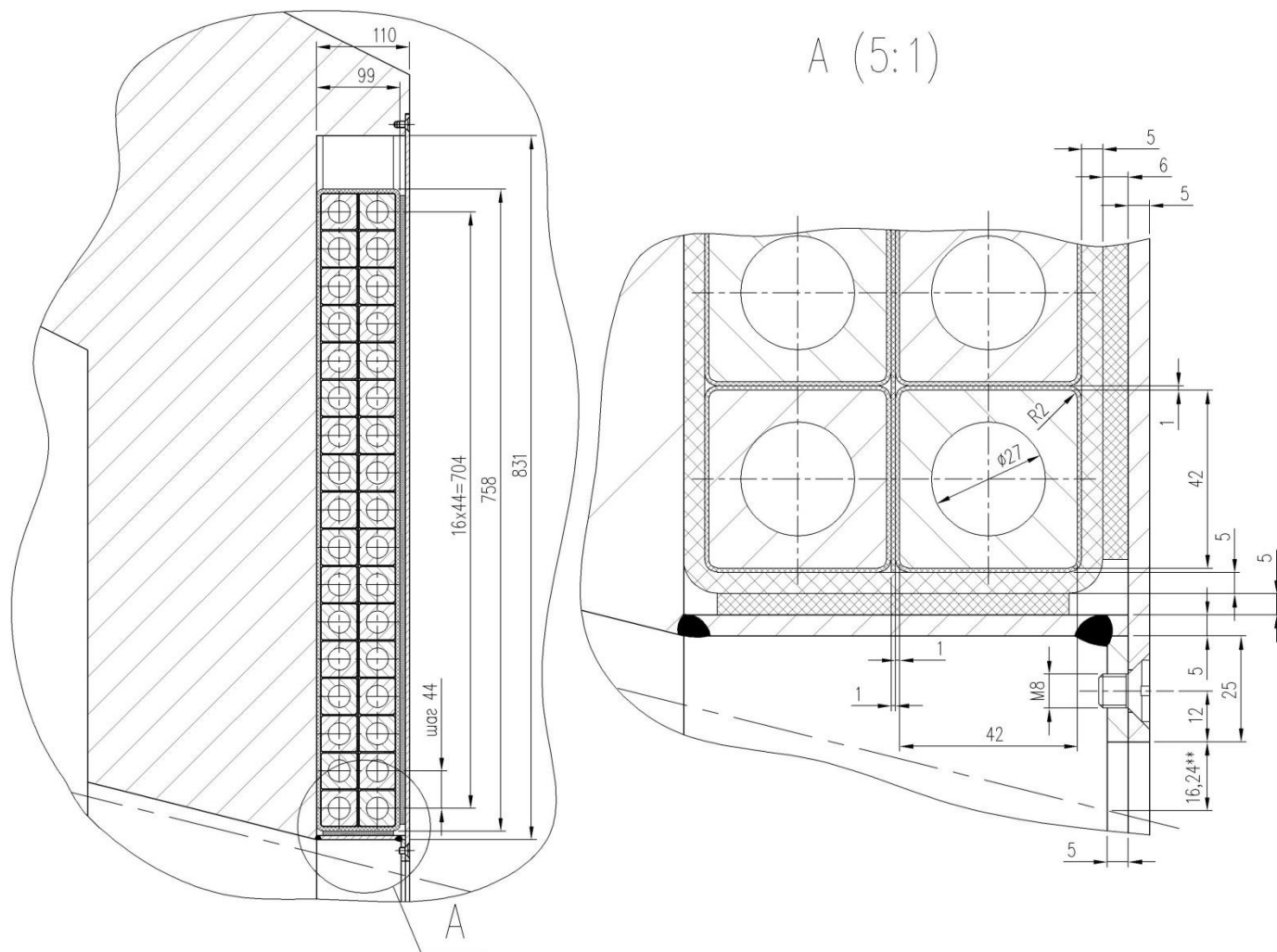


Fig. 2.4.12.1. Cross section of the trim coil in the pole recess

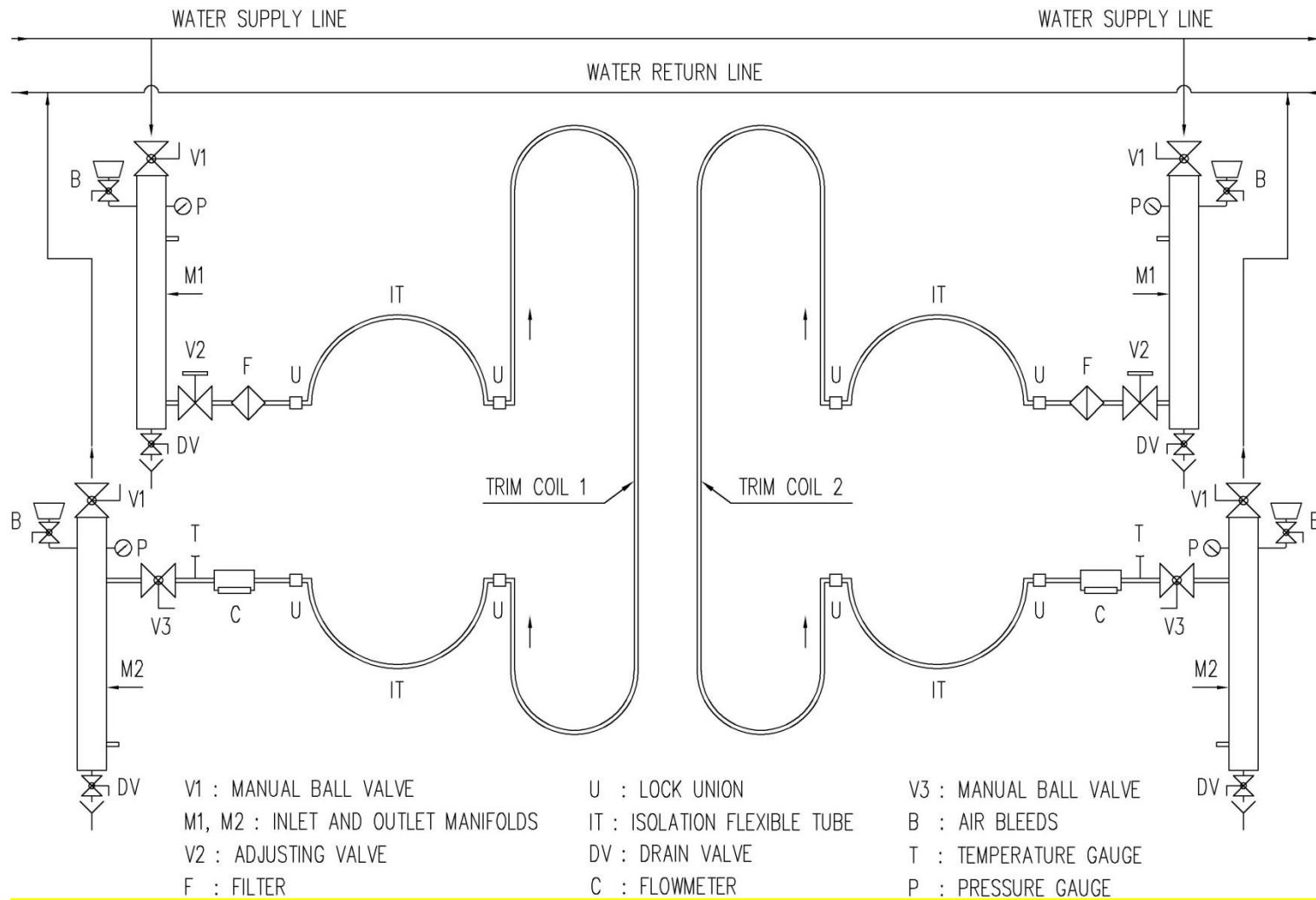


Fig. 2.4.12.2. Diagram of connection of the trim coils in the magnet poles to the return water supply system

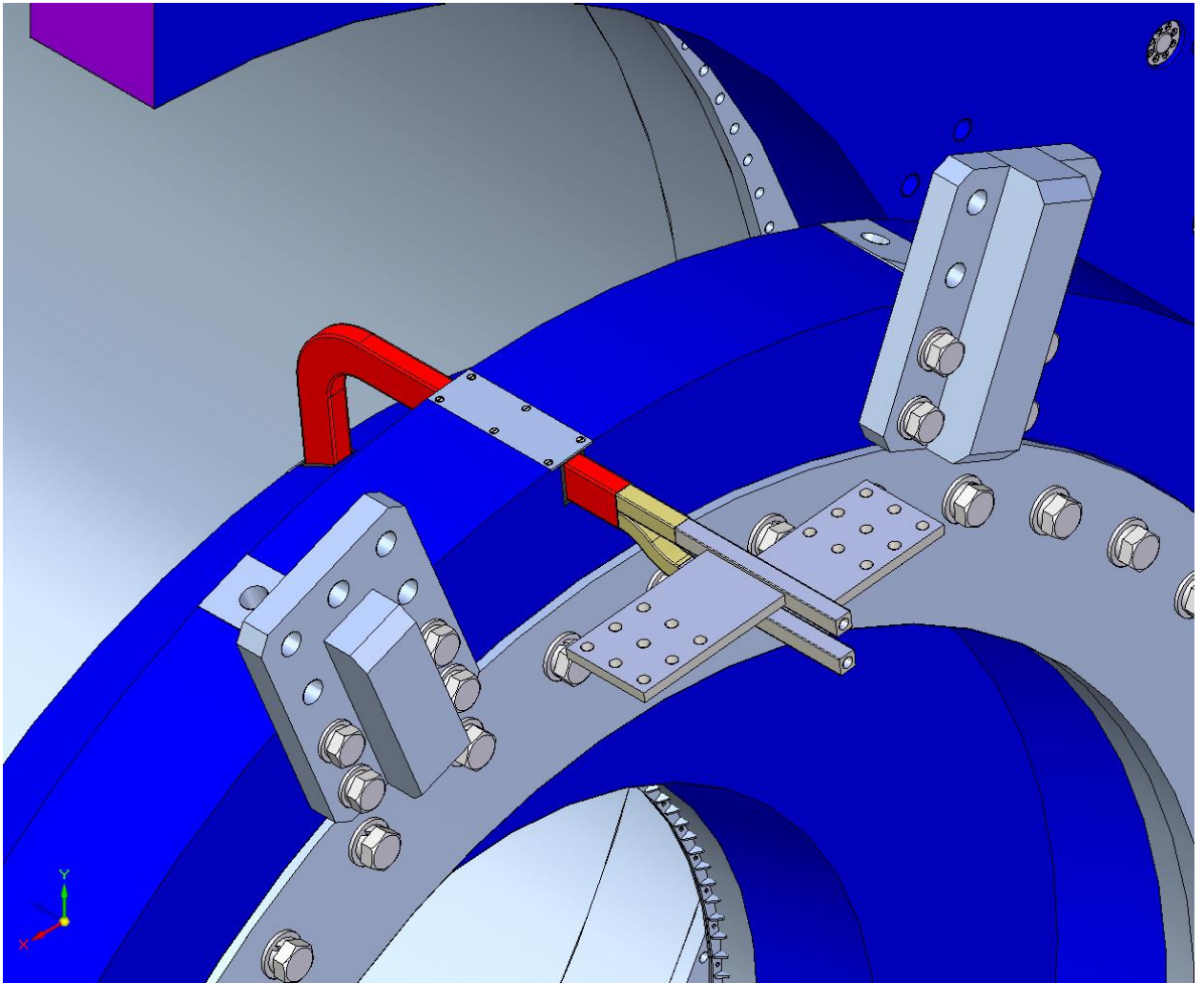


Fig. 2.4.12.3. Lead-outs of the pole trim coils

2.4.13 POWER SUPPLY OF THE MAGNET COILS

2.4.13.1 POWER SUPPLY SYSTEM OF THE MAGNET COILS

The power supply system of the superconducting coil L_s and pole trim coils L_{T1} and L_{T2} is schematically shown in Fig. 2.4.7.1.

The system consists of a power supply for the superconducting coil, two switches in the coil power supply circuit S_1 and S_2 (for increasing the reliability of the quench protection system operation), and dump resistors for de-energizing the coil R_{d1} and R_{d2} . The switch S_3 allows the discharge resistance to be varied for varying the coil de-energizing rate.

The switch S_{p1} is used to change the current polarity in the superconducting coil in synchronism with the change in the polarity of the pole trim coil power supplies. The power supply is connected to the current leads on the cap of the control Dewar by air-cooled aluminum buses.

Since the currents of the trim coils must be controlled separately, two power supplies PS_1 and PS_2 are needed. The overall loss power in both trim coils can be as high as 310 kW at the maximum loss power in one of the trim coil up to 155 kW. To change the power supply current polarity, there are switches S_{p2} and S_{p3} .

The pole trim coils and the superconducting coil have voltage limiters as shunts to prevent high voltage arising at the terminals of the coils when the polarity is changes at a low current in the coils.

When both trim coils are switched on/off simultaneously, the superconducting coil current changes as defined by the expression

$$\Delta I = 2 \times I_t \times M / L_s ,$$

where I_t is the trim coil current, M is the mutual inductance of the pole trim coil and the superconducting coil, and L_s is the solenoid coil inductance. Thus, the current varies by ~ 2.4 A.

During the emergency de-energizing of the superconducting coil with a time constant of 84 s (current variation rate 28.4 A/s), voltage arises at the open ends of the trim coils; it is defined as

$$U = M \times dI_s / dt$$

and amounts to ~ 0.065 V, which is appreciably lower than the maximum coil operating voltage of 35 V.

An additional axial force acting on the suspension system of the superconducting coil will be originated during emergency shutdown of one of the power supplies of the trim coils [10]. So when the coils powered by two independent power supplies in case of an emergency shutdown of one of them, the maximum force acting on the axial suspension of the sc coil (magnetic induction at the coil center 0.54 T), could be up to 273 kN, which exceeds the allowable force for the axial suspension in an emergency [248 kN]. The power supplies connection as shown in Fig. 2.4.7.1 is used to limit the forces acting on the axial suspension during emergency shutdown of a power supply. The power supply PS_1 produces the same current through the trim

coils, and the other power supply P_{S2} is used for the correction of technology deviations of the magnetic circuit parameters.

Center of the superconducting coil has to be shifted in the direction opposite chimney side, as the axial suspension rods work better for tension than for compression. For this reason, the power supply of P_{S2} will relate to the trim coil L_{T2} , located on the pole of the chimney side.

For example, the current of 4441 A in the “chimney side” trim coil and the current of 2441 A in the other trim coil are needed for the field correction in the TPC area in case of the worst combination of the technology deviations (magnet field in the coil center $B = 0.54$ T). In this case, the current 2441 A of a power supply is common for both trim coils and the current of the second power supply should be $4441 \text{ A} - 2441 \text{ A} = 2000$ A. The maximum force acting on the superconducting coil with the loss of the current 2441 A and with the remaining correction current 2000 A is 143 kN only.

An equivalent circuit (Figure 2.4.13.1) can be considered to define values of power supply voltages for the circuit in Fig. 2.4.7.1.

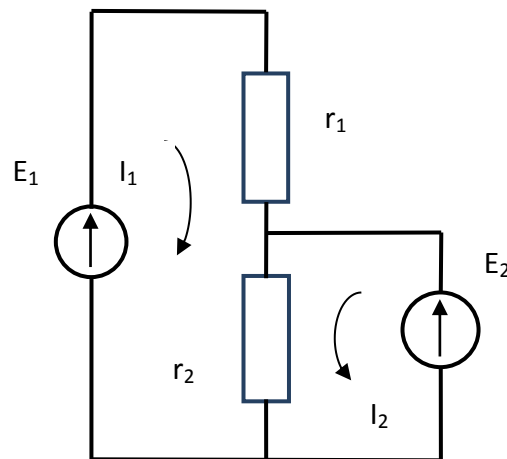


Fig. 2.4.13.1. Equivalent circuit of the trim coil power supply

EMF E_1 corresponds to the common power supply, and the EMF E_2 – to the additional one. Trim coils resistance r_1 and r_2 in this case are identical $r_1 = r_2 = r_0$.

The resistance of each coil at 20°C is 0.007299 Ohm, and at the temperature of 40°C (average temperature of the conductor during operation) - 0.007883 Ohm.

Contour currents I_1 and I_2 correspond to currents of the power supplies. Obviously, for the considered case $I_1 = 2441$ A, and the current $I_2 = 2000$ A. Let us write the expression for the EMF of power supplies in terms of contour currents:

$$E_1 = 2r \cdot I_1 + r \cdot I_2$$

$$E_2 = r \cdot I_1 + r \cdot I_2$$

For this case $E_1 = 54$ V, and $E_2 = 35$ V, and the of power losses of the trim coils compensated by current sources are:

$$P_1 = E_1 \cdot I_1 = 132 \text{ kW}$$

$$P_2 = E_2 \cdot I_2 = 70 \text{ kW}$$

It is obvious that the power supply P_{S1} should provide the maximum voltage up to 70 V, and the maximum power losses to be compensated by this source will correspond to the absence of technological deviations with the same maximum allowable values of the currents of 4441 kA in both correction coils (it corresponds to a field in center of the magnet 0.64 T):

$$P_{1max} = 2E_1 \cdot I_1 = 311 \text{ kW}.$$

The power supply P_{S2} should provide the maximum load voltage of 35 V, and the maximum power losses to be compensated by this source will correspond to a field in the center of the coil 0.54 T:

$$P_{2max} = 70 \text{ kW}.$$

2.4.13.2 SUPERCONDUCTING COIL POWER SUPPLY

The power supply of the superconducting coil must allow a long time of operation at the maximum solenoid current of 2.388 kA, which corresponds to a field of 0.66 T in the magnet operation region. The superconducting coil power supply should have an output voltage up to 10 V and stability better than 0.1% [12]. The supply line: three phases, 50 Hz, and 380 V.

A power supply that meets these conditions is, for example, Heinzinger [13] PNY 10-2500/M with an output voltage of 0 to 10 V at a maximum current of 0 to 2500 A.

Performance:

Current stabilization

Reproducibility: $\pm 0.1\% I_{nom}$

Stability over 8 h: $\leq 0.03\% I_{nom}$

Ripple: $\leq 1\%_{pp} \pm 1 \text{ mA } I_{nom}$

Temperature coefficient: $\leq 0.03\% I_{nom}/K$

Cooling

Water cooling of radiators of power transistors and thyristors

Water temperature at the entrance: $\sim 18^\circ\text{C}$

Pressure: 2–5 bar

Requirements on cooling water: appropriate water for cooling aluminum radiators

Coolant for the transformer and other equipment: air

Current and voltage displays: 3.5 digits (separately for voltage and current)

Output value setting: 10-turn potentiometers (separately for voltage and current)

Remote control through the integrated analogue interface of 0–10 V (digital interface as an option)

The following digital interface versions are possible:

RS232/IEEE488 combined interface (12bit for voltage, current, and control)

RS232/RS485 combined interface, (12bit for voltage, current, and control)

Outputs: constant current output at the top of the power supply backside

Input: connector (supply line cable with a CEE connector as an option)

Mainframe: 19 "rack

Dimensions: max. 1200×2000×800 mm (W×H×D)

Weight: 1200 kg

2.4.13.3 POWER SUPPLIES OF THE POLE TRIM COILS

Power supply PS_{T1} (Fig. 2.4.7.1) provides a current of the both correction coils up to 4441 A and compensates for power loss to 2x155 kW, at voltages up to 2x35 V. Power supply PS_{T2} shall ensure the maximum voltage across the load of 35 V and a maximum current of ~ 2000 A. The maximum power loss to be compensated for by this source has to be up to 70 kW.

The power supplies must allow the current stability no worse than $\pm 0.1\%$. The supply line: three phases, 50 Hz, 380 V.

A power supplies that meets these conditions is, for example, Heinzinger [13] PNY series.

Performance:

Current stabilization

Reproducibility: $\pm 0.1\% I_{nom}$

Stability over 8 h: $\leq 0.03\% I_{nom}$

Ripple: $\leq 1\%_{pp} \pm 1mA I_{nom}$

Temperature coefficient: $\leq 0.03\% I_{nom}/K$

Cooling

Water cooling of radiators of power transistors and thyristors

Water temperature at the entrance: $\sim 18^\circ C$

Pressure: 2–5 bar

Requirements on cooling water: appropriate water for cooling aluminum radiators

Coolant for the transformer and other equipment: air

Current and voltage displays: 3.5 digits (separately for voltage and current)

Output value setting: 10-turn potentiometers (separately for voltage and current)

Remote control through the integrated analogue interface of 0–10 V (digital interface as an option)

Возможны следующие варианты цифрового интерфейса:

RS232/IEEE488 combined interface, (12bit for voltage, current, and control)

RS232/RS485 combined interface, (12bit for voltage, current, and control)

Outputs: constant current output at the top of the power supply backside

Input: connector (supply line cable with a CEE connector as an option)

Mainframe: 19 "racks

2.4.14 Seismic safety of the magnet

Since NICA is not sited in an earthquake hazard zone and the installation itself is not liable, either in safety class or in seismic stability category (NP-01-97, item 2.5 and NP-031-01, item 2.6.3), to Requirements NP-064-05 "Allowance for Natural and Manmade Impacts on Nuclear Installations" (items 1.3 and 1.5), no seismic load calculations are needed for the MPD magnet.

In addition, there is no information on any danger arising from the earthquake-caused shift of the MPD magnet components which is needed for taking a decision to perform seismic stability calculations.

2.4.15 PASSAGES FOR RUNNING CABLING AND TUBING OUT OF THE MAGNET APERTURE

Radial passages between the cryostat but ends and the yoke support rings will be used for running cables and tubing out of the inner volume of the MPD magnet (Fig. 2.4.15.1). On passing the cryostat ends the tubing and the cabling go out of the magnet through slots (150×500 mm) in the yoke beams (Figs. 2.4.15.2 and 2.4.15.3). The passage cross section area should be no smaller than 12000 cm² on one side of the magnet.

Considering that the passages are partially blocked by 24 support beams of the inner detectors, the minimum cross section area of the gap between the cryostat but ends and the support rings which can be used for running cabling and tubing at the cryostat position closest to the support ring (160 mm) is $S \approx 16000 \text{ cm}^2$. With the nominal gap of 180 mm, the effective cross section area for running the cables increases to $S \approx 18000 \text{ cm}^2$. The slots in the barrel beams are round off at the angles to a radius of 50 mm. Beam B13 (Fig. 2.4.15.3) has a larger slot 520 × 320 mm in size for the cryogenic chimney and cables.

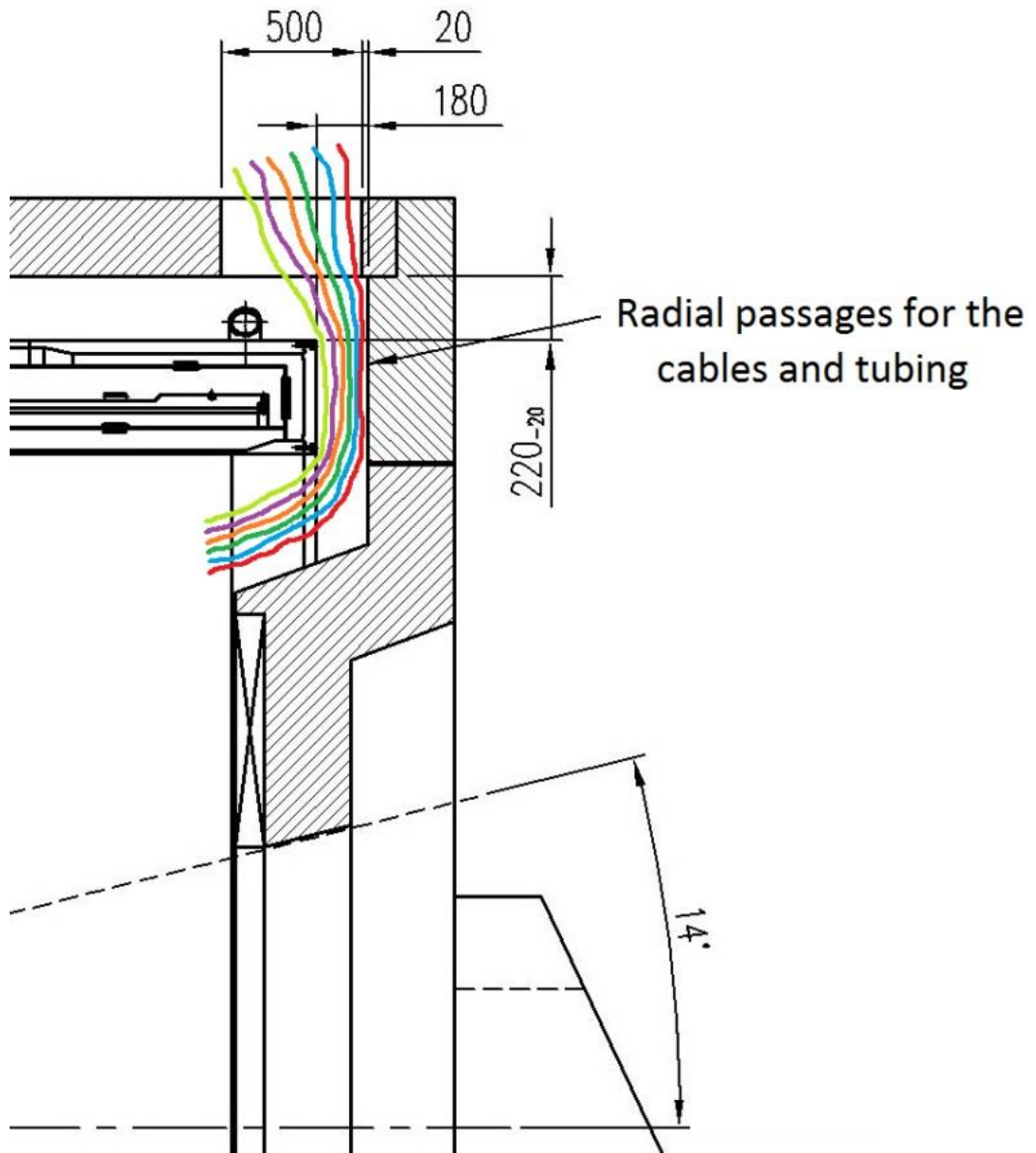


Fig. 2.4.15.1. Radial passages for cables and tubing (side view)

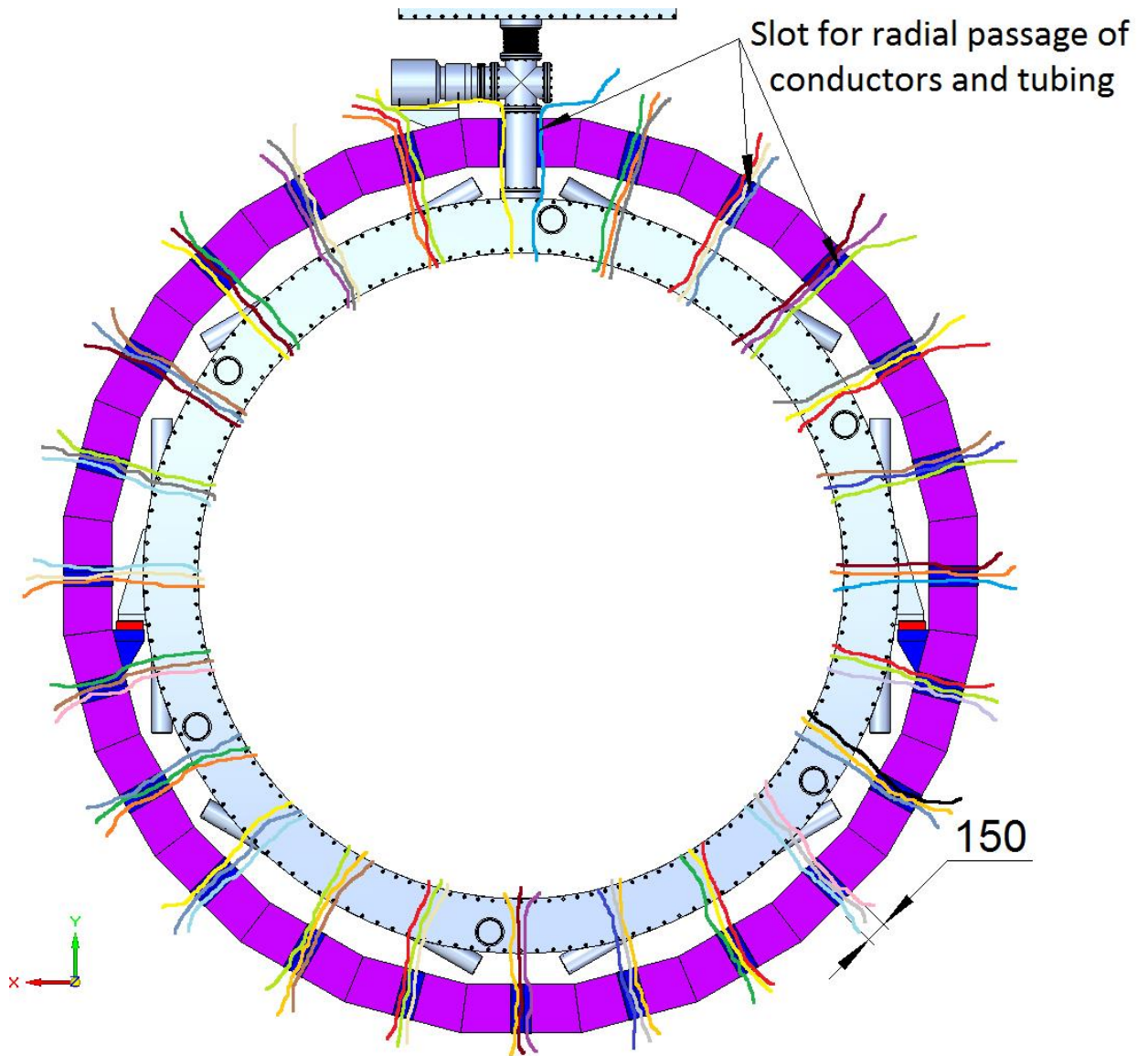


Fig. 2.4.15.2. Radial passages for cables and tubing (view from the magnet end)

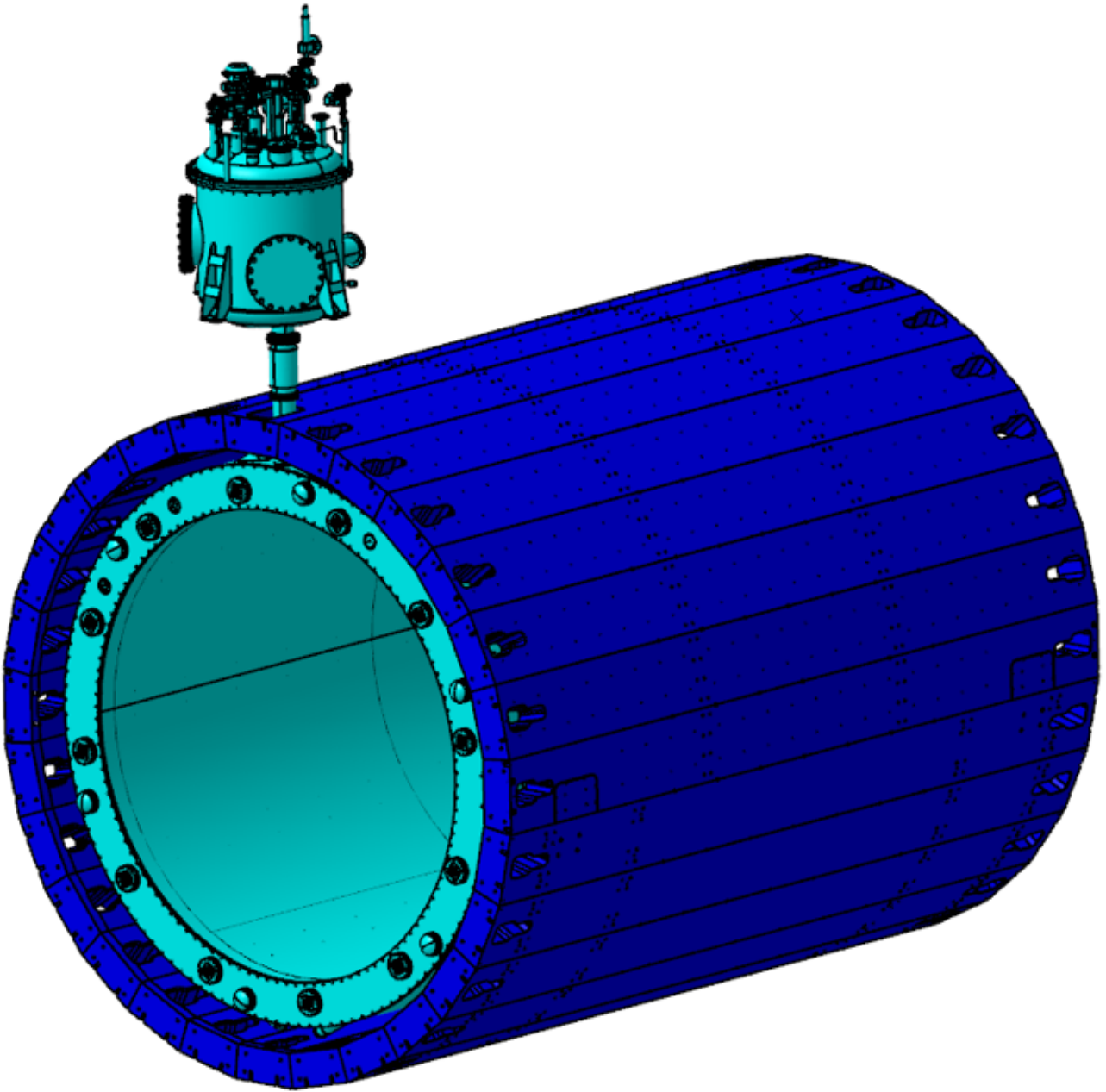


Fig. 2.4.15.3. Radial slots in the beams for running cables and tubing

2.4.16 The upper platform for the equipment of the magnet

Platform 8.7x7 m² (see Fig. 2.4.1.2) is placed on top of the magnet to host the vacuum pumps, equipment of the control Dewar, power supply, protection and control system of the sc coil, as well as for their service. Total weight of the equipment on the platform does not exceed 10 t.

Cutout in the platform deck provides access to service of the control Dewar mounted on the upper beam of the magnet barrel.

To access the hardware on the platform there are two ladders on the sides of the magnet. The low point the stairs on the south side of the magnet is located on the pit floor level and the stairs on the north side starts at the level of the top deck of the platform for the detector electronics and equipment that moves together with the magnet.

2.5 ASSEMBLING THE MAGNET

2.5.1 TEST ASSEMBLY OF THE YOKE AT THE MANUFACTURER'S

2.5.1.1 ASSEMBLING THE POLES

- 2.5.1.1.1 Mounting support rings horizontally
- 2.5.1.1.2 Setting poles on the supports in the support rings and centering them relative to the support ring boring
- 2.5.1.1.3 Inserting and tightening fastening bolts
- 2.5.1.1.4 Drilling holes for guide pins
- 2.5.1.1.5 Drilling out the holes of the guide pins in the support rings to allow for deformation of the support rings under the effect of the weight load
- 2.5.1.1.6 Performing test assembly of the poles on the transport platforms

2.5.1.2 ASSEMBLING THE YOKE BARREL IN THE VERTICAL POSITION

- 2.5.1.2.1 Setting one of the support rings in the horizontal position on an auxiliary support (Fig. 2.5.1.2.1).

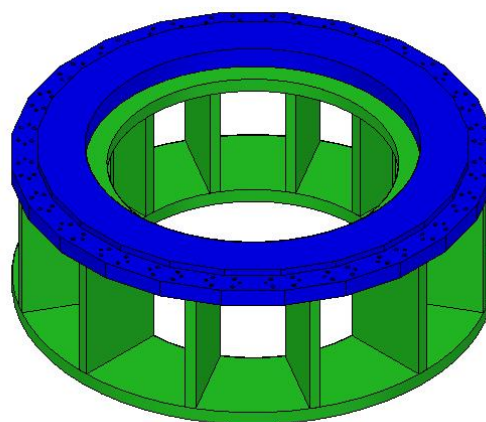


Fig. 2.5.1.2.1. Support ring set on an auxiliary support

- 2.5.1.2.2 Setting beams one by one in the vertical position in their corresponding places on the support ring (Fig. 2.5.1.2.2).

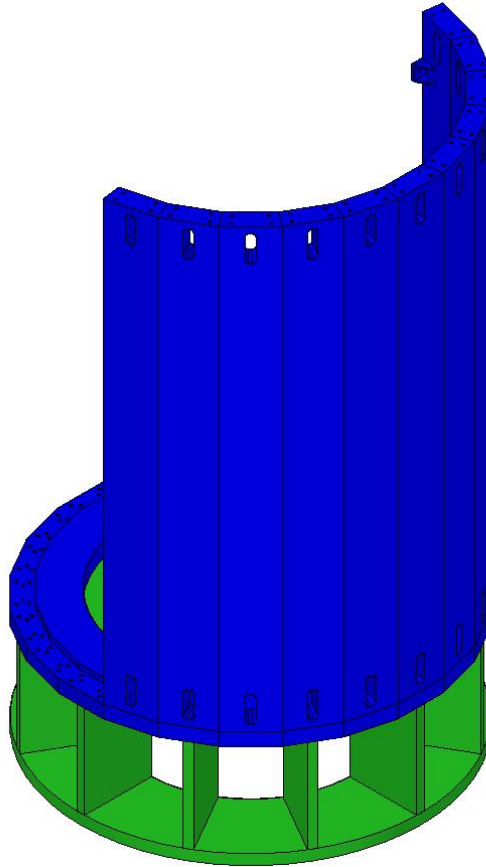


Fig. 2.5.1.2.2. One-by-one mounting of the yoke beams in the vertical position

- 2.5.1.2.3 Setting M48 studs with supernuts in the butt joints of the beams and the support ring and preliminarily tightening the supernuts on all beams as they are set (Fig. 2.5.1.2.3); adjusting the spatial position of the beams to meet the assembly drawing requirements; securing the beams in position to prevent their turning-over.

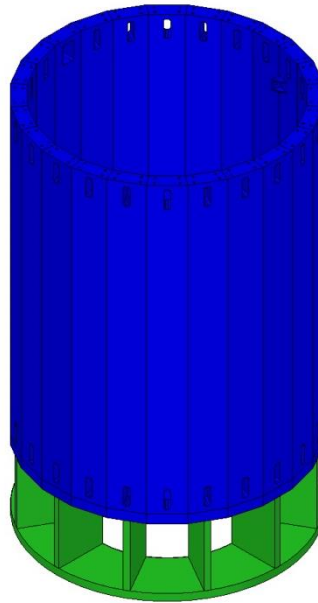


Fig. 2.5.1.2.3. Mounting of all beams

- 2.5.1.2.4 Setting the second support ring on the free ends of beams (using spacers if necessary to level the common end plane); setting M48 studs with supernuts in the butt joints of the beams and the second support ring and preliminarily tightening the supernuts (Fig. 2.5.1.2.4); checking the support rings for their spatial position to meet the assembly drawing requirements.

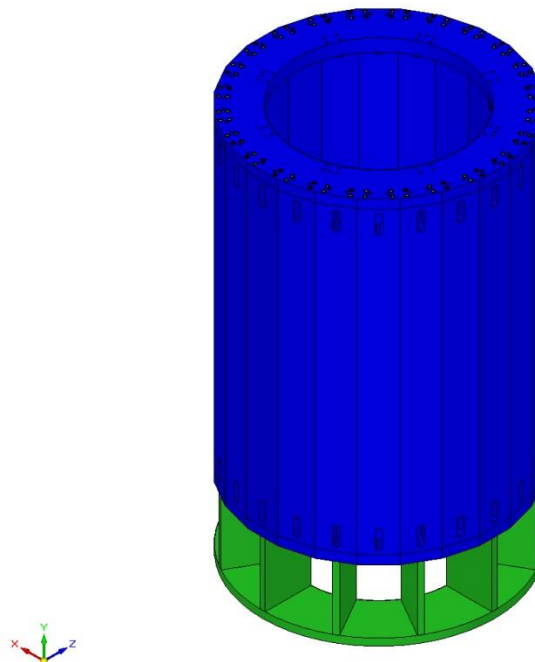


Fig. 2.5.1.2.4. Yoke barrel assembled in the vertical position

- 2.5.1.2.5 Bringing radial beam support surfaces of the beam into proper contact with support ring surfaces using tie rods; fully tightening all supernuts.
- 2.5.1.2.6 Checking support rings for their relative position in the fully assembled yoke barrel; drilling and finally preparing holes for pins through the support rings to the beam ends and setting the pins.
- 2.5.1.2.7 Disassembling the yoke and assembling it on the other support ring for fixing the beams and the support ring that was previously at the bottom by pins.
- 2.5.1.2.8 Setting cradles on the auxiliary supports and adjusting their position relative to the barrel in accordance with the drawing requirements (Fig. 2.5.1.2.5); using spacers to ensure contact of the cradle surfaces with the yoke beams.

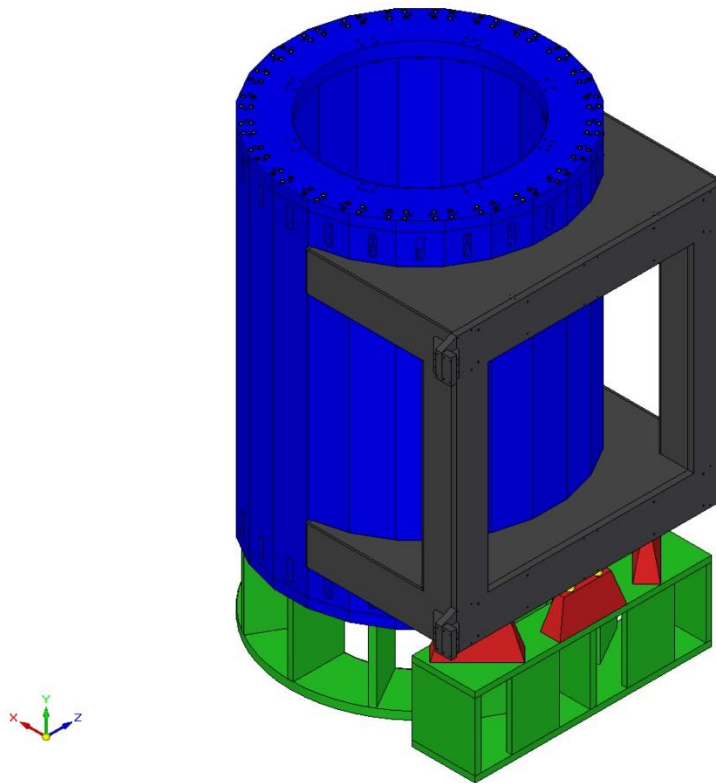


Fig. 2.5.1.2.5. Yoke assembled in the vertical position on the supports

- 2.5.1.2.9 Preparing holes for locating pins at the place of contact between the beams and the cradles.
- 2.5.1.2.10 Assembling the yoke in the horizontal position using pins and spacers between the yoke beams and the cradles.

2.5.1.3 ACCEPTANCE TESTS OF THE YOKE IN THE HORIZONTAL POSITION

- 2.5.1.3.1 Checking the rings for alignment, mutual parallelism, and perpendicularity to the magnet axis.
- 2.5.1.3.2 Checking the fit of the beams to mating surfaces of the support rings.
- 2.5.1.3.3 Checking coaxiality of the support rings and the poles. Checking the gaps between the poles and the support rings.

2.5.2 DISASSEMBLY AND TRANSPORTATION OF THE YOKE

- 2.5.2.1 Disassembly of the yoke.
- 2.5.2.2 Spacers between the beams and the cradles remain welded to the cradle surface.

2.5.3 FINAL ASSEMBLY OF THE MAGNET IN DUBNA

2.5.3.1 ASSEMBLING THE MAGNET WITH THE CRYOSTAT

- 2.5.3.1.1 Putting the magnet support cradles on the roller skates on the rail track in accordance with the requirements of the assembly drawing and the scheme of the magnet allocation at the assembly site (Fig. 2.5.3.1.1); adjusting the positions of the roller skates and their guide rollers.

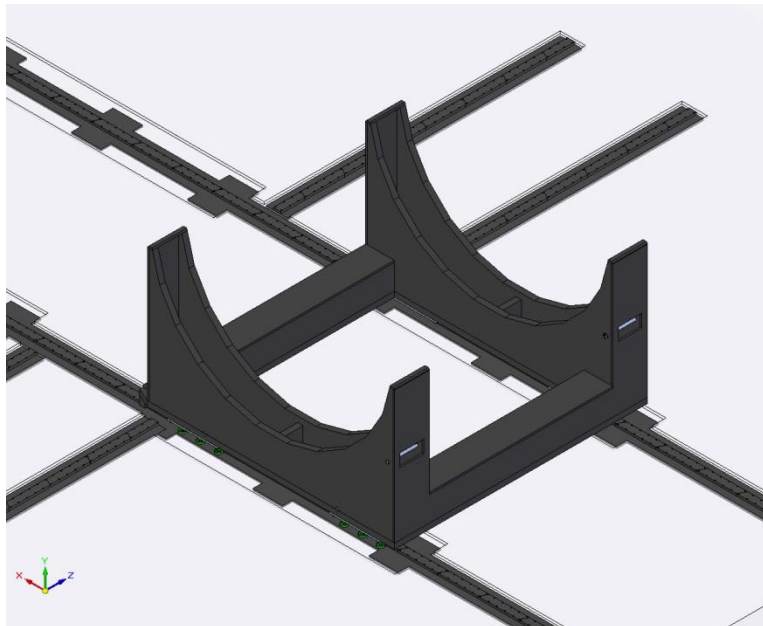


Fig. 2.5.3.1.1. Magnet cradles put on the roller skates

- 2.5.3.1.2 Transferring the magnet cradles to the stationary supports and adjusting their height using hydraulic jacks and shims between the stationary supports and the foundation in accordance with the assembly draw requirements (Fig. 2.5.3.1.2); checking the position of the cradle support planes.

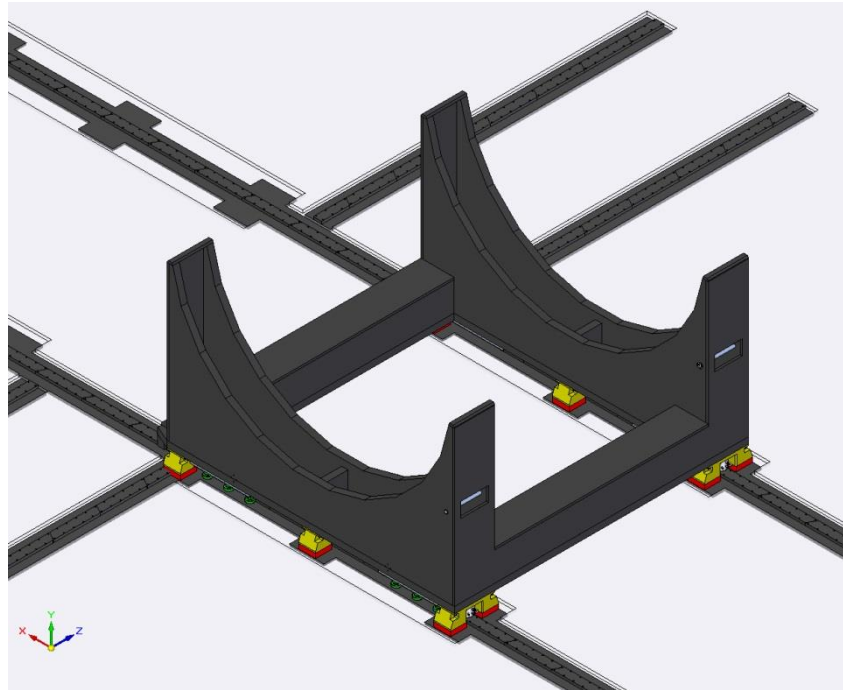


Fig. 2.5.3.1.2. Magnet cradles set on the stationary supports

- 2.5.3.1.3 Setting eleven lower beams with pins; checking the spatial arrangement of the barrel components for being in accordance with the assembly drawing requirements.
- 2.5.3.1.4 Mounting support rings, checking their relative position for meeting the assembly drawing requirements.
- 2.5.3.1.5 Mounting the upper distance spacer between the support rings.
- 2.5.3.1.6 Setting tie studs with supernuts and preliminarily tightening the supernuts on the mounted beams.
- 2.5.3.1.7 Checking relative position of the support rings.
- 2.5.3.1.8 Welding the beams to the cradle and to each other (Fig. 2.5.3.1.3).
- 2.5.3.1.9 Removing the upper distance piece between the support rings.
- 2.5.3.1.10 Mounting the cryostat (Fig. 2.5.3.1.4).

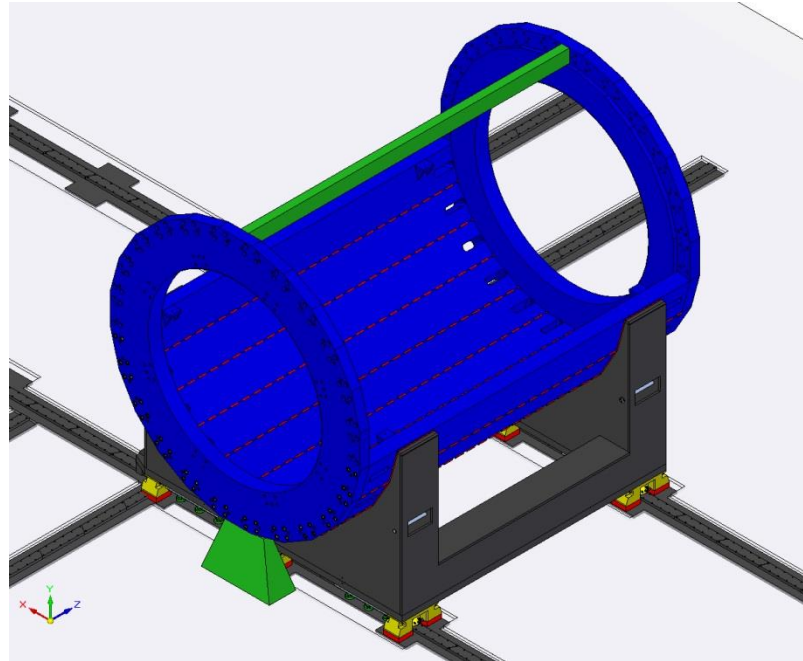


Fig. 2.5.3.1.3. Welding of eleven lower beams to the cradle and to each other (beam welding places are shown by red dashed lines)

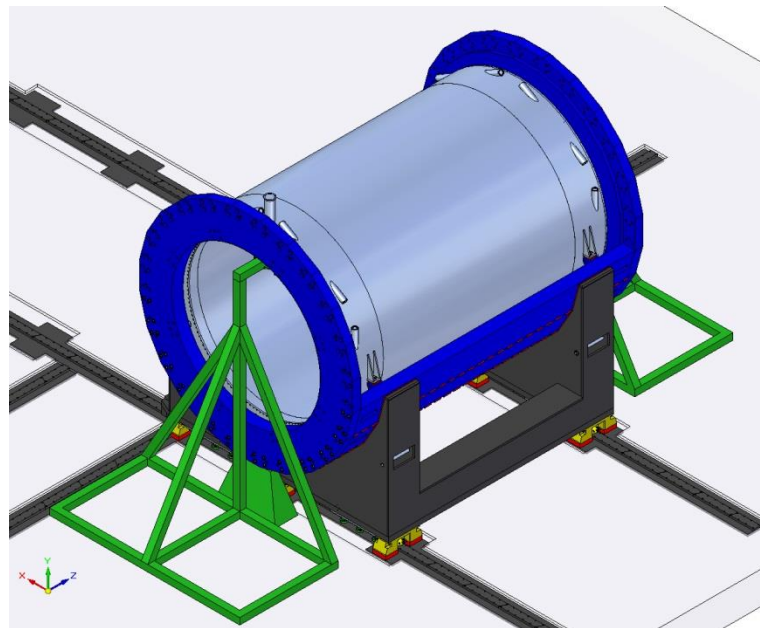


Fig. 2.5.3.1.4. Mounting of the cryostat after assembling eleven lower beams and the support rings

- 2.5.3.1.11 Checking the relative position of the support rings and adjusting it if necessary.
- 2.5.3.1.12 Adjusting the position of the cryostat relative to the support rings using spacers.
- 2.5.3.1.13 Mounting the remaining 13 barrel beams one by one, setting pins, and preliminarily tightening supernuts on the tie studs (Fig. 2.5.3.1.5); checking and adjusting, if necessary, the position of the support rings after mounting each of the remaining beams.

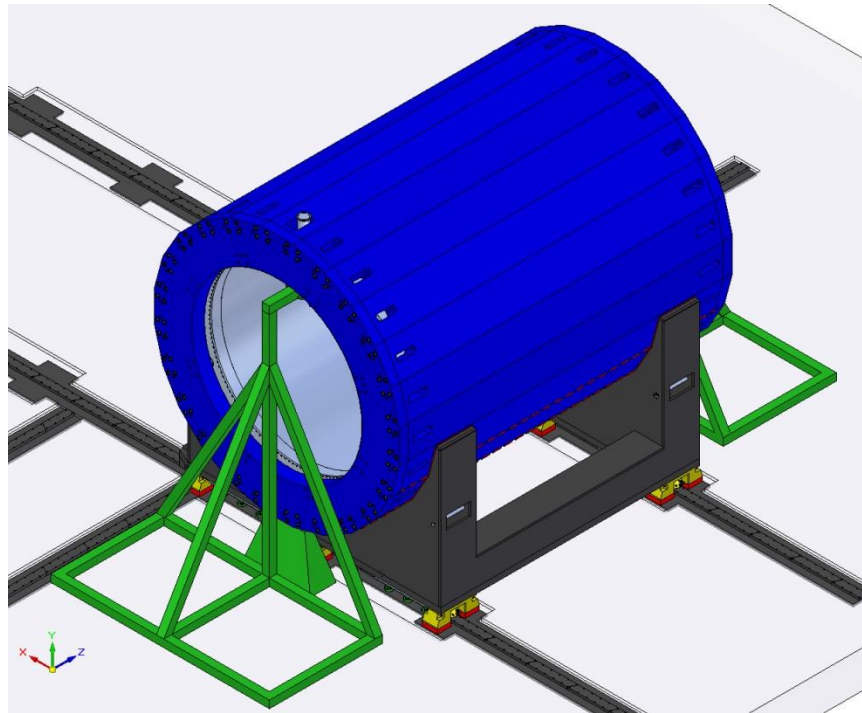


Fig. 2.5.3.1.5. Mounting of the remaining yoke beams after the mounting of the cryostat

- 2.5.3.1.14 Fully tightening all supernuts.
- 2.5.3.1.15 Checking the relative position of the support rings.
- 2.5.3.1.16 Checking the position of the cryostat relative the support rings.
- 2.5.3.1.17 Mounting the control Dewar, connecting cables and pipes in the chimney, welding the movable part of the chimney, and pumping out and checking vacuum.
- 2.5.3.1.18 Setting the upper platform on the yoke and mounting the equipment (vacuum pumps, power supplies, etc.) on the platform.
- 2.5.3.1.19 Assembling the platforms for moving solenoid poles.
- 2.5.3.1.20 Mounting the drives of the magnet and pole movement system; putting the hydraulic system of the magnet into operation.
- 2.5.3.1.21 Fitting trim coils into the recesses in the poles and securing them with caps.
- 2.5.3.1.22 Setting pole transport platforms on the rail tracks in the parking position; mounting counterweights.
- 2.5.3.1.23 Setting poles on the transport platforms (Figs. 2.4.8.2.1, 2.4.8.2.2, 2.4.8.3.5).
- 2.5.3.1.24 Moving the yoke to the pole mounting area.
- 2.5.3.1.25 Adjusting the position of the poles on the transport platforms relative to the borings in the support rings.
- 2.5.3.1.26 Inserting poles in the borings of the yoke support rings using the guide pins.
- 2.5.3.1.27 Adjusting the position of the poles relative the yoke support rings; bolting poles on the support rings with M48 bolts.
- 2.5.3.1.28 Checking poles for positioning relative to the support rings.
- 2.5.3.1.29 Adjusting the distance between the poles, their mutual parallelism, and perpendicularity to the magnet axis using spacers under axial stops of the poles.

- 2.5.3.1.30 Fitting off-loading stay wedges into the slots between the poles and the support rings. The assembled magnet in the operating position is shown in Fig. 2.4.8.3.6.
- 2.5.3.1.31 Detaching transport platforms from the poles and moving them to the parking position.
- 2.5.3.1.32 Moving the completely assembled magnet to the operating position.
- 2.5.3.1.33 Adjusting the position of the magnet relative to the beam axis in the horizontal plane using hydraulic cylinders of the movement system.
- 2.5.3.1.34 Transferring the magnet from the roller skates to the stationary supports.
- 2.5.3.1.35 Adjusting the position of the magnet relative to the axis beam in the vertical plane using spacers under the stationary supports.
- 2.5.3.1.36 Checking the magnet for the main geometrical parameters (relative position of the rings, position of the cryostat relative to support rings, position of the magnet relative to the beam axis).

2.5.3.2 ACCEPTANCE TESTS OF THE ASSEMBLED MAGNET

- 2.5.3.2.1 Checking the support rings for alignment and parallelism.
- 2.5.3.2.2 Checking the distance between the but ends of the rings.
- 2.5.3.2.3 Checking the beam ends for fitting to the support rings.
- 2.5.3.2.4 Checking the contact of the beams with the radial support surfaces of the support rings.
- 2.5.3.2.5 Checking the position of the superconducting coils (reference points on the cryostat outer shell) with respect to the support rings (alignment and radial position).
- 2.5.3.2.6 Checking the distance from the support ring to the cryostat flange on the chimney side.
- 2.5.3.2.7 Checking the relative position of the poles and their position relative to the support ring axis.
- 2.5.3.2.8 Checking the relative position of the poles, their position relative to the support ring axis, and the position of the cryostat relative the support rings after energizing the superconducting coil.

3 CRYOGENIC SYSTEM OF THE MPD MAGNET

3.1 COMPONENTS OF THE CRYOGENIC SYSTEM

The cryogenic system is intended for continuous cooling of the superconducting coil and the thermal shields of the MPD magnet in various modes of its operation. The main components of the cryogenic system are listed in Section 2.4.6.

3.2 COIL CRYOSTATTING EQUIPMENT

3.2.1 HELIUM SATELLITE REFRIGERATOR

A helium satellite refrigerator with a liquefaction performance of about 150 l/h of liquid helium will be used for cooling (heating) and cryostatting the superconducting winding of the MPD magnet. Diagram of the cryogenic supply system of the sc coil of the MPD magnet with the satellite refrigerator is shown in Fig. 2.4.6.1. Application of the satellite refrigerator allows the system to meet two contradictory requirements as high reliability and efficiency.

This type of refrigerator contains heat exchangers and vessel for liquid helium and doesn't include helium expander. It takes liquid helium from the main refrigerator and compressed gas for its operation.

The refrigerator is placed on the top platform of the magnet and connected with the main refrigerator of the NICA collider circuit by transfer lines.

The refrigerator provides operating modes with the parameters listed in Table 3.2.1.

Table 3.2.1. Parameters of the helium flows for various operation regimes

| Object | Stream | Parameters | Regime | | |
|-----------------------|---------------|---------------|------------------------------------|-----------------------|--|
| | | | steady-state (normal operation) | cool-down /warm-up | slow dump (refrigerator failure) |
| Cold mass | incoming flow | gas/liquid | LHe (saturated liquid) | GHe | - |
| | | flow | 4.34 g/s (129 l/h) | 16.2 g/s (1 K/h) | - |
| | | temperature | 4.5 K | 300 – 4.5 K | - |
| | | pressure | 1.3 bar | ≤ 10 bar | - |
| | | vapor quality | < 5 % | - | - |
| | return flow | gas/liquid | GHe (saturated vapor) | GHe | - |
| | | flow | 3.96 g/s (117.6 l/h) | 16.2 g/s (1 K/h) | - |
| | | temperature | 4.45 K | 300 – 4.5 K | - |
| pressure | | 1.25 bar | ≈ 1.5 bar | - | |
| Current leads | - | gas/liquid | GHe | - | GHe |
| | | flow | 0.38 g/s (11.3 l/h) | - | 0.38 g/s (11.3 l/h) |
| | | temperature | ≈ 300 K | - | ≈ 300 K |
| | | pressure | 1.25 bar | - | 1.25 bar |
| Thermal shield | incoming flow | gas/liquid | LN2 (saturated liquid) | GN2 | - |
| | | flow | 11.5 g/s | max 100 g/s * | - |
| | | temperature | 80 K | 300 – 80 K | - |
| | | pressure | 3 bar | 3 bar | - |
| | return flow | gas/liquid | GN2 (saturated vapor) | GN2 | - |
| | | flow | 11.5g/s | max 100 g/s * | - |
| | | temperature | 80 K | 300 – 80 K | - |
| | | pressure | 2.9 bar | ≈ 1.2 bar | - |
| Recovery line | - | gas/liquid | - | - | GHe |
| | | flow | - | - | 4.01 g/s (118.3 l/h) |
| | | temperature | - | - | 4.45 K |
| | | pressure | - | - | 1.25 bar |

* - during cool-down and warm-up regimes the value of the flow rate is regulated providing cooling speed of 1 K/h.

3.2.2 NITROGEN RE-CONDENSER FOR COOLING (HEATING) AND CRYOSTATTING THE THERMAL SCREENS

The nitrogen re-condenser is a part of cryogenic supply system of the magnet. It is located on the upper platform of the magnet and connected with the liquid nitrogen system circuit of the NICA collider by cryogenic tubes. The nitrogen re-condenser provides operating modes with the parameters presented in Table 3.2.1.

3.2.3 TRANSFER LINES

All connecting pipelines have vacuum multishield heat insulation and bayonet joints with the cryogenic system components.

3.3 OPERATING REGIMES

The following regimes are considered:

1. Coil cooling from 300 to 4.5 K
2. Steady-state regime and energizing/de-energizing regime
3. Warming-up
4. Emergency I (quench of the superconducting coil)
5. Cooling after a quench of the coil
6. Emergency II (refrigerator failure)
7. Emergency III (power loss)
8. Emergency IV (current lead voltage rise above the allowable level)
9. Emergency V (loss of vacuum)
10. Emergency VI (nitrogen re-condenser failure)

Calculations of cooling regimes for the MPD magnet winding are given in [21].

3.3.1 COOLING FROM 300 TO 4.5 K

Cold mass of the magnet is cooled with the satellite refrigerated by the helium flow of variable temperature from 300 K to 4.5 K. To avoid thermal deformations in the coil, the helium should be supplied with a temperature <20 K lower than the superconducting coil temperature. This temperature difference between the cooling gas and the coil should be provided within the entire cooling time period (approximate rate of cool-down is 1 K/hour). In the process of cooling the superconducting coil temperature should be continuously monitored and the cooling gas flow should be varied by the controlled valves of the control Dewar to maintain the necessary gas flow rate and pressure.

Thermal screens are cooled with a nitrogen stream of variable temperature from 300 K to 80 K from the nitrogen re-condenser. Over this temperature range the temperature of the thermal screens should be maintained at the temperature level of the sc coil.

In the process of cooling the control system of the magnet generates signals for the satellite refrigerator and nitrogen re-condenser corresponding to the required value of the flow and the temperature of the helium and nitrogen. The flows of cooling gases with the set parameters are provided by satellite refrigerator and nitrogen re-condenser. Schematic diagram of the cooling mode is shown in Fig. 3.3.1.

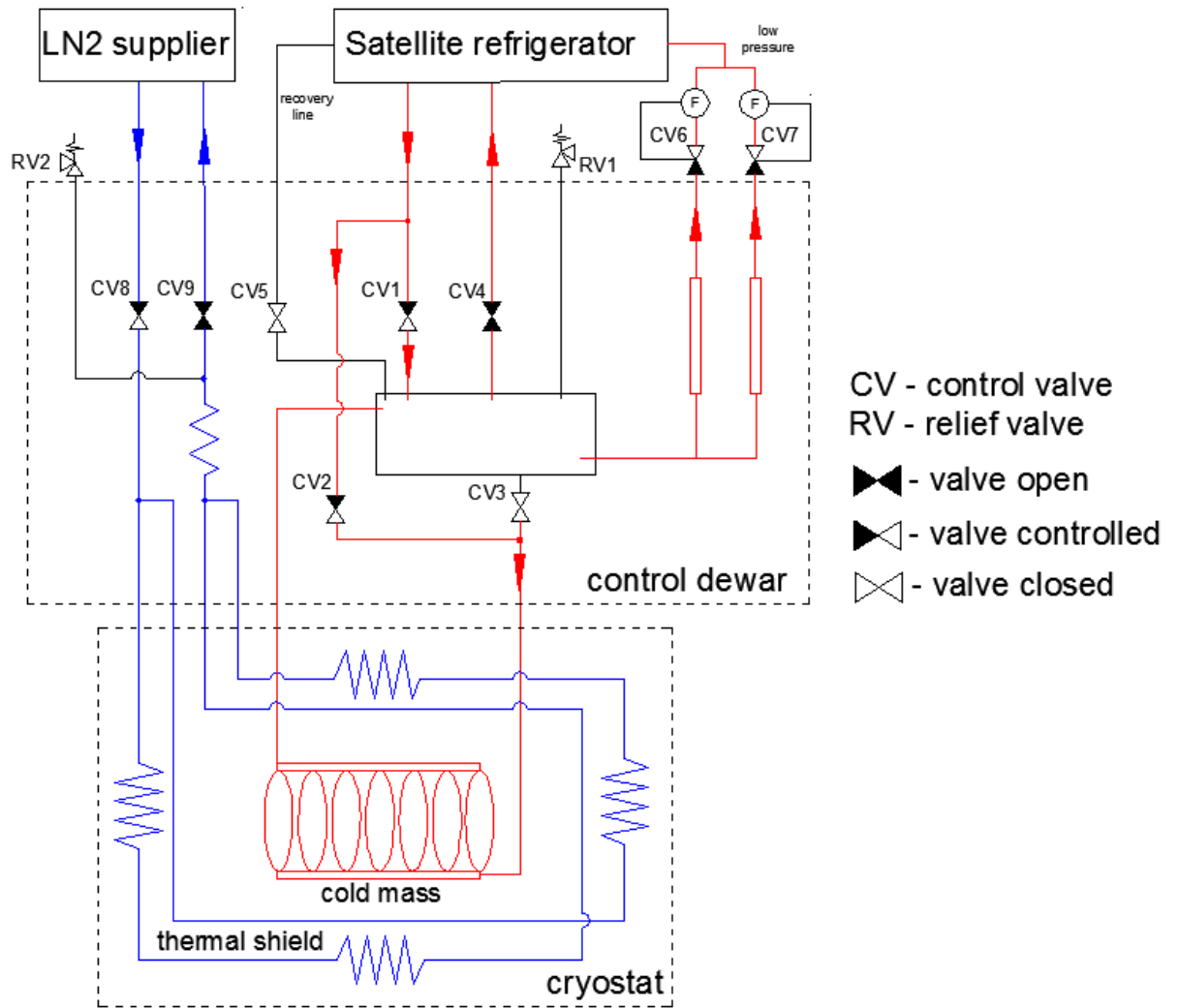


Fig. 3.3.1.1. The circuit provided cooling mode of the sc coil in the range from 300 K to 4.5 K

3.3.2 STEADY-STATE REGIME

The steady-state regime is schematically shown in Fig. 3.3.2.1.

In the stationary regime the liquid helium flux (130 l/h) at absolute pressure of 1.3 bar from satellite refrigerator through the transfer line and through the valve CV1 enters the helium bath of the control Dewar. From the helium bath the liquid helium through the valve CV3 on the supply pipe comes to the lower manifold of the heat exchanger. After passing through the heat exchanger parallel channels vapor-liquid mixture from the upper manifold of the heat exchanger comes into the upper part of the helium vessel of the control Dewar. In the vessel the liquid is separated from the steam. The circulation of the helium in the circuit is carried out because of the density difference of the helium flows in the supply and return pipes. Backflow in the form of saturated steam at absolute pressure of 1.25 bar returns through the valve CV4 back to the satellite refrigerator. Helium gas from the current leads heated up to 300 K is fed into the low pressure line (LP).

Nitrogen re-condenser is used for cooling the thermal screens by flow of liquid nitrogen that enters the control Dewar through the valve CV8. After passing through the thermal shields the nitrogen vapor-liquid mixture is returned through the valve CV9 to nitrogen re-condenser back, where the vapor phase is condensed and fed for cooling thermal screens (nitrogen closed system).

In the process of cooling the control system of the magnet generates signals for the satellite refrigerator and nitrogen re-condenser corresponding to the required values of the flows and the temperature of the helium and nitrogen. Schematic diagram of the cooling mode is shown in Fig. 3.3.2.1.

The excess of the helium refrigerator cooling power is used to maintain the liquid helium level in the helium bath of the control Dewar. The heater in the helium bath of the control Dewar is intended for speeding up evaporation of liquid helium from the bath, compensating for the cooling power excess, and controlling the amount of the return flux coming for the cold box from the helium bath of the control Dewar (maintaining heat balance).

The energizing/de-energizing regime is similar to the steady-state regime except for the additional heat load at a temperature level of 4.5 K resulting from the eddy currents that occur in the aluminium support cylinder. This heat load is compensated by the reserve of liquid helium in the helium bath of the control Dewar. The heat load in the support cylinder during the energizing per 1 hour is 4.2 W (considering the safety factor 2). That corresponds to a loss of about 7 liters of helium.

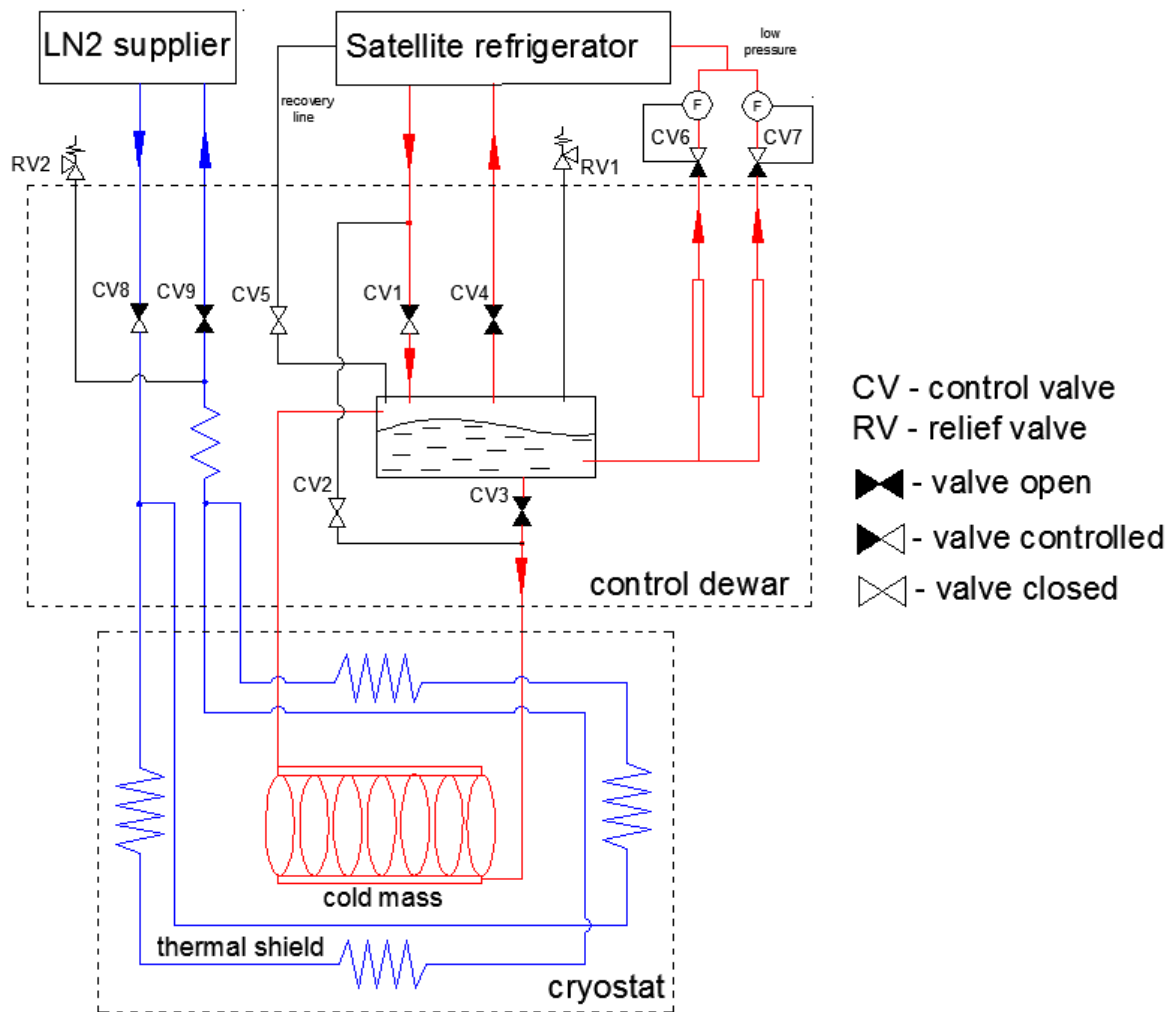


Fig. 3.3.2.1. Scheme of the steady-state regime

3.3.3 WARMING-UP REGIME

The warming-up regime is similar to the cooling regime. The heater shall be used for evaporation of the liquid helium from the control Dewar bath. The temperature of the helium flow will be gradually risen from 4.5 K to 300 K in the process of warming the superconducting coil and the control Dewar. The temperature of the flow will be changed due to changes of the operating parameters of the satellite refrigerator.

When the superconducting coil temperature rises up to ~ 80 K, warming-up of the thermal shields is started. Their temperature is raised by gradual rise of the nitrogen flow temperature from 80 K to 300 K.

The warming-up scheme is shown in Fig. 3.3.3.1. To prevent thermal deformations in the coil, the requirement on the temperature difference in the superconducting coil is the same as in the cooling regime: the difference between the maximum temperature of the gas and the minimum temperature of the support cylinder with the superconducting coil should not be higher than 20 K (the estimated heating rate is ~ 1 K/h). The superconducting coil temperature will be continuously monitored, and the warming-up gas flow will be varied using the control valves of the control Dewar to maintain the necessary gas flow rate, pressure, and

temperature. The superconducting coil can be heated by a low current from the power supply to speed up the warming-up process.

In the process of warming up the control system of the magnet generates signals for the satellite refrigerator and nitrogen re-condenser corresponding to the required values of the flows and the temperature of the helium and nitrogen.

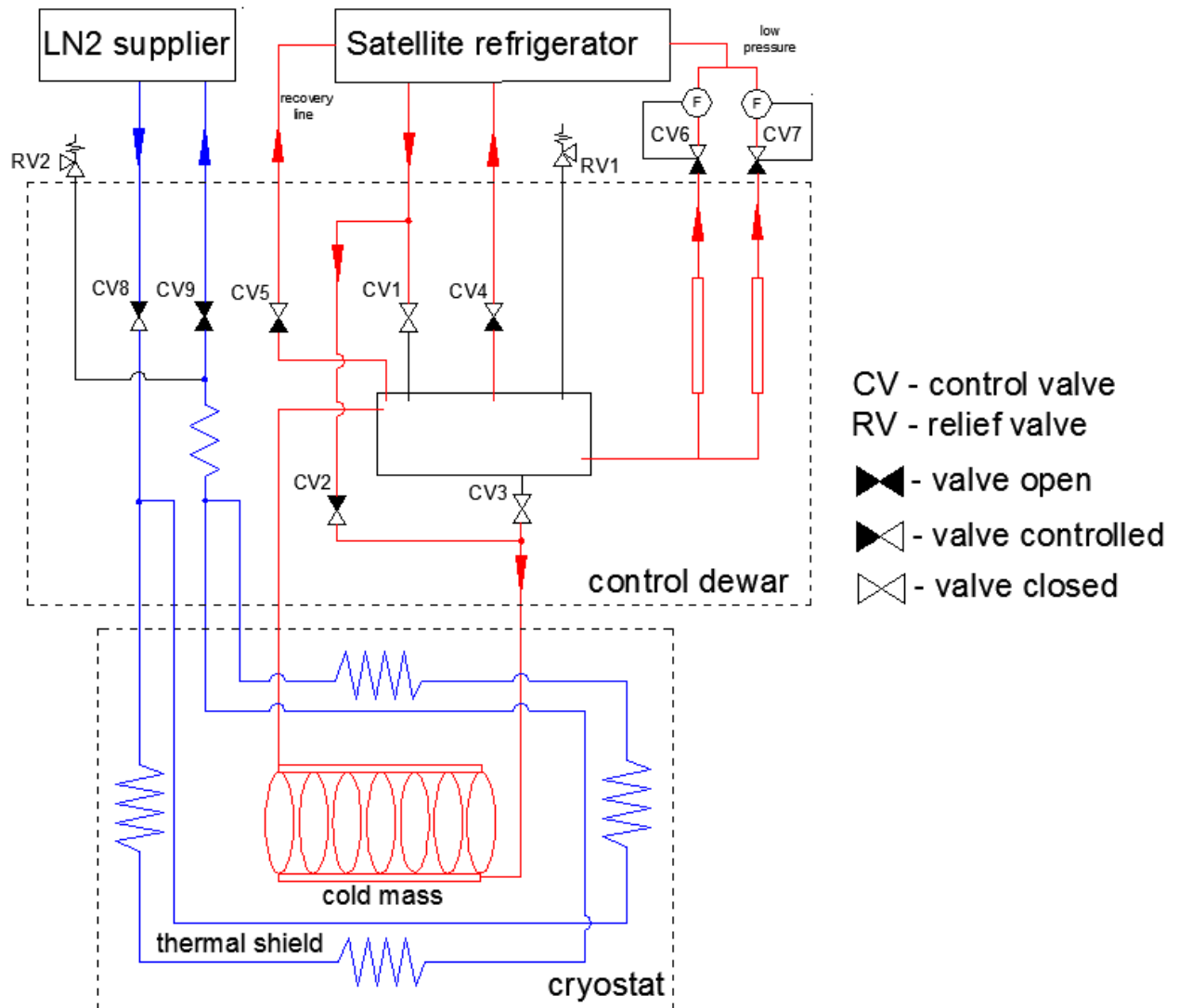


Fig. 3.3.3.1 Scheme provided warming mode of the superconducting coil

3.3.4 EMERGENCY REGIME I (SC COIL QUENCHING)

The energy stored in the superconducting coil at the maximum current is 24.3 MJ. After a quench has occurred, the protection system has to provide dump of the major part of the stored energy in the external discharge resistor within a time of ~ 3 min. The maximal temperature of the coil and the support cylinder after discharging the energy to the external resistor is 27 K. If the protection system failed to operate after quenching, all the stored energy is deposited in the cold mass of the cryostat, and the average temperature of the superconducting coil rises up to ~ 50 K.

After a quench the helium pressure in the heat exchanger pipe on the support cylinder drastically increases. The signal from the normal zone detection circuit stops helium supply

from the satellite refrigerator (closing valves CV1 and CV4). In addition, to avoid any damage the heat exchanger of the coil is cut off from the helium vessel of the control Dewar by closing the valve CV3. Discharge of helium gas from the heat exchanger to the helium recovery system is carried out through the relief valve CV5.

3.3.5 COOLING OF THE COIL AFTER QUENCHING

After the normal phase is detected and the sc coil is deenergized, the helium refrigerator is cut off from the control Dewar. When the gas pressure is released through the valve CV5 to the recovery line or through the relief valve vents to air, the coil recooling process can be started by the operator's decision. Cool down process of the winding after a quench can be started if the difference between the maximum and minimum temperature of the superconducting coil does not exceed 20 K.

Control of the sc coil temperature is carried out by sensors located on its inner surface and on the surface of the support cylinder. According to the calculations after an unprotected quench at the maximum design current the difference between the maximum and the minimum temperature in the winding can be up to 80 K [5]. So we have to wait for equalization of the winding temperature after a quench due to thermal diffusion (which may take several hours) to start cooling down process.

This process is almost the same as the cooling from 300 to 4.5 K, except that at the beginning of the cooling the return flow does not come back to the helium satellite refrigerator but goes to low pressure line since the temperature of the return flow is rather high and can strongly affect the operation of the satellite refrigerator.

3.3.6 EMERGENCY REGIME II (SATELLITE REFRIGERATOR FAILURE)

If the satellite refrigerator fails to operate or the working gas parameters change due to its malfunction, the direct and return flow valves between the refrigerator and the control Dewar (CV1, CV4) are to be closed.

After the trigger signal of refrigerator malfunction, the superconducting coil has to be de-energized. During the de-energizing the superconducting coil and the current leads are cooled by liquid helium from the control Dewar. The amount of helium in the Dewar is enough to allow normal (nonaccelerated) de-energizing of the coil in one hour using the power supply. The minimal level of liquid helium in the helium vessel before the coil de-energizing has to be 130 liters at least.

If the refrigerator doesn't restore its functionality during the time when the coil is de-energized, the solenoid is shifted to the passive warming-up regime by ambient heat inflows. The helium pipeline pressure is released to the collection and storage system through the relief valves.

The circuit which provides de-energizing the sc coil if the satellite refrigerator fails is presented in Fig. 3.3.6.1.

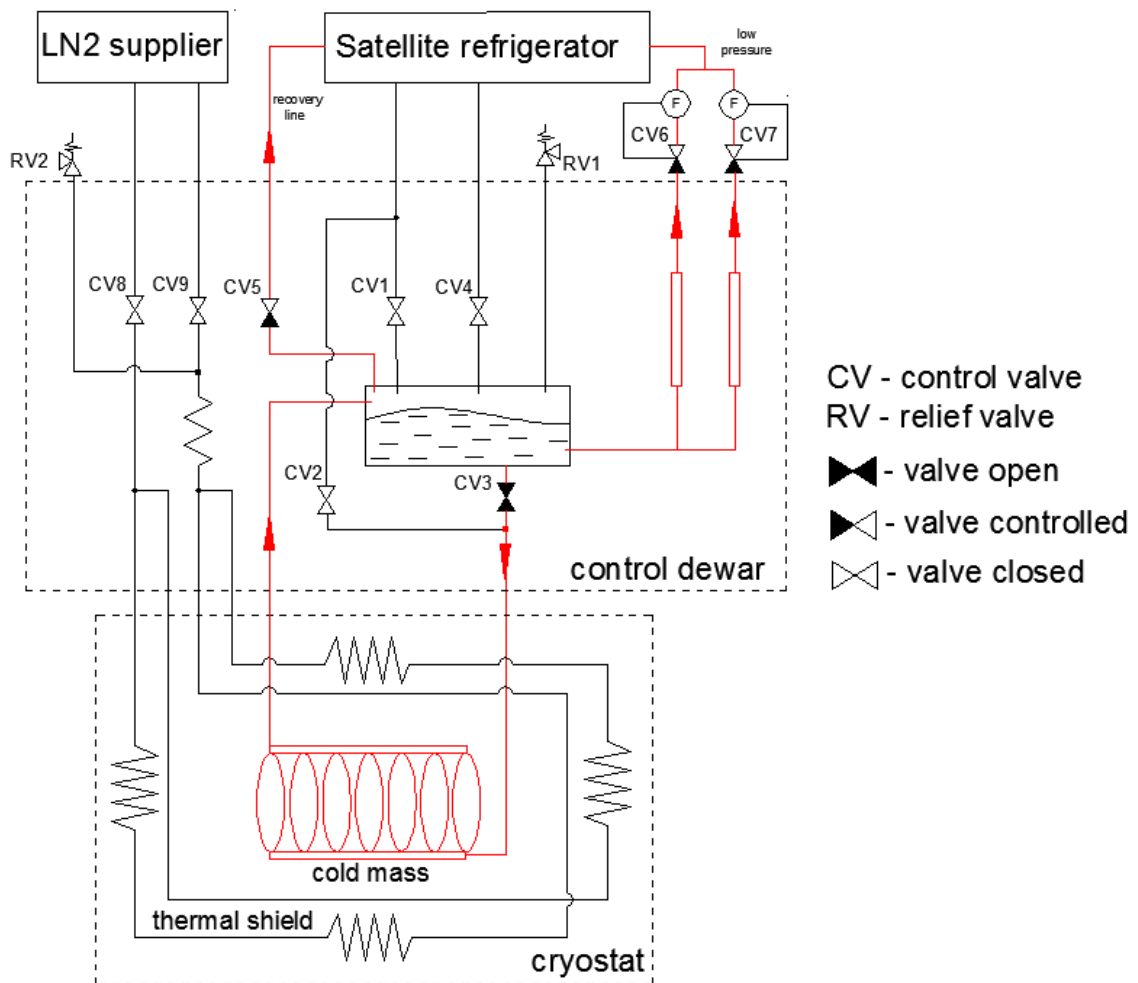


Fig. 3.3.6.1. The circuit which provides de-energizing the sc coil if the satellite refrigerator fails

3.3.7 EMERGENCY REGIME III (ON SITE POWER FAILURE)

If the power supply is violated in the experimental building, the cooling system will be automatically configured using controlled valves powered by uninterrupted power supplies and liquid helium from the control Dewar will be used for cooling the superconducting coil and current leads during the de-energizing period. Valves (CV1, CV4) cut off the helium refrigerator from the control Dewar. At the same time accelerated de-energizing of the superconducting coil without its quenching through the discharge resistor (during the time of ~20 minutes) is performed. After the de-energizing the coil, control Dewar, and thermal shields are warmed up by ambient heat inflows. The cooling circuit of the coil is similar to the scheme when satellite refrigerator is stopped.

3.3.8 EMERGENCY REGIME IV (CURRENT LEAD VOLTAGE RISE ABOVE ALLOWABLE LEVEL)

When the current lead voltage rises above the allowable level, emergency de-energizing of the superconducting coil through the discharge resistor is carried out.

If the current leads don't restore their functionality during the time when the coil is de-energized the solenoid is shifted to the warming-up regime by the operator's decision.

3.3.9 EMERGENCY REGIME V (LOSS OF VACUUM)

The control Dewar, chimney, and superconducting coil cryostat have a common vacuum volume. The causes for the loss of vacuum can be both "warm", when the ambient air leaks into the vacuum volume, and "cold", when the circulating helium leaks into the vacuum volume. In both cases the situation is identical except that in the "cold" case the pressure in the vacuum volume drastically increases because of expansion of cold helium vapor.

When sensors signal the loss of vacuum, the helium lines between refrigerator and the control Dewar are closed and the superconducting coil is de-energized through the discharge resistor. The valves (CV1, CV4) cut off the helium refrigerator from the control Dewar and the excess gas pressure in helium vessel is released to the recovery line or through the relief valve vents into the atmosphere. The valves (CV8, CV9) cut off the supply of liquid nitrogen from nitrogen re-condenser.

To avoid mechanical deformation due to increase of pressure in the vacuum volume (the vacuum shell of the superconducting coil cryostat is designed for the excessive pressure of 0.7 bar), relief valves (operate pressure 0.25 bar) and relief diaphragms (operate pressure 0.5 bar) are installed on the vacuum shell of the control Dewar and the chimney. As the maximum safe pressure of 0.25 bar in the vacuum volume is exceeded, the relief valves open, and as the pressure increases above 0.5 bar, the diaphragms are broken and the pressure is released into the atmosphere.

After de-energizing the solenoid is shifted to the warming-up regime: liquid helium in the control Dewar is evaporated using the heater and the winding is energized by a low current to prevent gases that leaked into the vacuum volume (air, water vapor, etc.) from condensing on the cold surface of the winding.

3.3.10 EMERGENCY REGIME VI (NITROGEN RE-CONDENSER FAILURE)

If the nitrogen re-condenser fails to operate or the working gas parameters change due to its malfunction, the direct and return flow valves between the re-condenser and the control Dewar (CV8, CV9) are to be closed.

After the trigger signal of re-condenser malfunction, the superconducting coil has to be de-energized. During the de-energizing the superconducting coil and the current leads are cooled by liquid helium from the control Dewar (satellite refrigerator continue to work). The amount of helium in the Dewar is enough to allow normal (nonaccelerated) de-energizing of the coil in one hour using the standard power supply. The minimal level of liquid helium in the helium vessel before the coil de-energizing has to be 130 liters at least.

If the re-condenser doesn't restore its functionality during the time when the coil is de-energized, the valves (CV1, CV4) cut off the helium refrigerator from the control Dewar and the

excess gas pressure in helium vessel is released to the recovery line or through the relief valve vents into the atmosphere.

After that the solenoid is shifted to the passive warming-up regime by ambient heat inflows.

3.4 CONTROLLED PARAMETERS AND CONTROL ACTIONS

Regime control and variation of flows through the heat exchangers of the coil and the shield are performed according to the scheme in Fig. 2.4.3.6.1 using control Dewar valves in accordance with Table 3.4.1, where modes of controlled valves of the control Dewar are indicated for each regime. The notation is given in Fig. 2.4.3.6.1

Operation parameters of the magnet cryogenic system are controlled by the sensors listed in Table 3.4.2.

The parameters of the magnet that do not relate to sc coil cooling are controlled by the sensors listed in Table 3.4.3.

Figure 3.4.2 shows the arrangements of the control Dewar and superconducting coil sensors.

Table 3.4.1. Positions of control Dewar valves for various MPD magnet operation regimes

| Valve | Regime | | | | | | | | | | |
|-------|-----------------|----------------------|--------------|------------|----------------------------|------------------------------|----------------------------------|------------------------|---|----------------------------|----------------------------------|
| | Initial setting | Cooling 300 to 4.5 K | Steady-state | Warming-up | Emergency (coil quenching) | Cooling after coil quenching | Emergency (refrigerator failure) | Emergency (power loss) | Emergency (current lead voltage rise above the allowable level) | Emergency (loss of vacuum) | Emergency (re-condenser failure) |
| CV1 | C | R | R | C | C | R | C | C | C | C | C |
| CV2 | C | R | C | R | C | R | C | C | C | C | C |
| CV3 | C | C | O | C | C | C | O | O | O | C | O |
| CV4 | C | O | O | R | C | O | C | C | C | C | C |
| CV5 | C | C | C | R | O | R | R | R | R | O | R |
| CV6 | C | R | R | R | C | R | R | R | R | C | R |
| CV7 | C | R | R | R | C | R | R | R | R | C | R |
| CV8 | C | R | R | R | R | R | C | C | R | C | C |
| CV9 | C | O | O | O | O | O | C | C | O | C | C |

O valve open

C valve closed

R valve in mode of adjustment (for pressure, temperature, flow rate or level of liquid helium)

Table 3.4.2. Sensors of the control Dewar and the superconducting coil for controlling the superconducting coil cooling regimes

| Sensor | Regimes | | | | | | | | | |
|----------|-------------------------|--------------|----------------|---|---------------------------|---|-------------------------------|---|------------------------------------|--|
| | Cooling 300 to 4.5 K | Steady-state | Warming- up | Emergency I (quench of the sc coil) | Cooling after a quench | Emergency II (refrigerator failure) | Emergency III (power loss) | Emergency IV (current lead voltage rise above allowable level) | Emergency V (loss of vacuum) | Emergency VI (nitrogen re- condenser failure) |
| T1 | C | C | C | | C | | | C | | C |
| T2 | C | V | C | V | C | C | C | V | V | V |
| T3, T4 | V | C | V | V | V | C | C | C | V | C |
| T5 | C | C | C | V | C | C | C | C | V | C |
| T6 | C | V | C | V | V | V | V | V | V | V |
| T7- T10 | V | V | V | V | V | V | V | V | V | V |
| T11 –T23 | C | C | V | V | C | C | C | C | V | C |
| T24- T31 | V | C | V | V | V | V | V | V | V | V |
| T32- T35 | V | C | V | V | V | V | V | V | V | V |
| T36-T39 | V | V | V | V | V | V | V | V | V | V |
| P1 | C | C | V | | C | | | | | |
| P2 | C | C | V | V | C | C | C | C | C | C |
| P3 | C | C | V | V | C | V | V | V | V | |
| F1,F2 | | C | | | | C | C | C | | C |
| L1 | | C | | C | | C | C | | C | C |
| V1,V2 | C | C | C | C | C | C | C | C | C | C |
| Q1 | | C | C | | | C | C | C | C | C |

V sensor in visualization mode

C sensor in regime control mode

T1–T10, T24 –T31 temperature sensors on the gas tubing

T11–T17 temperature sensors on the support cylinder (platinum)

T18–T23 temperature sensors on the support cylinder (carbon)

T32–T35 temperature sensors on the thermal shield of the cryostat

T36–T39 temperature sensors on the vacuum vessel of the cryostat

Table 3.4.3. Instrument sensors for measuring magnet parameters that do not relate to superconducting coil cooling

| Sensor | Regimes | | | | | | | | | |
|----------|-------------------------|--------------|----------------|---|---------------------------|---|-------------------------------|---|---------------------------------------|--|
| | Cooling 300 to 4.5 K | Steady-state | Warming- up | Emergency I (quench of the sc coil) | Cooling after a quench | Emergency II (refrigerator failure) | Emergency III (power loss) | Emergency IV (current lead voltage rise above allowable level) | Emergency V (loss of vacuum) | Emergency VI (nitrogen re- condenser failure) |
| T45–T48 | | X | | | | | | | | |
| T49 | | | | | X | | | | | |
| U1–U4 | | X | | X | | X | X | X | X | X |
| U5–U6 | X | X | X | X | X | X | X | X | X | X |
| X1–X2 | | | | | | | | | | |
| I1 | | X | X | X | | X | X | X | X | X |
| I2, I3 | | X | | X | | X | X | X | X | X |
| P10, P11 | | X | | X | | X | X | X | X | X |
| F4, F5 | | X | | X | | X | X | X | X | X |
| S1–S6 | | | | | | | | | | |

X sensor used for regime control

- T45–T48 temperature sensors on the inlets and outlets of the trim coil demineralized-water-cooling circuits
- T49 temperature of the superconducting coil dump resistor
- U1–U4 signals from potential leads in current lead sections
- U5–U6 signals from potential leads at the winding leads for determining winding voltage
- X1–X2 Hall probes to measure magnet field (used only in setting-up activities)
- I1 superconducting coil current sensor
- I2, I3 trim coil circuit current sensors
- P10, P11 trim coil cooling water pressure sensors
- F4, F5 trim coil cooling water flow rate sensors
- S1–S6 strain gauges on the axial tie rods (used only in setting-up activities)

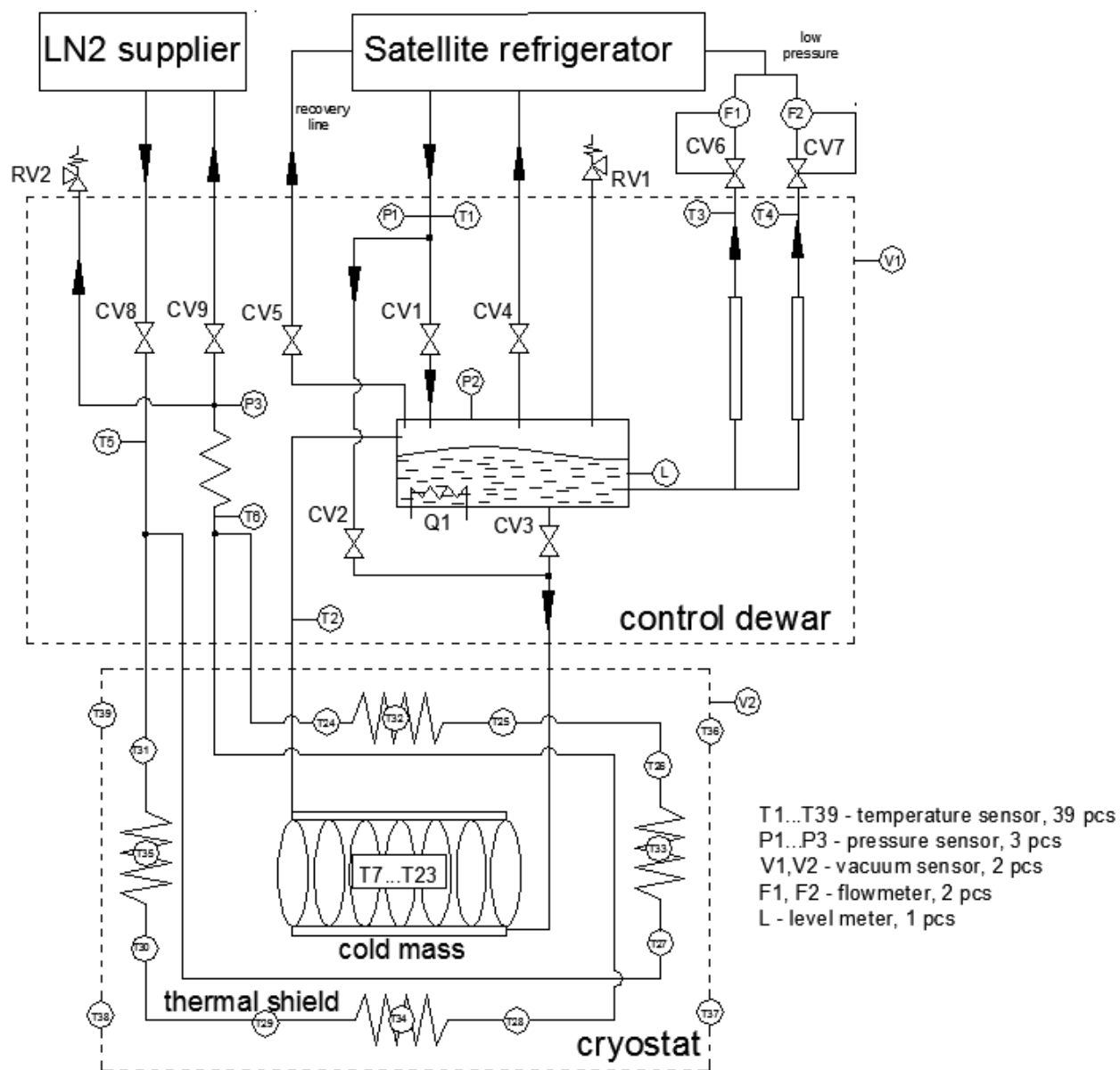


Fig. 3.4.2. Sensors of the control Dewar and the superconducting coil

4 CONTROL SYSTEM OF THE MAGNET

4.1 PURPOSE

- Collection, display, and logging of the main status parameters of the magnet systems.
- Coordinated control of the regimes of the magnet systems in the normal, pre-emergency, and emergency situations.
- Information exchange with the NICA control system.

4.2 GENERAL STRUCTURE

4.2.1 The system for monitoring the condition and controlling the regimes of the magnet systems has a three-level structure:

4.2.1.1 The lower level comprises primary transducers (sensors) to measure physical quantities and control actuators.

4.2.1.2 The middle level comprises controllers responsible for acquisition, processing, execution of control algorithms, formation of control signals for actuators, and interchange with other system controllers and upper-level servers.

4.2.1.3 The upper level comprises servers for general control over the system, visualization, registration, and data exchange with the collider control system.

4.2.2 The system is built as a distributed system with data acquisition and control (DAC) system controllers mounted in the immediate neighborhood of the primary sensors and controlled elements of particular systems.

4.2.2.1 Cabinets accommodating the DAC equipment have two independent power supply inputs.

4.2.2.2 Each DAC system controller is connected to the system server through two physically independent network interfaces.

4.2.2.3 The upper level of the system is a cluster of servers at the central magnet operator's panel that directly interact with the data display, logging, and accumulation system and exchange information with the upper-level collider control system.

The block diagram of the system is shown in Fig. 4.1.

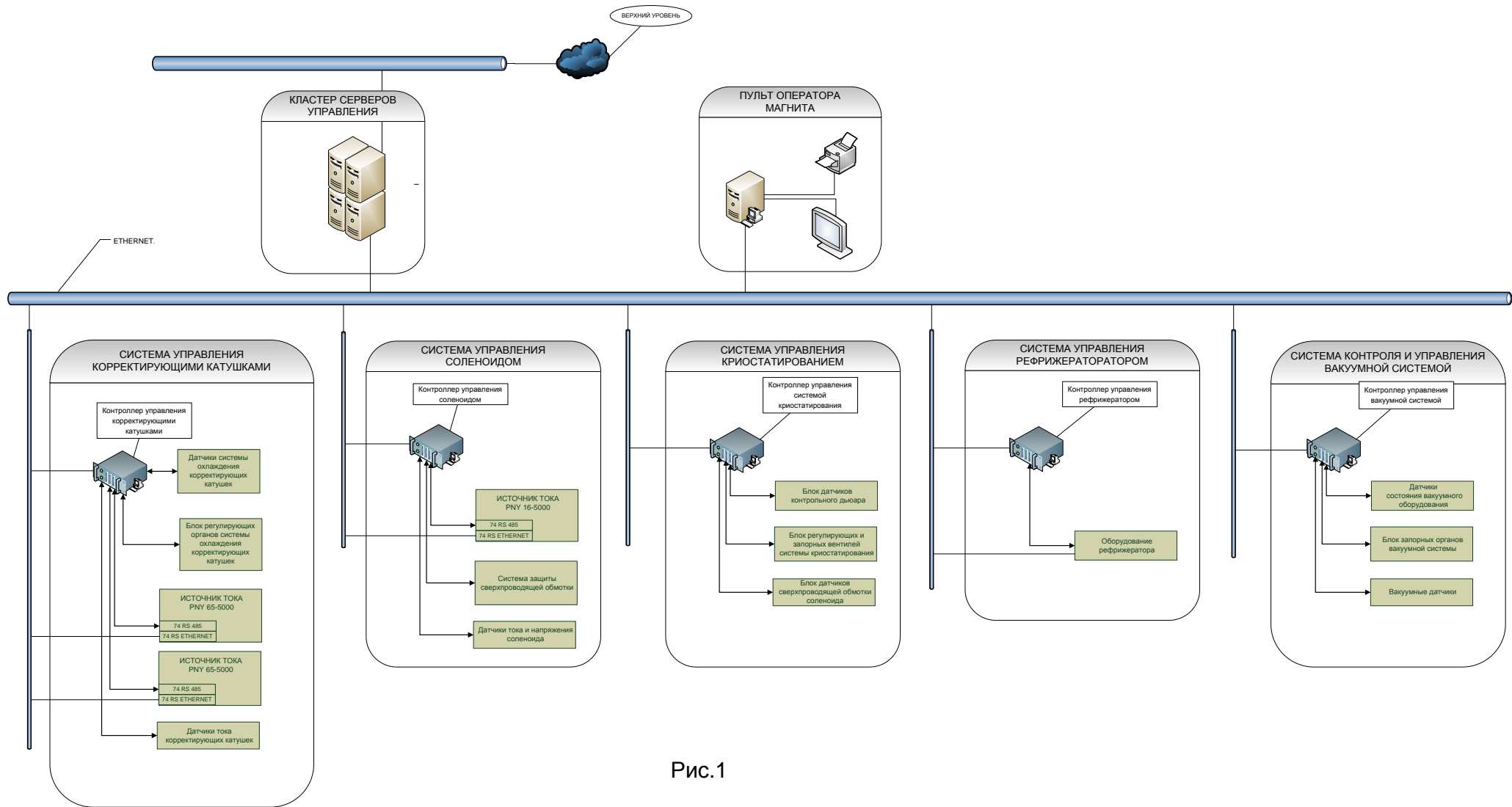


Рис.1

Fig. 4.1. Block diagram of the magnet condition monitoring and operation regime control system

4.3 Lower level structure (transducers and actuators)

- 4.3.1 Each subsystem has its own set of sensors (discrete and analogue), primary transducers, control actuators, or control interfaces if there are controllers built into the subsystem. The final list of sensors and actuators with their types and parameters will be made at the detailed design stage.
- 4.3.2 Sensors with nonstandard output signals are matched using normalizing converters to convert their outputs to unified input signals.
- 4.3.3 Actuators are equipped with power switches that connect discrete actuators to auxiliary contracts or limit switches to form status signals.
- 4.3.4 Adjusting actuators have unified input control signals (analogue or digital) and feedback signals (analogue or digital) for functioning in a closed control loop.

4.4 Middle level structure (master controllers)

- 4.4.1 Each middle-level subsystem has its own controller (controllers). A controller consists of a backplane, a processing module with the real-time operating system, input/output modules, and external interface modules.
- 4.4.2 The algorithm of a particular subsystem can be implemented using the National Instruments CompactRIO platform with an FPGA. Depending on its complexity, each subsystem can have one or several controllers working in parallel and the corresponding number of I/O modules (see Appendix 3).
- 4.4.3 Software tools and hardware features of National Instruments controllers (see Appendix 4) allow implementing complex distributed system control algorithms. Controllers perform real-time data acquisition from the first-level devices, analogue-to-digital conversion, synchronization of signals, data exchange over Ethernet between other controllers and with the upper-level servers, and formation and output of control actions to actuators.

4.5 Upper level structure (servers)

Physically, the upper level of the system consists of a fail-safe cluster of servers with the necessary system controller network support service, database server, timing service, and service of data exchange with the collider control system.

The workstation of the magnet operator's main control panel is connected to the local area network of domain controllers—a fail-safe cluster.

The software for the workstation of the magnet operator's main control panel provides regime control, visualization, logging, and adjustment and maintenance of magnet subsystems.

If necessary, the operator's control panel can be duplicated with all or some of the functions retained with the set priorities.

To adjust and attend to the equipment of the subsystems, there are points for connecting a portable operator's control panel with the necessary set of functions.

5 TRANSPORTATION OF THE MAGNET

Transportation of MPD magnet components to JINR, Dubna, is a difficult but quite solvable problem. The size and weight of the main yoke and cryostat components are presented in Table 2.4.8.4. Not special permission of the traffic police is needed for transporting most of the yoke components because their weight and size fall within the permitted limits. The yoke support rings with an outer diameter of 6.64 m and a weight of ~42 t and the poles with an outer diameter of 4.586 m and a weight of ~44 t will require a special oversized cargo platform and permission for their transportation along the agreed route under traffic police escort.

A more difficult problem is to transport the cryostat with its weight of 66 t, length of ~8 m, vertical dimension of ~6.6 m (from the shoulders for radial tie rods of the cold mass suspension at the bottom to the cryogenic inlet pipe at the top), and transverse dimension of ~5.75 m from the European manufacturer to Dubna. Obviously, the most efficient way is transportation by water followed by reloading onto a special platform and transportation to the installation place at NICA.

REFERENCES

1. MPD Magnet System Interface Control Document v. ??? 2013
2. Set of drawings 3HM1002.00.000
3. R. Brown et al., The STAR detector magnet subsystem, in 1997 Particle Accelerator Conference, Vancouver, BC, 1997, BNL-64461.
4. 3HM1002.00.000P4.1. Choice of parameters of the superconducting cable for the MPD winding.
5. 3HM1002.00.000P6. MPD magnet winding quench calculation. Winding stability calculation.
6. 3HM1002.00.000P1.3. Stress-strain state calculation of the superconducting MPD magnet coil.
7. 3HM1002.00.000P3. Calculation of the cryogenic parameters of the superconducting MPD magnet winding.
8. 3HM1002.00.000P1. Stress-strain state calculation of the structural MPD magnet elements.
9. 3HM1002.00.000P1.1. Choice of tie rods for the suspension of the MPD magnet cold mass.
10. 3HM1002.00.000P2. Optimization of the magnetic system of the MPD. Calculation of the magnetic fields and forces.
11. 3HM1002.00.000P5. Calculations of the MPD magnet pole trim coils.
12. Letter of V. M. Golovatyuk dated 17.05.2013
13. Power supplies. www.heinzinger.com
14. PB 03-576-03 Rules for structural arrangement and safe operation of vessels under pressure.
15. PB 03-584-03 Rules of design, manufacture, and acceptance of welded steel vessels and apparatuses.
16. PNAE G-7-002-86 Norms of strength calculation for equipment and pipelines of nuclear power plants.
17. PB 03-583-03 Rules for development, manufacture, and application of membranous protection devices.
18. 3HM1002.00.000P1.4. Bearing stress calculation of the concrete foundation plate under the supports and calculation of stops of the hydraulic cylinder for horizontal movement of the MPD magnet.
19. 3HM1002.00.000P1.5. Calculation of the trim coil mounting in the recess on the pole tip of the MPD magnet

20. 3HM1002.00.000P1.6. Stress-strain state calculation of the elements of the structural MPD magnet elements and the platforms for the movement of the magnet poles considering the weight load of the disc calorimeters.
21. 3HM1002.00.000P3.1. Calculation of the cryogenic parameters of the superconducting MPD magnet winding cooled in natural convection mode of liquid helium
22. 3HM1002.00.000TO. Technical description of the MPD magnet. Version of 2013

APPENDIX 1. SUPERBOLTS

SUPERBOLT fasteners (<http://www.superbolt.com/products.php>) are used for obtaining a high tightening force without producing a torque in studs (Fig. A1.1).



Fig. A1.1. Jamnut Tensioners

Types of these special fasteners are presented in Table A1.1. In the solenoid yoke design the barrel beams are supposed to be fastened to the support rings by M48 studs with the corresponding SJX-M48-4.5/w supernuts (see Table A1.2). These supernuts are used in structures with limited headroom available.

Table A1.1. Range of SUPERBOLT products





















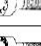



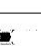




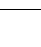

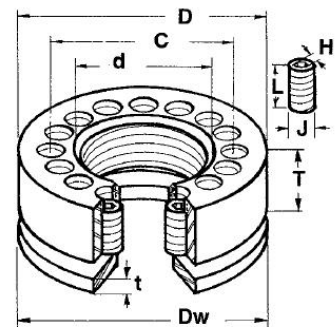
| | | | | | |
|---|--------------------------------------|--|--|---|---|
|  | MT Standard Torquenut® | For machinery applications. Replaces standard hex nuts. |  | H650 Med. temp. Torquenut® | Can be used on most B7 bolts or studs without modifications |
|  | CY High strength Torquenut® | CY tensioners can be used on grade 8 bolts and studs with high preload |  | H650X Med. temp. Torquenut® with Moly jackbolt lube | For bolts or studs at medium temperature. Features less jackbolts |
|  | MTSX Ultra high strength | For extra high loads. Torquenut |  | H650T, H650TX Med. temp. Torquenut® | For ambient and medium high temp. applications where space is limited |
|  | SJX Compact Jamnut | Where limited headroom is available. |  | H1215 High temp. Torquenut® Corrosion resistant | For high temp. applications where limited space is available |
|  | SMX Mill Motor Nut | For coupling and brake wheels on 600 and 800 series Mill Motors |  | H1216 High temp. Torquenut® Corrosion resistant | For high temp. applications where adequate space is available |
|  | NI Bearing Locknut | For direct replacement of std. AN series bearing locknuts |  | H1218 Stainless Steel Torquenut® Corrosion resistant | For food, corrosion, nonmagnetic applications and high temperatures |
|  | MTA Armored Torquenut® | For applications where jackbolts need to be protected from damage |  | High Temp. Bolting System Reduced diameter inconel studs at high prestress | Valves, steam flanges, steam turbines |
|  | STUDS Studs | OEM quality studs from all materials. Rolled threads to 6" dia. |  | Nuclear Series Approved nuclear materials | Valves, pumps, heaters, flanges, manways |
|  | EB Radial Expansion Bolts | To replace fitted bolts for large machines such as turbine couplings |  | Monel Series Approved marine and navy materials | Various naval and salt water applications |
|  | CN Crosshead Jamnuts | For reciprocating compressor crosshead connection. |  | Corrosion Protection Various platings available | wet applications or chemical service |
|  | SP Piston Endnuts | Low torque method to tighten piston to piston rods on all types of cylinders |  | Thrust Collars and Specials | |
|  | SB8 Standard Torquebolts® | Std. bolt type tensioner used mostly in Grade 5 and B7 applications |  | Tools Commercial and custom sockets | Custom sockets for higher torque values |
|  | SB12 High strength Torquebolts® | High strength bolt type tensioner used in demanding applications (Grade 8) |  | Lube JL-G (Graphite Lube) JL-M (Moly Lube) | For std. and high temp lube. For low torque on large jackbolts. |
|  | SBU High Strength Ultrabolts | The worlds strongest bolts made from exotic materials |  | Caps Plastic Caps, Metal Caps | Low cost plastic. avail. for most sizes. Metal caps designed and made to order. |
|  | SSJX Torquebolts® with set screws | Bolt type tensioners that fit in a std. counterbore of socket head capscrews | | | |
|  | SX8 Flexnuts | These nuts relieve the stress concentration on high strength bolts | | | |
|  | SX12 High strength Flexnuts | Designed for use at very high stress levels | | | |

Table A1.2. SJX Jamnut Tensioners (metric)

| Part No | Nominal Thread d In | O.D. D In | Body Thick T In | B.C. C In | OAL L In | Jackbolts | | | Washer | | Standard Pre-Load Moly Lube Lb | Jb Torq Lbft | Wt. Lb |
|--------------------------|---------------------|----------------|-----------------|---------------|---------------|--------------|----------------|--------------|---------------|----------------|--------------------------------|---------------|----------------|
| | | | | | | No Jb n | Size J In | Hex H In | O.D. Dw In | Thick t In | | | |
| Metric | mm | mm | mm | mm | mm | n | mm | mm | mm | mm | Lb | Lbft | Lb |
| SJX-M20-.../w | M20 | 43 | 18 | 31 | 16 | 4 | M8 | 4 | 41 | 3.3 | 20160 | 8.8 | .4 |
| SJX-M24-.../w | M24 | 50 | 18 | 35 | 16 | 6 | M8 | 4 | 48 | 4.8 | 29100 | 8.4 | .5 |
| SJX-M27-.../w | M27 | 56 | 18 | 38 | 16 | 8 | M8 | 4 | 51 | 4.8 | 38280 | 8.3 | .6 |
| SJX-M30-.../w | M30 | 63 | 23 | 44 | 20 | 8 | M10 | 5 | 57 | 4.8 | 46800 | 14 | 1.1 |
| SJX-M33-.../w | M33 | 69 | 23 | 47 | 20 | 10 | M10 | 5 | 60 | 4.8 | 58440 | 14 | 1.3 |
| SJX-M36-.../w | M36 | 75 | 30 | 53 | 25 | 8 | M12 | 6 | 67 | 4.8 | 68640 | 25 | 2.0 |
| SJX-M39-.../w | M39 | 81 | 30 | 56 | 25 | 10 | M12 | 6 | 70 | 4.8 | 82680 | 24 | 2.3 |
| SJX-M42-.../w | M42 | 88 | 30 | 59 | 25 | 10 | M12 | 6 | 73 | 4.8 | 94080 | 27 | 2.7 |
| SJX-M45-.../w | M45 | 91 | 30 | 62 | 25 | 12 | M12 | 6 | 80 | 6.4 | 111120 | 27 | 2.9 |
| SJX-M48-.../w | M48 | 100 | 38 | 70 | 35 | 8 | M16 | 8 | 89 | 6.4 | 124920 | 56 | 4.4 |
| SJX-M52-.../w | M52 | 107 | 38 | 74 | 35 | 10 | M16 | 8 | 95 | 6.4 | 150180 | 54 | 4.9 |
| SJX-M56-.../w | M56 | 113 | 38 | 78 | 35 | 10 | M16 | 8 | 95 | 6.4 | 173220 | 62 | 5.5 |
| SJX-M60-.../w | M60 | 119 | 42 | 82 | 40 | 10 | M16 | 8 | 108 | 6.4 | 197520 | 71 | 6.7 |
| SJX-M64-.../w | M64 | 126 | 42 | 86 | 40 | 12 | M16 | 8 | 114 | 8 | 229440 | 69 | 7.4 |
| SJX-M72-.../w | M72 | 151 | 46 | 100 | 45 | 12 | M20 | 10 | 121 | 8 | 299640 | 114 | 12 |
| SJX-M80-.../w | M80 | 157 | 52 | 108 | 45 | 12 | M20 | 10 | 133 | 10 | 379140 | 144 | 14 |
| SJX-M90-.../w | M90 | 177 | 64 | 124 | 60 | 12 | M24 | 12 | 152 | 10 | 491700 | 220 | 22 |
| SJX-M100-.../w | M100 | 183 | 76 | 134 | 60 | 14 | M24 | 12 | 163 | 10 | 618600 | 238 | 26 |
| SJX-M110-.../w | M110 | 202 | 79 | 144 | 60 | 16 | M24 | 12 | 175 | 10 | 741195 | 249 | 33 |
| SJX-M120-.../w | M120 | 208 | 79 | 154 | 60 | 16 | M24 | 12 | 188 | 10 | 744413 | 250 | 34 |
| SJX-M140-.../w | M140 | 221 | 91 | 174 | 60 | 18 | M24 | 12 | 213 | 13 | 833490 | 249 | 41 |
| SJX-M160-.../w | M160 | 240 | 95 | 194 | 60 | 20 | M24 | 12 | 239 | 13 | 932190 | 251 | 47 |



SJX Jamnuts are used for applications where limited headroom and/or limited thread engagement are required. On request, Jamnuts are available with Superbolt's patented captive set screws.

APPLICATIONS: Hydraulic cylinders, shaft mounts, pipe flanges, and inaccessible places.

APPENDIX 2. ROLLER SKATES

Low-profile roller skates with a high carrying capacity manufactured by the Boerkey Company (Germany) (<http://www.boerkey.com/>) are used to move heavy loads.

To move the MPD magnet and its poles, two types of roller skate were chosen:

- Models Vlv AS-H-50CrV4-FR-K (Fig. A2.1) and Vlv AS-H-50CrV4 (Fig. A2.2) to carry the 500-t load.
- Models V AS-H-50CrV4-FR-E and V AS-H-50CrV4 to carry the 85-t load.

The skates for the identical load differ by having guide rollers.

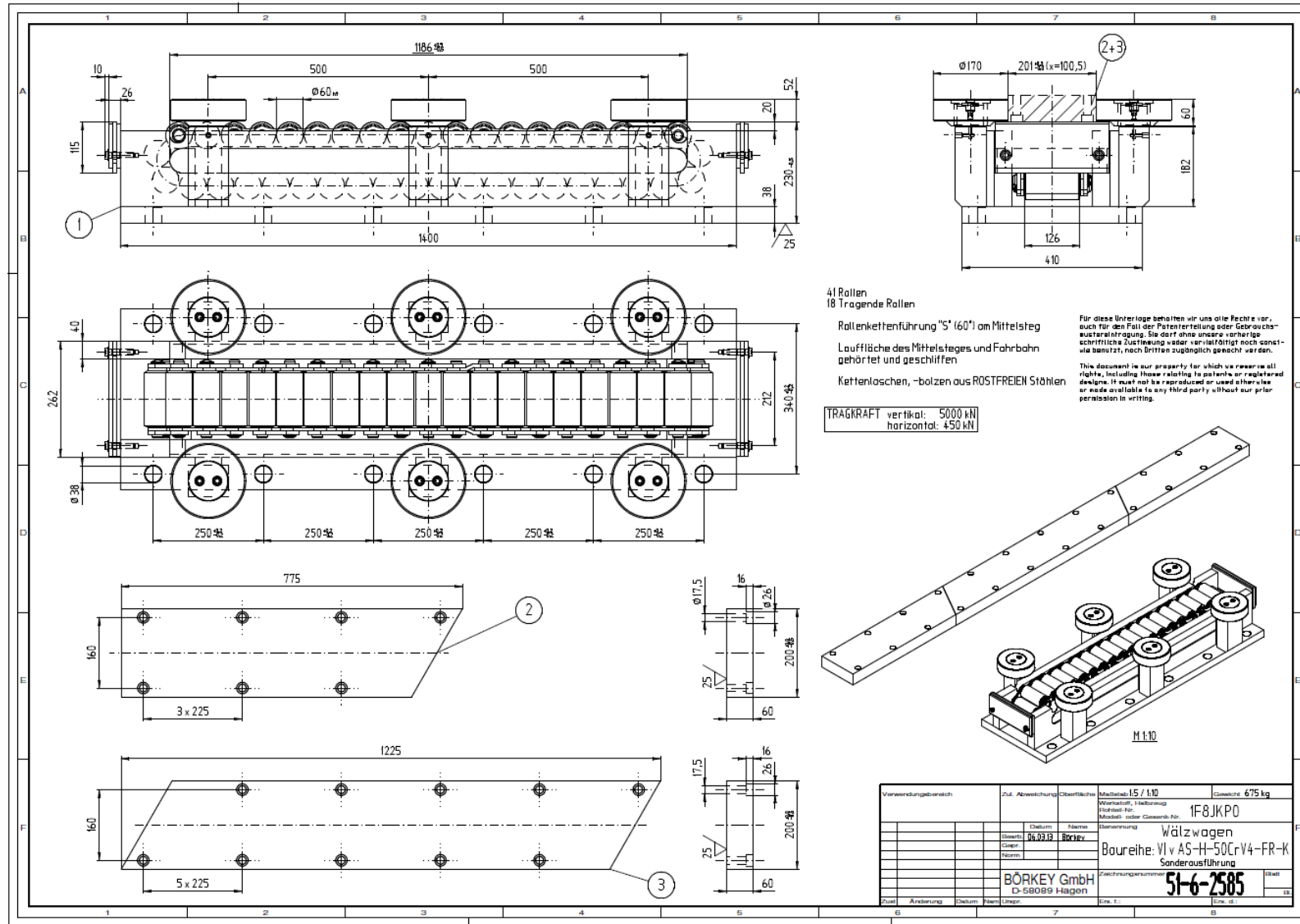


Fig. A2.1. Boerkey Vlv AS-H-50CrV4-FR-K roller skate with guide rollers to carry a load of 500 t

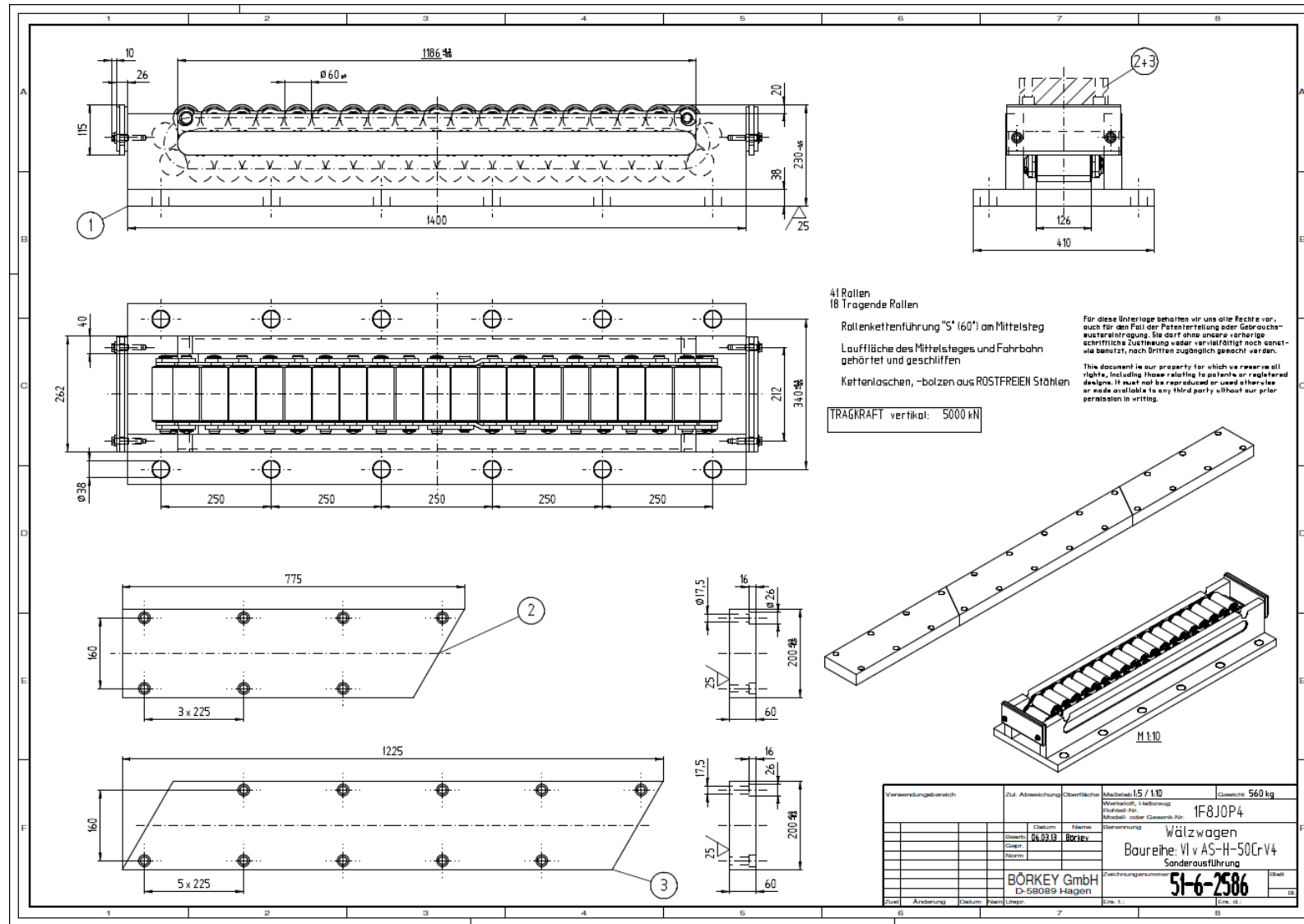


Fig. A2.2. Boerkey Vlv AS-H-50CrV4 roller skate without guide rollers to carry a load of 500 t

APPENDIX 3. INSTRUMENTATION SYSTEM HARDWARE

The CompactRIO platform is an architecture with open access to low-level hardware resources. It combines a real-time processor, a reconfigurable FPGA, and industrial input/output modules with built-in signal conditioning, which can be directly connected to sensors and are hot-swappable (while the controller is in operation).

The NI CompactRIO platform consists of more than ten cRIO-90xx real-time controllers based on heavy-duty floating-point processors, a family of cRIO-910x four-slot and eight-slot reconfigurable chassis housing an FPGA with 1 to 3 million logic gates, and over 50 I/O modules of various types, from thermocouple modules with a signal measuring range of ± 80 mV to 250 VAC/VDC universal digital input modules. The CompactRIO-based system combines a built-in real-time processor and a high-capacity FPGA for reconfigurable input/output. The FPGA nucleus of this system has built-in mechanisms for transferring data to the built-in real-time processor to be subsequently analyzed, processed, and stored and also for communicating with external computers. The CompactRIO platform allows direct hardware access to the electric circuits of each I/O module through the simplest functions. Each of the I/O modules has built-in connectors, a signal conditioning system, conversion circuits (like DAC and ADC), and galvanic isolation circuits. The reconfigurable FPGA built into the chassis is used to control, synchronize, and start the digital and analogue signal input/output. In this system the FPGA is connected to all measuring modules arranged in the star bus topology, which gives direct access to each of them and allows their flexible and precise synchronization, while the local PCI bus provides high-capacity connection between the FPGA and the real-time processor. The CompactRIO systems with a real-time controller use industrial Pentium processors with frequencies from 266 to 800 MHz. It runs Real-Time applications with the deterministic execution time for particular operations and participates in building hard real-time multithreaded control instrumentation systems. The controller also communicates with other controllers and the distributed network server through the Ethernet (10/100/1000 MB/s) interface and, in addition to the special-purpose software of a particular subsystem, has built-in WEB and FTP servers.

Figure A3.1 shows the CompactRIO-based systems consisting of a controller and I/O modules in the four-slot and eight-slot chassis.



Fig. A3.1. CompactRIO-based systems with a controller and I/O modules in the four-slot and eight-slot chassis

Each CompactRIO module consists of a built-in signal conditioning system, screw terminals, and BNC or D-Sub connectors. The range of currently available I/O modules is wide enough to meet the requirements of the projected control system, including the thermocouple module with an input range of ± 80 mV, simultaneous multichannel analogue I/O modules with a range of ± 10 V, digital I/O modules with an industrial voltage of 24 V and current up to 1 A, TTL digital modules with a controllable encoder output, and 250 Vrms universal digital input modules. A built-in signal conditioning system and support of an extended voltage range and various industrial types of signals allows sensors and controlled devices to be directly connected to the modules. Built on this platform, the distributed magnet control system is capable of solving various problems from simple logic of industrial automatic equipment to complex algorithms of multiloop PID controllers in the superconducting coil cryostatting system and integrating all subsystems into a single complex with centralized control.

The CompactRIO-based systems can be used at temperatures ranging from -40 to $+70^{\circ}\text{C}$ in potentially hazardous locations where there is a danger of explosion (Class I, Div 2) and withstand an impact load up to 50 g. Most modules have insulation up to 2300 Vrms. Each component is supplied with a set of the safety, EMC, climate, and environmental certificates.

- Operating temperature range -40 to $+70^{\circ}\text{C}$
- Insulation up to 2300 Vrms
- Impact loads up to 50 g
- International safety, EMC, climate, and environmental certificates
- Class I, Division 2 Hazardous Area Certification
- Supply voltage 11 to 30 V
- Standard power consumption 7 to 10 W (max. 17 W)

APPENDIX 4. RECONFIGURABLE INSTRUMENTATION SYSTEM SOFTWARE

Reconfigurable instrumentation systems usually consist of four main components:

- Reconfigurable application on the FPGA for signal input/output, implementation of communication protocols, and control over external systems and equipment.
- Cycle with the deterministic execution time for floating-point operations, signal processing, analysis, and step-by-step decision making.
- Normal priority cycle for transferring data to the real-time controller, remotely accessing the application through the Web, and communicating over Ethernet and a serial interface.
- Network control computer with a remote user interface, which stores and processes the acquired data.

Depending on the application requirements, one or all components are employed (Fig. A4.1).

In the system under discussion, cycles with critical execution time are used for synchronized input/output of data from primary transducers, computation of control actions in the PID controller loops, and processing of time-critical interrupts from other controllers of the complex. Normal priority cycles are used for communication between controllers and preparation of data for display and logging. The National Instruments reconfigurable input/output technology allows individual elements of the system to be developed at the hardware level using the reconfigurable FPGA with a resolution of 25 ns for timing and synchronization of instrumental circuits. Multiloop digital PID controllers will operate at a rate up to 100 kHz. The FPGA-based devices have a reconfigurable digital architecture with an array of configurable-logic blocks (CLB) surrounded by peripheral I/O units. Within the FPGA signals can be arbitrarily routed by controlling the programmable switches and the switching lines.

The applied software for the distributed system is developed for the real-time operating system environment. Each controller executes real-time data input from the primary transducers and external subsystem interfaces, data output to the actuators and external subsystem interfaces, and processing of software and hardware interrupts triggered by various events, signals from other controllers, and control commands from the upper-level subsystems. Control signals can arrive from other controllers, emergency control devices, and the operator's control panel and are processed by various controllers according to the given algorithm.

Final requirements on the software will be formulated after all sensors, actuators, and external interfaces are specified and the algorithms of the subsystems and the system as a whole are worked out in detail.

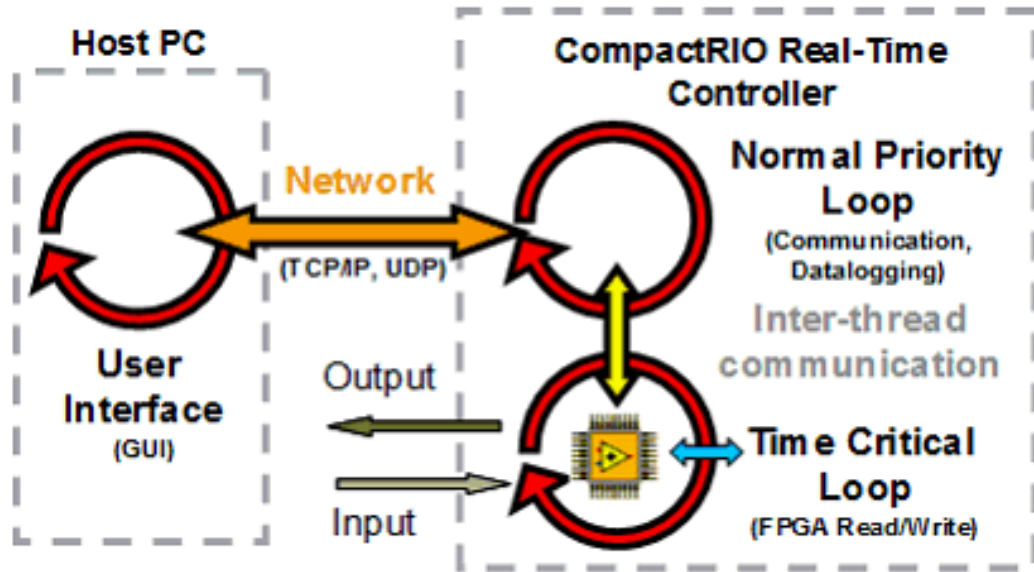
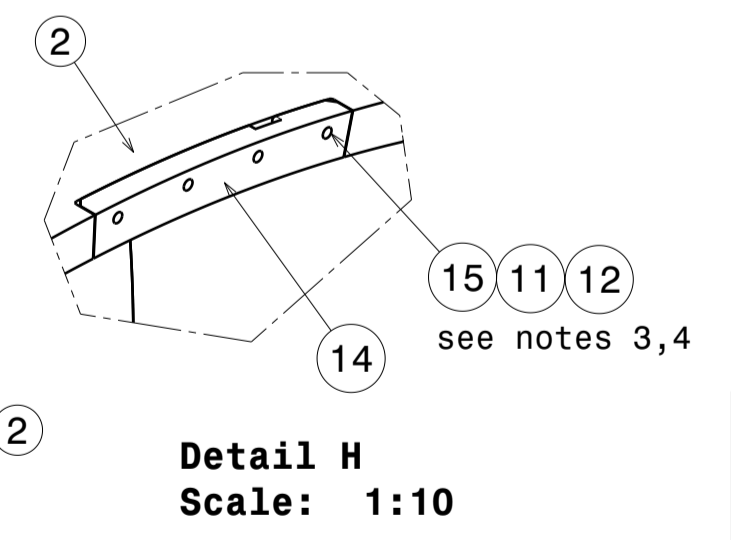
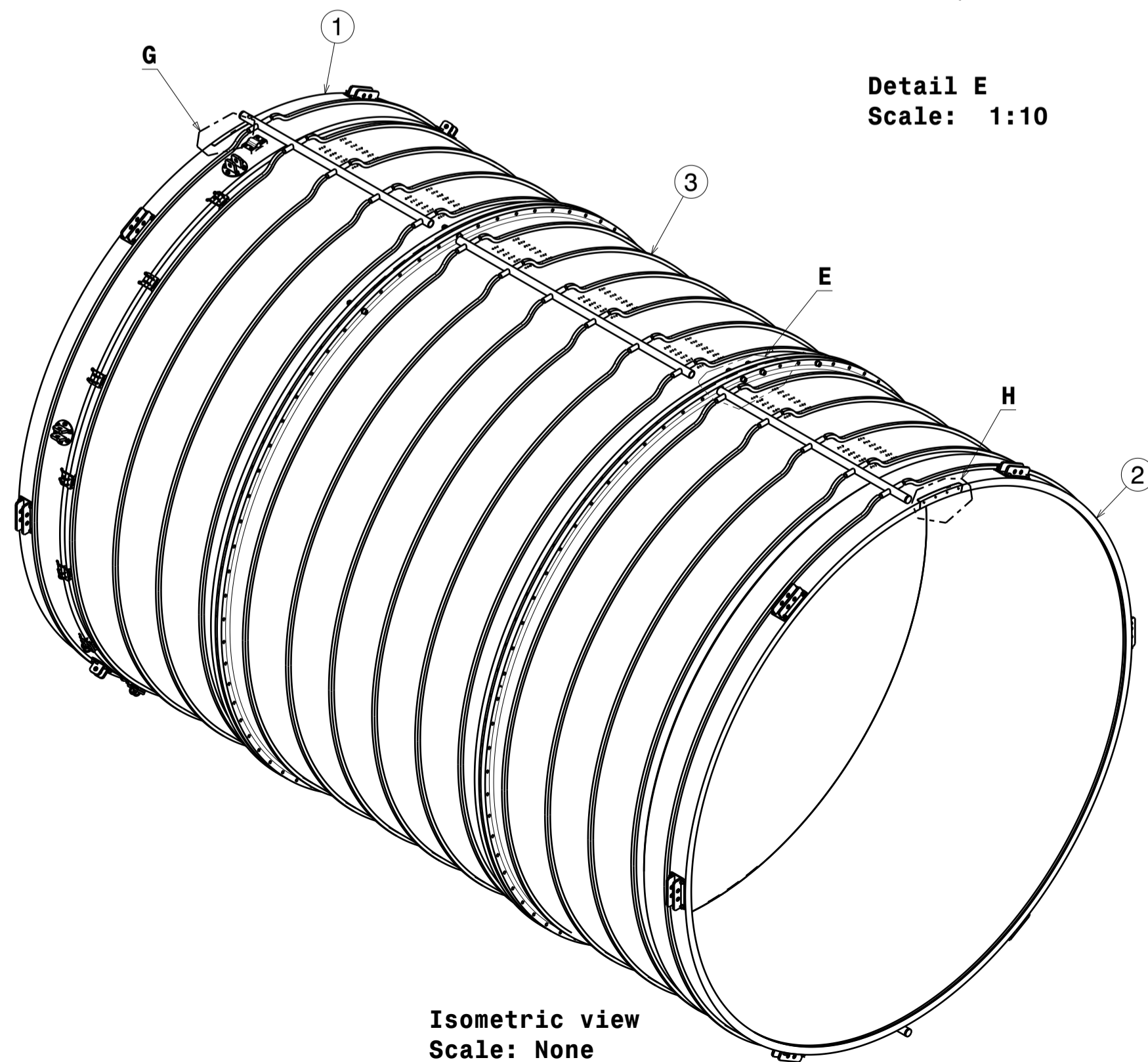
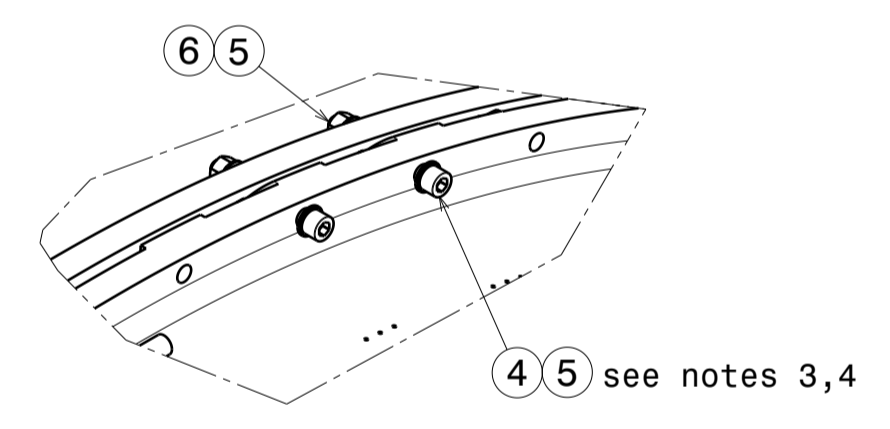
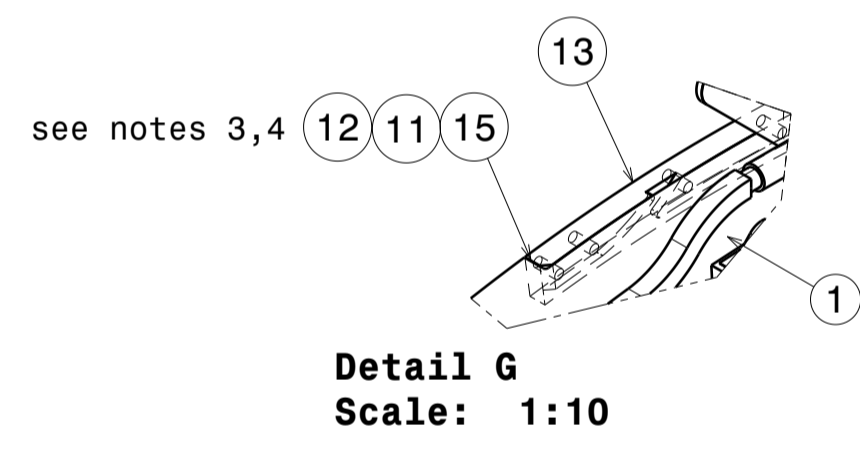
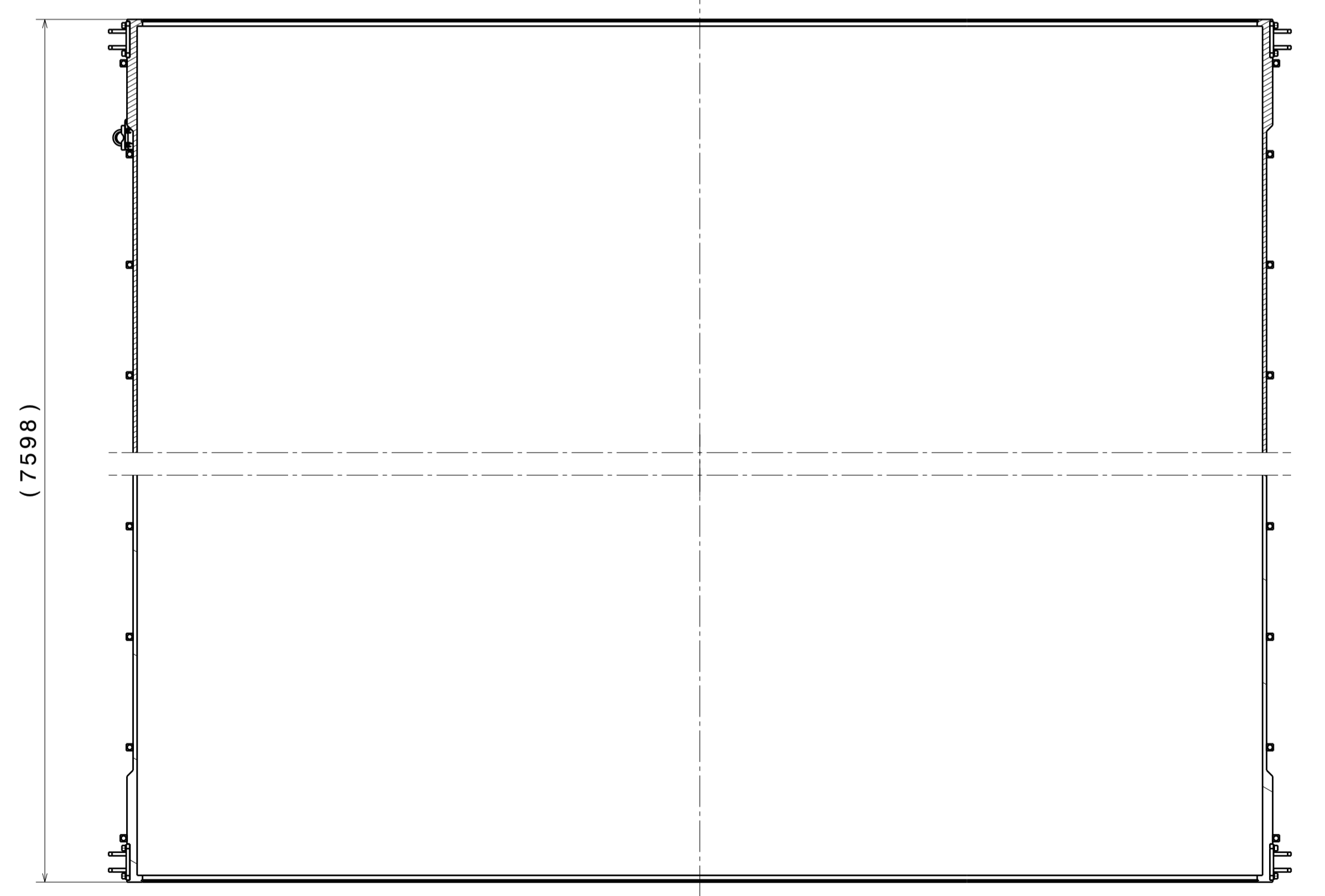
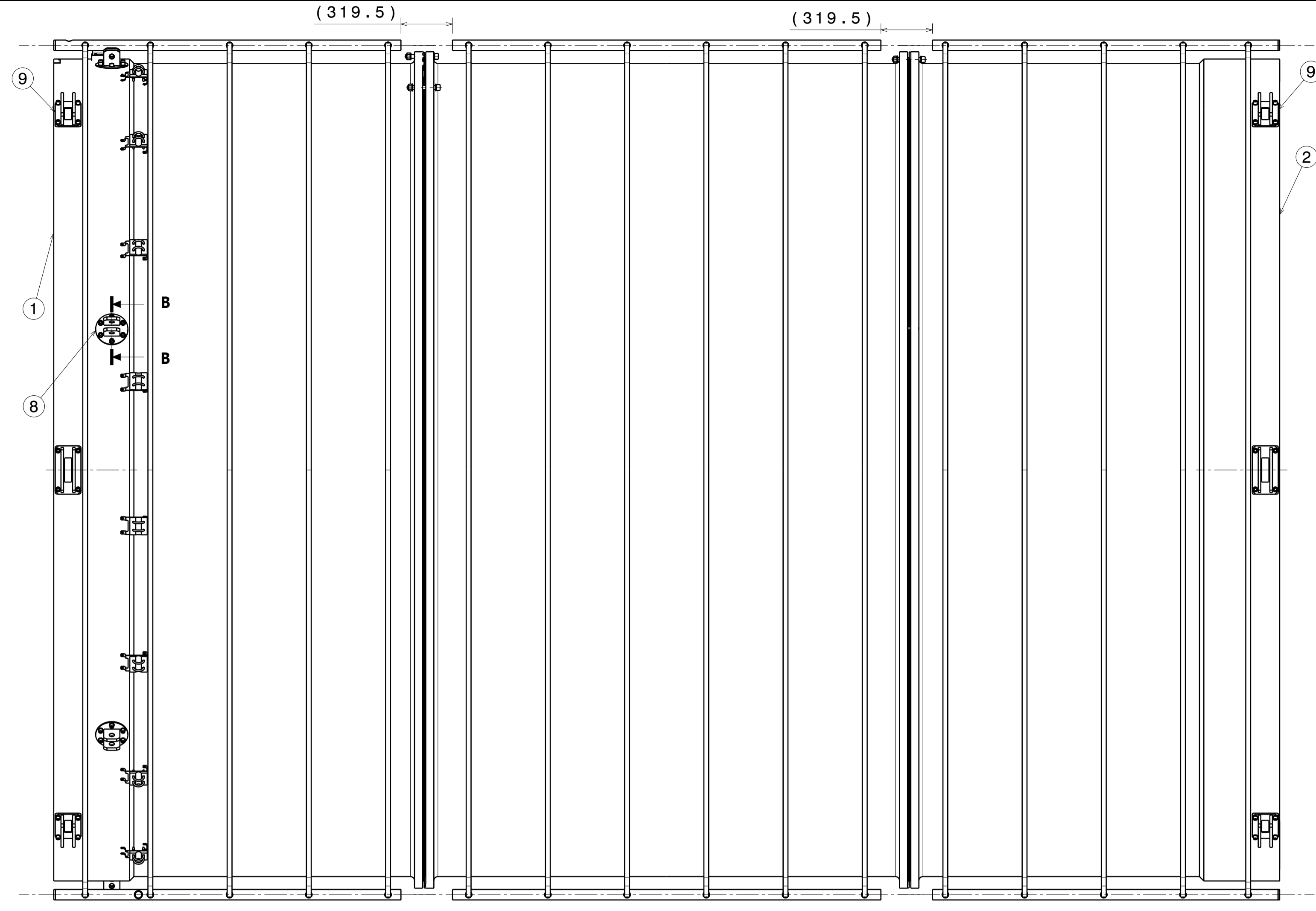
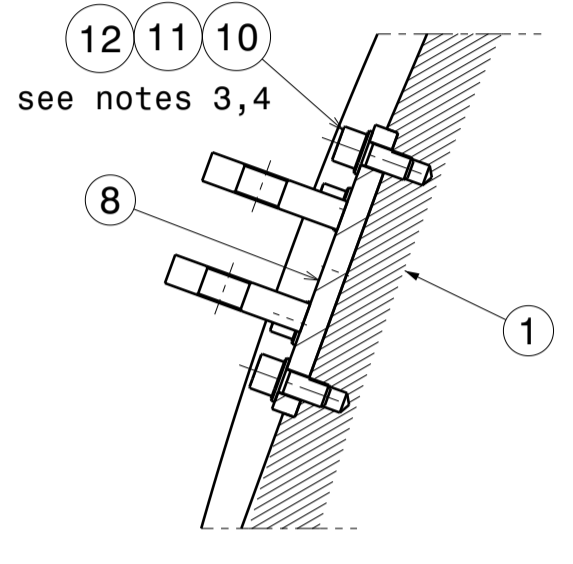
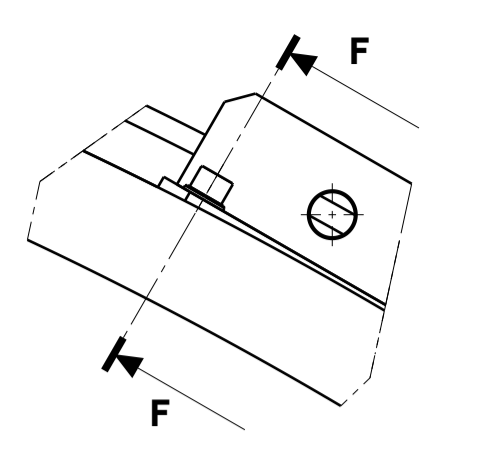
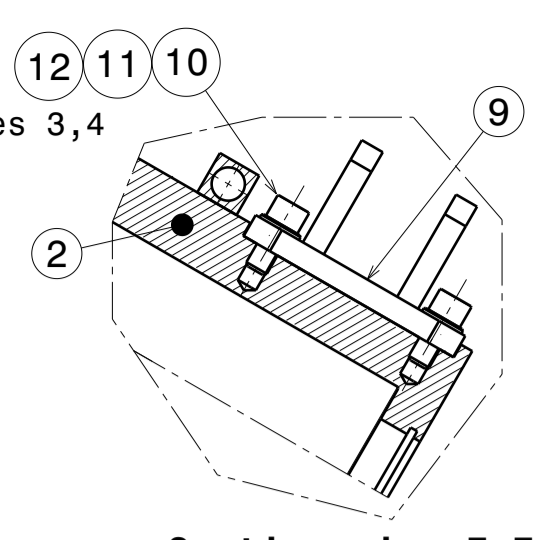
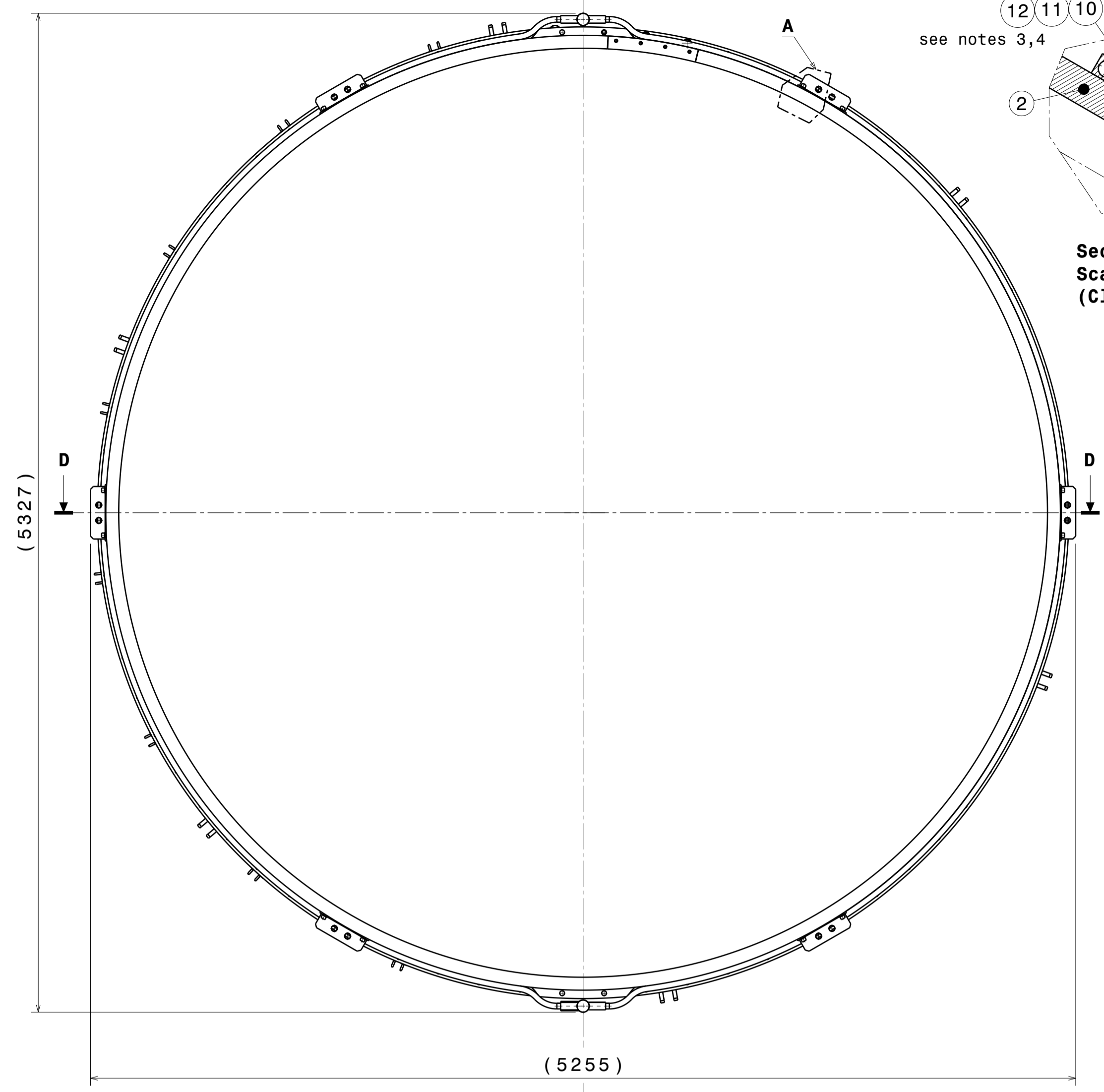


Fig. A4.1. Real-time software components implemented on the CompactRIO platform with an FPGA

APPENDIX 5. ASSEMBLY DRAWINGS OF THE SOLENOID



NOTE/REMARKS:

- 1) DISEGNO ASSIEME DI RIFERIMENTO: 600RM19699 / REFERENCE ASSEMBLY DRAWING see dwg. 600RM19699
- 2) MATERIALI CERTIFICATI SECONDO UNI-EN 10204-3.1 / MATERIALS CERTIFIED AFTER UNI EN 10204-3.1.
- 3) COPPIA DI SERRAGGIO SECONDO TAB.1 / TIGHTENING TORQUE ACCORDING TO TAB.1

| N° ITEM | QUANTITA' quantity | DEFINIZIONE definition | RIFERIMENTO reference | MATERIALE material | MASSA [kg] mass [kg] |
|---------|--------------------|---------------------------------|-----------------------|--------------------|----------------------|
| 15 | 8 | SCREW M16x65 | ISO 4762 | A2/70 | 1.0 |
| 14 | 1 | JUNCTION CLOSURE CASE #2 | 600RM19648 POS.2 | | |
| 13 | 1 | JUNCTION CLOSURE CASE #1 | 600RM19648 POS.1 | | |
| 12 | 92 | ELASTIC WASHER (GROWER) FOR M16 | DIN 127 B | A2 | 1.0 |
| 11 | 92 | WASHER FOR M16 | ISO 7092 | A2 | 1.0 |
| 10 | 84 | SCREW M16x40 | ISO 4762 | A2/70 | 8.4 |
| 9 | 12 | RADIAL TIE-ROD SUPPORT | 600RM19654 | | |
| 8 | 6 | LONGITUDINAL TIE-ROD SUPPORT | 600RM19653 | | |
| 7 | 46 | PIN Ø16x120-H0 | ISO 2809-B | A-4095 | |
| 6 | 144 | NUT M24 | ISO 4032 | AA 7075-T73 | 4.9 |
| 5 | 288 | WASHER Ø24x44 | ISO 7092 | AA 7075-T73 | 3.3 |
| 4 | 144 | SCREW M24X180 | ISO 4762 | AA 7075-T73 | 35.4 |
| 3 | 1 | CENTRAL MODULE | 600RM19506 | | |
| 2 | 1 | SIDE MODULE #2 | 600RM19508 | | |
| 1 | 1 | SIDE MODULE #1 | 600RM19507 | | |

| N° | ITEM | QUANTITA' | DEFINIZIONE | RIFERIMENTO | MATERIALE | MASSA |
|----|------|---------------------------------|------------------|-------------|-----------|-------|
| 15 | 8 | SCREW M16x65 | ISO 4762 | A2/70 | 1.0 | |
| 14 | 1 | JUNCTION CLOSURE CASE #2 | 600RM19648 POS.2 | | | |
| 13 | 1 | JUNCTION CLOSURE CASE #1 | 600RM19648 POS.1 | | | |
| 12 | 92 | ELASTIC WASHER (GROWER) FOR M16 | DIN 127 B | A2 | 1.0 | |
| 11 | 92 | WASHER FOR M16 | ISO 7092 | A2 | 1.0 | |
| 10 | 84 | SCREW M16x40 | ISO 4762 | A2/70 | 8.4 | |
| 9 | 12 | RADIAL TIE-ROD SUPPORT | 600RM19654 | | | |
| 8 | 6 | LONGITUDINAL TIE-ROD SUPPORT | 600RM19653 | | | |
| 7 | 46 | PIN Ø16x120-H0 | ISO 2809-B | A-4095 | | |
| 6 | 144 | NUT M24 | ISO 4032 | AA 7075-T73 | 4.9 | |
| 5 | 288 | WASHER Ø24x44 | ISO 7092 | AA 7075-T73 | 3.3 | |
| 4 | 144 | SCREW M24X180 | ISO 4762 | AA 7075-T73 | 35.4 | |
| 3 | 1 | CENTRAL MODULE | 600RM19506 | | | |
| 2 | 1 | SIDE MODULE #2 | 600RM19508 | | | |
| 1 | 1 | SIDE MODULE #1 | 600RM19507 | | | |

| | | | | |
|------------------|----------------|--------------------|-------------------|-----------------|
| progetto/project | cliente/client | materiale/material | quantita/quantity | massa/mass [kg] |
| MPD Dubna | JINR | | | 8445 |

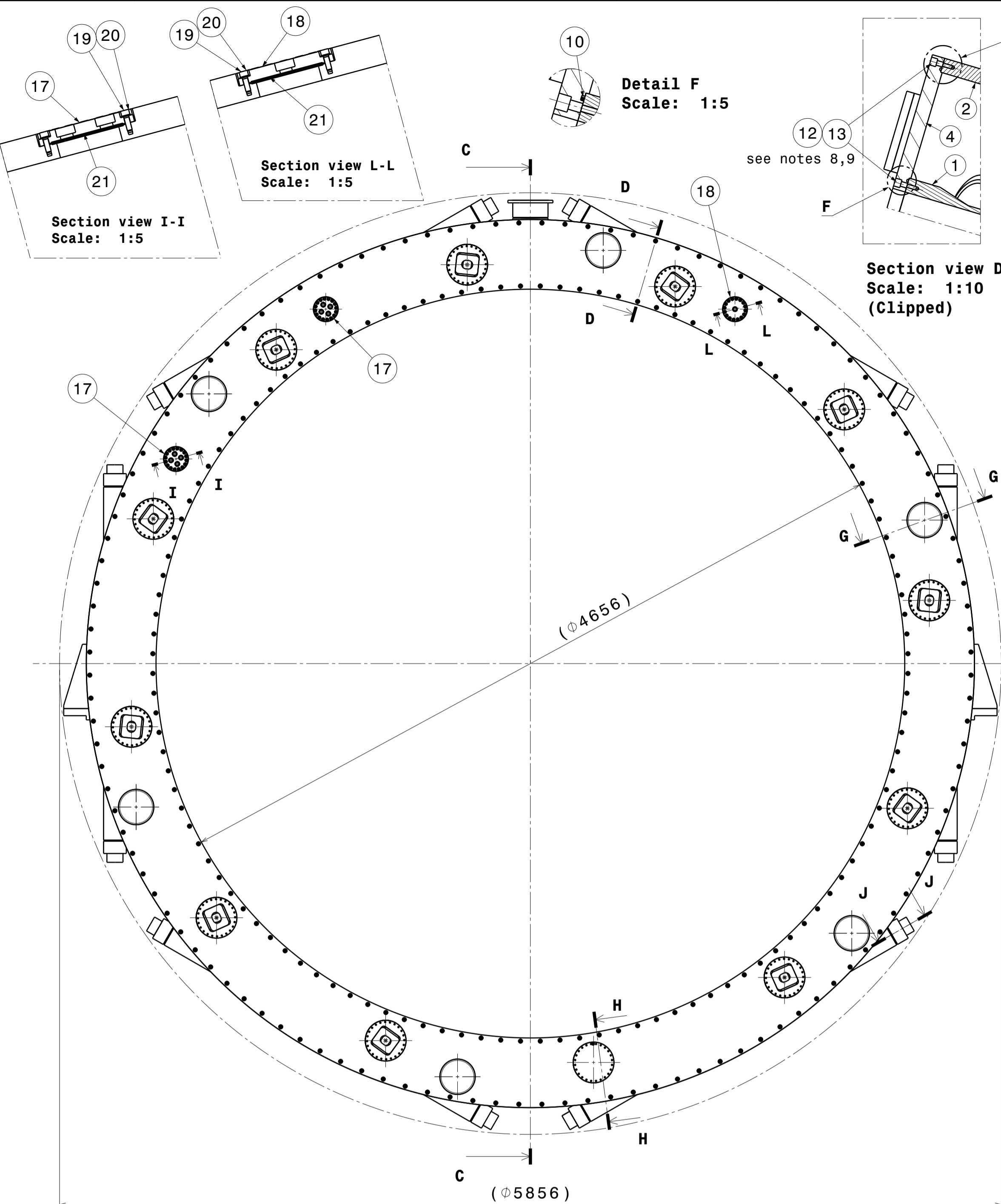
| | | | | | |
|-------------|-----------|---------|-------|--------------|------|
| commissa n° | emittente | formato | scala | derivato da | rev. |
| 2125 | DIS | A1 | 1:20 | Derived from | |

| | | | |
|---|--|--|-------------------|
| ASG Superconductors | | Mechanical Structure Ass.y | |
| Informazioni strettamente riservate, di proprietà ASG Superconductors S.p.A., da non utilizzare per scopi diversi da quelli per cui sono state fornite. | | Confidential information, property of ASG Superconductors S.p.A., not to be used for any purpose other than that for which it is supplied. | |
| Identificativo/document no. 600RM19505 | | rev. / rev. Foglio 0A 1 | Segue fg. di 1 |

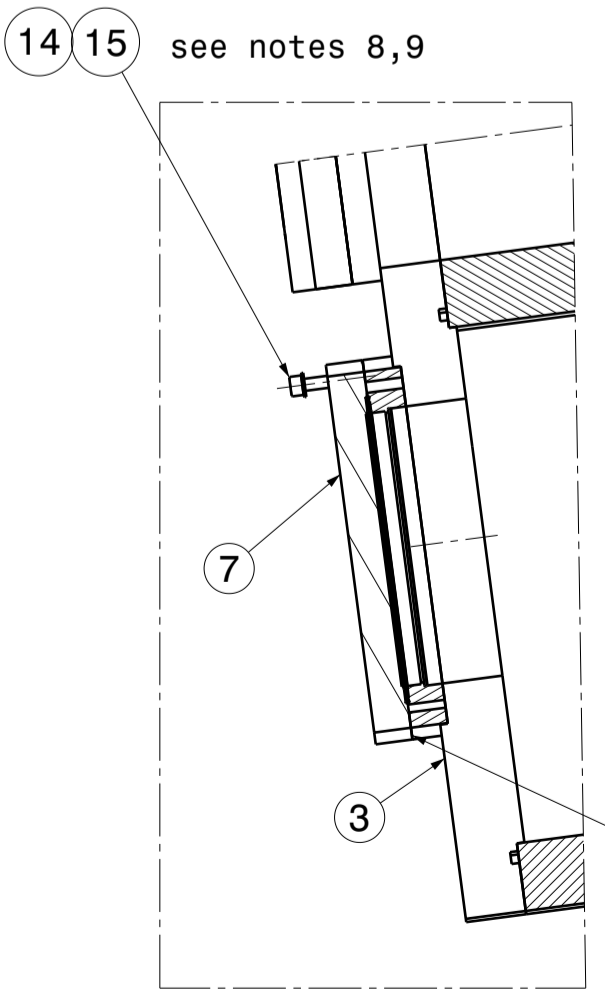
| TYPE | MAT. | T [Nm] |
|------|-------------|--------|
| M16 | A2/70 | 100 |
| M24 | AA 7075-T73 | 345 |

Tab.1: Tightening Torque

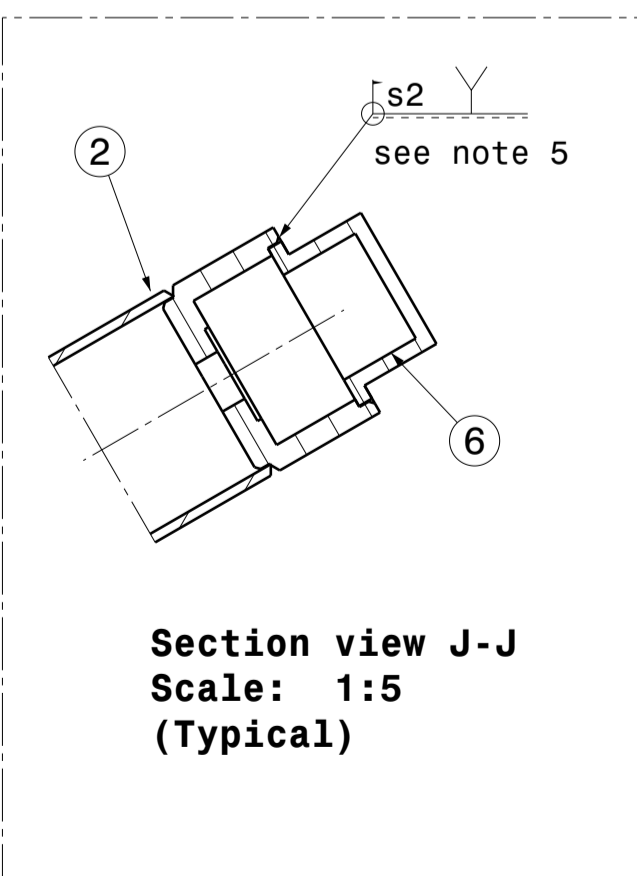
Simboli di rugosità secondo ISO 1302:2002
 Tolleranze di forma e di posizione secondo ISO 2768-2:1998
 Quote di lavorazione senza indicazione di tolleranza secondo ISO 2768-1:1999
 Classi di tolleranza M/K
 Simboli per rugosità secondo ISO 1302:2002
 Shape and position tolerances according to ISO 2768-2:1999
 Tolerances for non-limited dimensions for machining according to ISO 2768-1:1999
 Deviations grade M/K



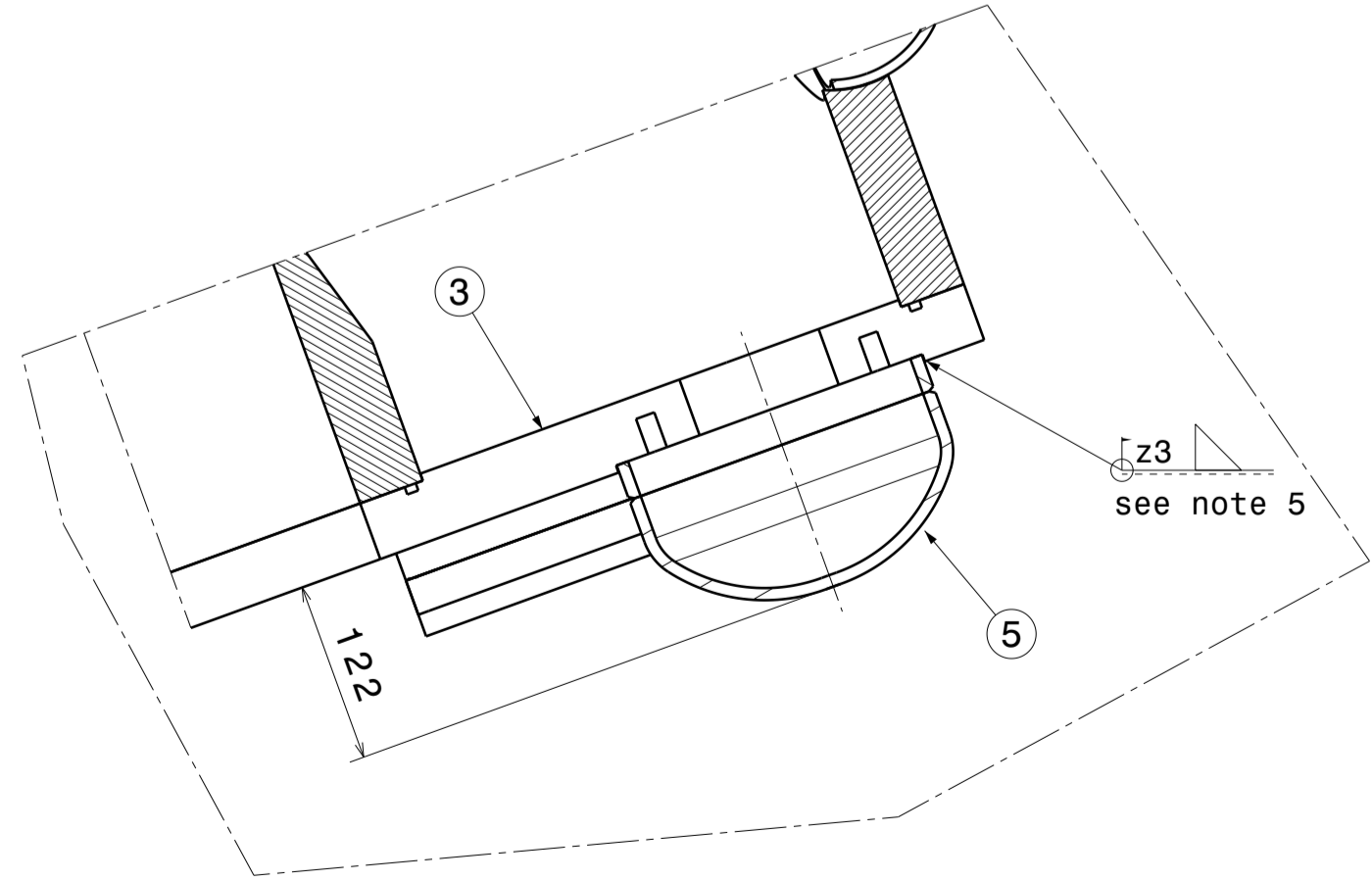
Front view in Operating Configuration
all sections except G-G and details
are typical for both sides



Section view H-H
Scale: 1:5
(Clipped)

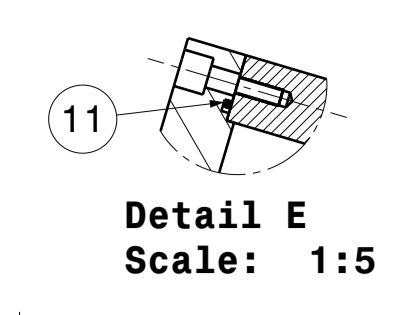


Section view J-J
Scale: 1:5
(Typical)

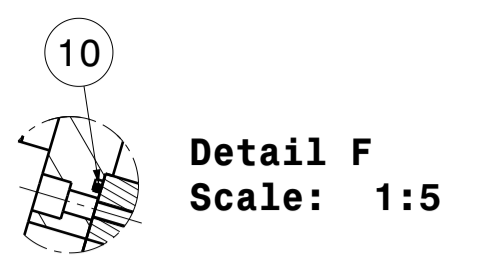


Section view G-G
Scale: 1:5
(Clipped)

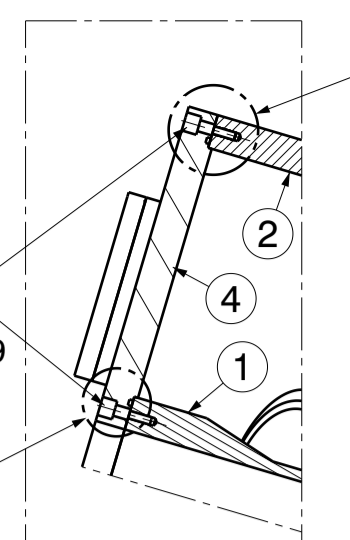
| | | | |
|--|--|--|------------------------------------|
| Simboli di rugosità secondo ISO 1302:2002 | Tolleranze di forma e di posizione sec. ISO 2768-2:1998 | Quote di lavorazione senza indicazioni di tolleranza secondo ISO 2768-1:1989 | Classi di tolleranza μM |
| Simboli for roughness according to ISO 1302:2002 | Shape and position tolerances according to ISO 2768-2:1998 | Tolerances for non-limited dimensions for machining according to ISO 2768-1:1989 | Deviations grade μm |



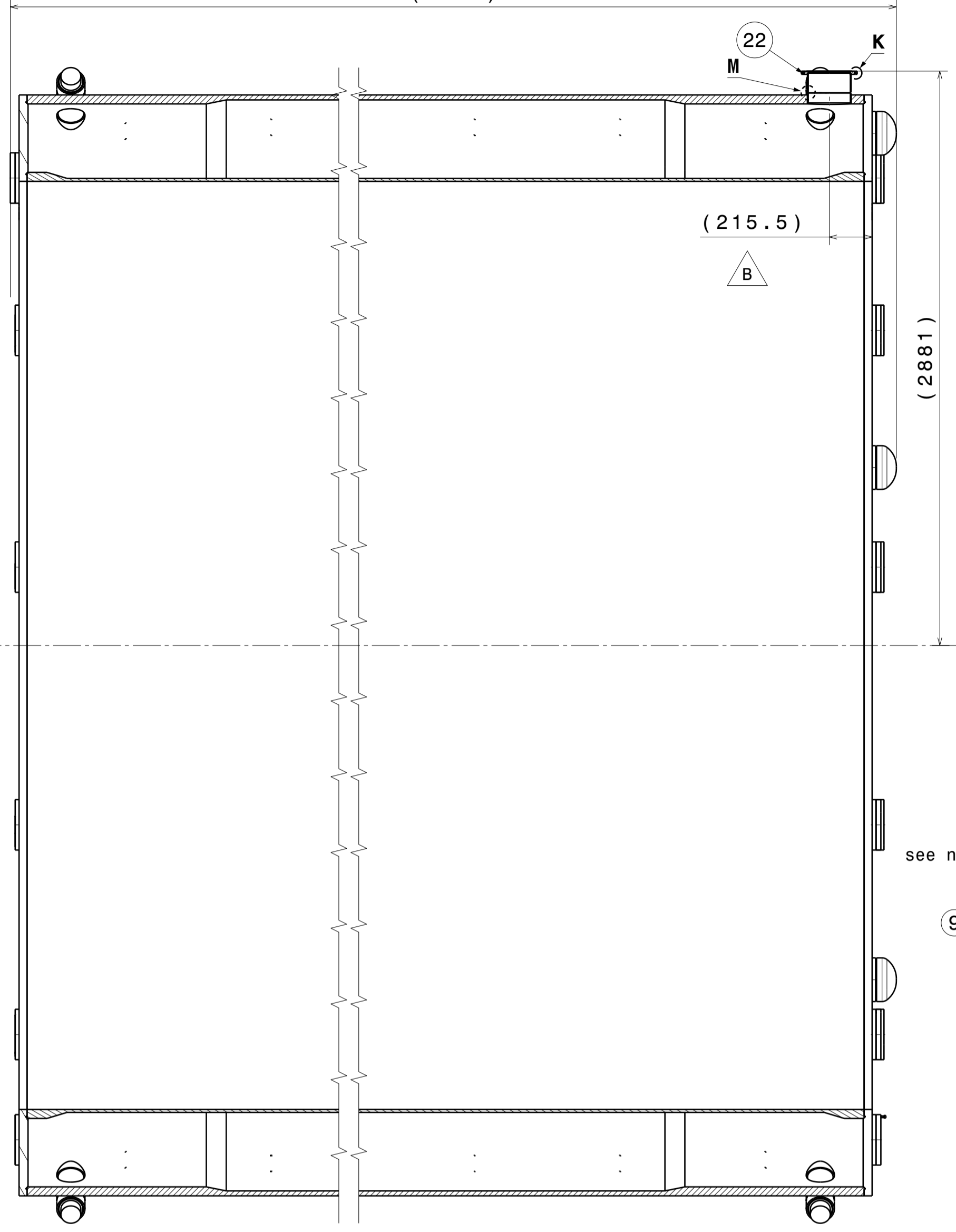
Detail E
Scale: 1:5



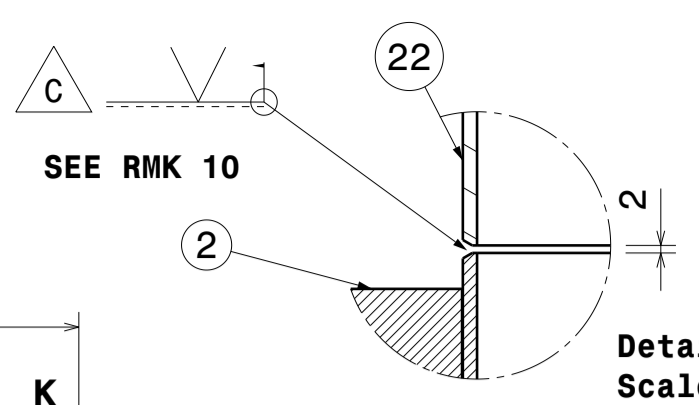
Detail F
Scale: 1:5



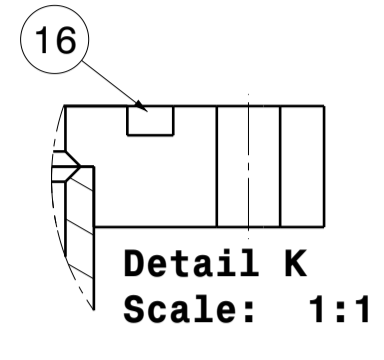
Section view D-D
Scale: 1:10
(Clipped)



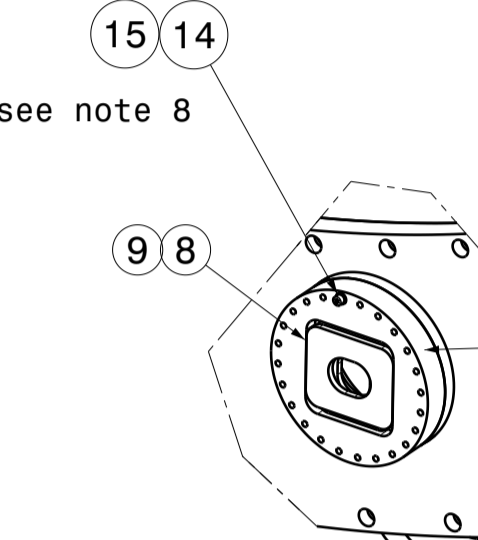
Section view C-C



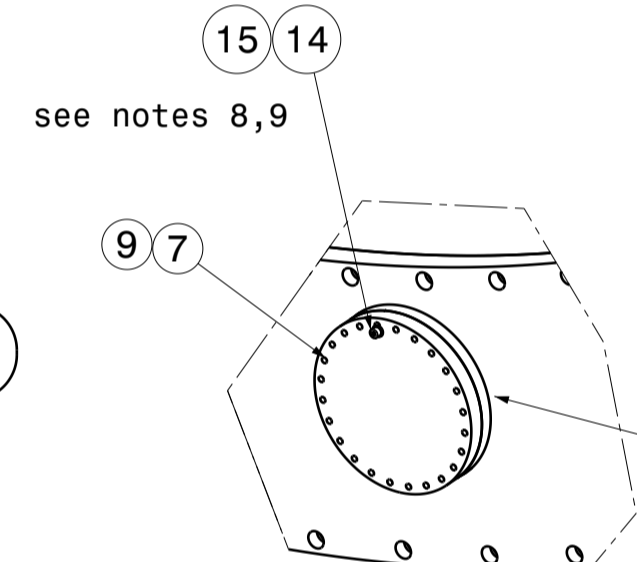
Detail M
Scale: 1:2



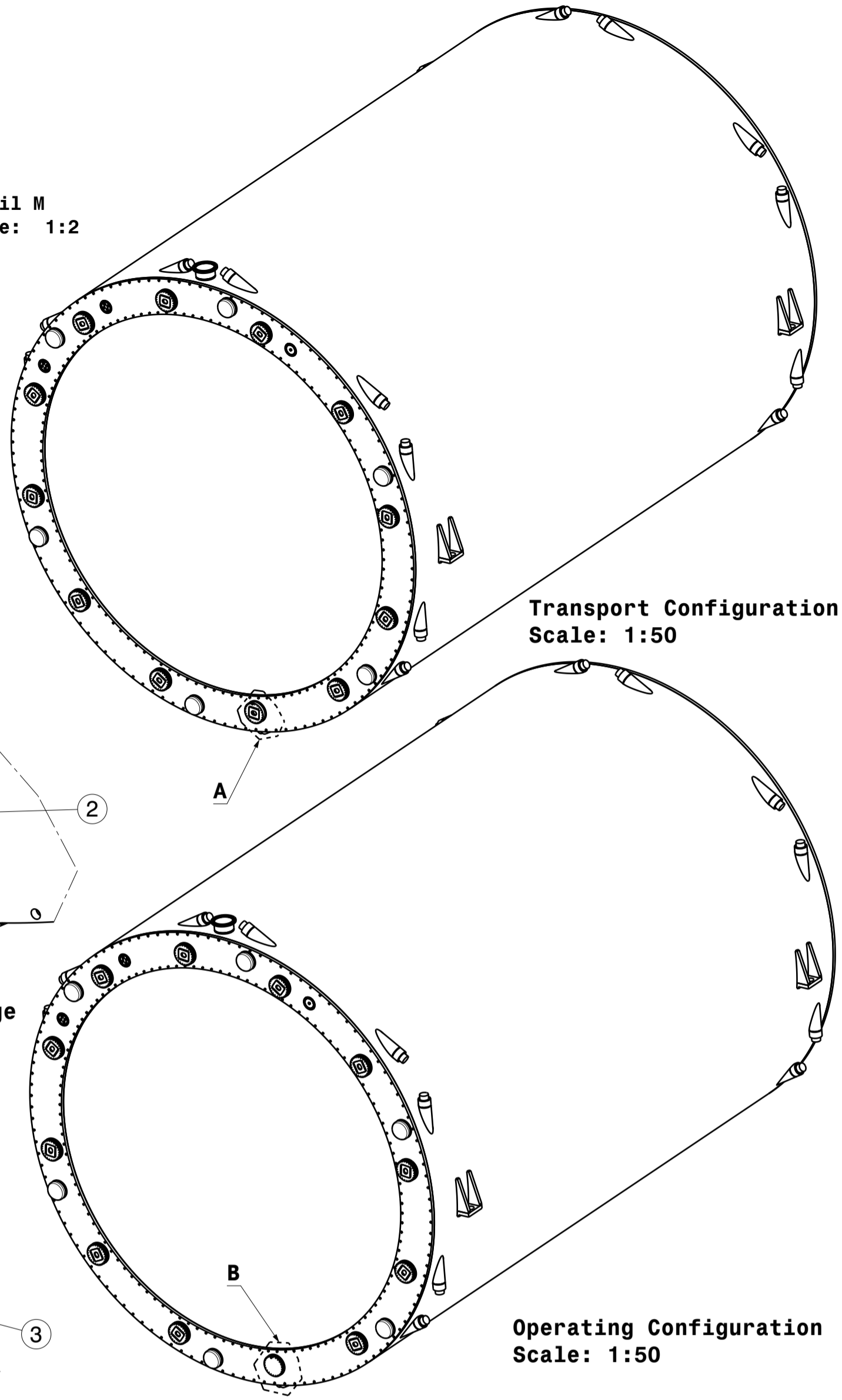
Detail K
Scale: 1:1



Detail A
Scale: 1:10
Transport Flange



Detail B
Scale: 1:10



Transport Configuration
Scale: 1:50

Operating Configuration
Scale: 1:50

Tab.1

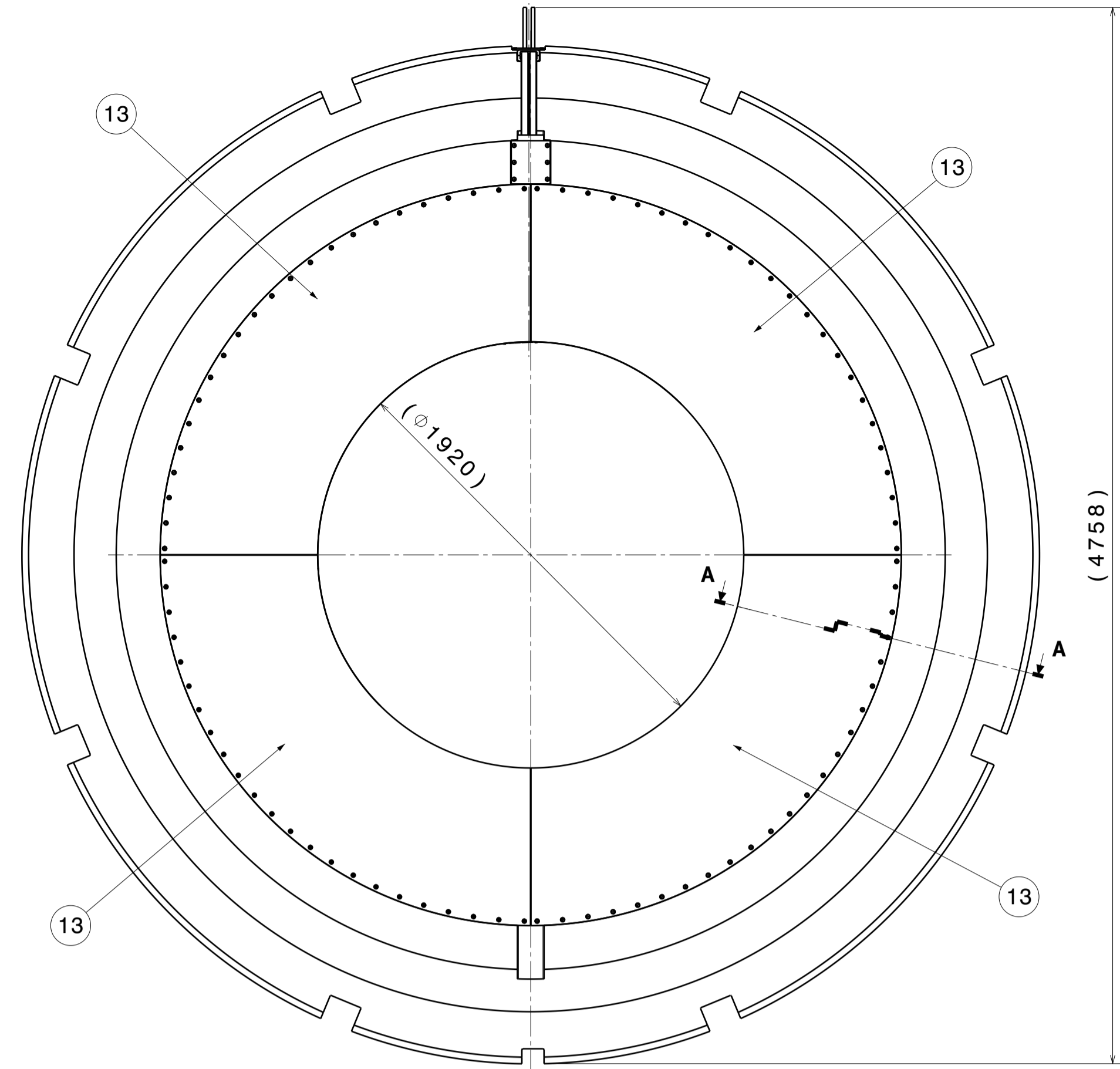
| type | mat. | Torque [Nm] |
|------|--------------------|-------------|
| M8 | A2/70 - AISI 316 L | 12 |
| M12 | A2/70 - AISI 316 L | 40 |

NOTE / REMARKS:

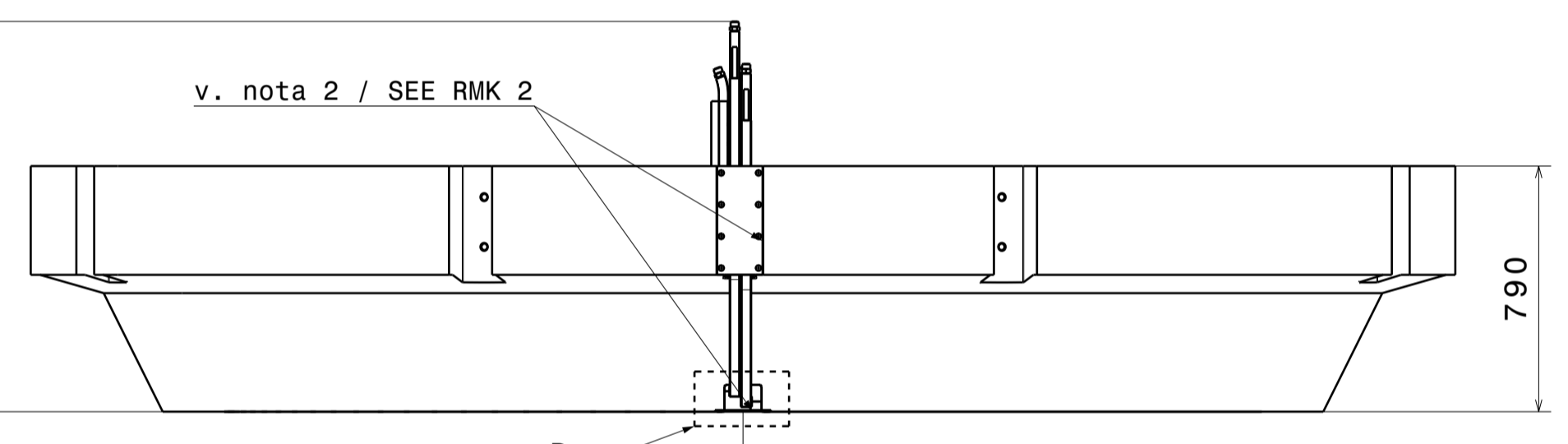
- DISEGNO ASSIEME DI RIFERIMENTO / REFERENCE ASSEMBLY DRAWING: 600RM19730
- ASSEMBLAGGIO FINALE COMPRENSIVO DI TUTTE LE SALDATURE A CURA DI ASG / FINAL ASSEMBLING INCLUDING ALL THE INDICATED WELDINGS BY ASG
- MATERIALI CERTIFICATI SECONDO UNI-EN 10204-3.1 / MATERIALS CERTIFIED AFTER UNI EN 1020-3.1.
- DIMENSIONI RIFERITE A TEMP. AMBIENTE 20 °C / DIMENSIONS ARE REFERRED TO AMB. TEMPERATURE 20 °C
- PREPARAZIONE SALDATURA SECONDO UNI EN 9692-1, CRITERIO DI ACCETTABILITA' SECONDO UNI EN 5817 LIV.B / PREPARATION ACCORDING TO UNI EN 9692-1 ACCEPTANCE CRITERIA UNI EN 5817 LIV.B
- PROGETTO, COSTRUZIONE E COLLAUDO IN CONFORMITA' ALLA NORMATIVA RUSSA PER I RECIPIENTI IN PRESSIONE ("ROSTEKHNADZOR") / DESIGN, MANUFACTURING AND TEST ACCEPTANCE IN AGREEMENT WITH RUSSIAN STANDARD CODE FOR PRESSURE VESSELS ("ROSTEKHNADZOR")
- FORNITURA COMPLETA DI CERTIFICATO DI CONFORMITA' NORMATIVA RUSSA EAC TR CU032 / SUPPLY COMPLETE OF CERTIFICATE OF CONFORMITY RUSSIAN EAC TR CU032.
- COPIA DI SERRAGGIO V. TAB.1 / TIGHTENING TORQUE SEE TAB.1
- APPLICARE BLOCCA FILETTI LOCTITE 243 MEDIA RESISTENZA A CURA DI ASG / APPLY THREAD LOCKER LOCTITE 243 MEDIUM STRENGTH BY ASG
- SALDATURA A CURA DI ASG/WELD TO BE PERFORMED BY ASG

| N° ITEM | QUANTITA' quantity | DEFINIZIONE definition | RIFERIMENTO reference | MATERIALE material | MASSA [kg] mass [kg] |
|---------|--------------------|-----------------------------------|--------------------------|--|----------------------|
| 22 | 1 | CHIMNEY MANIFOLD | v. dis. 600RM20008 | | |
| 21 | 6 | COPPER GASKET | CG100-NW 100CF | OFHC C10100 | |
| 20 | 128 | WASHER BX16 | ISO 7092 | A2/70 | |
| 19 | 128 | SCREW MBX25 | ISO 4762 | A2/70 | |
| 18 | 2 | CONNECTOR FLANGE - 1 HOLE | 600RM20819 | | |
| 17 | 4 | CONNECTOR FLANGE - 4 HOLES | 600RM20004 | | |
| 16 | 1 | O-RING Ø5.33 D227.96±1.3 | cod. PARKER 2-373 | V0494-70 | |
| 15 | 576 | WASHER FOR M8 | ISO 7090 | A2/70 | 1.0 |
| 14 | 576 | SCREW MBx50 | ISO 4762 | A2/70 | 14.0 |
| 13 | 480 | WASHER FOR M12 | ISO 7090 | A2 | 2.5 |
| 12 | 480 | SCREW M12x50 | ISO 4762 | A2/70 | 28.0 |
| 11 | 2 | O-RING De=5451.1 d6.99 (L=17.5 m) | ASTM D-2000 | Nitrile NBR Shore A 70 | |
| 10 | 2 | O-RING De=4720.0 d6.99 (L=15.0 m) | ASTM D-2000 | Nitrile NBR Shore A 70 Cu OFHC C10100 | |
| 9 | 24 | COPPER GASKET CF DN200 | ISO 3669-2 or equivalent | Cu OFHC C10100 | |
| 8 | 24 | TRANSPORT FLANGES | v. dis. 600RM19959 | | |
| 7 | 24 | CF FLANGE 200 BLIND | ISO 3669-2 or equivalent | AISI 316 L | 213.6 |
| 6 | 24 | RADIAL TIE-ROD CAP | v. dis. 600RM20003 | | |
| 5 | 6 | AXIAL TIE-ROD CAP | v. dis. 600RM20002 | | |
| 4 | 1 | SIDE FLANGE #2 ASS.Y | v. dis. 600RM20001 | | |
| 3 | 1 | SIDE FLANGE #1 ASS.Y | v. dis. 600RM19999 | | |
| 2 | 1 | OUTER WALL ASS.Y | v. dis. 600RM19998 | | |
| 1 | 1 | INNER WALL | v. dis. 600RM19997 | | |

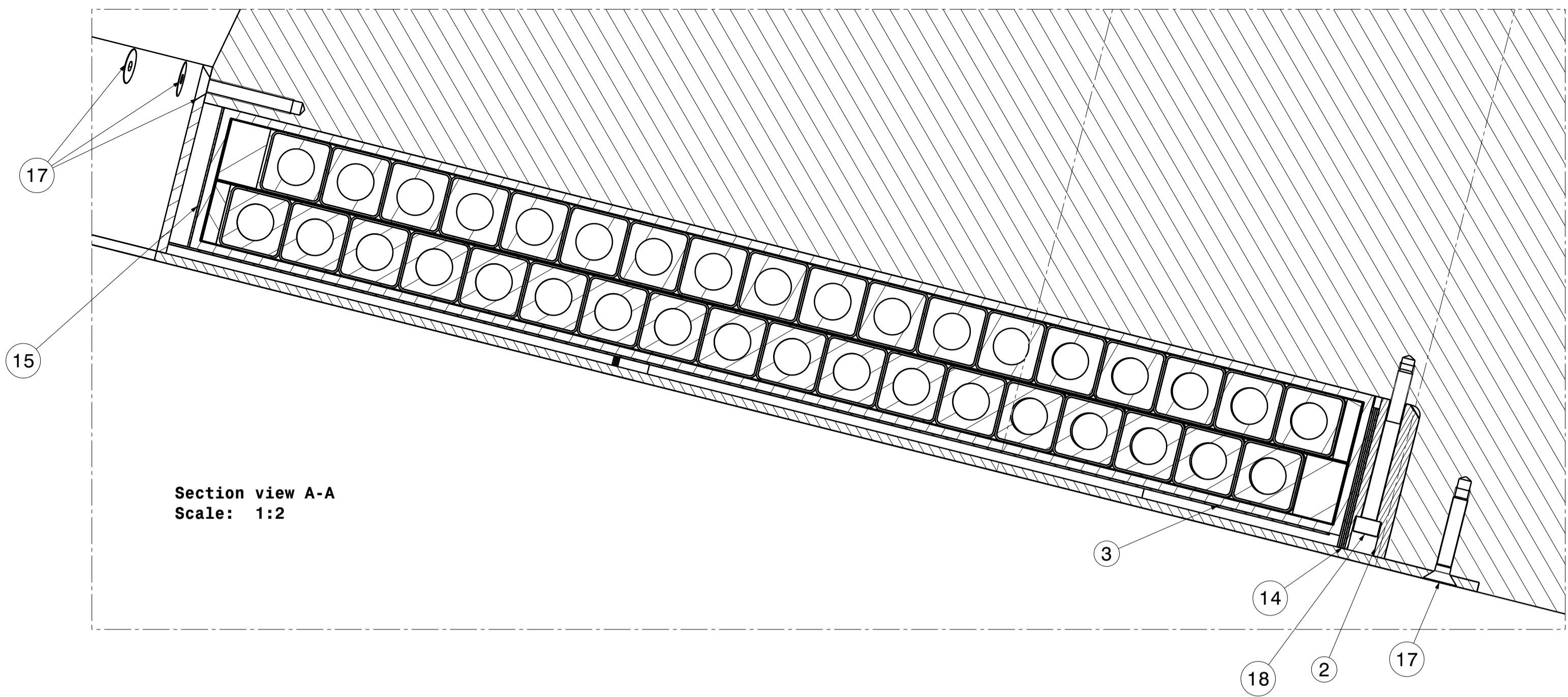
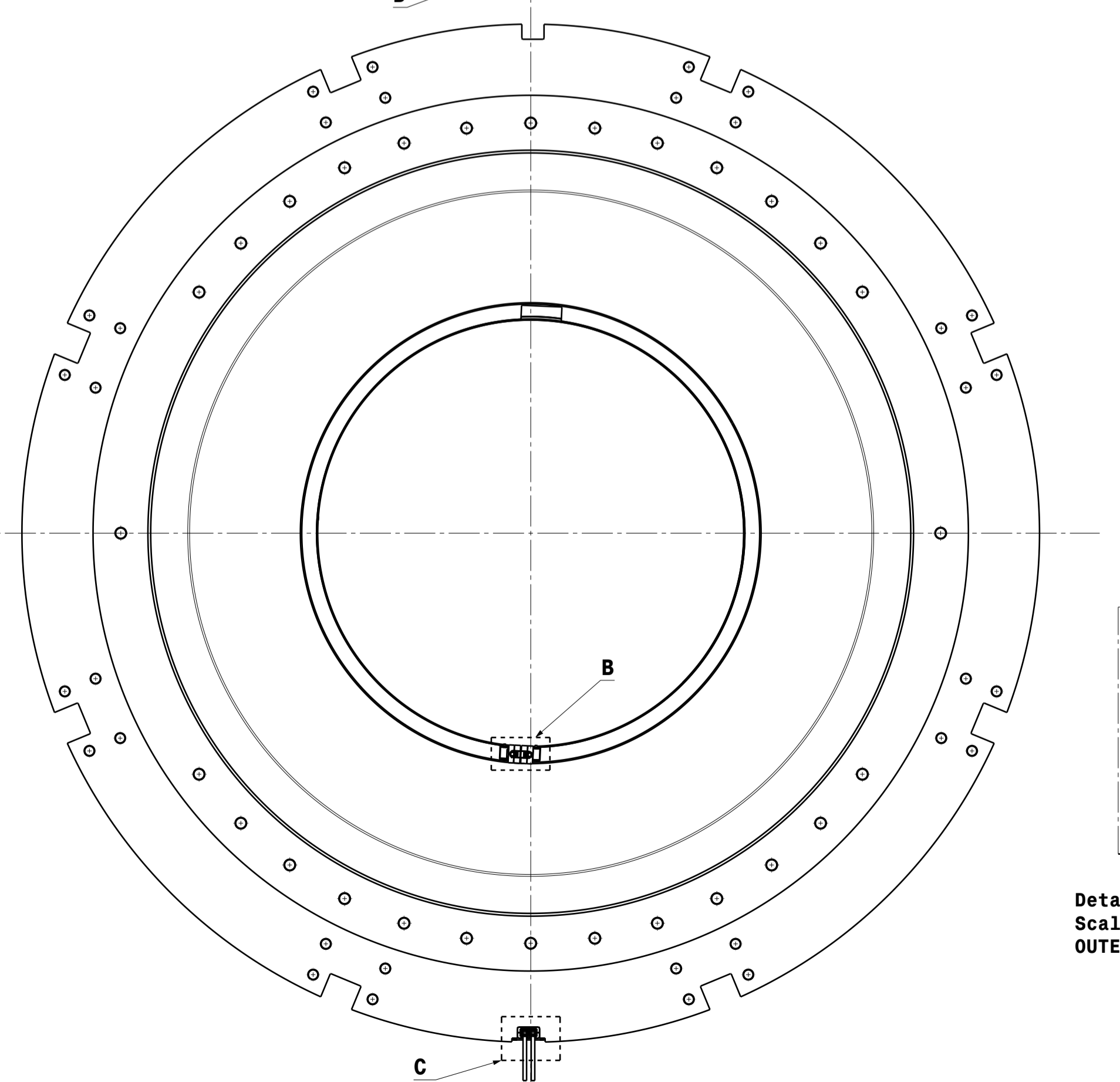
| | | | | | | | | | |
|---|-------------------------------|--|----------------|-----------------------------|----------------|---------------------|------------|-----------|----------|
| 20000Rev. 0. CATDrawing | C WELD MOD. Δ C | | Vercalli | Cuneo | Pesenti | Grillo | Valle | Marabotto | 24/11/17 |
| | B DIMENSION MOD. ITEM 22 ADD. | | Vercalli | Cuneo | Pesenti | Grillo | Valle | Marabotto | 28/07/17 |
| | A GENERAL REVIEW | | Salvitti | Cuneo | Pesenti | Grillo | Valle | Marabotto | 28/03/17 |
| | rev. st. sc. | Descrizione revisione | Preparato | Controllato | Verificato | Verificato | Verificato | Approvato | Data |
| progetto/project | cliente/client | materiale/material | | quantita/quantity | | massa/mass [t] | | | |
| commissa n° job n° | emittente issued by | formato size | scala scale | derivato da derived from | | rev. | | | |
| 2125 | DIS | A1 | 1:20 | | | | | | |
| ASG Superconductors | | titolo title | | Vacuum Vessel Ass.y | | | | | |
| Informazioni strettamente riservate, di proprietà ASG Superconductors S.p.A., da non utilizzare per scopi diversi da quelli per cui sono state fornite. | | Confidential information, property of ASG Superconductors S.p.A., not to be used for any purpose other than that for which it is supplied. | | | | | | | |
| Identificativo/document no. | | 600RM20000 | | rev. / rev. | Foglio / sheet | Segue fg. / di / of | | | |
| | | | | OAB | 1 | | | 1 | |



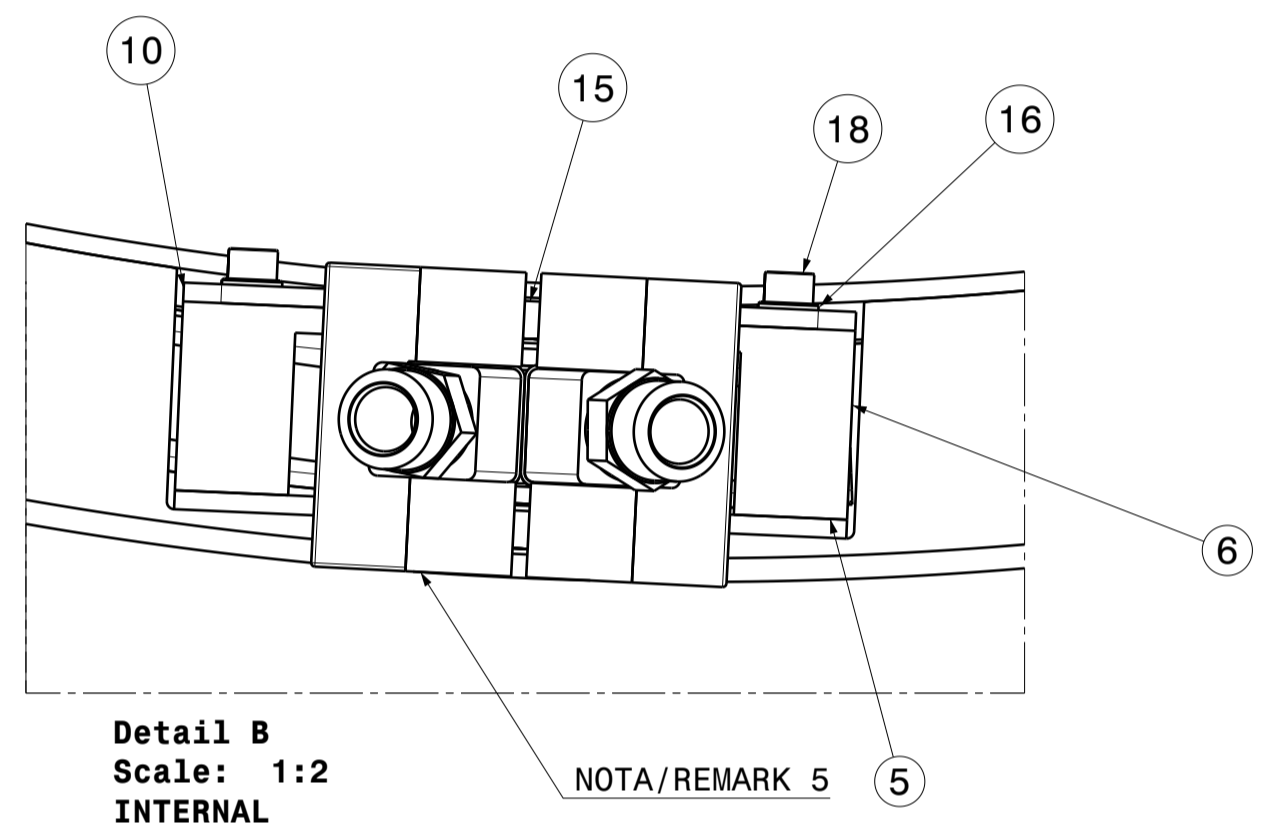
(4758)



v. nota 2 / SEE RMK 2

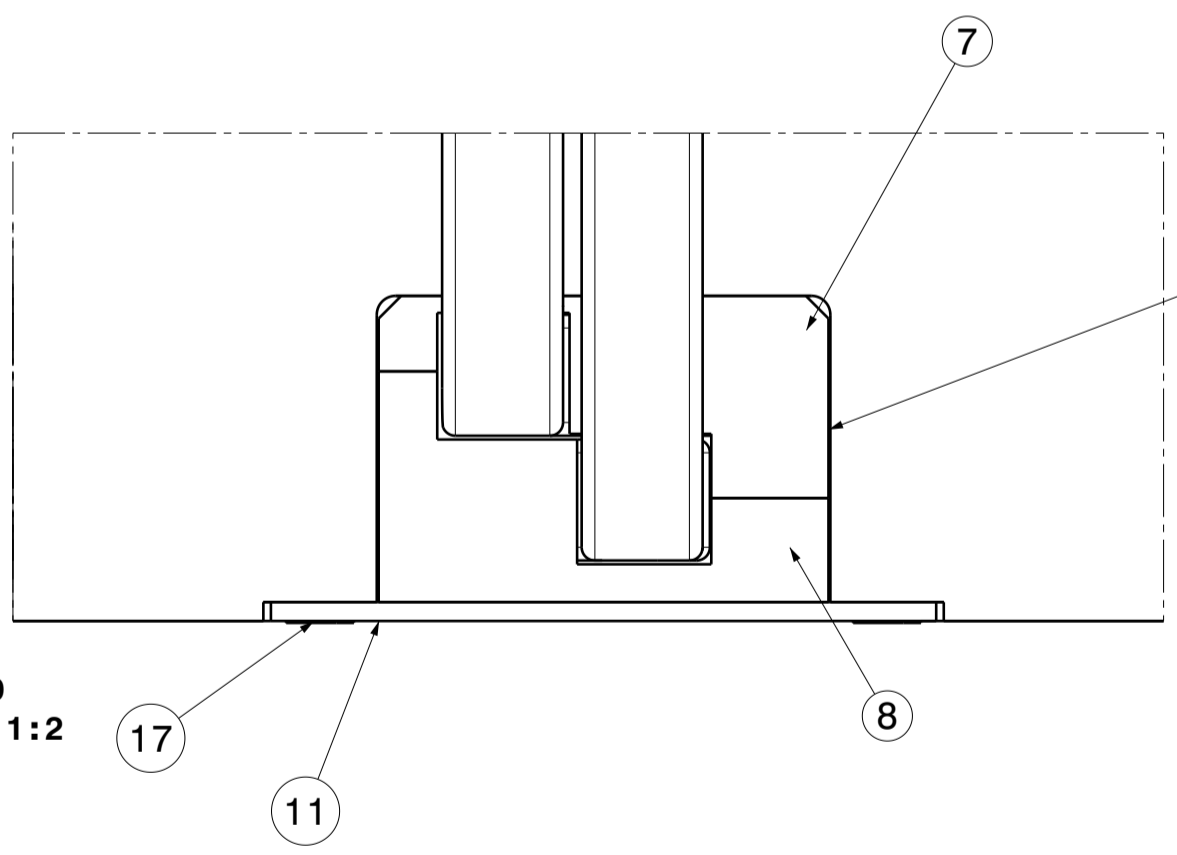
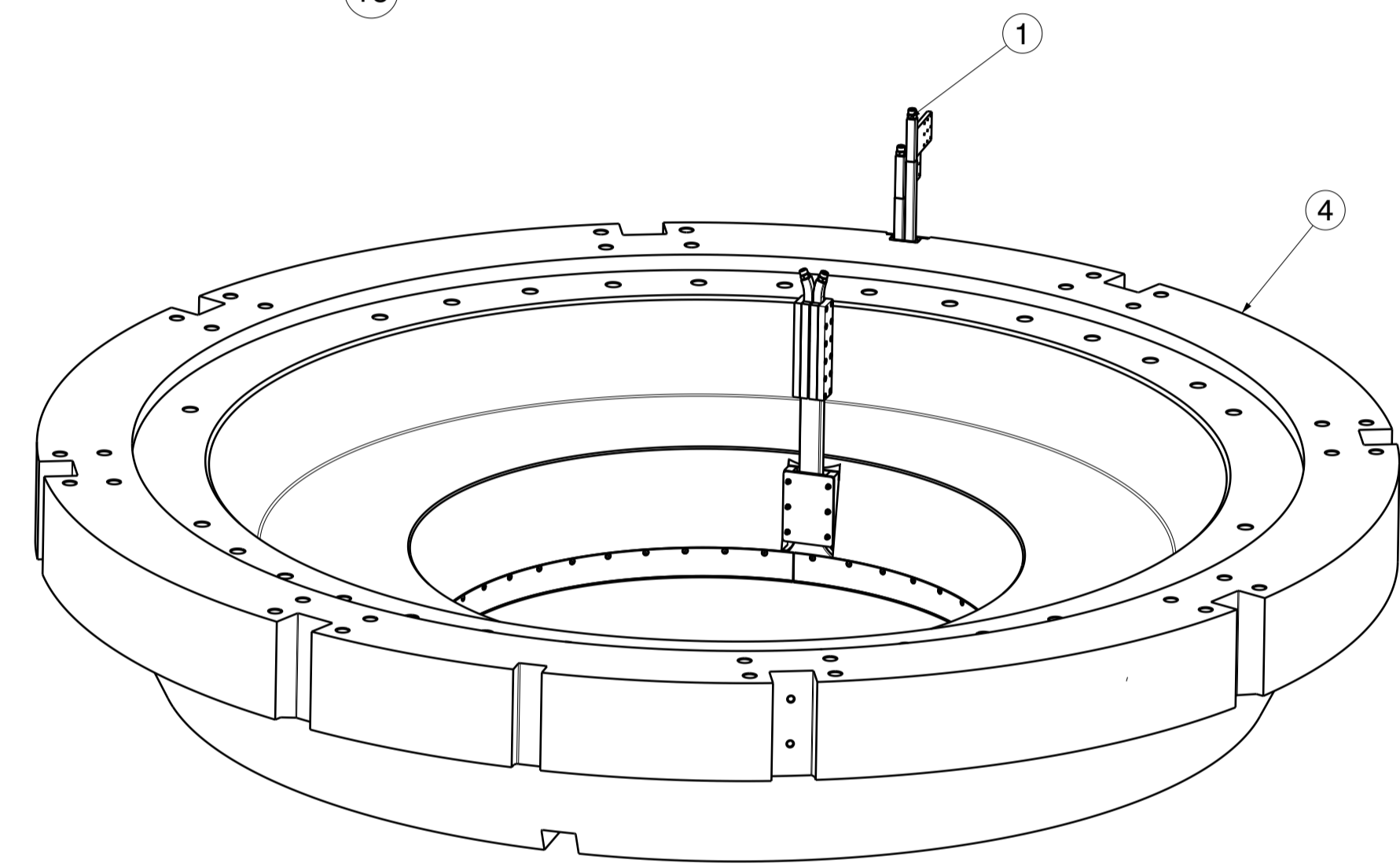


Section view A-A
Scale: 1:2



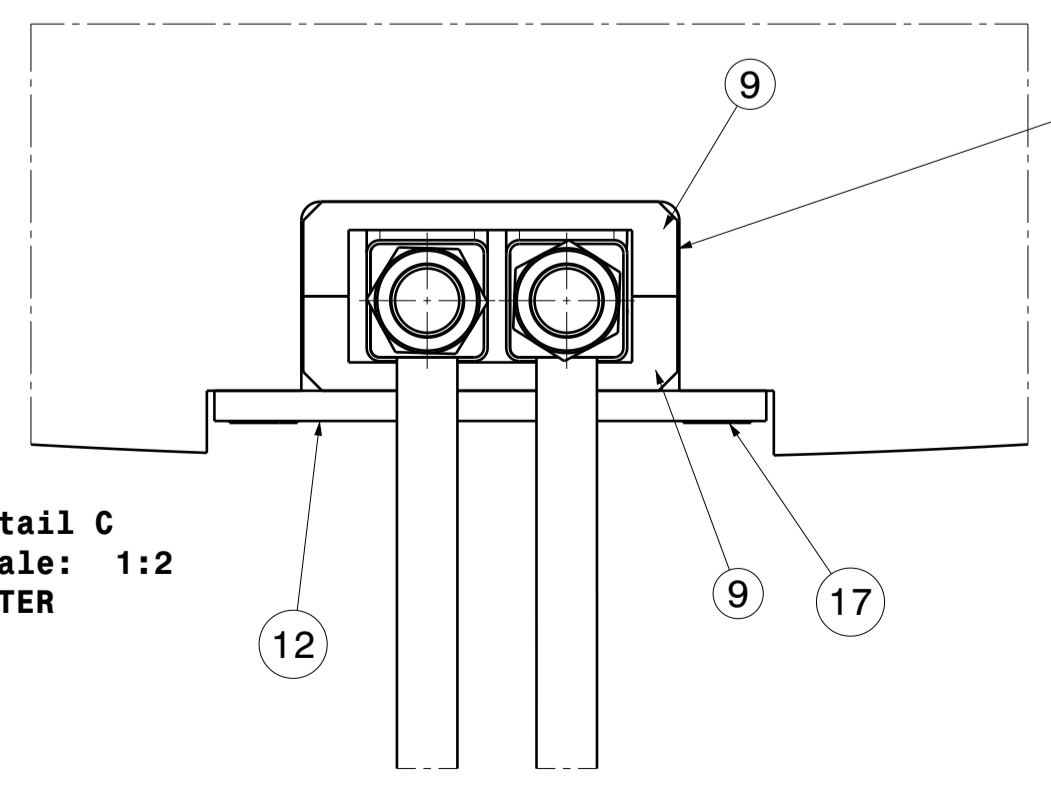
Detail B
Scale: 1:2
INTERNAL

NOTA/REMARK 5



Detail D
Scale: 1:2
MIDDLE

NOTA/REMARK 5



Detail C
Scale: 1:2
OUTER

NOTA/REMARK 5

Tab. 1

| TYPE | MATERIAL | TIGHTENING TORQUE [Nm] |
|------|----------|------------------------|
| M8 | A2/70 | 18.0 |

REMARKS / NOTE:

- ISOLARE LE TERMINAZIONI 2 NASTRATURE 1/2 SOVRAPPOSTE CON NASTRO DI VETRO 0.25x25 mm / TERMINATION INSULATION 2 LAYERS OF OVERLAPPING TAPE E-GLASS RIBBON 0.25x25 mm - PROLUNGARE IL TRATTO DI ISOLAMENTO FINO ALLA SUPERFICIE DEL POLO / EXTEND INSULATION TAPING UNTIL POLE SURFACE
- COPPIA DI SERRAGGIO VITI V. TABLE 1 / FOR SCREWS TIGHTENING TORQUE SEE TABLE 1
- INTERPORRE SPESSORI FINO A COMPENSARE EVENTUALE GAP COL DIAMETRO DEL DP / INSERT SHIMS TO COMPENSATE POSSIBLE GAP WITH RESPECT TO DP DIAMETER.
- QUANTITA' DA ADATTARE AL MONTAGGIO/QUANTITY TO BE ADJUSTED DURING ASSEMBLY.
- INTERPORRE SPESSORI IN NEMA G10 FINO A COMPENSARE EVENTUALE GAP. SPESS. 0.5mm/ INSERT SHIMS NEMA G10 TO COMPENSATE POSSIBLE GAP. THK 0.5mm

| N° ITEM | QUANTITA' quantity | DEFINIZIONE definition | RIFERIMENTO reference | MATERIALE material | MASSA [kg] mass [kg] |
|---------|--------------------|-----------------------------------|-------------------------------------|-----------------------------|----------------------|
| 18 | 30 | SCREW M8x80 | ISO 4762 | A2-70 | |
| 17 | 150 | SCREW M8x45 | ISO 10642 | A2-70 | |
| 16 | 6 | WASHER 8x16 | DIN 7980 | A2 | |
| 15 | 55 | TRIM COIL GASKET 1500x74x1 mm | (NOTA/REMARK 4) | E0540-80 Ethylene Propylene | |
| 14 | 64 | SHIM 700x75 th. 0.5mm | (NOTA/REMARK 4) | NEMA G10 | |
| 13 | 4 | TRIM COIL ENCLOSURE PLATE QUARTER | see dwg. 600RM19522 | | |
| 12 | 1 | OUTER CASE PLATE | see dwg. 600RM19520 POS.2 | | |
| 11 | 1 | MIDDLE CASE PLATE | see dwg. 600RM19520 POS.3 | | |
| 10 | 1 | INTERNAL CASE PLATE | see dwg. 600RM19520 POS.1 | | |
| 9 | 2 | OUTER INSULATED SUPPORT | see dwg. 600RM19519 POS.3 | | |
| 8 | 1 | MIDDLE INSULATED SUPPORT TOP | see dwg. 600RM19519 POS.5 | | |
| 7 | 1 | MIDDLE INSULATED SUPPORT BOTTOM | see dwg. 600RM19519 POS.4 | | |
| 6 | 1 | INTERNAL INSULATED SUPPORT TOP | see dwg. 600RM19519 POS.1 | | |
| 5 | 1 | INTERNAL INSULATED SUPPORT BOTTOM | see dwg. 600RM19519 POS.2 | | |
| 4 | 1 | TRIM COIL YOKE | see dwg. 672RM19497 | | |
| 3 | 56 | TRIM COIL FRONT GASKET SECTOR | see dwg. 600RM19518 (NOTA/REMARK 4) | | |
| 2 | 8 | CENTERING SECTOR | see dwg. 600RM19517 | | |
| 1 | 1 | TRIM COIL DOUBLE PANCAKE ASSEMBLY | see dwg. 600RM19332 | | |

| N° ITEM | QUANTITA' quantity | DEFINIZIONE definition | RIFERIMENTO reference | MATERIALE material | MASSA [kg] mass [kg] |
|---------|--------------------|-----------------------------------|-------------------------------------|-----------------------------|----------------------|
| 18 | 30 | SCREW M8x80 | ISO 4762 | A2-70 | |
| 17 | 150 | SCREW M8x45 | ISO 10642 | A2-70 | |
| 16 | 6 | WASHER 8x16 | DIN 7980 | A2 | |
| 15 | 55 | TRIM COIL GASKET 1500x74x1 mm | (NOTA/REMARK 4) | E0540-80 Ethylene Propylene | |
| 14 | 64 | SHIM 700x75 th. 0.5mm | (NOTA/REMARK 4) | NEMA G10 | |
| 13 | 4 | TRIM COIL ENCLOSURE PLATE QUARTER | see dwg. 600RM19522 | | |
| 12 | 1 | OUTER CASE PLATE | see dwg. 600RM19520 POS.2 | | |
| 11 | 1 | MIDDLE CASE PLATE | see dwg. 600RM19520 POS.3 | | |
| 10 | 1 | INTERNAL CASE PLATE | see dwg. 600RM19520 POS.1 | | |
| 9 | 2 | OUTER INSULATED SUPPORT | see dwg. 600RM19519 POS.3 | | |
| 8 | 1 | MIDDLE INSULATED SUPPORT TOP | see dwg. 600RM19519 POS.5 | | |
| 7 | 1 | MIDDLE INSULATED SUPPORT BOTTOM | see dwg. 600RM19519 POS.4 | | |
| 6 | 1 | INTERNAL INSULATED SUPPORT TOP | see dwg. 600RM19519 POS.1 | | |
| 5 | 1 | INTERNAL INSULATED SUPPORT BOTTOM | see dwg. 600RM19519 POS.2 | | |
| 4 | 1 | TRIM COIL YOKE | see dwg. 672RM19497 | | |
| 3 | 56 | TRIM COIL FRONT GASKET SECTOR | see dwg. 600RM19518 (NOTA/REMARK 4) | | |
| 2 | 8 | CENTERING SECTOR | see dwg. 600RM19517 | | |
| 1 | 1 | TRIM COIL DOUBLE PANCAKE ASSEMBLY | see dwg. 600RM19332 | | |

| progetto/project | cliente/client | materiale/material | quantità/quantity | massa/mass |
|------------------|----------------|--------------------|-------------------|------------|
| MPD DUBNA | JINR | - | 1 | 52 t |

19305Rev. 0. CADrawing

commissa n° 2125 DIS A1 1:20

emittente issued by: **ASG** Superconductors

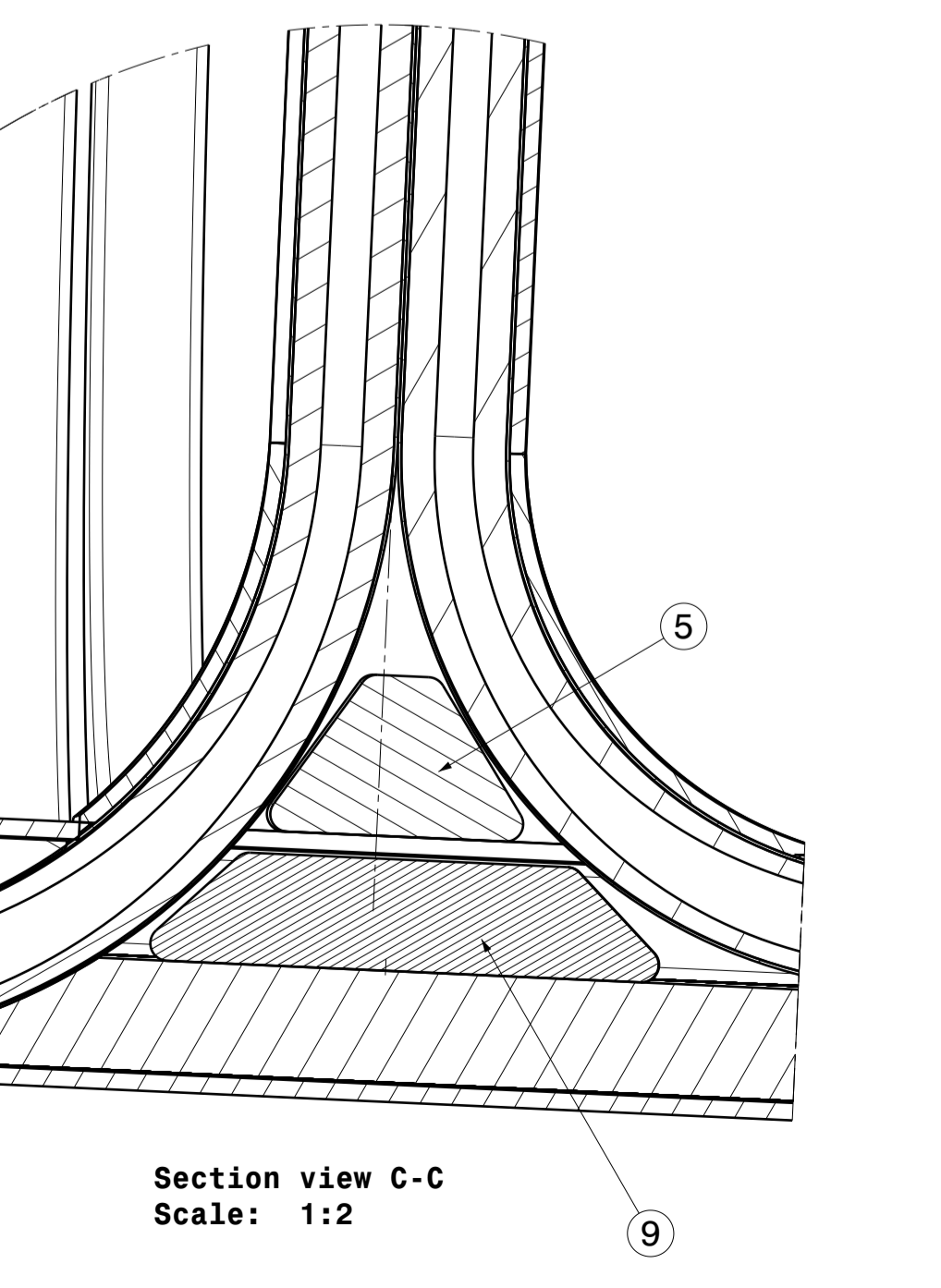
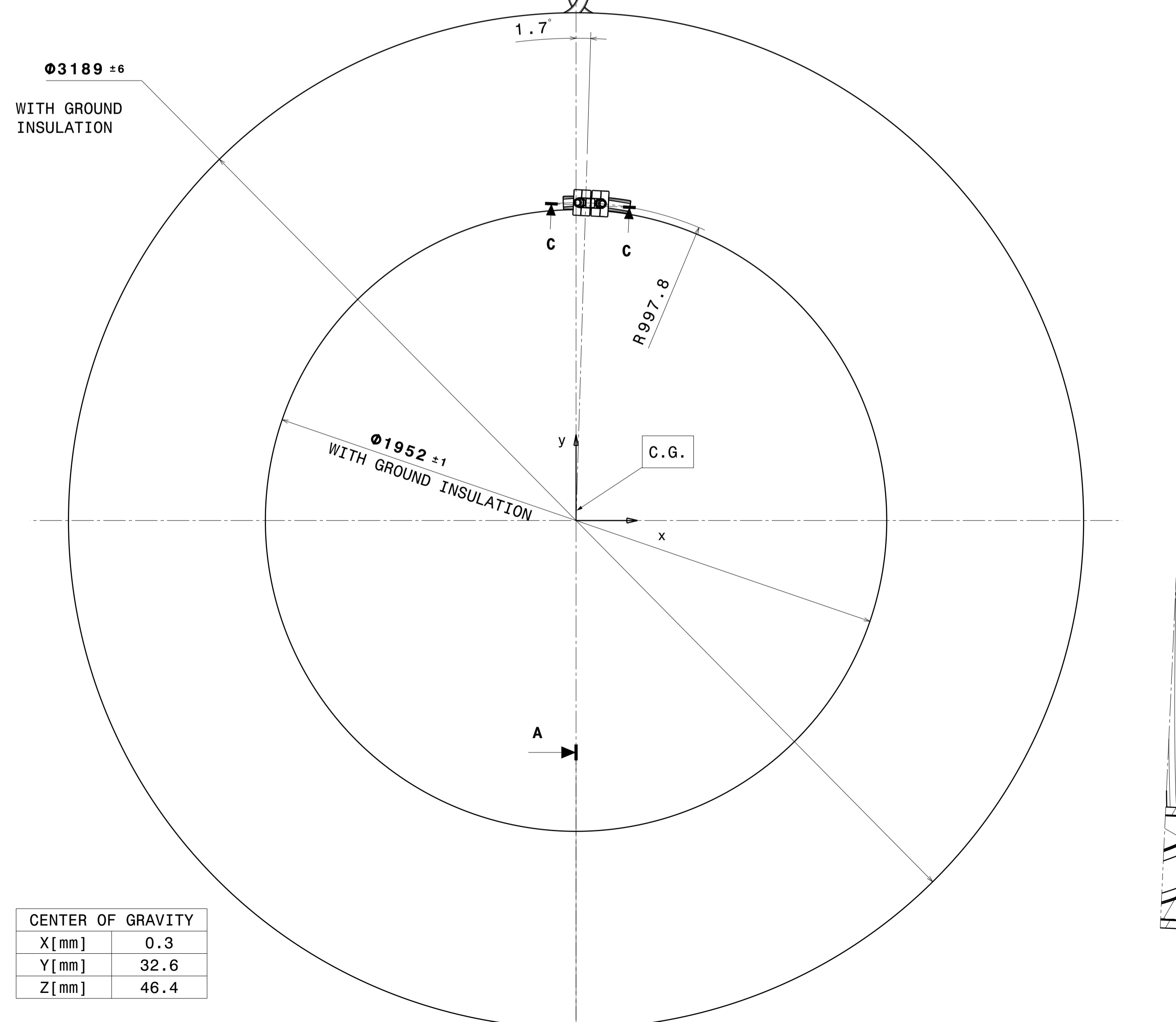
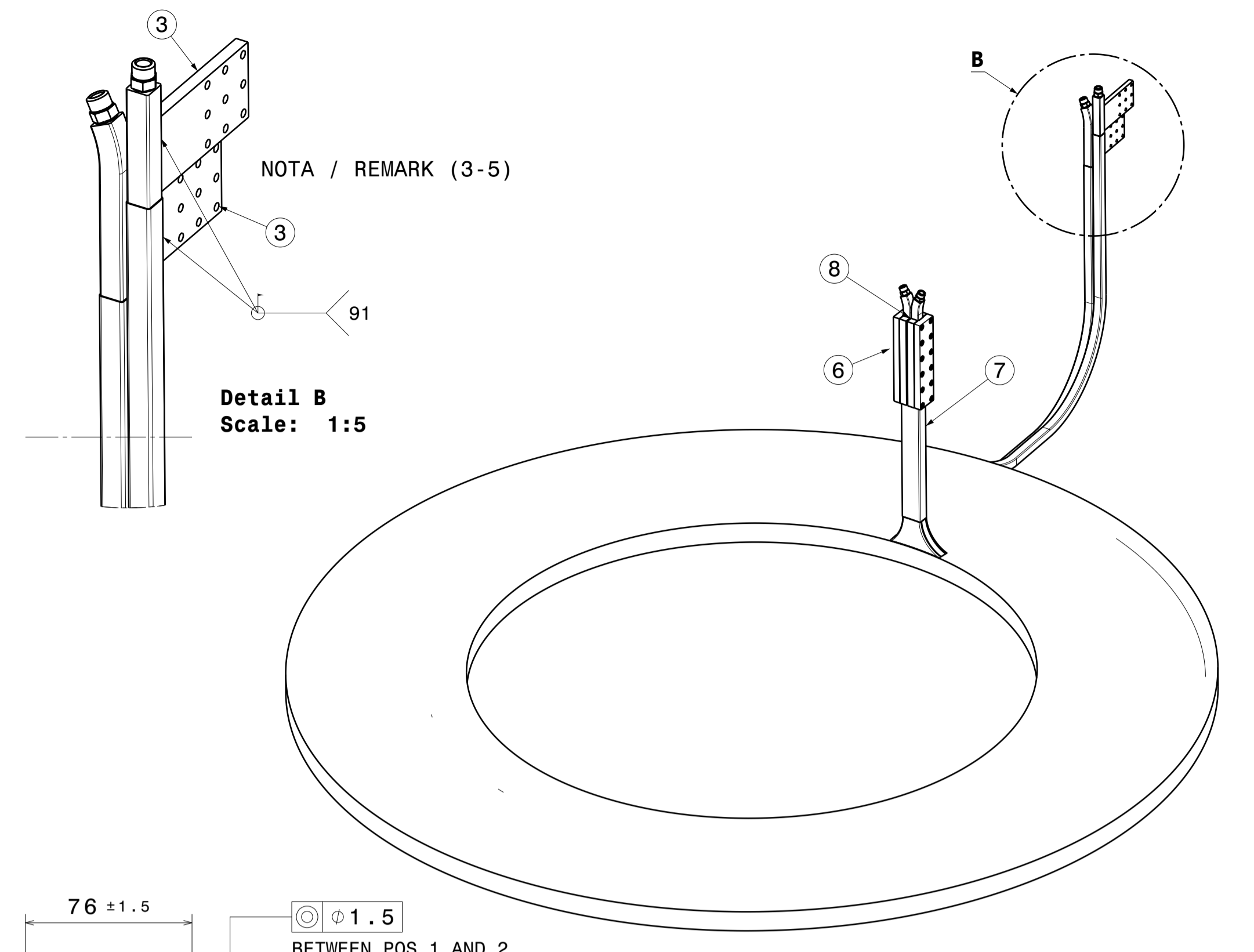
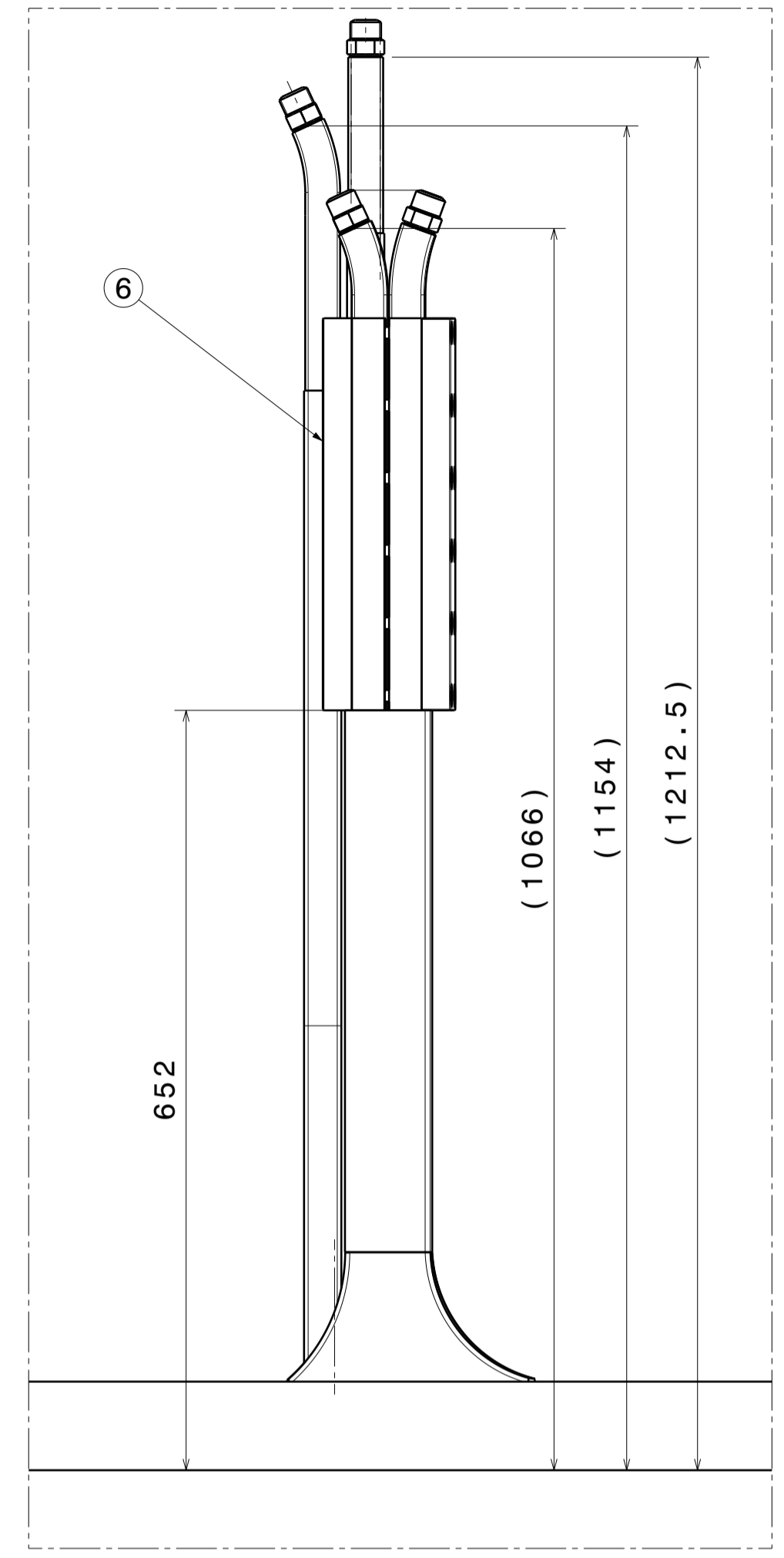
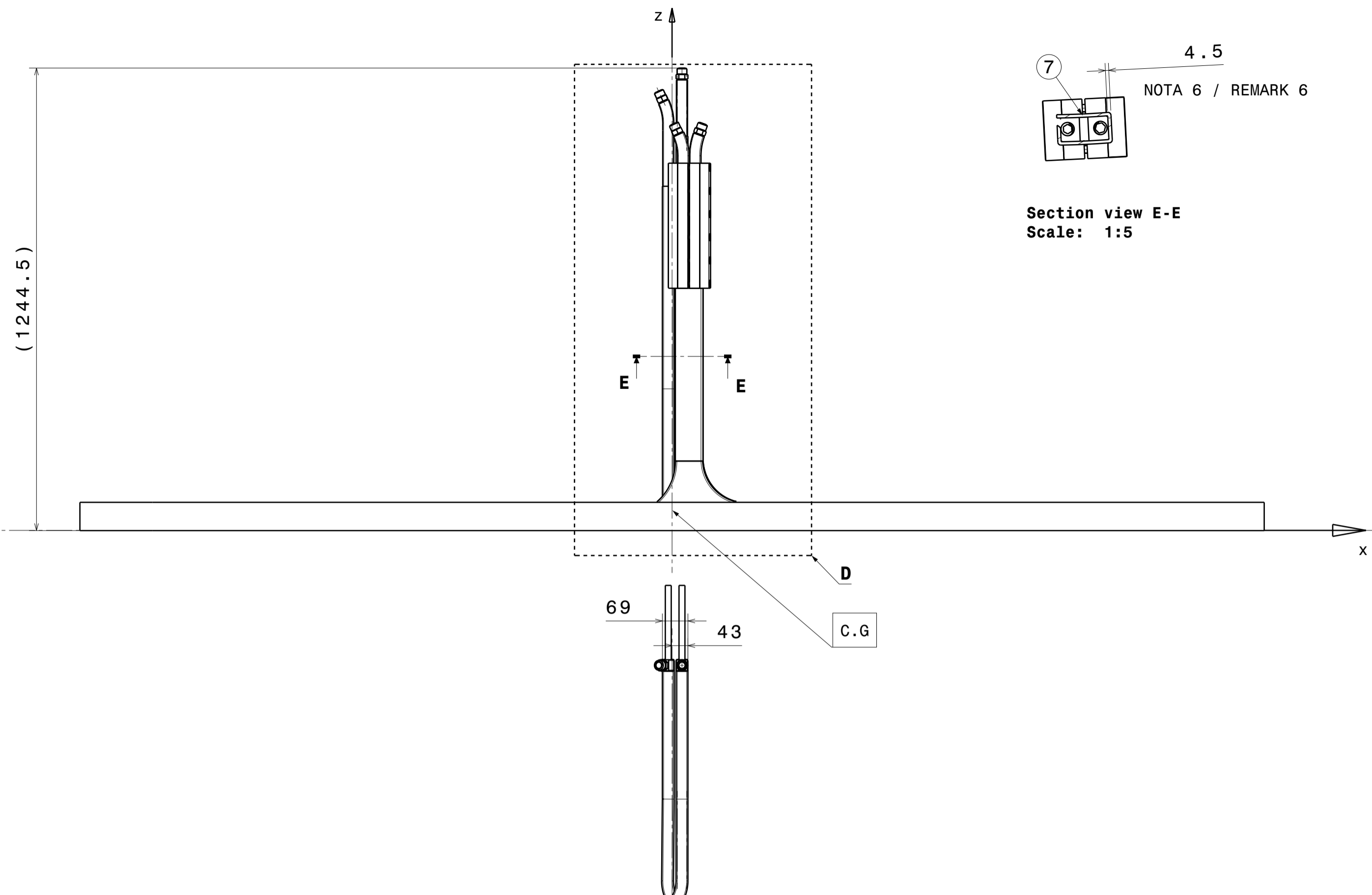
formato size: A1
scala scale: 1:20
derivato da derived from:

titolo title: **Trim Coil + Pole Assembly**

Informazioni strettamente riservate, di proprietà ASG Superconductors S.p.A., da non utilizzare per scopi diversi da quelli per cui sono state fornite.
Confidential information, property of ASG Superconductors S.p.A., not to be used for any purpose other than that for which it is supplied.

Identificativo/document no. **600RM19305**

rev. / rev. Foglio sheet 1 of 1



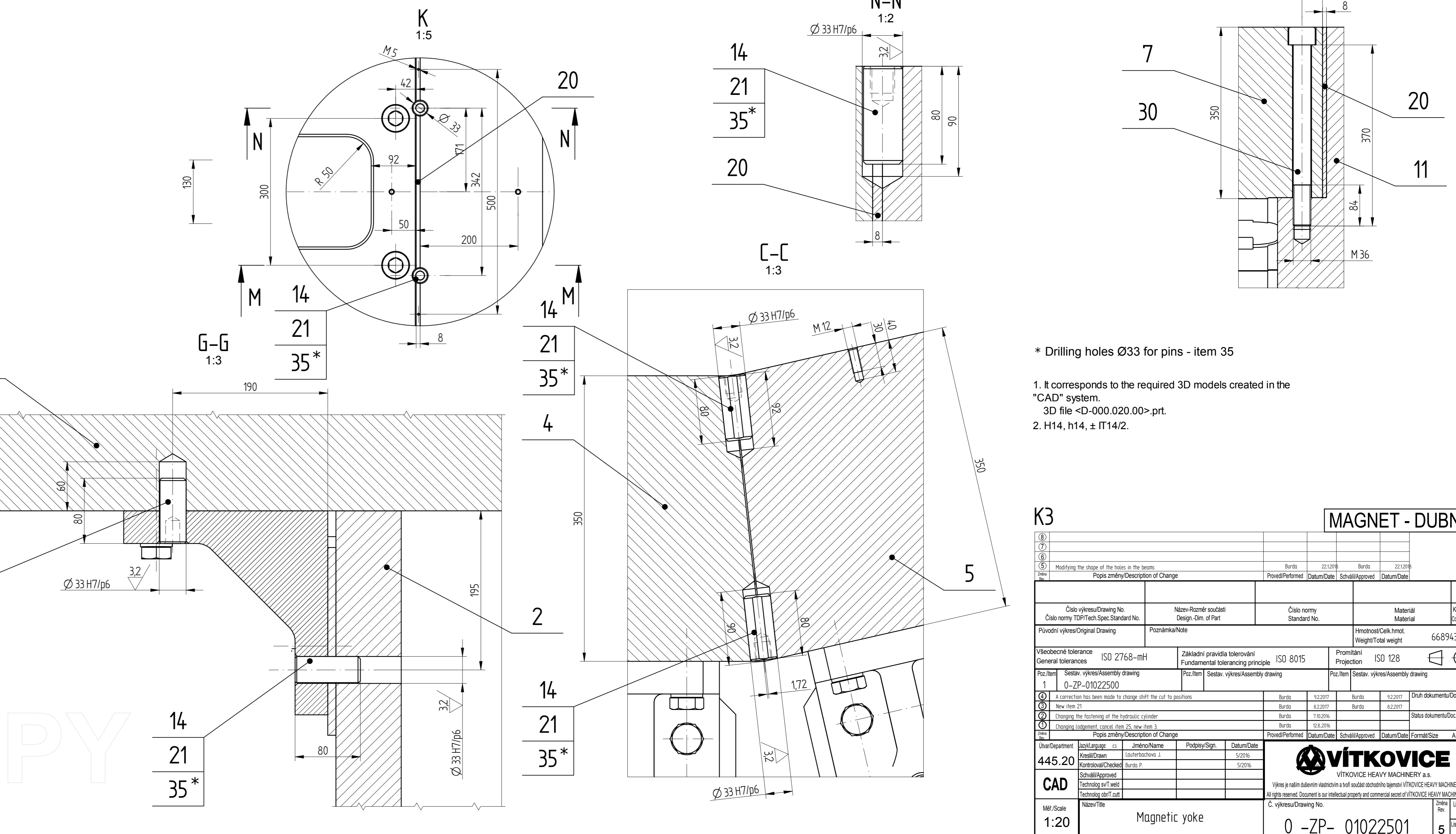
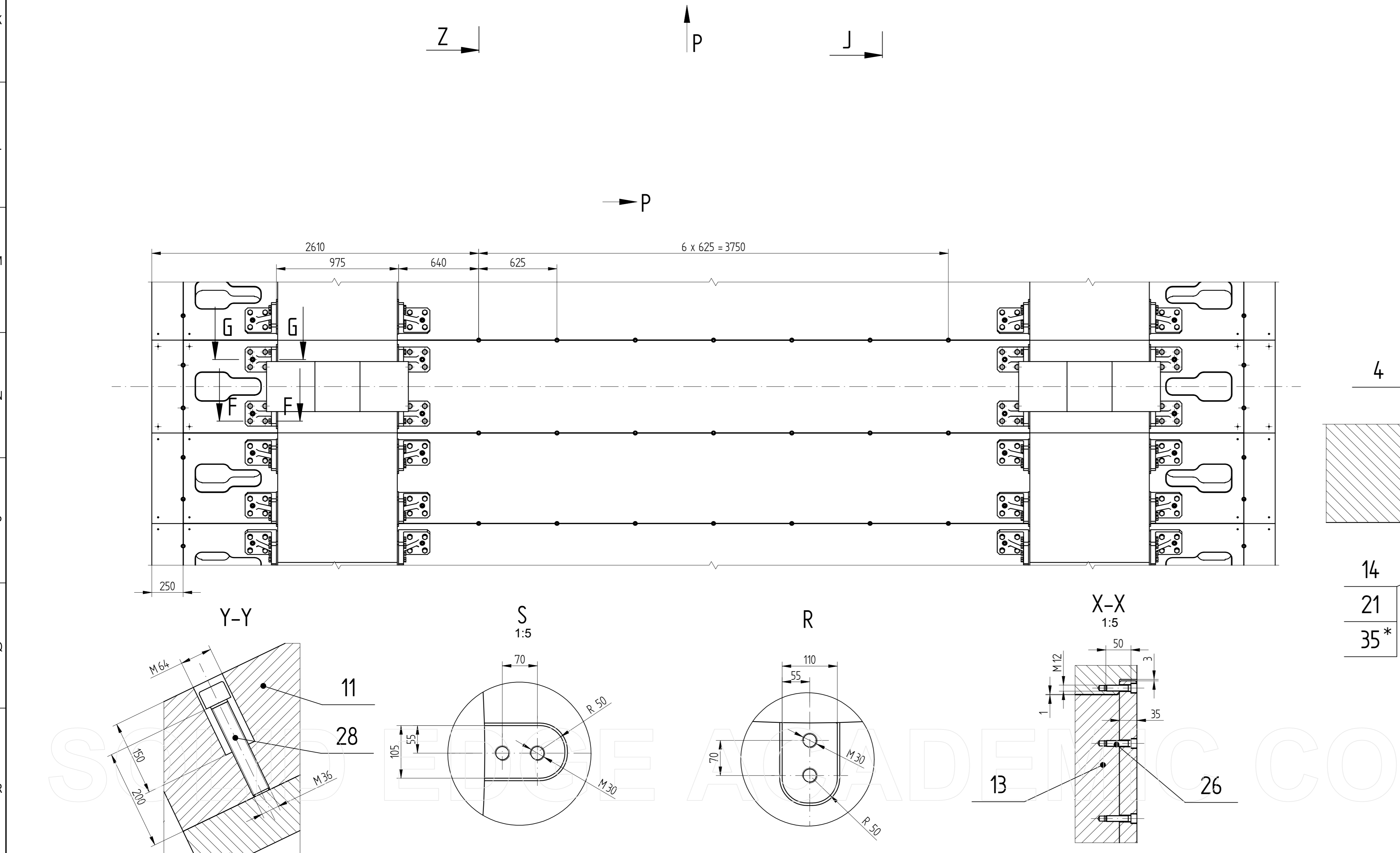
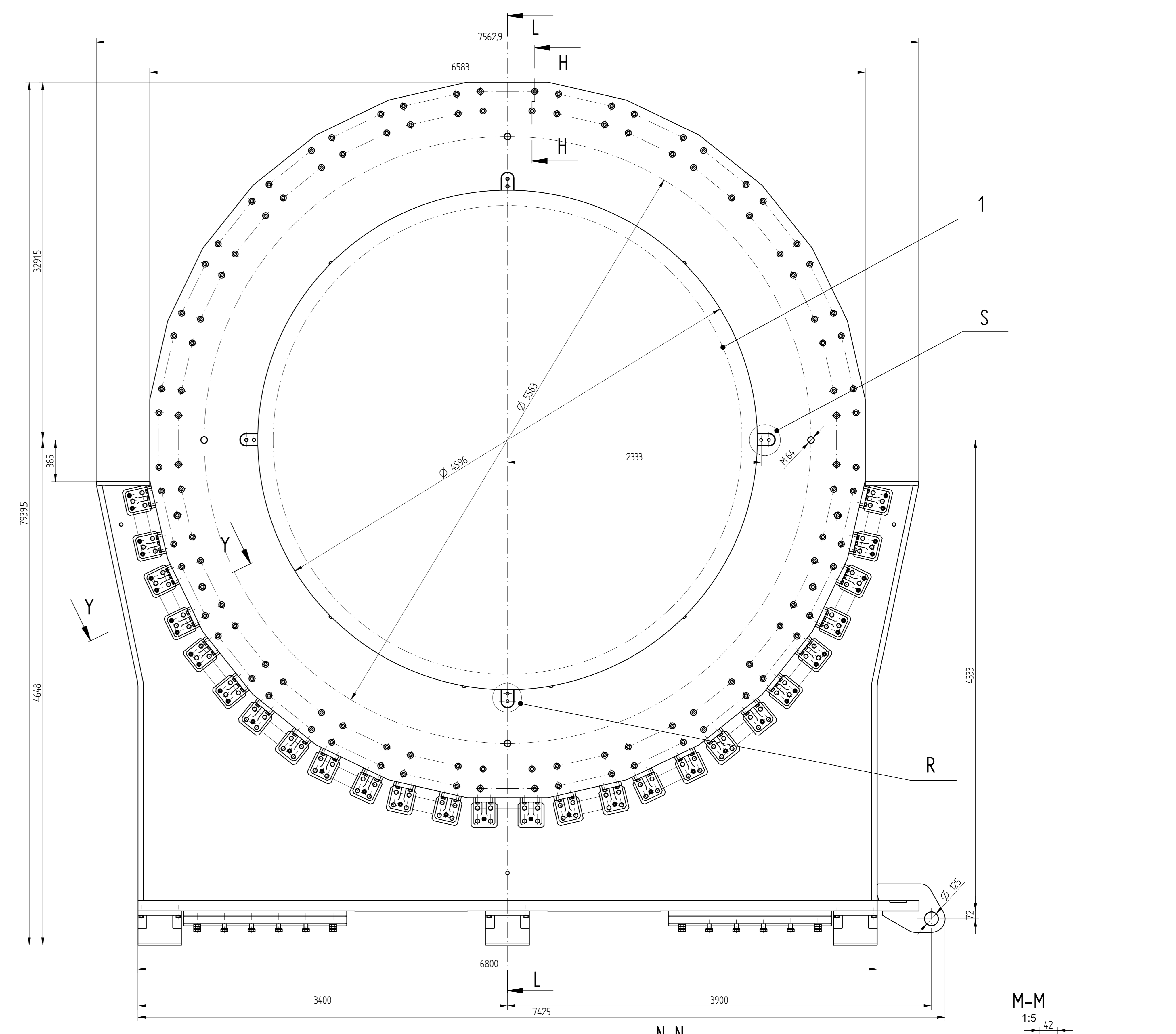
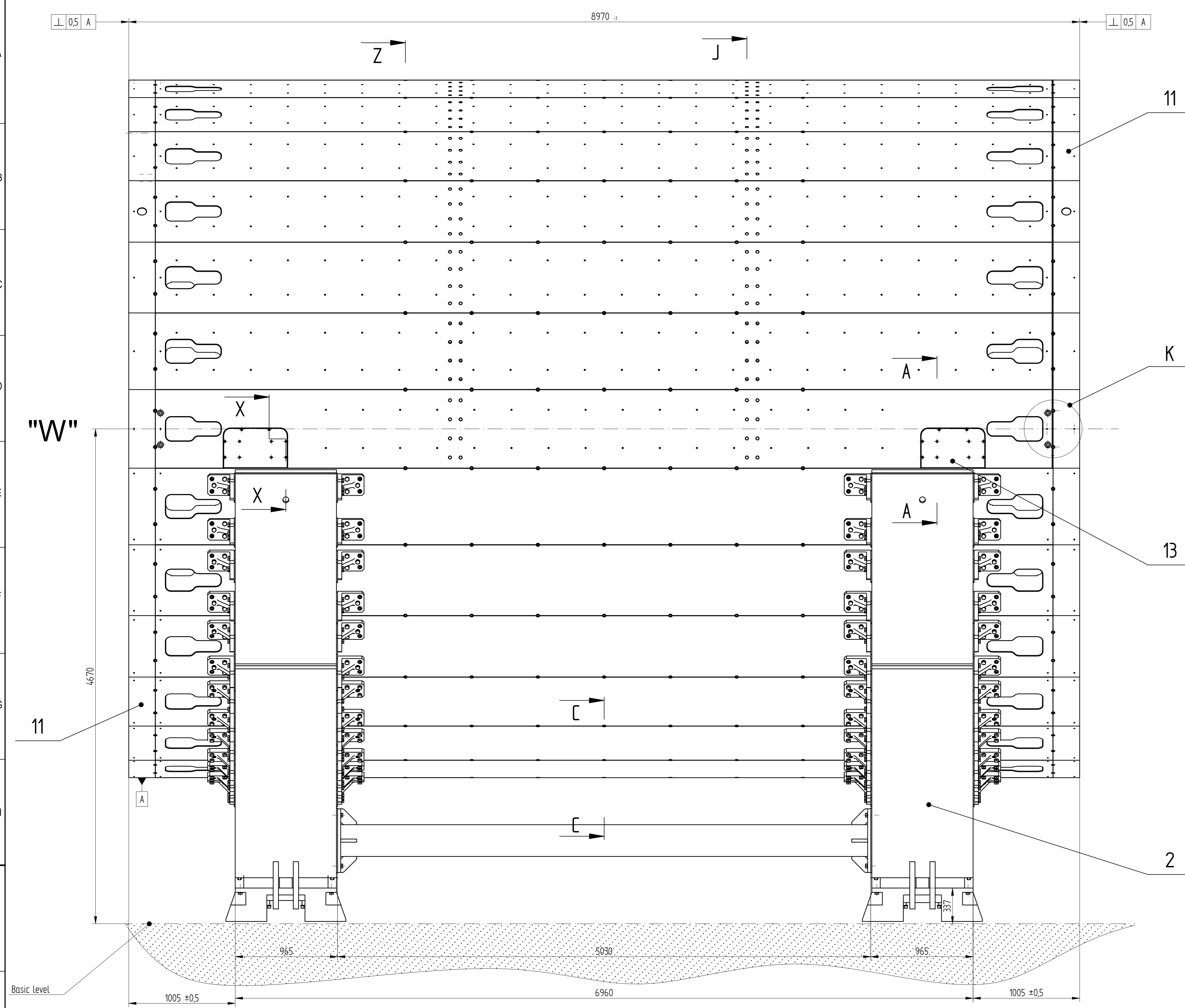
- NOTE / REMARKS:**
- DISEGNO ASSIEME DI RIFERIMENTO / REF. ASSEMBLY DWG 600RM19305
 - RIEMPIRE SPAZI VUOTI CON NASTRO DI VETRO-E 0.25mm CON RAPPORTO PIENO-VUOTO DI 50%.
FILL IN THE BLANKS WITH E-GLASS TAPE 0.25mm WITH 50% FILLING RATIO.
 - UNIRE LE BARRE DI CONNESSIONE (ITEM 3) AI SINGOLI PANCAKE (ITEM 1 E 2) MEDIANTE BRASATURA FORTE /
JOIN THE CONNECTION BAR (ITEM 3) TO THE SINGLE PANCAKE (ITEM 1 AND 2) USING HARD BRAZING:
- BRASARE CON SILFOS TIPO BRAZTEC 15 EN 1044 CP 102 (V. ANCHE SPEC. 701RM15229) / BRAZE BY BRAZTEC 15 EN 1044 CP 102 SILFOS (see also T.S. 701RM15229)
- DISOSSIDARE MECCANICAMENTE E PULIRE CON ACETONE LE PARTI / DEOXIDIZE AND CLEAN THE SURFACES BY ACETONE
- RISCALDARE LE PARTI A 800 °C CON FIAMMA OSSACETILENICA E AGGIUNGERE LEGA BRASANTE DA VERGELLA / HEAT THE PARTS UP TO 800 °C W. OXY-ACETYLENE TORCH AND ADD BRAZING ALLOY BY WIRE ROD
- ACCOPPIARE LE PARTI PREMENDOLE INSIEME E MANTENERE LA PRESSIONE FINO A RAFFREDDAMENTO COMPLETO / JOIN THE PARTS TOGETHER AND MANTAIN THE PRESSURE UNTIL COMPLETE COOLING
- PULIRE MECCANICAMENTE I PEZZI PER ELIMINARE LO STRATO DI OSSIDO SUPERFICIALE / CLEAN BY MACHINING THE PARTS TO REMOVE SURFACE OXIDATION LAYER
 - ISOLAMENTO DOPPIO PANCAKE: 9 NASTRATURE 1/2 SOVRAPPOSTE CON NASTRO DI VETRO-E 0.25mm E 1 NASTRATURA 1/2 SOVRAPPOSTA CON ACCOPPIATO NASTRO DI VETRO-E 0.25mm - KAPTON 0.025mm / DOUBLE PANCAKE INSULATION: 9 LAYER 1/2 HALF-OVERLAPPED WITH E-GLASS TAPE 0.25mm AND 1 LAYER 1/2 HALF-OVERLAPPED WITH E-GLASS TAPE 0.25mm - KAPTON 0.025mm
E RESINA A FREDDO.
ON THE CURRENT LEADS, RESTORE INSULATION, AFTER BRASING, WITH GLASS TAPE AND COLD CURING RESIN.
 - ISOLAMENTO USCITE ELETTRICHE: 8 NASTRATURE 1/2 SOVRAPPOSTE CON NASTRO DI VETRO-E 0.25mm E 1 NASTRATURA 1/2 SOVRAPPOSTA CON ACCOPPIATO NASTRO DI VETRO-E 0.25mm - KAPTON 0.025mm / CURRENT LEADS INSULATION: 9 LAYER 1/2 HALF-OVERLAPPED WITH E-GLASS TAPE 0.25mm AND 1 LAYER 1/2 HALF-OVERLAPPED WITH E-GLASS TAPE 0.25mm - KAPTON 0.025mm
 - TUTTE LE QUOTE SI RIFERISCONO ALLA BOBINA IMPREGNATA IN VUOTO E FINITA.
ALL DIMENSIONS REFER TO VACUUM-IMPREGNATED AND FINISHED COIL.

| Q | 1 | FILLER DOUBLE PANCAKE LONG | 600RM21413 | NEMA G10 | 0.15 |
|---|--------|-------------------------------|---------------------|----------------------|------|
| 8 | 1 | PLATE Cu 335x30x2mm | | Cu ETP 99.95% C11100 | |
| 7 | 1 | E-GLASS RIBBON 0.25mm | | | |
| 6 | 1 | TRIM COILS CLAMP BOX ASSEMBLY | see dwg. 653RM19559 | | |
| 5 | 1 | FILLER DOUBLE PANCAKE | 600RM19567 | NEMA G10 | 0.1 |
| 4 | 8.2 Km | E-GLASS RIBBON 0.25mm | | E-GLASS | 56 |
| 3 | 2 | CONNECTION PLATE | 600RM19339 | | |
| 2 | 1 | 2" PANCAKE ASSEMBLY | 600RM19331 | | |
| 1 | 1 | 1" PANCAKE ASSEMBLY | 600RM19330 | | |

| N° ITEM | QUANTITA' Quantity | DEFINIZIONE Definition | RIFERIMENTO Reference | MATERIALE Material | MASSA Mass [kg] | | | |
|---------|-------------------------------------|------------------------|-----------------------|--------------------|-----------------|-------|-----------|------------|
| D | RMK (2,4,5,6) MODIFIED, RMK 7 ADDED | VERCALLI | SPERDUTO | GRILLO | PESENTI | VALLE | MARABOTTO | 24/05/2018 |
| C | ITEM 4 AND 7 MOD. / RMK (4) MOD. | VERCALLI | CUNEO | GRILLO | PESENTI | VALLE | MARABOTTO | 27/11/17 |
| B | Section A-A mod. / ITEM 9 add. | VERCALLI | CUNEO | GRILLO | PESENTI | VALLE | MARABOTTO | 23/10/17 |

| | | | | |
|---|------------------------|---|-------------------|-----------------------------|
| progetto/project | cliente/client | materiale/material | quantità/quantity | massa/mass [kg] |
| MPD DUBNA | JINR | | | 1770 |
| commissa n° job n° | emittente issued by | formato size | scala scale | derivato da derived from |
| 2125 | DIS | A1 | 1:10 | - |
| | | DOUBLE PANCAKE ASSEMBLY ASSIEME DOPPIO PANCAKE | | |
| <small>Informazioni strettamente riservate, di proprietà ASG Superconductors S.p.A., da non utilizzare per scopi diversi da quelli per cui sono state fornite. Confidential information, property of ASG Superconductors S.p.A., not to be used for any purpose other than that for which it is supplied.</small> | | | | |
| Identificativo/document no. | | rev. / rev. Foglio page | | |
| 600RM19332 | | 1 1 1 | | |

APPENDIX 6. ASSEMBLY DRAWINGS OF THE YOKE

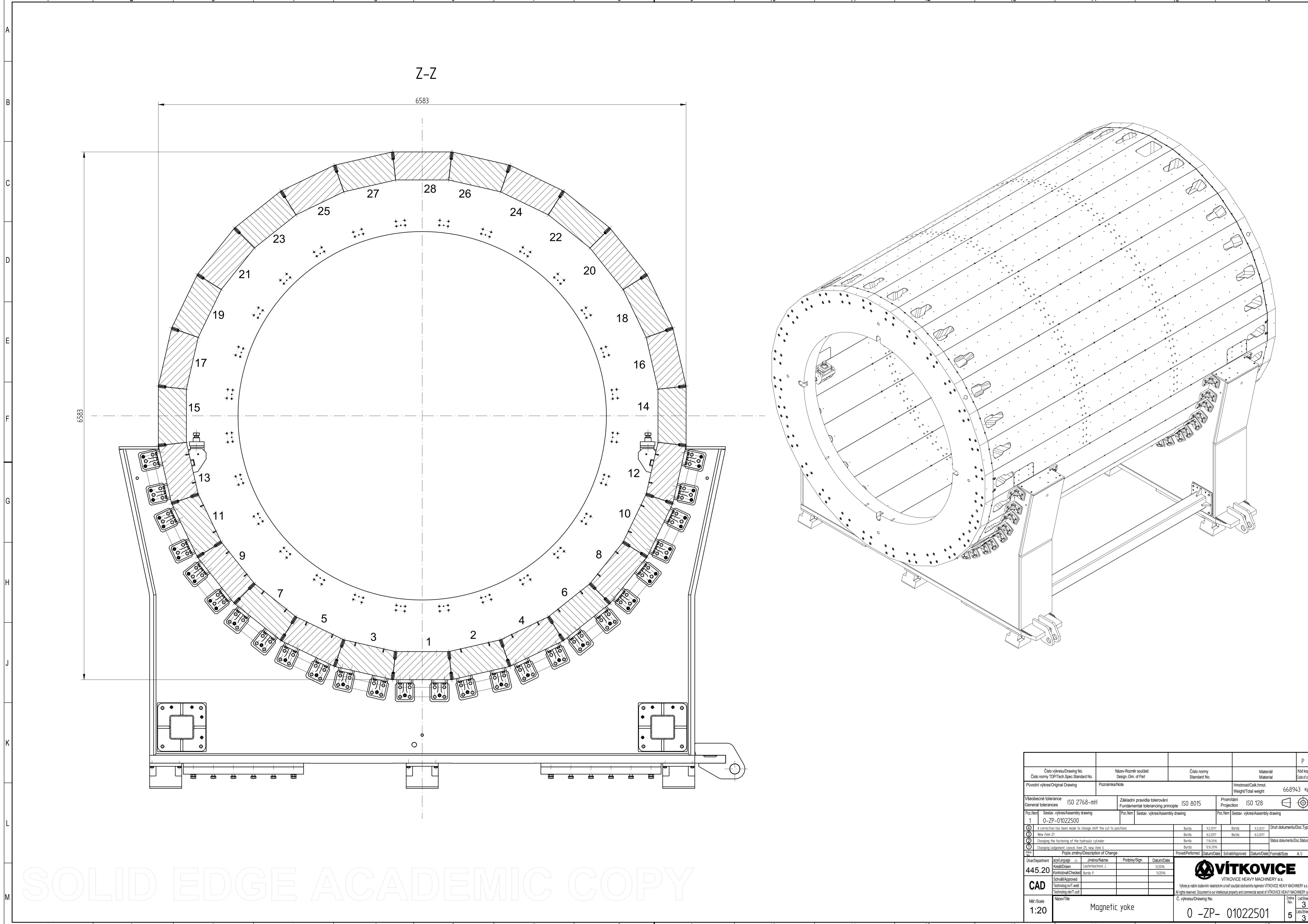


* Drilling holes Ø33 for pins - item 35
 1. It corresponds to the required 3D models created in the "CAD" system.
 - 3D file <D-000 020 00>.prt.
 2. H14, H14, ± IT14/2.

| MAGNET - DUBNA | | | | | | | | | |
|----------------|-----|-----|-----|-----|-----|-----|-----|-----|-----|
| № | № | № | № | № | № | № | № | № | № |
| 1 | 1 | 1 | 1 | 1 | 1 | 1 | 1 | 1 | 1 |
| 2 | 2 | 2 | 2 | 2 | 2 | 2 | 2 | 2 | 2 |
| 3 | 3 | 3 | 3 | 3 | 3 | 3 | 3 | 3 | 3 |
| 4 | 4 | 4 | 4 | 4 | 4 | 4 | 4 | 4 | 4 |
| 5 | 5 | 5 | 5 | 5 | 5 | 5 | 5 | 5 | 5 |
| 6 | 6 | 6 | 6 | 6 | 6 | 6 | 6 | 6 | 6 |
| 7 | 7 | 7 | 7 | 7 | 7 | 7 | 7 | 7 | 7 |
| 8 | 8 | 8 | 8 | 8 | 8 | 8 | 8 | 8 | 8 |
| 9 | 9 | 9 | 9 | 9 | 9 | 9 | 9 | 9 | 9 |
| 10 | 10 | 10 | 10 | 10 | 10 | 10 | 10 | 10 | 10 |
| 11 | 11 | 11 | 11 | 11 | 11 | 11 | 11 | 11 | 11 |
| 12 | 12 | 12 | 12 | 12 | 12 | 12 | 12 | 12 | 12 |
| 13 | 13 | 13 | 13 | 13 | 13 | 13 | 13 | 13 | 13 |
| 14 | 14 | 14 | 14 | 14 | 14 | 14 | 14 | 14 | 14 |
| 15 | 15 | 15 | 15 | 15 | 15 | 15 | 15 | 15 | 15 |
| 16 | 16 | 16 | 16 | 16 | 16 | 16 | 16 | 16 | 16 |
| 17 | 17 | 17 | 17 | 17 | 17 | 17 | 17 | 17 | 17 |
| 18 | 18 | 18 | 18 | 18 | 18 | 18 | 18 | 18 | 18 |
| 19 | 19 | 19 | 19 | 19 | 19 | 19 | 19 | 19 | 19 |
| 20 | 20 | 20 | 20 | 20 | 20 | 20 | 20 | 20 | 20 |
| 21 | 21 | 21 | 21 | 21 | 21 | 21 | 21 | 21 | 21 |
| 22 | 22 | 22 | 22 | 22 | 22 | 22 | 22 | 22 | 22 |
| 23 | 23 | 23 | 23 | 23 | 23 | 23 | 23 | 23 | 23 |
| 24 | 24 | 24 | 24 | 24 | 24 | 24 | 24 | 24 | 24 |
| 25 | 25 | 25 | 25 | 25 | 25 | 25 | 25 | 25 | 25 |
| 26 | 26 | 26 | 26 | 26 | 26 | 26 | 26 | 26 | 26 |
| 27 | 27 | 27 | 27 | 27 | 27 | 27 | 27 | 27 | 27 |
| 28 | 28 | 28 | 28 | 28 | 28 | 28 | 28 | 28 | 28 |
| 29 | 29 | 29 | 29 | 29 | 29 | 29 | 29 | 29 | 29 |
| 30 | 30 | 30 | 30 | 30 | 30 | 30 | 30 | 30 | 30 |
| 31 | 31 | 31 | 31 | 31 | 31 | 31 | 31 | 31 | 31 |
| 32 | 32 | 32 | 32 | 32 | 32 | 32 | 32 | 32 | 32 |
| 33 | 33 | 33 | 33 | 33 | 33 | 33 | 33 | 33 | 33 |
| 34 | 34 | 34 | 34 | 34 | 34 | 34 | 34 | 34 | 34 |
| 35 | 35 | 35 | 35 | 35 | 35 | 35 | 35 | 35 | 35 |
| 36 | 36 | 36 | 36 | 36 | 36 | 36 | 36 | 36 | 36 |
| 37 | 37 | 37 | 37 | 37 | 37 | 37 | 37 | 37 | 37 |
| 38 | 38 | 38 | 38 | 38 | 38 | 38 | 38 | 38 | 38 |
| 39 | 39 | 39 | 39 | 39 | 39 | 39 | 39 | 39 | 39 |
| 40 | 40 | 40 | 40 | 40 | 40 | 40 | 40 | 40 | 40 |
| 41 | 41 | 41 | 41 | 41 | 41 | 41 | 41 | 41 | 41 |
| 42 | 42 | 42 | 42 | 42 | 42 | 42 | 42 | 42 | 42 |
| 43 | 43 | 43 | 43 | 43 | 43 | 43 | 43 | 43 | 43 |
| 44 | 44 | 44 | 44 | 44 | 44 | 44 | 44 | 44 | 44 |
| 45 | 45 | 45 | 45 | 45 | 45 | 45 | 45 | 45 | 45 |
| 46 | 46 | 46 | 46 | 46 | 46 | 46 | 46 | 46 | 46 |
| 47 | 47 | 47 | 47 | 47 | 47 | 47 | 47 | 47 | 47 |
| 48 | 48 | 48 | 48 | 48 | 48 | 48 | 48 | 48 | 48 |
| 49 | 49 | 49 | 49 | 49 | 49 | 49 | 49 | 49 | 49 |
| 50 | 50 | 50 | 50 | 50 | 50 | 50 | 50 | 50 | 50 |
| 51 | 51 | 51 | 51 | 51 | 51 | 51 | 51 | 51 | 51 |
| 52 | 52 | 52 | 52 | 52 | 52 | 52 | 52 | 52 | 52 |
| 53 | 53 | 53 | 53 | 53 | 53 | 53 | 53 | 53 | 53 |
| 54 | 54 | 54 | 54 | 54 | 54 | 54 | 54 | 54 | 54 |
| 55 | 55 | 55 | 55 | 55 | 55 | 55 | 55 | 55 | 55 |
| 56 | 56 | 56 | 56 | 56 | 56 | 56 | 56 | 56 | 56 |
| 57 | 57 | 57 | 57 | 57 | 57 | 57 | 57 | 57 | 57 |
| 58 | 58 | 58 | 58 | 58 | 58 | 58 | 58 | 58 | 58 |
| 59 | 59 | 59 | 59 | 59 | 59 | 59 | 59 | 59 | 59 |
| 60 | 60 | 60 | 60 | 60 | 60 | 60 | 60 | 60 | 60 |
| 61 | 61 | 61 | 61 | 61 | 61 | 61 | 61 | 61 | 61 |
| 62 | 62 | 62 | 62 | 62 | 62 | 62 | 62 | 62 | 62 |
| 63 | 63 | 63 | 63 | 63 | 63 | 63 | 63 | 63 | 63 |
| 64 | 64 | 64 | 64 | 64 | 64 | 64 | 64 | 64 | 64 |
| 65 | 65 | 65 | 65 | 65 | 65 | 65 | 65 | 65 | 65 |
| 66 | 66 | 66 | 66 | 66 | 66 | 66 | 66 | 66 | 66 |
| 67 | 67 | 67 | 67 | 67 | 67 | 67 | 67 | 67 | 67 |
| 68 | 68 | 68 | 68 | 68 | 68 | 68 | 68 | 68 | 68 |
| 69 | 69 | 69 | 69 | 69 | 69 | 69 | 69 | 69 | 69 |
| 70 | 70 | 70 | 70 | 70 | 70 | 70 | 70 | 70 | 70 |
| 71 | 71 | 71 | 71 | 71 | 71 | 71 | 71 | 71 | 71 |
| 72 | 72 | 72 | 72 | 72 | 72 | 72 | 72 | 72 | 72 |
| 73 | 73 | 73 | 73 | 73 | 73 | 73 | 73 | 73 | 73 |
| 74 | 74 | 74 | 74 | 74 | 74 | 74 | 74 | 74 | 74 |
| 75 | 75 | 75 | 75 | 75 | 75 | 75 | 75 | 75 | 75 |
| 76 | 76 | 76 | 76 | 76 | 76 | 76 | 76 | 76 | 76 |
| 77 | 77 | 77 | 77 | 77 | 77 | 77 | 77 | 77 | 77 |
| 78 | 78 | 78 | 78 | 78 | 78 | 78 | 78 | 78 | 78 |
| 79 | 79 | 79 | 79 | 79 | 79 | 79 | 79 | 79 | 79 |
| 80 | 80 | 80 | 80 | 80 | 80 | 80 | 80 | 80 | 80 |
| 81 | 81 | 81 | 81 | 81 | 81 | 81 | 81 | 81 | 81 |
| 82 | 82 | 82 | 82 | 82 | 82 | 82 | 82 | 82 | 82 |
| 83 | 83 | 83 | 83 | 83 | 83 | 83 | 83 | 83 | 83 |
| 84 | 84 | 84 | 84 | 84 | 84 | 84 | 84 | 84 | 84 |
| 85 | 85 | 85 | 85 | 85 | 85 | 85 | 85 | 85 | 85 |
| 86 | 86 | 86 | 86 | 86 | 86 | 86 | 86 | 86 | 86 |
| 87 | 87 | 87 | 87 | 87 | 87 | 87 | 87 | 87 | 87 |
| 88 | 88 | 88 | 88 | 88 | 88 | 88 | 88 | 88 | 88 |
| 89 | 89 | 89 | 89 | 89 | 89 | 89 | 89 | 89 | 89 |
| 90 | 90 | 90 | 90 | 90 | 90 | 90 | 90 | 90 | 90 |
| 91 | 91 | 91 | 91 | 91 | 91 | 91 | 91 | 91 | 91 |
| 92 | 92 | 92 | 92 | 92 | 92 | 92 | 92 | 92 | 92 |
| 93 | 93 | 93 | 93 | 93 | 93 | 93 | 93 | 93 | 93 |
| 94 | 94 | 94 | 94 | 94 | 94 | 94 | 94 | 94 | 94 |
| 95 | 95 | 95 | 95 | 95 | 95 | 95 | 95 | 95 | 95 |
| 96 | 96 | 96 | 96 | 96 | 96 | 96 | 96 | 96 | 96 |
| 97 | 97 | 97 | 97 | 97 | 97 | 97 | 97 | 97 | 97 |
| 98 | 98 | 98 | 98 | 98 | 98 | 98 | 98 | 98 | 98 |
| 99 | 99 | 99 | 99 | 99 | 99 | 99 | 99 | 99 | 99 |
| 100 | 100 | 100 | 100 | 100 | 100 | 100 | 100 | 100 | 100 |



445.20
 CAD
 1:20
 Magnetic yoke
 0 - ZP - 01022501



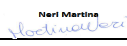

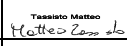
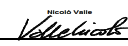

| | | | | | | | | | |
|---|---|--|----------------------------------|---|----------------------------------|------------------------|------------|-----------------------------|-----|
| Číslo výkresu/Drawing No. | | Název-Rozměr součásti Design-Dim. of Part | | Číslo normy Standard No. | | Materiál Material | | Kód kópi Code of copy | |
| Původní výkres/Original Drawing | | Poznámka/Note | | Hmotnost/Česká hmot. Weight/Total weight | | 668943 Kg | | | |
| Všeobecné tolerance General tolerances | | ISO 2768-mH | | Základní pravidla tolerování Fundamental tolerancing principle | | ISO 8015 | | Promítání Projection | |
| | | | | | | | | ISO 128 | |
| 1 | Sestava výkresu/Assembly drawing | 1 | Sestava výkresu/Assembly drawing | 1 | Sestava výkresu/Assembly drawing | | | | |
| 1 | | 0-ZP-01022500 | | | | | | | |
| A correction has been made to change shift the cut to positions | | | | Burda | 9.2.2017 | Burda | 9.2.2017 | Druh dokumentu/Doc. Type | |
| New item 21 | | | | Burda | 8.2.2017 | Burda | 8.2.2017 | | |
| Changing the fastening of the hydraulic cylinder | | | | Burda | 7.10.2016 | | | Status dokumentu/Doc Status | |
| Changing lodgement, capitol item 25, new item 3 | | | | Burda | 12.8.2016 | | | | |
| Popis změny/Description of Change | | | | Provedl/Performed | Datum/Date | Schválil/Approved | Datum/Date | Formát/Size | A 0 |
| Uživatel/Department | Jazyk/Language | Číslo kresla/Sheet No. | Jméno/Name | Podpis/Sign. | Datum/Date | | | | |
| 445.20 | cs | | Lochteschewer J. | | 9/2016 | | | | |
| Kontrolní/Kontrolled | Schválil/Schválil | | | | | | | | |
| | Burda P. | | | | | | | | |
| CAD | Technologie/Technology | | | | | | | | |
| | Technologický obrázek/Technical drawing | | | | | | | | |
| Mřížka/Scale | Název/Title | | | | | | | | |
| 1:20 | Magnetic yoke | | | | | | | | |
| | | | | | | Č. výkresu/Drawing No. | | Zobrazení/Sheet | |
| | | | | | | 0 -ZP- 01022501 | | 3 | |
| | | | | | | | | 5 | |
| | | | | | | | | 3 | |

SOLID EDGE ACADEMIC COPY



Všetky práva vyhrazena. Dokument je součástí duševního vlastnictví společnosti VITKOVICE HEAVY MACHINERY a.s. All rights reserved. Document is our intellectual property and commercial secret of VITKOVICE HEAVY MACHINERY a.s.

APPENDIX 7. THERMAL CALCULATION

| | | | | | | | | | |
|--|---|--|--|--|--|--|---|-----------------------|--------------|
| Titolo Title | | | Documento no. Document no. | | | Rev. Rev. | Pag. Page | Di Of | |
| Thermal Calculation MPD Dubna | | | 100RM19469 | | | 3 | 1 | 25 | |
| Altro Identificativo no. Other Identification no. | | | Rev. Rev. | | | | | | |
| Tipo doc. Doc. type | Emittente Issued by | Edizione in lingua Language | Derivato da Derived from | | | | Rev. Rev. | | |
| RT | ING | English | | | | | | | |
| Commissa Job no. | Progetto Project | | Cliente Customer | | | | | | |
| 2125 | MPD Dubna | | JINR | | | | | | |
| Rev. | Motivo Revisione Reason for revision | | | | | | | | |
| Rev. | | | | | | | | | |
| 0 | First issue | | | | | | | | |
| 1 | First Revision: wire parameters updated with the 1.73 mm strand diameter (par 3.4) | | | | | | | | |
| 2 | Second Revision: AC and Eddy Current losses (par 3.2.5) Local tie-rod effect (par 3.2.6) Update of the tie-rod design (par 3.5) | | | | | | | | |
| 3 | Third Revision: par.3.6 added: Former SIDE MODULE #1 as-built | | | | | | | | |
| Lista di Distribuzione Distribution List | | | | | | | | | |
| 3 | | |  M. Neri |  S. Grillo |  M. Tassisto |  N. Valle |  R. Marabotto | 06/12/2017 | |
| 0 | | | S. Grillo | M. Tassisto | N. Valle | | R. Marabotto | 08/07/2016 | |
| Rev. Rev. | Stato (W/R) Status | Classe Riserv (1/2/3) Confid. | Preparato Prepared | Controllato Reviewed | Verificato Verified | Verificato Verified | Verificato Verified | Approvato Approved | Data Date |

| | | | | |
|-------------------------------|--|--------------|--------------|----------|
| Titolo Title | Documento no. Document no. | Rev. Rev. | Pag. Page | Di Of |
| | 100RM19469 | 3 | 2 | 25 |
| Thermal Calculation MPD Dubna | Altro Identificativo no. Other Identification no. | Rev. Rev. | | |
| | | | | |

Summary

| | |
|--|----|
| 1. Introduction | 3 |
| 2. Thermal Input on cold mass..... | 3 |
| 2.1 JINR Study | 4 |
| 2.2 ASG Study | 6 |
| 2.3 Conclusion: thermal input | 8 |
| 3. SC coil temperature | 8 |
| 3.1 JINR study | 8 |
| 3.2 ASG study: steady state..... | 11 |
| 3.2.1 Study 1: only radiation thermal input | 12 |
| 3.2.2 Study 2: radiation thermal input + tie-rods | 13 |
| 3.2.3 Study 3: radiation thermal input + tie-rods + 2 more tube2 | 14 |
| 3.2.4 Study 4: effect of the thermal contact surface | 15 |
| 3.2.5 Study 5: effect of the AC and Eddy Current Losses..... | 16 |
| 3.2.6 Study 6: local tie-rod effects | 17 |
| 3.3 Conclusions: SC coil temperature distribution | 17 |
| 3.4 SC wire thermal properties: the new wire..... | 18 |
| 3.5 Update of the tie-rod design | 20 |
| 3.6 Former SIDE MODULE #1 as-built | 21 |
| 4. Cryogenic circuit parameters | 22 |
| 4.1 JINR Study | 22 |
| 4.2 ASG Study | 23 |
| 4.2.1 Mass flow in cool down regime..... | 23 |
| 4.2.2 Cooling circuit heat exchange – cool down | 24 |
| 4.2.3 Cooling circuit heat exchange – steady state | 24 |
| 4.3 Conclusions: cooling circuit parameters..... | 25 |

| | | | | |
|-------------------------------|--|--------------|--------------|----------|
| Titolo Title | Documento no. Document no. | Rev. Rev. | Pag. Page | Di Of |
| | 100RM19469 | 3 | 3 | 25 |
| Thermal Calculation MPD Dubna | Altro Identificativo no. Other Identification no. | Rev. Rev. | | |
| | | | | |

1. Introduction

The MPD magnet will be cooled through natural convection of liquid Helium flow (termosiphone mode). The superconductive coil is cooled indirectly via the thermal contact with the aluminum support cylinder on the outer surface of which the cooling pipes are welded.

The cooling circuit is a 'rib-type' heat exchanger, compound by 32 parallel branches. The cooling pipes are square aluminum tubes (cross-section 30x30 mm²) with a hole of 22 mm diameter.

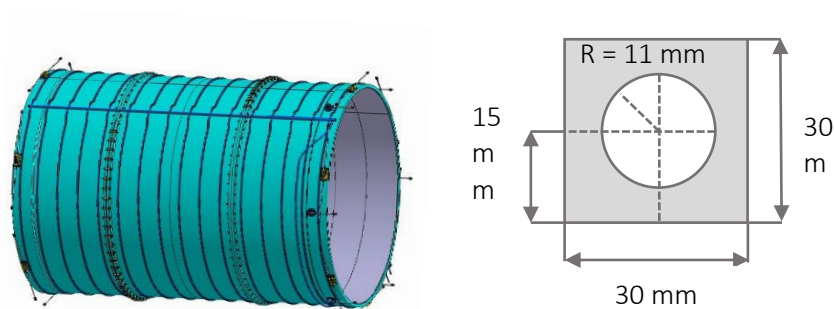


Figure 1: Cooling circuit on the cold mass and pipe cross-section.

A thermal study has been done with the goal to verify the design of the cooling circuit. The study is also compared with the previous studies done by JINR.

2. Thermal Input on cold mass

The cold mass is compound by the superconductive coil and the aluminum support cylinder. The thermal inputs on it are the following:

- Radiation Input
- Heat inflow to the cold mass supports (tie-rods)
- Conductor joints and wires
- Current Leads

These thermal inputs are present both in the steady-state and in the transition regime.

| | | | | |
|-------------------------------|--|--------------|--------------|----------|
| Titolo Title | Documento no. Document no. | Rev. Rev. | Pag. Page | Di Of |
| | 100RM19469 | 3 | 4 | 25 |
| Thermal Calculation MPD Dubna | Altro Identificativo no. Other Identification no. | Rev. Rev. | | |
| | | | | |

2.1 JINR Study

All the thermal inputs have been calculated by JINR in the documents 3HM1002.00.000P3.1 and 3HM1002.00.000P3.

Radiation Input

The radiation input has been calculated considering 10 Multi-layer insulation layers covering the cold mass.

Assuming this hypothesis, the heat flux is 0.07 W/m² on a surface of 240 m² (outer Al cylinder surface + inner SC coil surface). The radiation input on the cold mass is $Q_{rad}=0.07*240 = 16.8$ W.

Considering a safety factor of 2, $Q_r = 2*16.8 = 33.6$ W.

Heat inflow to the cold mass supports (tie-rods)

The cold mass is supported by 6 axial rods and 12 radial pairs of rods (30 rods total). All the tie-rods are secured to the thicker region of the support cylinder: the axial rods are secured only on one side while the radial rods are present in both sides.

The heat input due to the tie-rods can be calculated by:

$$Q_{tr} = \frac{Aq}{L_{cold}}$$

(A=cross-section; L_{cold} = equivalent length of the cold portion; q = integral thermal conductivity).

Axial tie-rods:

The MPD magnet is expected to have 6 axial rods on one side only. They are 24 mm diameter, 362 mm long rods made of Inconel 718 .

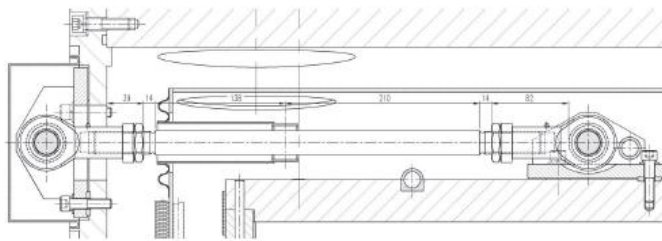


Figure 2: Axial Rod from 3HM1002.00.000P3 document.

$$A = 452 \text{ mm}^2$$

$$q = 0.031 \text{ W} \cdot \text{m} / \text{cm}^2 [4.2-77] \text{K}.$$

$$L_{eqv} = 265 \text{ mm}$$

Considering these values, the total thermal input due to one axial rod is: $Q = 0.55$ W.

Considering all the axial rods: $Q_{tr_ax} = 0.55*6 = 3.3$ W.

Considering a safety factor of 2 : $Q_{tr_ax} = 3.3*2 = 6.6$ W.

| | | | | |
|--------------------------------------|--|--------------|--------------|----------|
| Titolo Title | Documento no. Document no. | Rev. Rev. | Pag. Page | Di Of |
| | 100RM19469 | 3 | 5 | 25 |
| Thermal Calculation MPD Dubna | Altro Identificativo no. Other Identification no. | Rev. Rev. | | |
| | | | | |

Radial tie-rods:

The MPD magnet is expected to have 6 axial rods for each side (each radial tie-rod is compound by two symmetrical tie-rods for a total of 24 single tie-rods). They are 23 mm diameter, 785 mm long rods made of Inconel 718 .

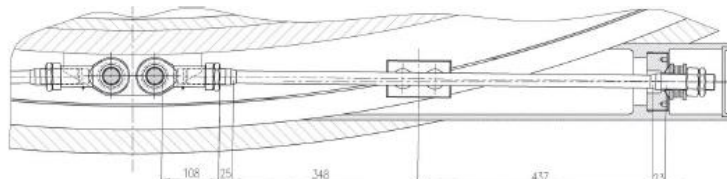


Figure 3: Radial Rod from 3HM1002.00.000P3 document.

$$A = 415 \text{ mm}^2$$

$$q = 0.031 \text{ W} \cdot \text{m} / \text{cm}^2 [4.2-77] \text{K}$$

$$L_{eqv} = 393 \text{ mm}$$

Considering these values, the total thermal input due to one axial rod is: $Q = 0.327 \text{ W}$.

Considering all the axial rods: $Q_{tr_rad} = 0.327 \cdot 24 = 7.85 \text{ W}$.

Considering a safety factor of 2 : $Q_{tr_rad} = 7.85 \cdot 2 = 15.7 \text{ W}$.

Conductor joints and wires

The heat power due to the wires, contacts and joints has been estimated to be 1 W.

Considering a security factor of 2: $Q_{wires} = 2 \text{ W}$.

Current Leads

Basing on the L 3000 American company Magnetics Inc. current lead properties, the flow of Helium required to cool the pair of current leads is 0.38 g/s at 1792 A (rated current value) and 0.23 g/s at zero current.

The heat load due to the current leads is 7 W (with operative current) and 4.2 W (without current).

| | | | | |
|-------------------------------|--|--------------|--------------|----------|
| Titolo Title | Documento no. Document no. | Rev. Rev. | Pag. Page | Di Of |
| | 100RM19469 | 3 | 6 | 25 |
| Thermal Calculation MPD Dubna | Altro Identificativo no. Other Identification no. | Rev. Rev. | | |
| | | | | |

2.2 ASG Study

Radiation input

The radiation input has been calculated considering 10 Multi-layer insulation layers covering the cold mass.

Assuming this hypothesis the heat flux at 4.5 K can be assumed equal to 0.05 W/m² (from coolcat2 RUAG documentation).

The radiation input on the cold mass (surface of 240 m² = outer Al cylinder surface + inner SC coil surface) is $Q_r = 0.05 \cdot 240 = 12$ W.

Heat inflow to the cold mass supports (tie-rods)

The heat input due to the tie-rods has been calculated by:

$$Q_{tr} = \frac{Aq}{L_{cold}}$$

(A=cross-section; L_{cold} = equivalent length of the cold portion; q = integral thermal conductivity).

Axial tie-rods:

The MPD magnet is expected to have 6 axial rods only on one side. They are 24 mm diameter, 362 mm long rods made of Inconel 718 .

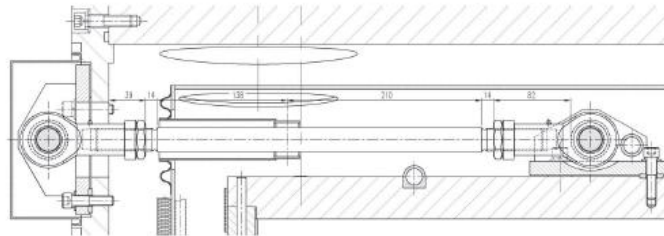


Figure 4: Axial Rod from 3HM1002.00.000P3 document.

A = 452 mm²

q = 0.033 W*m/cm² [4.2-77]K.

Leqv = 268.7 mm (Leqv = 2/3 L)

Considering these values the total thermal input due to one axial rod is: Q = 0.56 W.

Considering all the axial rods: $Q_{tr_ax} = 0.56 \cdot 6 = 3.36$ W.

Radial tie-rods:

The MPD magnet is expected to have 6 axial rods for each side (each radial tie-rod is compound by two symmetrical tie-rods for a total of 24 single tie-rods). They are 23 mm diameter, 785 mm long rods made of Inconel 718 .

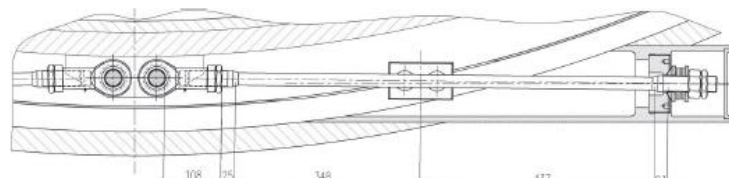


Figure 5: Radial Rod from 3HM1002.00.000P3 document.

| | | | | |
|---|--|-----------------------|-----------------------|--------------------|
| Titolo Title Thermal Calculation MPD Dubna | Documento no. Document no. 100RM19469 | Rev. Rev. 3 | Pag. Page 7 | Di Of 25 |
| | Altro Identificativo no. Other Identification no. | Rev. Rev. | | |

$A = 415 \text{ mm}^2$
 $q = 0.033 \text{ W} \cdot \text{m} / \text{cm}^2 [4.2-77] \text{K}$
 $L_{eqv} = 540 \text{ mm} (L_{eqv} = 2/3 L)$

Considering these values the total thermal input due to one axial rod is: $Q = 0.25 \text{ W}$.
 Considering all the axial rods: $Q_{tr_rad} = 0.25 \cdot 24 = 6 \text{ W}$.

Joins and wires

The heat power due to the joints can be calculated as $Q_{joints} = RI^2$.
 Joint process qualifications made by ASG for CMS verified that 1m long joints (TIG welded pieces of conductor) have a resistance of 0.7-0.8 nΩ @ B=1T (measurements done by INFN and CEA laboratories).
 Considering 1 nΩ over a meter of joint, a half-turn joint (L=7.75 m) has a resistance of 0.13 nΩ.
 In the operative regime (I=1828 A) the heat budget generates by one joint is 0.4 mW.

In the SC coil there are 7 inter-module joints and 2 intra-module joints: the total heat due to the joints at operative current is 3.6 mW.

To check the cold mass temperature several temperature sensors will be placed on magnet. From TDR (3HM1002.00.000TO) there will be 16 sensors on the only cold mass; since each of them has 4 wires there are in total 64 wires. Considering also 2 voltage traps on each joint of the 9 joints, the total number of wires is 82.

For a 0.051 mm² cross-section, 3.5 m long wire (awg 30) the heat load, without any thermalization, is $Q_{wires} = 0.18 \text{ W}$ (at operative current).

The total heat due to joints and wires at operative current is 0.1836 W.

Current leads

An optimized current lead cooled by the return flow has a specific heat load of 1.2 W/kA.
 Considering 2 current leads, in the operative current regime (I=1.82 kA), the heat load is $Q_{CL} = 4.4 \text{ W}$ while in maximum current regime (I=2388 A) $Q_{CL} = 5.7 \text{ W}$.
 At zero current the thermal input is estimated to be 60% of the input with maximum current. At zero current 2 current leads generate a heat of 3.42 W.

| | | | | |
|-------------------------------|--|--------------|--------------|----------|
| Titolo Title | Documento no. Document no. | Rev. Rev. | Pag. Page | Di Of |
| | 100RM19469 | 3 | 8 | 25 |
| Thermal Calculation MPD Dubna | Altro Identificativo no. Other Identification no. | Rev. Rev. | | |
| | | | | |

2.3 Conclusion: thermal input

The comparison of the thermal inputs on the cold mass calculated by JINR and by ASG is shown in the Table 1:

| Thermal Input | JINR | ASG |
|-------------------------------------|--------------------------------------|---------------------------------------|
| Radiative [W] | 16.8 | 12 |
| Axial tie-rods [W] | 3.3 | 3.36 |
| Radial tie-rods [W] | 15.7 (sf = 2) | 6 |
| Joints, wires, cables [W] | 1 | 0.1836 |
| Current leads [W] (Nominal current) | 7.0 (with current)/ 4.2 (no current) | 4.4 (with current) |
| Current leads [W] (Maximum current) | | 5.7 (with current)/ 3.42 (no current) |

Table 1: comparison between the thermal inputs calculated by JINR team and by ASG. The fs factor is a security factor.

3. SC coil temperature

A study on the maximum temperature reached by the coil has been done. This study is necessary to define the temperature margin on the wire.

3.1 JINR study

The model considered for the study includes the coil, with its insulation, the support cylinder (Al 5083) and the cooling tubes (Al 1100). In the original project the cooling tubes were glued to the support cylinder with a layer (0.2 mm) of epoxy resin.

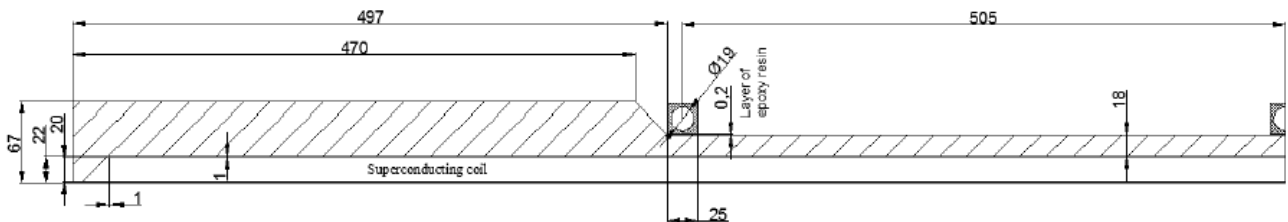


Figure 6: system considered for the thermal calculations by the JINR team¹.

The study was carried out with the following assumptions:

- the superconducting coil with interturn insulation is considered as an anisotropic cylinder with equivalent thermal conductivity in the axial, radial and azimuthal directions;
- the determination of the thermal conductivity of the superconducting coil is not taken into account the thermal conductivity of the copper matrix superconducting wire and the thermal conductivity of a superconductor;

| | | | | |
|-------------------------------|--|--------------|--------------|----------|
| Titolo Title | Documento no. Document no. | Rev. Rev. | Pag. Page | Di Of |
| | 100RM19469 | 3 | 9 | 25 |
| Thermal Calculation MPD Dubna | Altro Identificativo no. Other Identification no. | Rev. Rev. | | |
| | | | | |

- heat gain to the cold mass at the suspension rods are removed by thermal shunts and does not affect the temperature distribution in the winding.

The input data are reported in Table 2.

| Thermal loads | steady-state regime (normal operation) | Transit regime |
|--|---|----------------|
| Radiation, W/m ² | 0.14 | 0.14 |
| Eddy current losses in the Al support cylinder, W/m ³ | - | 3.3 |

Table 2: input data used in the thermal calculations made by the JINR team (3HM1002.00.000P3.1).

The radiation has been calculated considering 10 layers of Multi-layer insulation + a security factor of 2 and it has to be applied on the whole cold mass surface, 240 m² (as described in the document 3HM1002.00.000P3). The radiative input is 33.6 W.

The material used are described by their thermal conductivity reported in Table 3, where the main columns are:

Temperature [K], Epoxy glue Kt [W/(m*K)], Al 1100 Kt [W/(m*K)], Al 5083 Kt [W/(m*K)], Insulation Kt [W/(m*K)], SC wire Kt [W/(m*K)] and Cable matrix (Al RRR1000) Kt [W/(m*K)].

Табл. 12. Коэффициент теплопроводности материалов, используемых в расчете

| Тем-ра, К | Коэффициент теплопроводности, Вт/м*К | | | | | | |
|--------------|--------------------------------------|-----------------------------------|--------------------------------|----------|----------------------------|---|---|
| | Эпоксидный клей | Охлаждающая трубка, Al-1100 | Опорный цилиндр, Al-5083 | Изоляция | Сверхпроводящая обмотка | | Матрица кабеля, Алюминий (RRR=1000) |
| | | | | | аксиальное направление | радиальное и азимутальное направление | |
| 4 | 0.05 | 54.1 | 3.2 | 0.055 | 0.61 | 3629 | 3992 |
| 6 | 0.052 | 83.3 | 4.8 | 0.07 | 0.77 | 5283 | 5811 |
| 8 | 0.054 | 113.5 | 6.4 | 0.09 | 0.99 | 6612 | 7273 |
| 10 | 0.056 | 142 | 8.0 | 0.105 | 1.2 | 7461 | 8207 |
| 15 | 0.06 | 214 | 12.0 | 0.13 | 1.4 | 7545 | 8299 |
| 20 | 0.065 | 283 | 16.0 | 0.15 | 1.7 | 6249 | 6874 |
| 30 | 0.074 | 372 | 23.9 | 0.2 | 2.2 | 3511 | 3862 |
| 40 | 0.083 | 389 | 31.5 | 0.24 | 2.6 | 1796 | 1976 |
| 50 | 0.092 | 369 | 38.4 | 0.265 | 2.9 | 989 | 1088 |
| 70 | 0.104 | 308 | 49.5 | 0.325 | 3.6 | 461 | 507 |
| 100 | 0.114 | 250 | 62.4 | 0.437 | 4.7 | 273 | 300 |
| 120 | 0.119 | 231 | 70.0 | 0.47 | 5.1 | 238 | 262 |
| 160 | 0.129 | 218 | 83.8 | 0.52 | 5.6 | 221 | 243 |
| 200 | 0.136 | 215 | 95.7 | 0.54 | 5.8 | 218 | 238 |
| 300 | 0.15 | 212 | 121.4 | 0.63 | 6.8 | 215 | 237 |

Table 3: Thermal conductivity of the material used in the model (3HM1002.00.000P3.1).

| | | | | |
|-------------------------------|--|--------------|--------------|----------|
| Titolo Title | Documento no. Document no. | Rev. Rev. | Pag. Page | Di Of |
| | 100RM19469 | 3 | 10 | 25 |
| Thermal Calculation MPD Dubna | Altro Identificativo no. Other Identification no. | Rev. Rev. | | |
| | | | | |

The results of this study are shown in *Figure 7: Results obtained by JINR study: temperature distribution in the cold mass (3HM1002.00.000P3.1).* and are reported in the Table 4.

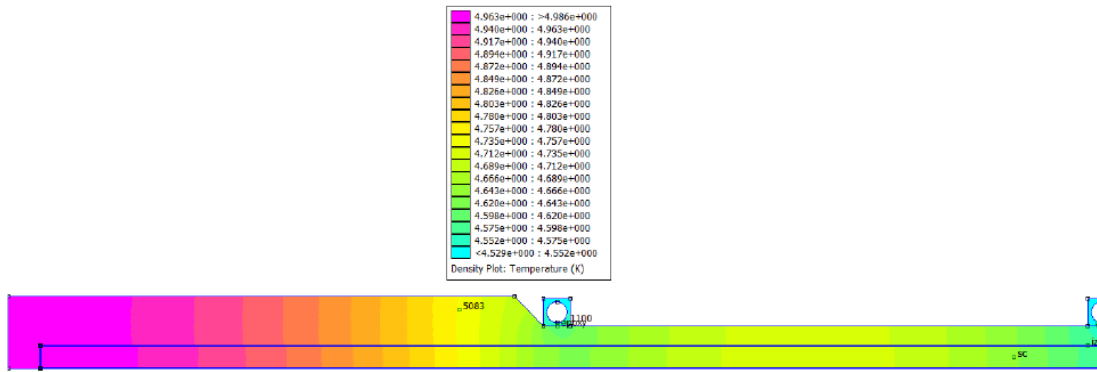


Рис. 19. Распределение температуры для варианта: ввод тока, уровень в гелиевой ванне контрольного дьюада 700 мм.

Figure 7: Results obtained by JINR study: temperature distribution in the cold mass (3HM1002.00.000P3.1).

| № | Mode of solenoid operation | Level in helium bath, mm | Helium mass flow, g/s | Heat transfer coefficient, W/m2*K | Thermal load | | Maximal temperature in the coil, K | Temperature increase, above 4.5 K, K | Temperature drop on the epoxy glue connection of a rib, K |
|---|----------------------------|--------------------------|-----------------------|-----------------------------------|-----------------|--------------------|------------------------------------|--------------------------------------|---|
| | | | | | Radiation, W/m2 | Eddy current, W/m3 | | | |
| 1 | Steady state | 100 | 1.24 | 77 | 0.14 | - | 4.84 | 0.34 | 0.04 |
| | | 700 | 1.60 | 95 | 0.14 | - | 4.83 | 0.33 | 0.04 |
| 2 | Current ramping | 100 | 1.30 | 80 | 0.14 | 3.3 | 4.99 | 0.49 | 0.06 |
| | | 700 | 1.66 | 98 | 0.14 | 3.3 | 4.98 | 0.48 | 0.06 |

Table 4: Maximum temperature reached by the coil in the steady state and in the transient regime.

The maximum temperature reached by the coil is:

- steady state = 4.84 K;
- transient regime = 4.99 K

| | | | | |
|-------------------------------|--|--------------|--------------|----------|
| Titolo Title | Documento no. Document no. | Rev. Rev. | Pag. Page | Di Of |
| | 100RM19469 | 3 | 11 | 25 |
| Thermal Calculation MPD Dubna | Altro Identificativo no. Other Identification no. | Rev. Rev. | | |
| | | | | |

3.2 ASG study: steady state

The basic system considered includes the SC coil with the insulation, the support cylinder (Al 5083-O) and the cooling tubes (approx.: Al 5083-O). The cooling tubes are thought to be welded to the support cylinder.

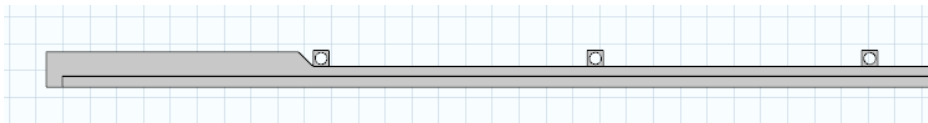


Figure 8: system modeled with Comsol software.

Different studies have been carried out, all with the following assumptions:

- the impregnated fiberglass layer between the coil and the support cylinder has been taken into account as G10;
- the thermal properties of the SC winding have been calculated as equivalent bulk properties: an isotropic C_p [J/(kg*K)] and an anisotropic K [W/(m*K)];
- only the steady state has been studied;
- a perfect thermal contact between the whole cooling tube surface and the support cylinder has been considered.

Focusing on the steady state study, the input data used in all the simulations are:

- a temperature of 4.5 K fixed on the internal radius of tubes;
- a radiation input of 0.14 W/m^2 (to be comparable with JINR calculations)

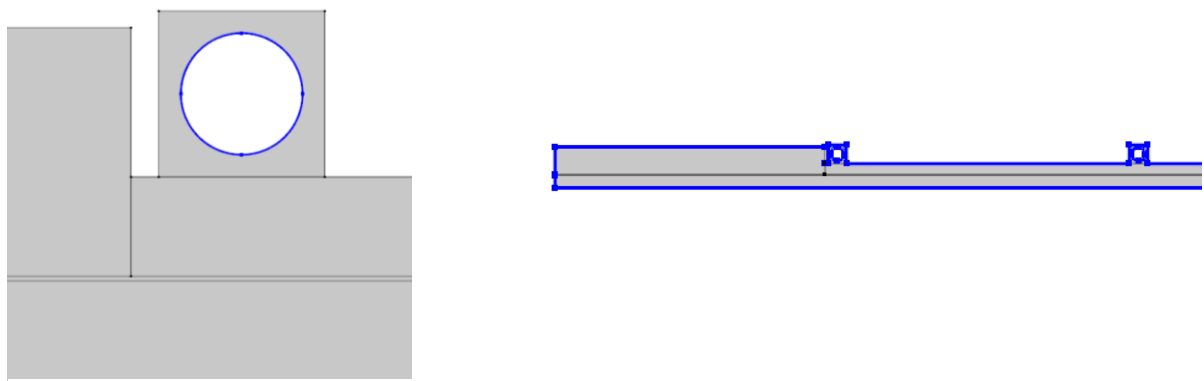


Figure 9: Thermal input data: a fixed temperature (4.5 K) in the inner surface of the cooling tube and the radiation input on the whole cold mass surface.

| | | | | |
|---|--|------------------------------|-------------------------------|---------------------------|
| Titolo Title Thermal Calculation MPD Dubna | Documento no. Document no. 100RM19469 | Rev. Rev. 3 | Pag. Page 12 | Di Of 25 |
| | Altro Identificativo no. Other Identification no. | Rev. Rev. | | |

The material properties, in particular the thermal conductivity, have been calculated using CRYOCOMP Software. The SC coil material properties have been calculated as equivalent bulk properties; the thermal conductivity has been considered as anisotropic. The materials that compose the SC wire are NbTi, Cu (RRR =100) and Al (RRR=1000) with a ratio of NbTi/Cu/Al=1/0.9/100.

3.2.1 Study 1: only radiation thermal input

The first study focuses on the effect of the only radiation thermal input. Considering a surface of 240 m², the total thermal input is $0.14 \text{ W/m}^2 \cdot 240 \text{ m}^2 = 33.6 \text{ W}$, where a safety factor of 2 has been introduced ($0.07 \cdot 2 \text{ W/m}^2$).

In this configuration the temperature of the coil reaches 4.75 K at the end of the winding where there are not cooling tubes. The temperature distribution is symmetric with respect to the median plane.

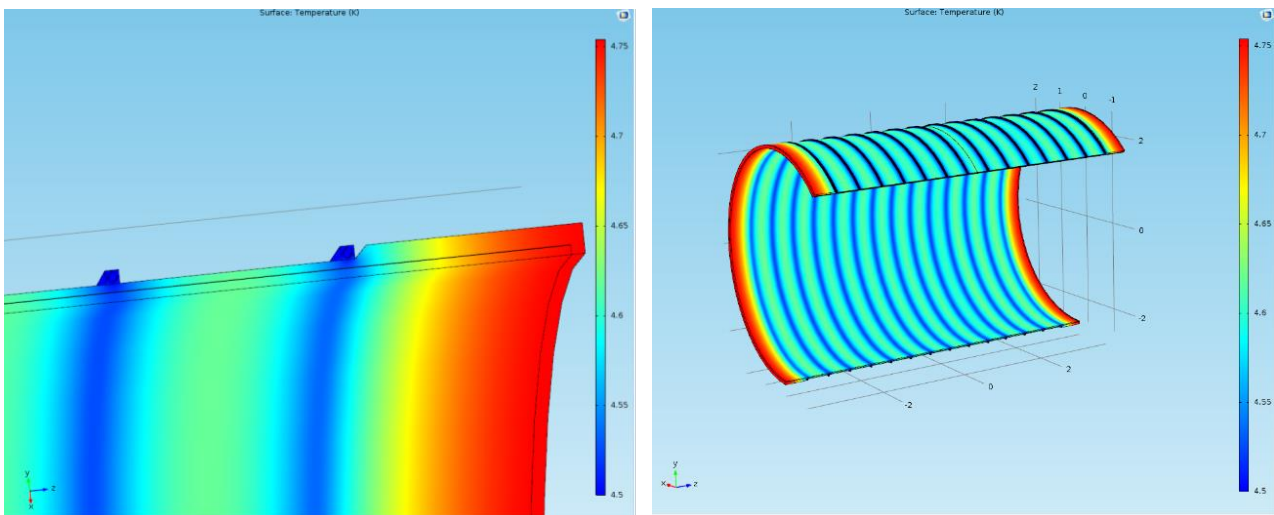


Figure 10: Temperature distribution calculated with the only radiation input.

| | | | | |
|-------------------------------|--|--------------|--------------|----------|
| Titolo Title | Documento no. Document no. | Rev. Rev. | Pag. Page | Di Of |
| | 100RM19469 | 3 | 13 | 25 |
| Thermal Calculation MPD Dubna | Altro Identificativo no. Other Identification no. | Rev. Rev. | | |
| | | | | |

3.2.2 Study 2: radiation thermal input + tie-rods

The second study adds the thermal input due to the tie-rods calculated in the previous section (axial rods $Q_{tr_ax}= 3.7$ W; radial rods $Q_{tr_rad}= 6.6$ W, with a safety factor of 1.1).

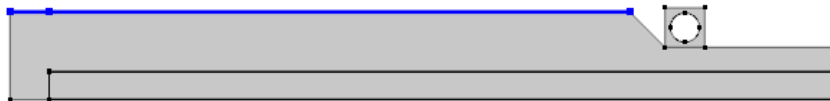


Figure 11: Thicker region of the support cylinder where the thermal input due to the tie-rods is applied.

In the model the thermal input due to the tie-rods is applied to the thicker portion of the support cylinder: the axial rods contribute only on one side, while the radial ones contribute on both the sides.

In this configuration the temperature of the coil reaches 5.5 K on the side where both axial and radial tie-rods are present, and 5.1 K on the other side.

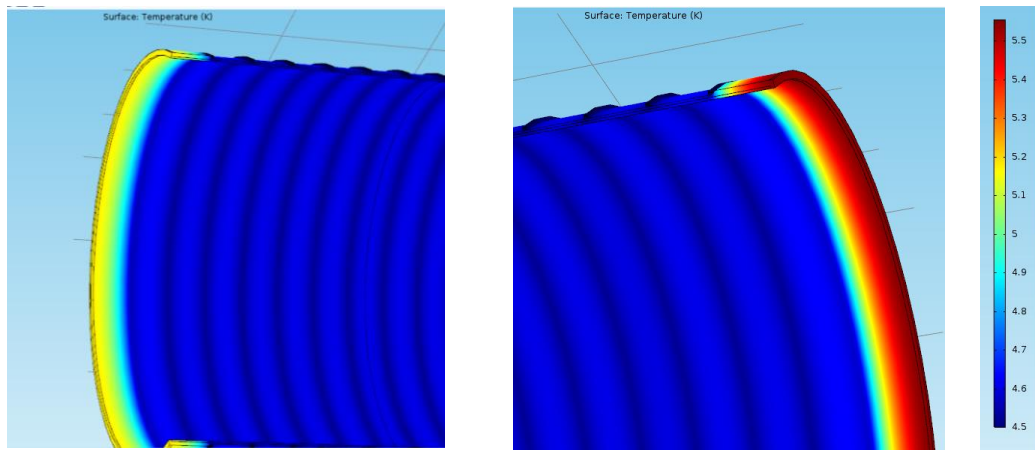


Figure 12: Temperature distribution considering both the radiation and the tie-rods thermal inputs.

The temperature reached by the coil is too high: one more cooling pipe has been added on each side of the support cylinder.

| | | | | |
|-------------------------------|--|--------------|--------------|----------|
| Titolo Title | Documento no. Document no. | Rev. Rev. | Pag. Page | Di Of |
| | 100RM19469 | 3 | 14 | 25 |
| Thermal Calculation MPD Dubna | Altro Identificativo no. Other Identification no. | Rev. Rev. | | |
| | | | | |

3.2.3 Study 3: radiation thermal input + tie-rods + 2 more tube2

To reduce the temperature in the end of the winding two more cooling tubes have been positioned on the thicker region of the support cylinder. They are supposed to be at about 0.18 m from the edge of the support cylinder.

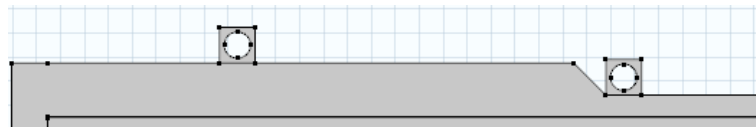


Figure 13: model with the cooling tubes on the thicker region of the support cylinder.

In this configuration the coil reaches 4.71 K on the side with both axial and radial tie-rods and 4.6 K on the other side.

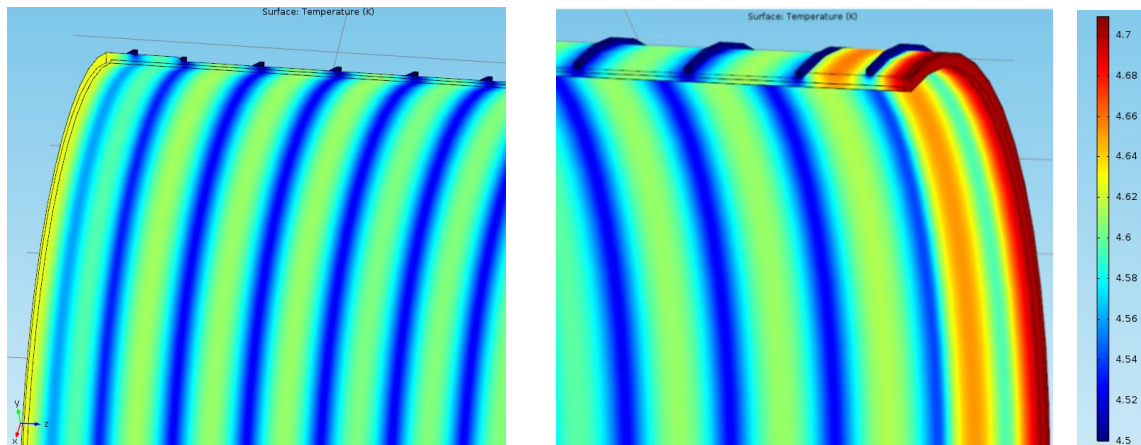


Figure 14: Temperature distribution with two more cooling tubes.

The two additional cooling pipes are necessary to reduce the temperature of the SC coil.

| | | | | |
|-------------------------------|--|--------------|--------------|----------|
| Titolo Title | Documento no. Document no. | Rev. Rev. | Pag. Page | Di Of |
| | 100RM19469 | 3 | 15 | 25 |
| Thermal Calculation MPD Dubna | Altro Identificativo no. Other Identification no. | Rev. Rev. | | |
| | | | | |

3.2.4 Study 4: effect of the thermal contact surface

The cooling tubes would be welded in alternately positions with respect to their axis. In this configuration the not welded region could be lifted and could be not more in contact with the support cylinder.



Figure 15: Schematic example of the welding typology of the cooling tube.

To take into account a not perfect contact, a layer (0.1 mm) of air has been introduced between half (or 2/3) cooling tube surface and the support cylinder.

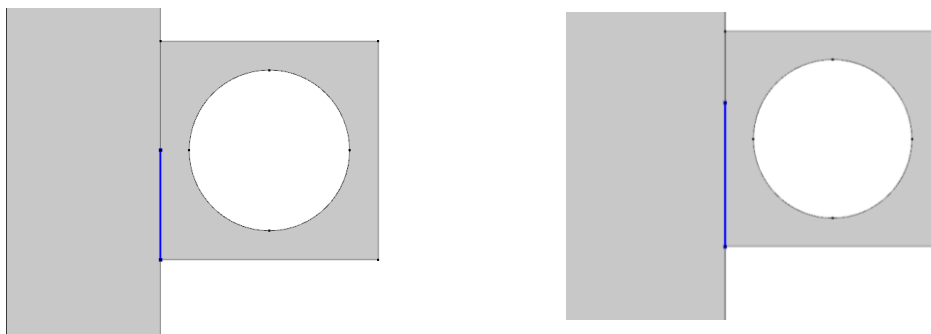


Figure 16: part of the cooling tube surface that is not in contact with the support cylinder. A layer of air has been introduced.

The thermal input considered are the same of section 3.2.3.

- Considering half cooling tube surface in contact the coil reaches a maximum temperature of 4.74 K on the side with both axial and radial tie-rods and at 4.65 K on the other side.

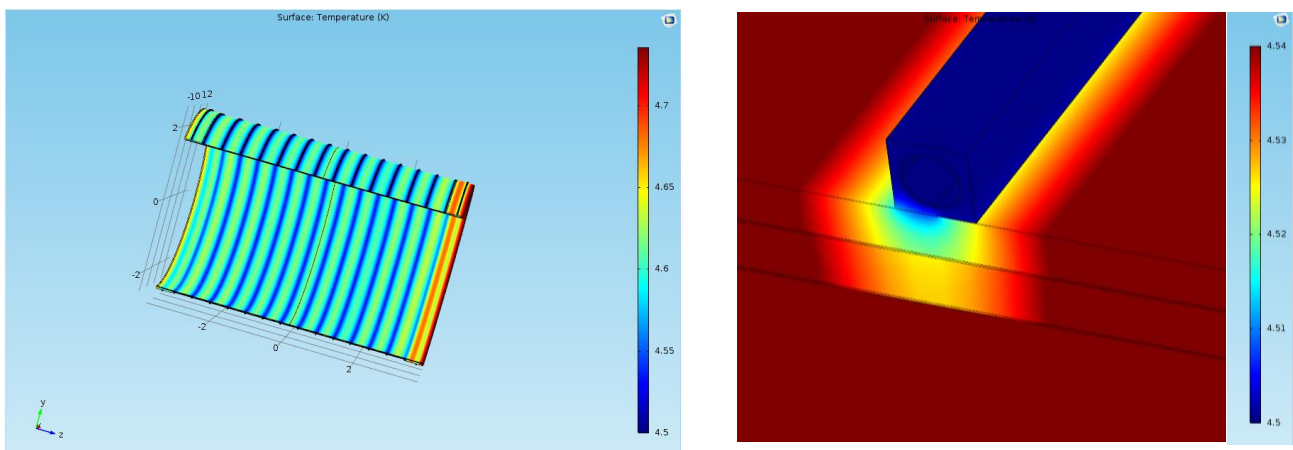


Figure 17: Temperature distribution on the cold mass (left) and focus on one cooling tube (right).

- Considering 1/3 cooling tube surface in contact the coil reaches a maximum temperature of 4.76 K on the side with both axial and radial tie-rods and at 4.68 K on the other side.

| | | | | |
|---|--|------------------------------|-------------------------------|---------------------------|
| Titolo Title Thermal Calculation MPD Dubna | Documento no. Document no. 100RM19469 | Rev. Rev. 3 | Pag. Page 16 | Di Of 25 |
| | Altro Identificativo no. Other Identification no. | Rev. Rev. | | |

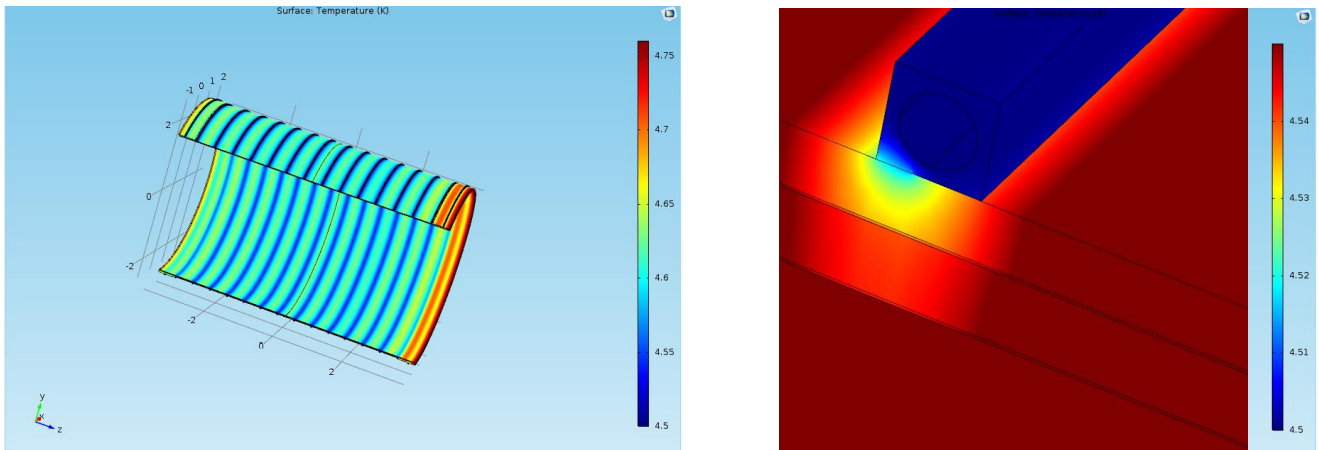


Figure 18: Temperature distribution on the cold mass (left) and focus on the in contact cooling tube surface (right).

3.2.5 Study 5: effect of the AC and Eddy Current Losses

During the magnet charging, the conducting masses are affected by eddy current losses and the coil is affected by AC losses.

In order to study the thermal effect of an additional power deposition on these surfaces, a batch of simulations has been run.

In figure 19 there is the maximum coil temperature as function of AC losses and eddy current losses on the Aluminium former.

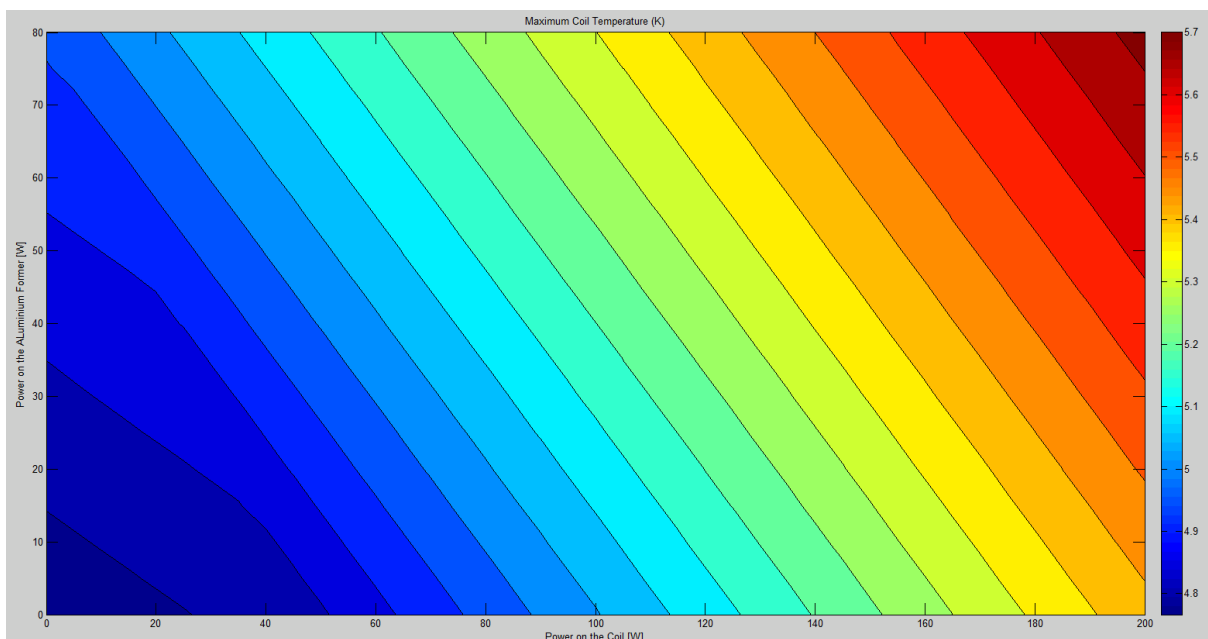


Figure 19: maximum temperature of the coil as function of the AC and Eddy Current Losses.

| | | | | |
|--------------------------------------|--|--------------|--------------|----------|
| Titolo Title | Documento no. Document no. | Rev. Rev. | Pag. Page | Di Of |
| | 100RM19469 | 3 | 17 | 25 |
| Thermal Calculation MPD Dubna | Altro Identificativo no. Other Identification no. | Rev. Rev. | | |
| | | | | |

Considering a 5 hours ramp up from 0 to the maximum current, the estimated losses are:

- 0.09 W of eddy currents
- 0.3 W AC losses

The graph in figure 19 shows how these two values are perfectly compatible with a negligible increase of the maximum temperature of the superconductive coil.

3.2.6 Study 6: local tie-rod effects

The local tie-rod effect has been evaluated by a 3D thermal calculation: on the aluminium former the radiation thermal input and the 12 tie-rod side have been simulated; the coil and the counter mass insulation have not been taken into account.

The local temperature pick below the tie-rod (considered as a perfect contact thermal input) is about 5.2K.

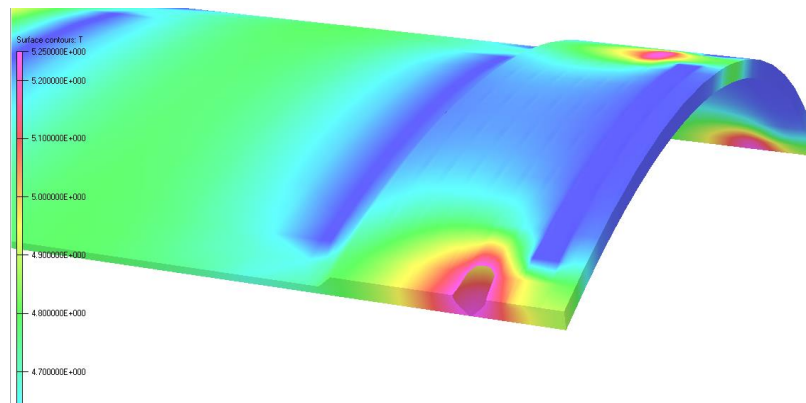


Figure 20: Local temperature pick below the tie-rod anchoring point.

The local radial heat flux is around 1 W/m².

Considering the high thermal impedance ($k \sim 0.2$ W/m/K) of the counter mass (thickness 0.8 mm), it is possible to estimate a thermal gradient of 0.4 K.

It means that the maximum local effect on the coil is negligible in the maximum temperature (2D calculated) coil areas.

3.3 Conclusions: SC coil temperature distribution

The thermal study focused on the temperature distribution on the cold mass.

Considering a perfect thermal contact between the cooling tubes and the support cylinder surfaces, the results of this study are:

- at least 10 layers of Multi-layer insulations are necessary to reduce the radiative input on the cold mass;
- the thermal input due to the tie-rods can not be neglected;
- with the supposed cooling system and the radiative and tie-rod thermal inputs, the coil reaches 5.5 K on the side with both axial and radial tie-rods and 5.1 K on the other side.

| | | | | |
|--------------------------------------|--|--------------|--------------|----------|
| Titolo Title | Documento no. Document no. | Rev. Rev. | Pag. Page | Di Of |
| | 100RM19469 | 3 | 18 | 25 |
| Thermal Calculation MPD Dubna | Altro Identificativo no. Other Identification no. | Rev. Rev. | | |
| | | | | |

Another cooling tube must be added on each thicker region of the support cylinder. In this configuration the coil reaches 4.71 K on the side with both axial and radial tie-rods and 4.6 K on the other side.

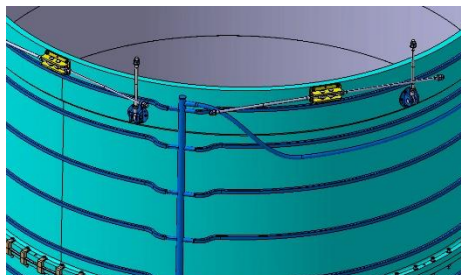


Figure 21: Zoom on the thicker part of the aluminium support cylinder in which a pipe has been added.

A not perfect contact between cooling tubes and support cylinder produces an increase of the maximum temperature reached of 0.05 K (4.76 K VS 4.71 K).

3.4 SC wire thermal properties: the new wire

In order to guarantee the requirements on the critical current, the wire has been changed. In particular the strand diameter has been increased (from 1.5 mm to 1.73 mm), fixing the NbTi/Cu ratio (1/0.9) but changing the Strand/Al ratio (from 1.9/100 to 1.9/65). The material properties have been re-calculated: the comparison with the old ones shows that the wire change has not a relevant effect on the material properties (Figure 22 and Figure 23).

Since the material properties have not a relevant change, also the thermal behavior of the wire does not change. The thermal calculations, done taking into account the new wire, give the same temperature distribution.

| | | | | |
|---|--|------------------------------|-------------------------------|---------------------------|
| Titolo Title Thermal Calculation MPD Dubna | Documento no. Document no. 100RM19469 | Rev. Rev. 3 | Pag. Page 19 | Di Of 25 |
| | Altro Identificativo no. Other Identification no. | Rev. Rev. | | |

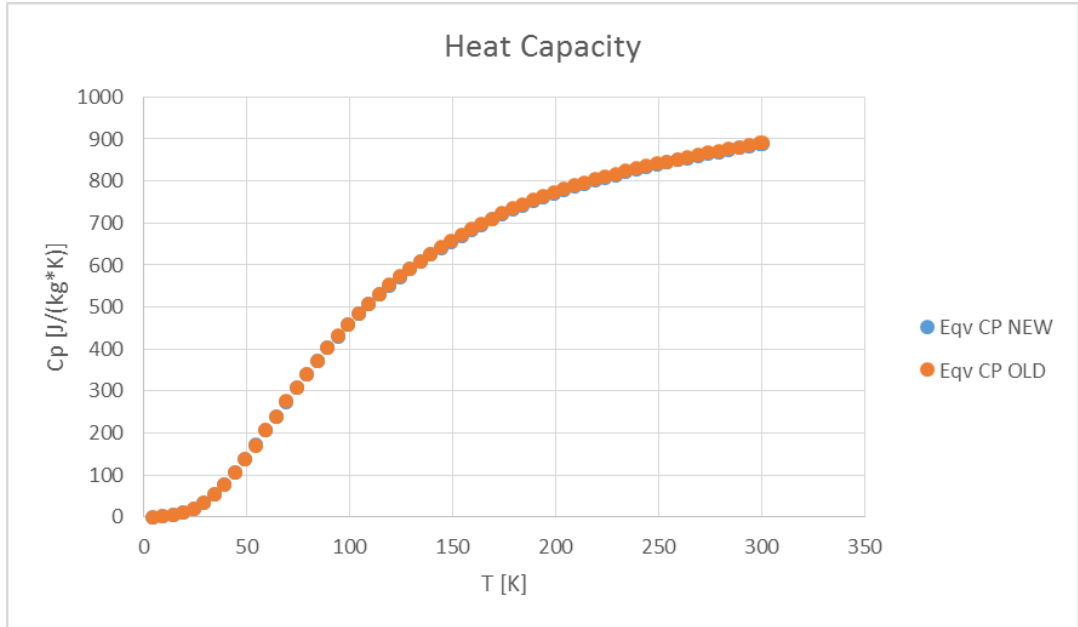


Figure 22: Comparison between the heat capacities of the two different wires.

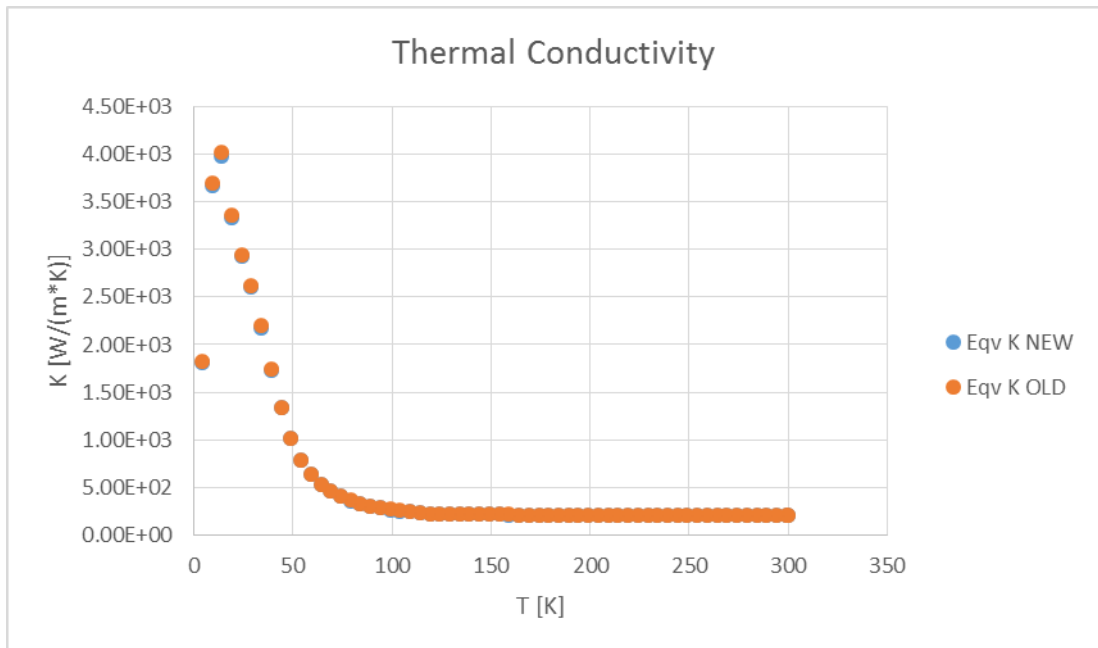


Figure 23: Comparison between the thermal conductivities of the two different wires.

| | | | | |
|-------------------------------|--|--------------|--------------|----------|
| Titolo Title | Documento no. Document no. | Rev. Rev. | Pag. Page | Di Of |
| | 100RM19469 | 3 | 20 | 25 |
| Thermal Calculation MPD Dubna | Altro Identificativo no. Other Identification no. | Rev. Rev. | | |
| | | | | |

3.5 Update of the tie-rod design

The design of the tie-rods has been updated: the impact of this update on the thermal input carried by the tie-rod has been verified.

Axial tie-rods:

The MPD magnet is expected to have 6 axial rods only on one side. They are 24 mm diameter, 415.5 mm long rods made of Inconel 718 .

In order to calculate the thermal input due to a tie-rod, the formula is:

$$Q_{tr} = \frac{Aq}{L_{cold}}$$

where A=cross-section; Lcold = equivalent length of the cold portion; q = integral thermal conductivity.

$$A = 459 \text{ mm}^2$$

$$q = 309 \text{ W/m [4.2-77]K.}$$

$$Leqv = 277 \text{ mm (Leqv} = 2/3 L)$$

Considering these values the total thermal input due to one axial rod is: $Q = 0.512 \text{ W.}$

Considering all the axial rods: $Q_{tr_ax} = 0.512 * 6 = 3.1 \text{ W.}$

Radial tie-rods:

The MPD magnet is expected to have 6 radial rods for each side (each radial tie-rod is compound by two symmetrical tie-rods for a total of 24 single tie-rods). Each couple is formed by two tie-rods of 24 mm diameter made of Inconel 718. The length is slightly different: the top radial tie-rod is 959 mm long, while the bottom tie-rod is 963 mm long.

$$A = 459 \text{ mm}^2$$

$$q = 309 \text{ W/m [4.2-77]K.}$$

$$Leqv_top = 639.3 \text{ mm (Leqv} = 2/3 L); Leqv_bottom = 642 \text{ mm (Leqv} = 2/3 L)$$

Considering these values the total thermal input due to one radial rod is: $Q_{top} = Q_{bottom} = 0.22.$

Considering all the radial rods: $Q_{tr_rad} = 0.22 * 24 = 5.28 \text{ W.}$

Since the thermal input due to the updated tie-rods is less than the old one, it is not necessary to calculate the temperature distribution on the cold mass. The calculations reported in the previous paragraphs can be considered as conservative.

| | | | | |
|-------------------------------|--|--------------|--------------|----------|
| Titolo Title | Documento no. Document no. | Rev. Rev. | Pag. Page | Di Of |
| | 100RM19469 | 3 | 21 | 25 |
| Thermal Calculation MPD Dubna | Altro Identificativo no. Other Identification no. | Rev. Rev. | | |
| | | | | |

3.6 Former SIDE MODULE #1 as-built

Former SIDE MODULE 1# was built with the path of the cooling circuit shown in Figure 24.

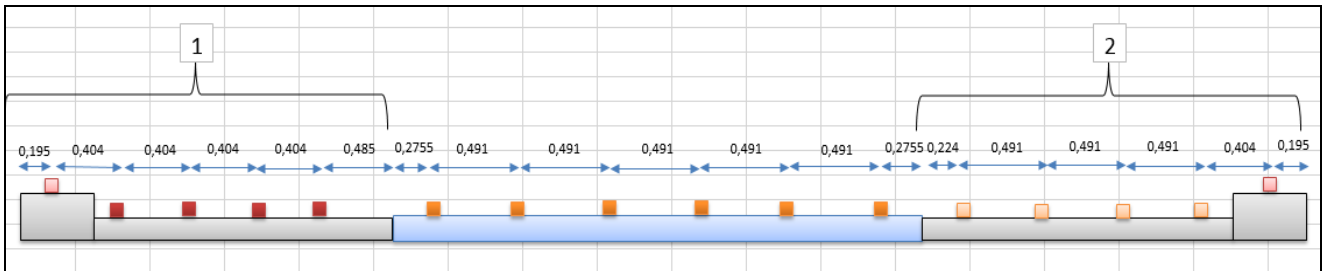


Figure 24: Formers cooling circuit path. SIDE MODULE #1 as-built on the left.

In particular, red tubes in Figure 24 (on the left) are closer to the thicker part of the former compared to tubes in SIDE MODULE #2 (light orange, on the right). Distance between tubes in former SIDE MODULE #1 is 404 mm for all the tubes, while in former SIDE MODULE #2 the distance between the tubes in the thinner part is 491mm.

On the SIDE MODULE #1 are installed both the axial and the radial tie-rods, while in the SIDE MODULE #2 only radial tie-rods are installed.

Considering the same input used in previous paragraphs, the calculations show that **the temperature doesn't rise above 4.8K**, the maximum temperature considered in operating mode of the magnet to calculate the temperature margins of the superconductive cable. In particular, the difference on the maximum temperature calculated using the as-built path and the original path is less than 0.002K.

Figure 25 shows the thermal behavior of the magnet in steady state. The colors exalt the difference of temperature between the tubes.

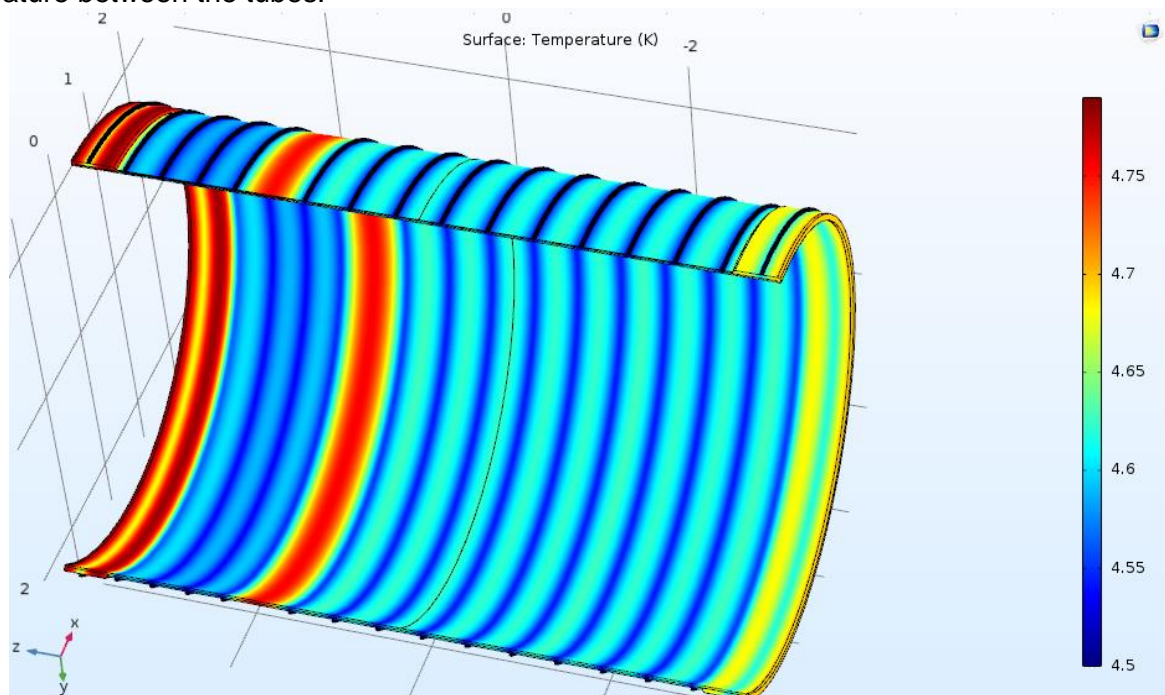


Figure 25: Temperature distribution in the coil during steady state. SIDE MODULE #1 as-built on the left.

| | | | | |
|-------------------------------|--|--------------|--------------|----------|
| Titolo Title | Documento no. Document no. | Rev. Rev. | Pag. Page | Di Of |
| | 100RM19469 | 3 | 22 | 25 |
| Thermal Calculation MPD Dubna | Altro Identificativo no. Other Identification no. | Rev. Rev. | | |
| | | | | |

4. Cryogenic circuit parameters

The cooling circuit of the cold mass is a 'rib-cage' type in direct contact with the aluminum support cylinder. The dimensions of the cooling circuit must be verified to guarantee the correct cooling of the SC coil.

This verify has to be done in the cool-down regime and in particular at room temperature.

4.1 JINR Study

In the 3HM1002.00.000TO document, in Table 3.2.1 at page 115, a flow of 16.2 g/s is indicated as incoming flow to guarantee the cool-down (300 to 4.5 K) with a rate of 1 K/h.

The flow value has been calculated using a finite element analysis, described in 3HM1002.00.000P3.1 document.

The model is a 2D axialsymmetric model of the cold mass (SC coil + support cylinder).

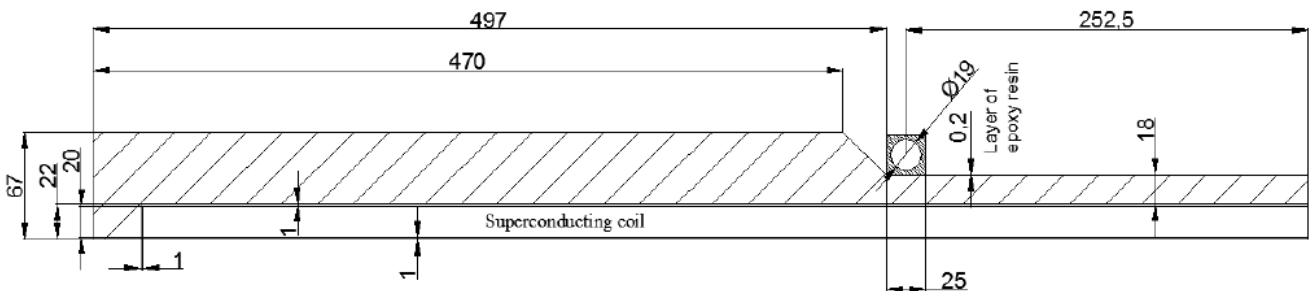


Figure 26: finite element model used for the study of the He flow necessary for the cool-down.

The SC coil material properties (thermal conductivity, heat capacity and density) have been calculated as equivalent. The SC coil thermal conductivity has been considered anisotropic (radial, axial and azimuthal components).

This study was carried out considering a the cool-down of the cold mass from 300 to 80 K, with a rate of 1 K/h and keeping a maximum temperature difference between He gas and support cylinder of 20 K. The stream of He cooling the cold mass is considered at variable temperature at a pressure of 3 bar.

Assuming these initial data, the necessary gas flow is 0.6 g/s for pipe. Considering 27 pipes, the total flow is 16.2 g/s.

With a flow of 16.2 g/s and a rate of 1 K/h the full cooling of the cold mass needs 230 hours.

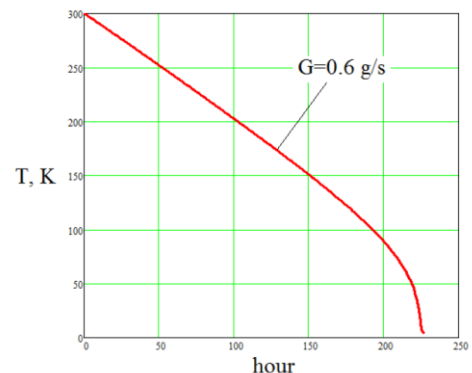


Figure 27: SC winding temperature VS time, considering a cooling rate of 1 K/h and a gas flow of 0.6 g/s.

| | | | | |
|-------------------------------|--|--------------|--------------|----------|
| Titolo Title | Documento no. Document no. | Rev. Rev. | Pag. Page | Di Of |
| | 100RM19469 | 3 | 23 | 25 |
| Thermal Calculation MPD Dubna | Altro Identificativo no. Other Identification no. | Rev. Rev. | | |
| | | | | |

4.2 ASG Study

4.2.1 Mass flow in cool down regime

The He gas flow necessary to guarantee the cool-down can be calculated at room temperature. The mass to be cooled is formed by SC coil and by the aluminum support cylinder. It has a mass of $m_{CM}=15 \cdot 10^3$ kg and an equivalent heat capacity (at 300 K) of 900 J/(kg*K). Assuming a cooling rate of 1 K/h, the power necessary to cool down the cold mass is:

$$P = \frac{m_{CM} C_{PCM} \dot{T}}{3600} = 3750 \text{ W}$$

The cooling circuit is formed by 32 pipes (28 ribs on the thinner part and 4 on the thicker part of the support cylinder), each with a diameter of 22 mm, a length of 7914 mm and a cross-section of 380 mm.

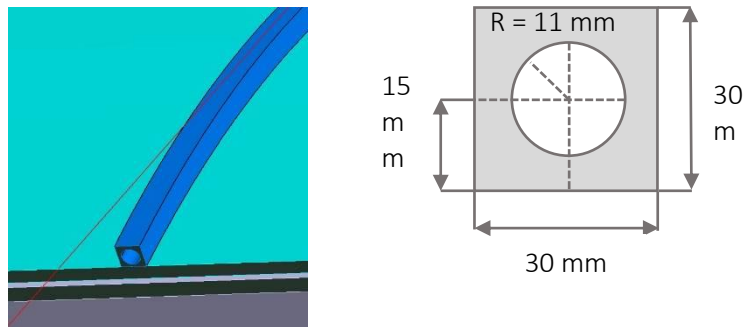


Figure 28: Cross-section of the cooling circuit pipe.

Considering a negligible pressure drop in the pipes, the total power necessary to cool down the cold mass can be divided for the pipes: each pipe must absorb

$$P_i = \frac{P}{32} = 117 \text{ W}$$

Considering a temperature difference, between the cooling gas and the cold mass, $\Delta T = 20 \text{ K}$, the He flow (\dot{m}_{He}), for a single pipe, necessary to cool down the cold mass is given by:

$$P = \dot{m}_{He} C_{p_{He}} \Delta T$$

The mass flow is $\dot{m}_{He} = 0.0011 \text{ Kg/s}$.

Considering 32 pipes, the total gas flow is $0.0011 \cdot 32 = 0.0352 \text{ Kg/s}$.

| | | | | |
|-------------------------------|--|--------------|--------------|----------|
| Titolo Title | Documento no. Document no. | Rev. Rev. | Pag. Page | Di Of |
| | 100RM19469 | 3 | 24 | 25 |
| Thermal Calculation MPD Dubna | Altro Identificativo no. Other Identification no. | Rev. Rev. | | |
| | | | | |

4.2.2 Cooling circuit heat exchange – cool down

To verify the right dimensions of the cooling circuit, the allowable heat exchange has been calculated. The cooling circuit pipes have a lateral surface of $S_{Lat} = 0.55 \text{ m}^2$. The exchangeable power by the pipe can be calculated as:

$$P_{exc} = f_{HTC} \overline{\Delta T} S_{Lat}$$

where f_{HTC} is the heat transfer coefficient depending on the pipe dimensions (diameter D) and on the coolant gas properties (thermal conductivity λ and Nusselt's number Nu):

$$f_{HTC} = \frac{\lambda Nu}{D}$$

while $\overline{\Delta T}$ is the difference between the cold mass temperature (300 K) and the average temperature of the gas (290 K considering 300 K for the outflow gas and 280 K for the inflow gas).

With this assumptions each pipe could exchange up to 490 W, that is about 4 times greater than the necessary (117 W). To exchange the required power (117 W) a lateral surface of 0.131 m^2 is enough. The cooling circuit pipes have a latera surface 4 times greater.

4.2.3 Cooling circuit heat exchange – steady state

This study has been done considering the following heat flows: 40 W due to radiation and about 15 W due to conduction (tie-rods).

The heat flows for branch can be divided in two components:

- 1.25 W due to radiation acting on all the 32 pipes (internal + external branches)
- 3.75 W due to conduction, acting only on the 4 more external pipes

Assuming a heat transfer surface of 0.1375 m^2 (25% of the pipe lateral surface), the specific heats for branch are:

- 9.1 W/m^2 (internal branch) = $1.25/0.1375$
- 36.4 W/m^2 (external branch) = $(1.25+3.75)/0.1375$

The total heat flow for each branch is much lower than 1000 W/m^2 , the regime is boiling-off.

In steady state conditions, the heat transfer is mainly due to convective effects along the cooling branches.

| | | | | |
|---|--|-----------------------|------------------------|--------------------|
| Titolo Title Thermal Calculation MPD Dubna | Documento no. Document no. 100RM19469 | Rev. Rev. 3 | Pag. Page 25 | Di Of 25 |
| | Altro Identificativo no. Other Identification no. | Rev. Rev. | | |

4.3 Conclusions: cooling circuit parameters

The study on the cooling circuit has verified that the circuit is sized to cool the cold mass. It could absorb a power rate 4 times greater than the required.






The gas helium mass flow necessary to cool down the cold mass, calculated at 300 K, has been estimated to be 36 g/s. This value is 2.2 times the value calculated by JINR team.

The mass flow can be reduced decreasing the temperature rate: considering a rate of 0.5 K/h the mass flow is reduced to 19 g/s.

APPENDIX 8. Magnetic verification

| | | | | | | |
|--|------------------------|--------------------------------|--|--------------|--------------|--------------|
| Titolo Title | | | Documento no. Document no. | Rev. Rev. | Pag. Page | Di Of |
| Magnetic verification of the new yoke configuration | | | 100RM19902 | 1 | 1 | 21 |
| | | | Altro Identificativo no. Other Identification no. | Rev. Rev. | | |
| Tipo doc. Doc. type | Emittente Issued by | Edizione in lingua Language | Derivato da Derived from | | | Rev. Rev. |
| RT | ING | English | | | | |
| Commissa Job no. | Progetto Project | | Cliente Customer | | | |
| 2125 | MPD Dubna | | JINR | | | |

| Rev. Rev. | Motivo Revisione Reason for revision |
|--------------|--|
| 0 | First issue |
| 1 | First Revision: magnetic force calculations (par. 7) |

| Lista di Distribuzione Distribution List | | | | | | | | | |
|---|--------------------------|---|---|---|--|---|------------------------|-----------------------|--------------|
| 1 | |  |  |  |  |  | | 12/12/2016 | |
| 0 | | S. Grillo | A. Capelluto | N.Valle | | R.Marabotto | | 13/10/2016 | |
| Rev. Rev. | Stato (W/R) Status | Classe Riserv (1/2/3) Confid. | Preparato Prepared | Controllato Reviewed | Verificato Verified | Verificato Verified | Verificato Verified | Approvato Approved | Data Date |

| | | | | |
|---|--|-----------------------|-----------------------|--------------------|
| Titolo Title Magnetic verification of the new yoke configuration | Documento no. Document no. 100RM19902 | Rev. Rev. 1 | Pag. Page 2 | Di Of 21 |
| | Altro Identificativo no. Other Identification no. | Rev. Rev. | | |

Summary

| | | |
|-----|--|----|
| 1. | Introduction..... | 3 |
| 2. | Yoke description | 4 |
| 2.1 | Pole description | 4 |
| 3. | BH curve..... | 5 |
| 4. | Magnetic check..... | 9 |
| 4.1 | No modular configuration – Nominal configuration | 9 |
| 4.2 | No modular configuration – Technological Deviation | 10 |
| 4.3 | Modular configuration – Nominal configuration..... | 10 |
| 4.4 | Modular configuration – Technological deviation | 11 |
| 5. | Cradle effect | 15 |
| 6. | Conclusion..... | 17 |
| 7. | Magnetic Forces | 18 |
| 7.1 | Conclusions | 21 |

| | | | | |
|--|--|--------------|--------------|----------|
| Titolo Title | Documento no. Document no. | Rev. Rev. | Pag. Page | Di Of |
| | 100RM19902 | 1 | 3 | 21 |
| Magnetic verification of the new yoke configuration | Altro Identificativo no. Other Identification no. | Rev. Rev. | | |
| | | | | |

1. Introduction

The magnet of the Multi-Purpose Detector is requested to have a highly homogeneous magnetic field of 0.5 T in an aperture of 4596 mm in diameter. The asked requirements, which are reported in Table 1, have to be respected also taking into account all the possible technological deviations due to the positioning and assembly procedures.

| | | |
|--|---|----------------------------|
| $0 < Z < Z_{max} = 1700 \text{ mm}$ $403 \text{ mm} < r < 1203 \text{ mm}$ | $INT = \int_z^{z_{max}} \frac{B_r}{B_z} dz$ | $ INT < 0.775 \text{ mm}$ |
| $Z_{min} = -1700 \text{ mm} < Z < 0$ $403 \text{ mm} < r < 1203 \text{ mm}$ | $INT = \int_z^{z_{min}} \frac{B_r}{B_z} dz$ | $ INT < 0.775 \text{ mm}$ |
| Homogeneity | $\delta = \frac{ B_{max} - B_{min} }{2B_0}$ | $3 \cdot 10^{-4}$ |

Table 1: MPD magnet requirements. All the requirements are defined inside the TPC, Charged Particle Tracker, volume ($Z = [-1700;1700]$ mm ; $r = [403;1203]$ mm).

All the requirements are defined inside the cylindrical volume of the Charged Particle Tracker (TPC: $Z = [-1700;1700]$ mm and $r = [403;1203]$ mm).

In the 100RM18955 document, a magnetic configuration respecting all the requirements is described. This configuration was optimized considering Copper TRIM coils, 24 beam iron yoke and 2 poles made both of Steel AISI-1006.

Since a new yoke configuration has been defined, a magnetic check is necessary.

| | | | | |
|--|--|--------------|--------------|----------|
| Titolo Title | Documento no. Document no. | Rev. Rev. | Pag. Page | Di Of |
| | 100RM19902 | 1 | 4 | 21 |
| Magnetic verification of the new yoke configuration | Altro Identificativo no. Other Identification no. | Rev. Rev. | | |
| | | | | |

2. Yoke description

In order to consider structural stability a new yoke configuration has been designed. The greatest difference between the old and the new yoke design is the beam number: in the old configuration there were 24 beams that have been increased to 28 in the new one.

2.1 Pole description

With the new yoke configuration, the poles have been also slightly modified: in particular, in order to close on the yoke, they are divided in 28 sectors. The comparison with the old configuration shows that the pole dimensions and position are not changed.

The pole design given us by JINR is optimized for the Al TRIM coils. In order to fit the pole with the Cu TRIM coils (see 100RM18955 document), the gap of the pole has been changed.

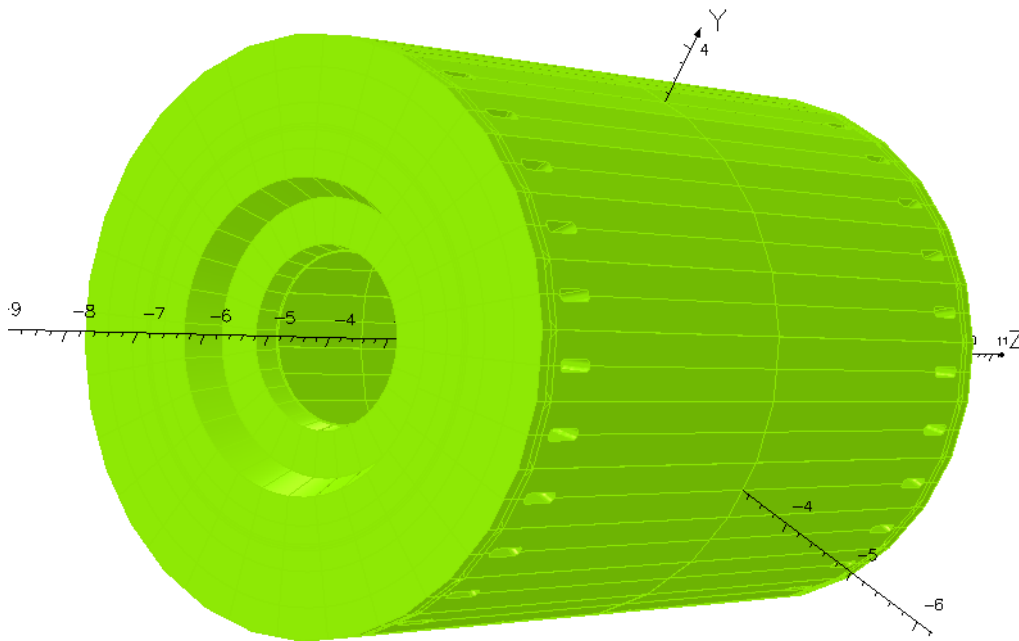


Figure 1: Yoke model in opera software.

| | | | | |
|---|--|------------------------------|------------------------------|---------------------------|
| Titolo Title Magnetic verification of the new yoke configuration | Documento no. Document no. 100RM19902 | Rev. Rev. 1 | Pag. Page 5 | Di Of 21 |
| | Altro Identificativo no. Other Identification no. | Rev. Rev. | | |

3. BH curve

The magnetic configuration described in 100RM18955 document was optimized with the yoke/poles made of Steel AISI-1006.

Since the yoke material has been bought, the magnetic verify has been done using the measured BH curve.

A measurement of magnetic induction has been done on 14 of the 28 yoke beams by ALPHYSICA (in according with GOST 8.377-80 standards). The measured BH curves are shown in Figure 2.

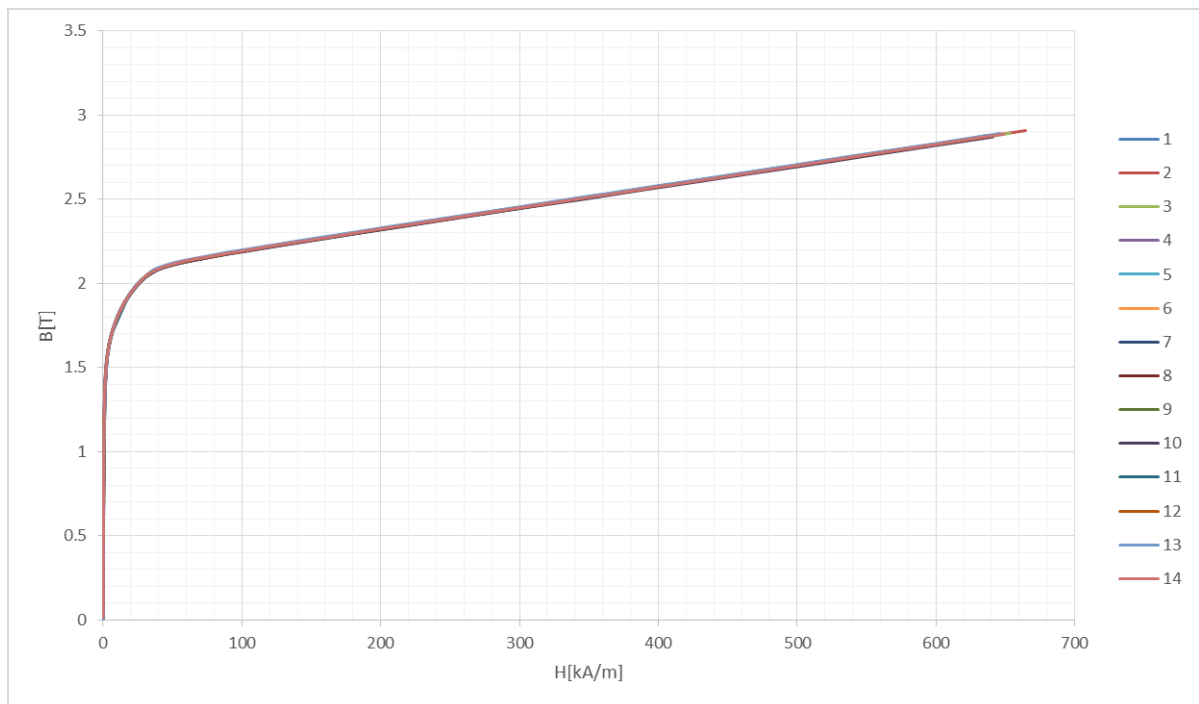


Figure 2: Measured BH curves of 14 beams (on 28).

In the finite element model of the MPD magnet, the yoke material has been described with the BH curve obtained as “best-fit” of all the measured curves. This curve is shown in

Figure 3, where it is compared with the AISI 1006 curve and with the BH curve present in the first Opera model received by JINR.

| | | | | |
|--|--|--------------|--------------|----------|
| Titolo Title | Documento no. Document no. | Rev. Rev. | Pag. Page | Di Of |
| | 100RM19902 | 1 | 6 | 21 |
| Magnetic verification of the new yoke configuration | Altro Identificativo no. Other Identification no. | Rev. Rev. | | |
| | | | | |

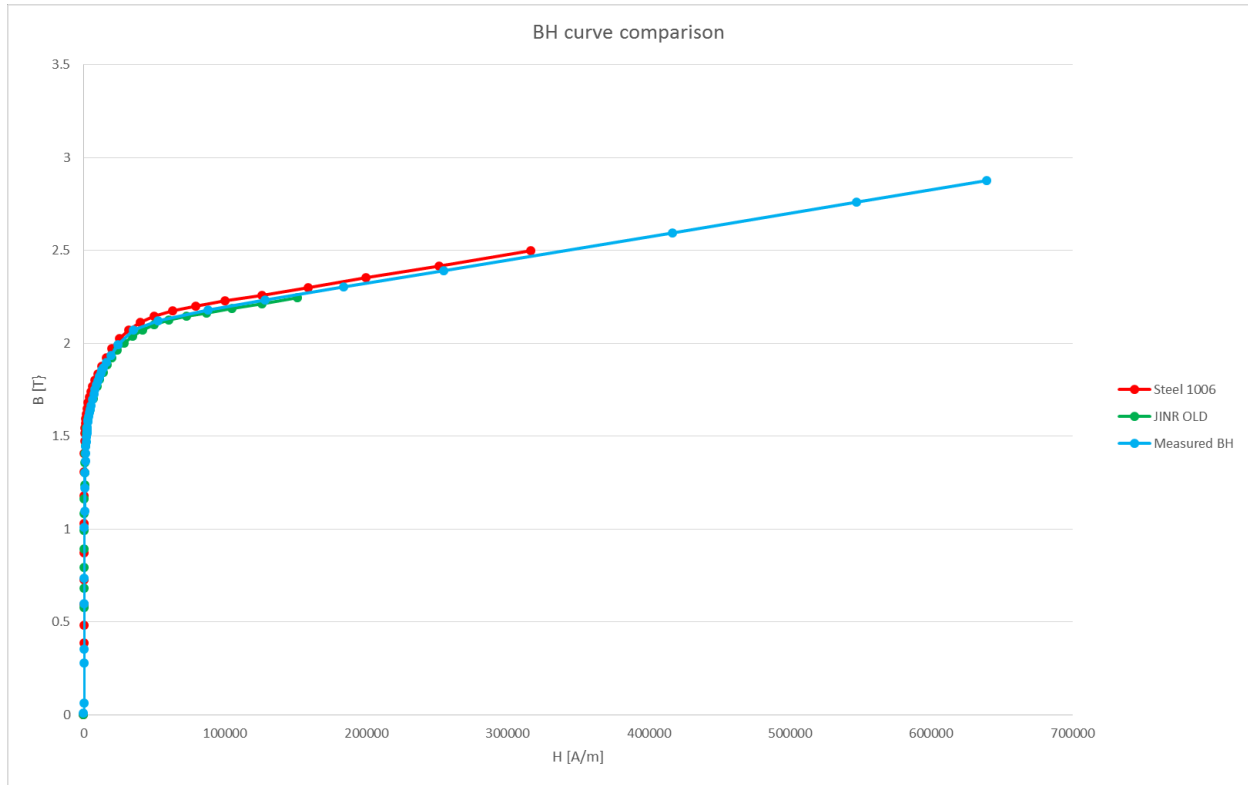


Figure 3: BH curve comparison. The red curve corresponds to Steel AISI-1006 and it was used in the previous magnetic configuration. The cyan curve is the curve that has been measured on the real beams. The green curve is the curve present in the first Opera model received by JINR.

In the 3HM1002.00.000TO document the yoke material is described to have a BH curve including the following points:

| Induction [T] | Magnetizing Field [A/m] |
|---------------|-------------------------|
| 1.55 | <2179 |
| 2.01 | <23881 |

Table 2:Iron yoke magnetic properties required in 3HM1002.00.000TO.

The measured steel does not respect these requirements: the comparison between the required and the real values is reported in Table 3 . The real values refer to the "best-fit" BH curve.

| Induction [T] | Required Magnetizing Field [A/m] | Real Magnetizing Field [A/m] |
|---------------|----------------------------------|------------------------------|
| 1.55 | <2179 | > 2660 |
| 2.01 | <23881 | > 24213 |

Table 3: Comparison between the required and the real magnetic requirements for the yoke steel. The real values refer to the "best-fit" of the measured BH curves.

| | | | | |
|--|--|--------------|--------------|----------|
| Titolo Title | Documento no. Document no. | Rev. Rev. | Pag. Page | Di Of |
| | 100RM19902 | 1 | 7 | 21 |
| Magnetic verification of the new yoke configuration | Altro Identificativo no. Other Identification no. | Rev. Rev. | | |
| | | | | |

The ring material was also been measured. The ring is the circular component of the yoke which connects the beams to the poles. The measurements were done by Laboratorio Elettrofisico (Walker LDJ Scientific) on some material samples in according to GOST 8473-70 standard. The BH curves are reported in Figure 4.

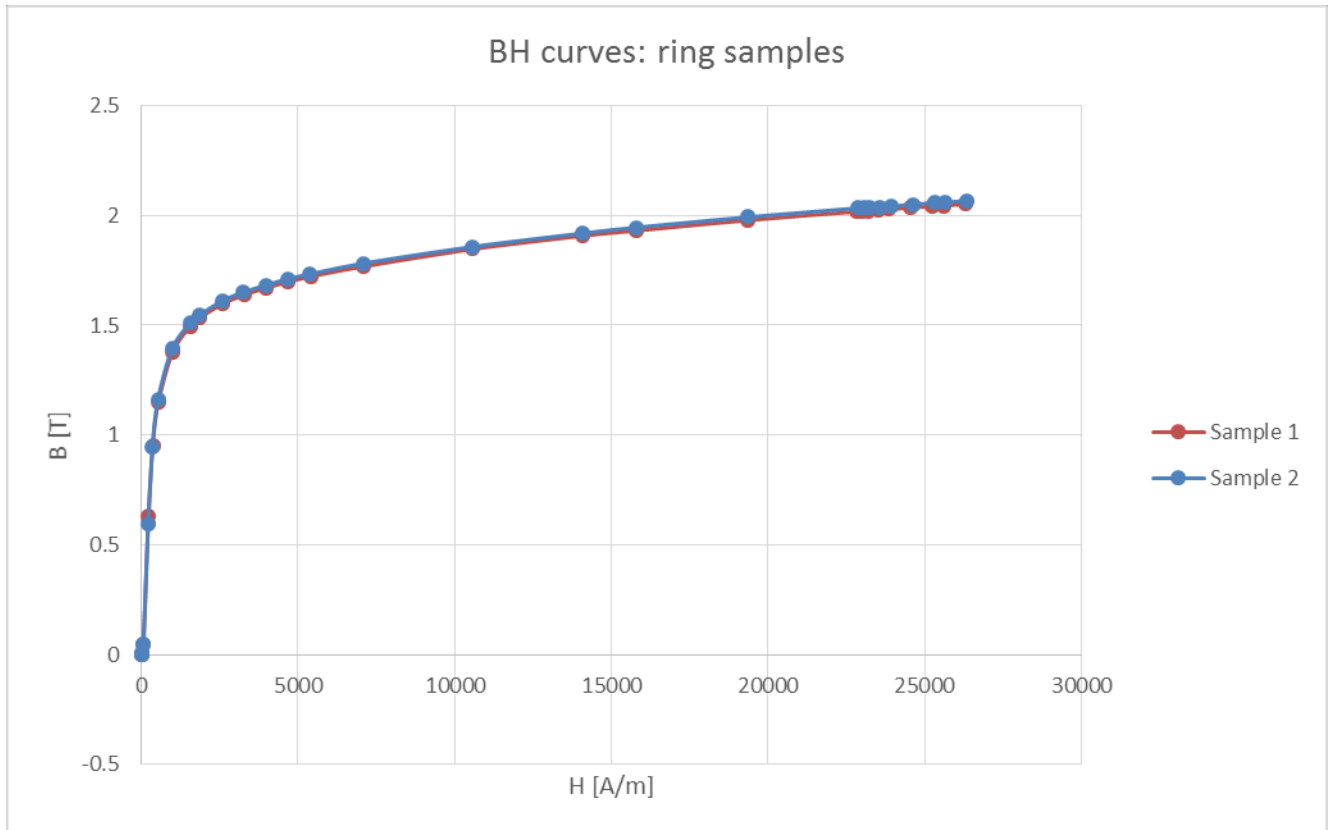


Figure 4: Ring material BH curves.

The ring material respects the required magnetic properties (certified by Laboratorio Elettrofisico).

| Magnetizing Field [A/m] | Required Induction [T] | Real Induction [T] Sample 1 | Real Induction [T] Sample 2 |
|-------------------------|------------------------|--------------------------------|--------------------------------|
| <2179 | 1.55 | 1.56 | 1.58 |
| <23881 | 2.01 | 2.02 | 2.04 |

Table 4: Comparison between the required and the real magnetic properties for the rings.

In Figure 5 it is shown the comparison between the “best-fit” on the 14 beams and the two ring BH curves.

| | | | | |
|---|--|------------------------------|------------------------------|---------------------------|
| Titolo Title Magnetic verification of the new yoke configuration | Documento no. Document no. 100RM19902 | Rev. Rev. 1 | Pag. Page 8 | Di Of 21 |
| | Altro Identificativo no. Other Identification no. | Rev. Rev. | | |

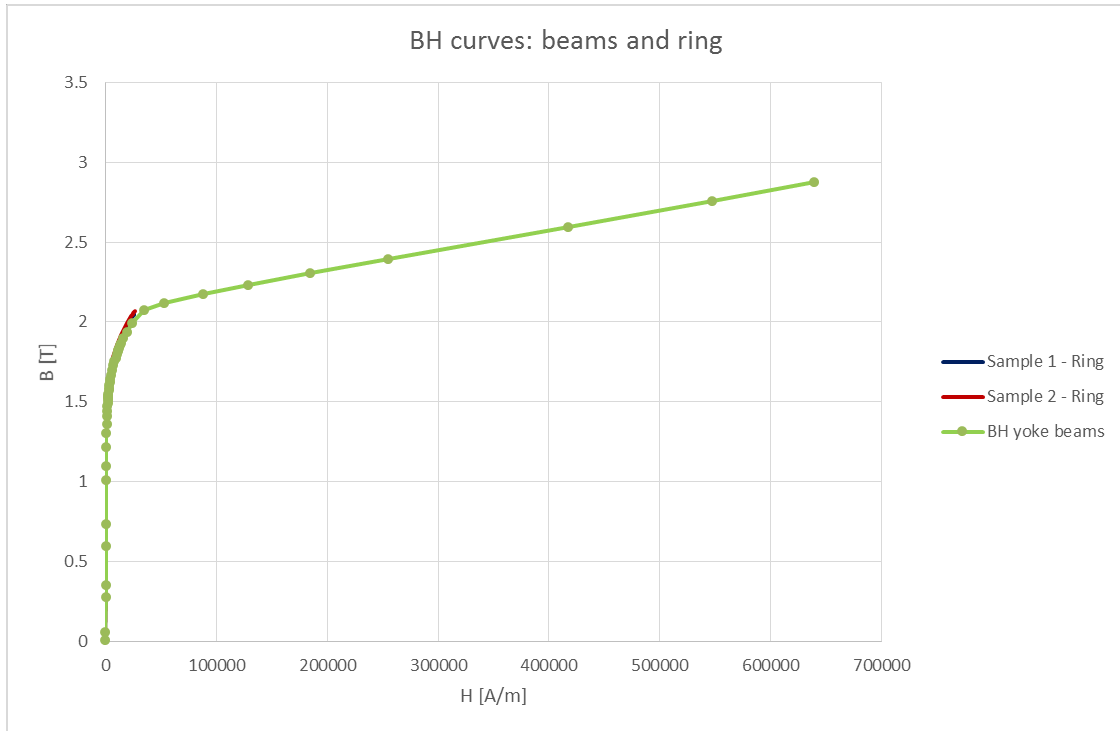


Figure 5: BH curves of the rings compared with the yoke curve.

Since the beam and ring materials are quite similar and the ring material is much less than the beam material it has been decided to use the beam BH curve for all the iron components (beam, rings and poles).

| | | | | |
|--|--|--------------|--------------|----------|
| Titolo Title | Documento no. Document no. | Rev. Rev. | Pag. Page | Di Of |
| | 100RM19902 | 1 | 9 | 21 |
| Magnetic verification of the new yoke configuration | Altro Identificativo no. Other Identification no. | Rev. Rev. | | |
| | | | | |

4. Magnetic check

The previous magnetic configuration was tested on a several number of configurations (see 100RM18955 the check of the magnetic quality with the new yoke configuration has been done on only some chosen configurations (

Table 1Table 5).

The TRIM coils were defined in the previous magnetic study: they are copper coils formed by 36 turns in 2 layers (for details see 100RM18955 document).

| Modular/No modular SC | Nominal Configuration | Technological Deviation |
|-----------------------------|-----------------------|---|
| No modular SC configuration | Tested | Pole + TRIM coil axial shift (2x5 mm increasing interpole distance) |
| Modular SC configuration | Tested | Radial Shift, 2 external modules (± 5 mm along X direction) |
| | | Ovalization, 1 central module (-20 mm) |
| | | Ovalization, 1 external module (-20 mm) |
| | | Complex deviation 1 (+ 10 mm along Z direction + $\nabla J = +1\%$ towards Z<0) |
| | | Complex deviation 2 (+ 20 mm along Z direction + $\nabla J = +1\%$ towards Z>0) |

Table 5: Chosen configurations for the magnetic check.

4.1 No modular configuration – Nominal configuration

In the No modular configuration a unique solenoid has been considered.

The nominal configuration corresponds to the nominal positioning of all the conductors, without any technological deviation.

In the previous study the magnetic configuration found was characterized by the following parameters:

| Configuration | J sol [A/mm ²] | J trim [A/mm ²] | B0 [T] | INT [mm] | homogeneity |
|---------------|----------------------------|-----------------------------|--------|----------|-------------|
| Old-Nominal | 20.25 | 1.7 | 0.5031 | 0.05 | 0.53E-04 |

Table 6: Magnetic configuration that was defined in the previous study in the nominal configuration with the unique solenoid.

Applying the same current densities in the new yoke configuration the magnetic quality gets worse.

| Configuration | J sol [A/mm ²] | J trim [A/mm ²] | B0 [T] | INT [mm] | homogeneity |
|---------------|----------------------------|-----------------------------|--------|----------|-------------|
| New-Nominal | 20.25 | 1.7 | 0.5033 | 0.29 | 1E-04 |

Table 7: Magnetic quality of the new configuration with the current densities that were optimized in the previous study.

| | | | | |
|--|--|--------------|--------------|----------|
| Titolo Title | Documento no. Document no. | Rev. Rev. | Pag. Page | Di Of |
| | 100RM19902 | 1 | 10 | 21 |
| Magnetic verification of the new yoke configuration | Altro Identificativo no. Other Identification no. | Rev. Rev. | | |
| | | | | |

The required magnetic quality is simply obtained tuning the TRIM coil current density:

| Configuration | J sol [A/mm ²] | J trim [A/mm ²] | B0 [T] | INT [mm] | homogeneity |
|---------------|----------------------------|-----------------------------|--------|----------|-------------|
| New-Nominal | 20.25 | 1.77 | 0.5035 | 0.059 | 0.59E-04 |

Table 8: Magnetic quality in the new yoke configuration after the TRIM coil current optimization.

The effect on the magnetic quality is principally due to the kind of iron used in the yoke and not to the beam number. This conclusion has been deduced through an additional analysis in which the old model has been studied with the measured BH curve and the new model has been analysed with the AISI-1006 BH curve. The results are reported in Table 9.

| Yoke Model | BH curve | J sol [A/mm ²] | J trim [A/mm ²] | B0 [T] | INT [mm] | homogeneity |
|----------------|-----------|----------------------------|-----------------------------|--------|----------|-------------|
| Old – 24 beams | Measured | 20.25 | 1.7 | 0.5023 | 0.27 | 9.50E-05 |
| New – 28 beams | Measured | 20.25 | 1.7 | 0.5033 | 0.29 | 1E-04 |
| Old – 24 beams | AISI-1006 | 20.25 | 1.7 | 0.5031 | 0.05 | 0.53E-04 |
| New – 28 beams | AISI-1006 | 20.25 | 1.7 | 0.5043 | 0.04 | 5.20E-05 |

Table 9: Comparison between old and new yoke models with different BH curves. The principal effect on the magnetic quality is due to the kind of iron used in the yoke and not to the beam number.

4.2 No modular configuration – Technological Deviation

Increase of the interpole distance

In the No modular configuration a unique solenoid has been considered.

The considered technological deviation is the increase of the interpole distance: each pole, with the related TRIM coil, has been moved 5 mm away from its nominal position.

In the new yoke configuration, this technological deviation has a quite relevant effect even though the requirements are always respected without a tuning of the TRIM coil currents:

| Configuration | J sol [A/mm ²] | J trim [A/mm ²] | B0 [T] | INT [mm] | homogeneity |
|-----------------|----------------------------|-----------------------------|--------|------------------|-------------|
| New-PoleAxShift | 20.25 | 1.77 | 0.5032 | 0.34=0.059+0.281 | 1.07E-04 |

Table 10: Magnetic quality in the new yoke configuration taking into account an increase in the interpole distance of 2x5 mm.

4.3 Modular configuration – Nominal configuration

In the Modular configuration a solenoid formed by 10 modules has been considered. The module number corresponds to the number of SC wire lengths that will be wound. The real SC coil will have 7 intra-module joints and 2 inter-module joints. In the Finite Element model, the intra-module joints have been built as a single turn with opposite current while the inter-module joints will be simulated as a couple of half-turns with opposite current.

The nominal configuration corresponds to the nominal positioning of all the conductors, without any technological deviation.

| | | | | |
|--|--|--------------|--------------|----------|
| Titolo Title | Documento no. Document no. | Rev. Rev. | Pag. Page | Di Of |
| | 100RM19902 | 1 | 11 | 21 |
| Magnetic verification of the new yoke configuration | Altro Identificativo no. Other Identification no. | Rev. Rev. | | |
| | | | | |

In the previous study the magnetic configuration was characterized by the following parameters:

| Configuration | J sol [A/mm ²] | J trim [A/mm ²] | B0 [T] | INT [mm] | homogeneity |
|---------------------|----------------------------|-----------------------------|--------|----------|-------------|
| Old-Modular-Nominal | 20.40 | 1.62 | 0.5025 | 0.087 | 0.60E-04 |

Table 11: Magnetic quality in the old yoke configuration with the modular SC coil in the nominal position.

Applying the same current densities in the new yoke configuration the magnetic quality gets worse.

| Configuration | J sol [A/mm ²] | J trim [A/mm ²] | B0 [T] | INT [mm] | homogeneity |
|---------------------|----------------------------|-----------------------------|--------|----------|-------------|
| New-Modular-Nominal | 20.40 | 1.62 | 0.5020 | 0.12 | 0.57E-04 |

Table 12: Magnetic quality with the new yoke configuration in which the old configuration current densities have been applied. The SC coil is in the modular configuration but in the nominal position.

The required magnetic quality is simply obtained tuning the TRIM coil current density:

| Configuration | J sol [A/mm ²] | J trim [A/mm ²] | B0 [T] | INT [mm] | homogeneity |
|---------------------|----------------------------|-----------------------------|--------|----------|-------------|
| New-Modular-Nominal | 20.40 | 1.65 | 0.5020 | 0.08 | 0.47E-04 |

Table 13: Magnetic quality in the new yoke configuration with the optimized TRIM coil current densities.

4.4 Modular configuration – Technological deviation

Radial Shift of 2 external modules

The 10 sub-modules are divided in 3 groups, corresponding to the 3 modules in which the support cylinder is divided. One of the possible technological deviation is the radial shift of one or more modules with respect to the nominal position.

The studied technological deviation concerns the radial shift (5 mm along the X direction) of both the 2 external modules. In particular the module at $Z > 0$ has been moved of 5 mm along $X > 0$, while the other module has been moved of 5 mm along $X < 0$.

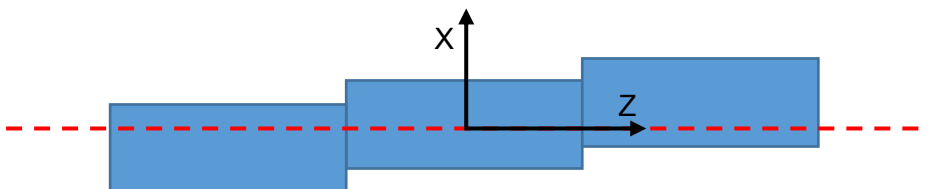


Figure 6: Radial shift of 2 external modules.

| | | | | |
|--|--|--------------|--------------|----------|
| Titolo Title | Documento no. Document no. | Rev. Rev. | Pag. Page | Di Of |
| | 100RM19902 | 1 | 12 | 21 |
| Magnetic verification of the new yoke configuration | Altro Identificativo no. Other Identification no. | Rev. Rev. | | |
| | | | | |

With this technological deviation and without aTRIM coil current density tuning the magnetic field quality is within the requirements.

| Configuration | J sol [A/mm ²] | J trim [A/mm ²] | B0 [T] | INT [mm] | homogeneity |
|---------------------------|----------------------------|-----------------------------|--------|-----------------|-------------|
| New-Modular-RadShift-2Ext | 20.40 | 1.65 | 0.5020 | 0.53=0.08+ 0.45 | 0.62E-04 |

Table 14: Magnetic quality in the new yoke configuration considering a radial shift of the 2 external modules.

Ovalization of the central module or of 1 external module

Another possible technological deviation is the ovalization of the SC coil.

In this study the central module or one of the two external modules have been ovalized decreasing their radius of 20 mm in the X direction.

Also without aTRIM coil current density tuning the magnetic field quality is within the requirements. The results are reported in

Table 15, where P is referred to the integral at $Z > 0$ and N to the integral at $Z < 0$.

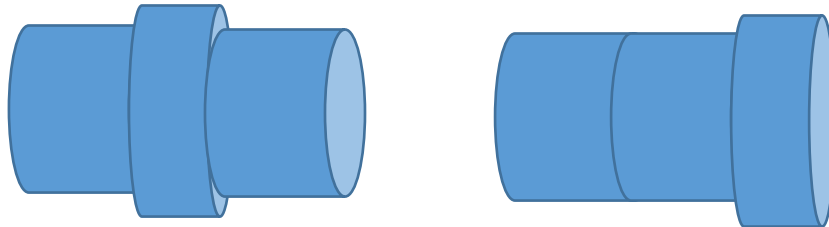


Figure 7: Ovalization of one module: the central or the external one.

| Configuration | J sol [A/mm ²] | J trim [A/mm ²] | B0 [T] | INT [mm] | homogeneity |
|-------------------------|----------------------------|-----------------------------|--------|--------------------------------------|-------------|
| New-Modular-Oval-1Centr | 20.40 | 1.65 | 0.5017 | P:0.58=0.08+0.5 N:0.69=0.08+0.61 | 1.90E-04 |
| New-Modular-Oval-1Ext | 20.40 | 1.65 | 0.5015 | P:0.42=0.08+0.34 N:0.27=0.08+0.19 | 2.26E-04 |

Table 15: Magnetic quality in the new yoke configuration with the ovalization of 1 central module or 1 external module.

| | | | | |
|--|--|--------------|--------------|----------|
| Titolo Title | Documento no. Document no. | Rev. Rev. | Pag. Page | Di Of |
| | 100RM19902 | 1 | 13 | 21 |
| Magnetic verification of the new yoke configuration | Altro Identificativo no. Other Identification no. | Rev. Rev. | | |
| | | | | |

Complex 1: axial shift and current density linear variation

In this technological deviation two effects have been taken into account: an axial shift of the whole SC coil and a linear variation of the SC current density.

- Axial shift: SC coil is moved of 10 mm along $Z > 0$.
- Linear variation of J: 1% of variation along each SC module length in the $Z < 0$ direction.

The linear variation has been calculated considering that the current density changes from its nominal value $- 0.5\%$ to its nominal value $+ 0.5\%$ along each module.

Each of the two external modules are formed by 3 sub-modules, while the central module is formed by 4 sub-modules: in the next figure the calculation of the linear variation of J is described.

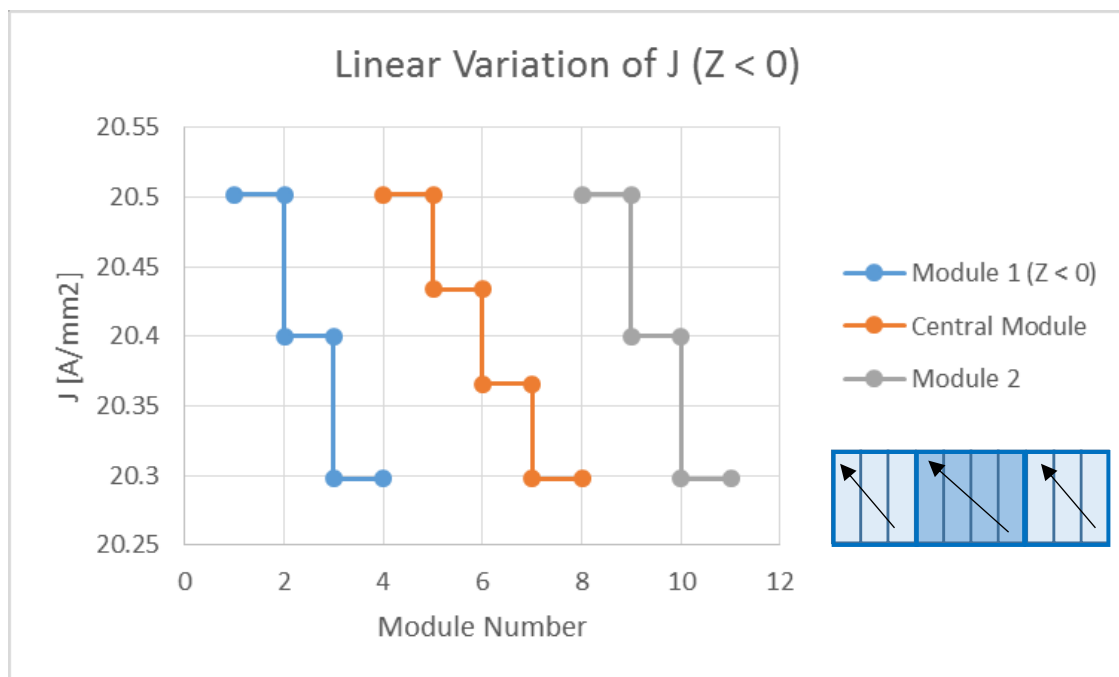


Figure 8: Current density linear variation ($Z < 0$) along each module.

In this configuration the magnetic quality is guaranteed without the TRIM coil current tuning:

| Configuration | J sol [A/mm²] | J trim [A/mm²] | B0 [T] | INT [mm] | homogeneity |
|-----------------------|---------------|----------------|--------|--------------------------------------|-------------|
| New-Modular-Complex 1 | 20.40 | 1.65 | 0.5021 | P:0.44=0.08+0.36 N:0.29=0.08+0.21 | 1.90E-04 |

Table 16: Magnetic quality in the new yoke configuration and complex technological deviation 1.

| | | | | |
|--|--|--------------|--------------|----------|
| Titolo Title | Documento no. Document no. | Rev. Rev. | Pag. Page | Di Of |
| | 100RM19902 | 1 | 14 | 21 |
| Magnetic verification of the new yoke configuration | Altro Identificativo no. Other Identification no. | Rev. Rev. | | |
| | | | | |

Complex 2: axial shift and current density linear variation

In this technological deviation two effects have been taken into account: an axial shift of the whole SC coil and a linear variation of the SC current density.

- Axial shift: SC coil is moved of 20 mm along $Z > 0$.
- Linear variation of J: 1% of variation along each SC module length in the $Z > 0$ direction.

The linear variation of J is described in Figure 9:

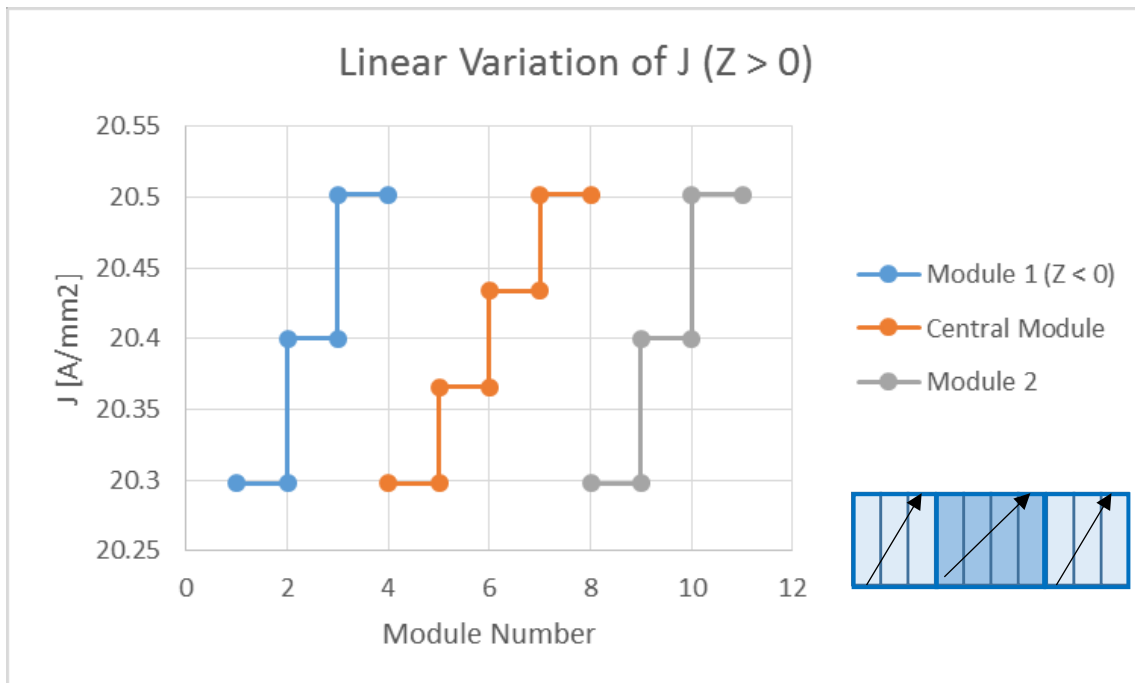


Figure 9: Current density linear variation in the $Z > 0$ direction.

In this configuration the magnetic quality is guaranteed only with a TRIM coil current tuning. The tuning is different for the two TRIM coils, in Table 17 the Trim+ is referred to the TRIM at $Z > 0$, while the Trim- to the TRIM coil at $Z < 0$.

| Configuration | J sol [A/mm²] | J trim [A/mm²] | B0 [T] | INT [mm] | homogeneity |
|-----------------------|---------------|--------------------------|--------|-----------------------------------|-------------|
| New-Modular-Complex 2 | 20.40 | Trim + =1.3 Trim - =2 | 0.5020 | P:0.25=0.08+0.17 N:0.08=0.08+0 | 2.01E-04 |

Table 17 : Magnetic quality in the new yoke configuration and in the complex technological deviation 2.

| | | | | |
|--|--|--------------|--------------|----------|
| Titolo Title | Documento no. Document no. | Rev. Rev. | Pag. Page | Di Of |
| | 100RM19902 | 1 | 15 | 21 |
| Magnetic verification of the new yoke configuration | Altro Identificativo no. Other Identification no. | Rev. Rev. | | |
| | | | | |

5. Cradle effect

Since the MPD magnet is supported by an iron cradle, its effect has been studied. In order to use the symmetry of the cradle, a quarter of model has been built. The cradle has been modeled considering the BH curve of Fe360. The conductors have been considered in the nominal positions with the optimized current densities.

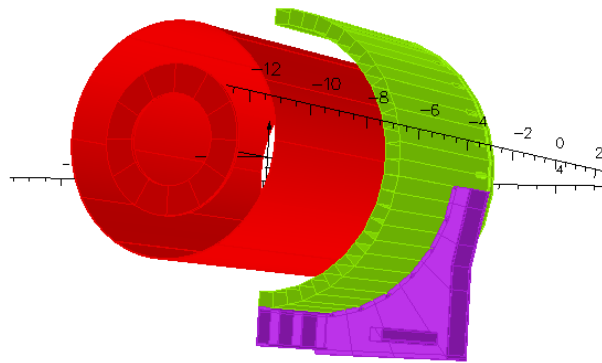


Figure 10: Finite Element model of the system with the cradle.

The magnetic field quality with the cradle has been compared to the quality without it. The presence of the cradle has not an effect on the value of B_0 but it has a not negligible effect on the integral value. The requirements are always respected but the integral reaches the value of 0.16 mm. The cradle breaks also the symmetry of the system, as it is visible in the next figures. In Figure 11 and Figure 12 the radial component (B_r) of the magnetic field in the configuration without and with the cradle are reported. The radial component has been calculated at $r=\pm 0.803$ m and at $z=[-1.7;1.7]$ m: in the no cradle configuration the B_r value does not change with the angular position (at fixed radius), unlike the cradle configuration.

| | | | | |
|---|--|------------------------------|-------------------------------|---------------------------|
| Titolo Title Magnetic verification of the new yoke configuration | Documento no. Document no. 100RM19902 | Rev. Rev. 1 | Pag. Page 16 | Di Of 21 |
| | Altro Identificativo no. Other Identification no. | Rev. Rev. | | |

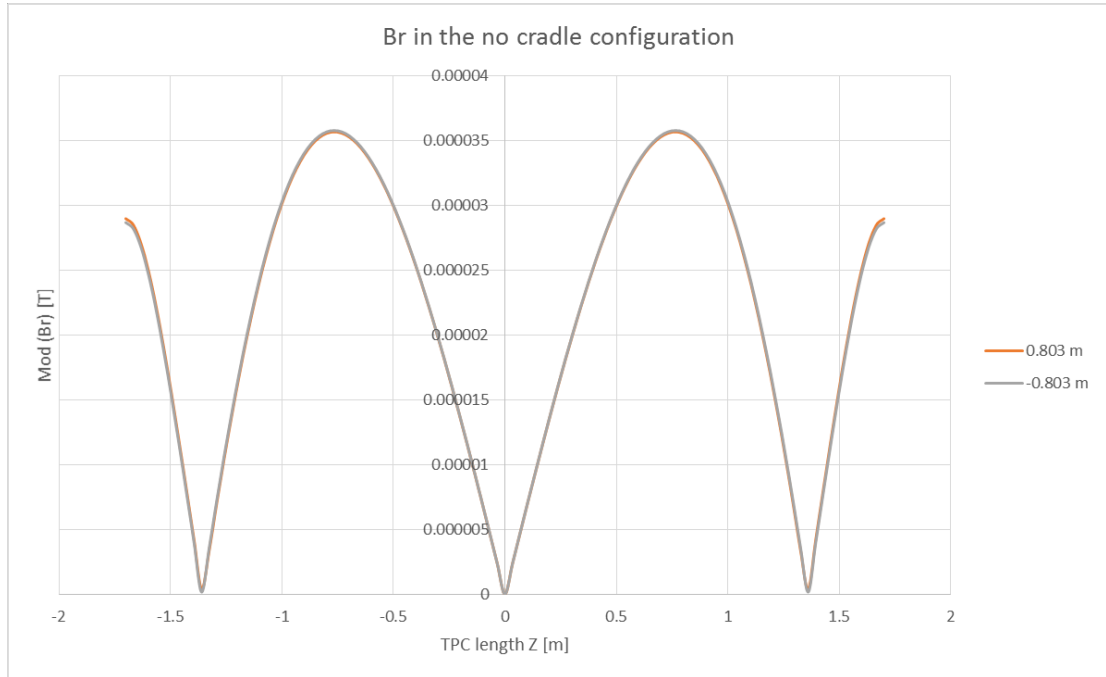


Figure 11: Br values calculated at $r = \pm 0.803$ m in the no cradle configuration.

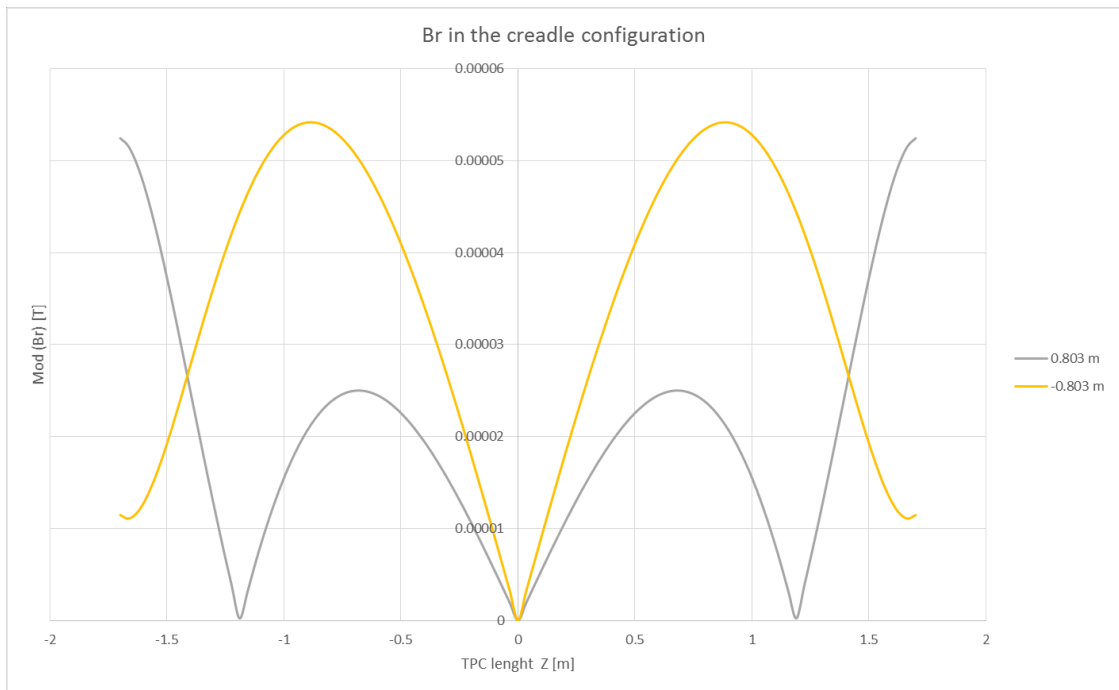


Figure 12: Br value calculated at $r = \pm 0.803$ m in the configuration with the cradle.

| | | | | |
|--|--|--------------|--------------|----------|
| Titolo Title | Documento no. Document no. | Rev. Rev. | Pag. Page | Di Of |
| | 100RM19902 | 1 | 17 | 21 |
| Magnetic verification of the new yoke configuration | Altro Identificativo no. Other Identification no. | Rev. Rev. | | |
| | | | | |

6. Conclusion

The study of the new yoke configuration has shown that there is a not negligible effect on the magnetic quality of the MPD magnet due principally to the material (BH curve).

This effect can be correct with a simply TRIM coil current density tuning, while the SC current can be kept constant. In particular:

- Nominal configuration – No modular SC coil: the TRIM coil current density has been increased fom 1.7 to 1.77 A/mm² (+ 4 %);
- Nominal configuration – Modular SC coil: the TRIM coil current density has been increased fom 1.62 to 1.65 A/mm² (+ 2 %);

Given the new nominal configuration, the technological deviations can be corrected with finer TRIM coil current tunings.

| Configuration | J sol [A/mm ²] | J trim [A/mm ²] | B0 [T] | INT [mm] | homogeneity |
|---------------------------|----------------------------|-----------------------------|--------|--------------------------------------|-------------|
| New-Modular-Nominal | 20.40 | 1.65 | 0.5020 | 0.08 | 0.47E-04 |
| New-Modular-RadShift-2Ext | 20.40 | 1.65 | 0.5020 | 0.53=0.08+0.45 | 0.62E-04 |
| New-Modular-Oval-1Centr | 20.40 | 1.65 | 0.5017 | P:0.58=0.08+0.5 N:0.69=0.08+0.61 | 1.90E-04 |
| New-Modular-Oval-1Ext | 20.40 | 1.65 | 0.5015 | P:0.42=0.08+0.34 N:0.27=0.08+0.19 | 2.26E-04 |
| New-Modular-Complex 1 | 20.40 | 1.65 | 0.5021 | P:0.44=0.08+0.36 N:0.29=0.08+0.21 | 1.90E-04 |
| New-Modular-Complex 2 | 20.40 | Trim + =1.3 Trim - =2 | 0.5020 | P:0.25=0.08+0.17 N:0.08=0.08+0 | 2.01E-04 |

Table 18: Magnetic quality for all the studied situations with the new yoke configuration.

Finally, the presence of the cradle has a not negligible effect, which means an increase in the integral value and a symmetry break, even thought all the requirements are respected.

| Configuration | J sol [A/mm ²] | J trim [A/mm ²] | B0 [T] | INT [mm] | homogeneity |
|---------------|----------------------------|-----------------------------|--------|----------|-------------|
| New-Cradle | 20.25 | 1.77 | 0.5035 | 0.16 | 0.74E-04 |

Table 19: Magnetic quality of the model with the cradle.

| | | | | |
|--|--|--------------|--------------|----------|
| Titolo Title | Documento no. Document no. | Rev. Rev. | Pag. Page | Di Of |
| | 100RM19902 | 1 | 18 | 21 |
| Magnetic verification of the new yoke configuration | Altro Identificativo no. Other Identification no. | Rev. Rev. | | |
| | | | | |

7. Magnetic Forces

Both the main coil and the TRIM coils are subjected to magnetic forces.

Since the magnetic system is symmetric, the magnetic force on the main coil is null. In order to design the tie-rods supporting the cold mass, the magnetic forces have been calculated in two unbalanced configurations, for which a magnetic force on the main coil appears.

The two unbalanced configurations are described by an axial shift of the main coil, a current density linear variation along the main coil and a pole-TRIM coil axial shift.

| Configuration | Axial Shift (main coil) | J variation | Pole Shift |
|---------------|-------------------------|--|--------------|
| Case 1 | 20 mm in Z>0 | [-0.5;0.5]% increasing in positive Z | 5 mm outside |
| Case 2 | 10 mm in Z>0 | [-0.5;0.5]% increasing in negative Z | 0 |

Table 20: The two unbalanced configurations taken into account in the magnetic force calculations.

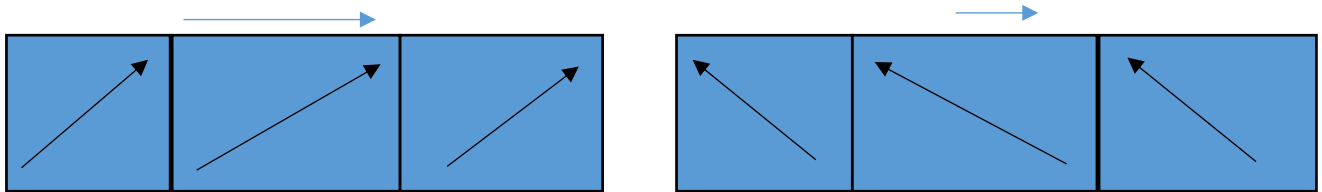


Figure 13: Case 1 (Left) and Case 2 (Right). The blue arrow shows the axial shift direction while the black arrows show the current density variation.

Since the main coil will be formed by three modules and ten wire lengths, the current density variation has been calculated on each module. In particular each module has been divided in sub-modules, corresponding to the wire lengths, and on each sub-module the current density has been considered fixed.

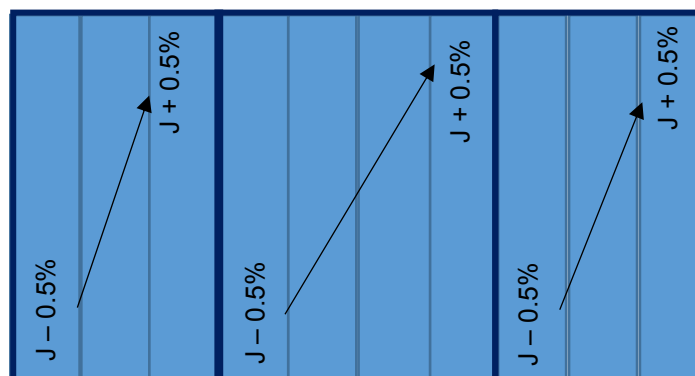


Figure 14: Schematic view of the current density linear variation calculation.

| | | | | |
|--|--|--------------|--------------|----------|
| Titolo Title | Documento no. Document no. | Rev. Rev. | Pag. Page | Di Of |
| | 100RM19902 | 1 | 19 | 21 |
| Magnetic verification of the new yoke configuration | Altro Identificativo no. Other Identification no. | Rev. Rev. | | |
| | | | | |

The two unbalanced configurations have been considered for different working regimes: operative, test and failure.

| Regime | Main coil J [A/mm ²] | TRIM coil J [A/mm ²] |
|-----------|----------------------------------|----------------------------------|
| Operative | Nominal = 20.40 | Nominal = 1.65 (both trim coils) |
| Test 1 | Nominal = 20.40 | Maximum = 2.81 (both trim coils) |
| Test 2 | Maximum = 26.77 | OFF (both trim coils) |
| Failure 1 | OFF | Nominal = 1.65 (both trim coils) |
| Failure 2 | OFF | Maximum = 2.81 (both trim coils) |
| Failure 3 | Nominal = 20.40 | OFF (both trim coils) |

Table 21: Regimes (operative, test and failure) in which the magnetic forces have been calculated.

In these configurations there is only the axial component of the force.

The TRIM + is the TRIM coil at positive Z positions and the TRIM- is the TRIM coil at negative Z positions.

| Regime | Case | Fz [kN] Main coil | Fz [kN] TRIM + | Fz [kN] TRIM- |
|-----------|--------|-------------------|----------------|---------------|
| Operative | Case 1 | 107 | 13 | -14.5 |
| | Case 2 | 36 | 13 | -13 |
| Test 1 | Case 1 | 106.7 | 65.4 | -67.7 |
| | Case 2 | 35.5 | 65.6 | -64.5 |
| Test 2 | Case 1 | 150.7 | 0 | 0 |
| | Case 2 | 50.3 | 0 | 0 |
| Failure 1 | Case 1 | 0 | 51.9 | -52 |
| | Case 2 | 0 | 51.8 | -51.5 |
| Failure 2 | Case 1 | 0 | 129.9 | -130.2 |
| | Case 2 | 0 | 129.7 | -128.9 |
| Failure 3 | Case 1 | 108.4 | 0 | 0 |
| | Case 2 | 36.3 | 0 | 0 |

Table 22: Magnetic forces for the different regimes and configurations.

The maximum force on the main coil is 151 kN in test mode 2, while the maximum force on the TRIM coils is 130 kN if, during the test mode 1, the main coil switches off.

In all these situations the force on the main coil is toward positive Z positions and the forces on the TRIM coils push them against the poles.

In all these situations only axial forces are generated. In order to check the magnitude of a possible radial force, a study has been done considering a radial shift of the main coil.

| Configuration | Radial Shift (main coil) | J variation | Pole Shift |
|---------------|--------------------------|-------------|------------|
| Case 3 | 5 mm in X>0 | 0 | 0 |

Table 23: Case 3: the main coil has been radially shifted.

The forces have been calculated only in operative and test regimes.

| | | | | |
|--|--|--------------|--------------|----------|
| Titolo Title | Documento no. Document no. | Rev. Rev. | Pag. Page | Di Of |
| | 100RM19902 | 1 | 20 | 21 |
| Magnetic verification of the new yoke configuration | Altro Identificativo no. Other Identification no. | Rev. Rev. | | |
| | | | | |

| Regime | Case | Fx [kN] Main coil | Fz [kN] TRIM + | Fz [kN] TRIM- |
|-----------|--------|-------------------|----------------|---------------|
| Operative | Case 3 | -4.6 | 13 | -12 |
| Test 1 | Case 3 | -4.6 | 65.5 | -64 |
| Test 2 | Case 3 | -7.5 | 0 | 0 |

Table 24: Magnetic forces generated by a radial shift of the main coil.

Finally, unbalanced TRIM coils have been considered. Actually, if there will be a complex deviation (axial shift and current density variation), in order to keep the system within the magnetic requirements, the TRIM coils will have two different currents. As described in 4.4, considering a 20 mm axial shift and a [-0.5;0.5]% variation of the main coil current density, the magnetic requirements are respected with a current density of 1.3 A/mm² in the negative TRIM coil and with a current density of 2 A/mm² in the positive TRIM coil. In order to be conservative, the magnetic forces have been also calculated with other two TRIM coil current densities: 1.2 A/mm² in the negative TRIM coil and with a current density of 2.1 A/mm² in the positive TRIM coil.

The unbalanced TRIM coils are related to the complex deviation 2 (axial shift of 20 mm) while they are not necessary in the complex deviation 1 (axial shift of 10 mm). The only studied configuration is Case 1.

| Configuration | Main coil J [A/mm ²] | TRIM + coil J [A/mm ²] | TRIM - coil J [A/mm ²] |
|---------------|----------------------------------|------------------------------------|------------------------------------|
| Case 1 -1 | 20.40 | 1.3 | 2 |
| Case 1 -2 | 20.40 | 1.2 | 2.1 |

Table 25: Unbalanced TRIM coil current density configurations.

The unbalanced TRIM coils are possible only in the operative regime and in the failure mode 1.

| Regime | Case | Fz [kN] Main coil | Fz [kN] TRIM + | Fz [kN] TRIM- |
|-----------|----------|-------------------|----------------|---------------|
| Operative | Case 1-1 | 64.4 | -0.2 | -23 |
| | Case 1-2 | 52 | -2 | -27.5 |
| Failure 1 | Case 1-1 | 0 | 28 | -66 |
| | Case 1-2 | 0 | 24 | -72 |

Table 26: Magnetic forces in the unbalanced TRIM coil configurations.

Unbalanced TRIM coils generate forces which can push them also toward the center of the system. The TRIM coils have to be hold by the caps.

The last check has taken into account the possibility that the power supplier of the base current switches off without the safety device. The TRIM+ coil current density decreases up to zero while the other TRIM coil current density decreases up to 0.7 A/mm².

| Configuration | Main coil J [A/mm ²] | TRIM + coil J [A/mm ²] | TRIM - coil J [A/mm ²] |
|---------------|----------------------------------|------------------------------------|------------------------------------|
| Case 1 -3 | 20.40 | 0 | 0.7 |

Table 27: TRIM coil current density configuration in case of base current power supplier failure.

| Regime | Case | Fz [kN] Main coil | Fz [kN] TRIM + | Fz [kN] TRIM- |
|-----------|----------|-------------------|----------------|---------------|
| Operative | Case 1-3 | 64.6 | 0 | 6 |

Table 28: Magnetic forces in the case of one TRIM off.

| | | | | |
|--|--|--------------|--------------|----------|
| Titolo Title | Documento no. Document no. | Rev. Rev. | Pag. Page | Di Of |
| Magnetic verification of the new yoke configuration | 100RM19902 | 1 | 21 | 21 |
| | Altro Identificativo no. Other Identification no. | Rev. Rev. | | |

7.1 Conclusions

The maximum magnetic force on the main coil is 151 kN in test mode 2, when the coil current is maximum. The principal component of the force is the axial one, the radial component appears only if there is a radial shift but it is less than 10 kN.







With the considered tolerances in the positioning of the coil, the two extreme axial shifts are 5 and 20 mm. In these situations the axial force on the main coil is always directed in the positive Z direction.

The magnetic forces on balanced TRIM coils are always directed towards the poles: the TRIM coils are pushed against the poles.

Only with unbalanced TRIM coils there are forces pushing the coils towards the center of the system and so against the caps.

The maximum force on the TRIM coils is: 130 kN against the poles in the failure mode 2 and 6 kN against the caps in the unbalanced case.

APPENDIX 9. Magnet Power Supply System

| | | | | | | | | | |
|--|---|---|---|---|---|--|---|-----------------------|--------------|
| Titolo Title | | | Documento no. Document no. | | | | Rev. Rev. | Pag. Page | Di Of |
| MPD Magnet Power Supply System | | | 700RM20220 | | | | 1 | 1 | 15 |
| Altro Identificativo no. Other Identification no. | | | Rev. Rev. | | | | | | |
| Tipo doc. Doc. type | Emittente Issued by | Edizione in lingua Language | | Derivato da Derived from | | | | Rev. Rev. | |
| TS | ING | English | | | | | | | |
| Commessa Job no. | | Progetto Project | | Cliente Customer | | | | | |
| 2125 | | MPD Dubna | | JINR | | | | | |
| Rev. Rev. | Motivo Revisione Reason for revision | | | | | | | | |
| 0 | First issue | | | | | | | | |
| 1 | Scheme review, QD power supply to UPS, fast discharge passive system detailed | | | | | | | | |
| Lista di Distribuzione Distribution List | | | | | | | | | |
| 1 | |  |  |  |  |  |  | 18/04/2017 | |
| | | S. Grillo | M. Modica | N. Valle | | | R. Marabotto | | |
| 0 | | | | | | | | | |
| | | S. Grillo | M. Modica | N. Valle | | | R. Marabotto | 13/02/2017 | |
| Rev. Rev. | Stato (W/R) Status | Classe Riserv (1/2/3) Confid. | Preparato Prepared | Controllato Reviewed | Verificato Verified | Verificato Verified | Verificato Verified | Approvato Approved | Data Date |

| | | | | |
|--|--|------------------------------|------------------------------|---------------------------|
| Titolo Title MPD Magnet Power Supply System | Documento no. Document no. 700RM20220 | Rev. Rev. 1 | Pag. Page 2 | Di Of 15 |
| | Altro Identificativo no. Other Identification no. | Rev. Rev. | | |

Summary

| | | |
|-------|---|----|
| 1. | Introduction..... | 3 |
| 1.1 | Power supply system component..... | 3 |
| 2. | SC Power Supply..... | 3 |
| 3. | Coil discharge..... | 5 |
| 3.1 | Emergency discharge: Dump Resistor..... | 5 |
| 3.2 | Fast discharge system..... | 5 |
| 3.2.1 | Modular dump resistor..... | 6 |
| 3.2.2 | Diodes array..... | 6 |
| 4. | TRIM Coil Power Supply..... | 7 |
| 5. | QD system..... | 8 |
| 6. | Protection System..... | 10 |
| 7. | Polarity Switch System..... | 12 |
| 7.1 | SC Current Switch..... | 12 |
| 8. | Control Software..... | 13 |
| 9. | ASG personnel training..... | 13 |
| 10. | Test and acceptance..... | 13 |
| 11. | Supplier Guarantee and Support..... | 14 |
| 12. | Documentation..... | 14 |
| 13. | Identification and packing..... | 15 |
| 14. | ASG Reference personnel..... | 15 |

| | | | | |
|--|--|------------------------------|------------------------------|---------------------------|
| Titolo Title MPD Magnet Power Supply System | Documento no. Document no. 700RM20220 | Rev. Rev. 1 | Pag. Page 3 | Di Of 15 |
| | Altro Identificativo no. Other Identification no. | Rev. Rev. | | |

1. Introduction

The MPD magnet is composed by a Superconductive solenoid coil (SC) and two resistive coil (TRIM coils) at the ends, disponed as shown in Fig 1.

The SC is a solenoid that produce the main magnetic field. At both side of the SC there is a TRIM coil, a resistive copper spiral used for the fine tuning and correction of the magnetic field.

The Power Supply System should energize the system during the normal operation of the magnet, discharge it and also protect it in case of failure.



Fig 1: Magnet configuration

1.1 Power supply system component

The Power Supply System main components are summarized in these main items:

- SC power supply (SC PS)
- SC quench detector (SC QD)
- Current Breaker
- Dump resistor
- Fast passive discharge system
- TRIM coil main power supply (TRIM PS1)
- TRIM coil correction power supply (TRIM PS2)
- Polarity Switch System
- Control Software

Hardwired communication trough an interlock is required between the SC power supply and Trim coil power supplies in order to ramp down / shut down the system in case of failure. The main issue of the protection system should be to protect the coil in case of quench and to avoid a scenario with a TRIM coil and the SC ON and the other TRIM coil OFF.

The system should be a “plug and play” system, wired by the supplier.

2. SC Power Supply

The superconductive coil should be energized using a power supply and protected from the quench by a quench detection system that, in case of quench, should open a breaker/contactors system to discharge the coil in a dump resistor.

If a quench occurs, the voltage in the coil is unbalanced. A Quench Detection System detect the quench monitoring the difference between voltage of the solenoid through voltage taps. Fig 2 shows the SC power supply and protection system proposed; each component will be described in following paragraphs:

| | | | | |
|---------------------------------------|--|--------------|--------------|----------|
| Titolo Title | Documento no. Document no. | Rev. Rev. | Pag. Page | Di Of |
| | 700RM20220 | 1 | 4 | 15 |
| MPD Magnet Power Supply System | Altro Identificativo no. Other Identification no. | Rev. Rev. | | |
| | | | | |

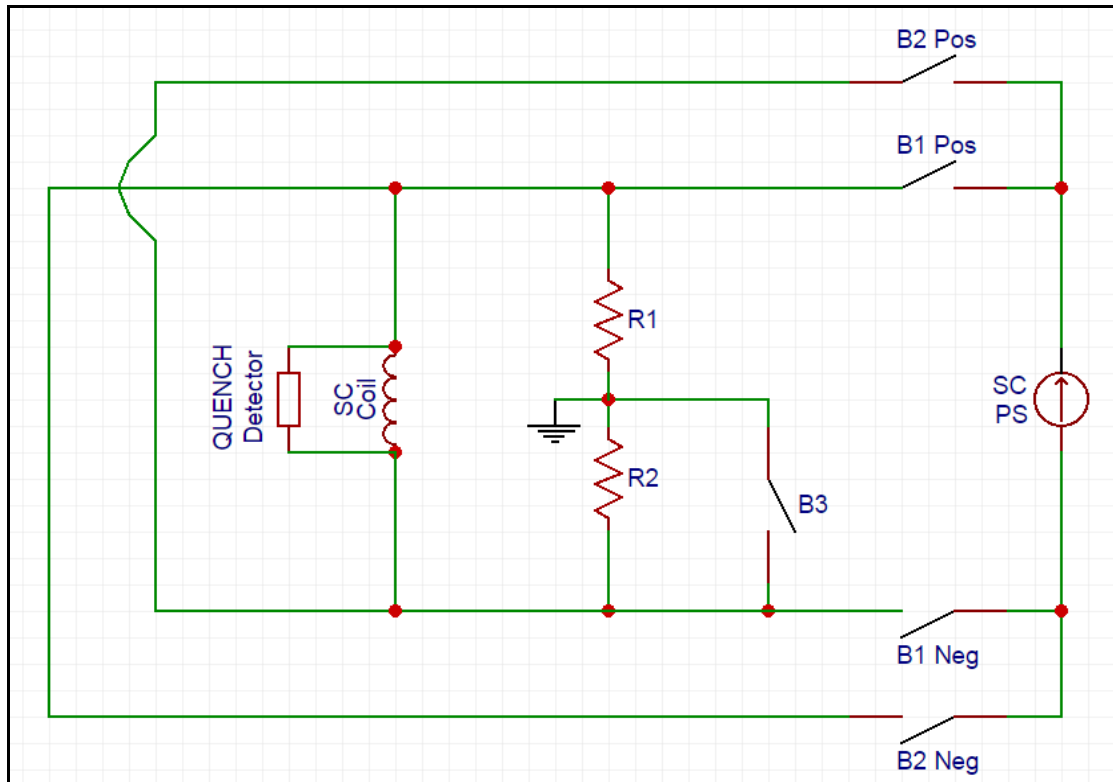


Fig 2: SC Power Supply System

With this electric connections, if a failure occurs, the breakers/contactors open the circuit and the coil could discharge on the dump resistors, excluding the Power Supply. The grounding device is connected to the mid point of the dump resistor, to halve the voltage during the magnet discharge.

The power supply connections have to be floating.

The main characteristics of the system are:

- Max current: 2500A
- Max voltage: 10V
- Stability over 8h < 0.03% Inom
- Reproducibility: +0.1% Inom
- Current Ripple: $\leq 1\%_{pp} \pm 1\text{mA Inom}$
- Lcoil = 9H
- Max ramp-up rate: 1 Amp/sec
- Communication: Profibus / Profinet
- Max ramp-down rate from max current to 0Amp: 1 Amp/sec

| | | | | |
|---------------------------------------|--|--------------|--------------|----------|
| Titolo Title | Documento no. Document no. | Rev. Rev. | Pag. Page | Di Of |
| | 700RM20220 | 1 | 5 | 15 |
| MPD Magnet Power Supply System | Altro Identificativo no. Other Identification no. | Rev. Rev. | | |
| | | | | |

Shunt or DCCT shall be put in the circuit to monitor the current.

The SC power supply system includes:

- a controllable ramp rate;
- a quench detection system, integrated with the power supply cabinet;
- a dump resistor;
- breakers/contactors system;
- fast passive discharge system;
- 2 external interlock to ramp down / ramp stop / breaker open.

The system should have a passive safety device that allows a fast discharge of the magnet also in case of a Main Power Line failure avoiding the discharge on the complete dump resistor. A fast ramp down from 2500Amp to 0Amp should be done in 20 minutes using a passive discharge system (diodes array or dump resistor). The design of this system should be done in accordance with ASG.

3. Coil discharge

During normal operation, the magnet should be de-energized, driven by the power supply, with a ramp rate of 1 Amp/sec. If the system has a failure during the normal operation, there could be two more different discharge option that protect the magnet and the other auxiliary system:

- **Emergency discharge:** ≈ 4 min, necessary in case of major failure of the magnet, provided by dump resistor;
- **Fast discharge:** ≈ 20 min, necessary in case of minor failure of auxiliary system that allows a discharge of the magnet slower than the emergency discharge but faster than the PS controlled discharge.

3.1 Emergency discharge: Dump Resistor

The dump resistor should provide to the **emergency discharge** of the magnet during emergency and major failure of the system. The energy will be dissipated in the dump resistor. Its maximum temperature should be limited to $\approx 300^{\circ}\text{C}$. It will be cooled by natural air convection.

The resistance of the dump should be $\approx 0.104\Omega$.

3.2 Fast discharge system

In case of minor failure, (i.e. LHe Refrigerator failure) the magnet should be de-energized in ≈ 20 min. According with ASG, the supplier should propose two different passive system that provide this **fast discharge**, not driven by the power supplies: a small dump resistor or a diodes array. ASG will choose which system will be used.

| | | | | |
|--------------------------------|--|--------------|--------------|----------|
| Titolo Title | Documento no. Document no. | Rev. Rev. | Pag. Page | Di Of |
| | 700RM20220 | 1 | 6 | 15 |
| MPD Magnet Power Supply System | Altro Identificativo no. Other Identification no. | Rev. Rev. | | |
| | | | | |

3.2.1 Modular dump resistor

The total dump resistor should be composed by two resistor connected in series: R1 and R2 as reported in Fig 2.

The fast discharge of the coil should be provided by R1 resistor. The supplier should compose the main dump resistors (0.104 Ω) with two parts. In Fig 2 is described the dump resistor connection.

A circuit with a breaker B3 splits the dump in two parts. The R1 will provide to the fast discharge of the coil in 20min. The R1+R2 will provide to the emergency discharge of the system.

B3 should be breaker that must interrupt the circuit when there is the max current in the system, as ABB model IORR3200-10-CC or equivalent.

$$R1 = 0.052 \Omega \quad R2 = 0.052 \Omega \quad R1 + R2 = 0.104$$

The configurations of the breakers/contactors in different operating conditions are described in Table 1:

Table 1: Breakers operating conditions

| Operating Condition | B1/B2 | B3 |
|---------------------------|--------|--------|
| Normal Operation | CLOSED | OPEN |
| Normal discharge | CLOSED | OPEN |
| Emergency discharge | OPEN | OPEN |
| Fast discharge | OPEN | CLOSED |
| SAFE CONFIGURATION | OPEN | OPEN |

The breakers/contactors B1 and B2 are better described in Par.7 *Polarity Switch System*.

3.2.2 Diodes array

The fast discharge of the coil could also be provided by a diodes array. The supplier could provide a passive system that allows a ramp down rate ≈ 120 Amp/min.

It is preferred an air convection cooled system.

In case of failure of one diode a short circuit must be guarantee.

| | | | | |
|--|-------------------------------|--------------|--------------|----------|
| Titolo Title | Documento no. Document no. | Rev. Rev. | Pag. Page | Di Of |
| | 700RM20220 | 1 | 7 | 15 |
| Altro Identificativo no. Other Identification no. | | Rev. Rev. | | |

4. TRIM Coil Power Supply

The MPD Magnet needs two resistive TRIM coils to reach the field homogeneity in the requested area. The cold mass (support cylinder and SC coil) is fixed to the Cryostat by an asymmetric suspension system (axial and radial tie rods). To avoid an unbalanced axial force on the cold mass, the system must avoid the scenario with a TRIM coil ON and the other one OFF.

The circuit is described in Fig 3.

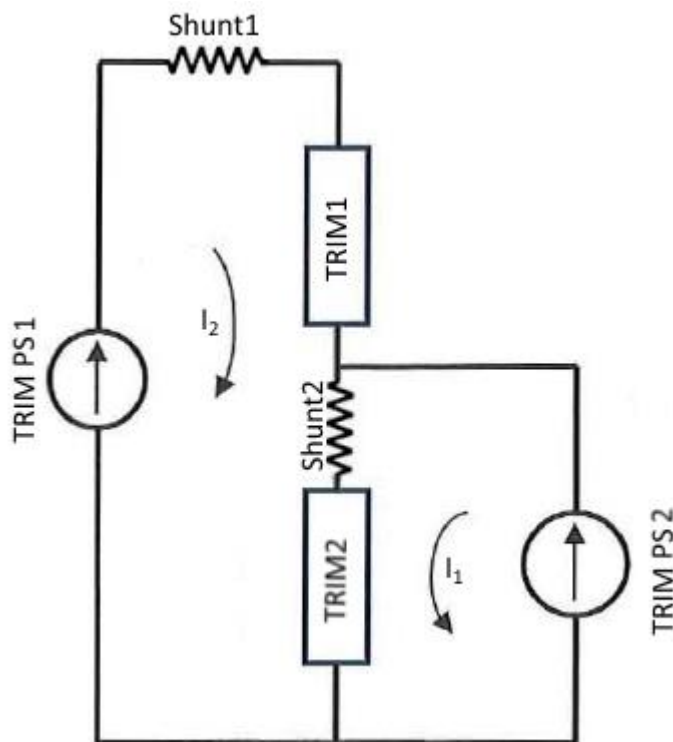


Fig 3: TRIM Coils Power Supply System

The power supply TRIM PS1 (main) produces the same current through the trim coils (I_2). The power supply TRIM PS2 (correction), is used for the correction of technology deviations of the magnetic circuit parameters, unbalancing the current in the TRIM2 coil.

The shunts or DCCT are a redundant safety control system.

The max current is 4500A but the final current of the coils will be different. It's required a fine current tuning for each coil. During normal operation of the magnet, the PS TRIM1 will be ramped up to reach the base current in both TRIM coils. Then the PS TRIM2 will be ramped up to tuning the magnetic field.

Whenever a trim coil ramp down or shut down (also in case of failure), the second one must do the same, simultaneously. The system should not allow a configuration with only one TRIM coil ON. During controlled ramp-down, PS TRIM2 will be ramped down first, then the PS TRIM1 will be ramped down.

| | | | | |
|--|--|------------------------------|------------------------------|---------------------------|
| Titolo Title MPD Magnet Power Supply System | Documento no. Document no. 700RM20220 | Rev. Rev. 1 | Pag. Page 8 | Di Of 15 |
| | Altro Identificativo no. Other Identification no. | Rev. Rev. | | |

The main characteristics of the system are:

- PS TRIM1 Max current: 4500A
- PS TRIM1 Max voltage: 50V
- PS TRIM1 Current Ripple: $\leq 1\%pp \pm 1mA$ Inom

- PS TRIM2 Max current: 2500A
- PS TRIM2 Max voltage: 30V
- PS TRIM2 Current Ripple: $\leq 1\%pp \pm 1mA$ Inom

- Reproducibility (for both PS): $\pm 0.1\%$ Inom
- Stability over 8 h (for both PS): $< 0.03\%$ Inom
- Communication:
 - RS232/IEEE488 combined interface (12bit for voltage, current, and control)
 - Profibus / Profinet

- Ltrim: 0.007H
- Mutual inductivity of the SC coil and each of the TRIM coils : 0.05H

5. QD system

The SC coil has quench detector system hardwired. The QD has an output signal normally closed (safety mode) connected with the breakers, the power supplies and the magnet control system, as reported in Fig 6.

The quench detector must have a dedicated power line (220Amp) under a **UPS** (UPS is not in the scope of supply) to guarantee his correct operability also during a black out. The power absorption should be indicated by the supplier.

The quench detector has to be based on the mid-point protection system. The signals taken from the voltage taps on the solenoid are:

- a voltage tap on the top (T);
- a voltage tap on the bottom (B);
- voltage tap on the modules junctions (V_{tap2} and V_{tap3}) (C1 and C2).

The solenoid is divided into 3 modules. A mid voltage tap is between the first and the second modules, another one is between the second and the third modules, in the external module-module junction. The mid-point for this system is unbalanced and divides the coil in $\approx 1/3 \ 1/3 \ 1/3$.

To avoid the possibility that a quench occurs under a mid point voltage tap and the system could not detect it, the QD should compare two different voltage, one using as central taps the V_{tap2} and the other using the V_{tap3} . (Fig 4):

| | | | | |
|--|--|------------------------------|------------------------------|---------------------------|
| Titolo Title MPD Magnet Power Supply System | Documento no. Document no. 700RM20220 | Rev. Rev. 1 | Pag. Page 9 | Di Of 15 |
| | Altro Identificativo no. Other Identification no. | Rev. Rev. | | |

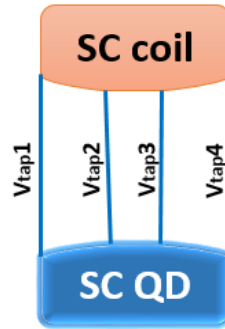


Fig 4: QD and voltage taps connections

| | | | | |
|--------------------------------|--|--------------|--------------|----------|
| Titolo Title | Documento no. Document no. | Rev. Rev. | Pag. Page | Di Of |
| | 700RM20220 | 1 | 10 | 15 |
| MPD Magnet Power Supply System | Altro Identificativo no. Other Identification no. | Rev. Rev. | | |
| | | | | |

6. Protection System

The protection system manages all the signals and the logic protections that avoids the dangerous scenarios.

All the output interlocks must be normally closed (safe configuration). The power supplies are ON only with all signals are closed.

Magnet Control System (MCS) is a PLC system that manages the signals of all the magnetic system, included the Power Supply System described in this document.

The system connections are sketched in Fig 5. The SC coil is connected with a Quench Detector (SC QD). The QD signal pilot all the power supplies. If QD signal goes DOWN, the power supplies must shut down immediately, **the breaker must OPEN** and the information must be sent to MCS.

The first stage of this protection system is the direct connection of QD with the breakers(contactors). The signal is used as interlock for the breakers(contactors) that opens if the signal is DOWN. So if QD signal goes DOWN the breakers(contactors) will OPEN.

The second stage is the connection with the Power Supplies. The QD signal is used as input for interlock of each power supply. If the signal goes DOWN, each power supplies SHUT DOWN.

The third stage is the connection with the Magnet Control System (MCS). The QD signal is used as input for interlock of the MCS. If signal goes DOWN, the MCS interlock goes DOWN.

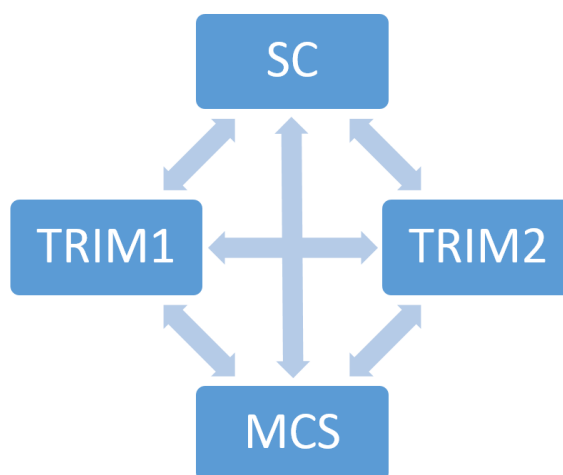


Fig 5: Protection System connections

| | | | | |
|---------------------------------------|--|--------------|--------------|----------|
| Titolo Title | Documento no. Document no. | Rev. Rev. | Pag. Page | Di Of |
| | 700RM20220 | 1 | 11 | 15 |
| MPD Magnet Power Supply System | Altro Identificativo no. Other Identification no. | Rev. Rev. | | |
| | | | | |

The Fig 5 is a scheme of the protection system that shows inputs and interlocks from and to PS. The scheme highlights the function of the QDs that, with the three signals in series, drive Power Supplies, Breaker and MCS.

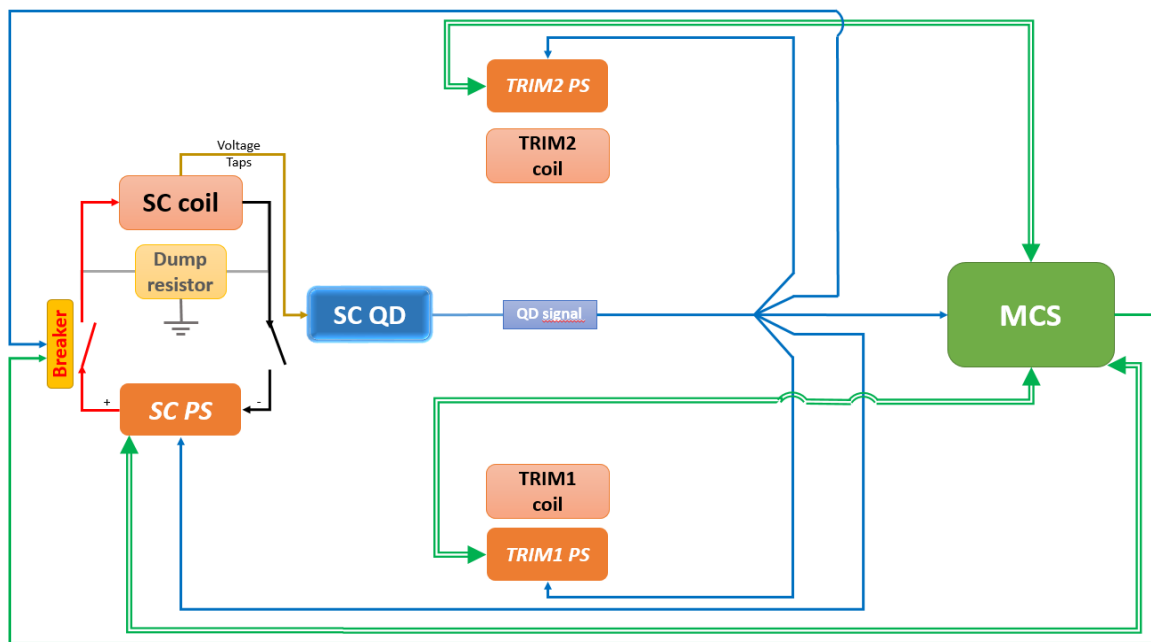


Fig 6: PS protection system scheme

NOTE: In this scheme, the TRIM coils power supplies are not electrical connected.

-  Single QD signal
-  Interlock from and to the PS
-  Signal from MCS to Breakers

| | | | | |
|--------------------------------|--|--------------|--------------|----------|
| Titolo Title | Documento no. Document no. | Rev. Rev. | Pag. Page | Di Of |
| | 700RM20220 | 1 | 12 | 15 |
| MPD Magnet Power Supply System | Altro Identificativo no. Other Identification no. | Rev. Rev. | | |
| | | | | |

7. Polarity Switch System

The magnetic system is placed in a laboratory with a particle accelerator. The power supply system will not be easily reached by personnel after the first experiment because it will be in a dangerous radiation zone.

Due to the requirements of polarity switch of the system (always at zero current, with all power supplies OFF), current switches that could be remote driven should be included in the power supply system and should allow the polarity switch of all the power supplies.

The polarity of the power supplies must always be changed together, so there could be only two possible operating configurations.

The TRIM coil Current Switch shall be design in accordance with ASG.

7.1 SC Current Switch

The superconductive connections include breakers for the protection of the superconductive coil and contactors for the polarity switch.

Fig 7 shows a proposal for the SC Current Switch that the supplier should analyze. Modifications and implementations of the system should be agreed with ASG.

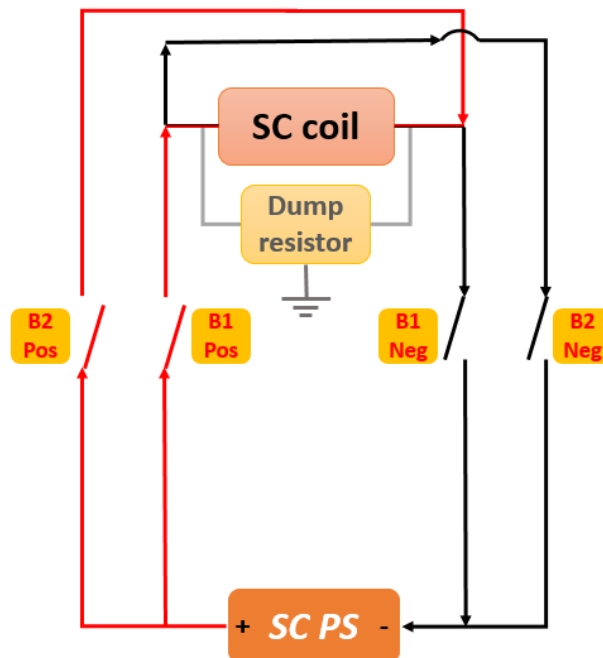


Fig 7: SC Current Switch

B1 Pos and **B2 Pos** should be breakers that must interrupt the circuit when there is the max current in the system. The breaker should be ABB model IORR3200-10-CC or equivalent.

The **B1 Neg** and **B2 Neg** should be contactor that change the polarity of the system. The design of those contactor should be done in accordance with ASG. They will always operate at 0 current with power supplies off, only to change polarity to the system and not to protect it during a failure.

| | | | | |
|---------------------------------------|--|--------------|--------------|----------|
| Titolo Title | Documento no. Document no. | Rev. Rev. | Pag. Page | Di Of |
| | 700RM20220 | 1 | 13 | 15 |
| MPD Magnet Power Supply System | Altro Identificativo no. Other Identification no. | Rev. Rev. | | |
| | | | | |

The Table 2 shows the configuration of the breakers/contactors in three configurations:

Table 2: Breaker configurations

| Switch configuration | B1 Pos | B1 Neg | B2 Pos | B2 Neg |
|---------------------------|--------|--------|--------|--------|
| Configuration 1 | CLOSED | CLOSED | OPEN | OPEN |
| Configuration 2 | OPEN | OPEN | CLOSED | CLOSED |
| SAFE CONFIGURATION | OPEN | OPEN | OPEN | OPEN |

The protection system **must open all breakers** if a failure occurs, for example if the SC Quench Detector detects a quench, to protect the magnet.

8. Control Software

A control software for the power supply system should be provided, to remote drive all the Power Supply System components, using the communication protocols defined in previous paragraph.

9. ASG personnel training

The supplier should include in the offer the ASG personnel training for the system set up, first run, tests, in accordance with ASG.

The technical description of the system should be included, with electrical schemes of the main components.

10. Test and acceptance

The Supplier will have to do, at his own expenses and under his own responsibility, in addition to what foreseen by applicable codes and guidelines, the tests listed below, mandatory for the acceptance, and supply the relevant documentation.

Two series of test will be performed: the Factory Acceptance Test at the supplier factory (FAT) and the Site Acceptance Test in ASG (SAT). Both FAT and SAT will be performed under the supplier responsibility and by supplier personnel. During the test the ASG personnel will be trained in the correct use and maintenance of the system.

The FAT is a complete functional test of all the power supply system and of each unit that composes the system.

All the interlocks interactions should be tested, simulating different failures in the system. Breakers and contactors must be tested to control their correct operation also at max current, both individually and in the system.

| | | | | |
|---------------------------------------|--|--------------|--------------|----------|
| Titolo Title | Documento no. Document no. | Rev. Rev. | Pag. Page | Di Of |
| | 700RM20220 | 1 | 14 | 15 |
| MPD Magnet Power Supply System | Altro Identificativo no. Other Identification no. | Rev. Rev. | | |
| | | | | |

Each power supply should be tested performing:

- the ramp up to max current at different ramp rate;
- the steady state at max current, **16 hours**;
- the ramp down from max current to 0 at different ramp rate;
- the emergency ramp stop, ramp down, shut down;
- the measurements of all the main characteristics of the power supplies, described in Par. 2 (SC Power Supply) and Par. 4 (TRIM coil Power Supplies);
- the interlock interactions, simulating failures in the quench detector and in each power supply.

All test procedure shall be agreed with ASG.

The SAT is a complete functional test of all the power supply system and of each unit that composes the system in ASG. No difference will be accepted between the result of FAT and SAT. The supplier must guarantee the presence of his personnel in ASG during the SAT.

The shipment of the Supply to the Client's address, or other address agreed, will be possible only after the certificates have been received by ASG and only after their written consent.

11. Supplier Guarantee and Support

The Supply should have a Guarantee of 24 months after the SAT acceptance.

The supplier should guarantee the support for the installation and test at the final customer site (Dubna, Russia). If needed, the supplier should also guarantee the presence of personnel in case of failure and technical issues in short term.

The spare parts of the power supply have to be stored by the supplier warehouse and must be available in short term.

12. Documentation

The documentation, unless more stringent requirements are specified by applicable codes, will include as minimum:

- Manufacturing plan (a preliminary release is expected with the offer);
- Quality Control Plan, to be submitted to ASG for comments and approval (a preliminary release is expected with the offer);
- Test procedures, to be submitted to ASG for comments and approval;
- Tests certificates;
- Block scheme of the system;
- Detailed electrical schemes of each component;
- 3D CAD model of each component for their overall dimensions;
- Full set of detailed drawings
- Certificate of compliance.

Quality documents will have to be sent as original copy to the address indicated in ASG purchasing order (certificates@as-g.it).

| | | | | |
|--|--|--------------------------|---------------------------|-----------------------|
| Titolo Title MPD Magnet Power Supply System | Documento no. Document no. 700RM20220 | Rev. Rev. 1 | Pag. Page 15 | Di Of 15 |
| | Altro Identificativo no. Other Identification no. | Rev. Rev. | | |

A copy will have to be sent to ASG Superconductors, attached to the shipped material.

13. Identification and packing

The components will have to be identified so that materials could be traced back.

The components will be packaged on standard wood pallets and will have to be covered, so that they are protected against environmental agents during transport.

The assembly will be protected in a plastic sealed bag, to protect it against environmental agents. The bag will have de-moisturing salt bags inside and filled with Nitrogen at room pressure and temperature.

The delivery address is: ASG Superconductors Via Melara, 40 I-La Spezia

14. ASG Reference personnel

- *Technical Dept.:*

Dr. S. Grillo Tel. +39 010 6489218 grillo.simone@as-g.it

Dr. M. Modica Tel. +39 010 6489327 modica.marco@as-g.it

Dr. N. Valle Tel. +39 010 6489238-158 valle.nicolo@as-g.it

- *Purchasing Dept.:*

Sig.ra D. Grillo Tel. +39 010 6489213 - Fax +39 010 6489275 grillo.daniela@as-g.it

- *Quality Assurance:*

Ing. F. Terzi Tel. +39 010 6489317 - Fax +39 010 6489275 terzi.franco@as-g.it

APPENDIX 10. Power supplies general specifications and performances



Magnet Power Supply system

Magnet Power Supplies

**Power supplies
general specifications
and performances**

v.01

| | | |
|-----|--|----|
| 1 | SC POWER SUPPLY SPECIFICATION | 3 |
| 1.1 | General specifications..... | 3 |
| 1.2 | Performance | 4 |
| 1.3 | Water cooling circuit..... | 5 |
| 1.4 | Cabinet specifications | 5 |
| 2 | TRIM PS1 POWER SUPPLY SPECIFICATION..... | 6 |
| 2.1 | General specifications..... | 6 |
| 2.2 | Performance | 7 |
| 2.3 | Water cooling circuit..... | 8 |
| 2.4 | Cabinet specifications | 8 |
| 3 | TRIM PS2 POWER SUPPLY SPECIFICATION..... | 9 |
| 3.1 | General specifications..... | 9 |
| 3.2 | Performance | 10 |
| 3.3 | Water cooling circuit..... | 11 |
| 3.4 | Cabinet specifications | 11 |

1 SC POWER SUPPLY SPECIFICATION

1.1 General specifications

| General specifications | |
|---|---|
| Unit/Type | Super conductive coil power supply |
| Basic topology | AC/DC power converter with 12 pulses SCR controlled rectifiers (SEM single pulse control) |
| Current Sensor | DCCT |
| Power line input voltage | - Europe 400 V ±10%, 3-phase + PE for power - 230 V ±10% from UPS for control racks |
| Input frequency | 50 / 60 Hz |
| Maximum current consumption | 95A/ph; 66kVA on 3-phase line < 1k VA on 230 V UPS |
| Nominal output current (Inom) | ±2500A _{dc} (polarity reversing switch*) |
| Output current ramp rate | Adjustable 0.1A/s – 1A/s |
| Maximum output power | 25000 W |
| Operation mode | DC constant current. |
| Maximum line voltage distortion acceptable | <5% RMS |
| Total harmonic distortion (current) | <30% |
| | $THD_i = \sqrt{\sum_{h=2}^H \left(\frac{I_h}{I_1} \right)^2}$ |
| Inrush current | 10 x Inominal, limited by soft start sequence to 3 x Inominal |
| Phase imbalance | ±3%, balanced by SEM |
| Line protection/Main breaker | Main Manual Switch |
| Inrush current limitation | AC contactor plus series resistors |
| Load | Super conductive magnet. (Tests at Sigmaphi done on a resistive load) |

Table 1 - General Specifications SCPS

*Reversing the polarity is only possible at zero current. Reversing the output polarity is a system functionality, all the power supplies outputs shall be reversed together.

1.2 Performance

| Performance | |
|--|---|
| Current control range | 0.1 A to 100% of I_{dcmax} |
| Maximum output voltage | 10 V |
| Voltage limitation range | 100% of V_{dcmax} |
| Line regulation +/-1% (fast <0.2 sec) | ± 300 ppm of I_{nom} |
| Load regulation (+/-10% resistance variation) | ± 300 ppm of I_{nom} |
| Power factor (estimated) | Nominal |
| | $V_{out}=10V$ 0.6 |
| Efficiency (estimated) | Nominal line |
| | $V_{out}=10V$ 0.45 |
| Output stability at nominal current : (DC to 1Hz) Long term 8 hours (Under constant conditions of line, load and temperature) | ± 300 ppm of I_{nom} |
| Output current ripple | $\leq 1\%pp \pm 1mA$ of I_{nom}^* |
| Reproducibility | $\pm 0.1\%$ I_{nom} |
| Warm up time (from cold) | 1 hour |
| Temperature coefficient (ambient air) | 100ppm of $I_{max} / ^\circ C$ |
| Setting value resolution | 18bits |
| Overload protection | Yes , adjusted at 110% of I nominal |
| Filter discharge | After 10s $\rightarrow \leq 48V$ & $\leq 20J$ |
| Acoustic noise (f< 20 kHz) | < 65dBA at three meters from the unit |
| Transformer | 12 pulses, air cooled, with screen, heating type F, insulation type H |
| Semiconductors | SCRs |
| MTBF | 50000 hours typical |

Table 2 - Performance Specifications SCPS

1.3 Water cooling circuit

| Water cooling circuit | |
|-----------------------------------|--|
| Water | Water de-ionized, de-gassed |
| Conductivity | Max 40uS/meter for indirect cooled systems |
| Input temperature | 25°C ±1°C |
| Δ In/Out typ. | 10°C |
| Approx. flow | 15 l/min |
| Max. absolute pressure | 12 bars |
| Min. differential pressure | 5 bars |
| Test pressure | 16 bars/20 min |
| Flow meter | Yes |
| Material | CU, stainless steel, plastic (no brass) |

Table 3 – Water cooling circuit Specifications SCPS

1.4 Cabinet specifications

| Cabinet specifications | |
|-------------------------------|--|
| Material | Steel |
| Color | RAL7035 (light grey) |
| Support | Stands |
| Handling | Overhead crane via lifting eyes, fork lift |
| Width (approximative) | 3000mm |
| Depth (approximative) | 1000mm |
| Height (approximative) | 1800mm |
| Weight (approximative) | TBD |

Table 4 – Cabinet Specifications SCPS

2 TRIM PS1 POWER SUPPLY SPECIFICATION

2.1 General specifications

| General specifications | |
|--|---|
| Unit/Type | Resistive coil power supply |
| Basic topology | AC/DC power converter with 12 pulses SCR controlled rectifiers (SEM single pulse control) |
| Power line input voltage | Europe 400 V ±10%, 3-phase + PE |
| Input frequency | 50 / 60 Hz |
| Maximum current consumption | 500A/ph; 350kVA |
| Nominal output current (Inom) | ±3000Adc (polarity reversing switch*) |
| Output current ramp rate | Adjustable 0.1A/s – 1A/s |
| Maximum output power | 210 000 W |
| Operation mode | DC constant current. |
| Maximum line voltage distortion | <5% RMS |
| Total harmonic distortion (current) | <30% |
| | $THD_i = \sqrt{\sum_{h=2}^H \left(\frac{I_h}{I_1} \right)^2}$ |
| Inrush current | 10 x Inominal, limited by soft start sequence to 3 x Inominal |
| Phase imbalance | ±3%, balanced by SEM |
| Line protection/Main breaker | Fuses and Manual Switch |
| Inrush current limitation | AC contactor plus series resistors |
| Load | Resistive magnet. |

Table 4 - General Specifications TRIM PS1

*Reversing the polarity is only possible at zero current. Reversing the output polarity is a system functionality, all the power supplies outputs shall be reversed together.

2.2 Performance

| Performance | | | | |
|---|--|--------------|---------|-------------|
| Current control range | 0.1 A to 100% of Idcmax | | | |
| Maximum output voltage | 70 V | | | |
| Voltage limitation range | 100% of Vdcmx | | | |
| Line regulation +/-1% (fast <0.2 sec) | < 300 ppm of Inom | | | |
| Load regulation (+/-10% resistance variation) | < 300 ppm of Inom | | | |
| Power factor (estimated) | | Line -10% | Nominal | Line +10% C |
| | Vout=50V | 0,85 | 0,78 | 0,7 |
| | Vout=40V | 0,63 | 0,56 | 0,5 |
| | Vout=30V | 0,28 | 0,26 | 0,24 |
| Efficiency (estimated) | | Nominal line | | |
| | Vout=70V | 0.70 | | |
| | Vout=50V | 0.51 | | |
| | Vout=20V | 0.20 | | |
| Output stability at current Nom: (DC to 1Hz) Long term 8 hours (Under constant conditions of line, load and temperature) | +/-300 ppm of Inom | | | |
| Output current ripple | ≤1%pp ±1mA of Inom | | | |
| Reproducibility | ±0.1% Inom | | | |
| Warm up time (from cold) | 3 hours | | | |
| Temperature coefficient (ambient air) | 100ppm of Inom/°C | | | |
| Setting value resolution | 18bits | | | |
| Overload protection | Yes , adjusted at 110% of I nominal | | | |
| Filter discharge | After 10s → ≤ 48V & ≤20J | | | |
| Acoustic noise (f< 20 kHz) | < 65dBA at three meters from the unit | | | |
| Transformer | 12 pulses, with screen, heating type F , insulation type H | | | |
| Semiconductors | SCRs | | | |
| Sensors | DCCT | | | |
| MTBF | 50000 hours typical | | | |

Table 5 - Performance Specifications TRIM PS2

2.3 Water cooling circuit

| Water cooling circuit | |
|--|---|
| Water | Water de-ionized, de-gassed |
| Conductivity | 10 to 100 μ S/meter for direct cooled systems |
| Input temperature | 25°C \pm 1°C |
| Δ In/Out typ. | 10°C |
| Approx. flow | 30 l/min |
| Max. absolute pressure | 12 bar |
| Min. differential pressure | 5 bar |
| Test pressure | 16 bar/20 min |
| Flow meter | Yes |
| Material | CU, stainless steel, plastic (no brass) |

Table 6 – Water cooling circuit Specifications

2.4 Cabinet specifications

| Cabinet specifications | |
|-------------------------------|--|
| Material | Steel |
| Color | RAL7035 (light grey) |
| Support | Stands |
| Handling | Overhead crane via lifting eyes, fork lift |
| Width (approximative) | 3000mm |
| Depth (approximative) | 1000mm |
| Height (approximative) | 1800mm |
| Weight (approximative) | TBD |

Table 4 – Cabinet Specifications TRIM PS1

3 TRIM PS2 POWER SUPPLY SPECIFICATION

3.1 General specifications

| General specifications | |
|--|---|
| Unit/Type | Resistive coil power supply |
| Basic topology | AC/DC power converter with 12 pulses SCR controlled rectifiers (SEM single pulse control) |
| Power line input voltage | Europe 400 V ±10%, 3-phase + PE |
| Input frequency | 50 / 60 Hz |
| Maximum current consumption | 145A/ph; 101kVA |
| Nominal output current (Inom) | ±1300Adc (polarity reversing switch*) |
| Output current ramp rate | Adjustable 0.1A/s – 1A/s |
| Maximum output power | 58500 W |
| Operation mode | DC constant current. |
| Maximum line voltage distortion | <5% RMS |
| Total harmonic distortion (current) | <30% |
| | $THD_i = \sqrt{\sum_{h=2}^H \left(\frac{I_h}{I_1} \right)^2}$ |
| Inrush current | 10 x Inominal, limited by soft start sequence to 3 x Inominal |
| Phase imbalance | ±3%, balanced by SEM |
| Line protection/Main breaker | Fuses and Manual Switch |
| Inrush current limitation | AC contactor plus series resistors |
| Load | Resistive magnet. |

Table 7 - Mains Specifications

*Reversing the polarity is only possible at zero current. Reversing the output polarity is a system functionality, all the power supplies outputs shall be reversed together.

3.2 Performance

| Performance | | | | |
|---|---|--------------|---------|-------------|
| Current control range | 0.1 A to 100% of Idcmax | | | |
| Maximum output voltage | 45 V | | | |
| Voltage limitation range | 100% of Vdcmx | | | |
| Line regulation +/-1% (fast <0.2 sec) | < 300 ppm of Inom | | | |
| Load regulation (+/-10% resistance variation) | < 300 ppm of Inom | | | |
| Power factor (estimated) | | Line -10% | Nominal | Line +10% C |
| | Vout=45V | 0,87 | 0,8 | 0,69 |
| | Vout=30V | 0,61 | 0,56 | 0,50 |
| | Vout=15V | 0,34 | 0,32 | 0,30 |
| Efficiency (estimated) | | Nominal line | | |
| | Vout=45V | 0.70 | | |
| | Vout=30V | 0.47 | | |
| | Vout=15V | 0.23 | | |
| Output stability at current Nom: (DC to 1Hz) Long term 8 hours (Under constant conditions of line, load and temperature) | +/-300 ppm of Inom | | | |
| Output current ripple | ≤1%pp ±1mA of Inom | | | |
| Reproducibility | ±0.1% Inom | | | |
| Warm up time (from cold) | 2 hours | | | |
| Temperature coefficient (ambient air) | 100ppm of I max /°C | | | |
| Setting value resolution | 18bits | | | |
| Overload protection | Yes , adjusted at 110% of I nominal | | | |
| Filter discharge | After 10s → ≤ 48V & ≤20J | | | |
| Acoustic noise (f< 20 kHz) | < 65dBA at three meters from the unit | | | |
| Transformer | 12 pulses, water cooled, with screen, heating type F, insulation type H | | | |
| Semiconductors | SCRs | | | |
| Sensors | DCCT | | | |
| MTBF | 50000 hours typical | | | |

Table 8 - Performance Specifications TRIM PS2

3.3 Water cooling circuit

| Water cooling circuit | |
|--|---|
| Water | Water de-ionized, de-gassed |
| Conductivity | 10 to 100 μ S/meter for direct cooled systems Max 40 μ S/meter for indirect cooled systems |
| Input temperature | 25°C \pm 1°C |
| Δ In/Out typ. | 10°C |
| Approx. flow | 12 l/min |
| Max. absolute pressure | 12 bar |
| Min. differential pressure | 5 bar |
| Test pressure | 16 bar/30 min |
| Flow meter | Yes |
| Material | CU, stainless steel, plastic (no brass) |

Table 9 – Water circuit Specifications TRIM PS2

3.4 Cabinet specifications

| Cabinet specifications | |
|-------------------------------|--|
| Material | Steel |
| Color | RAL7035 (light grey) |
| Support | Stands |
| Handling | Overhead crane via lifting eyes, fork lift |
| Width (approximative) | 1800mm |
| Depth (approximative) | 1000mm |
| Height (approximative) | 1800mm |
| Weight (approximative) | TBD |

Table 4 – Cabinet Specifications TRIM PS2

APPENDIX 11. Quench Calculation

| | | | | |
|-------------------------------------|-------------------------------|--|--------------|----------|
| Titolo Title | Documento no. Document no. | Rev. Rev. | Pag. Page | Di Of |
| | 100RM19300 | 1 | 1 | 24 |
| Quench Calculation MDP Dubna | | Altro Identificativo no. Other Identification no. | | |
| | | Rev. Rev. | | |

| | | | | |
|------------------------|------------------------|--------------------------------|-----------------------------|--------------|
| Tipo doc. Doc. type | Emittente Issued by | Edizione in lingua Language | Derivato da Derived from | Rev. Rev. |
| RT | ING | English | | |

| | | |
|---------------------|---------------------|---------------------|
| Commissa Job no. | Progetto Project | Cliente Customer |
| 2125 | MDP Dubna | JINR |

| Rev. Rev. | Motivo Revisione Reason for revision |
|--------------|---|
| 0 | First issue |
| 1 | Updated Wire Parameters |

| Lista di Distribuzione Distribution List | | | | | | | | | |
|---|--------------------------|--|-----------------------|-------------------------|------------------------|------------------------|------------------------|-----------------------|--------------|
| | | <i>A. Capelluto</i> | <i>S. Grillo</i> | <i>N. Valle</i> | XXXXXXXXXX | XXXXXXXXXX | XXXXXXXXXX | <i>R. Marabotto</i> | |
| 1 | | A. Capelluto | S. Grillo | N. Valle | | | | R. Marabotto | 12/09/2016 |
| Rev. Rev. | Stato (W/R) Status | Classe Riserv (1/2/3) Confid. | Preparato Prepared | Controllato Reviewed | Verificato Verified | Verificato Verified | Verificato Verified | Approvato Approved | Data Date |

| | | | | |
|--|--|------------------------------|------------------------------|---------------------------|
| Titolo Title Quench Calculation MDP Dubna | Documento no. Document no. 100RM19300 | Rev. Rev. 0 | Pag. Page 2 | Di Of 24 |
| | Altro Identificativo no. Other Identification no. | Rev. Rev. | | |

Summary

| | |
|--|----|
| 1. Introduction | 3 |
| 1.1 SC Equivalent Properties | 4 |
| 1.2 Minimum Quench Energy estimation | 4 |
| 1.3 Circuital and protection system | 6 |
| 2. Full 3D VS Quasi-2D | 7 |
| 3. Quench Configuration | 8 |
| 3.1 Case1: Yes Quench Back, Yes Iron Yoke, No Dump Resistor | 9 |
| 3.2 Case2: Yes Quench Back, Yes Iron Yoke, Yes Dump Resistor | 11 |
| 3.3 Case3: Yes Quench Back, Yes Iron Yoke, No Dump Resistor | 14 |
| 3.4 Case4: Yes Quench Back, Yes Iron Yoke, Yes Dump Resistor | 18 |
| 4. Conclusions | 21 |

| | | | | |
|------------------------------|--|--------------|--------------|----------|
| Titolo Title | Documento no. Document no. | Rev. Rev. | Pag. Page | Di Of |
| | 100RM19300 | 0 | 3 | 24 |
| Quench Calculation MDP Dubna | Altro Identificativo no. Other Identification no. | Rev. Rev. | | |
| | | | | |

1. Introduction

The study of the transition to the normal state has been implemented in different configurations as described in Table 1.

All the calculations have been implemented under the following assumptions:

- the AC losses have not been considered;
- no heat exchange with the helium circuit;
- the quench has been induced with a constant heat flow up to 10 K in a small region in the maximum field zone (end turns of the winding);
- the starting current has been set to 2385 A (132% operative current).

| Label | Aluminum Former | Insulation layer: SC-Former | Dump Resistor | Iron Yoke | I (kA) | Starting Point |
|--------------|-----------------|-----------------------------|---------------|-----------|--------|----------------|
| Quench_Case1 | YES | YES | NO | YES | 2.385 | End turns |
| Quench_Case2 | YES | YES | YES | YES | 2.385 | End turns |
| Quench_Case3 | YES | NO | NO | YES | 2.385 | End turns |
| Quench_Case4 | YES | NO | YES | YES | 2.385 | End turns |

Table 1: Quench study configurations.

The study of the transition to normal state has been implemented with a finite element (F.E.) model developed with QUENCH/ELEKTRA tool of Opera® Software. The F.E. model of the system includes the coil, simplified iron yoke and support cylinder and the TRIM coils, that have been modeled as filamentary circuital components to avoid calculation problems due to their proximity to the iron yoke.

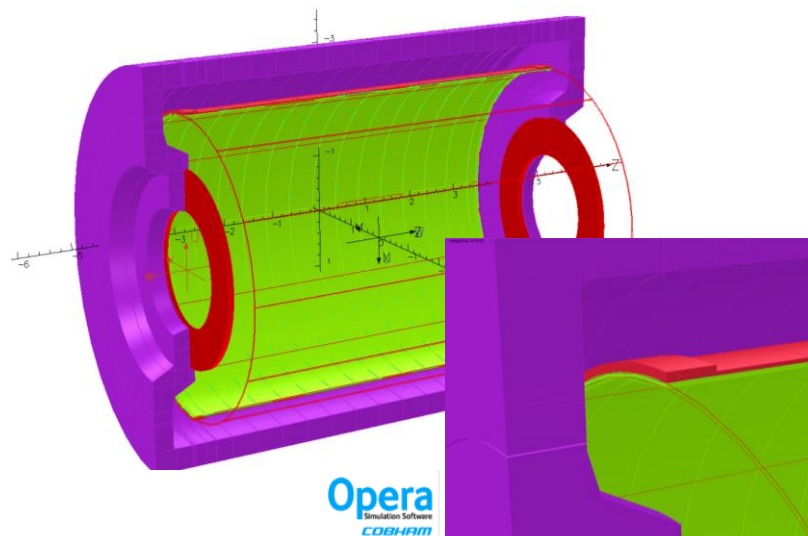


Figure 1: F.E. model of the system used to study the transition to normal state.

| | | | | |
|-------------------------------------|--|--------------|--------------|----------|
| Titolo Title | Documento no. Document no. | Rev. Rev. | Pag. Page | Di Of |
| | 100RM19300 | 0 | 4 | 24 |
| Quench Calculation MDP Dubna | Altro Identificativo no. Other Identification no. | Rev. Rev. | | |
| | | | | |

The coil is made by a superconductive wire (NbTi in a Cu matrix) stabilized with high pure Aluminum (RRR>1000). The Al/Cu/NbTi ratio is 100/0.9/1. The wire is insulated with fiberglass (G10). The iron yoke is made of Steel 1006. The support cylinder is made of Al 5083 and it is divided from the coil by 1 mm thick impregnated fiberglass insulation layer. The TRIM coils are made of copper wire.

1.1 SC Equivalent Properties

In order to perform the quench analysis the equivalent SC coil bulk properties have been calculated. The equivalent heat capacity and electrical conductivity have been considered as isotropic properties while the equivalent thermal conductivity has been considered anisotropic.

The SC wire critical currents have been calculated using Bottura's Formula.

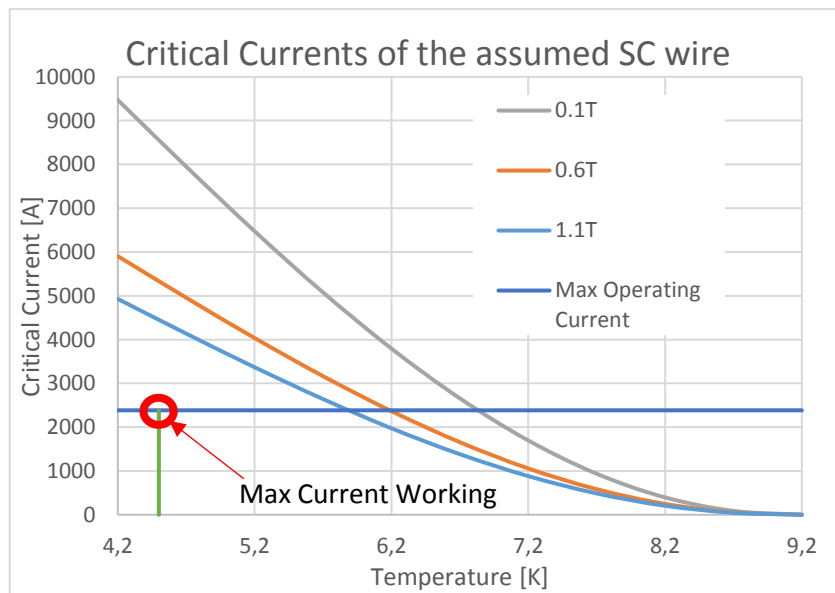


Figure 2: SC wire critical currents calculated with Bottura's Formula

The minimum temperature margin in the maximum field area is about 1.7K at 4.5K while the current margin in maximum current condition is up to 3000 A (>300% operative current).

1.2 Minimum Quench Energy estimation

The minimum quench energy (M.Q.E.) is the minimum energy needed to induce the quench in the wire. To estimate this value a specific F.E. model has been built. The modeled system includes a 4 turns straight SC wire: the wire is detailed with turns and turn-to-turn insulation (0.2 mm thick fiberglass). To take into account the quench back effect due to the support cylinder, the relative volume of aluminum (Al 5083) has been put above the wire (Figure 3).

| | | | | |
|------------------------------|--|--------------|--------------|----------|
| Titolo Title | Documento no. Document no. | Rev. Rev. | Pag. Page | Di Of |
| | 100RM19300 | 0 | 5 | 24 |
| Quench Calculation MDP Dubna | Altro Identificativo no. Other Identification no. | Rev. Rev. | | |
| | | | | |

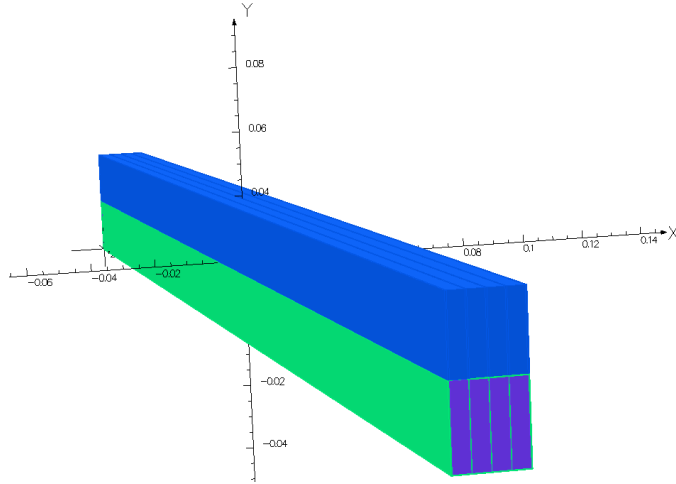


Figure 3: F.E. model used to estimate the M.Q.E. of the wire. In purple there is the wire, detailed in turns divided by the insulation (green) while in blue there is the aluminum volume.

In all the wire volume a generation power ($G=\rho j^2$, where “ ρ ” is the electrical resistivity of the wire and “ j ” is the current density) is produced.

Different heat flows have been inserted as an input over a small area (one turn cross-section) highlighted in red in Figure 4. The heat input duration is less than 0.1 s.

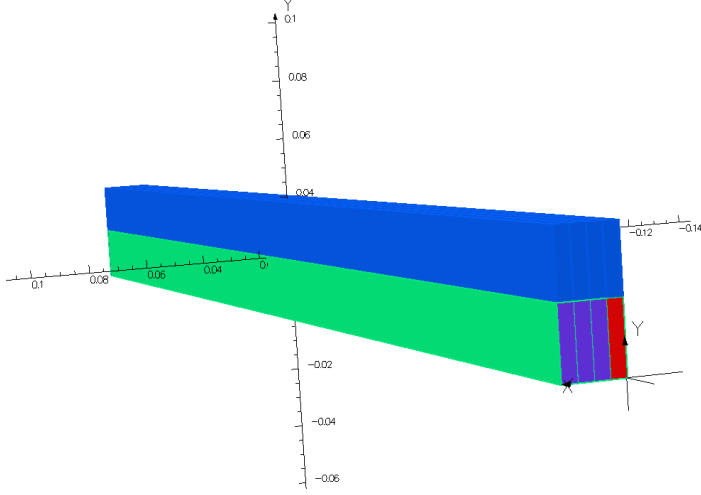


Figure 4: The red area is the surface over which the heat flow is pumped.

To estimate the M.Q.E., the SC wire temperature trend has been studied. If after the heat input is stopped the temperature increases the quench is induced. The estimated M.Q.E. is about 1700 mJ.

| | | | | |
|------------------------------|--|--------------|--------------|----------|
| Titolo Title | Documento no. Document no. | Rev. Rev. | Pag. Page | Di Of |
| | 100RM19300 | 0 | 6 | 24 |
| Quench Calculation MDP Dubna | Altro Identificativo no. Other Identification no. | Rev. Rev. | | |
| | | | | |

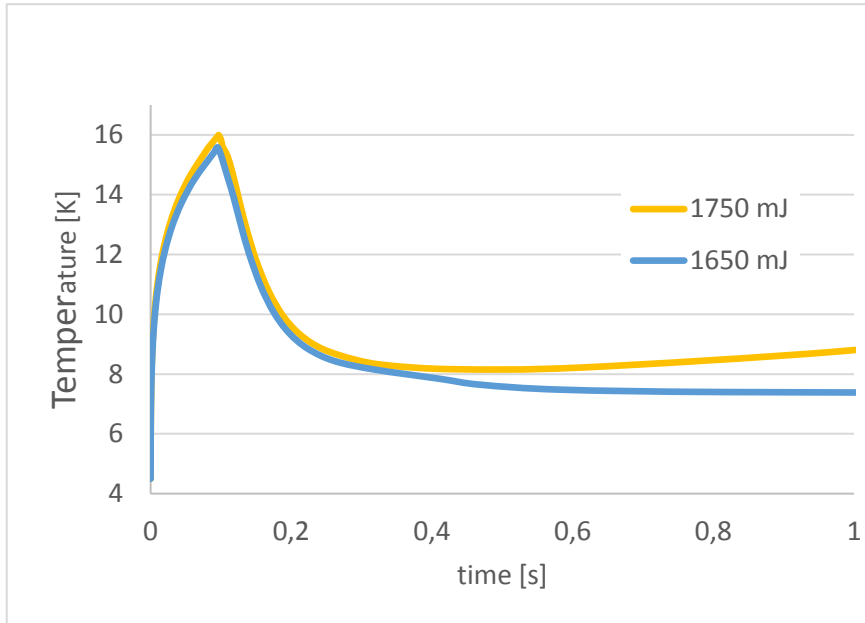


Figure 5: SC wire temperature trend for 2 different heat inputs.

1.3 Circuital and protection system

The circuital and protection system used in the quench calculations is described in Figure 6. The SC coil (MAIN) is powered by a Power Supply (PS), if the MAIN voltage reaches 1V a Quench Detection System commands the Switch to open. When the Switch is open the MAIN SC Coil discharges itself on the Dump (0.103 Ω) and Lead (1 mΩ) Resistances.

The quench calculations have been implemented with and without the Dump Resistor.

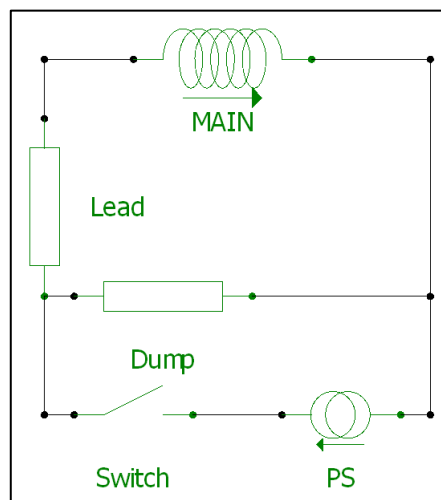


Figure 6: Protection circuit. The switch opens when the voltage reaches 1 V.

| | | | | |
|------------------------------|--|--------------|--------------|----------|
| Titolo Title | Documento no. Document no. | Rev. Rev. | Pag. Page | Di Of |
| | 100RM19300 | 0 | 7 | 24 |
| Quench Calculation MDP Dubna | Altro Identificativo no. Other Identification no. | Rev. Rev. | | |
| | | | | |

2. Full 3D VS Quasi-2D

Starting from the SC wire thermal conductivity study, it could be noticed that the azimuthal/longitudinal ratio of this property reaches values close to 1000, in particular at low temperatures.

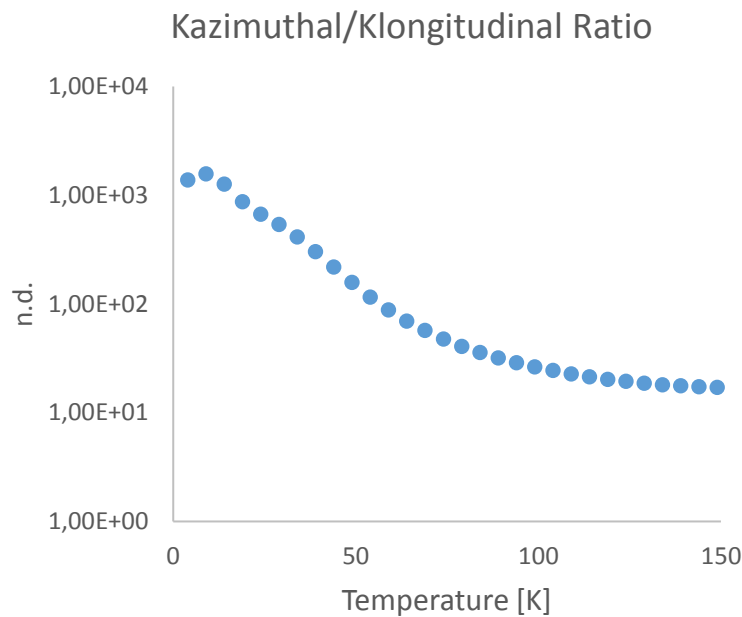


Figure 7: Azimuthal/Longitudinal ratio of the wire thermal conductivity.

This thermal trend could justify the assumption of the system as a quasi-2D system (axial-symmetrical). The thermal propagation is much faster along the turn than across adjacent turns. In the winding direction the thermal propagation could be assumed as instantaneous.

To verify this hypothesis, a comparison between a full 3D and a quasi-2D model has been done. The quasi-2D model consists in a 1 element thick slice of the system as described in Figure 8.

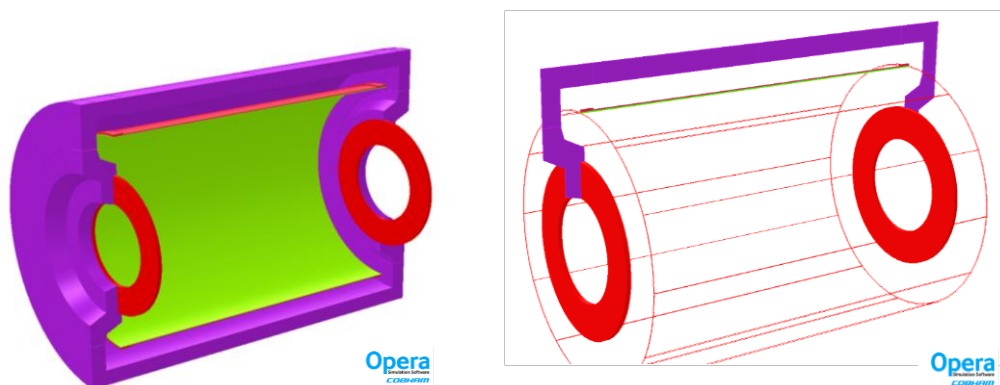


Figure 8: Full 3D model VS Quasi-2D model.

| | | | | |
|--|--|------------------------------|------------------------------|---------------------------|
| Titolo Title Quench Calculation MDP Dubna | Documento no. Document no. 100RM19300 | Rev. Rev. 0 | Pag. Page 8 | Di Of 24 |
| | Altro Identificativo no. Other Identification no. | Rev. Rev. | | |

The considered system for this comparison includes the whole system without the dump resistor. Comparing the temperature trend obtained with the two models it is evident that the two models are comparable. The temperature differences are negligible, there is only a temporal shift. All the quench calculations have been implemented with the quasi-2D model.

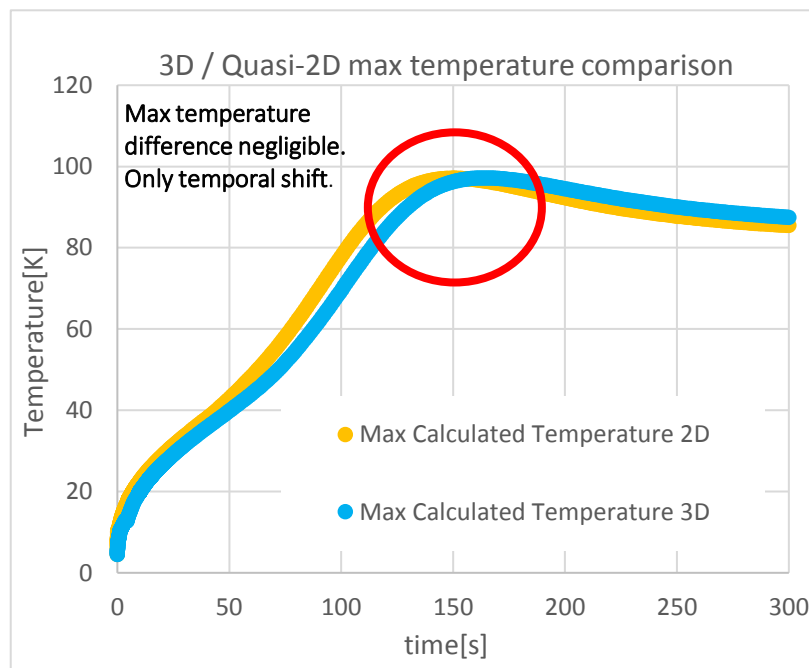


Figure 9: Temperature trend obtained with the full 3D (blue) and quasi-2D (orange) models.

3. Quench Configuration

In this section the results obtained by the quench study are shown.

In all the considered configurations the assumptions are:

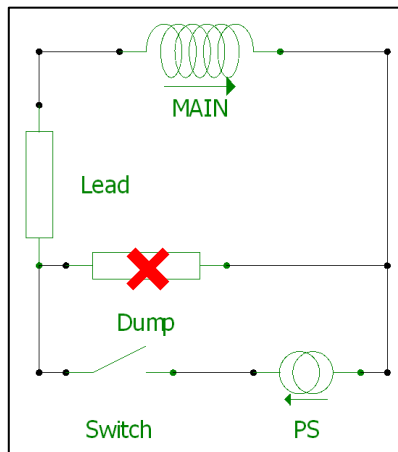
- the iron yoke has been taken into account only for the magnetic field and inductance calculations (no iron electrical conductivity);
- eddy currents in the support cylinder have been included (aluminum electrical conductivity);
- the non linear inductance has been automatically calculated by the software code.

| | | | | |
|------------------------------|--|--------------|--------------|----------|
| Titolo Title | Documento no. Document no. | Rev. Rev. | Pag. Page | Di Of |
| | 100RM19300 | 0 | 9 | 24 |
| Quench Calculation MDP Dubna | Altro Identificativo no. Other Identification no. | Rev. Rev. | | |
| | | | | |

3.1 Case1: Yes Quench Back, Yes Iron Yoke, No Dump Resistor

Impregnated fiberglass insulation layer between SC coil and Support Cylinder

The first considered configuration, without the Dump Resistor, is the worst from the temperature point of view. In this configuration the SC coil discharges itself only on the Lead Resistor (1 mΩ).



In this configuration the SC coil temperature remains below 100K.

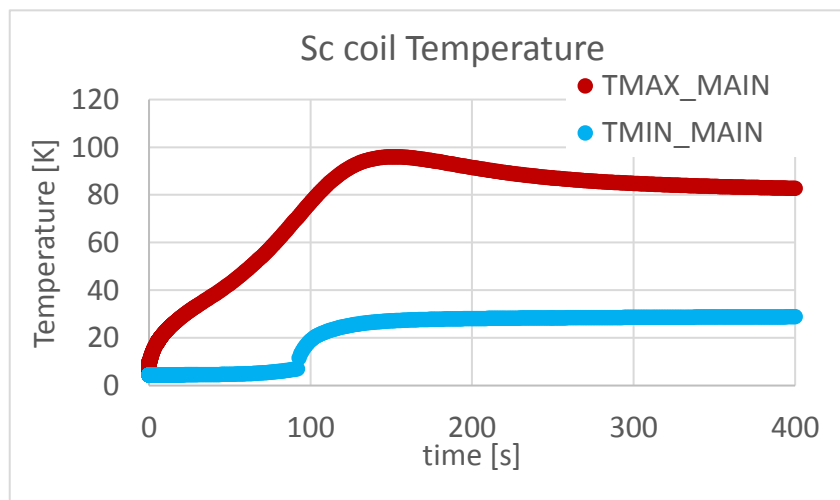


Figure 10: : Maximum and minimum temperature trends of the SC coil (without Dump Resistor).

| | | | | |
|------------------------------|--|--------------|--------------|----------|
| Titolo Title | Documento no. Document no. | Rev. Rev. | Pag. Page | Di Of |
| | 100RM19300 | 0 | 10 | 24 |
| Quench Calculation MDP Dubna | Altro Identificativo no. Other Identification no. | Rev. Rev. | | |
| | | | | |

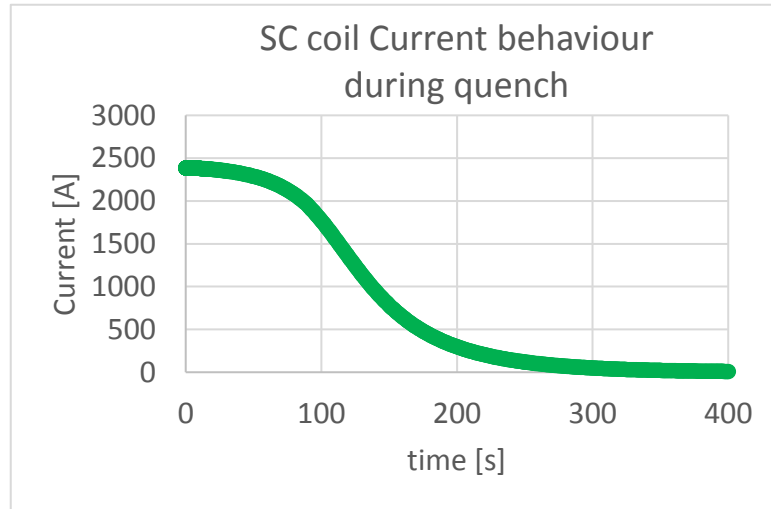


Figure 11: SC coil current behaviour during the quench.

Considering the turn resistance (σ = electrical conductivity, $l=2\pi R_{coil}$ and $S=Area_{turn}$)

$$R_{turn}(T) = \frac{1}{\sigma(T)} \frac{l}{S}$$

the inter-turn drop voltage can be calculated as:

$$\Delta V_{turn} = R_{turn}(T) I_{coil}(T)$$

In this configuration the maximum inter-turn voltage drop is 8 V.

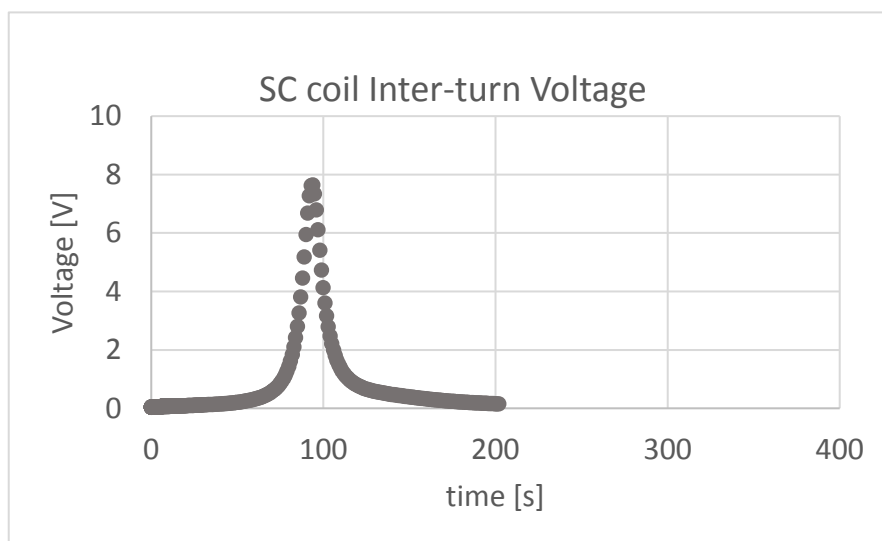


Figure 12: Inter-turn Voltage Drop.

| | | | | |
|--|--|-----------------------|------------------------|--------------------|
| Titolo Title Quench Calculation MDP Dubna | Documento no. Document no. 100RM19300 | Rev. Rev. 0 | Pag. Page 11 | Di Of 24 |
| | Altro Identificativo no. Other Identification no. | Rev. Rev. | | |

The inductive voltage drop across each TRIM coil is less than 2 V.

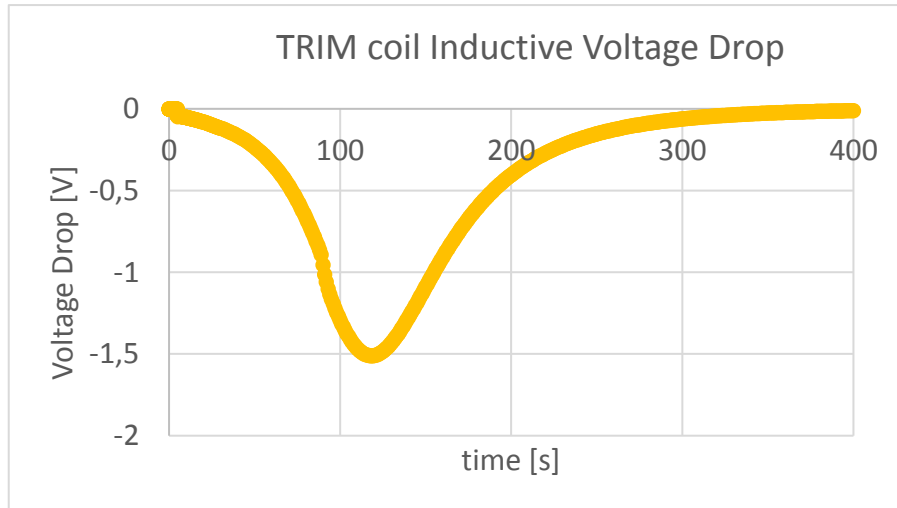
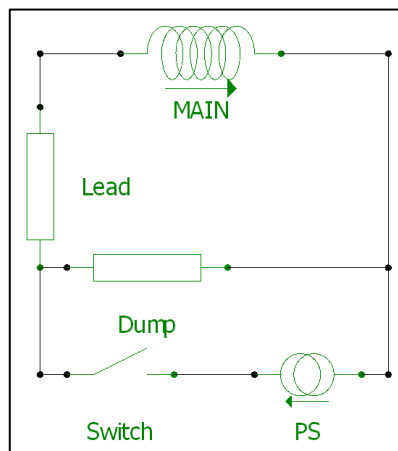


Figure 13: TRIM coil Inductive Voltage Drop.

3.2 Case2: Yes Quench Back, Yes Iron Yoke, Yes Dump Resistor

Impregnated fiberglass insulation layer between SC coil and Support Cylinder

The second considered configuration, with also the Dump Resistor, is the worst from the voltage point of view. In this configuration the SC coil discharges itself on the Dump (0.103 Ω) and Lead (1 mΩ) Resistors.



| | | | | |
|--|--|------------------------------|-------------------------------|---------------------------|
| Titolo Title Quench Calculation MDP Dubna | Documento no. Document no. 100RM19300 | Rev. Rev. 0 | Pag. Page 12 | Di Of 24 |
| | Altro Identificativo no. Other Identification no. | Rev. Rev. | | |

In this configuration the SC coil temperature remains below 35 K and the voltage drop across it is 245 V.

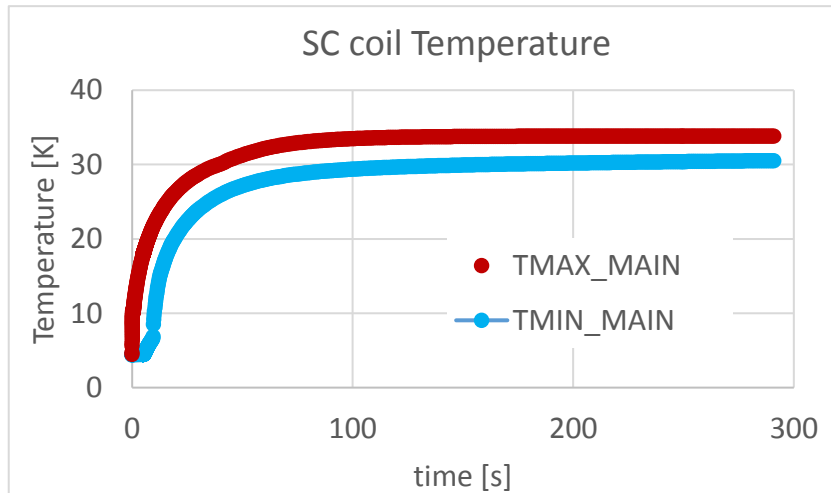


Figure 14: Maximum and minimum temperature trends of the SC wire in the protected configuration.

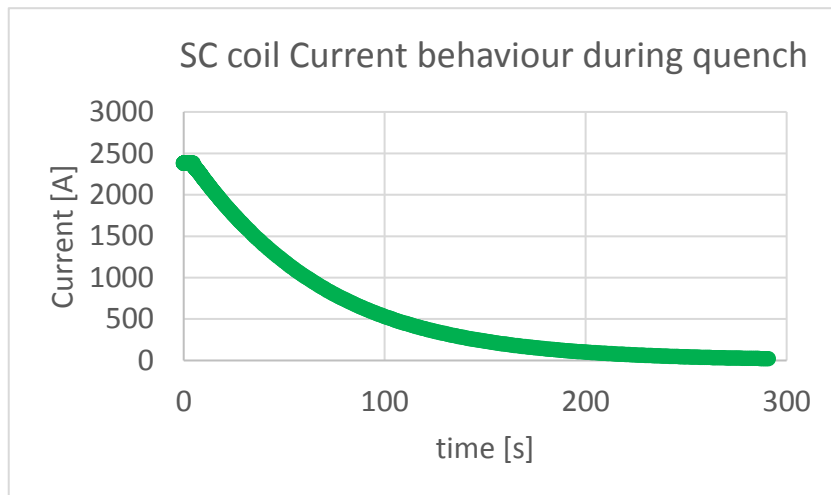


Figure 15: SC coil current behaviour during quench.

Titolo
Title

Quench Calculation MDP Dubna

Documento no.
Document no.

100RM19300

Rev.
Rev.

0

Pag.
Page

13

Di
Of

24

Altro Identificativo no.
Other Identification no.

Rev.
Rev.

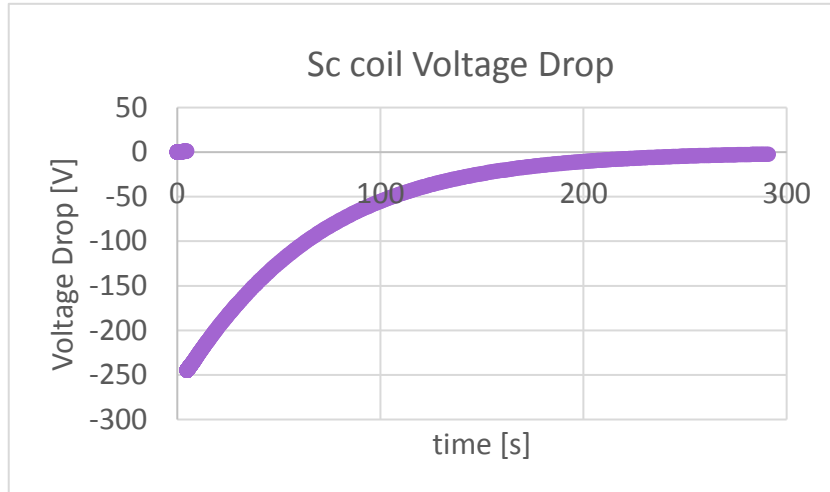


Figure 16: Voltage Drop across the SC coil.

In this configuration the maximum inter-turn voltage drop is below 0.1 V.

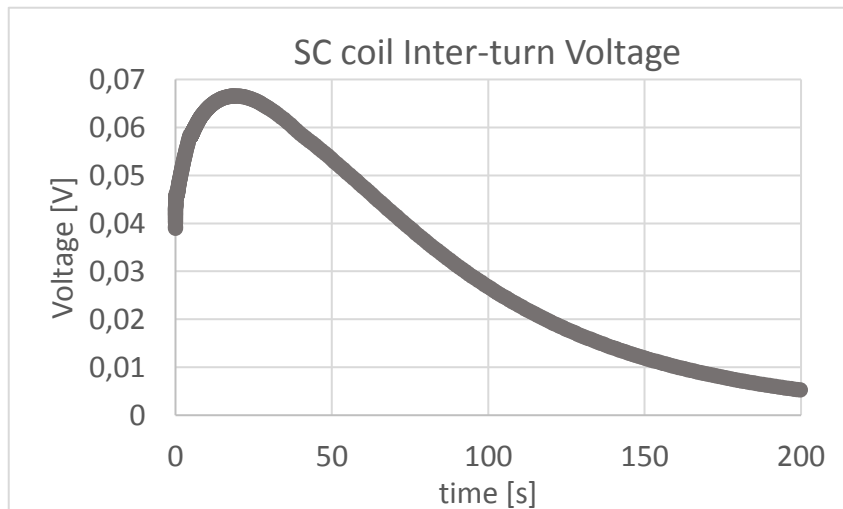


Figure 17: Inter-turn Voltage Drop.

| | | | | |
|--|--|------------------------------|-------------------------------|---------------------------|
| Titolo Title Quench Calculation MDP Dubna | Documento no. Document no. 100RM19300 | Rev. Rev. 0 | Pag. Page 14 | Di Of 24 |
| | Altro Identificativo no. Other Identification no. | Rev. Rev. | | |

The inductive voltage drop across each TRIM coil is less than 2 V.

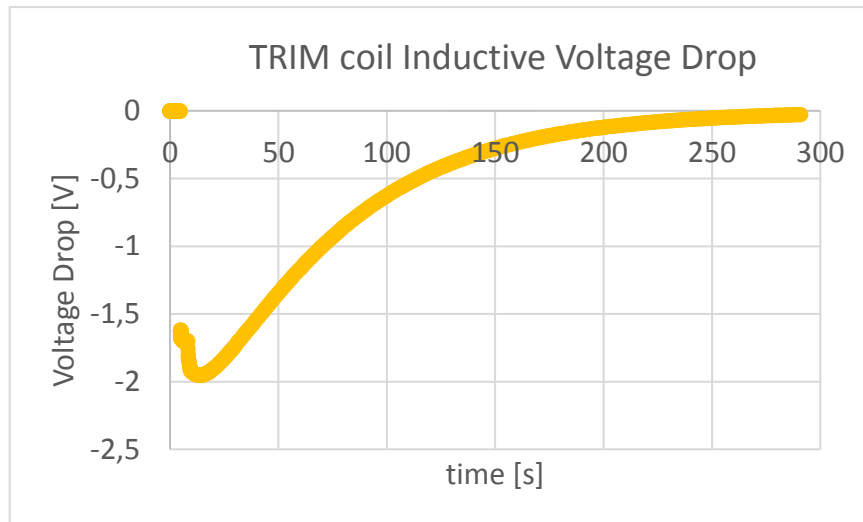


Figure 18: TRIM coil inductive voltage drop.

3.3 Case3: Yes Quench Back, Yes Iron Yoke, No Dump Resistor

Without impregnated fiberglass insulation layer between SC coil and Support Cylinder

This configuration is similar to Case 1 (No Dump Resistor) but without the impregnated fiberglass insulation layer between the SC coil and the support cylinder. The coil and the Al cylinder remains coupled from an electromagnetic point of view (eddy currents are induced in the aluminum former) but they have not more thermal coupling.

| | | | | |
|--|--|------------------------------|-------------------------------|---------------------------|
| Titolo Title Quench Calculation MDP Dubna | Documento no. Document no. 100RM19300 | Rev. Rev. 0 | Pag. Page 15 | Di Of 24 |
| | Altro Identificativo no. Other Identification no. | Rev. Rev. | | |

In this configuration the SC coil temperature reaches 152 K.

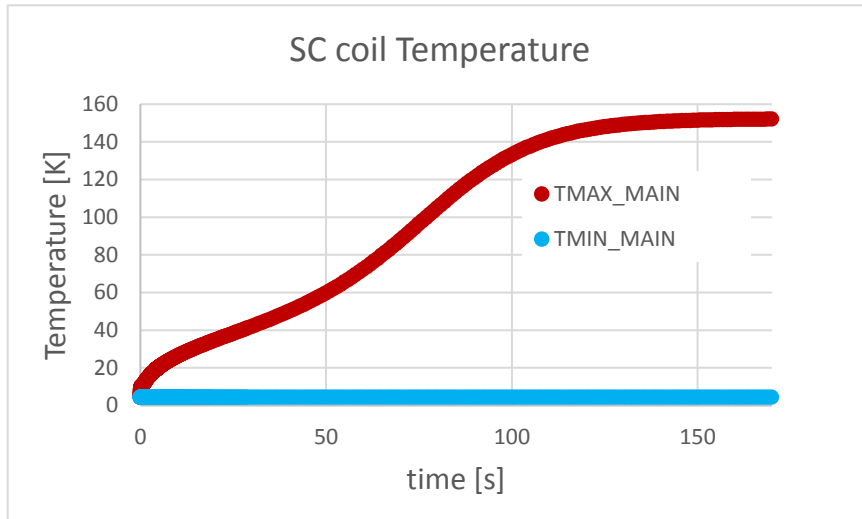


Figure 19: SC coil maximum and minimum temperatures.

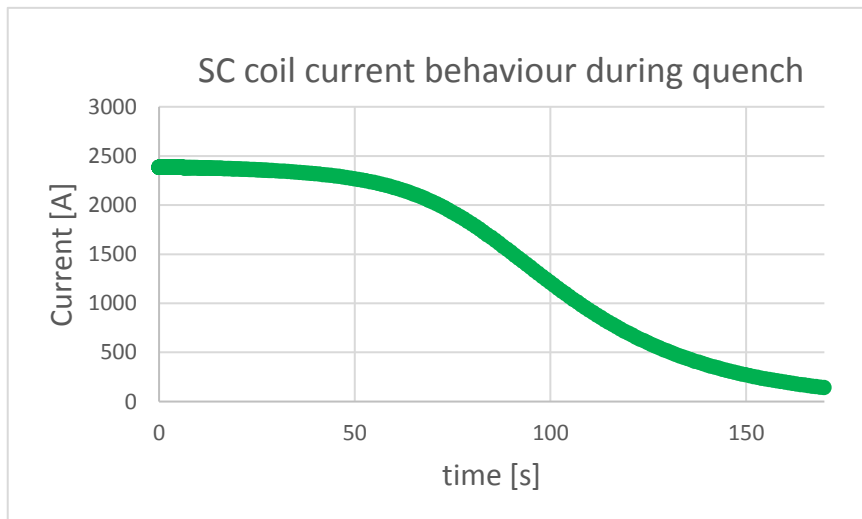


Figure 20: SC coil current behaviour during quench.

| | | | | |
|--|--|------------------------------|-------------------------------|---------------------------|
| Titolo Title Quench Calculation MDP Dubna | Documento no. Document no. 100RM19300 | Rev. Rev. 0 | Pag. Page 16 | Di Of 24 |
| | Altro Identificativo no. Other Identification no. | Rev. Rev. | | |

In this configuration the maximum inter-turn voltage drop is below 9 V.

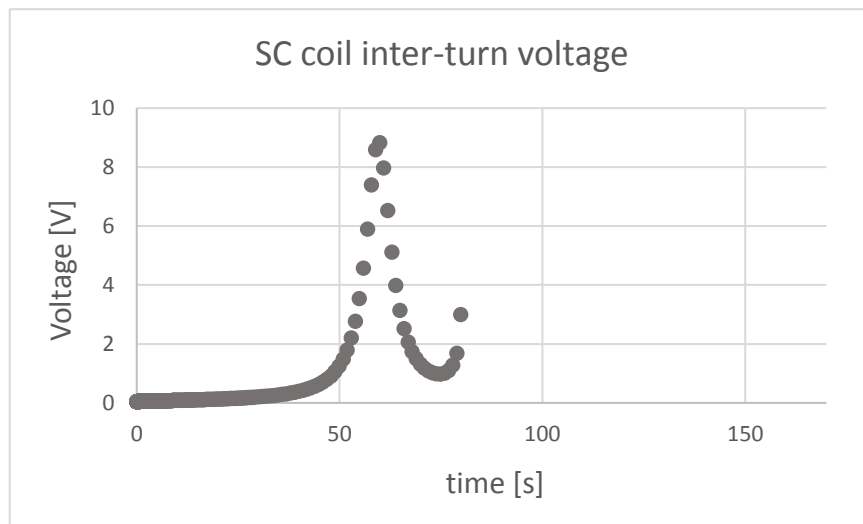


Figure 21: SC coil inter-turn voltage drop.

The inductive voltage drop across each TRIM coil is below 2.5 V.

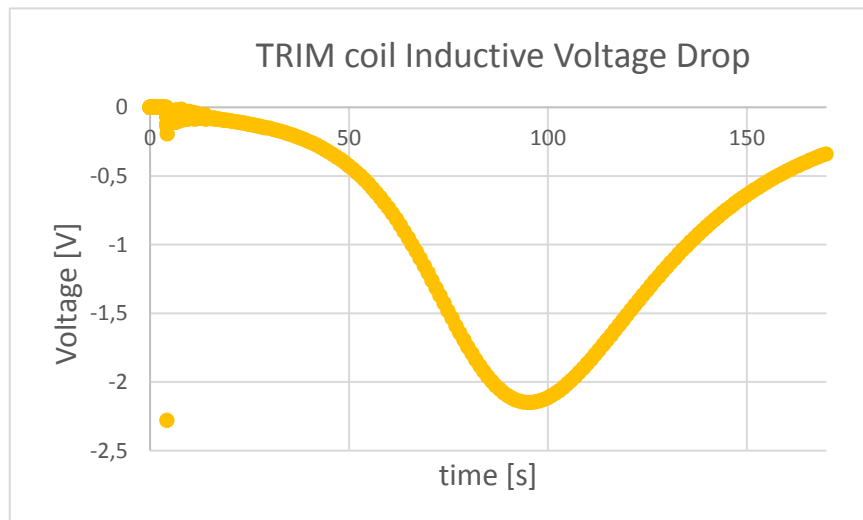


Figure 22: TRIM coil inductive voltage drop.

Comparing this configuration with Case 1 it is evident that the insulation layer allows the thermal propagation between the coil and the support cylinder. Without the insulation layer the coil reaches temperature values above 150 K while the whole support cylinder reaches 20 K. With the insulation layer the SC coil remains below 100 K while the aluminium former is not uniformly warmed. It warms up to 82 K with a temperature difference of about 50 K.

| | | | | |
|--|--|------------------------------|-------------------------------|---------------------------|
| Titolo Title Quench Calculation MDP Dubna | Documento no. Document no. 100RM19300 | Rev. Rev. 0 | Pag. Page 17 | Di Of 24 |
| | Altro Identificativo no. Other Identification no. | Rev. Rev. | | |

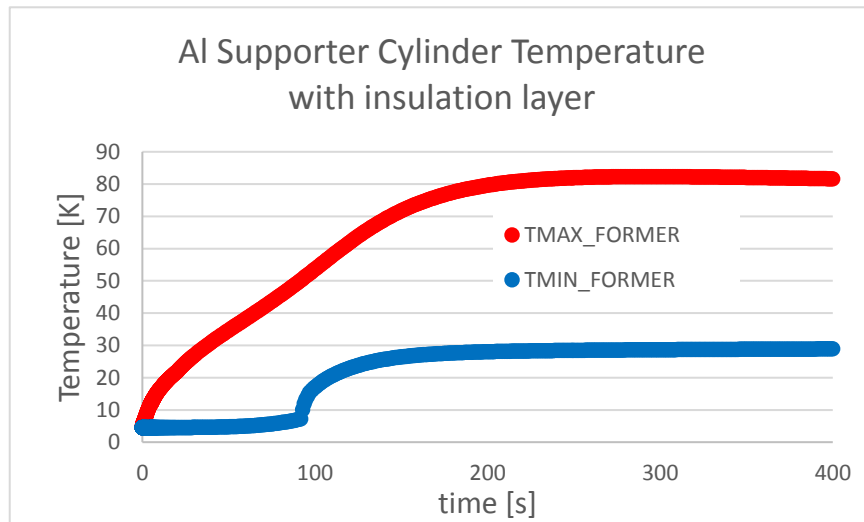


Figure 23: Aluminum support cylinder maximum and minimum temperatures in the configuration with the insulation layer.

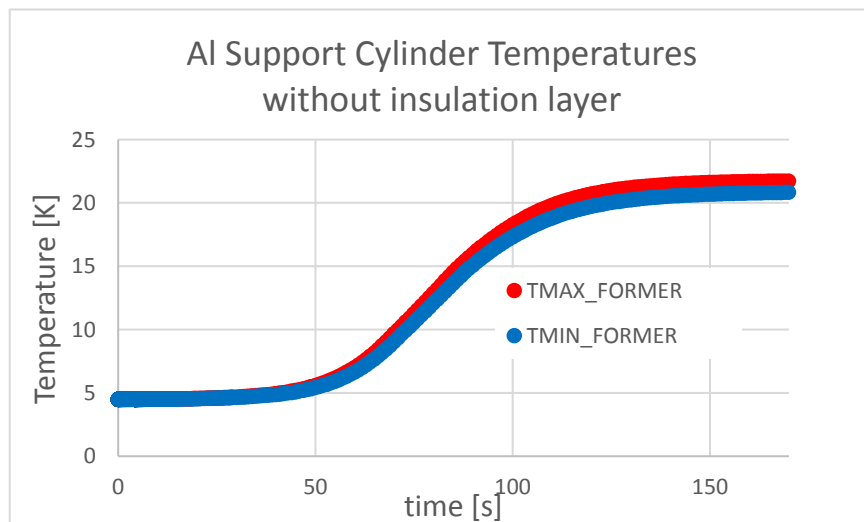


Figure 24: Aluminum support cylinder maximum and minimum temperatures in the configuration without the insulation layer.

| | | | | |
|------------------------------|--|--------------|--------------|----------|
| Titolo Title | Documento no. Document no. | Rev. Rev. | Pag. Page | Di Of |
| | 100RM19300 | 0 | 18 | 24 |
| Quench Calculation MDP Dubna | Altro Identificativo no. Other Identification no. | Rev. Rev. | | |
| | | | | |

3.4 Case4: Yes Quench Back, Yes Iron Yoke, Yes Dump Resistor

Without impregnated fiberglass insulation layer between SC coil and Support Cylinder

This configuration is similar to Case 2 (with Dump Resistor) but without the impregnated fiberglass insulation layer between the SC coil and the support cylinder. The coil and the Al cylinder remains coupled from an electromagnetic point of view (eddy currents are induced in the aluminum former) but they have not more thermal coupling.

In this configuration only the protection system (Dump Resistor) mitigates the degradation of the SC coil. In this configuration the SC coil temperature reaches 54 K.

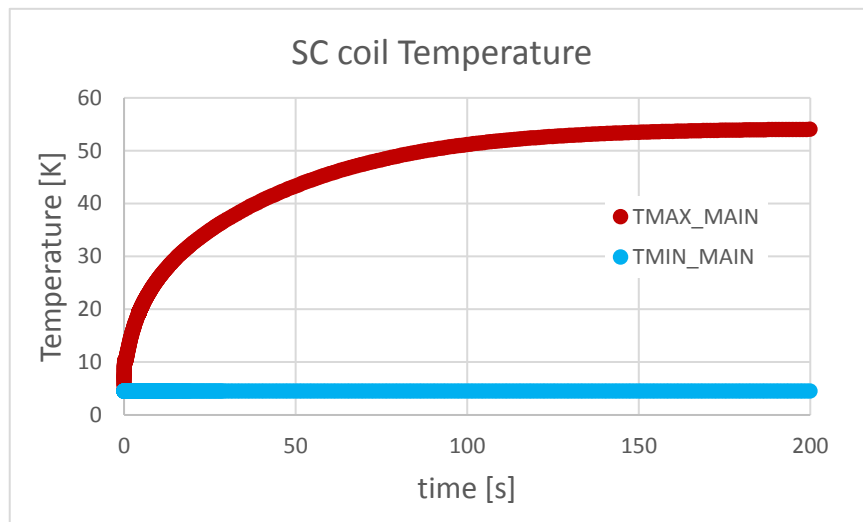


Figure 25: SC coil maximum and minimum temperatures.

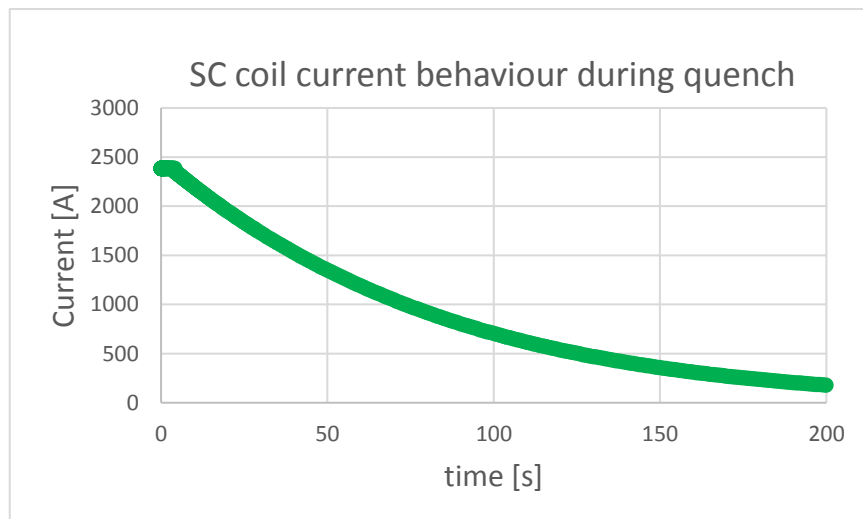


Figure 26: SC coil current behaviour during the quench.

| | | | | |
|--|--|------------------------------|-------------------------------|---------------------------|
| Titolo Title Quench Calculation MDP Dubna | Documento no. Document no. 100RM19300 | Rev. Rev. 0 | Pag. Page 19 | Di Of 24 |
| | Altro Identificativo no. Other Identification no. | Rev. Rev. | | |

The voltage drop across the SC coil is 245 V.

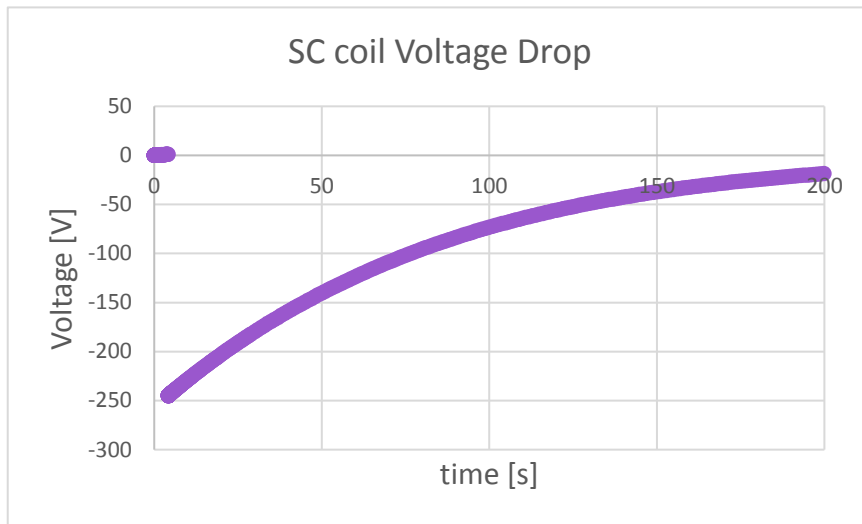


Figure 27: Voltage Drop across the main SC coil.

In this configuration the maximum inter-turn voltage drop is below 0.2 V.

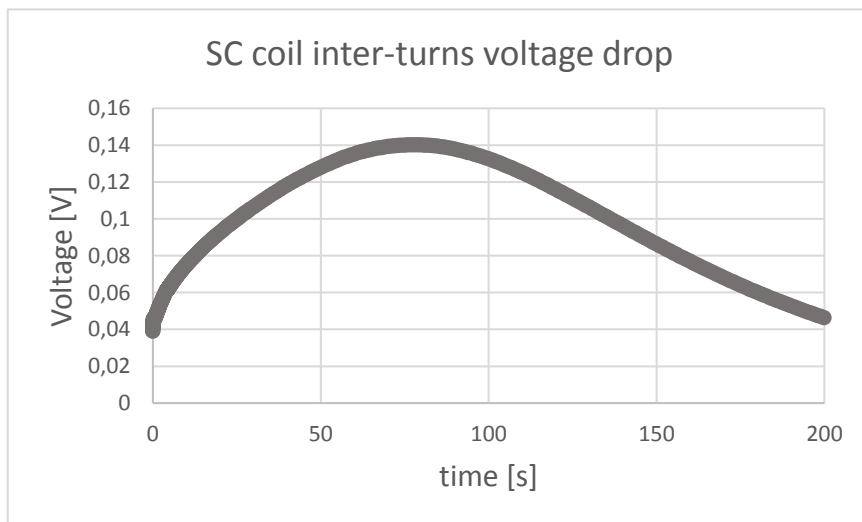


Figure 28: Inter-turn voltage drop.

| | | | | |
|--|--|------------------------------|-------------------------------|---------------------------|
| Titolo Title Quench Calculation MDP Dubna | Documento no. Document no. 100RM19300 | Rev. Rev. 0 | Pag. Page 20 | Di Of 24 |
| | Altro Identificativo no. Other Identification no. | Rev. Rev. | | |

The inductive voltage drop across each TRIM coil is below 4 V.

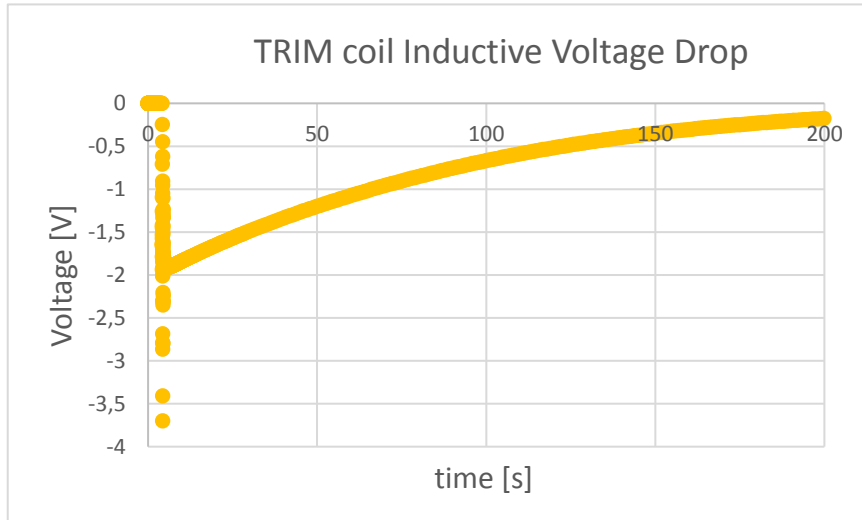


Figure 29: Voltage drop induced across each TRIM coil.

The comparison between this configuration and Case2, beyond highlighting the importance of the insulation layer in the thermal propagation, shows also the predominant effect of the Dump Resistor with respect to the quench back. The presence of the Dump Resistor guarantees that the SC coil temperature remains below 60 K.

Without the insulation layer the aluminum support cylinder is warmed uniformly up to 20 K while with the insulation fiberglass it has a temperature difference of about 4K.

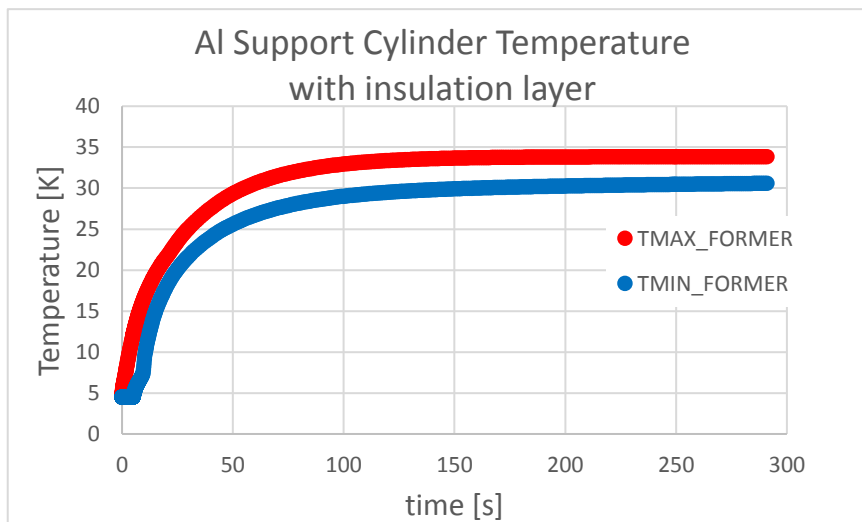


Figure 30: Al support cylinder maximum and minimum temperature in the configuration with the insulation layer.

| | | | | |
|------------------------------|--|--------------|--------------|----------|
| Titolo Title | Documento no. Document no. | Rev. Rev. | Pag. Page | Di Of |
| | 100RM19300 | 0 | 21 | 24 |
| Quench Calculation MDP Dubna | Altro Identificativo no. Other Identification no. | Rev. Rev. | | |
| | | | | |

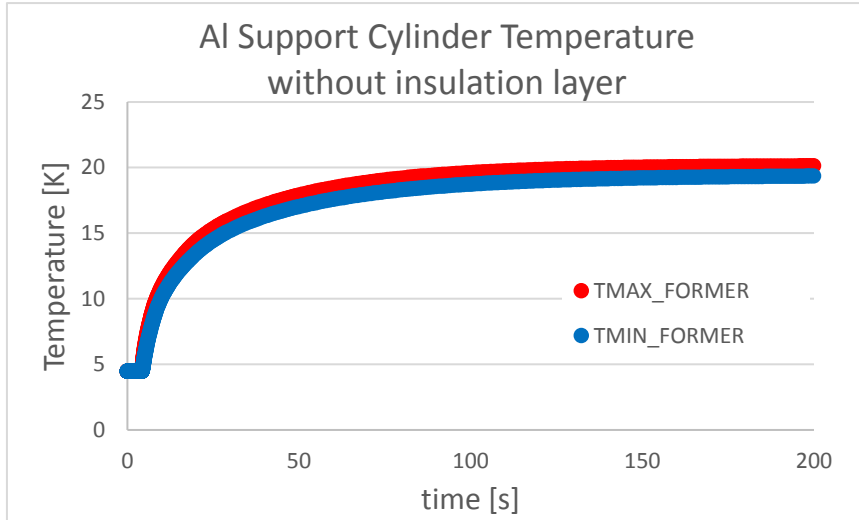


Figure 31: Al support cylinder temperature in the configuration without the insulation layer.

4. Conclusions

All the quench calculations have been implemented with quasi-2D models based on one element thick slice of the system. It has been demonstrated that the quasi-2D model is comparable with the full 3D model: the same quench simulation has been implemented with both the models giving as result a negligible temperature difference.

The minimum quench energy (M.Q.E.) has been calculated with a specific F.E. model in which a detailed wire, with turns and turn-to-turn insulation, is taken into account. The M.Q.E. found is about 1700 mJ.

All the calculations have been implemented under the following assumptions:

- the AC losses have not been considered;
- no heat exchange with the helium bath;
- the quench has been induced with a constant heat flow up to 10 K in a small region in the maximum field zone (end turns of the winding);
- starting current 2385 A.

The transition to normal state has been studied in 4 different configurations (Table 1).

| | | | | |
|-------------------------------------|--|--------------|--------------|----------|
| Titolo Title | Documento no. Document no. | Rev. Rev. | Pag. Page | Di Of |
| | 100RM19300 | 0 | 22 | 24 |
| Quench Calculation MDP Dubna | Altro Identificativo no. Other Identification no. | Rev. Rev. | | |
| | | | | |

The results of this study are reported in Table 2.

| Case | Tmax SC coil [K] | SC coil ΔV [V] | Discharge time [s] | Inter-turn ΔV [V] |
|-------|---------------------|---------------------------|-----------------------|------------------------------|
| Case1 | 97 | | 400 | <8 |
| Case2 | 35 | 245 | 300 | <0.1 |
| Case3 | 152 | | 200 | <9 |
| Case4 | 54 | 245 | 200 | <0.2 |

Table 2: Results obtained for the quench calculations in the different configurations.

In all the considered configurations the aluminium support cylinder is present while the impregnated fiberglass layer between it and the SC coils is not always taken into account. Eddy currents are always induced in the support cylinder while the thermal contact is not always present. For simplicity the configuration with the fiberglass layer will be indicated as “with quench back” while the configuration without the insulation layer will be referred as “without quench back”.

- The only warring situation is the Case3, in which neither the Dump Resistor nor the quench back effect are present. This is a vary unrealistic situation.
- Comparing Case1 (No Dump Resistor – Yes Quench Back) and Case4 (Yes Dump Resistor – No Quench Back), it is evident that the more relevant role in the coil protection is the presence of the Dump Resistor: the system with the Dump Resistor and without the quench back reaches only 54K. Anyway the only quench back effect (Case1) is enough to have a safe situation, reaching a temperature near to the 100K limit.
- The presence of the impregnated fiberglass insulation layer between the SC coil and the support cylinder is fundamental to guarantee the thermal propagation without which the SC coil is warmed up.
- Considering both the Dump Resistor and the quench back effect the system does not reach 40K.
- The Voltage Drop across the SC coil reaches 245V in the configuration with the Dump Resistor while it is very low in the others because the SC coil discharges itself only on the Lead Resistor.
- The inter-turn voltage drop is very low with the Dump Resistor and it reaches 9V without it.
- Considering the induced voltage drop on each TRIM coil, it is always below 2V except to Case4 (Dump Resistor and not quench back) in which it reaches 4V.

5. Updated Wire Parameters

After a lot of iterations with the wire supplier some wire parameters have been changed respect to the starting hypothesis.

The overall wire section dimension have not been modified, but changed the Stabilized/Superconductor ratio: the NbTi area is 1.24 mm², and the Cu/Sc ratio is 0.9; the Al/Sc ratio is about 64.

The Aluminium RRR didn't changed (is about 1000).

| | | | | |
|-------------------------------------|--|--------------|--------------|----------|
| Titolo Title | Documento no. Document no. | Rev. Rev. | Pag. Page | Di Of |
| | 100RM19300 | 0 | 23 | 24 |
| Quench Calculation MDP Dubna | Altro Identificativo no. Other Identification no. | Rev. Rev. | | |
| | | | | |

Following the result of the chapter 2 only the quasi-2D model has been run, in order to speed up the simulation without worries about the output.
 Only the case 1 (YES Quenchcack, YES Yoke, NO Dump Resistor) has been run, because is the most critical concerning the coil temperatures.
 The protection circuit didn't changed (fig.32)

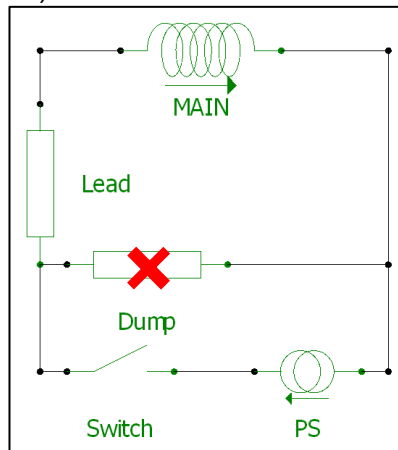


Figure 32: protection circuit scheme

The temperature result is show in fig. 33

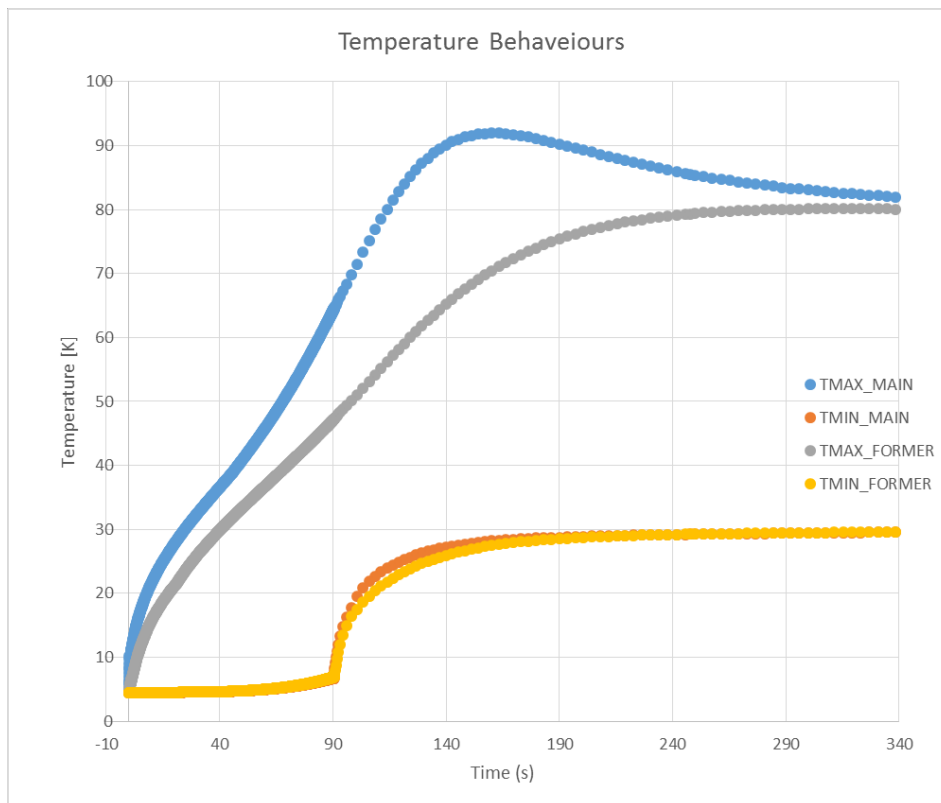


Figure 33: temperature result of quench simulation

The maximum temperature is less of 100K, confirming the good stability of the system.
 The current profile is almost identical to previous simulation (fig 34)

| | | | | |
|--|--|------------------------------|-------------------------------|---------------------------|
| Titolo Title Quench Calculation MDP Dubna | Documento no. Document no. 100RM19300 | Rev. Rev. 0 | Pag. Page 24 | Di Of 24 |
| | Altro Identificativo no. Other Identification no. | Rev. Rev. | | |

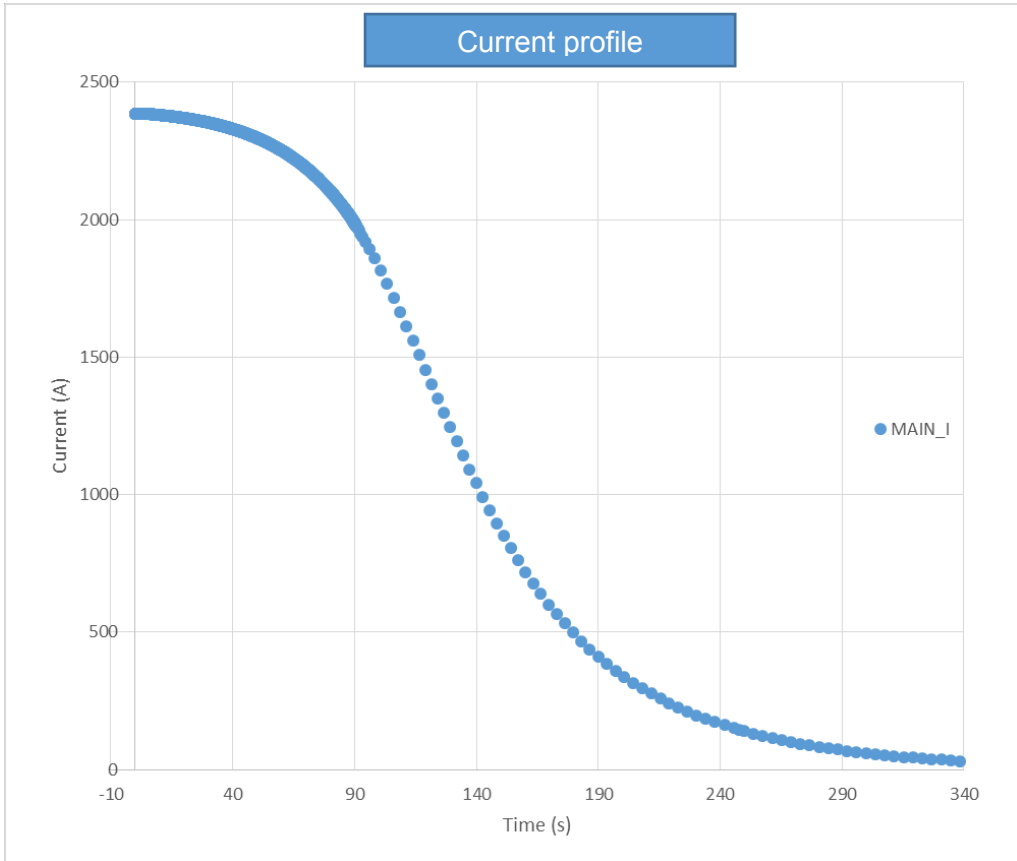


Figure 34: current behaviour in case of quench

APPENDIX 12. HELIUM REFRIGERATOR DESCRIPTION



Technical report

ILK-B-1-16-319a **confidential**

Rev2

31.01.2017

pages 53

First development report – Part A

Helium Refrigerator for MPD cooling

Customer: Joint Institute for Nuclear Research, Dubna, Russia


Editor of technical report: Dr.-Ing. N. Gust, Dr. rer. nat. A. Kade
Dr. rer. nat. M. Schneider, Dipl.-Ing. M. Kuhn
Dipl.-Ing. D. Schmidt

| Revision | Date | Content | Name |
|----------|------------|---------------------------------|----------|
| 0 | 31.03.2016 | | |
| 1 | 26.10.2016 | WEKA valves, vacuum vessel | Kade, A. |
| 2 | 30.01.2017 | schematic drawing vacuum vessel | Kade, A. |



Table of Contents

| | |
|--|-----------|
| 1 Introduction – General notes | 3 |
| 1.1 Overview | 3 |
| 1.2 Definition of the different operating modes | 4 |
| 2 Scope of Supply | 7 |
| 3 Dimensioning of the heat exchangers and the main components | 7 |
| 3.1 Dimensioning of the pipes | 10 |
| 3.2 Parameters of the plate heat exchanger (PHE) | 10 |
| 3.3 Dimensioning of the liquid bath heat exchanger | 16 |
| 4 Dimensioning of the Valves | 19 |
| 4.1 Calculation of the K_v -value | 19 |
| 4.2 JT Valve (V3) | 20 |
| 4.3 Control valves V1, V7, V10, V12, V13 and V14 | 20 |
| 4.4 Table of valves | 21 |
| 5 Vessels and overpressure protection | 22 |
| 5.1 Vacuum vessel | 23 |
| 5.2 LHe Vessel | 24 |
| 5.3 LN ₂ Vessel | 30 |
| 5.4 Overpressure protection — summary | 34 |
| 6 Design | 35 |
| 6.1 Drawings of the refrigerator system for the MPD | 35 |
| 6.2 Female siphons | 39 |
| 6.3 Control and safety valves | 39 |
| 6.4 Thermal shield | 39 |
| 6.5 List of Suppliers | 40 |
| 7 Measurement and control technology | 42 |
| 7.1 Operation modes | 43 |
| 7.2 Control scheme | 45 |
| 7.3 Hardware | 52 |
| 7.4 Sensors | 53 |

| | | | |
|-------------------------------------|------|-------------------|---|
| Rev. 2 | Page | Document no. |  |
| 31.01.2017 | 3 | ILK-B-1-16-319a_v | ILK Dresden |
| Title | | | |
| Helium Refrigerator for MPD cooling | | | |

1 Introduction – General notes

1.1 Overview

The Joint Institute for Nuclear Research (JINR) in Dubna, Russia, is an international intergovernmental scientific research organisation. The main fields of JINR's activity are theoretical and experimental studies in elementary particle physics, nuclear physics, and condensed matter physics. A new project of a Nuclotron-based Ion Collider fAcility (NICA) is proposed at JINR. For this project, a new helium satellite refrigerator for a Multi-Purpose-Detector (MPD) is required.

The scope of this work is the development and manufacturing of an enhanced new helium “satellite” refrigerator (SRU) for cooling of the MPD. This development comprises calculations, dimensioning and design of this special refrigerator system for dipole cooling with a cooling power of 100 W at 4.5 K. Initial point of the development is the compressor pressure for the helium flow of up to 15 bar(abs). The acceptable system pressure is set to 20 bar(abs).

1.2 Definition of the different operating modes

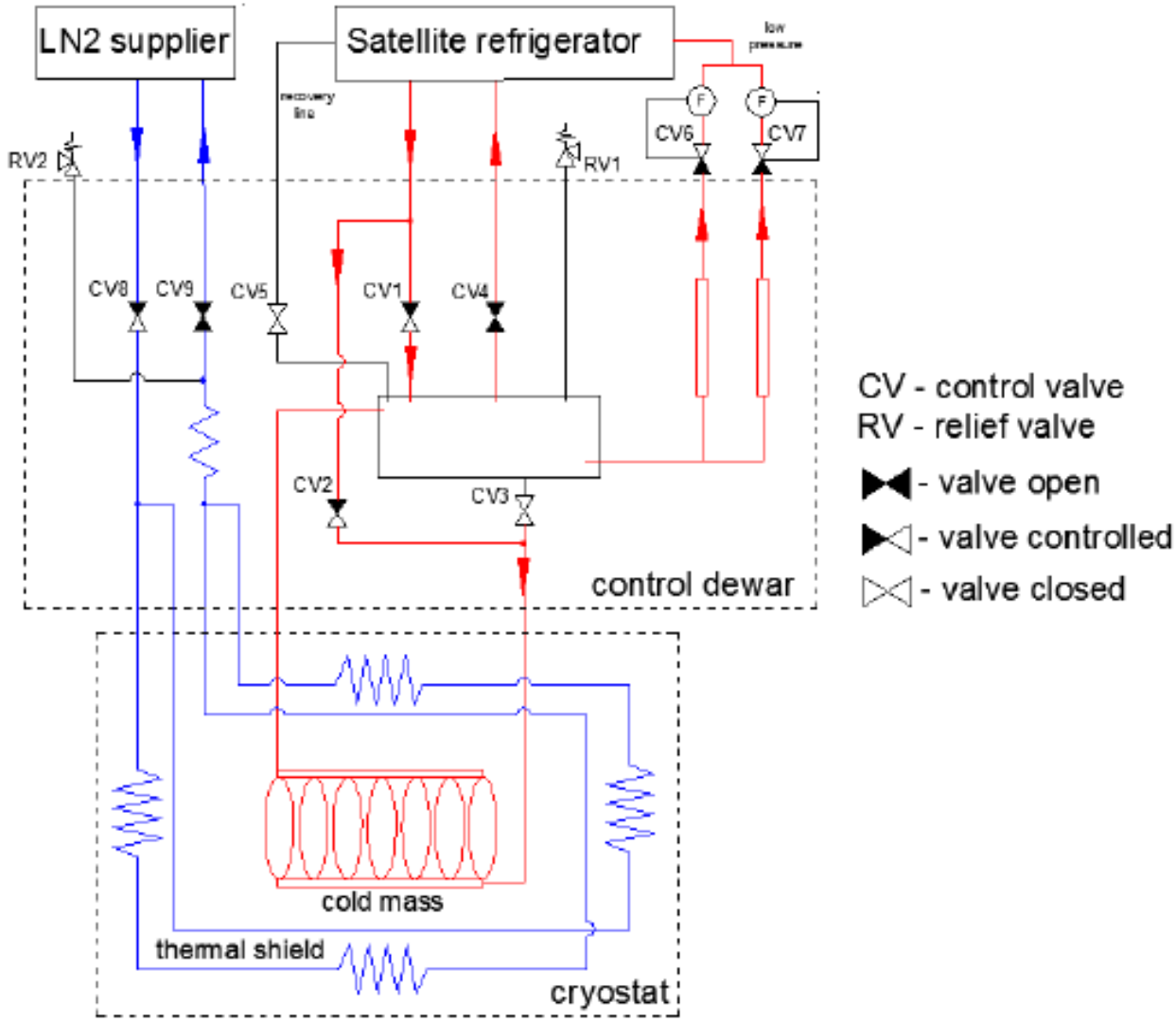



Figure 1: Schematic drawing of the cooling circuit of the refrigerator system for the MPD [JINR]

| | | | |
|-------------------------------------|------|-------------------|---|
| Rev. 2 | Page | Document no. |  |
| 31.01.2017 | 5 | ILK-B-1-16-319a_v | ILK Dresden |
| Title | | | |
| Helium Refrigerator for MPD cooling | | | |

For the dimensioning of the components (heat exchanger, valves and pipes), mainly two operating modes were defined (see Figure 1 and Table 1):

- cool-down and warm-up operation mode: high-pressure helium gas (13 bar(a)); flow rate delivered to the experiment with variable decompression (16.2 g/s)
- normal operation mode (5 g/s): 13 bar(a) high pressure helium gas max. 5 g/s, decompressed to below 2 bar(a), liquefied and delivered to the MPD
Requirement: power 100 W @ 4.5 K

For these operating modes the valve settings in, depending on temperature regime and cooling load, are possible.



| | | | |
|-------------------------------------|------|-------------------|---|
| Rev. 2 | Page | Document no. |  |
| 31.01.2017 | 6 | ILK-B-1-16-319a_v | |
| Title | | | |
| Helium Refrigerator for MPD cooling | | | |

Table 1: Parameters of the helium flows for various operation regimes [JINR]

| Object | Stream | Parameters | Regime | | |
|----------------|---------------|---------------|------------------------------------|-----------------------|-------------------------------------|
| | | | steady-state (normal operation) | cool-down /warm-up | slow dump (refrigerator failure) |
| Cold mass | incoming flow | gas/liquid | LHe (saturated liquid) | GHe | - |
| | | flow | 4.34 g/s (129 l/h) | 16.2 g/s (1 K/h) | - |
| | | temperature | 4.5 K | 300 – 4.5 K | - |
| | | pressure | 1.3 bar | ≤ 10 bar | - |
| | | vapor quality | < 5 % | - | - |
| | return flow | gas/liquid | GHe (saturated vapor) | GHe | - |
| | | flow | 3.96 g/s (117.6 l/h) | 16.2 g/s (1 K/h) | - |
| | | temperature | 4.45 K | 300 – 4.5 K | - |
| | | pressure | 1.25 bar | ≈ 1.5 bar | - |
| | | Current leads | - | gas/liquid | GHe |
| | | flow | 0.38 g/s (11.3 l/h) | - | 0.38 g/s (11.3 l/h) |
| | | temperature | ≈ 300 K | - | ≈ 300 K |
| | | pressure | 1.25 bar | - | 1.25 bar |
| Thermal shield | incoming flow | gas/liquid | LN2 (saturated liquid) | GN2 | - |
| | | flow | 11.5 g/s | max 100 g/s * | - |
| | | temperature | 80 K | 300 – 80 K | - |
| | | pressure | 3 bar | 3 bar | - |
| | | vapor quality | < 5 % | - | - |
| | return flow | gas/liquid | GN2 (saturated vapor) | GN2 | - |
| | | flow | 11.5g/s | max 100 g/s * | - |
| | | temperature | 80 K | 300 – 80 K | - |
| | | pressure | 2.9 bar | ≈ 1.2 bar | - |
| | | vapor quality | 100% | - | - |
| Recovery line | - | gas/liquid | - | - | GHe |
| | | flow | - | - | 4.01 g/s (118.3 l/h) |
| | | temperature | - | - | 4.45 K |
| | | pressure | - | - | 1.25 bar |

* - during cool-down and warm-up regimes the value of the flow rate is regulated providing cooling speed of 1 K/h.

| | | | |
|-------------------------------------|------|-------------------|---|
| Rev. 2 | Page | Document no. |  |
| 31.01.2017 | 7 | ILK-B-1-16-319a_v | ILK Dresden |
| Title | | | |
| Helium Refrigerator for MPD cooling | | | |


2 Scope of Supply

The ILK will supply the following components:

- Satellite refrigerator unit for the MPD cooling with cooling power of 100 W at a temperature of 4.5 K with a liquid Helium flow of 5 g/s (see Figure 1)
- Geometrical dimensions are comparable to those of SRU 2 and 3
- Programmable logic controller, Human machine interface (7" monitor)
- Electrical power switchboard
- Safety devices (valves and rupture disk)
- Tests and acceptance
 - Welding examination
 - Leakage tests
 - Functional test of valves and instruments
 - Dimensional control
 - Pressure tests
- Selected material certificates and documents

3 Dimensioning of the heat exchangers and the main components

The SRU for the MPD needs different kinds of heat exchangers (plate heat exchangers for the pre-cooling operating mode; type Compact36-C-10 from company AIREC) and the main helium/helium heat exchangers Compact36-C-10 and 4 units of type H29-C for the normal operating mode (HEX I and II in Figure 2). Each assembly follows a liquid bath heat exchanger (dimensioned and calculated by the ILK Dresden).

| | | | |
|---|------|-------------------|---|
| Rev. 2 | Page | Document no. |  ILK Dresden |
| 31.01.2017 | 8 | ILK-B-1-16-319a_v | |
| Title Helium Refrigerator for MPD cooling | | | |

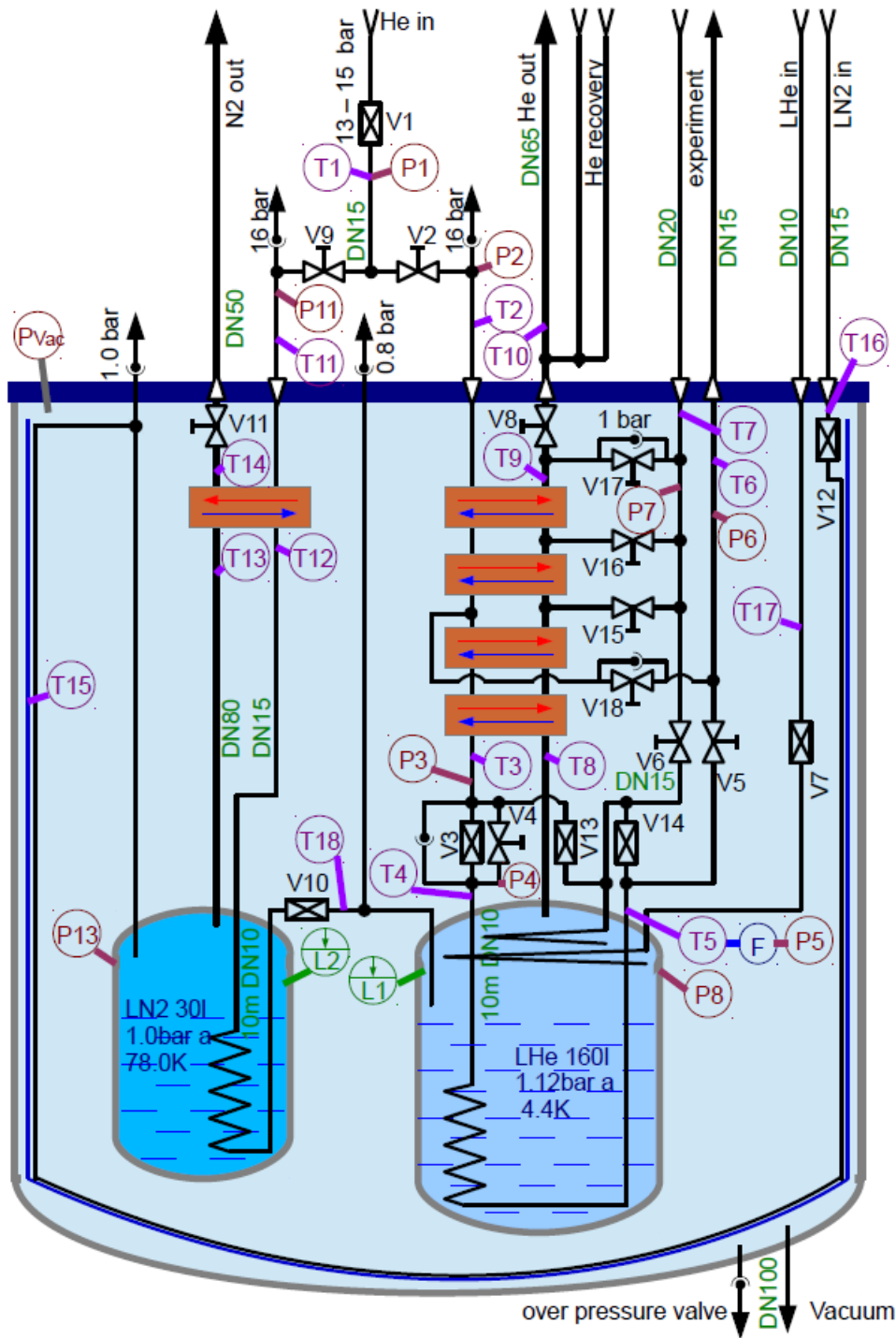


Figure 2: Schematic installation layout of the refrigerator system for the MPD [ILK Dresden] (left HEX II, right HEX I)



| | | | |
|--|------|-------------------|---|
| Rev. 2 | Page | Document no. |  |
| 31.01.2017 | 9 | ILK-B-1-16-319a_v | |
| Title Helium Refrigerator for MPD cooling | | | |

Table 2: Description of the installation layout of the MPD-SRU (see Figure 2)

| | |
|---|---|
| F | venturi tube (mass flow meter) |
| L1 | capacitive level meter (CMT Manufacturing for LHe) |
| L2 | capacitive level meter (CMT Manufacturing for LN ₂) |
| Valves (V) | see Table 11 |
| Sensors (Pressure-P and Temperature-T) | see Table 16 and Table 17 |
| Heat exchangers HEX I | helium/helium heat exchanger from company AIREC (right side) |
| Heat exchangers HEX II | helium/nitrogen heat exchanger from company AIREC (left side) |
| liquid bath heat exchanger inside LN ₂ | coiled tube 10 m, Cu |
| liquid bath heat exchanger inside LHe | coiled tube 10 m, Cu |
| LN ₂ | vessel 30-100 liters usable volume – design pressure 2.5 bar(abs) |
| LHe | vessel 160 liters usable volume – design pressure 2 bar(abs) |
| pressure relief devices | see chapter 5 |

| | | | |
|--|------|-------------------|---|
| Rev. 2 | Page | Document no. |  |
| 31.01.2017 | 10 | ILK-B-1-16-319a_v | |
| Title Helium Refrigerator for MPD cooling | | | |

3.1 Dimensioning of the pipes

Table 3: Diameter of pipelines (see Table 2)

| # | | ID [mm] | |
|---|---|---------|-------|
| 1 | Return helium pipeline (He out) | 65 | DN 65 |
| 2 | Compressed helium pipeline (He in) | 15 | DN 15 |
| 3 | Liquid nitrogen pipeline from an external cryogenic storage tank (LN2 in) | 15 | DN 15 |
| 4 | Liquid helium pipeline from an external cryogenic storage tank (LHe in) | 10 | DN 10 |
| 5 | Return nitrogen pipeline (N2 out) | 50 | DN 50 |
| 6 | Siphon for transferring liquid helium to the control dewar (experiment) | 15 | DN 15 |
| 7 | Siphon for transferring of the helium return flow from the control dewar (experiment) | 20 | DN 20 |
| 8 | Helium recovery (external pipeline) | 30 | DN 30 |

All these dimensions must be approved by the JINR.

3.2 Parameters of the plate heat exchanger (PHE)

3.2.1 Assembly of PHE for the Pre-Cooling operating mode

The assembly consists of six plate heat exchangers of the type Compact36-C-10 from the company AIREC. The dimensioning was done in accordance with AIREC and is summarized in Table 4 to Table 6 and shown in Figure 3.

Table 4: Application data (a) of the Pre-Cooler HEX II (from comp. AIREC)

| Fluid A | Fluid B |
|--------------------------------|-----------------|
| Single phase | Single phase |
| Helium @13 bar(a) – Pre-Cooler | Nitrogen – COLD |



| | | | |
|--|------|-------------------|---|
| Rev. 2 | Page | Document no. |  |
| 31.01.2017 | 11 | ILK-B-1-16-319a_v | |
| Title Helium Refrigerator for MPD cooling | | | |

Table 5: Application data (b) of the Pre-Cooler HEX II (from comp. AIREC)

| | |
|------------------------|----------|
| Fouling factor | 5.0 % |
| Heat transferred | 3.247 kW |
| Temperature efficiency | 99.7 % |
| Max plate temperature | 299.67 K |

Table 6: Plate heat exchangers – Pre-Cooling operation mode

| parameter | | index | unit | side A | side B |
|---------------------|--------|-----------------------------------|------|------------|--------------|
| fluid | | | | helium gas | nitrogen gas |
| mass flow | | \dot{m}_{He} | kg/s | 0.005 | 0.014 |
| pressure | | p | bar | 13.0 | 1.0 |
| temperature | inlet | T_{in} | K | 300.00 | 78.80 |
| | outlet | T_{out} | K | 176.47 | 299.38 |
| heat transferred | | \dot{Q} | W | 3247 | |
| pressure drop | | Δp | mbar | 13.49 | 8.77 |
| plate material | | see below | | | |
| heat exchanger type | | 6 x Compact36-C-10 | | | |
| assembly | | FD1-NS6-PA1-PB1 (counter current) | | | |
| safety reserve | | % | -- | 5 | |

| | | | |
|---|------|-------------------|---|
| Rev. 2 | Page | Document no. |  ILK Dresden |
| 31.01.2017 | 12 | ILK-B-1-16-319a_v | |
| Title Helium Refrigerator for MPD cooling | | | |

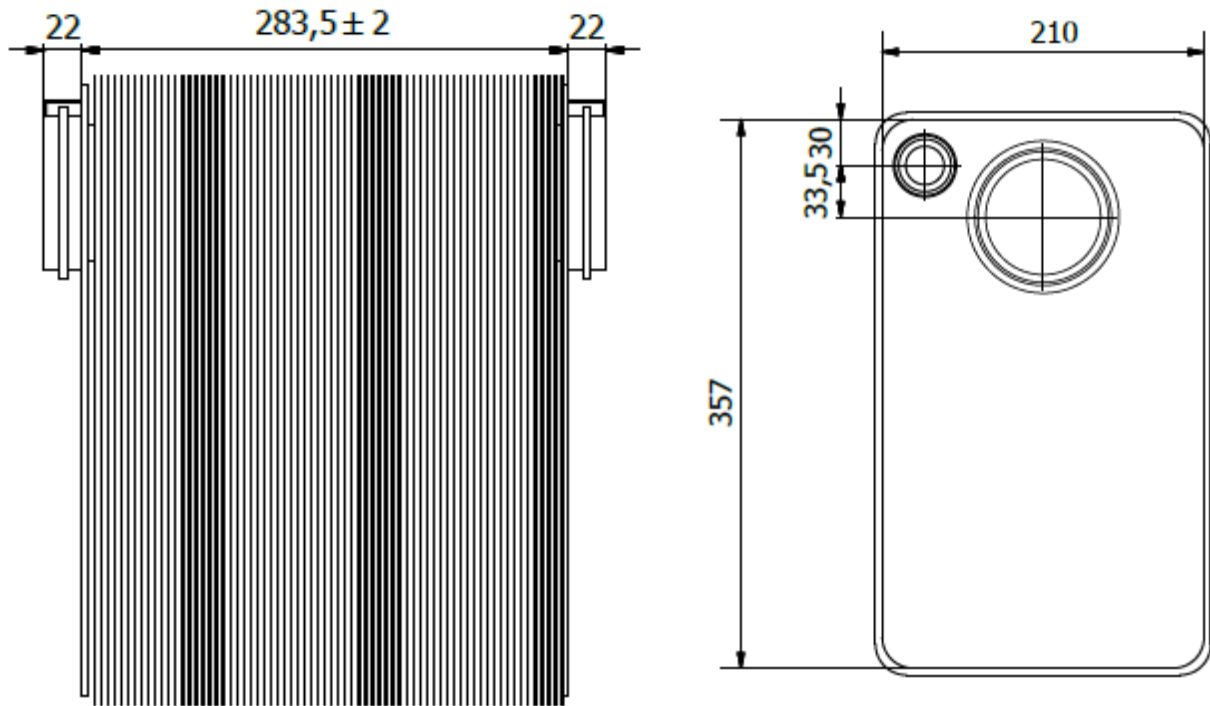



Figure 3: Pre-Cooler for nitrogen (PHE) (© AIREC)

Material of the Pre-Cooler (Compact 36-C-6x10): 316L/1.4404 with copper as brazing material.
 Minimum temperature: 77 K

| | | | |
|--|------|-------------------|---|
| Rev. 2 | Page | Document no. |  ILK Dresden |
| 31.01.2017 | 13 | ILK-B-1-16-319a_v | |
| Title Helium Refrigerator for MPD cooling | | | |

3.2.2 Assembly of plate heat exchangers for the normal operating mode

The dimensioning is summarized in Table 7 for step 1 and Table 8 for step 2.

Table 7: Plate heat exchangers (PHE) – normal operation mode – step 1 (from comp. AIREC)

| parameter | | index | unit | side A | side B |
|---------------------|--------|--------------------|------|------------|------------|
| fluid | | | | helium gas | helium gas |
| mass flow | | \dot{m}_{He} | kg/s | 0.005 | 0.006 |
| pressure | | p | bar | 13.0 | 1.0 |
| temperature | inlet | T_{in} | K | 290.00 | 44.00 |
| | outlet | T_{out} | K | 48.00 | 247.00 |
| heat transferred | | \dot{Q} | W | 6399 | |
| pressure drop | | Δp | mbar | < 30 | < 30 |
| plate material | | AISI 316Ti, 1.4404 | | | |
| heat exchanger type | | Compact36-C-10 | | | |
| assembly | | | | | |
| safety reserve | | % | -- | | |

The pressure drop for one Compact36-C unit is 150 mbar at a helium mass flow of 14 g/s at 14 bar and 300 K, respectively 30 mbar at 80 K and 14 bar.


| | | | | |
|--|------|-------------------|---|--|
| Rev. 2 | Page | Document no. |  | |
| 31.01.2017 | 14 | ILK-B-1-16-319a_v | | |
| Title Helium Refrigerator for MPD cooling | | | | |

Table 8: Plate heat exchangers – normal operation mode – step 2 (from comp. AIREC)


| parameter | | index | unit | side A | side B |
|---------------------|--------|------------------------------|------|------------|------------|
| fluid | | | | helium gas | helium gas |
| mass flow | | \dot{m}_{He} | kg/s | 0.005 | 0.006 |
| pressure | | p | bar | 13.0 | 1.0 |
| temperature | inlet | T_{in} | K | 48.00 | 44.00 |
| | outlet | T_{out} | K | 5.50 | 4.50 |
| heat transferred | | \dot{Q} | W | 3247 | |
| pressure drop | | Δp | mbar | < 20 | < 20 |
| plate material | | AISI 316Ti, 1.4404 | | | |
| heat exchanger type | | H29-C-20, H29-C-30, H29-C-40 | | | |

A schematic drawing of the heat exchanger flow regime is given in Figure 4.

Experimental studies with two Compact36 units and four H29 units inside the first satellite refrigerator units shows outlet temperatures T (high-pressure side) between 4.7 K and 5.1 K with a helium flow of 5 g/s.

The maximum operational pressure of the heat exchanger is 20 bar(g).

Experimental studies show an efficiency of the main heat exchanger of approx. 99.85 %.

| | | | |
|---|------|-------------------|---|
| Rev. 2 | Page | Document no. |  ILK Dresden |
| 31.01.2017 | 15 | ILK-B-1-16-319a_v | |
| Title Helium Refrigerator for MPD cooling | | | |

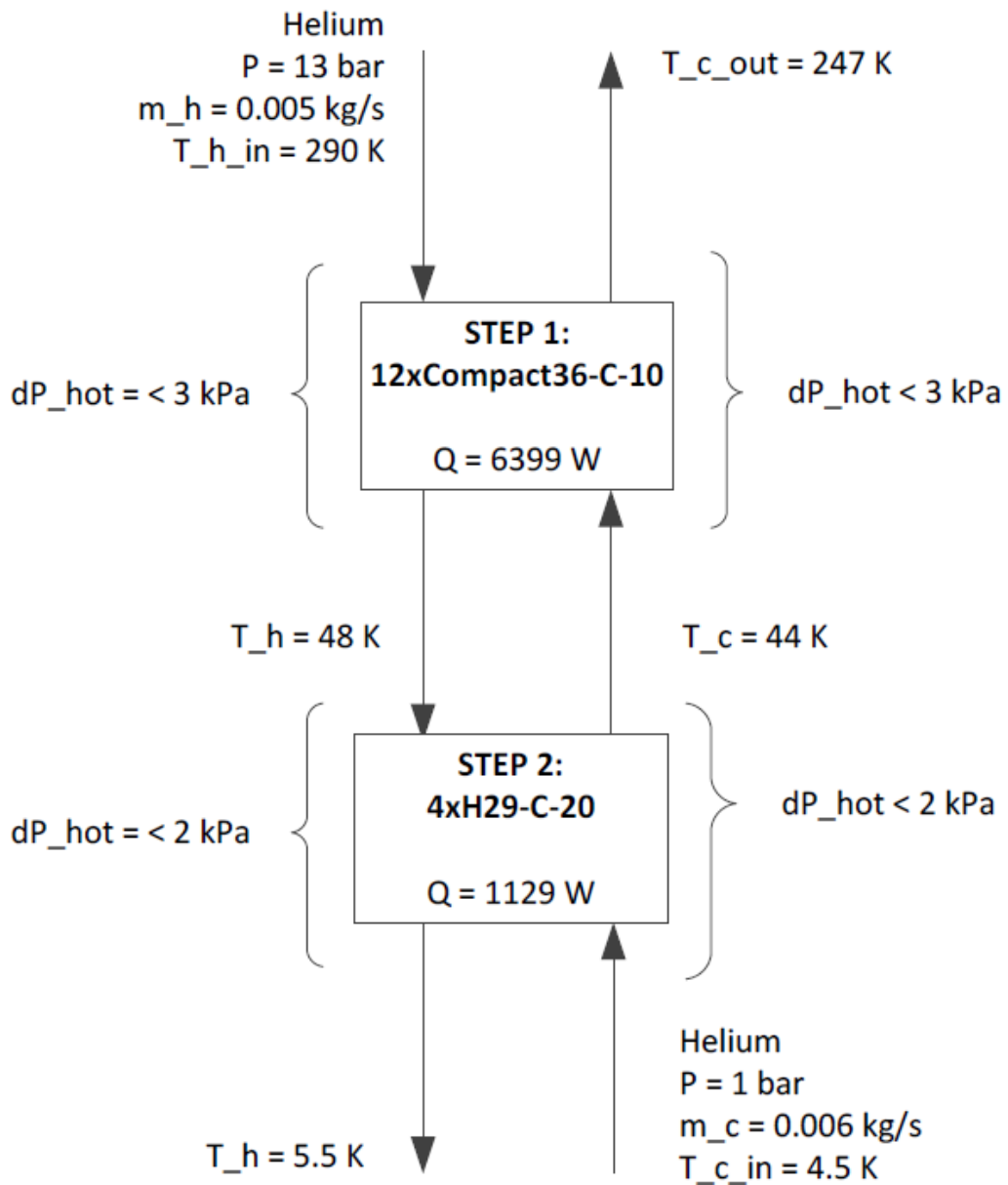



Figure 4: Typical schematic drawing of the main heat exchanger behaviour

| | | | |
|--|------|-------------------|---|
| Rev. 2 | Page | Document no. |  |
| 31.01.2017 | 16 | ILK-B-1-16-319a_v | |
| Title Helium Refrigerator for MPD cooling | | | |

3.2.3 Bypass functionality V18

The pressure loss at 300 K and 16.2 g/s helium flow is 0.6 bar for the HEX unit and approximately 4 bar in the sub-cooler and venturi tube. The total pressure loss would be too high for the required pressure at the magnet inlet of 10 bar. Therefore we suggest implementing a high-pressure bypass with V18 after the second stage of the main HEX I directly to the inlet of the magnet. This bypass reduces the pressure drop from room temperature down to 60 K below 2 bar. Below 60 K the total pressure drop is below 2 bar and the bypass can be closed completely.

3.3 Dimensioning of the liquid bath heat exchanger


The heat exchangers in the liquid baths are coiled tubes. To determine the required area for the heat transfer, the diameter and length of the tube and the heat transfer coefficient has to be calculated. The heat transfer is calculated according to Newton's law of cooling, see equation (1) and following.

$$\dot{Q} = h \cdot A \cdot \Delta T_m \quad (1)$$

$$\text{with } \Delta T_m = \frac{T_{He,in} - T_{He,out}}{\ln \frac{T_W - T_{He,in}}{T_W - T_{He,out}}} \quad \text{and } h = \frac{k \cdot Nu}{d_i} \quad (2)$$

$$Nu = 0.0235 (Re^{0.8} - 230) \left(1 + \left(\frac{d_i}{L} \right)^{2/3} \right) (1.8 \cdot Pr^{0.3} - 0.8) \quad (3)$$

$$Re = \frac{\omega \cdot d_i}{\nu} \quad (4)$$


| | | | |
|--|------|-------------------|---|
| Rev. 2 | Page | Document no. |  |
| 31.01.2017 | 17 | ILK-B-1-16-319a_v | |
| Title Helium Refrigerator for MPD cooling | | | |

3.3.1 Dimensioning of the heat exchanger in the liquid nitrogen bath

This heat exchanger consists of a coiled tube, which inlet is connected with the outlet of side A of the plate heat exchanger described in chapter 3.2.1 (precooling operating mode). The wall temperature corresponds to the saturation temperature of the liquid nitrogen. Inside the tube, the helium gas cools down to about 80 K for the precooling of the liquid helium vessel (see Table 9). Due to the cool-down of the helium gas, the liquid nitrogen evaporates and thus generates the volume flow for side B of the mentioned plate heat exchanger. In the normal operation mode these heat exchangers are not working as controlled by valves (V9, V10).

Table 9: Heat exchanger in the liquid nitrogen bath

| parameter | | index | unit | value |
|-----------------------------------|--------|-----------------|--------------------|-------|
| temperature | inlet | $T_{He,in}$ | K | 150.0 |
| | outlet | $T_{He,out}$ | K | 80.1 |
| pressure | | p_{He} | MPa | 1.3 |
| pressure drop | | Δp | mbar | 75 |
| wall temperature | | T_w | K | 79.6 |
| He mass flow | | \dot{m}_{He} | kg/s | 0.002 |
| tube outer diameter | | d_i | mm | 10 |
| tube wall thickness | | δ | mm | 1 |
| tube length | | l | m | 10 |
| tube material | | Copper (DHP) | | |
| heat load | | \dot{Q} | W | 730 |
| corresponding N ₂ flow | | \dot{V}_{N_2} | m ³ /hr | 2.28 |
| safety reserve | | % | -- | 240 |


| | | | |
|--|------|-------------------|---|
| Rev. 2 | Page | Document no. |  |
| 31.01.2017 | 18 | ILK-B-1-16-319a_v | |
| Title Helium Refrigerator for MPD cooling | | | |

3.3.2 Dimensioning of the heat exchanger in the liquid helium bath

This heat exchanger consists of a coiled tube (parameters, see Table 10), which inlet is connected with the outlet of side A of the main heat exchanger, step 2 (normal operating mode) with the Joule-Thomson (JT) valve in between. The wall temperature corresponds to the saturation temperature of the liquid helium. Inside the tube, the helium gas cools down to the required condition for the experiment (1.2 bar to 1.8 bar absolute). Due to the cool down of the helium gas, the liquid helium evaporates and generates an additional volume flow to the volume flow of the helium gas coming from the experiment. The total volume flow goes to the inlet of side B of the mentioned main heat exchanger. The temperature of this mixed flow should be controlled carefully to avoid temperatures above 5 K at the low-pressure inlet of the main heat exchanger.

Table 10: Heat exchanger in the liquid helium bath

| parameter | | index | unit | value |
|---|--------|----------------|------|--------|
| temperature | inlet | $T_{He,in}$ | K | 5.03 |
| | outlet | $T_{He,out}$ | K | 4.5 |
| pressure | | p_{He} | MPa | 0.2 |
| pressure drop | | Δp | mbar | 66 |
| wall temperature | | T_w | K | 4.42 |
| He mass flow | | \dot{m}_{He} | kg/s | 0.005 |
| tube inner diameter | | d_i | mm | 10 |
| tube wall thickness | | δ | mm | 1 |
| tube length | | l | m | 10 |
| tube material | Copper | | | |
| heat load | | \dot{Q} | W | 46.6 |
| corresponding He mass flow | | \dot{m} | kg/s | 0.0022 |
| safety reserve | | % | -- | 100 |
| outlet temperature without safety reserve | | $T_{He,out}$ | K | 4.42 |

| | | | |
|--|------|-------------------|---|
| Rev. 2 | Page | Document no. |  |
| 31.01.2017 | 19 | ILK-B-1-16-319a_v | |
| Title Helium Refrigerator for MPD cooling | | | |

4 Dimensioning of the Valves

4.1 Calculation of the K_V -value

To select the proper control valves, the flow coefficient K_V must be calculated^{1,2}. K_V describes the relationship between the pressure drop across an orifice, valve or other assembly and the corresponding flow rate. The calculation of the K_V for gases depends on the pressure regime, whether it is super- or subcritical. This condition is defined in equation (5).

$$\text{subcritical: } p_2 > \frac{p_1}{2} \quad \text{or supercritical: } p_2 < \frac{p_1}{2} \quad (5)$$

For the subcritical pressure regime the K_V -value is calculated according to equation (6), for the supercritical pressure regime equation (7) applies,

$$K_V = \frac{\dot{V}_G}{515} \sqrt{\frac{\rho_G \cdot T_1}{\Delta p \cdot p_2}} \quad (6)$$

$$K_V = \frac{\dot{V}_G}{259.5 \cdot p_1} \sqrt{\rho_G \cdot T_1} \quad (7)$$


with K_V and \dot{V} in $\frac{\text{m}^3}{\text{h}}$, p in bar, ρ in $\frac{\text{kg}}{\text{m}^3}$ and T in K

\dot{V}_G and ρ_G must be defined at 273 K and 1.013 bar. Index 1 indicates the condition at the inlet, index 2 at the outlet, respectively. For the calculation with fluids, refer to equation (8).

$$K_V = \dot{V} \sqrt{\frac{\rho}{1000 \cdot \Delta p}} \quad (8)$$

¹ http://www.mankenberg.de/UPLOAD/pdf/s33_0.pdf

² DIN IEC 534

| | | | |
|--|------|-------------------|---|
| Rev. 2 | Page | Document no. |  ILK Dresden |
| 31.01.2017 | 20 | ILK-B-1-16-319a_v | |
| Title Helium Refrigerator for MPD cooling | | | |

4.2 JT Valve (V3)

The dimensioning of the Joule-Thomson (JT) expansion valve (V3) (see Table 11) is the most critical part, due to the two-phase flow regime. The pressure regime is supercritical.

4.3 Control valves V1, V7, V10, V12, V13 and V14

V1 controls the inlet pressure of the gaseous He input. It reduces the pressure from a maximum value of 20 bar to the normal operating pressure of 13 bar. V7 regulates the liquid helium input to the system (LHe inlet). V12 (LN2 in) does the same for the liquid nitrogen input and is connected directly before the radiation shield. Both liquid inlet valves are designed for a liquid nitrogen mass flow of 8 g/s plus evaporated flow from pipe line heat load. This heat load must be defined for the final valve design. Valve V10 operates only in the precooling mode and reduces the pressure from 13 to about 1.5 bar, before the gas enters the liquid helium vessel (over pressure protection!), it is designed for a mass flow of 4 g/s 300 K warm helium. V13 and V14 are bypass valves. V13 is a bypass valve between high-pressure outlet and low-pressure inlet of HEX II (no mass flow over subcooler and experiment, subcooler bypass) and must therefore reduce the pressure from 13 to about 1.5 bar. V14 is a bypass between the inlet and the outlet of the experiment and is essential if no experiment is in place (experiment bypass).


Please note:

Valves from company WEKA with electric actuator from company Haselhofer.

4.4 Table of valves

Table 11: Valve list of the MPD-SRU

| Qty | Valve | Type (seat) | off state(power-off and pressure less) | DN | Fluid | PN [bar(a)] | Pressure Inlet [bar(a)] | Pressure Outlet [bar(a)] | Operating Temperature [K] | Mass-flow [g/s] | K_{vs} -value (max. K_v -value with 100% opening) [m ³ /h] | A-size [mm] |
|-----|-------|-------------|--|----|-----------------------|-------------|-------------------------|--------------------------|---------------------------|-----------------|---|-------------|
| 1 | V1 | variable | manual | 15 | GHe | 20 | 13,5 - 20 | 13 | 300 | 30 | max | - |
| 1 | V2 | on/off | last | 15 | GHe | 20 | 13 | 13 | 300 | 16,2 | max | - |
| 1 | V3 JT | variable | last | 10 | GHe + LHe | 20 | 13 | 2 | 5 - 10 | 5 | 0.06 | 800 |
| 1 | V4 | on/off | last | 10 | GHe | 20 | 13 | 13 | 10 - 300 | 16,2 | max | 800 |
| 1 | V5 | on/off | last | 15 | GHe / LHe | 20 | 13 / 2 | 13 / 2 | 4,2 - 300 | 5 / 16,2 | max | 800 |
| 1 | V6 | on/off | last | 15 | GHe / LHe | 20 | 1 – 1.5 | 1 – 1.5 | 4,2 - 300 | 5 / 16,2 | max | 800 |
| 1 | V7 | variable | last | 10 | GHe + LHe | 3 | | 1 – 1.5 | 4,5 | 8 | 0,26 | 800 |
| 1 | V8 | on/off | last | 65 | GHe | 3 | 1,2 | 1 | 240 - 300 | 16,2 | max | 350 |
| 1 | V9 | on/off | last | 15 | GHe | 20 | 13 | 13 | 300 | 14 | max | - |
| 1 | V10 | variable | last | 10 | GHe | 20 | 13 | 1 – 1.5 | 77 - 300 | 14 / 4 | 0,124 | 350 |
| 1 | V11 | on/off | last | 50 | GN ₂ | 3 | 1 – 1.5 | 1 – 1.1 | 240 - 300 | 3 + GN2_V12 | max | 350 |
| 1 | V12 | variable | last | 15 | GN ₂ + LN2 | 3 | | | 77 | 8 | 1,20 | 350 |
| 1 | V13 | variable | last | 10 | GHe | 20 | 13 | 1 – 1.5 | 4,2 - 300 | 5 / 16,2 | 0.06 / 0.48 | 800 |
| 1 | V14 | variable | last | 10 | GHe | 20 | 13 / 2 | 1 – 1.5 | 4,2 - 300 | 5 / 16,2 | 0.06 / 0.48 | 800 |
| 1 | V15 | on/off | last | 20 | GHe | 20 | <2 | 1,3 | 10 - 120 | 16,2 | max | 800 |
| 1 | V16 | on/off | last | 20 | GHe | 20 | <2 | 1,2 | 100 - 250 | 16,2 | max | 350 |
| 1 | V17 | on/off | last | 20 | GHe | 20 | <2 | 1,1 | 230 - 300 | 16,2 | max | 350 |
| 1 | V18 | on/off | last | 15 | GHe | 20 | 13 | 12,5 | 60 - 300 | 16,2 | max | 350 |

| | | | |
|---|------|-------------------|---|
| Rev. 2 | Page | Document no. |  ILK Dresden |
| 31.01.2017 | 22 | ILK-B-1-16-319a_v | |
| Title Helium Refrigerator for MPD cooling | | | |

5 Vessels and overpressure protection

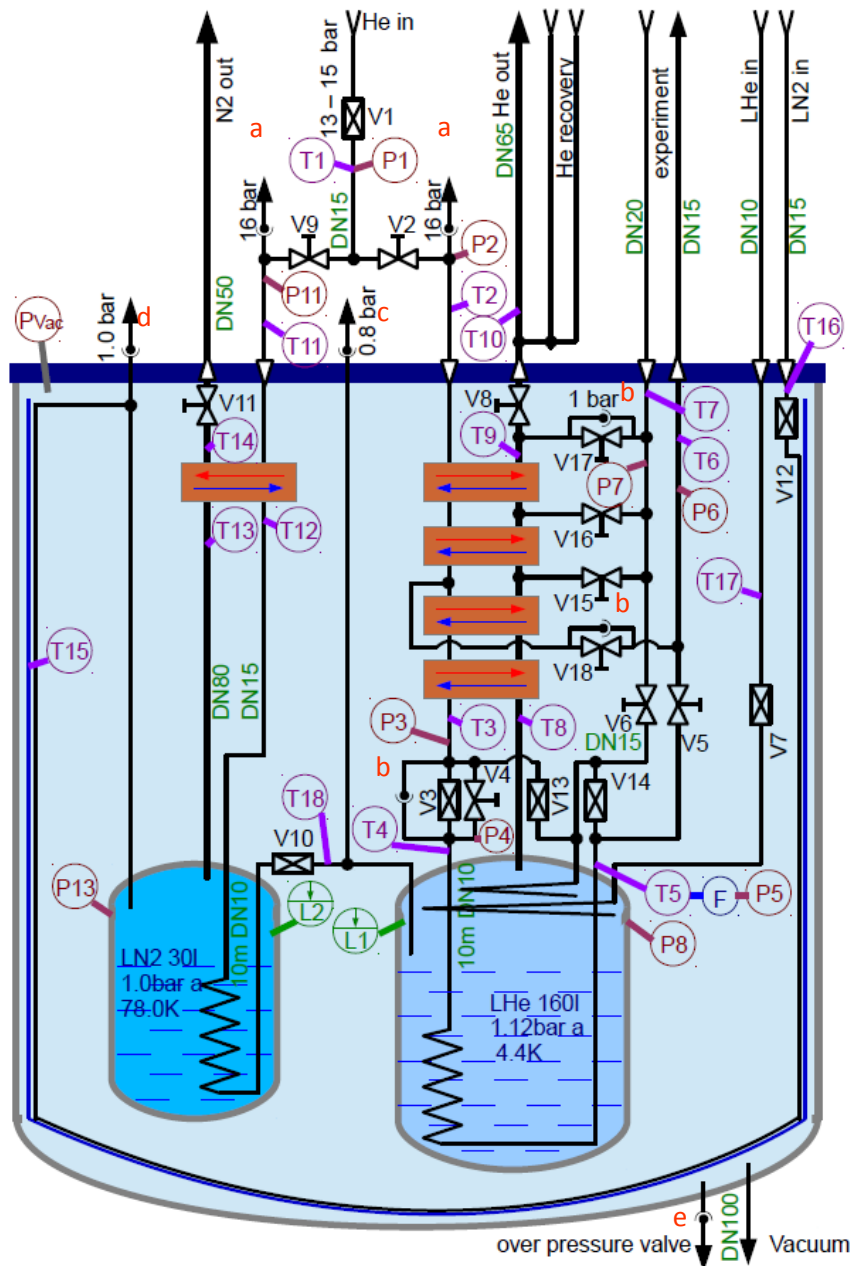



Figure 5: Schematic drawing of the MPD-SRU with overpressure relief devices (a - e)


| | | | |
|--|------|-------------------|---|
| Rev. 2 | Page | Document no. |  ILK Dresden |
| 31.01.2017 | 23 | ILK-B-1-16-319a_v | |
| Title Helium Refrigerator for MPD cooling | | | |

5.1 Vacuum vessel

To reduce heat deposition to the inner cold parts, the MPD-SRU has to be equipped with a vacuum insulated jacket. To reach a suitable vacuum pressure ($< 1 \times 10^{-4}$ mbar) a vacuum pump (pre-pump plus turbomolecular pump) has to be used. Therefore the vacuum jacket is equipped with an ISO100B104-316 flange and a TU50K70 flange for the Pirani vacuum gauge (DN 25) and the pressure relief valve DN 50 KF (via T-piece).

Before beginning of operation and during the operation a stable vacuum ($< 1 \times 10^{-4}$ mbar) inside the SRU must always be ensured. In the case of non-compliance, a risk of condensation with heat load and strong evaporation of cryogenic substances occurs (helium and nitrogen)!

According to CGA S-1.3 (CGA - Compressed Gas Association) and EN 13458-2 (EN-European standard) the jacket of the containers (vacuum) shall be protected by a suitable PRD (pressure release devices) to release internal pressure. The total discharge area of vacuum jacket relief devices on a container shall be at least $0.3414 \text{ mm}^2/\text{kg}$ of water capacity of the container (cryogenic vessels, overall volume 328 liter) minimum DN 10. Therefore the vacuum container has to be equipped with a pressure relief valve DN 50 KF from company STÖHR with a self-actuating open and close behaviour (response pressure 0.3 bar, type 50KF-ES) (see Figure 6). For an extreme leakage the vacuum jacket has to be equipped with two relief valves (DN 50 KF-flange) from the company Jakob Vakuumentchnik (see Figure 7, response pressure < 0.5 bar) but without self-actuating close behavior. During the operation of the MPD-SRU leakage gases can aggregate on cold surfaces. During warm-up of the refrigerator substantial amount of these gases will release into the vacuum volume. In order to ensure the vacuum during the entire warm-up phase, a suitable vacuum pump should be operated continuously.

| | | | |
|--|------|-------------------|---|
| Rev. 2 | Page | Document no. |  |
| 31.01.2017 | 24 | ILK-B-1-16-319a_v | |
| Title Helium Refrigerator for MPD cooling | | | |

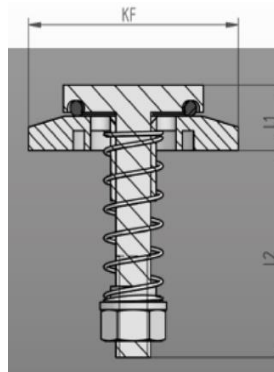


Figure 6: Small flange vacuum pressure relief valve from the company STÖHR³.

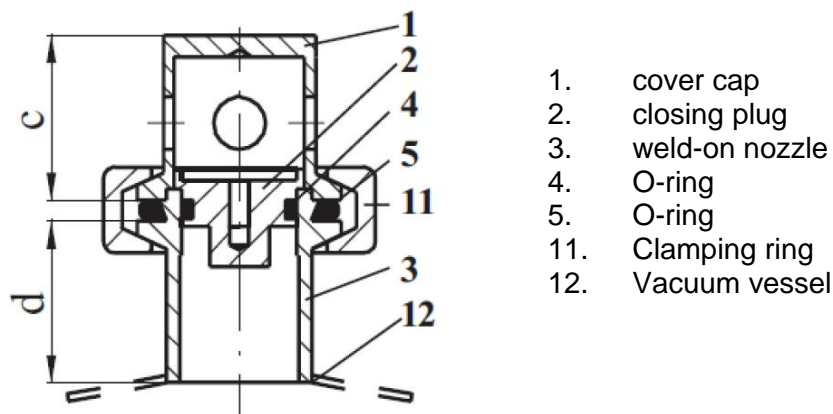



Figure 7: Vacuum pressure relief valve from the company Jakob Vakuumtechnik⁴.

5.2 LHe Vessel

| | |
|------------------|---|
| Overall volume: | 198 liter |
| Usable volume: | 160 liter |
| Surface area: | 2 m ² |
| Design pressure: | 2 bar(abs) |
| Design: | according to EN 13458 and AD 2000 specifications (working group for pressure vessels) |

³ http://www.stoehr-valves.de/medien/katalog/StoehrArmaturen_Produktkatalog_DE.pdf, page 64, 26/08/13

⁴ http://www.jakobvakuumtechnik.de/downloads/katalog_5.pdf, page 2, 26/08/13

| | | | |
|--|------|-------------------|---|
| Rev. 2 | Page | Document no. |  |
| 31.01.2017 | 25 | ILK-B-1-16-319a_v | |
| Title Helium Refrigerator for MPD cooling | | | |

The continuous operation helium flow (< 7 g/s) will release over the main heat exchanger outlet (always open line). According to the EN 13648-3 (Cryogenic vessels — Safety devices for protection against excessive pressure) and the AD 2000-A2 rules, the helium vessel has to be protected with a valve D₀ 14 mm from company HEROSE (safety valve, type: 06850 (G ½)) with 1.8 bar(abs) response pressure and a rupture disc (rupture disk, CF40-UKB-LS) DN 40 from company REMBE according to PED 97/23/EG gridline with 2.2 bar(abs).

Calculations according to EN 13648 (without impacts of fire):

See EN 13648 – 3.2.2: vacuum-insulated vessels with loss of vacuum, heat transition

$$W_2 = (T_a - T) \times U_2 \Sigma$$

With:

$U_2 \equiv$ coefficient of heat transfer

$$U_2 = \frac{\lambda_2}{e_2}$$

$\lambda_2 \equiv$ thermal conductivity of the insulating material at atmospheric pressure, in W m⁻¹K⁻¹

$e_2 \equiv$ minimum thickness of the insulating material, in m

$\Sigma \equiv$ arithmetic average of the inner and outer area of the insulating material of the vessel, in m²

| |
|--|
| Thermal conductivity λ_{MLI} of the MLI (multilayer insulation) at atmospheric pressure 0.02 W/m K ⁵ |
|--|

Insulation (30 layers type RUAG Coolcat 2 NW): 9 mm practical thickness after installation (company RUAG)

Saturation temperature (2 bar) LHe: 5.04 K

$$W_2 = \frac{\lambda_{\text{MLI}}}{e_{\text{MLI}}} (300 \text{ K} - 5.04 \text{ K}) \cdot 2 \text{ m}^2 = 1311 \text{ W}$$


| |
|--|
| <u>For comparison only:</u> coupling of helium atmosphere to the MLI (average heat conductivity of helium $\lambda = 0.113 \text{ W/m K}$ ⁶ between 80 K and 300 K): |
|--|

$$W_2 = \frac{\lambda_{\text{He}}}{e_{\text{MLI}}} \cdot (300 \text{ K} - 5.04 \text{ K}) \cdot 2 \text{ m}^2 = 7409 \text{ W}$$

| |
|-----------------------------|
| Protection by rupture disc! |
|-----------------------------|

⁵ H. Frey, R. A. Haefer, Tieftemperaturtechnologie, VDI Verlag, page 238

⁶ <http://webbook.nist.gov/chemistry/fluid/>

| | | | |
|--|------|-------------------|---|
| Rev. 2 | Page | Document no. |  |
| 31.01.2017 | 26 | ILK-B-1-16-319a_v | |
| Title Helium Refrigerator for MPD cooling | | | |

See EN 13648 – 3.2.3: Heat transition per time (Watt) through vessel mountings and pipelines in space between

$$W_3 = (T_a - T) \times (w_1 + w_2 + \dots + w_n + \dots)$$

With:

$W_3 \equiv$ thermal loss per K due to vessel mountings and pipelines, in W K⁻¹

$$w_n = \lambda_n \frac{S_n}{l_n}$$

$\lambda_n \equiv$ thermal conductivity of vessel mountings or pipelines between T and T_a , in W m⁻¹K⁻¹

$S_n \equiv$ cross-section area of the vessel mountings and pipelines

$l_n \equiv$ length of the vessel mountings or pipelines in space between, in m

All pipelines equipped with MLI. All connections in stainless steel.

(Previous assumption of heat transition per time: 250 W)

See EN 13648 – 3.2.4:

Evaporating helium from the inner helical tube can stream over the AIREC heat exchanger He/He system.

Mass flow helium in normal operation mode: 5 g/s

According to the calculation of the company AIREC: pressure loss < 0.2 bar.

Summary:

The heat load for the calculation of the mass flow for the valves was found to be 1561 W.

See EN 13648 –4.1: The blow-out pressure p is smaller than 40 % of the critical pressure (2.28 bar):

$$Q_m = 3.6 \times \frac{W}{L}$$

With:

$L \equiv$ latent enthalpy of vaporization of the cryogenics fluid at blow out conditions, in kJ kg⁻¹


See EN 13648 –4.1: The blow out pressure p is smaller than the critical pressure (2.28 bar), but equal or larger than 40% of this pressure:

$$Q_m = 3.6 \times \left(\frac{v_g - v_l}{v_g} \right) \frac{W}{L}$$

With:

$v_g \equiv$ specific volume of the saturated gas at blow out pressure p , in m³ kg⁻¹

$v_l \equiv$ specific volume of the saturated liquid at blow out pressure p , in m³ kg⁻¹

| | | | |
|--|------|-------------------|---|
| Rev. 2 | Page | Document no. |  |
| 31.01.2017 | 27 | ILK-B-1-16-319a_v | |
| Title Helium Refrigerator for MPD cooling | | | |

Enthalpy of vaporization (1.8 bar): 14.56 kJ/kg ⁷

$$\dot{m} = \frac{1.56 \text{ kW}}{14.56 \frac{\text{kJ}}{\text{kg}}} = 0.11 \frac{\text{kg}}{\text{s}} = 386 \frac{\text{kg}}{\text{h}}$$

This value was taken into account for the calculation of the valves.

For comparison: Coupling of the He atmosphere to the MLI

$$\dot{m} = \frac{7.66 \text{ kW}}{14.56 \frac{\text{kJ}}{\text{kg}}} = 0.53 \frac{\text{kg}}{\text{s}} = 1904 \frac{\text{kg}}{\text{h}}$$

Protection over rupture disc (see Table 13)!

Rules for the installation of safety devices EN 13648 –5: fulfilled

The loss of pressure inside the periphery was calculated to be 0.02 bar.

⁷ REFPROP – NIST Reference Fluid Properties



| | | | |
|--|------|-------------------|---|
| Rev. 2 | Page | Document no. |  |
| 31.01.2017 | 28 | ILK-B-1-16-319a_v | |
| Title Helium Refrigerator for MPD cooling | | | |

Table 12: Calculation of the required cross section of safety valves according to AD 2000, chapter 10.4.1 (page 85), 1.56 kW heat load

| | | |
|-------------------------------|--------------------------|--|
| pa - back pressure | 0.10 MPa | $A_0 = \frac{q_m}{\psi \cdot \alpha_w \cdot \sqrt{2 \frac{p_0}{v}}}$ |
| p0 - vessel pressure | 0.18 MPa | |
| Helium - vapour density | 32.96 kg/m ³ | $\frac{p_a}{p_0} > \left(\frac{2}{k+1} \right)^{\frac{k}{k-1}} = \frac{p_k}{p_0}$ |
| isentropic exponent | 1.87 | |
| area | 2.00 m ² | subcritical pressure relation |
| heat load | 1.56 kW | |
| enthalpy of vaporisation | 14.56 kJ/kg | |
| mass flow | 0.11 kg/s | |
| volume flow | 0.0033 m ³ /s | |
| | 11.71 m ³ /h | |
| free cross section | 0.000154 m ² | |
| flow rate | 21.13 m/s | |
| Ψ – function of discharge | 0.52 | $\psi = \sqrt{\frac{k}{k-1}} \cdot \sqrt{\left(\frac{p_a}{p_0}\right)^{\frac{2}{k}} - \left(\frac{p_a}{p_0}\right)^{\frac{k+1}{k}}}$ |
| αw - coefficient of discharge | 0.70 see data sheet | |
| necessary cross section | 0.000085 m ² | type 06850 |
| | 85.14 mm ² | |
| Type 06850 - 1 piece | 153.94 mm ² | |

Result: safety valve type Herose 06850, D₀ 14 mm, 1 pcs (G ½)


Table 13: Calculation of the required cross section of the rupture disc according to AD 2000, 10.17 kW heat load

| | | | |
|--|------|-------------------|---|
| Rev. 2 | Page | Document no. |  |
| 31.01.2017 | 29 | ILK-B-1-16-319a_v | |
| Title Helium Refrigerator for MPD cooling | | | |

| | | |
|-------------------------------|--------------------------|--|
| pa - back pressure | 0.10 MPa | $A_0 = \frac{q_m}{\psi \cdot \alpha_w \cdot \sqrt{2 \frac{p_0}{v}}}$ |
| p0 - vessel pressure | 0.22 | |
| Helium - vapour density | 49.29 kg/m ³ | $\frac{p_a}{p_0} > \left(\frac{2}{k+1} \right)^{\frac{k}{k-1}} = \frac{p_k}{p_0}$ |
| isentropic exponent | 2.20 | |
| Zarge | 1413717 mm ² | $\psi = \sqrt{\frac{k}{k-1}} \cdot \sqrt{\left(\frac{p_a}{p_0} \right)^{\frac{2}{k}} - \left(\frac{p_a}{p_0} \right)^{\frac{k+1}{k}}}$ |
| h1 | 31416 mm ² | |
| flange | 90956 mm ² | Innendurchmesser 66 mm minus Querschnitt weiblicher Siphon |
| cage | 159388.2 mm ² | |
| Area | 1.70 m ² | |
| heat load | 10.17 kW | |
| enthalpy of vaporisation | 7.71 kJ/kg | |
| mass flow | 1.32 kg/s | |
| volume flow | 0.03 m ³ /s | |
| | 96.41 m ³ /h | |
| free cross section | 0.0028 m ² | |
| flow rate | 9.56 m/s | |
| Ψ - function of discharge | 0.56 | |
| αw - coefficient of discharge | 0.6 | |
| necessary cross section | 0.000845 m ² | |
| | 8.45 cm ² | |
| necessary diameter | 32.80 mm | |

Result: Reverse rupture disc from company Rembe⁸ (CF40-UKB-LS, material 1.4301/Ni).

⁸ <http://www.rembe.de/produkte/prozesssicherheit/umkehr-berstscheiben/ukb-ls/> (17.03.2016)

| | | | |
|--|------|-------------------|---|
| Rev. 2 | Page | Document no. |  ILK Dresden |
| 31.01.2017 | 30 | ILK-B-1-16-319a_v | |
| Title Helium Refrigerator for MPD cooling | | | |

5.3 LN₂ Vessel

| | |
|------------------|-----------------------------------|
| Overall volume: | 130 liter |
| Usable volume: | 30-100 liter |
| Surface area: | < 1.7 m ² |
| Design pressure: | 2.5 bar(abs) |
| Design: | according to EN 13458 and AD 2000 |

The continuous operation flow of nitrogen during the cool down mode will release over the pre-cooler heat exchanger outlet (power off state / valve open). According to the EN 13648-3 (Cryogenic vessels — Safety devices for protection against excessive pressure) and the AD 2000-A2 rules the nitrogen vessel has to be protected with a HEROSE safety valve D₀ 10 mm (type: 06316.X.N000/N020 (G ½)) with 2.0 bar(abs) response pressure. Please note: The design pressure was used for the calculations.

Calculations according to EN 13648 (without impacts of fire):

See EN 13648 – 3.2.2: vacuum-insulated vessels with loss of vacuum, heat transition

$$W_2 = (T_a - T) \times U_2 \Sigma$$

With:

$U_2 \equiv$ coefficient of heat transfer

$$U_2 = \frac{\lambda_2}{e_2}$$

$\lambda_2 \equiv$ thermal conductivity of the insulating material at atmospheric pressure, W m⁻¹ K⁻¹

$e_2 \equiv$ minimum thickness of the insulating material, in m

$\Sigma \equiv$ arithmetic average of the inner and outer area of the insulating material of the vessel, in m²


See thermal conductivity of the MLI (multilayer insulation) at atmospheric pressure:
0.02 W/m K⁹

Thickness of 20 layers MLI (type RUAG Coolcat 2 NW): 6 mm practical thickness after installation (RUAG space company)

Saturation temperature (2.5 bar) LN₂: 85.93 K

$$W_2 = \frac{\lambda_{MLI}}{e_{MLI}} \cdot (300 \text{ K} - 85.93 \text{ K}) \cdot 1.7 \text{ m}^2 = 1213 \text{ W}$$

⁹ H. Frey, R. A. Haefer, Tieftemperaturtechnologie, VDI Verlag, page 238

| | | | |
|--|------|-------------------|---|
| Rev. 2 | Page | Document no. |  ILK Dresden |
| 31.01.2017 | 31 | ILK-B-1-16-319a_v | |
| Title Helium Refrigerator for MPD cooling | | | |

For comparison: coupling of helium atmosphere to the MLI (average heat conductivity of helium $\lambda = 0.113 \text{ W/m K}^{10}$ between 80 K and 300 K):

$$W_2 = \frac{\lambda_{\text{He}}}{e_{\text{MLI}}} \cdot (300 \text{ K} - 85.93 \text{ K}) \cdot 1.7 \text{ m}^2 = 6854 \text{ W}$$

See EN 13648 – 3.2.3: Heat transition per time (Watt) through vessel mountings and pipelines in space between

$$W_3 = (T_a - T) \times (w_1 + w_2 + \dots + w_n + \dots)$$

With:

$W_3 \equiv$ thermal loss per K due to vessel mountings and pipelines, in W K^{-1}

$$w_n = \lambda_n \frac{S_n}{l_n}$$

$\lambda_n \equiv$ thermal conductivity of vessel mountings or pipelines between T and T_a , in $\text{W m}^{-1}\text{K}^{-1}$

$S_n \equiv$ cross-section area of the vessel mountings and pipelines

$l_n \equiv$ length of the vessel mountings or pipelines in space between, in m

All pipelines are equipped with MLI. All connections are made of stainless steel. The heat load into the LN2 reservoir was experimentally found to be 60 W.

Assumption: 250 W

See EN 13648 – 3.2.4:

Evaporating nitrogen from the inner helical tube can stream over the AIREC heat exchanger (pre-cooler He/N2 system):

Mass flow helium in normal operation mode: 5 g/s, 10 g/s

Evaporation rate N_2 through the pre-cooler: 14 g/s (50 kg/h) at 5 g/s He-mass flow


According to the calculation of the company AIREC: pressure loss < 10 mbar

Summary: The heat load for the calculation of the mass flow was found to be 7104 W.

See EN 13648 –4.1: The blow out pressure p is smaller than 40 % of the critical pressure (34 bar):

$$Q_m = 3.6 \times \frac{W}{L}$$

¹⁰ <http://webbook.nist.gov/chemistry/fluid/>

| | | | |
|--|------|-------------------|---|
| Rev. 2 | Page | Document no. |  |
| 31.01.2017 | 32 | ILK-B-1-16-319a_v | |
| Title Helium Refrigerator for MPD cooling | | | |

With:

$L \equiv$ latent enthalpy of vaporization of the cryogenics fluid at blow out conditions, in kJ kg^{-1}

Enthalpy of vaporization (2.5 bar): 187.19 kJ/kg

Coupling of the He Atmosphere to the MLI

$$\dot{m} = \frac{7.1 \text{ kW}}{187.19 \frac{\text{kJ}}{\text{kg}}} = 0.038 \frac{\text{kg}}{\text{s}} = 136.5 \frac{\text{kg}}{\text{h}}$$

Rules for the installation of safety devices EN 13648 –5: fulfilled

The loss of pressure inside the pipelines was calculated to be 0.053 bar.



| | | | |
|-------------------------------------|------|-------------------|--|
| Rev. 2 | Page | Document no. |  ILK Dresden |
| 31.01.2017 | 33 | ILK-B-1-16-319a_v | |
| Title | | | |
| Helium Refrigerator for MPD cooling | | | |

Table 14: Calculation of the required cross section of safety valves according to AD 2000, chapter 10.4.1, page 85, 7 kW heat load (135 kg/h):

| | | |
|-------------------------------|--------------------------|---|
| pa - back pressure | 0.10 MPa | $A_0 = \frac{q_m}{\psi \cdot \alpha_w \cdot \sqrt{2 \frac{p_0}{v}}}$ |
| p0 - vessel pressure | 0.25 MPa | |
| Helium- steam density | 10.67 kg/m ³ | $\frac{p_a}{p_0} > \left(\frac{2}{k+1} \right)^{\frac{k}{k-1}} = \frac{p_k}{p_0}$ |
| isentropic exponent | 1.39 | |
| area | 1.7 m ² | überkritisches Druckverhältnis overcritical pressure relation |
| heat load | 7.00 kW | |
| enthalpy of vaporisation | 187.09 kJ/kg | Für überkritische Druckverhältnisse ist |
| mass flow | 0.0374 kg/s | |
| volume flow | 0.0035 m ³ /s | $\psi = \psi_{\max} = \sqrt{\frac{k}{k+1}} \cdot \left(\frac{2}{k+1} \right)^{\frac{1}{k-1}} \approx 0,431k^{0,346}$ |
| free cross section | 12.62 m ³ /h | |
| flow rate | 0.000079 m ² | type 06316 |
| Ψ – function of discharge | 44.64 m/s | |
| αw - coefficient of discharge | 0.48 | data sheet |
| necessary cross section | 0.50 | |
| | 6.72E-05 m ² | type 06316 |
| | 67.15 mm ² | |
| 1 pcs type 06316 | 78.54 mm ² | |


Result: safety valve type Herose 06316, D₀ 10 mm, 1 pcs, (06316.X.N000/N020 (G ½))

The static heat load into the LN2 reservoir: approx. 60 W.

| | | | |
|--|------|-------------------|---|
| Rev. 2 | Page | Document no. |  ILK Dresden |
| 31.01.2017 | 34 | ILK-B-1-16-319a_v | |
| Title Helium Refrigerator for MPD cooling | | | |

5.4 Overpressure protection — summary

- Compressed helium pipeline
Integration of one valve MG84 S from company Air Liquide (16 bar(g) response pressure) in each pipeline, (see 'a' in Figure 5)
- Liquid helium vessel
Safety valve type Herose 06850 D₀ 14 mm, 1 pcs, with 0.8 bar(g) response pressure and a reverse bursting disc from company Rembe (CF40-UKB-LS, material 1.4301/Ni, 1.14 – 1.32 bar(g) response pressure at room temperature), (see 'c' in Figure 5)
- Liquid nitrogen vessel
Safety valve type Herose 06316 D₀ 10 mm, 1 pcs with 1 bar(g) response pressure, (see 'd' in Figure 5)
- Vacuum vessel (< 0.5 bar), (see 'e' in Figure 5)
- Pipelines for transferring cryogenic helium, check valves, (see 'b' in Figure 5)

| | | | |
|---|------|-------------------|---|
| Rev. 2 | Page | Document no. |  ILK Dresden |
| 31.01.2017 | 35 | ILK-B-1-16-319a_v | |
| Title Helium Refrigerator for MPD cooling | | | |

6 Design

6.1 Drawings of the refrigerator system for the MPD

Due to changing of the valves from STÖHR type to WEKA type and a double wall vacuum vessel in October 2016 as requested by JINR, the height of the refrigerator system and the positions of certain parts on the cover can slightly change. Figure 8, Figure 9 and Figure 10 show the design version from the 31th of March 2016.

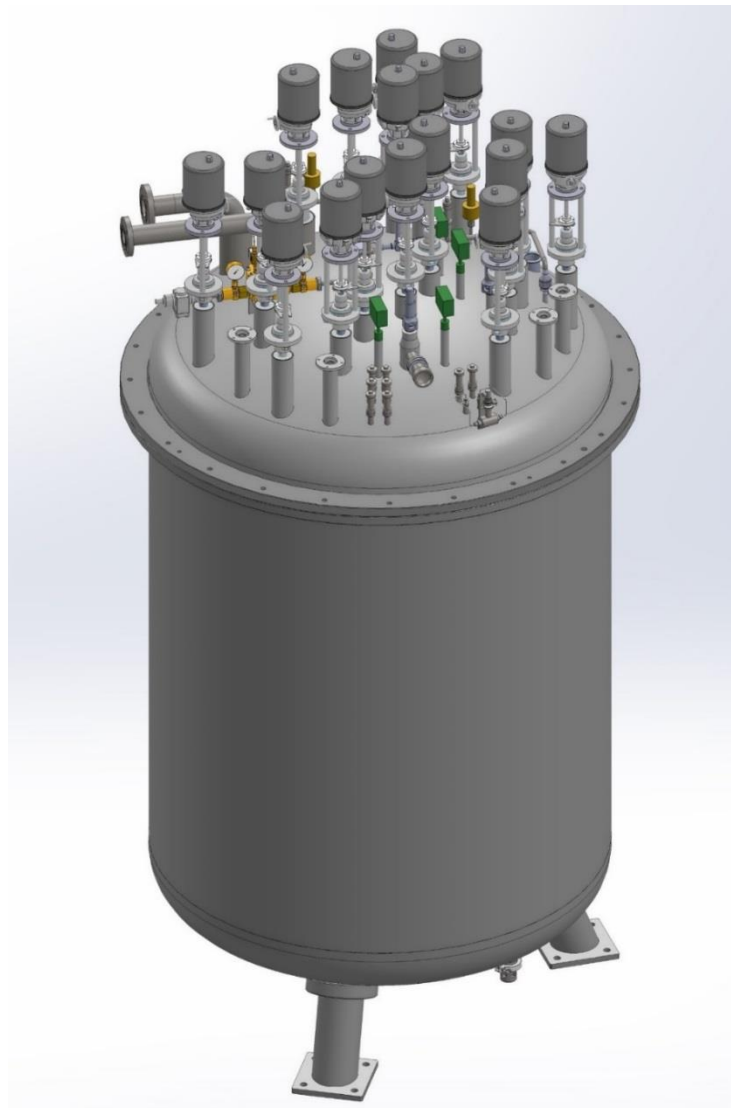



Figure 8: Design drawing of the refrigerator system for the MPD [ILK Dresden].

| | | | |
|---|------|-------------------|---|
| Rev. 2 | Page | Document no. |  ILK Dresden |
| 31.01.2017 | 36 | ILK-B-1-16-319a_v | |
| Title Helium Refrigerator for MPD cooling | | | |

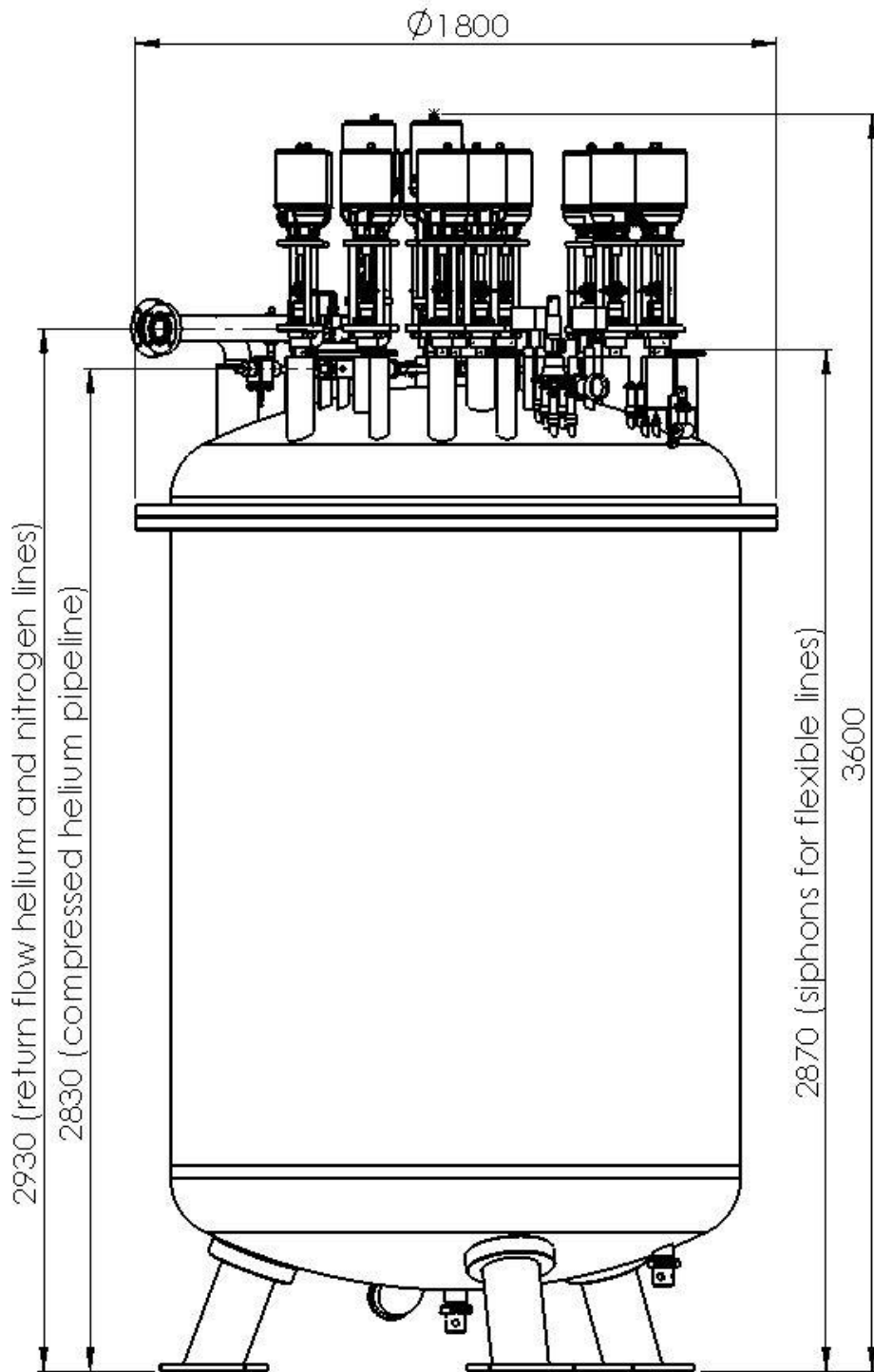


Figure 9: Side view of the refrigerator system for the MPD with geometrical dimensions (standard vacuum vessel) [ILK Dresden].


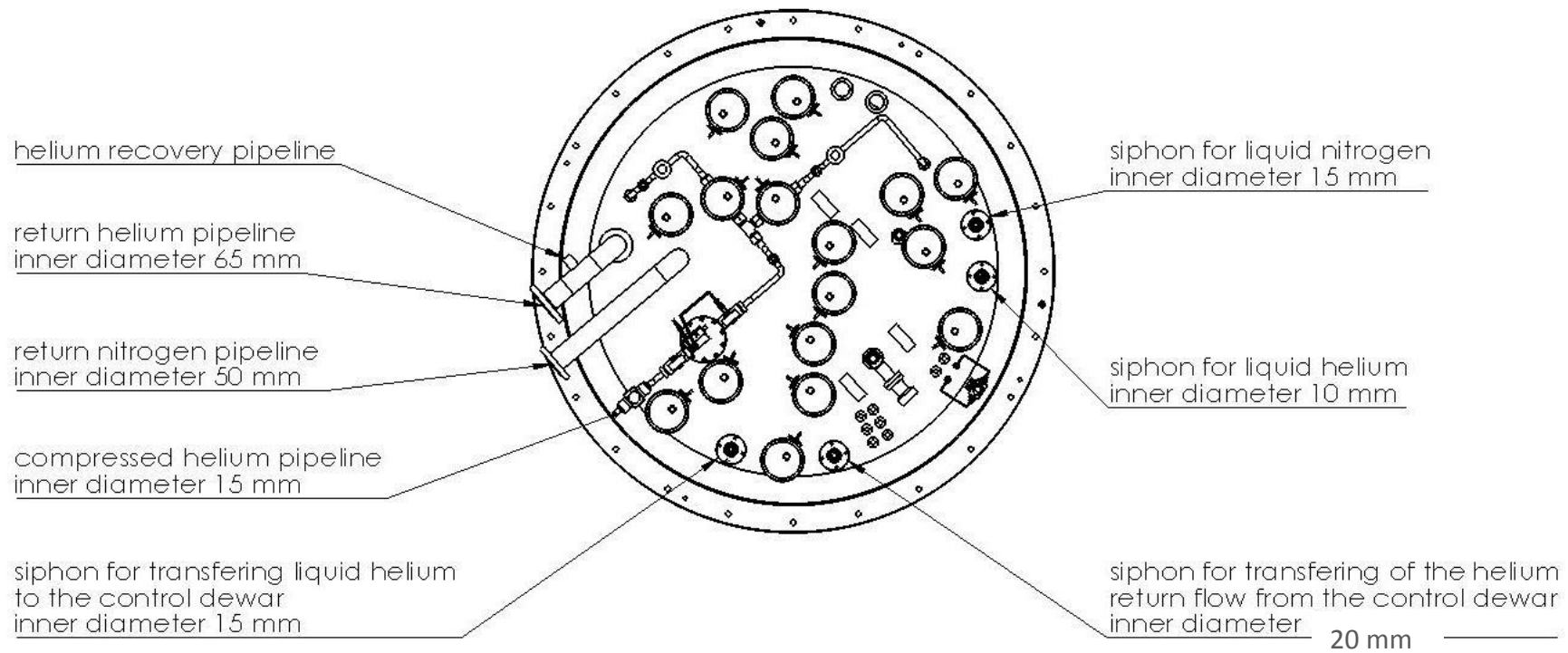

| | | | |
|--|------|-------------------|--|
| Rev. 2 | Page | Document no. |  ILK Dresden |
| 31.01.2017 | 37 | ILK-B-1-16-319a_v | |
| Title Helium Refrigerator for MPD cooling | | | |

Figure 10: Top view of the refrigerator system for the MPD [ILK Dresden].



| | | | |
|---|------|-------------------|---|
| Rev. 2 | Page | Document no. |  ILK Dresden |
| 31.01.2017 | 38 | ILK-B-1-16-319a_v | |
| Title Helium Refrigerator for MPD cooling | | | |

With reference to new inquiries (the e-mail from Nikita Emelianov on the 3rd of October 2016), the MPD SRU will be equipped with a double wall vacuum vessel, with ISO-K 100 flanges for pumping. A first schematic drawing of the special vacuum vessel is shown in

Figure 11.

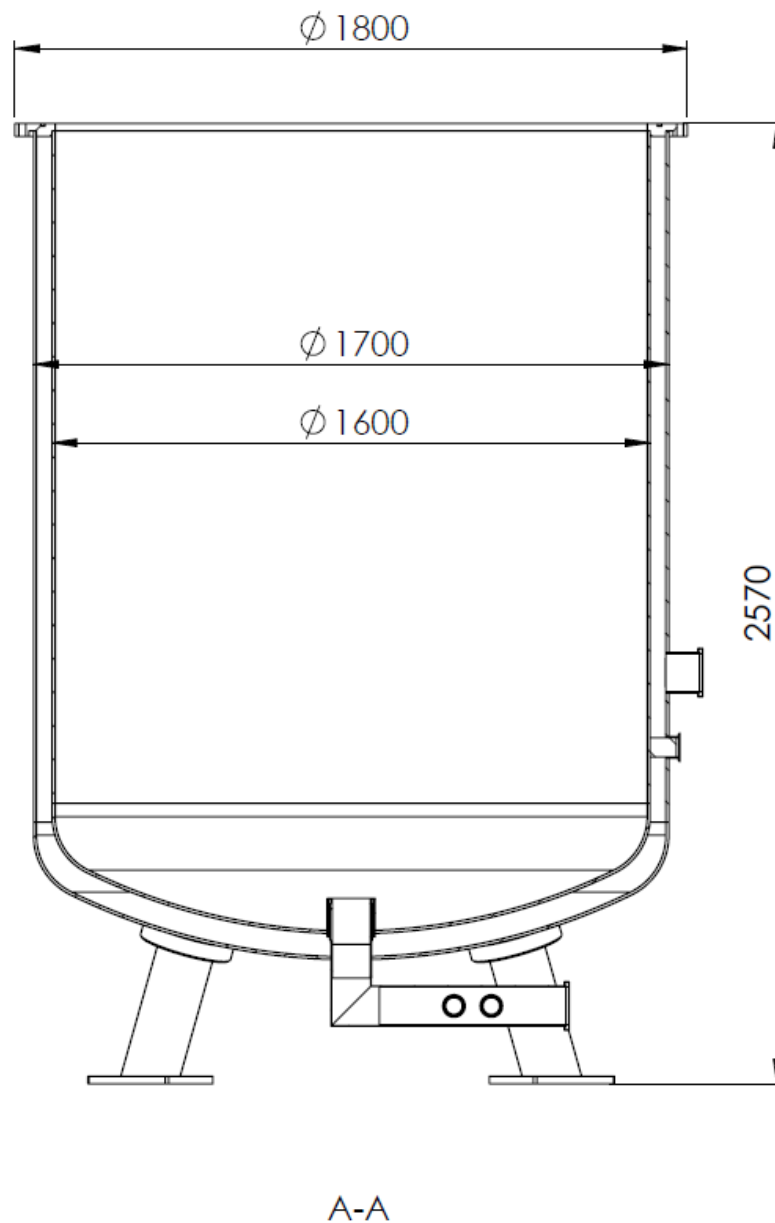



Figure 11: Schematic drawing of the double wall vacuum vessel with ISO-K 100 flanges.

| | | | |
|--|------|-------------------|---|
| Rev. 2 | Page | Document no. |  ILK Dresden |
| 31.01.2017 | 39 | ILK-B-1-16-319a_v | |
| Title Helium Refrigerator for MPD cooling | | | |

6.2 Female siphons

As already used for the SRU 1, 2 and 3 the helium refrigerator for the MPD cooling will be equipped with female Johnson-couplings from the company STÖHR ARMATUREN.

6.3 Control and safety valves


- WEKA for the control valves with electric actuator from company Haselhofer
According to the statement of the supplier, these electric actuators should be robust against electromagnetic radiation (10 Gray).
- HEROSE and AIR LIQUIDE for the safety valves
- REMBE for the burst disks
- WITT for the dome-loaded pressure regulator

6.4 Thermal shield

To reduce the heat load by radiation the MPD-SRU will be equipped with an active cooled shield (with liquid nitrogen) made of copper. Consequently, we expect a heat load of several Watt into the cryostat.


Please note:

The design drawings, as it was done for SRU 1, 2 and 3, will be included in the manual of the complete helium refrigerator unit for the MPD cooling after the completion of the Part B.


| | | | |
|---|------|-------------------|---|
| Rev. 2 | Page | Document no. |  ILK Dresden |
| 31.01.2017 | 40 | ILK-B-1-16-319a_v | |
| Title Helium Refrigerator for MPD cooling | | | |

6.5 List of Suppliers

| Name | Adress | Web-page |
|-------------|--|--|
| WITT | WITT-GASETECHNIK GmbH & Co KG Salinger Feld 4-858454 Witten / Germany | witt@wittgas.com |
| Air Liquide | AIR LIQUIDE Deutschland GmbH Fritz-Klatte-Straße 6 D – 65933 Frankfurt / Germany | awz@airliquide.com |
| WEKA | WEKA AG Schürlistrasse 8 8344 Bäretswil / Schweiz | www.weka-ag.ch |
| HEROSE | HEROSE GMBH ARMATUREN UND METALLE Elly-Heuss-Knapp-Straße 12 23843 Bad Oldesloe / Germany | www.herose.com |
| ROVAK | ROVAK GmbH Zum Teich 4 01723 Grumbach / Germany | www.rovak.de |
| REMBE | REMBE® GMBH SAFETY + CONTROL Gallbergweg 21 59929 Brilon / Germany | www.rembe.de |
| STÖHR | Stoehr Armaturen GmbH & Co. KG Dornierstrasse 4 86343 Koenigsbrunn / Germany | www.stoehr-valves.de |
| JAKOB | Jakob Vakuumtechnik GmbH Daimler Ring 42 Industriegebiet 63839 Kleinwallstad / Germany | info@jakobvakuumtechnik.de |
| allectra | Allectra GmbH Traubeneichenstr. 62-66 D-16567 Schönfließ b. Berlin / Germany | www.allectra.com |
| FESTO | Festo AG & Co. KG Verkaufsbüro Berlin Franz-Jacob-Straße 4 10369 Berlin / Germany | www.festo.com |
| Lakeshore | Cryophysics GmbH Dolivostrasse 9 D-64293 Darmstadt / Germany | www.lakeshore.com info@cryophysics.de |
| Keller | Keller & Kalmbach GmbH Siemensstraße 19 85716 Unterschleißheim / Germany | info@keller-kalmbach.com |


| | | | |
|---|------|-------------------|---|
| Rev. 2 | Page | Document no. |  ILK Dresden |
| 31.01.2017 | 41 | ILK-B-1-16-319a_v | |
| Title Helium Refrigerator for MPD cooling | | | |

| Name | Adress | Web-page |
|----------------|--|--|
| CMT | CMT Manufacturing BV Hakselseweg 50 NL-6713 KW EDE The Netherlands | info@cmtbv.nl |
| KIT | Karlsruher Institut für Technologie Hermann-von-Helmholtz-Platz 1 76344 Eggenstein-Leopoldshafen / Germany | www.itep.kit.edu/index.php |
| Leybold Vacuum | Oerlikon Leybold Vacuum GmbH Bonner Str. 498 50968 Koeln / Germany | www.oerlikon.com |
| Farnell | Karl-Hammerschmidt-Str. 38 85609 Aschheim / Germany | http://de.farnell.com/ |
| RUAG Space | RUAG Space GmbH (Wien) Stachegasse 16 1120 Wien / Austria | http://www.ruag.com/space/at |
| FLEXOMAT | Flexomat GmbH Nossen Gewerbegebiet Heynitz-Lehden Lindigtstraße 2 01683 Nossen / Germany | www.flexomat.de/ |
| SAXONIA | Saxonia Edelstahltechnik und -handels GmbH Salzburger Str. 38-40 ▪ 01279 Dresden / Germany | www.saxonia-edelstahl.de/ |

| | | | |
|-------------------------------------|------|-------------------|---|
| Rev. 2 | Page | Document no. |  |
| 31.01.2017 | 42 | ILK-B-1-16-319a_v | ILK Dresden |
| Title | | | |
| Helium Refrigerator for MPD cooling | | | |

7 Measurement and control technology


A programmable logic controller (PLC) is used for monitoring and control of the MPD-SRU. There are 9 pressure sensors, two level sensors, one mass-flow sensor, 18 temperature sensors and one vacuum sensor, whose values are monitored in real time (see Table 17). According to the current operation mode and the state of the MPD-SRU, 18 electrical control valves are controlled and adjusted as required (see Table 11).

| | | | |
|--|------|-------------------|---|
| Rev. 2 | Page | Document no. |  |
| 31.01.2017 | 43 | ILK-B-1-16-319a_v | |
| Title Helium Refrigerator for MPD cooling | | | |

7.1 Operation modes


Table 15: Operation modes, for valve numbering see Table 11

| <u>valve</u> | 0 off state | 1 clean state | 2 cool down/warm up | 3 normal operation | 4 stand by (no magnet) |
|--------------|--------------------|----------------------|----------------------------|---------------------------|----------------------------------|
| V1 | fixed | fixed | fixed | fixed | fixed |
| V2 | closed | open | open | open | open |
| V3 | 50 % open | 100 % open | P4 regulator | P4 JT regulator | P4 JT regulator |
| V4 | closed | 2 % open | P4 regulator | closed | closed |
| V5 | closed | 100 % open | 100 % open | 100 % open | closed |
| V6 | closed | 100 % open | open if T7 < 40 K | 100 % open | closed |
| V7 | closed | closed | LHe temperature regulator | LHe level regulator | LHe level regulator |
| V8 | 100 % open | 100 % open | 100 % open | 100 % open | 100 % open |
| V9 | closed | 100 % open | open if T8 > 78 K | closed | closed |
| V10 | 5 % open | 10 % open | LN2 temperature regulator | 5 % open | 5 % open |
| V11 | 100 % open | 100 % open | 100 % open | 100 % open | 100 % open |

| | | | |
|--|------|-------------------|---|
| Rev. 2 | Page | Document no. |  |
| 31.01.2017 | 44 | ILK-B-1-16-319a_v | |
| Title Helium Refrigerator for MPD cooling | | | |

Operation modes, for valve numbering see Table 11 (continued from Table 15)

| <u>valve</u> | 0 off state | 1 clean state | 2 cool down/warm up | 3 normal operation | 4 stand by (no magnet) |
|--------------|--------------------|----------------------|---|---------------------------|-------------------------------|
| V12 | closed | closed | LN2 level regulator | LN2 level regulator | LN2 level regulator |
| V13 | 5 % open | 5 % open | closed | closed | closed |
| V14 | 5 % open | 5 % open | closed | closed | fixed |
| V15 | closed | 100 % open | open if $120\text{ K} > T7 > 40\text{ K}$ | closed | closed |
| V16 | closed | 100 % open | open if $250\text{ K} > T7 > 120\text{ K}$ | closed | closed |
| V17 | closed | 100 % open | open if $T7 > 250\text{ K}$ | closed | closed |
| V18 | closed | 100 % open | open if $P6 < \text{set_value} - 0.5\text{ bar}$ | closed | closed |

| | | | |
|---|------|-------------------|---|
| Rev. 2 | Page | Document no. |  ILK Dresden |
| 31.01.2017 | 45 | ILK-B-1-16-319a_v | |
| Title Helium Refrigerator for MPD cooling | | | |

7.2 Control scheme

7.2.1 LN2 Liquid nitrogen level control with V12

The liquid nitrogen level is controlled with the LN2 inlet valve V12 and the level sensor L2:

Set value: $75\% < \text{set_value_L2} < 95\%$

Priority 1: LN2 over pressure P13 → close V12

LN2 level > 100 % → close V12

Priority 2: In cool down and warm up mode maximum temperature gradient surveillance

T12, T13, T14, T15, T16 is active:

$dT/dt < -5 \text{ K/h} \rightarrow \text{decrease V12}$

$dT/dt > 5 \text{ K/h} \rightarrow \text{increase V12}$

Priority 3: LN2 level < $\text{set_value_L2} - 2\%$ → slowly increase V12

LN2 level > $\text{set_value_L2} + 2\%$ → decrease V12

7.2.2 Liquid helium level control with V7

The liquid helium level is controlled by the LHe inlet valve V7 and the level sensor L1 in normal operation mode:

Set value: $45\% < \text{set_value_L1} < 95\%$

Priority 1: LHe over pressure P8 → close V7

LHe Level > 100 % → close V7


Priority 2: LHe Level < $\text{set_value_L1} - 2\%$ → slow increase V7

LHe Level > $\text{set_value_L1} + 2\%$ → slow decrease V7

During cool down and warm up there is no or little liquid helium inside the SRU and V7 is controlled with the LHe temperature regulator.

7.2.3 LN2 temperature control with V10

During cool down or warm up, temperature of the experiment is controlled. The maximum absolute temperature difference between inlet T6 and outlet T7 must be below 10 K and the maximum absolute temperature gradient below 1 K/h. The experiment temperature is determined as average of T6 and T7. LN2 temperature control with V10 is active (V9 open) as long as the experiment inlet temperature T6 is above 78 K.

| | | | |
|--|------|-------------------|--|
| Rev. 2 | Page | Document no. |  ILK Dresden |
| 31.01.2017 | 46 | ILK-B-1-16-319a_v | |
| Title Helium Refrigerator for MPD cooling | | | |

All changes are done very slowly to avoid temperature jumps:

Set value: Automatic adjustment with 1 K/h if $|T7-T6| < 10$ K:
 $78 \text{ K} < \text{set_value_T_experiment} < 300 \text{ K}$

Priority 1: He over pressure P8 → close V10

Priority 2: He pressure P8 regulation: if $P8 > \text{set_value_P8}$ → decrease V10

Priority 3: $T6 < 78 \text{ K}$ → close V10 slowly

Priority 4: $dT18/dt > 5 \text{ K/h}$ → increase V10


$dT18/dt < -5 \text{ K/h}$ → decrease V10

Priority 5: $T7 - T6 > 10 \text{ K}$ → decrease V10

$T7 - T6 < -10 \text{ K}$ → increase V10

Priority 6: $(T7+T6)/2 > \text{set_value_T_experiment} + 0.2 \text{ K}$ → increase V10

$(T7+T6)/2 < \text{set_value_T_experiment} - 0.2 \text{ K}$ → decrease V10

| | | | |
|--|------|-------------------|---|
| Rev. 2 | Page | Document no. |  ILK Dresden |
| 31.01.2017 | 47 | ILK-B-1-16-319a_v | |
| Title Helium Refrigerator for MPD cooling | | | |

7.2.4 LHe temperature control with V7

During cool down or warm up, temperature of the experiment is controlled. The maximum absolute temperature difference between inlet T6 and outlet T7 must be below 10 K and the maximum absolute temperature gradient below 1 K/h. The experiment temperature is determined as average of T6 and T7. LHe temperature control with V7 is active as long as the experiment inlet temperature T6 is below 80 K or $T6 < T17$.

All changes are done very slowly to avoid temperature jumps:

Set value: Automatic adjustment with 1 K/h if $|T7-T6| < 10$ K:
 $4.5 \text{ K} < \text{set_value_T_experiment} < 80 \text{ K}$

Priority 1: He over pressure P8 → close V7
Liquid Helium level L1 > 100 % → close V7

Priority 2: He pressure surveillance P8 > 0.1 bar + set_value_P8 → decrease V7
Liquid Helium level L1 > 40 % → decrease V7

Priority 3: $dT17/dt > 5 \text{ K/h}$ → increase V7
 $dT17/dt < -5 \text{ K/h}$ → decrease V7


Priority 4: $T6 + 1 \text{ K} < T17$ → increase V7

Priority 5: $T6 > 80 \text{ K}$ → close V7 slowly

Priority 6: $T7 - T6 > 10 \text{ K}$ → decrease V7
 $T7 - T6 < -10 \text{ K}$ → increase V7

Priority 7: $(T7+T6)/2 > \text{set_value_T_experiment} + 0.2 \text{ K}$ → increase V7
 $(T7+T6)/2 < \text{set_value_T_experiment} - 0.2 \text{ K}$ → decrease V7

If $(T6+T7)/2 < 5 \text{ K}$ and cool-down mode then the normal operation mode is started.

| | | | |
|--|------|-------------------|---|
| Rev. 2 | Page | Document no. |  ILK Dresden |
| 31.01.2017 | 48 | ILK-B-1-16-319a_v | |
| Title Helium Refrigerator for MPD cooling | | | |

7.2.5 He liquefier valve control with V3

In normal operation mode the Joule-Thomson (JT) decompression of GHe from 13 bar (P3) to 1.1 – 2 bar (P4) is controlled by regulating V3. Valve 4 is completely closed in this mode:

Set value: $1.1 \text{ bar} < \text{set_value_P4} < 2.0 \text{ bar}$

Priority 1: He over pressure P8 → close V3

Priority 2: $P4 > \text{set_value_P4} + 50 \text{ mbar} \rightarrow \text{decrease V3}$
 $P4 < \text{set_value_P4} - 50 \text{ mbar} \rightarrow \text{increase V3}$

7.2.6 He decompression valve control with V3 and V4

In cool down and warm up operation mode the decompression of GHe from 13 bar (P3) to experiment pre-pressure (P4) is controlled by regulating V3 and V4. Valve 4 is used as extension of Valve 3 and starts opening if V3 is completely open:

Set value: $1.1 \text{ bar} < \text{set_value_P4} < 12.0 \text{ bar}$

Priority 1: He over pressure P8 → close V3 and V4

Priority 2: He pressure surveillance $P8 > 0.1 \text{ bar} + \text{set_value_P8} \rightarrow \text{decrease V3 and V4}$


Priority 3: $P4 > \text{set_value_P4} + 100 \text{ mbar} \rightarrow \text{decrease V3 and V4}$
 $P4 < \text{set_value_P4} - 100 \text{ mbar} \rightarrow \text{increase V3 and V4}$

7.2.7 He HEX by-pass control with V15, V16, V17, V18 and V6

In cool down and warm up mode the heat exchanger (HEX) by-pass valves V15, V16, V17, V18 and the return valve V6 are controlled according to experiment temperatures and pressure. All by-pass switching procedures are done very slowly to avoid temperature jumps. The following algorithms are implemented:

Switching temperatures: $T_{V17} = 250 \text{ K}$
 $T_{V16} = 120 \text{ K}$
 $T_{V15} = 40 \text{ K}$

Experiment pressure: $1.1 \text{ bar} < \text{set_value_P4} < 12 \text{ bar}$ depending on experiment temperature

| | | | |
|---|------|-------------------|---|
| Rev. 2 | Page | Document no. |  ILK Dresden |
| 31.01.2017 | 49 | ILK-B-1-16-319a_v | |
| Title Helium Refrigerator for MPD cooling | | | |

Priority 1: He over pressure P8 → open V17 and V6, close V18

Priority 2: He pressure surveillance:

- P8 > 0.2 bar + set_value_P8 → increase V15, decrease V18
- P8 > 0.3 bar + set_value_P8 → increase V16
- P8 > 0.4 bar + set_value_P8 → increase V17

Priority 3: He by-pass control with experiment return temperature T7:

- P6 < set_value_P4 – 0.6 bar → slowly increase V18
- P6 > set_value_P4 – 0.5 bar → slowly decrease V18
- T7 > T_V17 – 0.1 K → slowly increase V17
- T7 < T_V17 – 0.2 K → slowly decrease V17
- T7 < T_V17 + 0.1 K → slowly increase V16
- T7 > T_V17 + 0.2 K → slowly decrease V16
- T7 > T_V16 – 0.1 K → slowly increase V16
- T7 < T_V16 – 0.2 K → slowly decrease V16
- T7 < T_V16 + 0.1 K → slowly increase V15
- T7 > T_V16 + 0.2 K → slowly decrease V15
- T7 > T_V15 – 0.1 K → slowly increase V15
- T7 < T_V15 – 0.2 K → slowly decrease V15
- T7 < T_V15 + 0.1 K → slowly increase V6
- T7 > T_V15 + 0.2 K → slowly decrease V6

7.2.8 Warning and emergency control

The system is equipped with a high number of sensors, which can fail or sense values beyond specifications. Table 16 shows the normal operation conditions and the limits for **warnings** and **emergencies**. Warnings usually require human interaction to ensure a continued operation while the system keeps running, whereas emergencies can result in an immediate shut-down or insufficient cooling.



| | | | |
|--|------|-------------------|--|
| Rev. 2 | Page | Document no. |  ILK Dresden |
| 31.01.2017 | 50 | ILK-B-1-16-319a_v | |
| Title Helium Refrigerator for MPD cooling | | | |


Table 16: Warning and emergency conditions

| Sensors | on fail | normal range | cool down / warm up range | normal operation emergency range | cool down/ warm up emergency range |
|---------------|-----------------------------|---------------|--------------------------------------|----------------------------------|------------------------------------|
| T1 | warning, T2 & T11 redundant | 273 K - 325 K | 273 K - 325 K | | |
| T2 | warning, T1 redundant | 273 K - 325 K | 273 K - 325 K | | |
| T3 | warning, no redundant | 5 K - 10 K | 5 K - 325 K | | |
| T4 | warning, no redundant | 4.2 K - 6 K | 4.2 K - 325 K | | |
| T5 | warning, T6 redundant | 4.2 K - 4.7 K | 4.2 K - 325 K | > 6 K | |
| T6a, T6b, 16c | warning, T5 & T6 redundant | 4.2 K - 5.0 K | 4.2 K - 325 K, $ T7-T6 < 10$ K | > 6 K | $ T7-T6 > 11$ K |
| T7a, T7b, T7c | warning, T7 redundant | 4.2 K - 10 K | 4.2 K - 325 K, $ T7-T6 < 10$ K | > 11 K | $ T7-T6 > 11$ K |
| T8 | warning, no redundant | 4.2 K - 8.0 K | 4.2 K - 325 K | | |
| T9 | warning, T10 redundant | 230 K - 325 K | 200 K - 325 K | | |
| T10 | warning, T9 redundant | 230 K - 325 K | 200 K - 325 K | | |
| T11 | warning, T1 redundant | 273 K - 325 K | 273 K - 325 K | | |
| T12 | warning, no redundant | | 80 K - 325 K | | |
| T13 | warning, no redundant | 77 K - 100 K | 77 K - 325 K | | |
| T14 | warning, no redundant | 100 K - 325 K | 100 K - 325 K | | |
| T15a, T15b | warning, T15 redundant | 77 K - 120 K | 77 K - 325 K | | |
| T16 | warning, no redundant | 77 K - 100 K | 77 K - 325 K, ($< T7$) (< 80 K) | > 120 K | ($> T7 + 1$ K) & (> 81 K) |
| T17 | warning, no redundant | 4.1 K - 5.0 K | 4.1 K - 325 K, $< T7$ | > 6 K | $> T7 + 1$ K |

| | | | |
|--|------|-------------------|--|
| Rev. 2 | Page | Document no. |  ILK Dresden |
| 31.01.2017 | 51 | ILK-B-1-16-319a_v | |
| Title Helium Refrigerator for MPD cooling | | | |

Warning and emergency conditions, continued from Table 16:

| Sensors | on fail | normal range | cool down / warm up range | normal operation emergency range | cool down/ warm up emergency range |
|----------|----------------------------------|--------------------------|---------------------------|----------------------------------|------------------------------------|
| P1 | warning, P2 & P11 & P3 redundant | 11 - 15 bar (a) | 11 - 15 bar (a) | < 8 bar, > 20 bar | < 8 bar, > 20 bar |
| P2 | warning, P1 & P3 redundant | 11 - 15 bar (a) | 11 - 15 bar (a) | < 8 bar, > 20 bar | < 8 bar, > 20 bar |
| P3 | warning, P1 & P2 redundant | 11 - 15 bar (a) | 9 - 15 bar (a) | < 8 bar, > 20 bar | < 8 bar, > 20 bar |
| P4 | warning, P5a redundant | 1.1 - 2.5 bar (a) | 2 - 15 bar (a) | < 1.1 bar, > 20 bar | < 1.1 bar, > 20 bar |
| P5d | warning, no redundant | 0.01 - 0.1 bar | 0.01 - 1.0 bar | | |
| P5a | warning, P4 redundant | 1.1 - 2.5 bar (a) | 2 - 15 bar (a) | < 1.1 bar, > 20 bar | < 1.1 bar, > 20 bar |
| P6 | warning, P5 redundant | 1.1 - 2.5 bar (a) | 2 - 15 bar (a) | < 1.1 bar, > 20 bar | < 1.1 bar, > 20 bar |
| P7 | warning, P8 redundant | 0.9 - 1.5 bar (a) | 0.9 - 1.5 bar (a) | > 2 bar | > 2 bar |
| | | | | | |
| P8 | warning, P11/P7 redundant | 1.0 - 1.5 bar (a) | 0.9 - 1.5 bar (a) | > 1.6 bar | > 1.6 bar |
| P11 | warning, P1 & P2 redundant | 1.0 - 1.5 bar (a) | 1.0 - 15 bar (a) | > 20 bar | < 1.1 bar, > 20 bar |
| P13 | warning, no redundant | 0.9 - 1.5 bar (a) | 0.9 - 1.5 bar (a) | > 1.6 bar | > 1.6 bar |
| Pvac | warning, no redundant | <1x10 ⁻⁴ mbar | <1x10 ⁻⁴ mbar | > 1x10 ⁻² mbar | > 1x10 ⁻² mbar |
| | | | | | |
| L1a, L1b | warning, L1 redundant | 45 % < 100 % | -10 % < 100 % | < 40 %, > 105 % | > 105 % |
| L2a, L1b | warning, L2 redundant | 40 % < 100 % | -10 % < 100 % | > 105 % | > 105 % |

| | | | |
|--|------|-------------------|---|
| Rev. 2 | Page | Document no. |  ILK Dresden |
| 31.01.2017 | 52 | ILK-B-1-16-319a_v | |
| Title Helium Refrigerator for MPD cooling | | | |

7.3 Hardware

7.3.1 Programmable logic controller (PLC)

To be defined (t.b.d.)¹¹

7.3.2 Sensor interface

2 pieces 16x Temperature controller developed by ILK Dresden with cold multiplexer RS485 interface

1 piece 8 analog input 4-20 mA universal sensor interface (Level, Vacuum)

7.3.3 Valve interface

t.b.d.

7.3.4 Human machine interface (HMI)

t.b.d.


7.3.5 Data visualization and logging (PC)

Microsoft Windows PC software

Please note:

Required measurement data for communication have to be discussed with the JINR and the company ASG superconductors (manufacturer of the MPD).

¹¹ The final set-up will be defined after ordering of the valve interface.

| | | | |
|---|------|-------------------|---|
| Rev. 2 | Page | Document no. |  ILK Dresden |
| 31.01.2017 | 53 | ILK-B-1-16-319a_v | |
| Title Helium Refrigerator for MPD cooling | | | |

7.4 Sensors

Table 17: Sensor contractors and types

| Sensor | Contractor | Type |
|-----------|--------------------|-----------------------------|
| T1 - T2 | Farnell IST | 1266944 Pt1000 |
| T3 - T10 | JINR / ILK Dresden | 1 kOhm Carbon type |
| T11 - T16 | Farnell IST | 1266944 Pt1000 |
| T17 | JINR / ILK Dresden | 1 kOhm Carbon type |
| P1 - P4 | Keller Kalmbach | PAA-33X 30 bar MODBUS RTU |
| P5 | Keller Kalmbach | PRD-33X 1/40 bar MODBUS RTU |
| P6 - P7 | Keller Kalmbach | PAA-33X 30 bar MODBUS RTU |
| P8 | Keller Kalmbach | PAA-33X 3 bar MODBUS RTU |
| P11 | Keller Kalmbach | PAA-33X 30 bar MODBUS RTU |
| P13 | Keller Kalmbach | PAA-33X 3 bar MODBUS RTU |
| Pvac | Leybold Vacuum | Pirani DN 25 |
| F | ILK Dresden | Venturi tube 8/3.3 |
| L1 | CMT | C-Stic, capacitive type |
| L2 | CMT | C-Stic, capacitive type |